

1

Defining Enhanced Oil Recovery

Enhanced oil recovery (EOR) is oil recovery by the injection of materials not normally present in the reservoir. This definition covers all modes of oil recovery processes (drive, push-pull, and well treatments) and most oil recovery agents. Enhanced oil recovery technologies are also being used for in-situ extraction of organic pollutants from permeable media. In these applications, the extraction is referred to as cleanup or remediation, and the hydrocarbon as product. Various sections of this text will discuss remediation technologies specifically, although we will mainly discuss petroleum reservoirs. The text will also describe the application of EOR technology to carbon dioxide storage where appropriate.

The definition does not restrict EOR to a particular phase (primary, secondary, or tertiary) in the producing life of a reservoir. Primary recovery is oil recovery by natural drive mechanisms: solution gas, water influx, and gas cap drives, or gravity drainage. Figure 1-1 illustrates. Secondary recovery refers to techniques, such as gas or water injection, whose purpose is mainly to raise or maintain reservoir pressure. Tertiary recovery is any technique applied after secondary recovery. Nearly all EOR processes have been at least field tested as secondary displacements. Many thermal methods are commercial in both primary and secondary modes. Much interest has been focused on tertiary EOR, but the definition given here is not so restricted. The definition does exclude waterflooding but is intended to exclude all pressure maintenance processes. The distinction between pressure maintenance

and displacement is not clear, since some displacement occurs in all pressure maintenance processes. Moreover, agents such as methane in a high-pressure gas drive, or carbon dioxide in a reservoir with substantial native CO₂, do not satisfy the definition, yet both are clearly EOR processes. The same can be said of CO₂ storage. Usually the EOR cases that fall outside the definition are clearly classified by the intent of the process.

In the last decade, improved oil recovery (IOR) has been used interchangeably with EOR or even in place of it. Although there is no formal definition, IOR typically refers to any process or practice that improves oil recovery (Stosur *et al.*, 2003). IOR therefore includes EOR processes but can also include other practices such as waterflooding, pressure maintenance, infill drilling, and horizontal wells.

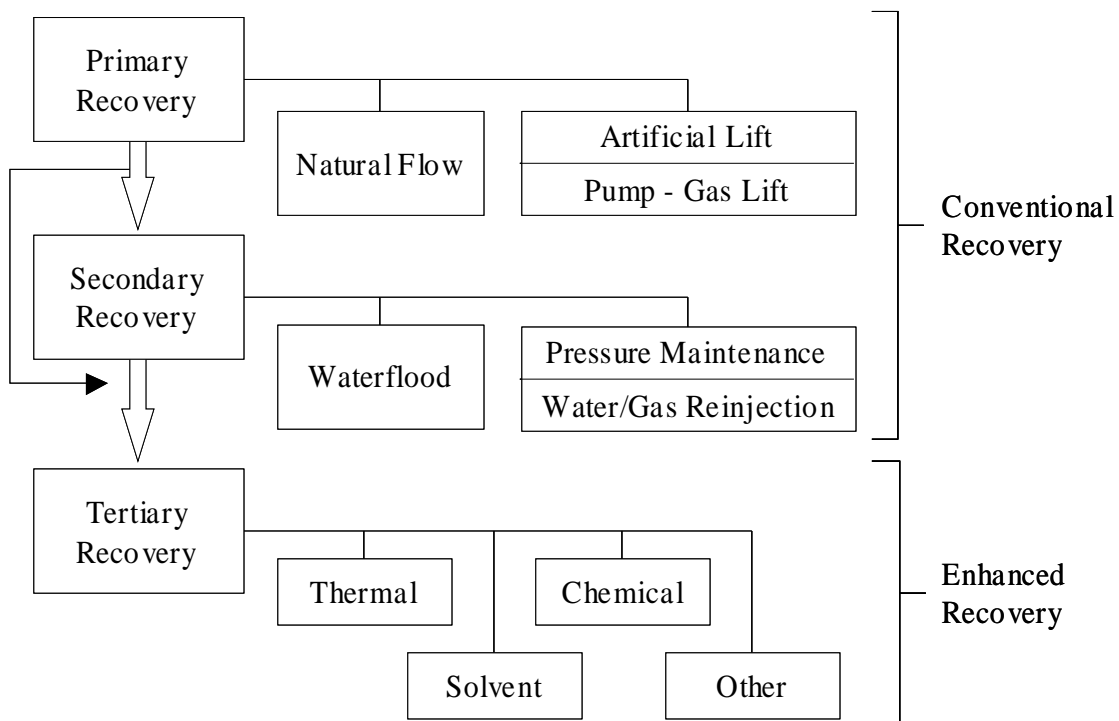


Figure 1-1. Oil recovery classifications (adapted from the Oil and Gas Journal biennial surveys).

1-1 EOR INTRODUCTION

The EOR Target

We are interested in EOR because of the amount of oil to which it is potentially applicable. This EOR target oil is the amount unrecoverable by conventional means (Fig. 1-1). A large body of statistics shows that conventional ultimate oil recovery (the percentage of the original oil in place at the time for which further conventional

recovery becomes uneconomic) is about 35%. This means for example that a field that originally contained 1 billion barrels will leave behind 650,000 barrels at the end of its conventional life. Considering all of the reservoirs in the U.S., this value is much larger than targets from exploration or increased drilling.

The ultimate recovery is shown in Fig. 1-2. This figure also shows that there is enormous variability in ultimate recovery within a geographic region, which is why we cannot target reservoirs with EOR by region. Reservoirs that have an exceptionally large conventional recovery are not good tertiary EOR candidates. Figure 1-2 shows also that the median ultimate recovery is the same for most regions, a fact no doubt bolstered by the large variability within each region.

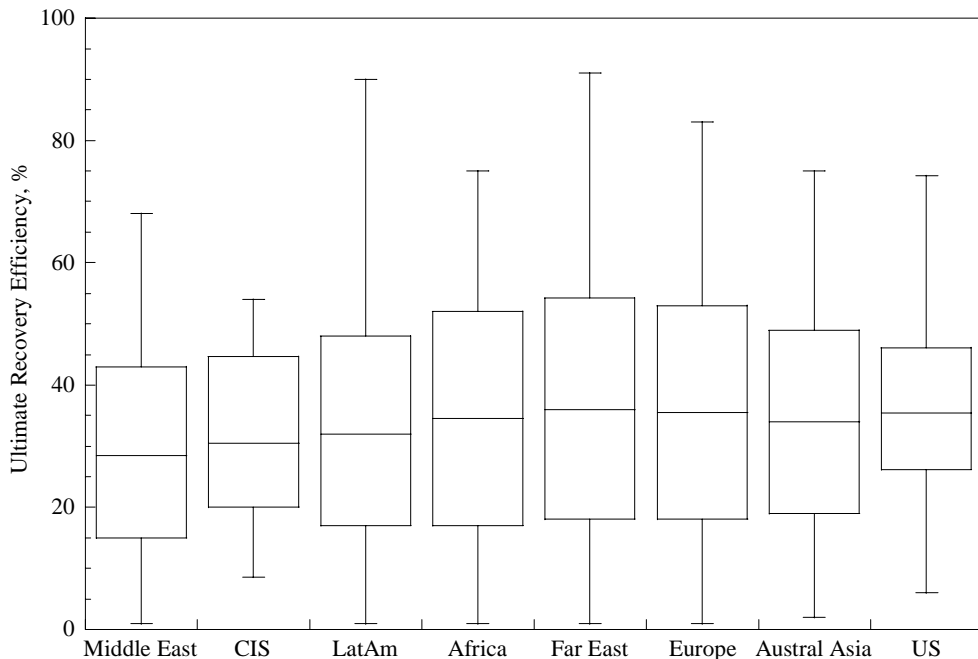


Figure 1-2. Box plots of ultimate oil recovery efficiency. 75% of the ultimate recoveries in a region fall within the vertical boxes; the median recovery is the horizontal line in the box; the vertical lines give the range. Ultimate recovery is highly variable, but the median is about the same everywhere (from Laherre, 2001).

1-2 THE NEED FOR EOR

Enhanced oil recovery is one of the technologies needed to maintain reserves.

Reserves

Reserves are petroleum (crude and condensate) recoverable from known reservoirs under prevailing economics and technology. They are given by the following material balance equation:

$$\left(\begin{array}{c} \text{Present} \\ \text{reserves} \end{array} \right) = \left(\begin{array}{c} \text{Past} \\ \text{reserves} \end{array} \right) + \left(\begin{array}{c} \text{Additions} \\ \text{to reserves} \end{array} \right) - \left(\begin{array}{c} \text{Production} \\ \text{from} \\ \text{reserves} \end{array} \right)$$

There are actually several categories of reservoirs (proven, etc.) which distinctions are very important to economic evaluation (Rose, 2001; Cronquist, 2001). Clearly, reserves can change with time because the last two terms on the right do change with time. It is in the best interests of producers to maintain reserves constant with time, or even to have them increase.

Adding to Reserves

The four categories of adding to reserves are

1. Discovering new fields
2. Discovering new reservoirs
3. Extending reservoirs in known fields
4. Redefining reserves because of changes in economics of extraction technology

We discuss category 4 in the remainder of this text. Here we substantiate its importance by briefly discussing categories 1 to 3.

Reserves in categories 1 to 3 are added through drilling, historically the most important way to add reserves. Given the 2% annual increase in world-wide consumption and the already large consumption rate, it has become evident that reserves can be maintained constant only by discovering large reservoirs.

But the discovery rate of large fields is declining. More importantly, the discovery rate no longer depends strongly on the drilling rate. Equally important, drilling requires a substantial capital investment even after a field is discovered. By contrast, the majority of the capital investment for EOR has already been made (if previous wells can be used). The location of the target field is known (no need to explore), and targets tend to be close to existing markets.

Enhanced oil recovery is actually a competitor with conventional oil recovery because most producers have assets or access to assets in all of the Fig. 1-1 categories. The competition then is joined largely on the basis of economics in addition to reserve replacement. At the present, many EOR technologies are competitive with drilling-based reserve additions. The key to economic competitiveness is how much oil can be recovered with EOR, a topic to which we next turn.

1-3 INCREMENTAL OIL

Definition

A universal technical measure of the success of an EOR project is the amount of incremental oil recovered. Figure 1-3 defines incremental oil. Imagine a field, reservoir, or well whose oil rate is declining as from A to B. At B, an EOR project is initiated and, if successful, the rate should show a deviation from the projected decline at some time after B. Incremental oil is the difference between what was actually recovered, B to D, and what would have been recovered had the process not been initiated, B to C. Since areas under rate-time curves are amounts, this is the shaded region in Fig. 1-3.

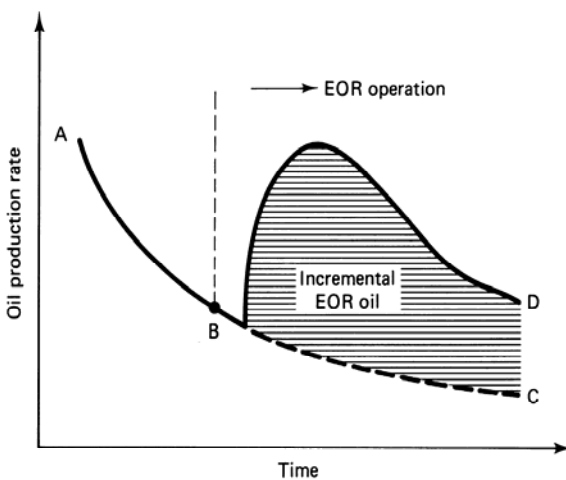


Figure 1-3. Incremental oil recovery from typical EOR response (from Prats, 1982)

As simple as the concept in Fig. 1-3 is, EOR is difficult to determine in practice. There are several reasons for this.

1. Combined (comingled) production from EOR and nonEOR wells. Such production makes it difficult to allocate the EOR-produced oil to the EOR project. Comingling occurs when, as is usually the case, the EOR project is phased into a field undergoing other types of recovery.
2. Oil from other sources. Usually the EOR project has experienced substantial well cleanup or other improvements before startup. The oil produced as a result of such treatment is not easily differentiated from the EOR oil.
3. Inaccurate estimate of hypothetical decline. The curve from *B* to *C* in Fig. 1-3 must be accurately estimated. But since it did not occur, there is no way of assessing this accuracy.

Ways to infer incremental oil recovery from production data range from highly sophisticated numerical models to graphical procedures. One of the latter, based on decine curve analysis, is covered in the next section.

Estimating Incremental Oil Recovery Through Decline Curves

Decline curve analysis can be applied to virtually any hydrocarbon production operation. The following is an abstraction of the practice as it applies to EOR. See Walsh and Lake (2003) for more discussion. The objective is to derive relations between oil rate and time, and then between cumulative production and rate.

The oil rate q changes with time t in a manner that defines a decline rate D according to

$$\frac{1}{q} \frac{dq}{dt} = -D \quad 1.3-1$$

The rate has units of (or [=]) amount or volume per time and D [=]1/time. Time is in units of days, months, or even years consistent with the units of q . D itself can be a function of rate, but we take it to be constant. Integrating Eq. 1.3-1 gives

$$q = q_i e^{-Dt} \quad 1.3-2$$

where q_i is the initial rate or q evaluated at $t = 0$. Equation 1.3-2 suggests a semilogarithmic relationship between rate and time as illustrated in Fig. 1-3. Exponential decline is the most common type of analysis employed.

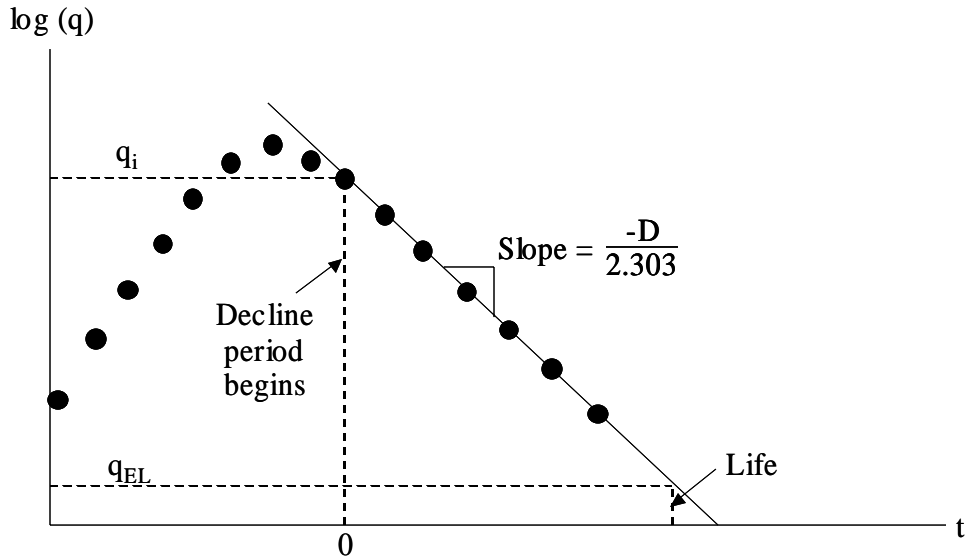


Figure 1-3. Schematic of exponential decline on a rate-time plot.

Figure 1-3 schematically illustrates a set of data (points) which begin an exponential decline at the ninth point where, by definition $t = 0$. The solid line represents the fit of the decline curve model to the data points. q_i is the rate given by the model at $t=0$, not necessarily the measured rate at this point. The slope of the model is the negative of the decline rate divided by 2.303, since standard semilog graphs are plots of base 10 rather than natural logarithms.

Because the model is a straight line, it can be extrapolated to some future rate. If we let q_{EL} designate the economically limiting rate (simply the *economic limit*) of the project under consideration, then where the model extrapolation attains q_{EL} is an estimate of the project's (of well's, etc.) economic life. The economic limit is a nominal measure of the rate at which the revenues become equal to operating expenses plus overhead. q_{EL} can vary from a fraction to a few hundred barrels per day depending on the operating conditions. It is also a function of the prevailing economics: as oil price increases, q_{EL} decreases, an important factor in reserve considerations.

The rate-time analysis is useful, but the rate-cumulative curve is more helpful. The cumulative oil produced is given by

$$N_p = \int_{\xi=0}^{\xi=t} q d\xi .$$

The definition in this equation is general and will be employed throughout the text, but especially in Chap. 2. To derive a rate -cumulative expression, insert Eq. 1.3-1, integrate, and identify the resulting terms with (again) Eq. 1.3-1. This gives

$$q = q_i - DN_p \quad 1.3-3$$

Equation 1.3-3 says that a plot of oil rate versus cumulative production should be a straight line on linear coordinates. Figure 1-4 illustrates.

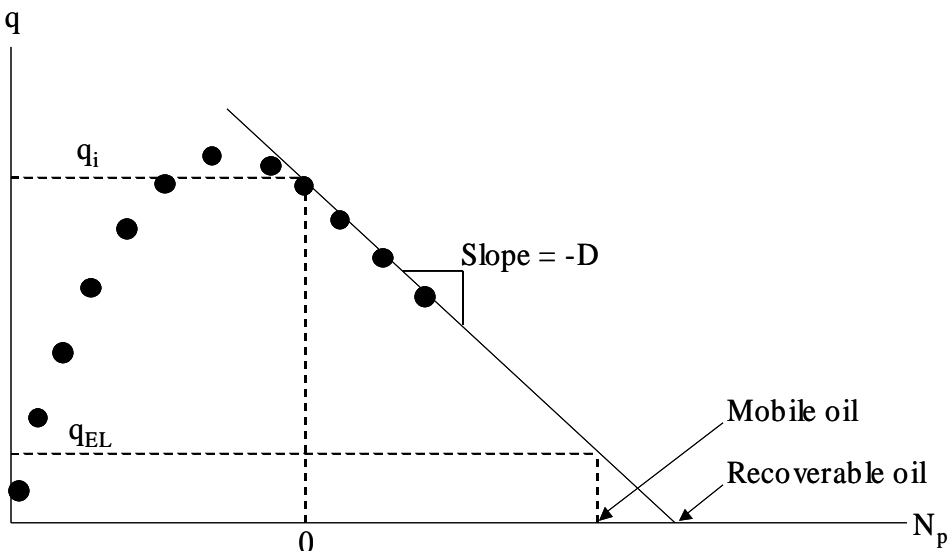


Figure 1-4. Schematic of exponential decline on a rate-cumulative plot.

You should note that the cumulative oil points being plotted on the horizontal axis of this figure are from the oil rate data, not the decline curve. If this were not so, there would be no additional information in the rate-cumulative plot. Calculating N_p normally requires a numerical integration with something like the trapezoid rule.

Using model Eqs 1.3-2 and 1.3-3 to interpret a set of data as illustrated in Figs. 1-3 and 1-4 is the essence of reservoir engineering practice, namely

1. Develop a model as we have done to arrive at Eqs. 1.3-2 and 1.3-3. Often the model equations are far more complicated than these, but the method is the same regardless of the model.
2. Fit the model to the data. Remember that the points in Figs. 1-3 and 1-4 are data. The lines are the model.
3. With the model fit to the data (the model is now calibrated), extrapolate the model to make predictions.

At the onset of the decline period, the data again start to follow a straight line through which can be fit a linear model. In effect, what has occurred with this plot is that we have replaced time on Fig. 1-3 with cumulative oil produced on Fig. 1-4, but there is one very important distinction: both axes in Fig. 1-4 are now linear. This has three important consequences.

1. The slope of the model is now $-D$ since no correction for log scales is required.
2. The origin of the model can be shifted in either direction by simple additions.
3. The rate can now be extrapolated to zero.

Point 2 simply means that we can plot the cumulative oil produced for all periods prior to the decline curve period (or for previous decline curve periods) on the same rate-cumulative plot. Point 3 means that we can extrapolate the model to find the total mobile oil (when the rate is zero) rather than just the recoverable oil (when the rate is at the economic limit).

Rate-cumulative plots are simple yet informative tools for interpreting EOR processes because they allow estimates of incremental oil recovery (IOR) by distinguishing between recoverable and mobile oil. We illustrate how this comes about through some idealized cases.

Figure 1-5 shows a rate-cumulative plot for a project having an exponential decline just prior to and immediately after the initiation of an EOR process.

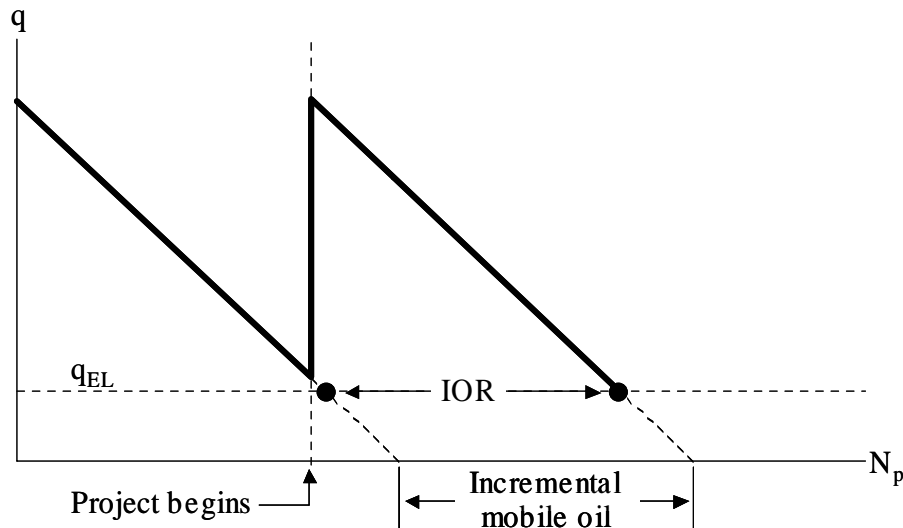


Figure 1-5. Schematic of exponential decline curve behavior on a rate-cumulative plot. The EOR project produces both incremental oil (IOR), and increases the mobile oil. The pre- and post-EOR decline rates are the same.

We have replaced the data points with the models only for ease of presentation. Placing both periods on the same horizontal axis is permissible because of the scaling arguments mentioned above. In this case, the EOR process did not accelerate the production because the decline rates in both periods are the same; however, the process did increase the amount of mobile oil, which in turn caused some incremental oil production. In this case, the incremental recovery and mobile oil are the same. Such idealized behavior would be characteristic of thermal, micellar-polymer, and solvent processes.

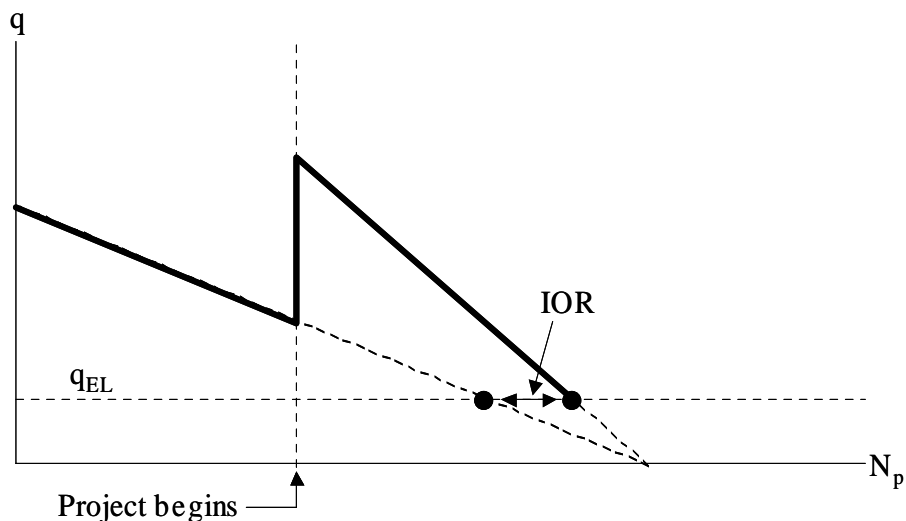


Figure 1-6. Schematic of exponential decline curve behavior on a rate-cumulative plot. The EOR project produces incremental oil at the indicated economic limit but does not increase the mobile oil.

Figure 1-6 shows another extreme where production is only accelerated, the pre- and post-EOR decline rates being different. Now the curves extrapolate to a common mobile oil but with still a nonzero IOR. We expect correctly that processes that behave as this will produce less oil than ones that increase mobile oil, but they can still be profitable, particularly, if the agent used to bring about this result is inexpensive. Processes that ideally behave in this manner are polymer floods and polymer gel processes, which do not affect residual oil saturation. Acceleration processes are especially sensitive to the economic limit; large economic limits imply large IOR.

Example 1-1. Estimating incremental oil recovery.

Sometimes estimating IOR can be fairly subtle as this example illustrates. Figure 1-7 shows a portion of rate-cumulative data from a field that started EOR about half-way through the total production shown.

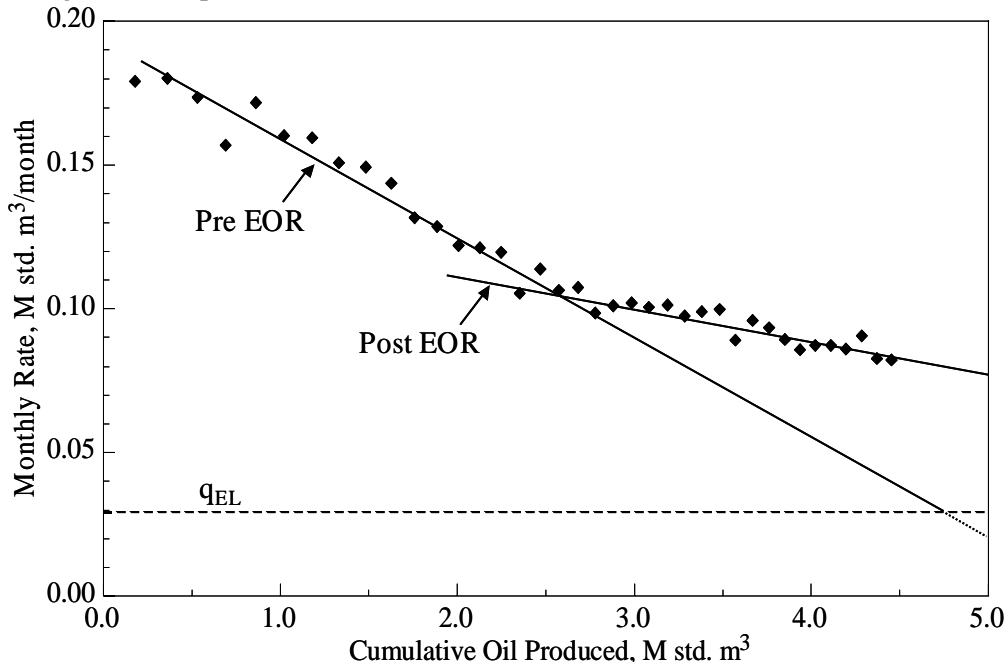


Figure 1-7. Rate (vertical axis) - cumulative (horizontal axis) plot for a field undergoing an EOR process.

- Identify the pre- and post-EOR decline periods.

The pre-EOR decline ends at about 2.5 M std. m³ of oil produced, at which time the post-EOR period begins. This point does not necessarily coincide with the start of the EOR process. The start cannot be inferred from the rate-cumulative plot.

- Calculate the decline rates ($= \text{mo}^{-1}$) for both periods.

Both decline periods are fitted by the straight lines indicated. The fitting is done through standard means; the difficulty is always identifying when the periods start and end. For the pre-EOR decline,

$$D = -\left(\frac{(0.11 - 0.18) \frac{\text{M std. m}^3}{\text{month}}}{(2.55 - 0) \text{M std. m}^3} \right) = 0.027 \text{ month}^{-1}$$

and for the post-EOR decline,

$$D = - \left(\frac{(0.09 - 0.11) \frac{\text{M std. m}^3}{\text{month}}}{(4 - 2.55) \text{M std. m}^3} \right) = 0.0137 \text{ month}^{-1}$$

The EOR project has about halved the decline rate even though there is no increase in rate.

c. Estimate the IOR ([=] M std. m³) for this project at the indicated economic limit.

The oil to be recovered by continued operations is 4.7 M std. m³. That from EOR is (by extrapolation) 7 M std. m³ for an incremental oil recovery of 2.3 M std. m³.

1-4 CATEGORY COMPARISONS

Comparative Performances

Most of this text covers the details of EOR processes. At this point, we compare performances of the three basic EOR processes and introduce some issues to be discussed later in the form of screening guides. The performance is represented as typical oil recoveries (incremental oil expressed as a percent of original oil in place) and by various utilization factors. Both are based on actual experience. Utilization factors express the amount of an EOR agent required to produce a barrel of incremental oil. They are a rough measure of process profitability.

Table 1-1 shows sensitivity to high salinities is common to all chemical flooding EOR. Total dissolved solids should be less than 100,000 g/m³, and hardness should be less than 2,000 g/m³. Chemical agents are also susceptible to loss through rock–fluid interactions. Maintaining adequate injectivity is a persistent issue with chemical methods. Historical oil recoveries have ranged from small to moderately large. Chemical utilization factors have meaning only when compared to the costs of the individual agents; polymer, for example, is usually three to four times as expensive (per unit mass) as surfactants.

TABLE 1-1 CHEMICAL EOR PROCESSES

Process	Recovery mechanism	Issues	Typical recovery (%)	Typical agent utilization*
Polymer	Improves volumetric sweep by mobility reduction	Injectivity Stability High salinity	5	0.3–0.5 lb polymer per bbl oil produced
Micellar polymer	Same as polymer plus reduces capillary forces	Same as polymer plus chemical availability, retention, and high salinity	15	15–25 lb surfactant per bbl oil produced

Alkaline polymer	Same as micellar polymer plus oil solubilization and wettability alteration	Same as micellar polymer plus oil composition	5	35–45 lb chemical per bbl oil produced
------------------	---	---	---	--

*1 lb/bbl \cong 2.86 kg/m³

Table 1-2 shows a similar comparison for thermal processes. Recoveries are generally higher for these processes than for the chemical methods. Again, the issues are similar within a given category, centering on heat losses, override, and air pollution. Air pollution occurs because steam is usually generated by burning a

TABLE 1-2 THERMAL EOR PROCESSES

Process	Recovery mechanism	Issues	Typical recovery (%)	Typical agent utilization*
Steam (drive and stimulation)	Reduces oil viscosity Vaporization of light ends	Depth Heat losses Override Pollution	50–65	0.5 bbl oil consumed per bbl oil produced
In situ combustion	Same as steam plus cracking	Same as steam plus control of combustion	10–15	10 Mscf air per bbl oil produced*

*1 Mscf/stb \cong 178std. m³ gas/std. m³ oil

portion of the resident oil. If this burning occurs on the surface, the emission products contribute to air pollution; if the burning is in situ, production wells can be a source of pollutants.

Table 1-3 compares solvent flooding processes. Only two groups are in this category, corresponding to whether or not the solvent develops miscibility with the oil. Oil recoveries are generally lower than for micellar-polymer recoveries. The solvent utilization factors as well as the relatively low cost of the solvents have brought these processes, particularly carbon dioxide flooding, to commercial application. The distinction between a miscible and an immiscible process is slight.

TABLE 1-3 SOLVENT EOR METHODS

Process	Recovery mechanism	Issues	Typical recovery (%)	Typical agent utilization*
Immiscible	Reduces oil viscosity Oil swelling Solution gas	Stability Override Supply	5–15	10 Mscf solvent per bbl oil produced
Miscible	Same as immiscible plus development of miscible	Same as immiscible	5–10	10 Mscf solvent per bbl oil produced

displacement

*1 Mscf/stb \equiv 178 std. m³ solvent/ std. m³ oil

Screening Guides

Many of the issues in Tables 1-1 through 1-3 can be better illustrated by giving quantitative limits. These screening guides can also serve as a first approximate for when a process would apply to a given reservoir. Table 1-4 gives screening guides of EOR processes in terms of oil and reservoir properties.

TABLE 1-4. SUMMARY OF SCREENING CRITERIA FOR EOR METHODS
(adapted from Taber *et al.*, 1997).

TABLE 3: SUMMARY OF SCREENING CRITERIA FOR EOR METHODS								
EOR Method	Oil Properties				Reservoir Characteristics			
	Gravity (°API)	Reservoir Viscosity mPa-s	Composition	Initial Oil Saturation (%PV)	Formation Type	Net Thickness (m)	Average Permeability (md)	Depth (m)
Solvent Methods								
Nitrogen and flue gas	>35	<0.4	Large % of C ₁ to C ₇	>40	NC	NC	NC	>1800
Hydrocarbon	>23	<3	Large % of C ₂ to C ₇	>30	NC	NC	NC	>1250
C ₂ O ₂	>22	<10	Large % of C ₅ to C ₁₂	>20	NC	NC	NC	>750
Immiscible gases	>12	<600	NC	>35	NC	NC	NC	>640
Chemical Methods								
Miscellar/polymer, ASP, and alkaline flooding	>20	<35	Light, intermediate, some organic acids for alkaline floods	>35	Sandstone preferred	NC	>10	<2700
Polymer Flooding	>15	10-150	NC	>50	Sandstone preferred	NC	>10	<2700
Thermal Methods								
Combustion	>10	<5,000	Some asphaltic components	>50		>3	>50	<3450
Steam	>8 to 13.5	<200,000	NC	>40		>6	>200	<1350
NC=not critical								

These should be regarded as rough guidelines, not as hard limits because special circumstances (economics, gas supply for example) can extend the applications.

The limits have a physical base as we will see. For example, the restriction of thermal processes to relatively shallow reservoirs is because of potential heat losses through lengthy wellbores. The restriction on many of the processes to light crudes comes about because of sweep efficiency considerations; displacing viscous

oil is difficult because of the propensity for a displacing agent to channel through the fluid being recovered. Finally, you should realize that some of categorizations in Table 1-7 are fairly coarse. Steam methods, in particular, have additional divisions into steam soak, steam drive, and gravity drainage methods. There are likewise several variations of combustion and chemical methods.

1-5 UNITS AND NOTATION

SI Units

The basic set of units in the text is the System International (SI) system. We cannot be entirely rigorous about SI units because many figures and tables have been developed in more traditional units. It is impractical to convert these; therefore, we give a list of the more important conversions in Table 1-7 and some helpful pointers in this section.

TABLE 1-5 AN ABRIDGED SI UNITS GUIDE (adapted from Campbell *et al.*, 1977)

SI base quantities and units			
Base quantity or dimension	SI unit	SI unit symbol	SPE dimensions symbol
Length	Meter	m	L
Mass	Kilogram	kg	m
Time	Second	s	t
Thermodynamic temperature	Kelvin	K	T
Amount of substance	Mole*	mol	

*When the mole is used, the elementary entities must be specified; they may be atoms, molecules, ions, electrons, other particles, or specified groups of such particles in petroleum work. The terms *kilogram mole*, *pound mole*, and so on are often erroneously shortened to mole.

Some common SI derived units			
Quantity	Unit	SI unit symbol	Formula
Acceleration	Meter per second squared	—	m/s^2
Area	Square meter	—	m^2
Density	Kilogram per cubic meter	—	kg/m^3
Energy, work	Joule	J	$\text{N} \cdot \text{m}$
Force	Newton	N	$\text{kg} \cdot \text{m/s}^2$
Pressure	Pascal	Pa	N/m^2
Velocity	Meter per second	—	m/s
Viscosity, dynamic	Pascal-second	—	$\text{Pa} \cdot \text{s}$
Viscosity, kinematic	Square meter per second	—	m^2/s
Volume	Cubic meter	—	m^3

Selected conversion factors			
-----------------------------	--	--	--

To convert from	To	Multiply by
Acre (U.S. survey)	Meter ² (m ²)	4.046 872 E+03
Acres	Feet ² (ft ²)	4.356 000 E+04
Atmosphere (standard)	Pascal (Pa)	1.013 250 E+05
Bar	Pascal (Pa)	1.000 000 E+05
Barrel (for petroleum 42 gal)	Meter ³ (m ³)	1.589 873 E-01
Barrel	Feet ³ (ft ³)	5.615 E+00
British thermal unit (International Table)	Joule (J)	1.055 056 E+03
Darcy	Meter ² (m ²)	9.869 232 E-13
Day (mean solar)	Second (s)	8.640 000 E+04
Dyne	Newton (N)	1.000 000 E-05
Gallon (U.S. liquid)	Meter ³ (m ³)	3.785 412 E-03
Gram	Kilogram (kg)	1.000 000 E-03
Hectare	Meter ² (m ²)	1.000 000 E+04
Mile (U.S. survey)	Meter (m)	1.609 347 E+03
Pound (lbm avoirdupois)	Kilogram (kg)	4.535 924 E-01
Ton (short, 2000 lbm)	Kilogram (kg)	9.071 847 E+02

TABLE 1-5 CONTINUED

Selected SI unit prefixes

Factor	SI prefix	SI prefix symbol (use roman type)	Meaning (U.S.)	Meaning outside US
10^{12}	tera	T	One trillion times	Billion
10^9	giga	G	One billion times	Milliard
10^6	mega	M	One million times	
10^3	kilo	k	One thousand times	
10^2	hecto	H	One hundred times	
10	deka	Da	Ten times	
10^{-1}	deci	D	One tenth of	
10^{-2}	centi	c	One hundredth of	
10^{-3}	milli	m	One thousandth of	
10^{-6}	micro	μ	One millionth of	
10^{-9}	nano	N	One billionth of	Milliardth

1. There are several cognates, quantities having the exact or approximate numerical value, between SI and practical units. The most useful for EOR are

$$\begin{aligned}
 1 \text{ cp} &= 1 \text{ mPa-s} \\
 1 \text{ dyne/cm} &= 1 \text{ mN/m} \\
 1 \text{ Btu} &\cong 1 \text{ kJ} \\
 1 \text{ Darcy} &\cong 1 \text{ } \mu\text{m}^2 \\
 1 \text{ ppm} &\cong 1 \text{ g/m}^3
 \end{aligned}$$

2. Use of the unit prefixes (lower part of Table 1-5) requires care. When a prefixed unit is exponentiated, the exponent applies to the prefix as well as the unit. Thus $1 \text{ km}^2 = 1(\text{km})^2 = 1(10^3 \text{ m})^2 = 1 \times 10^6 \text{ m}^2$. We have already used this convention where $1 \mu\text{m}^2 = 10^{-12} \text{ m}^2 \cong 1 \text{ Darcy}$.
3. Two troublesome conversions are between pressure (147 psia \cong 1 MPa) and temperature ($1 \text{ K} = 1.8 \text{ }^\circ\text{R}$). Since neither the Fahrenheit nor the Celsius scale is absolute, an additional translation is required.

$${}^\circ\text{C} = \text{K} - 273$$

and

$${}^\circ\text{F} = {}^\circ\text{R} - 460$$

The superscript ${}^\circ$ is not used on the Kelvin scale.

4. The volume conversions are complicated by the interchangeable use of mass and standard volumes. Thus we have

$$0.159 \text{ m}^3 = 1 \text{ reservoir barrel, or bbl}$$

and

$$0.159 \text{ std. m}^3 = 1 \text{ standard barrel, or stb}$$

The standard cubic meter, std. m^3 , is not standard SI; it represents the amount of mass contained in one cubic meter evaluated at standard temperature and pressure.

Consistency

Maintaining unit consistency is important in all exercises, and for this reason both units and numerical values should be carried in all calculations. This ensures that the unit conversions are done correctly and indicates if the calculation procedure itself is appropriate. In maintaining consistency, three steps are required.

1. Clear all unit prefixes.
2. Reduce all units to the most primitive level necessary. For many cases, this will mean reverting to the fundamental units given in Table 1-7.
3. After calculations are complete, reincorporate the unit prefixes so that the numerical value of the result is as close to 1 as possible. Many adopt the convention that only the prefixes representing multiples of 1,000 are used.

Example 1-2. Converting from Darcy units.

Maintaining unit consistency in an equation is easy. For example, suppose we want to use the typical oilfield units in Darcy's law: q in units of ($=$) bbl/day; k [=] md; A [=] ft^2 ; p [=] psia; μ [=] cp; and x [=] ft. First we write Darcy's law:

$$q = \frac{kA}{\mu} \frac{dp}{dx}$$

This is elementary form of Darcy's law is valid for 1-D horizontal flow Darcy's law is self-consistent in so-called Darcy's units; hence, a "units" balance for this equation is

$$\left(\frac{q - cm^3}{s} \right) = \frac{(k - D)(A - cm^2)}{(\mu - cp)} \left(\frac{dp - atm}{dx - cm} \right)$$

where $k-D$ means that the permeability k is in D or Darcys. The other units given in the equation are Darcy units. Note that the minus sign is unnecessary since we are dealing only with units. Next, we write this same equation into the units that we want , maintaining the unit consistency. That is,

$$\begin{aligned} & \left[\frac{q - bbl}{day} \right] \left\{ \frac{1 day}{24 hrs} \right\} \left\{ \frac{1 hr}{3600 s} \right\} \left\{ \frac{1 ft}{3600 s} \right\} \left\{ \frac{(30.48)^3 cm^3}{ft^3} \right\} = \\ & \frac{\left[k - md \right] \left\{ \frac{1 D}{1000 md} \right\} \left[A - ft^2 \right] \left\{ \frac{(30.48)^2 cm^2}{ft^2} \right\}}{[\mu - cp]} \times \\ & \quad \left[\frac{dp - psia}{dx - ft} \right] \left\{ \frac{1 atm}{14.70 psia} \right\} \left\{ \frac{1 ft}{30.48 cm} \right\} \end{aligned}$$

Although each term is written in the units we wish, each term reduces to the units of the original equation. This is illustrated in the above equation by canceling all similar units. By writing the above equation and checking the unit consistency, you are assured of making no errors. The equation also introduces the practice of putting ratios that are conversion factors in {}.

The last step is to rewrite the equation by grouping all numerical constants and calculating the appropriate constant that must appear before the right side of the equation. Darcy's law becomes

$$\left(\frac{q - bbl}{day} \right) = \left\{ \frac{(24)(3600)(30.48^2)}{(5.615)(30.48^3)(1000)(14.70)(30.48)} \right\} \frac{(k - md)(A - ft^2)}{(\mu - cp)} \left(\frac{dp - psia}{dx - ft} \right)$$

or

$$\left(\frac{q - bbl}{day} \right) = \left\{ 1.127 \times 10^{-3} \frac{(k - md)(A - ft^2)}{(\mu - cp)} \right\} \left(\frac{dp - psia}{dx - ft} \right).$$

The constant, which is accurate to four digits, is the well-known constant for Darcy's law written in oil field units. The above equation also illustrates a common practice in petroleum engineering--in our opinion bad and used sparingly in this text--of including a conversion factor directly in an equation.

The important point the above procedure is that there is no guessing involved. Any equation can be converted to the desired units as long as the procedure is followed exactly.

Naming Conventions

The diversity of EOR makes it possible to assign symbols to components without some duplication or undue complication. In the hope of minimizing the latter by adding a little of the former, Table 1-8 gives the naming conventions of phases and components used throughout this text. The nomenclature section defines other symbols.

Phase always carry the subscript j , which occupies the second position in a doubly subscripted quantity. $j = 1$ is always a water-rich, or the aqueous phase, thus freeing up the symbol w for wetting (and nw for nonwetting). The subscript s designates the solid, nonflowing phase.

A subscript i , occurring in the first position, indicates the component. Singly subscripted quantities indicate components. In general, $i = 1$ is always water; $i = 2$ is oil or hydrocarbon; and $i = 3$ refers to a displacing component, whether surfactant or light hydrocarbon. Component indices greater than 3 are used exclusively in Chaps. 8–10, the chemical flooding part of the text.

1-6 SUMMARY

No summary can do justice to what is a large, diverse, continuously changing, and complicated technology. The Oil and Gas Journal has provided an excellent service in documenting the progress of EOR, and you should consult those surveys for up to date information. The fundamentals of the processes change more slowly than the applications, and it is to these fundamentals that the remainder of the text is devoted.

TABLE 1-4 NAMING CONVENTIONS FOR PHASES AND COMPONENTS

Phases		
<i>j</i>	Identity	Text locations
1	Water-rich or aqueous	Throughout
2	Oil-rich or oleic	Throughout
3	Gas-rich, gaseous or light hydrocarbon	Secs. 5-6 and 7-7
	Microemulsion	Chap. 9
<i>s</i>	Solid	Chaps 2, 3, and 8 to 10
<i>w</i>	Wetting	Throughout
<i>nw</i>	Nonwetting	Throughout

Components		
<i>i</i>	Identity	Text locations
1	Water	Throughout
2	Oil or intermediate hydrocarbon	Throughout
3	Gas	Sec. 5-6
	Light hydrocarbon	Sec. 7-6
	Surfactant	Chap. 9
4	Polymer	Chaps. 8 and 9
5	Anions	Secs. 3-4 and 9-5
6	Divalents	Secs. 3-4 and 9-5
7	Divalent-surfactant component	Sec. 9-6
8	Monovalents	Secs. 3-4 and 9-5

EXERCISES

1A. Determining Incremental Oil Production. The easiest way to estimate incremental oil recovery IOR is through decline curve analysis, which is the subject of this exercise. The oil rate and cumulative oil produced versus time data for the Sage Spring Creek Unit A field is shown below (Mack and Warren, 1984)

Date	Oil Rate std. m ³ /day
1/76	274.0
7/76	258.1
1/77	231.0
7/77	213.5
1/78	191.2
7/78	175.2 (Start Polymer)
1/79	159.3
7/79	175.2
1/80	167.3
7/80	159.3
1/81	159.3
7/81	157.7

1/82	151.3
7/82	148.2
1/83	141.8
7/83	132.2
1/84	111.5
7/84	106.7
1/85	95.6
7/85	87.6
1/86	81.2
7/86	74.9
1/87	70.1
7/87	65.3

In 7/78 the ongoing waterflood was replaced with a polymer flood. (Actually, there was a polymer gel treatment conducted in 1984, but we neglect it here.) The economic limit is 50 std. m³/D in this field.

- (a) Plot the oil rate versus cumulative oil produced on linear axes. The oil rate axis should extend to $q = 0$.
- (b) Extrapolate the straight line portion of the data to determine the ultimate economic oil to be recovered from the field and the total mobile oil, both in Mstd. m³, for both the water and the polymer flood. Determine the incremental economic oil (IOR) and the incremental mobile oil caused by the polymer flood.
- (c) Determine the decline rates appropriate for the waterflood and polymer flood declines.
- (d) Use the decline rates in step c to determine the economic life of the polymer flood. Also determine what the economic life would have been if there were no polymer flood.

1B. Maintaining Unit Conversions (Darcy's Law). There are several unit systems used throughout the world and you should be able to convert equations easily between systems. Convert Darcy's Law for 1-D horizontal flow,

$$q = \frac{kA}{\mu} \frac{dp}{dx}$$

from Darcy units to the unit system where $q [=] \text{m}^3/\text{day}$, $k [=] \text{md}$, $A [=] \text{m}^2$, $\mu [=] \text{cp}$, $p [=] \text{kg}/\text{cm}^2$, and $x [=] \text{meters}$. This is the reverse of that in Example 1-2.

1C. Maintaining Unit Conversions (Dimensionless Time). A dimensionless time often appears in petroleum engineering. One definition for dimensionless time used in radial flow is

$$t_D = \frac{kt}{\phi \mu c_i r_w^2}$$

where the equation is written in Darcy units ($r_w [=] \text{cm}$, ϕ is dimensionless, $c_i [=] \text{atm}^{-1}$). Convert the equation for dimensionless time from Darcy units to

- (a) oil-field units.
- (b) SI units.

This means write the equation with a conversion factor in it so that quantities with the indicated units may be substituted directly.

1D. Maintaining Unit Conversions (Dimensionless Pressure). A dimensionless pressure often appears in petroleum engineering. One definition for dimensionless pressure is

$$p_D = \frac{2\pi kh\Delta p}{q\mu}$$

where the equation is written in Darcy units (h in cm, Δp in atm). Convert the equation for dimensionless pressure from Darcy units to

- (a) oil-field units.
- (b) SI units.

2

Basic Equations for Fluid Flow in Permeable Media

Successful enhanced oil recovery requires knowledge of equal parts chemistry, physics, geology and engineering. Each of these enters our understanding through elements of the equations that describe flow through permeable media. Each EOR process involves at least one flowing phase that may contain several components. Moreover, because of varying temperature, pressure, and composition, these components may mix completely in some regions of the flow domain, causing the disappearance of a phase in those regions. Atmospheric pollution and chemical and nuclear waste storage lead to similar problems.

This chapter gives the equations that describe multiphase, multicomponent fluid flow through permeable media based on conservation laws and linear constitutive theory. Initially, we strive for the most generality possible by considering the transport of each component in each phase. Then, special cases are obtained from the general equations by making additional assumptions. The approach in arriving at the special equations is as important as the equations themselves, since it will help to understand the specific assumptions--and the limitations--that are being made for a particular application.

The formulation initially contains two fundamentally different forms for the general equations: overall compositional balances, and the phase conservation equations. The overall compositional balances are useful for modeling how components are transported through permeable media in local thermodynamic equilibrium. The phase conservation equations are useful for modeling finite mass transfer among phases. Figure 2-1 illustrates the relationships among several equations developed as special cases in this chapter.

From the overall compositional balances, the list of special cases includes the multicomponent, single-phase flow equations (Bear, 1972) and the three-phase,

multicomponent equations (Crichlow, 1977; Peaceman, 1977; Coats, 1980). In addition, others (Todd and Chase, 1979; Fleming *et al.*, 1981; Larson, 1979) have presented multicomponent, multiphase formulations for flow in permeable media but with assumptions such as ideal mixing or incompressible fluids. Many of these assumptions must be made before the equations are solved, but we try to keep the formulation as general as possible as long as possible.

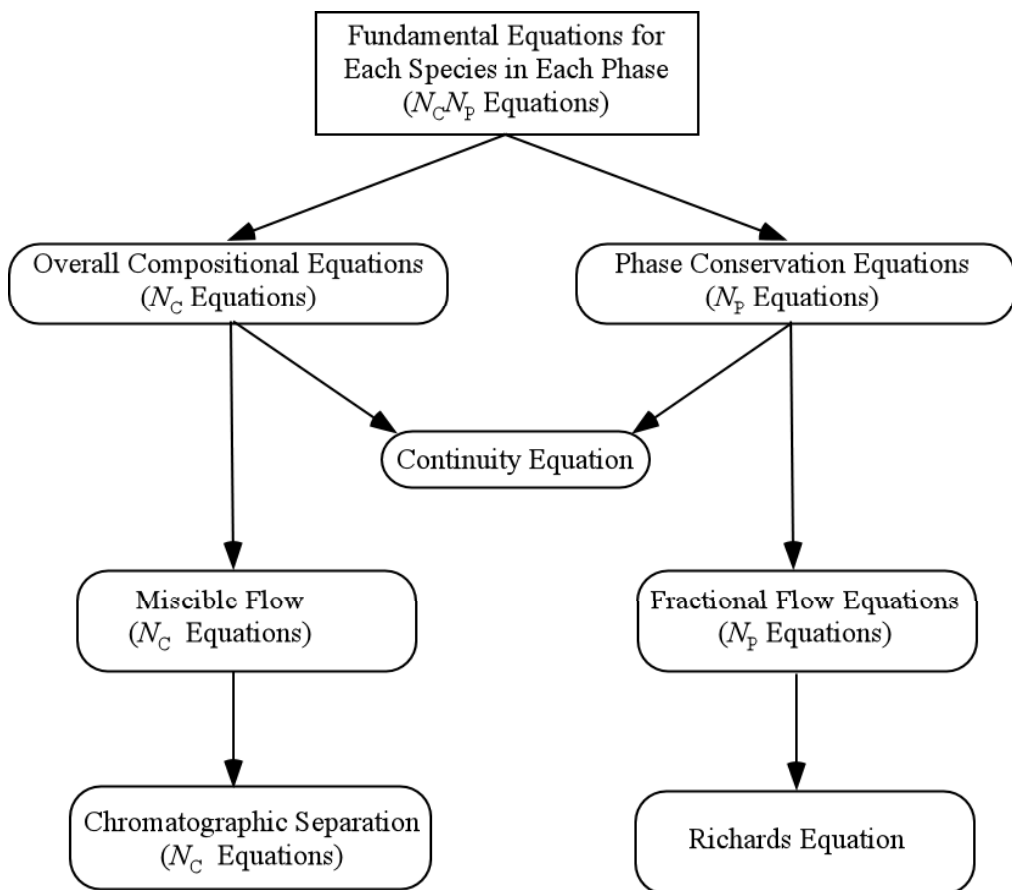


Figure 2-1 Flow diagram showing the relationships among the fundamental equations and selected special cases. There are N_C components and N_P phases.

2-1 MASS CONSERVATION

This section describes the conceptual nature of multiphase, multicomponent flows through permeable media and the mathematical formulation of the conservation equations.

The four most important mechanisms causing transport of chemical components in naturally occurring permeable media are viscous forces, gravity forces, dispersion (diffusion), and capillary forces. The driving forces for the first three are pressure, density, and concentration gradients, respectively. Capillary or surface forces are caused by high-curvature boundaries between the various homogeneous phases. This curvature is the result of such phases being constrained by the pore walls of the permeable medium. Capillary forces imply differing pressures in each homogeneous fluid phase so that the driving force for capillary pressure is, like viscous forces, pressure differences.

The ratios of these forces are often given as dimensionless groups and given particular names. For example, the ratio of gravity to capillary forces is the Bond number. When capillary forces are small compared to gravity forces, the Bond number is large and the process (or displacement) is said to be gravity dominated. The ratio of viscous to capillary forces is the capillary number, a quantity that will figure prominently through this text. The ratio of gravity to viscous forces is the gravity or buoyancy number. The magnitude of these and other dimensionless groups help in comparing or scaling one process to another; they will appear at various points throughout this text.

The Continuum Assumption

Transport of chemical components in multiple homogeneous phases occurs because of the above forces, the flow being restricted to the highly irregular flow channels within the permeable medium. The conservation equations for each component apply at each point in the medium, including the solid phase. In principle, given constitutive relations, reaction rates, and boundary conditions, it is possible to formulate a mathematical system for all flow channels in the medium. But the phase boundaries in such are extremely tortuous and their locations are unknown; hence, we cannot solve component conservation equations in individual channels except for only the simplest microscopic permeable media geometry.

The practical way of avoiding this difficulty is to apply a continuum definition to the flow so that a point within a permeable medium is associated with a representative elementary volume (REV), a volume that is large with respect to the pore dimensions of the solid phase but small compared to the dimensions of the permeable medium. The REV is defined as a volume below which local fluctuations in some primary property of the permeable medium, usually the porosity, become large (Bear, 1972). A volume-averaged form of the component conservation equations applies for each REV within the now-continuous domain of the macroscopic permeable medium. (Volume averaging is actually a formal process; see Bear, 1972; Gray, 1975; and Quintard and Whitaker, 1988.) The volume-averaged component conservation equations are identical to the conservation equations outside a permeable medium except for altered definitions for the accumulation, flux, and source terms. These definitions now include permeable media porosity, permeability, tortuosity, and dispersivity, all made locally smooth because of the definition of the

REV. Approximating the locally discontinuous permeable medium with a locally smooth one is called the *continuum assumption*.

A good way to understand the REV scale is to consider a microscopic view of pores and grains within a medium. Figure 2-2 illustrates a cube of small volume placed within a permeable medium. The porosity in the cube is defined as the pore volume within the cube divided by the bulk volume of the cube. If the cube volume is infinitesimally small, the porosity will be either 1.0 or 0.0 depending on whether it is initially located inside a grain or a pore. We now let the cube increase from its original size. As the cube volume increases, the porosity changes in an erratic fashion as more and more grains and pores pass inside the cube (see Figure 2-3).

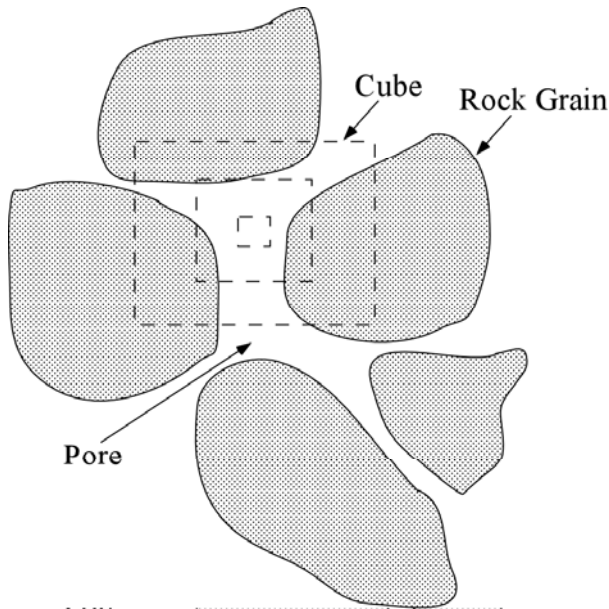


Figure 2-2 Illustration of microscopic cube placed within a permeable medium. The cube is initially within a pore so that its porosity is 1.0. As the cube volume increases, it takes in more grains so that its porosity decreases.

As the cube volume increases sufficiently, the porosity approaches a constant value representative of the porous medium. This is the porosity at the REV scale, which defines the onset of the permeable medium domain. Above the REV size, the cube porosity remains constant within the domain of the permeable medium. As the cube volume increases further, however, the cube porosity is affected by layering and other heterogeneities. The formation is homogeneous if the porosity remains fixed as the REV-sized cube is moved to any location within the permeable medium. A heterogeneous formation is one in which the porosity (or any other petrophysical property) varies from one spatial location to another when measured at the REV scale.

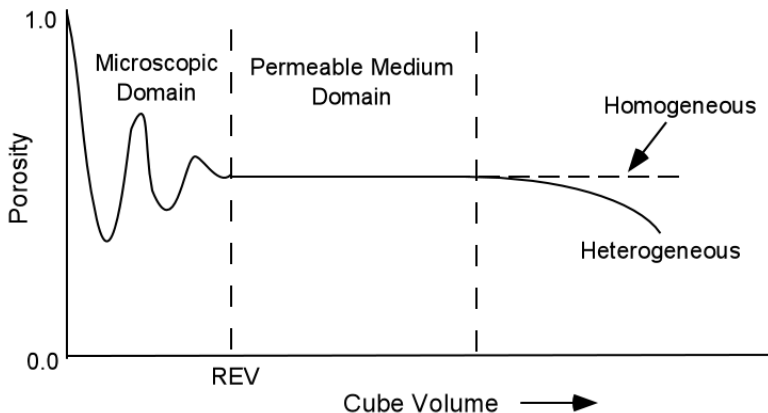


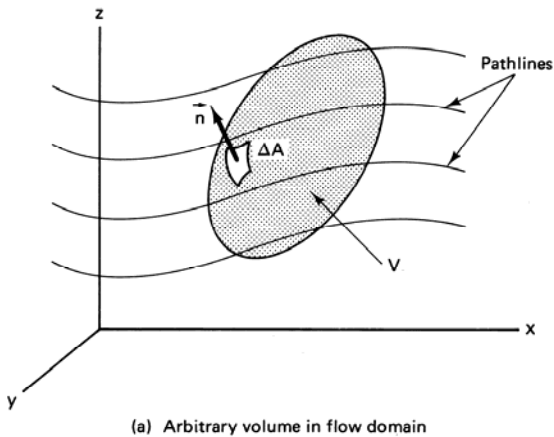
Figure 2-3 Idealization of the microscopic and permeable medium domains. The REV size separates these two domains.

Rather than beginning with the nonpermeable media flow equations, and then volume-averaging over the REV, we invoke the continuum assumption at the outset and derive the mass conservation on this basis. This approach skips over many of the physical insights obtained from volume averaging, but it is far more direct.

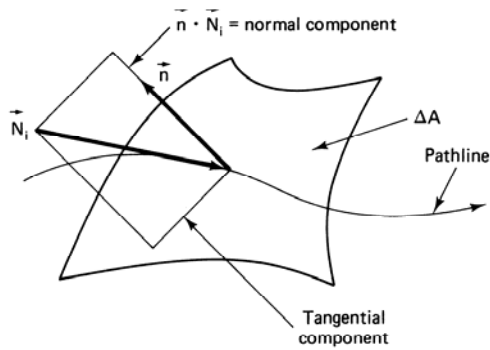
Mass Balance for a Component in a Phase

Consider an arbitrary, fixed volume V embedded within a permeable medium through which is flowing an arbitrary number of chemical components and phases. You must constantly be aware of the distinction between components and phases in this discussion. (This can be a source of confusion because under some circumstances phases and components are the same.) A *component* is any identifiable chemical entity. Components can be pure substances such as methane, a cation, or even combinations of elements. See Lake *et al.*, 2002 for more discussion. A *phase* is a physically distinct part of a region in space that is bound by interfaces with macroscopic physical properties, such as density and viscosity. A phase can consist of many components. There are up to $i = 1, \dots, N_C$ components, and up to $j = 1, \dots, N_P$ phases. The "up to" is because both components and phases can vanish in regions of the flow domain.

The conservation laws are written over a control volume V that is greater than or equal to the REV but smaller than or equal to the permeable medium dimensions. Except for some restrictions on the connectivity of the surface, V can be quite general. As Fig. 2-4 (a) shows, the surface area A



(a) Arbitrary volume in flow domain



(b) Surface element detail

Figure 2-4 Geometries for conservation law derivations.

of V is made up of elemental surface areas ΔA from the center of which is pointing a unit outward normal vector \vec{n} . The sum of all the surface elements ΔA is the total surface area A of V . This sum of all the ΔA becomes the total surface area A as the largest ΔA approaches zero.

The conservation equation for each component in each phase in volume V is

$$\left\{ \begin{array}{l} \text{Rate of} \\ \text{accumulation of } i \\ \text{in phase } j \text{ in } V \end{array} \right\} = \left\{ \begin{array}{l} \text{Net rate of } i \\ \text{in phase } j \\ \text{transported into } V \end{array} \right\} + \left\{ \begin{array}{l} \text{Net rate of} \\ \text{generation of } i \\ \text{in phase } j \text{ inside } V \end{array} \right\} \\ i = 1, \dots, N_C \quad j = 1, \dots, N_P . \quad (2.1-1)$$

There are a total of $N_C N_P$ equations represented by Eq. (2.1-1). This equation is the rate form of the conservation equation; an equivalent form based on cumulative flow follows from integrating Eq. (2.1-1) with respect to time (see Sec. 2-5). From left to right in Eq. (2.1-1) are the accumulation, flux, and source terms, respectively. A component can be transported within a phase by convection or hydrodynamic dispersion. The generation of a component in a given phase can be the result of chemical or biological reactions, injection or production of a component into or from wells, or mass transfer from one phase to the next owing to phase changes. These physical processes are discussed in more detail in Sec. 2.2.

The first term on the right side of Eq. (2.1-1) can be written as

$$\left\{ \begin{array}{l} \text{Net rate of } i \\ \text{in phase } j \\ \text{transported into } V \end{array} \right\} = \left\{ \begin{array}{l} \text{Rate of } i \\ \text{in phase } j \\ \text{transported into } V \end{array} \right\} - \left\{ \begin{array}{l} \text{Rate of } i \\ \text{in phase } j \\ \text{transported from } V \end{array} \right\} \\ i = 1, \dots, N_C \quad j = 1, \dots, N_P . \quad (2.1-2)$$

We give mathematical form to each term in the following paragraphs.

The accumulation term for component i in phase j is

$$\left\{ \begin{array}{l} \text{Rate of} \\ \text{accumulation of } i \\ \text{in phase } j \text{ in } V \end{array} \right\} = \frac{d}{dt} \left\{ \begin{array}{l} \text{Total mass of} \\ i \text{ in phase } j \\ \text{in } V \end{array} \right\} = \frac{d}{dt} \left\{ \int_V W_{ij} dV \right\} \quad (2.1-3)$$

where W_{ij} is the component concentration in units of mass of i in phase j per unit bulk volume. The units of Eq. (2.1-3) are mass per time. The volume integral represents the sum of infinitesimal volume elements in V weighted by the concentration.

Since V is stationary,

$$\frac{d}{dt} \left\{ \int_V W_{ij} dV \right\} = \int_V \frac{dW_{ij}}{dt} dV . \quad (2.1-4)$$

This entire development may be repeated with a time-varying V with the same result (Slattery, 1972).

The net flux term follows from considering the rate of transport across a single surface element into V as shown in Fig. 2-4(b). Let \vec{N}_{ij} be the flux vector of component i in phase j evaluated at the center of ΔA in units of mass of i in phase j per surface area-time. \vec{N}_{ij} consists of components normal and tangential to \vec{n} . However, only the normal component $\vec{n} \cdot \vec{N}_{ij}$ is crossing ΔA , and the rate of transport across ΔA is

$$\left\{ \begin{array}{l} \text{Rate of transport} \\ \text{of } i \text{ in phase } j \\ \text{across } \Delta A \text{ into } V \end{array} \right\} = -\vec{n} \cdot \vec{N}_{ij} \Delta A \quad (2.1-5)$$

The minus sign arises because \vec{n} and \vec{N}_{ij} are in opposing directions for transport across ΔA into V ($\vec{n} \cdot \vec{N}_{ij} < 0$), and this term must be positive from Eq. (2.1-1). An inherent assumption in Eq. (2.1-5) is that the flux across ΔA is uniform, an assumption that is valid as ΔA approaches zero. (Always remember that the continuum assumption assures continuity in taking limits.) The summation of infinitesimal surface elements yields

$$\left\{ \begin{array}{l} \text{Net rate of } i \\ \text{in phase } j \\ \text{transported into } V \end{array} \right\} = - \int_A \vec{n} \cdot \vec{N}_{ij} dA . \quad (2.1-6)$$

Since the surface integral is over the entire surface of V , both flow into and from V are included in Eq. (2.1-6).

The net rate of generation of i in phase j inside V is

$$\left\{ \begin{array}{l} \text{Net rate of} \\ \text{generation of } i \\ \text{in phase } j \text{ inside } V \end{array} \right\} = \int_V R_{ij} dV + \int_V r_{mij} dV , \quad (2.1-7)$$

where R_{ij} is the rate of mass generation in units of mass of i in phase j per bulk volume-time. This term can account for both generation ($R_{ij} > 0$) and destruction ($R_{ij} < 0$) of i , either through one or more chemical or biological reactions or through physical sources (wells) in V .

The term r_{mij} in Eq. (2.1-7) expresses the rate of mass transfer of component i from or into phase j owing to vaporization, condensation, or sorption. We must have $\sum_{j=1}^{N_p} r_{mij} = 0$, a relation following from the inability to accumulate mass at a volumeless phase interface. You can show that this is true by letting V be the interface itself. With no volume the fluxes must be continuous across an interface.

Substitution of Eqs. (2.1-3), (2.1-4), (2.1-6), and (2.1-7) into Eq. (2.1-1) gives the following scalar equation for the conservation of i in each phase:

$$\int_V \frac{dW_{ij}}{dt} dV + \int_A \vec{n} \cdot \vec{N}_{ij} dA = \int_V R_{ij} dV + \int_V r_{mij} dV, \\ i=1, \dots, N_C \quad j=1, \dots, N_P, \quad (2.1-8)$$

Equation (2.1-8) is an overall balance, or “weak” form of the conservation equation in each phase. Versions of this equation will be used in solving for solutions that have discontinuities, such as those that involve shocks or fronts. The weak form, which is called an overall balance in the last section of this chapter, is also useful in numerical simulation primarily because it is not tied to a particular coordinate system.

The surface integral in Eq. (2.1-8) converts to a volume integral through the divergence theorem

$$\int_V \vec{\nabla} \cdot \vec{B} dV = \int_A \vec{n} \cdot \vec{B} dA, \quad (2.1-9)$$

where B can be any scalar, vector, or tensor function of position in V (with appropriate changes in the operator definitions). The symbol $\vec{\nabla}$ is the divergence operator, a kind of generalized derivative, whose specific form depends on the coordinate system. Table 2-1 gives forms of $\vec{\nabla}$ in rectangular, cylindrical, and spherical coordinates. The function B must be single-valued in V , a requirement met by most physical solutions. Finally, implicit in the representation of the surface integral of Eqs. (2.1-8) and (2.1-9) is the requirement that the integrand be evaluated on the surface A of V .

Application of the divergence theorem to Eq. (2.1-8) gives

$$\int_V \left(\frac{\partial W_{ij}}{\partial t} + \vec{\nabla} \cdot \vec{N}_{ij} - R_{ij} - r_{mij} \right) dV = 0. \quad (2.1-10)$$

Using Eq. (2.1-10) restricts the formulation somewhat. V must now be simply connected (a point on the exterior surface of V is always exterior) and the spatial derivatives implied by the divergence exist because of the continuum assumption discussed above. But since V is arbitrary in location and size, the integrand must be zero:

$$\frac{\partial W_{ij}}{\partial t} + \vec{\nabla} \cdot \vec{N}_{ij} - R_{ij} - r_{mij} = 0 \quad i=1, \dots, N_C \quad j=1, \dots, N_P. \quad (2.1-11)$$

The time derivative in Eq. (2.1-11) is now a partial derivative, the introduction of other independent variables--the spatial coordinates--making this necessary. Equation (2.1-11) is the differential or “strong” form for the component conservation equation in each phase. It applies to any point (actually an REV) within the macroscopic dimensions of the permeable medium independent of the boundary conditions. From left to right in Eq. (2.1-11), the terms are now the *accumulation*, *transport*, and *source* terms, the last consisting of two types.

The strong form, Eq. (2.1-11), is useful in developing analytic solutions, a mainstay of this text. Equation (2.1-11) and its analogous conservation equations are called the strong form because they express conservation at a point (a REV) within a medium. The word "strong" means that if Eq. (2.1-11) is satisfied at all points within V, Eq. (2.1-8), the weak form, is also satisfied. The converse is not true. The exact form of the equations depends on the coordinate systems being used. The next section gives specific definitions to the component concentration W_{ij} , flux \bar{N}_{ij} , and source terms R_{ij} and r_{mij} .

TABLE 2-1 SUMMARY OF DIFFERENTIAL OPERATORS IN RECTANGULAR, CYLINDRICAL,
AND SPHERICAL COORDINATES

Rectangular coordinates (x, y, z)	Cylindrical coordinates (r, θ, z)	Spherical coordinates (r, θ, ϕ)
$\vec{\nabla} \bullet \vec{B} = \frac{\partial B_x}{\partial x} + \frac{\partial B_y}{\partial y} + \frac{\partial B_z}{\partial z}$	$\vec{\nabla} \bullet \vec{B} = \frac{1}{r} \frac{\partial(rB_r)}{\partial r} + \frac{1}{r} \frac{\partial B_\theta}{\partial \theta} + \frac{\partial B_z}{\partial z}$	$\vec{\nabla} \bullet \vec{B} = \frac{1}{r^2} \frac{\partial(r^2 B_r)}{\partial r} + \frac{1}{r \sin \theta} \frac{\partial}{\partial \theta}(B_\theta \sin \theta)$ $+ \frac{1}{r \sin \theta} \frac{\partial B_\phi}{\partial \phi}$
$[\vec{\nabla} S]_x = \frac{\partial S}{\partial x}$	$[\vec{\nabla} S]_r = \frac{\partial S}{\partial r}$	$[\vec{\nabla} S]_r = \frac{\partial S}{\partial r}$
$[\vec{\nabla} S]_y = \frac{\partial S}{\partial y}$	$[\vec{\nabla} S]_\theta = \frac{1}{r} \frac{\partial S}{\partial \theta}$	$[\vec{\nabla} S]_\theta = \frac{1}{r} \frac{\partial S}{\partial \theta}$
$[\vec{\nabla} S]_z = \frac{\partial S}{\partial z}$	$[\vec{\nabla} S]_z = \frac{\partial S}{\partial z}$	$[\vec{\nabla} S]_\phi = \frac{1}{r \sin \theta} \frac{\partial S}{\partial \phi}$
$\vec{\nabla}^2 S = \frac{\partial^2 S}{\partial x^2} + \frac{\partial^2 S}{\partial y^2} + \frac{\partial^2 S}{\partial z^2}$	$\vec{\nabla}^2 S = \frac{1}{r} \frac{\partial}{\partial r} \left(r \frac{\partial S}{\partial r} \right) + \frac{1}{r^2} \frac{\partial^2 S}{\partial \theta^2} + \frac{\partial^2 S}{\partial z^2}$	$\vec{\nabla}^2 S = \frac{1}{r^2} \frac{\partial}{\partial r} \left(r^2 \frac{\partial S}{\partial r} \right)$ $+ \frac{1}{r^2 \sin \theta} \frac{\partial}{\partial \theta} \left(\sin \theta \frac{\partial S}{\partial \theta} \right) + \frac{1}{r^2 \sin^2 \theta} \frac{\partial^2 S}{\partial \phi^2}$

Note: B = vector function
 S = scalar function

2-2 DEFINITIONS AND CONSTITUTIVE EQUATIONS FOR ISOTHERMAL FLOW

Each term in Eq. (2.1-11) represents an important physical process or mechanism. This section examines each of these processes in further detail and defines some key formation and fluid parameters. The units on Eq. (2.1-11) are amount per unit time. *Amount* means either mass or moles; we will continue to use mass generically to mean either mass or moles. When a distinction between the two is important, we will be explicit.

Consider first a bulk volume V at the REV scale where N_p phases exist. Figure 2.5 illustrates such a volume that contains three phases: a solid phase consisting of rock grains or soil, an aqueous phase, and an oleic phase. The porosity ϕ is defined as the fraction of the bulk permeable medium that is pore space, that is, the pore volume divided by the bulk volume V . The phase saturation S_j is defined as the fraction of the pore volume occupied by phase j .

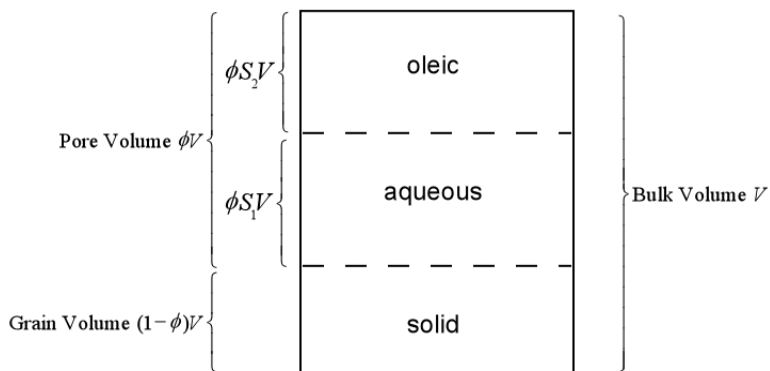


Figure 2-5 Representative bulk volume occupied by fluid and solid phases. The volume of the fluid phases are equal to $\phi S_j V$.

The volume fraction of phase j , ε_j , is the volume of phase j divided by the bulk volume V . For fluid phases such as liquids and vapors, $\varepsilon_j = \phi S_j$ where ϕS_j is also called the fluid *content*. For the solid phase, $\varepsilon_s = 1 - \phi$, which is the grain volume divided by the bulk volume V . By definition $\sum_{j=1}^{N_p} \varepsilon_j = 1$. The parameter ε_j is useful in writing general equations for any phase including the solid phase, as is done next. In summary, the fraction of the bulk volume that is occupied by phase j is

$$\varepsilon_j = \begin{cases} \phi S_j & \text{for fluid phases} \\ 1 - \phi & \text{for the solid phase} \end{cases} \quad (2.2-1)$$

Accumulation Term

The accumulation term in Eq. (2.1-11) contains the component concentration for a given phase (W_{ij}), which we write now in terms of the volume fraction ε_j . For solid or fluid phases the mass of phase j in any bulk volume V is given by $\varepsilon_j \rho_j V$. As before, the inherit assumption here is that the density of each phase is uniform in V , which is strictly valid only as V approaches the REV scale.

We now define the mass fraction of component i in V to be ω_{ij} . The parameter ω_{ij} is the mass of component i in phase j divided by the total mass of all components in that same phase. Hence, $\sum_{i=1}^{N_c} \omega_{ij} = 1$. With that definition the total mass of component i in phase j in V is $W_{ij}V$ where $W_{ij} = \varepsilon_j \rho_j \omega_{ij}$.

Flux Terms

For advective transport of component i we assume that phase j moves with its volume-averaged velocity \bar{u}_j . The component of the volumetric flow rate of component i that enters the elemental surface ΔA is $-\bar{n} \cdot \bar{u}_j \Delta A$. The mass flow rate of component i in phase j that enters V thru the elemental surface ΔA is therefore $-\bar{n} \cdot \rho_j \omega_{ij} \bar{u}_j \Delta A$. Again, phase j properties are assumed uniform across ΔA , which is valid as the elemental surface area becomes small. The component flux in phase j owing to advective transport alone is therefore equal to $\vec{j}_{cij} = \rho_j \omega_{ij} \bar{u}_j$. Note that the pore velocity for phase j is given by $\vec{v}_j = \bar{u}_j / \varepsilon_j$.

Hydrodynamic dispersion includes both molecular diffusion and mechanical dispersion. Molecular diffusion is independent of the direction or magnitude of flow, whereas mechanical dispersion in permeable media flows is anisotropic and depends on the magnitude of flow. Dispersion has the same form as does diffusion in nonpermeable media flows and, in fact, collapses to molecular diffusion in the limit of small \bar{u}_j (see Chap. 5). At larger \bar{u}_j , the components of $\vec{\bar{K}}_{ij}$, a second-order tensor, can be many times larger than molecular diffusion since they now contain contributions from fluctuations of the velocity \bar{u}_j and mass fraction ω_{ij} about their average values in the REV (Gray, 1975). Two components of $\vec{\bar{K}}_{ij}$ for a homogeneous, isotropic permeable medium (Bear, 1972) are

$$(K_{xx})_{ij} = \frac{D_{ij}}{\tau} + \frac{\alpha_{ij} u_{xj}^2 + \alpha_{ij} (u_{yj}^2 + u_{zj}^2)}{\phi S_j |\bar{u}_j|} \quad (2.2-2)$$

$$(K_{xy})_{ij} = \frac{(\alpha_{ij} - \alpha_{ij}) u_{xj} u_{yj}}{\phi S_j |\bar{u}_j|}, \quad (2.2-3)$$

where the subscript l refers to the spatial coordinate in the direction parallel, or longitudinal, to bulk flow, and t is any direction perpendicular, or transverse, to l . D_{ij} is the effective binary diffusion coefficient of component i in phase j (Bird *et al.*,

2002), α_{lj} and α_{tj} are the longitudinal and transverse dispersivities, and τ is the permeable medium tortuosity. (K_{tj}) is positive since $(\alpha_{lj} - \alpha_{tj})$ is always positive.

As is customary, hydrodynamic dispersion is assumed to have a Fickian form that is empirically modified for the volume fraction ε_j of each phase. The flux of component i in phase j with respect to volume-averaged velocity owing to hydrodynamic dispersion alone is taken to be $\vec{j}_{Dij} = -\varepsilon_j \vec{\tilde{K}}_{ij} \vec{\nabla}(\rho_j \omega_{ij})$ where the product $\rho_j \omega_{ij}$ is the mass concentration of component i in phase j . Alternatively, the flux with respect to mass-averaged velocity is $\vec{j}_{Dij} = -\varepsilon_j \rho_j \vec{\tilde{K}}_{ij} \vec{\nabla} \omega_{ij}$. The negative sign indicates that positive flux occurs in the direction of decreasing mass fraction. Note that $\vec{\nabla} \omega_{ij}$ has units of inverse length whereas $\vec{\tilde{K}}_{ij}$ has units of squared length per time.

The total mass flux owing to both advective and dispersive transport is the sum of the two. Thus, the component flux for phase j owing to both advective and hydrodynamic dispersive transport is $\vec{N}_{ij} = \rho_j \omega_{ij} \vec{u}_{ij} = \vec{j}_{Cij} + \vec{j}_{Dij} = \rho_j \omega_{ij} \vec{u}_j - \varepsilon_j \vec{\tilde{K}}_{ij} \vec{\nabla}(\rho_j \omega_{ij})$, where \vec{u}_{ij} is the statistical average apparent velocity of a component in phase j owing to both convection and dispersion. The velocity \vec{u}_{ij} therefore is the sum of the molecular velocities divided by the total number of molecules (Bird *et al.* 1960). The convective and dispersive flux for a component in the solid phase is negligible for most permeable media. The total mass flux of a component is just the sum of \vec{N}_{ij} over all phases.

Volume or mass-averaged velocities are sometimes used interchangeably in the literature even though the form of the dispersion term depends on the choice of velocity. The volume-averaged velocity \vec{u}_j for a multicomponent system is $\vec{u}_j = \sum_{i=1}^{N_c} \rho_j \omega_{ij} \vec{u}_j \hat{V}_{ij}$ where \hat{V}_{ij} is the partial mass volume of a component in phase j , where from thermodynamics $\sum_{i=1}^{N_c} \rho_j \omega_{ij} \hat{V}_{ij} = 1$. The partial mass volume depends on the mass fractions ω_{ij} , pressure, and temperature. The mass-averaged velocity is $\vec{u}_j = \sum_{i=1}^{N_c} \rho_j \omega_{ij} \vec{u}_j / \sum_{i=1}^{N_c} \rho_j \omega_{ij} = \sum_{i=1}^{N_c} \omega_{ij} \vec{u}_j$. Because the difference in the two velocities can be shown to be $\varepsilon_j \vec{\tilde{K}}_{ij} \cdot \vec{\nabla} \ln \rho_j$, the volume-averaged velocity is equal to the mass-averaged velocity for the case of an incompressible fluid. Experiments typically measure volume-averaged velocities since volumetric rates are directly measured at the inlet and outlet ends. Phase velocities, however, are never directly measured in situ and are approximated from empirical flux laws such as Darcy's law. Thus, the choice of volume or mass-averaged velocities likely does not result in significant errors for real mixtures owing to uncertainties in other formation parameters.

Source Terms

The source term R_{ij} in Eq. (2.1-11) accounts for the rate of appearance or generation of component i in phase j because of homogeneous chemical or biological reactions

within phase j (Levenspiel, 1999). Frequently, R_{ij} is used to represent reactions occurring at phase boundaries even though, strictly speaking, such reactions are the consequence of flux terms evaluated at phase boundaries in the volume-averaging procedures (Gray, 1975). In weak forms of the conservation laws it is also convenient to use R_{ij} to represent physical sources (wells) that are either specified or related to the phase pressures and saturations.

There is no general function for R_{ij} , although the volume fractions of each phase are handled through $R_{ij} = \varepsilon_j r_{ij}$ where r_{ij} is the reaction rate of component i in phase j . Both R_{ij} and r_{ij} have units of mass per volume per time, but r_{ij} is in terms of the phase volume not the bulk volume. Each r_{ij} could represent the sum of several reactions within phase j if component i participates in simultaneous reactions. In a given phase, mass is conserved so that $\sum_{i=1}^{N_c} r_{ij} = 0$ if the r_{ij} is in mass units. This is not correct if mole units are used to express the reaction rates because moles are not conserved in a chemical reaction. An example of a first-order reaction rate for radioactive decay or biodegradation is $r_{ij} = -k_i \rho_j \omega_j$ where k_i is the decay constant or reaction rate coefficient in units of inverse time.

The second source term r_{mij} in Eq. (2.1-11) allows for the appearance or disappearance of component i by mass transfer from phase j to another phase. This term is difficult to calculate without detailed analysis of the transport occurring within the phases. Thus, when mass transfer occurs, one typically simplifies the equations by using overall compositional balances as described later.

The total mass generation rate of component i in phase j per bulk volume of permeable medium is $R_{ij} + r_{mij}$. Injection and production of component i by wells is not explicitly included in this term and are better treated as boundary conditions or point sources.

Fundamental Conservation Equations for a Component in a Phase

A general set of partial differential equations for the conservation of component i in phase j is obtained upon substitution of the definitions for concentration W_{ij} , flux \vec{N}_{ij} , and source terms into Eq. (2.1-11):

$$\frac{\partial}{\partial t} (\varepsilon_j \rho_j \omega_{ij}) + \vec{\nabla} \cdot \left(\rho_j \omega_{ij} \vec{u}_j - \varepsilon_j \vec{K}_{ij} \vec{\nabla} (\rho_j \omega_{ij}) \right) = \varepsilon_j r_{ij} + r_{mij} \\ i = 1, \dots, N_c \quad j = 1, \dots, N_p . \quad (2.2-4)$$

The fundamental equations in Eq. (2.2-4) are the starting point for developing all equations for permeable media flows. The method used in this text is to simplify Eq. (2.2-4) by making the appropriate assumptions for the problem of interest. Several special cases or "working equations" are given in Sec. 2-4. There are a total of $N_c N_p$ equations represented by Eq. (2.2-4).

Example 2-1. Writing the conservation equations for each component and phase.

Consider two-component, three-phase flow in a permeable medium, where the components are component 1 and 2, and the phases are aqueous (w), oleic (o), and the solid phase (s). Write the specific conservation equations for each component and each phase assuming the solid phase is stationary (no deformation) and dispersive transport of each component in the solid phase is negligible.

Under these assumptions, Eq. (2.2-4) consists of the following set of six equations:

$$\left. \begin{aligned} \frac{\partial}{\partial t} (\phi S_1 \rho_1 \omega_{11}) + \vec{\nabla} \cdot \left(\rho_1 \omega_{11} \vec{u}_1 - \phi S_1 \vec{K}_{11} \vec{\nabla} (\rho_1 \omega_{11}) \right) &= \phi S_1 r_{11} + r_{m11} \\ \frac{\partial}{\partial t} (\phi S_1 \rho_1 \omega_{21}) + \vec{\nabla} \cdot \left(\rho_1 \omega_{21} \vec{u}_1 - \phi S_1 \vec{K}_{21} \vec{\nabla} (\rho_1 \omega_{21}) \right) &= \phi S_1 r_{21} + r_{m21} \\ \frac{\partial}{\partial t} (\phi S_2 \rho_2 \omega_{12}) + \vec{\nabla} \cdot \left(\rho_2 \omega_{12} \vec{u}_2 - \phi S_2 \vec{K}_{12} \vec{\nabla} (\rho_2 \omega_{12}) \right) &= \phi S_2 r_{12} + r_{m12} \\ \frac{\partial}{\partial t} (\phi S_2 \rho_2 \omega_{22}) + \vec{\nabla} \cdot \left(\rho_2 \omega_{22} \vec{u}_2 - \phi S_2 \vec{K}_{22} \vec{\nabla} (\rho_2 \omega_{22}) \right) &= \phi S_2 r_{22} + r_{m22} \\ \frac{\partial}{\partial t} ((1-\phi) \rho_s \omega_{1s}) &= (1-\phi) r_{1s} + r_{m1s} \\ \frac{\partial}{\partial t} ((1-\phi) \rho_s \omega_{2s}) &= (1-\phi) r_{2s} + r_{m2s} \end{aligned} \right\} \begin{array}{l} \text{aqueous phase} \\ \text{oleic phase} \\ \text{solid phase} \end{array}$$

The terms that remain in the solid phase equations allow for chemical reactions and mass transfer by adsorption. The above equations were arbitrarily grouped by the type of phase; they could have been grouped by the type of component.

Overall Compositional Balances

Important subsets of the fundamental equations are the overall compositional balance equations (see Fig. 2-1). Overall balances are written over all phases for each component. These set of N_C equations result from grouping Eqs. (2.1-11) or (2.2-4) by component type and then summing those grouped equations over all phases. The result of the summation of the component equations from Eq. (2.1-11) yields

$$\frac{\partial W_i}{\partial t} + \vec{\nabla} \cdot \vec{N}_i = R_i \quad i = 1, \dots, N_C, \quad (2.2-5)$$

where $\sum_{j=1}^{N_p} r_{mij} = 0$ and the equation has units of mass/bulk volume.. If we insert Eqs. (2.2-7) through (2.2-9) from Table 2-2 into Eq. (2.2-5), we arrive at a general form of the overall conservation equations

$$\begin{aligned} \frac{\partial}{\partial t} \left(\phi \sum_{j=1}^{N_p} \rho_j S_j \omega_{ij} + (1-\phi) \rho_s \omega_{is} \right) + \vec{\nabla} \cdot \left(\sum_{j=1}^{N_p} \left(\rho_j \omega_{ij} \vec{u}_j - \phi S_j \vec{\bar{K}}_{ij} \cdot \vec{\nabla} (\rho_j \omega_{ij}) \right) \right) \\ = \phi \sum_{j=1}^{N_p} S_j r_{ij} + (1-\phi) r_{is}, \quad i = 1, \dots, N_C. \end{aligned} \quad (2.2-6)$$

The compositional equations are useful for modeling the overall flow of component concentrations and are often used when mass transfer between fluid phases occurs. Of course, some detail is lost because of the disappearance of the interphase transport terms. The detail is partially restored by invoking the local equilibrium assumption (Lake *et al.*, 2002) that provides algebraic relations between concentrations in the phases. This assumption forms the justification for the discussion in Chap. 4. The local equilibrium assumption, used in the majority of the cases dealt with in this text and in the remainder of this chapter, is discussed more below.

Table 2-2 summarizes the overall balance equations needed for a complete description of isothermal, multicomponent, multiphase flow in permeable media. Column 1 in Table 2-2 gives the differential form of the equation named in column 2. Column 3 gives the number of scalar equations represented by the equation in column 1. Columns 4 and 5 give the identity and number of independent variables added to the formulation by the equation in column 1. N_D is the number of spatial dimensions ($N_D \leq 3$). The solid phase is a single homogeneous phase though more than one solid can exist.

Example 2-2. Writing the overall compositional equations for each component.

Combine the fundamental equations given in Example 2-1 to form the overall compositional balances. Use the same assumptions as in Example 2-1.

We first sort the equations listed in Example 2-1 by components 1 and 2. We then sum them over the phases to obtain the overall compositional balances in the form of Eq. (2.2-5). The resulting summation consists of the following set of two equations:

$$\left. \begin{aligned} & \frac{\partial}{\partial t} (\phi S_1 \rho_1 \omega_{11} + \phi S_2 \rho_2 \omega_{12} + (1-\phi) \rho_s \omega_{1s}) + \\ & \vec{\nabla} \cdot \left[\left(\rho_1 \omega_{11} \vec{u}_1 - \phi S_1 \vec{\bar{K}}_{11} \vec{\nabla} (\rho_1 \omega_{11}) \right) + \left(\rho_2 \omega_{12} \vec{u}_2 - \phi S_2 \vec{\bar{K}}_{12} \vec{\nabla} (\rho_2 \omega_{12}) \right) \right] \\ & = \phi S_1 r_{11} + \phi S_2 r_{12} + (1-\phi) r_{1s} \end{aligned} \right\} \text{component 1}$$

$$\left. \begin{aligned} & \frac{\partial}{\partial t} (\phi S_1 \rho_1 \omega_{21} + \phi S_2 \rho_2 \omega_{22} + (1-\phi) \rho_s \omega_{2s}) + \\ & \vec{\nabla} \cdot \left[\left(\rho_1 \omega_{21} \vec{u}_1 - \phi S_1 \vec{\bar{K}}_{21} \vec{\nabla} (\rho_1 \omega_{21}) \right) + \left(\rho_2 \omega_{22} \vec{u}_2 - \phi S_2 \vec{\bar{K}}_{22} \vec{\nabla} (\rho_2 \omega_{22}) \right) \right] \\ & = \phi S_1 r_{21} + \phi S_2 r_{22} + (1-\phi) r_{2s} \end{aligned} \right\} \text{component 2}$$

where we have used $\sum_{j=1}^{N_p} r_{mij} = 0$. The equations above can be rewritten as

$$\left. \begin{aligned} & \frac{\partial}{\partial t} \left(\phi \sum_{j=1}^2 S_j \rho_j \omega_{1j} + (1-\phi) \rho_s \omega_{1s} \right) + \vec{\nabla} \cdot \left[\sum_{j=1}^2 \left(\rho_j \omega_{1j} \vec{u}_j - \phi S_j \vec{\tilde{K}}_{1j} \vec{\nabla} (\rho_j \omega_{1j}) \right) \right] \\ &= \phi \sum_{j=1}^2 S_j r_{1j} + (1-\phi) r_{1s} \end{aligned} \right\} \text{component 1}$$

$$\left. \begin{aligned} & \frac{\partial}{\partial t} \left(\phi \sum_{j=1}^2 S_j \rho_j \omega_{2j} + (1-\phi) \rho_s \omega_{2s} \right) + \vec{\nabla} \cdot \left[\sum_{j=1}^2 \left(\rho_j \omega_{2j} \vec{u}_j - \phi S_j \vec{\tilde{K}}_{2j} \vec{\nabla} (\rho_j \omega_{2j}) \right) \right] \\ &= \phi \sum_{j=1}^2 S_j r_{2j} + (1-\phi) r_{2s} \end{aligned} \right\} \text{component 2}$$

TABLE 2-2 SUMMARY OF OVERALL CONSERVATION STRONG FORM EQUATIONS FOR ISOTHERMAL FLUID FLOW IN PERMEABLE MEDIA

Equation (1)	Name (2)	Number of independent scalar equations*	Dependent variables†	
		(3)	Identity (4)	Number (5)
(2.2-5) $\frac{\partial W_i}{\partial t} + \vec{\nabla} \bullet \vec{N}_i = R_i$	Component <i>i</i> conservation	N_C	W_i, R_i, \vec{N}_i	$2N_C + N_C N_D$
(2.2-7) $W_i = \phi \sum_{j=1}^{N_p} \rho_j S_j \omega_{ij} + (1-\phi) \rho_s \omega_{is}$	Overall concentration	$N_C - 1$	$\rho_j, S_j, \omega_{ij}, \omega_{is}$	$2N_P + N_P N_C + N_C$
(2.2-8) $\vec{N}_i = \sum_{j=1}^{N_p} \left(\rho_j \omega_{ij} \vec{u}_j - \phi S_j \vec{k} \bullet \vec{\nabla} (\rho_j \omega_{ij}) \right)$	Component <i>i</i> total flux	$N_C N_D$	\vec{u}_j	$N_P N_D$
(2.2-9) $R_i = \phi \sum_{j=1}^{N_p} S_j r_{ij} + (1-\phi) r_{is}$	Component <i>i</i> total source	$N_C - 1$	r_{ij}, r_{is}	$N_P N_C + N_C$
(2.2-10) $\sum_{i=1}^{N_C} R_i = 0$	Total reaction definition	1		
(2.2-11) $\vec{u}_j = -\lambda_{rj} \vec{k} \bullet (\vec{\nabla} P_j - \rho_j \vec{g})$	Darcy's law	$N_P N_D$	λ_{rj}, P_j	$2N_P$
(2.2-12) $\lambda_{rj} = \lambda_{rj}(S, \omega, \vec{u}_j, \vec{x})$	Relative mobility	N_P		
(2.2-13) $P_j - P_n = P_{cn}(S, \omega, \vec{x})$	Capillary pressure definition	$N_P - 1$		

* Total independent equations = $N_D(N_P + N_C) + 2N_P N_C + 4N_P + 4N_C$

† Total dependent variables = $N_D(N_P + N_C) + 2N_P N_C + 4N_P + 4N_C$

TABLE 2-2 CONTINUED

Equation (1)	Name (2)	Number of independent scalar equations*	Dependent variables†	
			Identity (4)	Number (5)
(2.2-14) $\sum_{i=1}^{N_c} \omega_{ij} = 1$	Mass fraction definition	N_P		
(2.2-15) $\sum_{i=1}^{N_c} \omega_{is} = 1$	Solid phase mass fraction definition	1		
(2.2-16) $\sum_{j=1}^{N_p} S_j = 1$	Saturation definition	1		
(2.2-17) $r_{ij} = r_j(\omega_{ij, P_j})$	Homogeneous kinetic reaction rates	$(N_C - 1)N_P$		
(2.2-18) $r_{is} = r_{is}(\omega_{is})$	Solid phase reaction rates	$N_C - 1$		
(2.2-19) $\sum_{i=1}^{N_c} r_{ij} = 0$	Total phase reaction definition	N_P		
(2.2-20) $\sum_{i=1}^{N_c} r_{is} = 0$	Solid phase total reaction rates	1		
(2.2-21) $\omega_{ij} = \omega_{ij}(\omega_{ik})_{k \neq j}$	Equilibrium relations (or phase balances)	$N_C(N_P - 1)$		
(2.2-22) $\omega_{is} = \omega_{is}(\omega_{ij})$	Solid phase equilibrium relations (or phase balances)	N_C		
(2.2-23) $\rho_j = \rho_j(T, P_j)$	Equations of state	N_P		

* Total independent equations = $N_D(N_P + N_C) + 2N_P N_C + 4N_P + 4N_C$

† Total dependent variables = $N_D(N_P + N_C) + 2N_P N_C + 4N_P + 4N_C$

A normally subscripted quantity (for example ω_{ij}) appearing without subscripts in Table 2-2 indicates a relationship involving, at most, all members of the subscripted set. In the listing of dependent variables, the primary media properties, such as porosity ϕ , and the permeability tensor \bar{k} , are given functions of position \bar{x} within the permeable medium. These quantities are, strictly speaking, functions of the fluid pressure within the medium (Dake, 1978), but for pressures nondestructive to the permeable medium, this effect is generally weak. We also assume the solid-phase density ρ_s is given, as is the dispersion tensor \bar{K}_{ij} , even though the latter is a function of the phase velocities and molecular diffusivities. The remaining terms in Table 2-2 are defined in the Nomenclature and below.

The first four equations in Table 2-2 are the component conservation Eq. (2.2-5) and definitions for the accumulation, flux, and source terms in this equation. We take the N_C conservation equations to be the independent set of equations; the conservation of overall mass or continuity equation, which follows from summing Eq. (2.2-5) from 1 to N_C , is not listed as an independent equation (see Sec. 2-4). In solving specific problems, it may be more convenient to take the problem statement as the continuity equation and $N_C - 1$ mass conservation equations with the major component (for example, water in flow of dissolved salts in an aqueous solution) being the one omitted.

Definition of Terms in the Overall Compositional Equations

The accumulation term W_i , the overall concentration of component i , represents the sum of the component i in the N_P flowing phases plus the solid phase as shown in Eq. (2.2-7). There are only $N_C - 1$ independent W_i , since summing on i with the mass fraction definitions of Eqs. (2.2-14) and (2.2-15) gives

$$\sum_{i=1}^{N_C} W_i = \phi \sum_{i=1}^{N_P} \rho_j S_j + (1-\phi)\rho_s \equiv \rho(\omega_i, P) \quad (2.2-24)$$

where ρ is the overall density of the permeable medium (total mass flowing plus solid phase divided by the bulk volume). We can regard the overall density as a complicated function of some local pressure P and the set of overall mass fractions defined as

$$\omega_i = \frac{W_i}{\sum_{i=1}^{N_C} W_i}. \quad (2.2-25)$$

Here ω_i is the mass of component i in all phases divided by the total mass of the permeable medium. The combination of Eqs. (2.2-24) and (2.2-25) yields a constraint on the W_i

$$\rho(W_1, \dots, W_{N_C}, P) = \sum_{i=1}^{N_C} W_i, \quad (2.2-26)$$

which means there are $N_C - 1$ independent W_i , not N_C . The notation on the left side of Eq. (2.2-26) indicates that ρ is a function of two variables, the set of overall concentrations and pressure. Equations (2.2-24) through (2.2-26) can be construed as a constraint on the mass fraction ω_{ij} , phase pressures P_j , and saturations S_j .

Auxiliary Relations

Equation (2.2-11) is a multiphase version of Darcy's law for flow in permeable media (Collins, 1976). The single-phase version of Darcy's law is actually a volume-averaged form of the momentum equation (Slattery, 1972; Hubbert, 1956). The form given in Eq. (2.2-11) assumes creeping flow in the permeable medium with no fluid slip at the solid phase boundaries. Corrections to account for non-Darcy effects appear in standard references (Collins, 1976; Bear, 1972). The potential function for the phase superficial velocity \bar{u}_j is the vectorial sum $\vec{\nabla}P_j + \rho_j\vec{g}$, where P_j is the pressure within the continuous phase j . \vec{g} is the gravitational vector, which is assumed constant and directed toward the Earth's center. Hereafter in this text, we assume the coordinate direction parallel to \vec{g} is positive upward, away from the Earth's center. The gravitational vector can be written as

$$\vec{g} = -g\vec{\nabla}D_z, \quad (2.2-27)$$

where g is the magnitude of the gravitational vector and D_z is a positive distance above some horizontal reference plane, typically depth. For Cartesian coordinate systems with a constant inclination with the reference plane, $\vec{\nabla}D_z$ becomes a vector consisting of cosines of the inclination angles between the respective axis and the vertical.

The tensorial form of the permeability \vec{k} implies an anisotropic permeable medium having coordinate axes unaligned with the principal axis of \vec{k} . With the inclusion of \vec{k} , we have now included all the primary permeable media properties, ϕ , \vec{k} , α_{lj} , α_{ij} , and τ , into the formulation. These properties, and their spatial distribution, are geologic in nature, being characterized by the details of the individual flow paths.

The other quantity in Eq. (2.2-11) is the relative mobility λ_{rj} of phase j , defined as the quotient of the relative permeability k_{rj} and viscosity μ_j .

$$\lambda_{rj} = \frac{k_{rj}(S, \omega, \vec{x})}{\mu_j(\omega, \bar{u}_j)}. \quad (2.2-28)$$

Equation (2.2-28) decomposes λ_{rj} into a rock–fluid property k_{rj} and a fluid property μ_j . k_{rj} is a function of the tendency of phase j to wet the permeable medium, of pore size distribution, and of the entire set of phase saturations (see Chap. 3). μ_j is a function of the phase composition and, if phase j is non-Newtonian, the magnitude of the superficial velocity \bar{u}_j (see Chap. 8). The relative permeabilities and viscosities

k_{rj} and μ_j are usually determined experimentally to give λ_{rj} . It is slightly more general to write the $\lambda_{rj}\vec{k}$ product in Eq. (2.2-11) as

$$\lambda_{rj}\vec{k} = \frac{\vec{k}_j}{\mu_j} \quad (2.2-29)$$

where \vec{k}_j is the phase permeability tensor. This form allows for anisotropic relative permeabilities, but little is known about the anisotropic nature of the relative permeabilities, so it remains a scalar function here, that is, $\vec{k}_j = k_{rj}\vec{k}$. Relative permeabilities and viscosities are chemical properties.

The difference between the phase pressures of any two phases flowing in the REV is the capillary pressure, defined as in Eq. (2.2-13). The capillary pressure between the phases j and n is a function of most of the same variables as the relative permeability (Fatt and Dykstra, 1951). That there are $N_p - 1$ independent relations follows from considering the set of all capillary pressures with j fixed, $P_{c1j}, P_{c2j}, \dots, P_{cN_p j}$. Ignoring the trivial case of $P_{cjj} (=0)$, there are clearly $N_p - 1$ capillary pressures. The capillary pressure P_{ckn} between any two other phases k and n may be expressed as a linear combination of members from the original set.

$$P_{ckn} = P_k - P_n = (P_k - P_j) + (P_j - P_n) = P_{ckj} + P_{cjn}. \quad (2.2-30)$$

Hence there are only $N_p - 1$ independent capillary pressure relations, usually determined experimentally under static conditions. We discuss capillary pressure in more detail in Chap. 3.

The pressures P_j are the continuous phase pressures, not the pressures that would exist in disconnected “globules” of phase j . In the latter case, the phase pressure differences still exist but, being a reflection of the local permeable medium pore configuration, are not uniquely determined by the functions given in Eq. (2.2-13).

Equations (2.2-14), (2.2-15), and (2.2-16) follow from the definitions of mass fraction and phase saturation, respectively.

Equations (2.2-17) through (2.2-20) are definitions of the reaction rate of component i in phase j or in the solid phase. As was true for R_i , there can be no net accumulation of mass in a phase owing to chemical reaction. Then the reaction rate terms r_{ij} and r_{is} sum to zero as indicated by Eqs. (2.2-18) and (2.2-19) if the equation is written in mass units.

Local Equilibrium

Equations (2.2-21) and (2.2-22) are relations among the mass fractions of the N_p flowing phases and the solid phase present in the REV. These relations arise from solving the conservation equation for each component in each phase

$$\frac{\partial W_{ij}}{\partial t} + \vec{\nabla} \cdot \vec{N}_{ij} = R_{ij} + r_{mij}. \quad (2.1-11)$$

Since the sum of the conservation equations over all flowing phases for component i is Eq. (2.2-5), there are $N_C(N_P - 1)$ such independent phase balances. Since there are also N_C phase balances for the solid phase, the total number of independent relations is $N_C N_P$. There are a similar number of additional unknowns, the r_{mij} , which must be independently specified.

The phase balance is formally correct, but requires considerable additional work to be useful. A much more practical approach is to assume local thermodynamic equilibrium; that is, the mass fractions of component i are related through thermodynamic equilibrium relations (Pope and Nelson, 1978). For flow through naturally occurring permeable media, the assumption of local equilibria among phases is usually adequate (Raimondi and Torcaso, 1965). Exceptions are flows at very high rates or leachant flows such as might occur in alkaline floods. The local equilibrium approximation, or LEA, is discussed further in Lake et al., 2002.

If local equilibrium applies, the number $N_C N_P$ of independent scalar equations may be derived from the phase rule (see Chap. 4). The equilibrium relations themselves are very strong functions of the particular EOR process, and much of the behavior and many of the important features of a given process can be understood from these considerations. Chapter 4 discusses phase behavior generally; we reserve more specifics for the relevant sections on solvent, chemical, and thermal flooding.

The final set of equations in Table 2-2 are the equations of state, Eq. (2.2-23), which relate each phase density to its composition, temperature, and pressure. For LEA flows, the equilibrium relations for the flowing phases, Eqs. (2.2-21) and (2.2-22), can be derived from the equation of state as discussed in Chap. 4. This practice enforces internal consistency between the equilibrium relations and the equations of state. In the text, however, we will often invoke simpler equilibrium relations for pedagogical purposes.

Phase Conservation Equations

Another important set of equations are the phase conservation equations, which are derived from the fundamental Eqs. (2.1-11) or (2.2-4) (see Fig. 2-1). This set of N_P equations result from grouping the equations by each phase and then summing those grouped equations over each component. The result of the summations on Eq. (2.2-4) gives

$$\frac{\partial}{\partial t} (\varepsilon_j \rho_j) + \vec{\nabla} \cdot (\rho_j \vec{u}_j) = \sum_{i=1}^{N_C} r_{mij} \quad j = 1, \dots, N_P, \quad (2.2-31)$$

where we used Eqs. (2.2-19) and (2.2-20) and $\sum_{i=1}^{N_C} \vec{\nabla} \cdot \vec{j}_{D_{ij}} = 0$ (net dispersive flux in a phase is zero). The dispersive flux term vanishes strictly only for the case when the

flux is written with respect to mass-averaged velocity (see exercise 2D). Nevertheless, we assume this is also approximately correct when the dispersive flux is written with respect to volume-averaged velocity. The phase conservation equations are useful for modeling fluid flow of several phases. In general, this is the case when fluids are immiscible so that the phase compositions are fixed.

Under the assumption of no mass transfer and sorption, $r_{mij} = 0$, Eq. (2.2-31) reduces to the immiscible phase conservation equations,

$$\frac{\partial}{\partial t}(\varepsilon_j \rho_j) + \vec{\nabla} \cdot (\rho_j \vec{u}_j) = 0 \quad j = 1, \dots, N_p, \quad (2.2-32)$$

where $\varepsilon_j = \phi S_j$ from Eq. (2.2-1) and N_p represents only flowing phases. The solid phase equation is omitted because its solution is trivial when it is non-deformable, that is, $(1-\phi)\rho_s$ is constant temporally.

Example 2-3. Writing the phase conservation equations for each phase.

Combine the fundamental equations given in Example 2-1 to form the phase conservation equations for the aqueous, oleic, and solid phases. Use the same assumptions as in Example 2-1.

The equations in Example 2-1 are already sorted by phase. Thus, we simply sum each set of grouped equations over the components to obtain the form of Eq. (2.2-31). The resulting summation consists of the following three equations:

$$\left. \begin{aligned} & \frac{\partial}{\partial t}(\phi S_1 \rho_1 \omega_{11} + \phi S_1 \rho_1 \omega_{21}) + \\ & \vec{\nabla} \cdot [\rho_1 \omega_{11} \vec{u}_1 + \rho_1 \omega_{21} \vec{u}_1] = \phi S_1 r_{11} + \phi S_1 r_{21} + r_{m11} + r_{m21} \\ & \frac{\partial}{\partial t}(\phi S_2 \rho_2 \omega_{12} + \phi S_2 \rho_2 \omega_{22}) + \\ & \vec{\nabla} \cdot [\rho_2 \omega_{12} \vec{u}_2 + \rho_2 \omega_{22} \vec{u}_2] = \phi S_2 r_{12} + \varepsilon_2 r_{22} + r_{m12} + r_{m22} \\ & \frac{\partial}{\partial t}((1-\phi) \rho_s \omega_{1s} + (1-\phi) \rho_s \omega_{2s}) = (1-\phi) r_{1s} + (1-\phi) r_{2s} + r_{m1s} + r_{m2s} \end{aligned} \right\} \begin{array}{l} \text{aqueous phase} \\ \text{oleic phase} \\ \text{solid phase} \end{array}$$

where we have used $\sum_{i=1}^{N_c} \vec{\nabla} \cdot \vec{j}_{D_i} = 0$. These equations can be further simplified by combining terms and using Eqs. (2.2-14), (2.2-15), (2.2-19), and (2.2-20). The final result is

$$\left. \begin{aligned} & \frac{\partial}{\partial t}(\phi S_1 \rho_1) + \vec{\nabla} \cdot (\rho_1 \vec{u}_1) = r_{m11} + r_{m21} \\ & \frac{\partial}{\partial t}(\phi S_2 \rho_2) + \vec{\nabla} \cdot (\rho_2 \vec{u}_2) = r_{m12} + r_{m22} \end{aligned} \right\} \begin{array}{l} \text{aqueous phase} \\ \text{oleic phase} \end{array}$$

$$\left. \frac{\partial}{\partial t} ((1-\phi) \rho_s) = r_{m1s} + r_{m2s} \right\} \text{solid phase} .$$

When flow is fully immiscible and there is no adsorption, the mass transfer terms in the above equations are zero. When there is no adsorption, the solid phase equation can be dropped, that is, its solution is again trivial. Eqs. (2.2-32) result under these additional assumptions.

Continuity Equation

We sum Eq. (2.2-6) over the N_C components to obtain the equation of *continuity*, or conservation of total mass. We could have also obtained the equation of continuity by summing the phase conservation equations, Eq. (2.2-31), over the N_P phases including the solid phase. The equation of continuity is

$$\frac{\partial}{\partial t} \left(\phi \sum_{j=1}^{N_p} \rho_j S_j + (1-\phi) \rho_s \right) + \vec{\nabla} \cdot \left(\sum_{j=1}^{N_p} \rho_j \vec{u}_j \right) = 0 . \quad (2.2-33)$$

Equation (2.2-33) can be written totally in terms of pressure and saturation derivatives using Eqs. (2.2-11) and (2.2-24); this equation is a form of the “pressure” equation. Equation (2.2-33) is strictly correct only when the velocity is the mass-averaged velocity, not volume-averaged.

2-3 ENERGY BALANCE EQUATIONS

For steam, hot water injection, and in situ combustion—some of the most important EOR and remediation processes—the temperature changes with both space and time. The equations of Table 2-2 apply equally well to nonisothermal flow but with an additional dependent variable, temperature, added to the formulation. The additional equation required to make the problem statement determinant is the conservation of energy, or the first law of thermodynamics. The first law is based on our every day observation that for any change of thermodynamic properties, total energy, which includes internal, potential, kinetic, heat, and work, is conserved.

A statement of the energy balance or first law of thermodynamics suitable for our purposes is

$$\left\{ \begin{array}{l} \text{Rate of} \\ \text{accumulation} \\ \text{of energy in } V \end{array} \right\} = \left\{ \begin{array}{l} \text{Net rate} \\ \text{of energy} \\ \text{transported into } V \end{array} \right\} + \left\{ \begin{array}{l} \text{Net rate of} \\ \text{generation of energy} \\ \text{inside } V \end{array} \right\} \quad (2.3-1)$$

where V is an arbitrary volume as in Fig. 2-4. From left to right in Eq. (2.3-1) are the accumulation, flux, and source terms, respectively. We use the parallel between the

component conservation Eq. (2.1-1) and Eq. (2.3-1) to shorten the following development. By analogy to the procedure in Sec. 2-2, the accumulation term in Eq. (2.3-1) for a stationary V can be written as

$$\left\{ \begin{array}{l} \text{Rate of} \\ \text{accumulation} \\ \text{of energy in } V \end{array} \right\} = \frac{d}{dt} \left\{ \begin{array}{l} \text{Total energy} \\ \text{in } V \end{array} \right\}$$

$$= \int_V \frac{d}{dt} \sum_{j=1}^{N_p} \left(\varepsilon_j \rho_j \left[U_j + \frac{1}{2} |\vec{v}_j|^2 - g D_z \right] \right) dV \quad (2.3-2)$$

where the total energy includes internal, kinetic, and potential energy. Equation (2.3-2) can also be written as

$$\left\{ \begin{array}{l} \text{Rate of} \\ \text{accumulation} \\ \text{of energy in } V \end{array} \right\} = \int_V \frac{d}{dt} \left(\rho U + \frac{1}{2} \rho |\vec{v}|^2 - \rho g D_z \right) dV \quad (2.3-3)$$

where U is an overall internal energy (total energy/total mass), and ρ is the overall density given by Eq. (2.2-24). In Eq. (2.3-3) the term $1/2(\rho|\vec{v}|^2)$ represents total kinetic energy per unit bulk volume and $-\rho g D_z$ total potential energy per unit bulk volume with reference to the depth below some horizontal plane.

The remaining terms in Eq. (2.3-1) are represented by

$$\int_V \frac{d}{dt} \left(\rho U + \frac{1}{2} \rho |\vec{v}|^2 - \rho g D_z \right) dV = - \int_V \vec{\nabla} \cdot \vec{E} dV + \dot{W} \quad (2.3-4)$$

where the terms \vec{E} and \dot{W} represent energy flux, and source, respectively, to which we give specific form below. The negative sign in front of the first term on the right is required to make energy flux positive when it flows into volume V . See Chap. 4 for more treatment of the first law of thermodynamics with application to phase behavior.

The source term requires more elaboration than do the other terms in Eq. (2.3-4). The form of the first law of thermodynamics for open systems expressed by Eq. (2.3-4) requires the \dot{W} term to be composed of work components only, in the absence of external heating sources. External heating sources can often be handled through boundary conditions. Heats of reaction, vaporization, and solution are, of course, important in several processes, but these are implicitly present in the equation in the concentration and flux terms. Here we consider only the rate of work done against a pressure field \dot{W}_{pv} , although other types of work could be included (see exercise 2P). In this derivation, there is no compression or expansion work done on volume V since it is assumed to be fixed.

Returning to Fig. 2-4(b), consider an element in the multiphase, multicomponent flow field crossing ΔA . Since work is the product of force times a distance, the rate of work is force times a velocity. The element crossing ΔA is, therefore, doing work $\Delta \dot{W}_{PV}$, where

$$\Delta \dot{W}_{PV} = - \sum_{j=1}^{N_p} P_j \Delta A \vec{n} \cdot \vec{u}_j . \quad (2.3-5)$$

The term $P_j \Delta A \vec{n}$ is the force exerted on ΔA by the pressure in phase j . The scalar product in Eq. (2.3-5) expresses a general definition of work rate when using vector forces and velocities. The negative sign in Eq. (2.3-5) is to satisfy the usual thermodynamic sign convention for work, since $\Delta \dot{W}_{PV}$ must be positive for work done on a fluid element flowing into $V (\vec{n} \cdot \vec{u}_j < 0)$. The total pressure-volume work is the sum of Eq. (2.3-5) over all surface elements, which, in the limit of the largest ΔA approaching zero, becomes a surface integral. Using the divergence theorem, Eq. (2.1-9), on this integral gives the final form for \dot{W}_{PV} .

$$\dot{W}_{PV} = - \int_V \sum_{j=1}^{N_p} \vec{\nabla} \cdot (P_j \vec{u}_j) dV . \quad (2.3-6)$$

The expression for work fits well into Eq. (2.3-4). After collecting all terms under the same volume integral and making the integrand zero because V is again arbitrary, we have

$$\frac{\partial}{\partial t} \left(\rho U + \frac{1}{2} \rho |\vec{v}|^2 - \rho g D_z \right) + \vec{\nabla} \cdot \vec{E} + \sum_{j=1}^{N_p} \vec{\nabla} \cdot (P_j \vec{u}_j) = 0 \quad (2.3-7)$$

The energy flux term is made up of convective contributions from the flowing phases (internal, kinetic, and potential energy), conduction, and radiation, all other forms being neglected.

$$\vec{E} = \sum_{j=1}^{N_p} \rho_j \vec{u}_j \left[U_j + \frac{1}{2} |\vec{v}_j|^2 - g D_z \right] + \vec{q}_c + \vec{q}_r . \quad (2.3-8)$$

For brevity, we neglect radiation in the following discussion, though this transport mechanism can be important in estimating heat losses from wells and in certain forms of EOR and remediation that involve electromagnetic sources. For multiphase flow, the conductive heat flux is from Fourier's law,

$$\vec{q}_c = -k_{Tt} \vec{\nabla} T , \quad (2.3-9)$$

where k_{Tt} is the scalar total thermal conductivity. k_{Tt} is a complex function of the phase saturations and phase k_{Tj} and solid k_{Ts} thermal conductivities, which we take to

be known (see Chap. 11). The parallel between Eq. (2.3-8) and the dispersive flux term in Eq. (2.2-8) is obvious. We have also invoked the requirement of local thermal equilibrium in this definition by taking the temperature T to be the same in all phases within the REV.

Inserting definitions (2.3-8) and (2.3-9) into Eq. (2.3-7) yields

$$\begin{aligned} \frac{\partial}{\partial t} \left(\rho U + \frac{1}{2} \rho |\vec{v}|^2 - \rho g D_z \right) + \vec{\nabla} \cdot \left(\sum_{j=1}^{N_p} \rho_j \vec{u}_j \left[U_j + \frac{1}{2} |\vec{v}_j|^2 - g D_z \right] \right) \\ - \vec{\nabla} \cdot (k_{T_l} \vec{\nabla} T) + \sum_{j=1}^{N_p} \vec{\nabla} \cdot (P_j \vec{u}_j) = 0 . \end{aligned} \quad (2.3-10)$$

The first sum in the energy flux and that in the pressure-volume work expression may be combined to give

$$\begin{aligned} \frac{\partial}{\partial t} \left(\rho U + \frac{1}{2} \rho |\vec{v}|^2 - \rho g D_z \right) + \vec{\nabla} \cdot \left(\sum_{j=1}^{N_p} \rho_j \vec{u}_j \left[H_j + \frac{1}{2} |\vec{v}_j|^2 - g D_z \right] \right) \\ - \vec{\nabla} \cdot (k_{T_l} \vec{\nabla} T) = 0 \end{aligned} \quad (2.3-11)$$

where $H_j = U_j + P_j/\rho_j$ is defined as the enthalpy of phase j per unit mass of j .

TABLE 2-3 SUMMARY OF ADDITIONAL STRONG FORM EQUATIONS FOR NONISOTHERMAL FLUID FLOW IN PERMEABLE MEDIA

Equation (1)	Name (2)	Number independent scalar* equations (3)	Dependent variables†	
			Identity (4)	Number (5)
(2.3-12) $\frac{\partial}{\partial t}(\rho U + \frac{1}{2} \rho \vec{v} ^2 - \rho g D_z) + \vec{\nabla} \cdot \left(\sum_{j=1}^{N_p} \rho_j \vec{u}_j \left[H_j + \frac{1}{2} \vec{v}_j ^2 - g D_z \right] \right) - \vec{\nabla} \cdot (k_{T_f} \vec{\nabla} T) = 0$	Energy conservation	1	U, H_j, T	$N_p + 2$
(2.3-13) $\rho U = \phi \sum_{j=1}^{N_p} \rho_j S_j U_j + (1-\phi) \rho_s U_s$	Total internal energy	1	U_j, U_s	$N_p + 1$
(2.3-14) $U_j = \sum_{i=1}^{N_c} \omega_{ij} U_{ij}$ $U_s = \sum_{i=1}^{N_c} \omega_{is} U_{is}$	Phase internal energy	N_p	U_{ij}	$N_p N_c$
(2.3-15) $H_j = \sum_{i=1}^{N_c} \omega_{ij} H_{ij}$	Phase enthalpy	N_p	H_{ij}	$N_p N_c$
(2.3-16) $U_{ij} = U_{ij}(T, P_j, \omega)$ $U_{is} = U_{is}(T, P_j, \omega)$	Partial mass internal energy	$N_p N_c$	N_c	

$$(2.3-17) \quad H_{ij} = H_{ij}(T, P_j, \omega)$$

Partial mass enthalpy

$N_P N_C$

*Total independent equations = $2(N_P N_C) + 2N_P + N_C + 3$

† Total dependent variables = $2(N_P N_C) + 2N_P + N_C + 3$

The conservation equation discussed in this section and in Table 2-3 are "overall" in the sense that the balances are written over a REV that contains all the phases. We could have written balances on each phase or each component just as was done in the previous section for mass conservation. These balances would have in them terms describing the rate of energy transport between phases and would not necessarily assume equality of temperature in all phases within a REV.

Equation (2.3-11) can also be obtained if the volume V is no longer stationary and both pressure-volume and compression-expansion work are present (see exercise 2Q). For example, consider a closed system where volume V expands or contracts at the same rate as the fluid flow velocity. In that case, compress-expansion work is done on the boundary of V as it deforms and pressure-volume work is zero. This type of work is given by $\Delta\dot{W}_{CE} = \vec{F}_{ext} \cdot \vec{u}$, where \vec{F}_{ext} is the component of external force acting along the velocity vector \vec{u} . Work is always related to the external pressure or force. If the external pressure were zero, there would be no work done by the system because the surroundings offer no resistance. The rate of work done on a surface element of V is therefore,

$$\Delta\dot{W}_{CE} = -\sum_{j=1}^{N_p} P_j \Delta A \vec{n} \cdot \vec{u}_j , \quad (2.3-18)$$

which is identical to Eq. (2.3-5) when the volume V deforms with the phase velocities. The development then proceeds as before, but with the accumulation term for a time-varying V deforming at a Darcy rate \vec{u}_j written as (Slattery, 1972)

$$\begin{aligned} \frac{\partial}{\partial t} \int_V \sum_{j=1}^{N_p} \left(\varepsilon_j \rho_j \left[U_j + \frac{1}{2} |\vec{v}_j|^2 - gD_z \right] \right) dV = \\ \int_{V(t)} \frac{\partial}{\partial t} \sum_{j=1}^{N_p} \left(\varepsilon_j \rho_j \left[U_j + \frac{1}{2} |\vec{v}_j|^2 - gD_z \right] \right) dV + \int_{A(t)} \nabla \cdot \sum_{j=1}^{N_p} \left(\rho_j \vec{u}_j \left[U_j + \frac{1}{2} |\vec{v}_j|^2 - gD_z \right] \right) dA . \end{aligned}$$

Equation (2.3-18) can be rewritten in a more familiar form by combining the surface element areas with the component of the velocity vector perpendicular to that surface element ($\Delta q_{j\perp} = \vec{n} \cdot \Delta A \vec{u}_j = \vec{n} \cdot \Delta \vec{q}_j$), summing over all surface elements, and taking the limit as the largest $\Delta q_{j\perp}$ approaches zero. The result is,

$$\dot{W}_{CE} = -\sum_{j=1}^{N_p} \int_{q_{j\perp} \in A(t)} P_j dq_{j\perp} . \quad (2.3-19)$$

Further, when the phase pressures are uniform along the boundary of V , the phase pressures can pass through the integral so that

$$\dot{W}_{CE} = -\sum_{j=1}^{N_p} P_j \frac{dV_j}{dt} . \quad (2.3-20)$$

V_j in Eq. (2.3-20) is now the total volume of phase j within V . Eq. (2.3-20) is valid no matter the shape or size of volume V .

Auxiliary Relations

Table 2-3 summarizes the equations that, together with those of Table 2-2, completely specify non-isothermal fluid flow problems. The first three equations we have already discussed.

The energy concentration per unit bulk volume must include internal energy contributions from all flowing phases and the solid phase,

$$\rho U = \phi \sum_{j=1}^{N_p} \rho_j S_j U_j + (1-\phi) \rho_s U_s \quad (2.3-13)$$

where U_j is the internal energy per unit mass of phase j . The total kinetic energy term includes kinetic energy contributions from all flowing phases,

$$\frac{1}{2} \rho |\vec{v}|^2 = \phi \sum_{j=1}^{N_p} \left(\frac{1}{2} \rho_j S_j |\vec{v}_j|^2 \right) \quad (2.3-21)$$

where the solid phase velocity is negligible.

The phase internal energies U_j and U_s and the enthalpies H_j are functions of temperature T , phase pressure P_j , and composition ω_{ij} . One form this dependency can take is Eq. (2.3-14), where the doubly subscripted internal energies (and enthalpies) are partial mass quantities. Partial mass quantities, Eq. (2.3-16), are analogous to partial molar quantities in solution thermodynamics (Denbigh, 1968). For example, the partial mass internal energy of component i in phase j is the change in U_j as ω_{ij} is changed, all other variables being held constant,

$$U_{ij} = \left(\frac{\partial U_j}{\partial \omega_{ij}} \right)_{P_j, T, \omega_{kj, k \neq i}} \quad (2.3-22)$$

and similarly for U_{is} and H_{ij} . The partial mass properties themselves may be calculated from equations of state, Eq. (2.2-23), or empirical correlations as functions of temperature, pressure, and composition.

Equations (2.3-14) and (2.3-15) readily revert to simple forms. For example, if phase j is an ideal solution, the partial mass quantities become pure component quantities, functions of temperature and pressure only. Further, if j is an ideal gas, the partial mass quantities are functions only of temperature.

The equations presented in Tables 2-2 and 2-3 are complete, but they can only be solved with the specification of a similarly complete set of initial and boundary conditions.

2-4 ENTROPY BALANCE EQUATIONS

The equations for conservation of total mass and energy are insufficient to solve many thermodynamic problems. For example, experience has shown that a pond on a hot summer day will not freeze, but instead will equilibrate to the temperature of its surroundings. The first law of thermodynamics, however, is satisfied whether the pond freezes (loses energy to surroundings) or heats up (gains energy from surroundings). That is, the direction of energy transfer is irrelevant to the first law of thermodynamics and there must be another equation that describes the approach to equilibrium.

More generally we observe that as long as there are no outside influences, gradients in concentration, temperature, and pressure eventually vanish reaching a time-invariant equilibrium state with its surroundings. The second law of thermodynamics provides a mathematical statement that describes this unidirectional nature of spontaneous processes. A new thermodynamic property, called entropy, is introduced to describe the tendency towards equilibrium. Although we are not as familiar with entropy, it is a property just like temperature and pressure. The main difference, however, is that we must infer its value from other measurable thermodynamic properties such as temperature and pressure.

Entropy increases in spontaneous processes until equilibrium is reached. For example, Figure 2-6 shows an initial state of a hypothetical closed volume that contains four molecules. The molecules are numbered 1 to 4 to aid in the accounting; in reality the molecules are indistinguishable from each other. The system is initially partitioned into two halves or subsystems, such that the molecules from one half cannot move into the other half. Thus, each subsystem has only one possible configuration at zero time, the initial state. The small number of possible configurations at the initial state corresponds to a well-ordered or small-entropy state.

When the partition is removed, the molecules from each subsystem are free to move into the other half of the system, say by random Brownian motion. When the elapsed time is short, the initial state is the most likely configuration. Over time, however, a total of 16 different equally-probable configurations are possible relative to the original partition location (see Figure 2-6). The increase in possible configurations of the system is related to an increase in entropy or disorder. A careful examination of the possible configurations shows further that a state with one or two molecules on each side is more likely to exist than the initial state, which has a probability of only 2^4 or 1/16, the initial state being just one of 16 possible states. A true equilibrium state with two molecules on either side of the original partition (no gradients) is also more likely to exist (probability of 6/16 or 3/8) than the initial state.

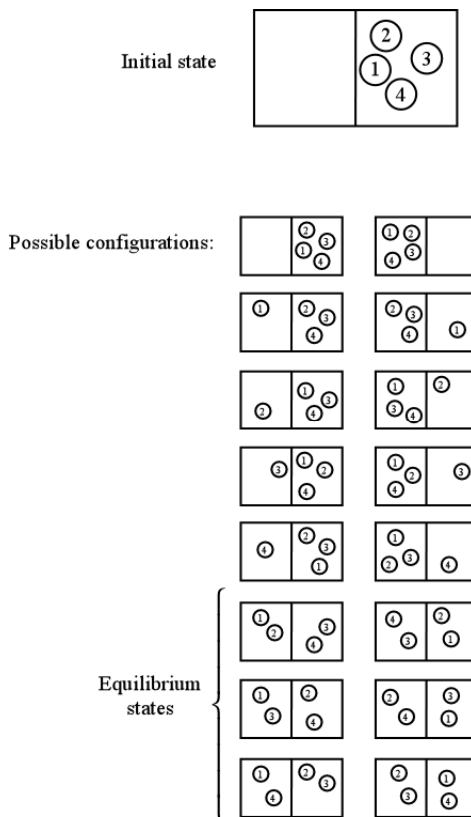


Figure 2-6: Illustration of configurations for four molecules in a closed composite system (after Smith et al. 2001). The molecules on each side of the partition are initially constrained by a partition.

The illustration of Figure 2-6 demonstrates in a simple way why equilibrium occurs in natural processes; equilibrium is the most likely state. A more realistic example, with many more molecules is even more convincing. For example, if one mole of a gas (6×10^{23} molecules) were present in the same partitioned volume, the probability for reaching equilibrium is astronomically close to 1.0. The apparent equilibrium state includes many unequal configurations where the number of molecules is not exactly the same on each side, but is sufficiently close in relative numbers that we cannot differentiate between those configurations. They all appear to be in equilibrium.

Let's consider an even simpler case to understand entropy and its relation to equilibrium. Entropy was defined by Boltzmann (1872) at the microscopic level by the mathematical function $S = -k \sum_i p_i \ln p_i$ where p_i is the state probability of a given configuration and k is an arbitrary constant. The negative sign is introduced so that entropy by this function is always positive, recognizing that probabilities must be between 0.0 and 1.0. There is nothing magical about this function, but it has the properties we desire in that entropy is always positive and increases uni-directionally

as equilibrium is approached. For example, applying this function to the simplest case of one molecule on the right hand side of the partition in Fig. 2-6, the probability initially is 1.0 that the molecule will be at the right-hand side of the partition just after it is removed and 0.0 that it will be at the left-hand side. Thus, entropy given by this function is initially $S = -k(0.0 \ln 0.0 + 1.0 \ln 1.0)$ or zero. As time advances, the probability that the molecule will be found at the right-hand side will decrease, whereas it will increase at the left-hand side. At some later time for example, the probabilities will be 0.9 and 0.1 giving $S = -k(0.1 \ln 0.1 + 0.9 \ln 0.9)$ or $0.33k$. Eventually at equilibrium, the molecule is equally-likely to exist on either side of the partition and entropy will achieve its maximum value of $S = -k(0.5 \ln 0.5 + 0.5 \ln 0.5) = -k \ln p_i$ or $0.69k$.

Once equilibrium has been reached, entropy remains fixed (because the probabilities are constant) as long as there are no other outside influences, such as the expansion of volume or addition of more molecules to the box in Fig. 2-6. For example, if a third equal volume is added to the other two, the probability that the molecule is contained in either is 0.33. The entropy at equilibrium is then $S = -k(0.33 \ln 0.33 + 0.33 \ln 0.33 + 0.33 \ln 0.33) = -k \ln p_i$ or $1.11k$, which is greater than the previous value of $0.69k$. Thus, an increase in volume increases the entropy at equilibrium since the equilibrium probabilities are decreased.

The microscopic entropy function defined by Boltzmann must be related to macroscopic thermodynamic properties for it to be practically useful. Fortunately, it is possible to relate entropy to changes in internal energy and volume (see for example, Schmidt *et al.* 2006). The easiest way to understand this is to think of the labeled molecules in Fig. 2-6 as representing different energy quanta. We can then assign probabilities for states based on the energy levels found on the left and right hand side of the box. For example, if the molecules are initially very near absolute zero, each molecule would have similar individual energies equal to the group average energy. The internal energy in the closed volume is then the sum of the individual molecule energies. The probability of finding a molecule at that energy state on the right-hand side of the box is 1.0 and will not change with time unless heat is added.

When heat is added to the box, the statistical distribution of individual molecule energies around a group average energy will spread out according to the Maxwell-Boltzmann distribution. That energy distribution shows that there will be a wider range of possible individual particle energies for a group of molecules that have a greater internal energy (or larger temperature). Hence, more possible energy levels or configurations results in lower probabilities, thereby increasing entropy in a similar fashion as in the molecule example of Fig. 2-6. This relationship between increasing entropy with increasing internal energy can be expressed by the partial derivative at constant volume $(\partial S / \partial U)_V = 1/T$. That is, the entropy change with internal energy is inversely proportional to temperature when the volume is fixed and will be greatest at temperatures near absolute zero. Similar logic leads to the relationship that for constant internal energy $(\partial S / \partial V)_U = P/T$. Because all properties

in these relationships are state functions (independent of the path), they can be combined to give the macroscopic definition of entropy as $dS = (\partial S / \partial U)_V dU + (\partial S / \partial V)_U dV = (1/T) dU + (P/T) dV$. Again, there is nothing magical about this definition except that like Boltzmann's microscopic definition it gives a value for entropy that is always positive and increasing monotonically towards equilibrium.

In summary, we have shown that the equilibrium state is the state of maximum entropy for an isolated system and statistically the most probable state. For example, it is possible, although highly improbable, that a lake of water will freeze on a hot summer day. The second law does not rule out this possibility, but instead gives us the most likely direction that nature will take. A good definition of the second law therefore is that the entropy of an isolated system will always increase from a state of high probability (well-ordered) to a state of lower probability (more disordered) until it reaches a state of minimum probability at equilibrium. This increase (or creation) of entropy is always related to initial gradients in the system, and overtime the rate of increase of entropy decreases as the fluids mix or heat is exchanged.

An entropy balance is used to mathematically represent the tendency of processes to approach equilibrium. The steps to write the entropy balance are similar to those for the first law of thermodynamics, except that entropy is created as fluids mix or heat is exchanged as illustrated in Figure 2-6. Entropy for a system that is not isolated can increase or decrease depending on the direction and magnitude of mass flow and heat exchange with its surroundings. A statement of the entropy balance is

$$\left\{ \begin{array}{l} \text{Rate of} \\ \text{accumulation} \\ \text{of entropy in } V \end{array} \right\} = \left\{ \begin{array}{l} \text{Net rate} \\ \text{of entropy} \\ \text{transported into } V \end{array} \right\} + \left\{ \begin{array}{l} \text{Rate of} \\ \text{generation of entropy} \\ \text{inside } V \end{array} \right\} \quad (2.4-1)$$

where V is an arbitrary volume as in Fig. 2-4. By analogy to the procedure for the first law of thermodynamics in Section 2-3, the accumulation term in Eq. (2.4-1) for a stationary V can be written as

$$\left\{ \begin{array}{l} \text{Rate of} \\ \text{accumulation} \\ \text{of entropy in } V \end{array} \right\} = \frac{d}{dt} \left\{ \begin{array}{l} \text{Total entropy} \\ \text{in } V \end{array} \right\} = \int_V \frac{\partial}{\partial t} \sum_{j=1}^{N_p} (\varepsilon_j \rho_j S_j) dV \quad (2.4-2)$$

where the total entropy includes contributions from all phases and S_j is the specific entropy of phase j . Equation (2.4-1) can now be expressed as

$$\int_V \frac{d}{dt} \sum_{j=1}^{N_p} (\varepsilon_j \rho_j S_j) dV = - \int_V \bar{\nabla} \cdot \bar{S} dV + \int_V \dot{\sigma}_G dV . \quad (2.4-3)$$

The first term on the right hand side is the entropy flux term. The second term is the rate of entropy generation per unit bulk volume.

The net rate of entropy transport into volume V is the result of heat and mass transfer into V from its surroundings. Entropy transport owing to convection of mass is handled similarly to energy. Further, from the definition of entropy, the entropy transport owing to heat exchange at fixed volume is proportional to the conductive heat flux divided by the temperature at which that transfer occurs, that is, $dS = dq/T$ since $dU = dq$ from the conservation of energy (see also Section 2.6). Thus, the total entropy transport owing to mass convection and heat exchange is

$$\vec{S} = \sum_{j=1}^{N_p} \rho_j \vec{u}_j S_j + \frac{\vec{q}_c}{T} . \quad (2.4-4)$$

Similar to the energy balance, we have invoked the requirement of local thermal equilibrium in Eq. (2.4-4) by taking the temperature T to be the same in all phases within the REV. Substitution of Eq. (2.4-4) into Eq. (2.4-3) gives,

$$\int_V \frac{d}{dt} \sum_{j=1}^{N_p} (\varepsilon_j \rho_j S_j) dV = - \int_V \vec{\nabla} \cdot \sum_{j=1}^{N_p} \rho_j \vec{u}_j S_j dV - \int_V \vec{\nabla} \cdot \frac{\vec{q}_c}{T} dV + \int_V \dot{\sigma}_G dV . \quad (2.4-5)$$

The desired result is obtained after collecting all terms under the same volume integral and making the integrand zero because V is again arbitrary,

$$\frac{\partial}{\partial t} \sum_{j=1}^{N_p} (\varepsilon_j \rho_j S_j) = - \vec{\nabla} \cdot \sum_{j=1}^{N_p} \rho_j \vec{u}_j S_j - \vec{\nabla} \cdot \frac{\vec{q}_c}{T} + \dot{\sigma}_G . \quad (2.4-6)$$

Analogous to the procedure in Sec. 2-4, Eq. (2.4-6) could also be obtained for a time-varying V .

Second Law of Thermodynamics

The inequality $\dot{\sigma}_G \geq 0$ is the second law of thermodynamics, the equality holding at equilibrium. This simple condition provides the restriction on bi-directional transport of energy. The creation of entropy is related to the gradients within the system.

The relationship between entropy generation and gradients within the system is most easily seen by assuming pure single-phase flow and neglecting changes in kinetic or potential energies. The mass, energy, and entropy balances become respectively,

$$\frac{\partial}{\partial t} (\phi \rho) = - \vec{\nabla} \cdot (\rho \vec{u})$$

$$\frac{\partial}{\partial t}(\phi\rho U) = -\vec{\nabla} \cdot (\rho \vec{u} U) - \vec{\nabla} \cdot (P \vec{u}) - \vec{\nabla} \cdot \vec{q}_c$$

and,

$$\frac{\partial}{\partial t}(\phi\rho S) = -\vec{\nabla} \cdot (\rho \vec{u} S) - \frac{1}{T} \vec{\nabla} \cdot \vec{q}_c + \frac{\vec{q}_c}{T^2} \cdot \vec{\nabla} T + \dot{\sigma}_G$$

where the conduction term in the entropy equation has been expanded and we used $H = U + P / \rho$. These equations can be combined and rearranged using the total derivative ($D / Dt = \partial / \partial t + \vec{v} \cdot \nabla$) to give,

$$\phi\rho \left(\frac{DS}{Dt} - \frac{1}{T} \frac{DU}{Dt} - \frac{P}{T} \frac{DV}{Dt} \right) = \frac{1}{T} \vec{u} \cdot \vec{\nabla} P + \frac{\vec{q}_c}{T^2} \cdot \vec{\nabla} T + \dot{\sigma}_G \quad (2.4-7)$$

where $V = 1 / \rho$ and under the assumption of constant porosity $\vec{\nabla} \cdot \vec{u} = \phi\rho DV / Dt$.

The left-hand side of Eq. (2.4-7) gives temporal changes in thermodynamic properties and is zero from the definition of entropy. The right-hand side of Eq. (2.4-7) involves terms that depend on the gradient of pressure and temperature. Thus, since entropy creation is the result of gradients, we must have

$$\dot{\sigma}_G = -\frac{1}{T} \vec{u} \cdot \vec{\nabla} P - \frac{\vec{q}_c}{T^2} \cdot \vec{\nabla} T \quad (2.4-8)$$

Substitution of Darcy's law for horizontal single-phase flow, $\vec{u} = -\left(\frac{\vec{k}}{\mu}\right) \cdot \nabla P$, and Fourier's law of heat conduction, $\vec{q}_c = -h \nabla T$, into Eq. (2.4-8) gives our desired result,

$$\dot{\sigma}_G = \frac{\vec{k}}{T\mu} \vec{\nabla} P \cdot \vec{\nabla} P + \frac{h}{T^2} \vec{\nabla} T \cdot \vec{\nabla} T \quad (2.4-9)$$

Equation (2.4-9) shows that entropy creation is proportional to the square of the pressure and temperature gradients. Thus, entropy creation is minimized when gradients are small, as they are when equilibrium is approached. Last, Eq. (2.4-9) shows that $\dot{\sigma}_G \geq 0$ since the properties in Eq. (2.4-9) and the square of the gradients are always positive. The expression for entropy creation can be extended to account for multiple components, diffusive flux, and other processes.

2-5 SPECIAL CASES OF THE STRONG FORM

We now turn to several important special cases of the phase conservation equations, Eqs. (2.2-31), and the overall compositional equations, Eqs. (2.2-4) and Tables 2-2 and 2-3 (see Fig. 2-1). Each special case is applied in practice to describe various EOR processes occurring in permeable media fluid flow. These special cases can be

accurately approximated by much simpler forms of the above general equations with fewer and simpler associated auxiliary equations and boundary conditions. All flows discussed here are in local thermodynamic equilibrium.

Fractional Flow Equations

Consider isothermal flow (T constant) with no interphase mass transfer so that $r_{mij} = 0$ (including sorption). Because flow is immiscible, only the fluid saturations change because phase compositions are fixed. Thus, we apply the above assumptions to the phase conservation equations, Eq. (2.2-31), which were derived from Eq. (2.2-4) (see Fig. 2-4). For this case, the energy conservation equation and the solid phase equation are trivial, and Eq. (2.2-31) reduces to Eq. (2.2-32).

$$\frac{\partial}{\partial t} (\phi S_j \rho_j) + \vec{\nabla} \cdot (\rho_j \vec{u}_j) = 0 \quad j = 1, \dots, N_p. \quad (2.2-32)$$

We specialize the equation next for one-dimensional linear flow in a medium dipping at a constant angle α and constant rock and fluid properties (ϕ constant temporally and ρ_j constant temporally and spatially). Because porosity and phase densities are constant, these properties can be removed from the respective derivatives and the phase densities cancelled. Equation (2.2-32) is then further simplified to

$$\phi \frac{\partial S_j}{\partial t} + \frac{\partial u_j}{\partial x} = 0, \quad j = 1, \dots, N_p. \quad (2.5-1)$$

To eliminate the need to solve for pressure, Eq. (2.5-1) is usually written in terms of a fractional flow function, which can be defined for the case of equal phase pressures ($P_{cjn} = 0$) as

$$f_j = \frac{u_j}{u} = \frac{\lambda_{rj}}{\sum_{k=1}^{N_p} \lambda_{rk}} \left[1 - \frac{kg \sin \alpha}{u} \sum_{k=1}^{N_p} \lambda_{rk} (\rho_j - \rho_k) \right], \quad (2.5-2)$$

where $u = \sum_{j=1}^{N_p} u_j$ and α is the dip angle $\tan \alpha = dD_z/dx$. The right side of Eq. (2.5-2) results by substitution of Darcy's law into the fractional flow definition. This equation will be derived and developed further in Chap. 5.

It is easily shown (Chap. 5) by summing the phase equations given in Eq. (2.5-1) that u is a function of time only and f_j is a function of saturation only. The sum being a form of the pressure equation, we can write Eq. (2.5-1) in a final form.

$$\frac{\partial S_j}{\partial t} + \frac{u}{\phi} \frac{\partial f_j}{\partial x} = 0, \quad j = 1, \dots, N_p. \quad (2.5-3)$$

To solve Eq. (2.5-3) for the phase saturations $S_j(x, t)$, the total volumetric fluid flux u injected at the inflow boundary and the experimentally measured fractional flow dependences of $N_p - 1$ phases (note $\sum_{j=1}^{N_p} f_j = 1$) are needed. Buckley and Leverett (1942) first solved this equation for two-phase flow, and the resulting estimation of waterflood oil recovery is called the Buckley-Leverett theory (see Chap. 5). Other similar cases, including three-phase flow and compositional effects such as interphase mass transfer and adsorption, have been solved in closed form (e.g. Pope, 1980). We discuss these solutions in detail in Chaps. 7 to 9.

Miscible Flow

The above fractional flow case applies to the simultaneous flow of immiscible fluids. We now treat the analogous but opposite case of many components flowing simultaneously in a single fluid phase in isothermal flow. Thus only one phase flows regardless of composition, but both convection and dispersion of these components must be included. Miscible processes of interest include (1) true (first-contact) miscible displacement of oil by a solvent from a reservoir; (2) chromatographic processes of various sorts such as analytical chromatography, separation chromatography, ion exchange processes, and adsorption of chemicals as they percolate through soils and other naturally occurring permeable media; (3) leaching processes such as the in situ mining of uranium; and (4) chemical reaction processes of many types in fixed-bed reactors.

Equation (2.2-6) for single-phase flow is

$$\frac{\partial(\phi\rho\omega_i)}{\partial t} + \frac{\partial}{\partial t}[(1-\phi)\rho_s\omega_{is}] + \vec{\nabla} \cdot [\rho\omega_i \vec{u} - \phi \vec{\bar{K}}_i \cdot \vec{\nabla}(\rho\omega_i)] = R_i \quad i = 1, \dots, N_c . \quad (2.5-4)$$

This equation arises because the saturations for all phases but one are zero and the saturation of the remaining phase is one. The second subscript j is now superfluous and has been dropped. The auxiliary Eqs. (2.2-11), (2.2-12), (2.2-14), (2.2-15), and (2.2-17) through (2.2-23) are still needed, but the others are no longer pertinent. The principal one of these, Eq. (2.2-11) or Darcy's law, has a considerably simpler form as well, namely,

$$\vec{u} = -\frac{\vec{k}}{\mu} \cdot (\vec{\nabla} P + \rho \vec{g}) . \quad (2.5-5)$$

Because the relative permeability is now constant (typically unity), it is lumped with \vec{k} .

For miscible solvents (see Chap. 7), the sorption term, the second term in Eq. (2.5-4), is negligible. That assumption coupled with no chemical reactions ($R_i = 0$), gives

$$\frac{\partial(\phi\rho\omega_i)}{\partial t} + \vec{\nabla} \cdot \left[\rho\omega_i \bar{u} - \phi \vec{\bar{K}}_i \cdot \vec{\nabla} (\rho\omega_i) \right] = 0, \quad i = 1, \dots, N_c . \quad (2.5-6)$$

A special one-dimensional linear case of Eq. (2.5-6) is obtained when the porosity is constant, and $\vec{\bar{K}}_i$ is a constant. Letting $C_i = \rho\omega_i$ be the mass concentration of component i , it follows that

$$\phi \frac{\partial C_i}{\partial t} + u \frac{\partial C_i}{\partial x} = \phi K_{li} \frac{\partial^2 C_i}{\partial x^2}, \quad i = 1, \dots, N_c , \quad (2.5-7)$$

where K_{li} , the longitudinal dispersion coefficient, is now a scalar,

$$K_{li} = \frac{D_i}{\tau} + \frac{\alpha_i |u|}{\phi} \quad (2.5-8)$$

as a special case of the more general definition given by Eq. (2.2-2). Moreover, u is at most a function of time, depending on the boundary conditions specified. D_i is usually taken as a constant, yielding the linear convection–diffusion (CD) equation, which is alternatively termed the advection-dispersion equation. Several closed-form solutions for simple initial and boundary conditions are available for the CD equation (see Chaps. 5 and 7).

Chromatographic Equations

Several chromatographic processes are special cases of Eq. (2.5-7). We must restore the C_{is} term ($C_{is} = \rho\omega_{is}$) that describes the accumulation of component i owing to sorption reactions, for this is the essence of a chromatographic process. These sorption reactions may be adsorption, the exchange of one ion by another on the solid substrate, or precipitation–dissolution reactions (see Chaps. 8 to 10 and Lake et al., 2002). All these processes lead to selective separation of the components as they percolate through the permeable medium. Dispersion does not alter the separation in chromatographic columns, so we neglect the second-order term, a step that results in a set of strongly coupled (via the sorption term) first-order partial differential equations

$$\phi \frac{\partial C_i}{\partial t} + (1-\phi) \frac{\partial C_{is}}{\partial t} + u \frac{\partial C_i}{\partial x} = 0, \quad i = 1, \dots, N_c . \quad (2.5-9)$$

For linear sorption Eq. (2.5-9) can be rewritten in terms of a retardation factor by first collecting like terms:

$$\frac{\partial}{\partial t} (\phi C_i + (1-\phi) C_{is}) + u \frac{\partial C_i}{\partial x} = 0, \quad i = 1, \dots, N_c . \quad (2.5-10)$$

The retardation factor for each component is defined as

$$D_i = \frac{(1-\phi)C_{is}}{\phi C_i} = \frac{(1-\phi)}{\phi} \rho_s K_{di} \quad (2.5-11)$$

where $K_{di} = \frac{\omega_{is}}{C_i}$ is the partition coefficient for component i that relates the mass fraction of the component adsorbed onto the solid divided by the concentration of the component in the single-phase mixture. Substitution of the definition for the retardation coefficient into Eq. (2.5-10) gives

$$\frac{\partial}{\partial t} (\phi C_i (1+D_i)) + u \frac{\partial C_i}{\partial x} = 0, \quad i = 1, \dots, N_C. \quad (2.5-12)$$

When the retardation factor and porosity are temporally constant,

$$\phi \frac{\partial C_i}{\partial t} + \frac{u}{1+D_i} \frac{\partial C_i}{\partial x} = 0, \quad i = 1, \dots, N_C. \quad (2.5-13)$$

This equation and Eq. (2.4-7) with dispersion neglected are nearly identical. The only difference is that the flow rate is divided by $1+D_i$, resulting in an effective flow rate of $u_{ei} = u/(1+D_i)$ for each component. The retardation factor is aptly named because it causes an apparent reduction in the velocity at which the component moves through the chromatographic column. With no sorption, the retardation factor is zero and the component moves at the average flow rate of the fluid. Because of the slowing of the velocity, the retardation factor is sometimes called a delay factor (Lake *et al.*, 2002).

Semimiscible Systems

In several EOR applications, a description of flow in permeable media based on strictly miscible or immiscible flow is insufficient. For these situations, the equations in Table 2-2 reduce to a simpler form consistent with the known complexities of the flow behavior. As an example of this, consider the isothermal flow of N_C components in up to N_P phases in the absence of chemical reaction. Such flows are characteristic of solvent (see Chap. 7) and micellar-polymer flooding (see Chap. 9) EOR applications.

We first assume that the change in pressure over the displacement length has negligible effect on phase behavior. Equation (2.2-6) may then be divided by the respective pure component density ρ_i^o to give

$$\frac{\partial}{\partial t} \left(\phi \sum_{j=1}^{N_p} C_{ij} S_j + (1-\phi) C_{is} \right) + \vec{\nabla} \cdot \left(\sum_{j=1}^{N_p} C_{ij} \vec{u}_j - \phi S_j \vec{K}_{ij} \cdot \vec{\nabla} C_{ij} \right) = 0 \\ i = 1, \dots, N_c \quad (2.5-14)$$

where, under the additional assumption of ideal mixing, $C_{ij} = \rho_j \omega_{ij} / \rho_i^o$ is the volume fraction of component i in phase j . Ideal mixing states that the volume of a mixture is equal to the sum of the pure component volumes weighted by the component mass fractions (Chap. 4).

We can sum Eq. (2.5-14) over the N_c components as for the development of Eq. (2.2-33), that is,

$$\frac{\partial}{\partial t} \left(\phi \sum_{i=1}^{N_c} \left(C_{ij} \sum_{j=1}^{N_p} S_j \right) + (1-\phi) \sum_{i=1}^{N_c} C_{is} \right) + \vec{\nabla} \cdot \left(\sum_{i=1}^{N_c} \left(C_{ij} \sum_{j=1}^{N_p} \vec{u}_j \right) \right) = 0, \\ i = 1, \dots, N_c, \quad (2.5-15)$$

where the dispersive flux term vanishes. The additional assumption of constant porosity in time leads to the result that

$$\vec{\nabla} \cdot \left(\sum_{j=1}^{N_p} \vec{u}_j \right) = \vec{\nabla} \cdot \vec{u} = 0, \quad (2.5-16)$$

where we have used Eq. (2.2-16), $\sum_{i=1}^{N_c} C_{ij} = 1$, and $\sum_{i=1}^{N_c} C_{is}$ is constant. For one-dimensional flow, Eq. (2.5-16) implies that the total flow rate is only a function of time. Thus, Eq. (2.5-16) can be used along with the definition of fractional flow (2.5-2) to write Eq. (2.5-14) in one-dimensional form.

$$\frac{\partial}{\partial t} \left(\phi \sum_{j=1}^{N_p} C_{ij} S_j + (1-\phi) C_{is} \right) + u \frac{\partial}{\partial x} \left(\sum_{j=1}^{N_p} C_{ij} f_j \right) - \frac{\partial}{\partial x} \left(\sum_{j=1}^{N_p} \phi S_j K_{ij} \frac{\partial C_{ij}}{\partial x} \right) = 0, \\ i = 1, \dots, N_c. \quad (2.5-17)$$

Even with the above assumptions, Eq. (2.5-17) is still fairly general and must be solved simultaneously with Darcy's law and with the definitions for relative mobility, capillary pressure, mass fractions, saturations, equations of state, and equilibria relations, [Eqs. (2.2-11), (2.2-16), (2.2-21), (2.2-22), and (2.2-23)]. This form is particularly convenient because many cases of binary and ternary phase equilibria are more conventionally represented as volume fractions rather than mass fractions (see Chap. 4).

We often define the overall component volume fraction to be $C_i = \sum_{j=1}^{N_p} C_{ij} S_j$ and the overall component fractional flow $F_i = \sum_{j=1}^{N_p} C_{ij} f_j$. With those definitions, constant porosity, and the assumption of dispersion-free flow with no sorption, Eq. (2.5-17) becomes

$$\phi \frac{\partial C_i}{\partial t} + u \frac{\partial F_i}{\partial x} = 0, \quad i = 1, \dots, N_c . \quad (2.5-18)$$

This equation is used in Chap. 7 to develop analytical solutions and basic insights for miscible flooding theory.

Richards Equation for Unsaturated Flow in Aquifers

The general equations developed here also apply to groundwater flow. As an example, consider the flow of water in the unsaturated (i.e. where both water and air exist) zone of aquifers. Aquifers are divided into two regions, an unsaturated region near the Earth's surface where both water and air are present and a saturated region near and below this where only the aqueous phase is present. The surface separating the two zones is near the water table. The water table is also known as the phreatic surface because water freely flows to this level in wells drilled through the aquifer.

We begin the development of the unsaturated flow equation by assuming no mass transfer $r_{mij} = 0$ in the phase conservation equations, Eqs. (2.2-31):

$$\frac{\partial}{\partial t} (\phi S_j \rho_j) + \vec{\nabla} \cdot (\rho_j \vec{u}_j) = 0 \quad j = 1, \dots, N_p , \quad (2.2-32)$$

where there are only two phases, an aqueous phase and an air phase. The two phases are immiscible; hence, phases and components are synonymous in this example. Because air near the Earth's surface is at low pressure, its density and viscosity are near zero and it provides little resistance to water flow (except through a physical restriction in the pore volume available for water flow). This is equivalent to assuming that the air phase is at atmospheric pressure everywhere in the aquifer. Thus, since only the aqueous phase flows, the solution to the air phase equation is trivial and can be dropped along with the subscripts for the aqueous phase.

$$\frac{\partial}{\partial t} (\phi S \rho) + \vec{\nabla} \cdot (\rho \vec{u}) = 0 . \quad (2.5-19)$$

The aqueous phase density is also assumed constant, a good assumption since the water pressure remains near atmospheric even under flowing conditions. Equation (2.5-19) becomes

$$\frac{\partial}{\partial t} (\phi S) + \vec{\nabla} \cdot \vec{u} = 0 . \quad (2.5-20)$$

Richards equation is often formally written in terms of the moisture content ($\theta = \phi S$), hydraulic head, and the hydraulic conductivity. The hydraulic head, which is often defined with reference to atmospheric pressure and surface elevation, is

$$h = \frac{P - P_{atm}}{\rho g} + z - z_{gs} . \quad (2.5-21)$$

The hydraulic conductivity tensor is defined as $\vec{K} = \bar{k} \rho g / \mu$. With those definitions and the use of Eq. (2.2-11), Eq. (2.5-20) gives Richards equation,

$$\frac{\partial \theta}{\partial t} - \vec{\nabla} \cdot \left(k_r \vec{K} \cdot \vec{\nabla} h \right) = 0 , \quad (2.5-22)$$

where $\vec{\nabla} h = \vec{\nabla} P / \rho g$ and k_r is the relative permeability of the aqueous phase, which is a function of the water saturation (moisture content). Note that although we dropped the air phase equation, the air phase does impact the flow of the aqueous phase through relative permeability.

Philips (1957) wrote Richards equation in a form commonly used by soil scientists. He split the hydraulic head into two parts: the suction head and elevation head where $\vec{\nabla} h = -\vec{\nabla} \psi + \vec{\nabla} z$ and $\psi = P_c / \rho g = -P / \rho g$. The capillary pressure is equal to the negative of the water pressure because the air pressure is assumed constant at atmospheric (taken as zero). The suction head is always positive because water is in tension above the phreatic surface, e.g. the aqueous phase pressure is less than atmospheric above the water table. The unsaturated flow equation used by Phillips as derived from Eq. (2.5-22) is then

$$\frac{\partial \theta}{\partial t} + \vec{\nabla} \cdot \left(k_r \vec{K} \cdot \vec{\nabla} \psi \right) = \vec{\nabla} \cdot \left(k_r \vec{K} \cdot \vec{\nabla} z \right) . \quad (2.5-23)$$

For Cartesian coordinates aligned in the principal flow directions, the term on the right side of Eq. (2.5-23) can be simplified to give

$$\frac{\partial \theta}{\partial t} + \vec{\nabla} \cdot \left(k_r \vec{K} \cdot \vec{\nabla} \psi \right) = \frac{\partial}{\partial z} (k_r K_{zz}) , \quad (2.5-24)$$

where K_{zz} is the component of the hydraulic conductivity in the z-direction. Finally, we can rewrite Eq. (2.5-24) in terms of the capillary diffusivity $\vec{D} = -\vec{K} \Psi'$, where Ψ' is the derivative of the suction head with respect to the moisture content.

$$\frac{\partial \theta}{\partial t} = \vec{\nabla} \cdot \left(k_r \vec{D} \cdot \vec{\nabla} \theta \right) + \frac{\partial}{\partial z} (k_r K_{zz}) . \quad (2.5-25)$$

The capillary diffusivity is positive and has units of length squared per time (hence its name). Phillips used Eq. (2.5-25) to develop semi-analytical solutions for rainfall infiltration.

Standard Black-Oil Equations

A common representation (Peaceman, 1977) of the flow of fluids in oil and gas reservoirs is the “black oil” equations wherein up to three phases, aqueous ($j = 1$), oleic ($j = 2$), and gaseous ($j = 3$), flow simultaneously. The aqueous and gaseous phases each consist of a single pseudocomponent, water ($i = 1$) and gas ($i = 3$), respectively. The oleic phase consists of two pseudocomponents, oil ($i = 2$) and a dissolved gas component. The components are *pseudocomponents* because each is really a group of true components whose composition remains constant.

The use of pseudocomponents is quite common in EOR descriptions, since this simplification often results in greater understanding of the processes and can significantly reduce the computational effort involved in numerical simulation with little loss of accuracy. Because of these advantages, the black-oil equations are used often to model many EOR processes, including those where the black-oil assumptions may not strictly apply. Black-oil equations, for example, may not accurately model miscible EOR processes or other processes that significantly deviate from the black-oil assumption of pseudocomponents having constant composition. In those cases, more rigorous fully compositional simulators are used, although they require significant computation time.

Figure 2-6 illustrates the black-oil assumptions. The model relates downhole reservoir volumes to standard temperature and pressure (STP) conditions. Definitions for STP vary slightly, but typical values are 14.7 psia and 60°F. Formation volume factors are defined that express the ratio between volumes at STP conditions and reservoir conditions as indicated by the dashed lines in Fig. 2-6. The solution gas-oil ratio is the volume of gas that evolves from a known volume of oil at STP conditions.

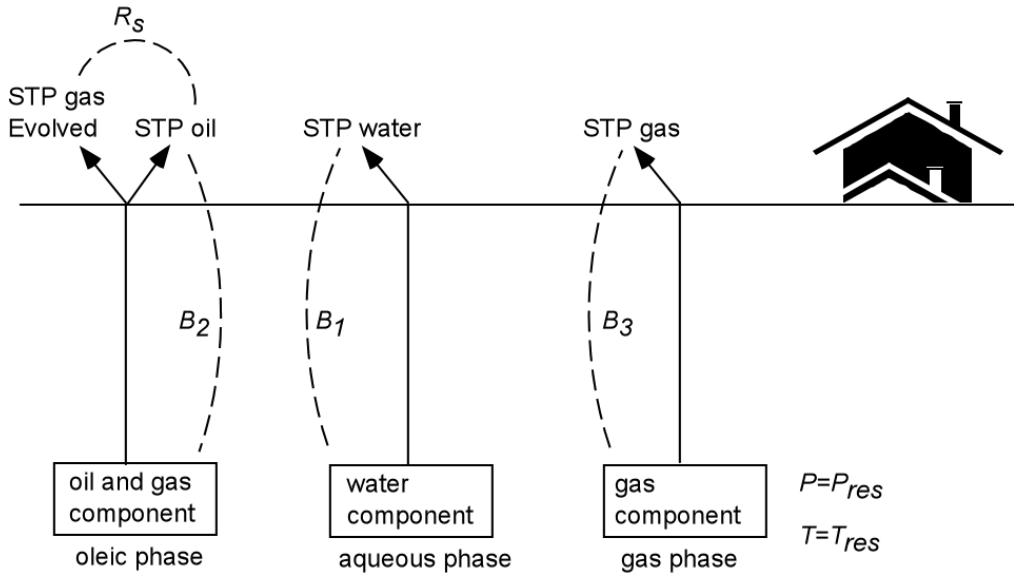


Figure 2-7: Illustration of standard black-oil assumptions. STP is standard temperature and pressure.

The black-oil equations are compositional equations in that they are developed from the overall compositional equations, Eq. (2.2-6). We invoke the following additional assumptions: no reaction ($R_i = 0$), no dispersion ($\bar{K}_{ij} = 0$), and no adsorption ($\omega_{is} = 0$). The black oil assumption itself becomes the following: the aqueous phases contains only water ($\omega_{11} = 1$, $\omega_{21} = 0$, $\omega_{31} = 0$), the oleic phase contains only oil and gas ($\omega_{12} = 0$, $\omega_{22} > 0$, $\omega_{32} > 0$), and the gas phase contains only the gas component ($\omega_{13} = 0$, $\omega_{23} = 0$, $\omega_{33} = 1$). For component 1 (the water component), Eq. (2.2-6) becomes

$$\frac{\partial}{\partial t}(\phi\rho_1 S_1) + \vec{\nabla} \cdot (\rho_1 \vec{u}_1) = 0 . \quad (2.5-26)$$

For component 2 (the oil component), Eq. (2.2-6) gives

$$\frac{\partial}{\partial t}(\phi\rho_2 S_2 \omega_{22}) + \vec{\nabla} \cdot (\rho_2 \omega_{22} \vec{u}_2) = 0 . \quad (2.5-27)$$

For component 3 (the gas component), Eq. (2.2-6) gives

$$\frac{\partial}{\partial t}(\phi[\rho_2 S_2 \omega_{32} + \rho_3 S_3]) + \vec{\nabla} \cdot (\rho_2 \omega_{32} \vec{u}_2 + \rho_3 \vec{u}_3) = 0 . \quad (2.5-28)$$

We now want to eliminate the mass fractions and rewrite Eqs. (2.5-26) to (2.5-28) in favor of formation volume factors and the solution gas-oil ratio. B_1 is the water formation volume factor (volume of a given mass of water at the prevailing temperature and pressure divided by the volume of the same mass of water at standard temperature and pressure).

$$B_1 = \frac{\rho_1^s}{\rho_1} .$$

B_2 is the oil formation volume factor (volume of a given mass of oil at prevailing temperature and pressure divided by the volume of the same mass of oil at standard conditions).

$$B_2 = \frac{\rho_2^s}{\omega_{22}\rho_2} .$$

B_3 is the gas formation volume factor (volume of a given mass of gas at prevailing temperature and pressure divided by the volume of the same mass at standard temperature and pressure).

$$B_3 = \frac{\rho_3^s}{\rho_3} .$$

R_s is the solution gas–oil ratio (volume of dissolved gas divided by volume of oil phase, with both volumes evaluated at standard temperature and pressure).

$$R_s = \frac{\omega_{32}\rho_2^s}{\omega_{22}\rho_3^s} .$$

The above definitions may be introduced into the mass balances of Table 2-2 by dividing each by their respective standard densities ρ_j^s and recognizing that each ρ_j^s is time and space independent. Equations (2.5-26) to (2.5-28) become

$$\frac{\partial}{\partial t} \left(\frac{\phi S_j}{B_j} \right) + \vec{\nabla} \cdot \left(\frac{\vec{u}_j}{B_j} \right) = 0, \quad j = 1, 2$$

and, for gas,

$$\frac{\partial}{\partial t} \left(\phi \left[\frac{S_3}{B_3} + \frac{S_2 R_s}{B_2} \right] \right) + \vec{\nabla} \cdot \left(\frac{R_s}{B_2} \vec{u}_2 + \frac{\vec{u}_3}{B_3} \right) = 0 .$$

Modified black-oil models, where CO₂ is added as a fourth component, are sometimes used to account for oil displacement by carbon dioxide or other miscible gases (Todd and Longstaff, 1972).

Steam Flooding Equations

As a special case of nonisothermal flow, we derive the “steam” equations given by Stegemeier *et al.* (1977). We assume at most $N_P = 3$ phases—an aqueous phase $j = 1$, a hydrocarbon phase $j = 2$, and a gas phase $j = 3$ —are present. Further, at most two unreactive, nonsorbing pseudocomponents—water and oil—are present. We restrict the hydrocarbon phase to contain only oil, and the aqueous and gaseous phases to contain only water, assumptions that eliminate volatile hydrocarbons from the equations. With these assumptions, the mass conservation equations, Eqs. (2.2-6), become, for water,

$$\frac{\partial}{\partial t} [\phi(\rho_1 S_1 + \rho_3 S_3)] + \vec{\nabla} \cdot (\rho_1 \vec{u}_1 + \rho_3 \vec{u}_3) = 0 \quad (2.5-29)$$

and, for oil,

$$\frac{\partial}{\partial t} (\phi \rho_2 S_2) + \vec{\nabla} \cdot (\rho_2 \vec{u}_2) = 0 . \quad (2.5-30)$$

The dispersion terms are absent from these equations since the phase compositions are constant. The conservation of energy Eq. (2.3-11) becomes

$$\begin{aligned} \frac{\partial}{\partial t} [\phi(\rho_1 S_1 U_1 + \rho_2 S_2 U_2 + \rho_3 S_3 U_3) + (1-\phi)\rho_s U_s] \\ + \vec{\nabla} \cdot (\rho_1 H_1 \vec{u}_1 + \rho_2 H_2 \vec{u}_2 + \rho_3 H_3 \vec{u}_3) - \vec{\nabla} \cdot (k_{T_t} \nabla T) = 0 , \end{aligned} \quad (2.5-31)$$

where kinetic and potential energy terms have been neglected. We further neglect pressure-volume work by letting the enthalpies equal internal energies and by taking porosity to be constant. The derivatives in Eq. (2.5-31) may then be expanded to give

$$\begin{aligned} (1-\phi) \frac{\partial(\rho_s H_s)}{\partial t} + \phi \rho_1 S_1 \frac{\partial H_1}{\partial t} + \phi \rho_2 S_2 \frac{\partial H_2}{\partial t} + \phi \rho_3 S_3 \frac{\partial H_3}{\partial t} + \phi(H_3 - H_1) \frac{\partial(\rho_3 S_3)}{\partial t} \\ + \rho_1 \vec{u}_1 \cdot \vec{\nabla} H_1 + \rho_2 \vec{u}_2 \cdot \vec{\nabla} H_2 + (H_3 - H_1) \vec{\nabla} \cdot (\rho_3 \vec{u}_3) + \rho_3 \vec{u}_3 \cdot \vec{\nabla} H_3 - \vec{\nabla} \cdot (k_{T_t} \vec{\nabla} T) = 0 , \end{aligned} \quad (2.5-32)$$

where Eqs. (2.5-29) and (2.5-30) have been used to eliminate several terms. The term $(H_3 - H_1)$ equals L_V , the latent heat of vaporization of water, and we assume enthalpies are independent of pressure $dH_j = C_{pj}dT$, where C_{pj} is the specific heat of phase j . If the C_{pj} are constant, Eq. (2.5-32) becomes

$$M_{T_t} \frac{\partial T}{\partial t} + (\rho_1 C_{p1} \vec{u}_1 + \rho_2 C_{p2} \vec{u}_2) \cdot \vec{\nabla} T - \vec{\nabla} \cdot (k_{T_t} \vec{\nabla} T)$$

$$= -L_V \left\{ \phi \frac{\partial(\rho_3 S_3)}{\partial t} + \vec{\nabla} \cdot (\rho_3 S_3 \vec{u}_3) \right\}, \quad (2.5-33)$$

where M_{T_l} is the overall volumetric heat capacity

$$M_{T_l} = \phi(\rho_1 C_{p1} S_1 + \rho_2 S_2 C_{p2}) + (1-\phi)\rho_s C_{ps}. \quad (2.5-34)$$

In this definition and in Eq. (2.5-33), the terms involving the gaseous phase density ρ_3 have been neglected since gas densities are usually much smaller than liquid densities. The term on the right side of Eq. (2.5-33) represents the production or destruction of the steam phase times the latent heat; it serves as a source term for the energy equation. If steam disappears (condenses), the source term is positive, which causes the temperature to rise. This results in a decrease in oil viscosity, the primary recovery mechanism in thermal flooding (see Chap. 11). The latent heat, phase pressures, and temperature are related through the vapor pressure curve for water and capillary pressure relations.

2-6 OVERALL BALANCES

A common and useful way to apply the equations in the previous sections is in the form of macroscopic or overall balances (Bird *et al.*, 1960). Rather than balances written for each point within the permeable medium, overall balances are spatially integrated forms of the differential balances that thereby apply to finite volumes within a reservoir, such as a cell in numerical simulation, or even, as is the case here, the entire reservoir. Since the spatial component is absent from the equations, overall balances are much simpler and far easier to integrate than differential balances. This simplification is achieved at the expense of losing spatial detail of the concentration variables; therefore, to be useful, overall balances must be supplemented with independently derived or analytical correlations.

Material Balance

To derive the overall mass balance for component i , begin with the weak form written on volume V in the compositional form of Eq.(2.2-4). The result is

$$\int_V \frac{\partial W_i}{\partial t} dV + \int_A \vec{n} \cdot \vec{N}_i dA = \int_V R_i dV, \quad i = 1, \dots, N_c. \quad (2.6-1)$$

We then identify V with the total bulk volume V_b exclusive of the small volumes associated with a finite number of sources and sinks embedded within. The boundary of V_b may also be a fluid source or sink term, as would be the case of an oil column abutting an aquifer or a free gas cap. If we assume the fluxes across the boundaries of V are normal to the cross-sectional area, Eq. (2.6-1) becomes

$$V_b \frac{d\bar{W}_i}{dt} + \dot{N}_{pi} - \dot{N}_{ji} = V_b \bar{R}_i, \quad i = 1, \dots, N_C, \quad (2.6-2)$$

where the superscript bar denotes volume-averaged quantities. The terms \dot{N}_{pi} and \dot{N}_{ji} are the mass production and injection rates of component i for all the source and sink terms in V_b . These are functions of time, since they are evaluated at fixed positions on V_b . \bar{R}_i is the volume-averaged reaction rate term of component i and is also a function of time. We integrate Eq. (2.6-2) with respect to time to arrive at a cumulative form of material balance

$$V_b (\bar{W}_i - \bar{W}_{il}) = N_{ji} - N_{pi} + V_b \int_0^t \bar{R}_i dt, \quad i = 1, \dots, N_C. \quad (2.6-3)$$

In writing Eq. (2.6-3), we have assumed the cumulative injection and production of component i at $t = 0$ is zero. In what follows, we ignore the cumulative reaction rate term.

The most common application of Eq. (2.6-3) is to calculate N_{pi} with W_i , \bar{W}_{il} , and N_{ji} specified. In particular, $\bar{W}_i(t)$ is difficult to evaluate without actually integrating the differential balances. This difficulty is circumvented by defining E_{ri} , the recovery efficiency of component i , as

$$E_{ri} \equiv \frac{N_{pi} - N_{ji}}{V_b \bar{W}_{il}}. \quad (2.6-4)$$

E_{ri} is the net amount of component i produced expressed as a fraction of the amount of component initially present. For a component injected into the reservoir, E_{ri} is negative, but for a component to be recovered, oil or gas (to which it is almost exclusively applied), E_{ri} is positive and lies between 0 and 1. From Eq. (2.6-3), \bar{W}_i is

$$\bar{W}_i = \bar{W}_{il} (1 - E_{ri}). \quad (2.6-5)$$

For either Eqs. (2.6-4) or (2.6-5) to be useful, E_{ri} must be expressed independently as a function of time. This is commonly done by decomposing E_{ri} into the displacement efficiency E_{di} and volumetric sweep efficiency E_{vi} of component i

$$E_{ri} = E_{di} E_{vi} \quad (2.6-6)$$

where

$$E_{di} = \frac{\text{Amount of } i \text{ displaced}}{\text{Amount of } i \text{ contacted}} \quad (2.6-7)$$

$$E_{vi} = \frac{\text{Amount of } i \text{ displaced}}{\text{Amount of } i \text{ in place}} \quad (2.6-8)$$

These quantities in turn must be specified independently: E_{Di} as a function of time and fluid viscosities, relative permeabilities, and capillary pressures (see Chap. 5) and E_{Vi} as a function of time, viscosities, well arrangements, heterogeneity, gravity, and capillary forces (see Chap. 6).

Energy Balance

A similar procedure applied to the energy conservation Eq. (2.3-11) yields

$$V_b \frac{d}{dt}(\overline{\rho U}) + \dot{H}_p - \dot{H}_J = - \int_A \vec{q}_c \cdot \vec{n} dA = -\dot{Q} \quad (2.6-9)$$

where kinetic and potential energy terms have been neglected and \dot{H}_p and \dot{H}_J represent the rates of enthalpy production and injection into and from V . \dot{Q} is positive when heat is lost from the reservoir. This equation, of course, is a version of the first law of thermodynamics that, depending on the selection of V , will be useful in calculating heat losses to wellbores (with the potential energy term restored) and the overburden and underburden of a reservoir (see Chap. 11).

The time integrated or cumulative form of Eq. (2.6-9) is

$$V_b((\overline{\rho U}) - (\overline{\rho U})_I) = H_J - H_p - Q \quad (2.6-10)$$

from which we may define a thermal efficiency \bar{E}_{hs} as the ratio of thermal energy remaining in the volume V_b to the net thermal energy injected.

$$\bar{E}_{hs} = \frac{V_b((\overline{\rho U}) - (\overline{\rho U})_I)}{H_J - H_p} = 1 - \frac{Q}{H_J - H_p} \quad (2.6-11)$$

Equation (2.6-11) is used to independently calculate Q .

Another more familiar form of the overall energy balance pertains to phase equilibrium thermodynamics (see Chap. 4). For brevity, we again neglect potential and kinetic energies, but allow for both pressure-volume and compression-expansion work (see exercise 2Q). The mass that enters volume V flows at a relative flow rate of \vec{u}_{fi} , which is the difference between the actual flow rate and the rate of deformation of V . Further, we rewrite the accumulation term to account for a deforming V using the weak form. The result is

$$\frac{d}{dt} \int_V (\rho U) dV = - \int_A \vec{n} \cdot \sum_{j=1}^{N_p} \rho_j \vec{u}_{fi} H_j dA - \int_A \vec{n} \cdot \vec{q}_c dA - \sum_{j=1}^{N_p} P_j \frac{dV_j}{dt} \quad (2.6-12)$$

From left to right, the terms are the accumulation, energy flux owing to mass inflow, energy flux owing to conduction, and compression-expansion work. The first three terms in Eq. (2.6-12) must now be evaluated. The accumulation term is

$$\frac{d}{dt} \int_V (\rho U) dV = \frac{\partial U}{\partial t} ,$$

where U is the total energy within volume V . The energy flux term is evaluated with the assumption that the enthalpy of the flowing mass for any phase is constant over the entrance or exit for mass flow. The result is

$$-\int_A \vec{n} \cdot \sum_{j=1}^{N_p} \rho_j \vec{u}_{fj} H_j dA = -\sum_{j=1}^{N_p} H_j \int_A \vec{n} \cdot (\rho_j \vec{u}_{fj}) dA = \sum_{j=1}^{N_p} H_j \dot{m}_j$$

where \dot{m}_j is the total net mass inflow of phase j into the system. The sign is positive to allow for the convention that mass flow rate is positive into the system. Finally, the conduction term is,

$$-\int_A \vec{n} \cdot \vec{q}_c dA = \dot{Q} .$$

With these additional assumptions, Eq. (2.6-12) reduces to

$$\frac{dU}{dt} = \sum_{j=1}^{N_p} H_j \dot{m}_j + \dot{Q} - \sum_{j=1}^{N_p} P_j \frac{dV_j}{dt} . \quad (2.6-13)$$

When only one phase exists, Eq. (2.6-13) reduces to a more familiar form of the first law of thermodynamics,

$$\frac{dU}{dt} = H\dot{m} + \dot{Q} - P \frac{dV}{dt} . \quad (2.6-14)$$

The pressure at the boundary of the system in Eq. (2.6-14) is equal to the pressure in the system when pressure gradients are negligible within the system. Along with the entropy balance discussed next, this equation will be used in Chap. 4 to determine the equilibrium conditions for phase behavior calculations.

Entropy Balance

To derive the overall entropy balance, we start by rewriting Eq. (2.4-5) as

$$\frac{d}{dt} \int_V \sum_{j=1}^{N_p} (\varepsilon_j \rho_j S_j) dV = -\int_A \vec{n} \cdot \sum_{j=1}^{N_p} \rho_j \vec{u}_j S_j dA - \int_A \vec{n} \cdot \frac{\vec{q}_c}{T} dA + \int_V \dot{\sigma}_G dV . \quad (2.6-15)$$

Following the same procedure as for the overall energy balance,

$$\frac{dS}{dt} = \sum_{j=1}^{N_p} S_j \dot{m}_j + \frac{\dot{Q}}{T} + \dot{S}_G , \quad (2.6-16)$$

where we have assumed that both temperature and phase entropies along the system boundary are independent of position. The term \dot{S}_G is now the total entropy generated within the system, that is, $\dot{S}_G = \int_V \dot{\sigma}_G dV$.

When only one phase exists, Eq. (2.6-16) reduces to,

$$\frac{dS}{dt} = S\dot{m} + \frac{\dot{Q}}{T} + \dot{S}_G . \quad (2.6-17)$$

This equation will be used in Chap. 4 to determine the equilibrium conditions for phase behavior calculations. As before, the Second Law of thermodynamics is $\dot{S}_G \geq 0$, the equality applying at equilibrium.

2-7 SUMMARY

We will use the equations introduced and developed in this chapter in the remainder of the text. Introducing all of the equations here eliminates repetitive derivation in later chapters. The compilation also emphasizes one of the main points of this text: the behaviors of all EOR and remediation processes are described by specializations of the same underlying conservation laws. Solving these specializations and deducing physical observations from the solutions will occupy much of the remainder of this text. You should keep in mind that all of the relationships discussed above and hence forth are ways of quantifying the chemical, physical and geologic bases of EOR.

EXERCISES

- 2A. Overall Compositional Equations.** A simplified form of the conservation equation can be obtained by summing Eq. (2.1-1) over all phases. The result is the mass conservation equation for component i in volume V :

$$\left\{ \begin{array}{l} \text{Rate of} \\ \text{accumulation} \\ \text{of } i \text{ in } V \end{array} \right\} = \left\{ \begin{array}{l} \text{Net rate of } i \\ \text{transported} \\ \text{into } V \end{array} \right\} + \left\{ \begin{array}{l} \text{Rate of} \\ \text{production} \\ \text{of } i \text{ in } V \end{array} \right\}, \quad i = 1, \dots, N_c .$$

Show starting with the above expression that the differential form for the component conservation equation is

$$\frac{\partial W_i}{\partial t} + \vec{\nabla} \cdot \vec{N}_i - R_i = 0, \quad i = 1, \dots, N_c$$

where W_i is the overall concentration of each component, \vec{N}_i is the overall flux of each component, and R_i is the overall production of each component. Indicate all units in the derivation.

- 2B.** **Volatile Oil Equations.** The text derived the "black oil" equations wherein the oleic and gaseous phases are immiscible and constant composition except for the solubility of a hydrocarbon gas in the oleic phase. The next step up in complexity is the "volatile oil" equations that allow for the vaporization of the oil into the gaseous phase (Walsh and Lake, 2003).

Derive the volatile oil equations in terms of the oil vaporization ratio R_v where

$$R_v = \frac{S \tan dard volumes of oil in gaseous phase}{S \tan dard volumes of gas}$$

State all assumptions and show all work.

- 2C.** **Hydrostatics.** Show that for static ($\vec{u}_j = 0$) conditions, Eq. (2.2-11) reduces to

$$\frac{dP_c}{dD_z} = (\rho_1 - \rho_2)g$$

for two-phase flow where P_c is the oil–water capillary pressure curve.

- 2D.** **Net Dispersion in a Phase.** Show that in a given phase $\sum_{i=1}^{N_c} \nabla \cdot \vec{j}_{Dij} = 0$ when dispersive flux is defined with respect to mass-averaged velocity. Use the relations given for the average-component velocity owing to convective and dispersive transport.
- 2E.** **Single-Phase Flow.** Show that for the flow of a single phase ($j = 2$) in the presence of an immiscible, immobile phase ($j = 1$) the isothermal mass balance equations in one-dimensional radial coordinates reduce to

$$\frac{\phi c_t}{\lambda_{r2} k} \frac{\partial P}{\partial t} - \frac{1}{r} \frac{\partial}{\partial r} \left(r \frac{\partial P}{\partial r} \right) = 0,$$

where

$$c_t = S_1 c_1 + S_2 c_2 + c_f$$

$$c_j = \frac{1}{\rho_j} \left(\frac{\partial \rho_j}{\partial P} \right)_T$$

$$c_f = \frac{1}{\phi} \left(\frac{\partial \phi}{\partial P} \right)_T$$

The above equation, the “diffusivity” equation, has been derived assuming that terms of the form $c_2(\partial P/\partial r)^2$ are negligible and the reservoir is homogeneous with constant thickness. The diffusivity equation forms the basis for a large variety of well test techniques (Earlougher, 1977).

- 2F.** *Confined Flow of Water in an Aquifer.* Show that the final result for problem 2E can be rewritten for fully saturated soil as

$$\frac{1}{r} \frac{\partial}{\partial r} \left(r \frac{\partial h}{\partial r} \right) = \frac{1}{\eta} \frac{\partial h}{\partial t},$$

where

$$c_t = c_1 + c_f$$

$$\eta = \frac{K}{S_s} = \frac{T}{S}$$

$$K = \frac{k \rho g}{\mu}$$

$$S_s = \phi c_t \rho g$$

The parameter S_s is the specific storage coefficient for the aquifer in units of inverse length. The dimensionless storage coefficient of the aquifer is equal to $T = S_s b$ where b is the thickness of the confined aquifer. A confined aquifer is an aquifer fully saturated with water that cannot escape at the top and bottom. The storage coefficient is defined as the volume of water stored (or released) per unit area of aquifer per unit increase (or decrease) in the hydraulic head h . The aquifer transmissivity is $T = Kb$. Finally, the parameter η is known as the diffusivity constant.

- 2G.** *Unconfined Flow in an Aquifer.* An unconfined aquifer is an unsaturated aquifer that contains both air and water. The water table (phreatic surface where capillary pressure is zero) can rise and fall as water is pumped from the aquifer. A common assumption to model the rising or falling water table is to assume that the hydraulic head is constant vertically and is a function only of the horizontal coordinates (this is a vertical equilibrium assumption as is discussed in Chap. 6). Show that under this assumption, the equation for flow in a 2-D unconfined homogeneous aquifer is

$$\frac{\partial}{\partial x} \left(h \frac{\partial h}{\partial x} \right) = \frac{S_y}{K} \frac{\partial h}{\partial t},$$

where

$$K = \frac{k \rho g}{\mu}$$

$$S_y = \phi(1 - S_{lr})$$

The parameter S_y is the specific yield of the aquifer, defined as the volume of water added (or lost) due to a unit increase (or decrease) in the water table height per unit horizontal area of aquifer. It is dimensionless. The residual water S_{lr} is assumed constant whether the water table is rising or falling. The water saturation above the water table is assumed constant at S_{lr} .

To derive the unconfined flow equation start with the equation for a confined aquifer given in 2F but expressed in x - and z -coordinates and integrate it vertically from the base of the aquifer to the water table. Use the Liebnitz's rule to evaluate integral expressions that result. Last, let the water table surface be given by $F(x, z, t) = z - a(x, t) = 0$, where $a(x, t)$ is the elevation of the water table as measured from the assumed horizontal base of the aquifer. The unit total derivative of $F(x, z, t)$ must be zero, which allows one to relate the movement of the water table in the horizontal and vertical directions to the time rate of change of the water table. State all assumptions clearly.

- 2H.** ***Convection-Dispersion Equation with Retardation.*** Show that when dispersion is constant, the one dimensional convection-dispersion equation with adsorption becomes

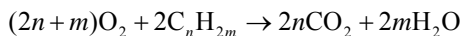
$$\phi \frac{\partial C_i}{\partial t} + \frac{u}{1+D_i} \frac{\partial C_i}{\partial x} - \frac{\phi K_l}{1+D_i} \frac{\partial^2 C_i}{\partial x^2} = 0, \quad i = 1, \dots, N_c,$$

where the delay factor $D_i = (1-\phi)C_{is}/\phi C_i$ is constant temporally and K_l is the longitudinal dispersion coefficient. State all assumptions required to obtain this equation. How does adsorption affect the transport of a component?

- 2I.** ***Simplified Combustion Model.*** Based on two-phase ($j = 2$ = liquid, $j = 3$ = gas), four-component ($i = 1$ = water, $i = 2$ = oil [C_nH_{2m}], $i = 3$ = CO_2 , $i = 4$ = O_2), one-dimensional flow show that the energy conservation equations in Table 2-3 reduce to

$$M_{T_l} \frac{\partial T}{\partial t} + (\rho_2 C_{p2} u_2 + \rho_3 C_{p3} u_3) \frac{\partial T}{\partial x} - \frac{\partial T}{\partial x} \left(k_{T_l} \frac{\partial T}{\partial x} \right) = \phi S_3 \Delta H_{RXN}$$

where ΔH_{RXN} is the heat of reaction for the gaseous phase reaction



$$\Delta H_{RXN} = -\sum_{i=1}^4 H_{io} r_{i3}$$

Further assumptions for the above equation are there is only oil present in liquid phase, no sorption or dispersion, ideal solution behavior (specific heat of gaseous phase is the mass fraction – weighted sum of the component specific heats), no heat of vaporization of oil ($H_{22} = H_{23}$), enthalpies and internal energies are equal, kinetic and potential energies are negligible, and solid phase density and porosity are constant.

- 2J.** **Total Velocity.** Show that for immiscible flow, constant porosity, and incompressible flow

$$\vec{\nabla} \cdot \vec{u} = 0$$

and that for one-dimensional flow the total velocity is a function only of time.

- 2K.** **Continuity Equation.** Derive Eq. (2.2-33) from the phase conservation equations, Eq. (2.2-31).

- 2L.** **Volume Change on Mixing.** The development of the semimiscible equations assumed no volume change on mixing to obtain volume fractions. When volume changes upon mixing, the total velocity can change spatially and temporally and the use of volume fractions is not needed. Relax the no-volume-change assumption and rederive the equations in a form similar to Eq. (2.5-18). You may neglect dispersion.

- 2M.** **Formation Volume Factor.** Show that in a black oil model equation that the oil formation volume factor can also be written as

$$B_2 = \frac{\rho_2^s + R_s \rho_3^2}{\rho_2}$$

- 2N.** **Oil Recovery by NH_3 Injection.** An inventor believes that he has discovered a new enhanced oil recovery technique that you are to simulate. The process involves the injection of anhydrous (water-free) ammonia (NH_3), which is to dissolve in and vaporize some of the connate water. This mass transfer is highly non-ideal in that there is a substantial heat of mixing. The heat released by this mixing will raise the temperature of the crude and cause it to flow more readily, just as in a thermal process.

There might also be some benefit from a pH increase, but the main objective is to increase temperature. To this end, the inventor has commissioned a commercial laboratory to do some displacements in a laboratory core. The

initial condition of the core is uniform temperature T_0 and 100% water saturation. The injected ammonia is pure and at the same temperature T_0 .

Beginning with the general equations, develop a set of working equations that will describe the experiment. There will several equations but these should be as simple as possible without omitting the important features discussed above. You should state all assumptions you made and ensure that the number of equations and unknowns are equal.

- 2O.** **Work Done by Gravity.** The derivation of Eq. (2.3-11) included potential energy directly. This need not be the case if gravity work on a fluid element in V is included in the source term by the work sum $\dot{W} = \dot{W}_{PV} + \dot{W}_G$. To account for the gravity work, take a scalar product of a velocity and the gravity vector \vec{g} ,

$$\Delta\dot{W}_G = \sum_{j=1}^{N_p} \rho_j \vec{u}_j \cdot \vec{g} \Delta V .$$

The positive sign arises in this equation since a fluid phase flowing against gravity ($\vec{u}_j \cdot \vec{g} < 0$) is having work done on it. Note the distinction between the elemental forms in Eqs. (2.3-5) and the equation above. Equation (2.3-5) is appropriate for work done against forces on the surface of V , whereas the above equation is appropriate for work done against body forces.

Show that the potential energy terms in Eq. (2.3-11) can be derived by inclusion as a work term, where the total work done by gravity in the volume V is

$$\dot{W}_G = \int_V \sum_{j=1}^{N_p} \rho_j \vec{u}_j \cdot \vec{g} dV .$$

Hint: You must use Eq. (2.2-33) and the identity

$$\sum_{j=1}^{N_p} \rho_j \vec{u}_j \cdot \vec{g} = -g \sum_{j=1}^{N_p} \vec{\nabla} \cdot (\rho_j \vec{u}_j D_z) + g \sum_{j=1}^{N_p} D_z \vec{\nabla} \cdot (\rho_j \vec{u}_j) .$$

- 2P.** **First Law of Thermodynamics.** Derive Eq. (2.6-12) for the first law of thermodynamics that includes both compression-expansion and pressure-volume work. Show that the equation reduces to Eq. (2.3-11) when the system is stationary. Also, derive the energy equation when the system deforms at the same rate as the phase velocities. Neglect kinetic and potential energies in your derivations.

- 2Q. ***Thermal Diffusivity Equation.*** From Eq. (2.5-33), state the necessary assumptions required to obtain the thermal diffusivity equation,

$$\vec{\nabla}^2 T = \frac{M_{Tr}}{k_{Tr}} \frac{\partial T}{\partial t} ,$$

where

$$M_{Tr} = \phi \rho_l C_{pl} S_l + (1 - \phi) \rho_s C_{ps} .$$

4

Phase Behavior and Fluid Properties

The phase behavior of crude oil, water, and enhanced oil recovery fluids is a common basis of understanding the displacement mechanisms of EOR processes. Such behavior includes the two- and three-phase behavior of surfactant–brine–oil systems, the two or more phases formed in crude-oil–miscible-solvent systems, and the steam–oil–brine phases of thermal flooding. This chapter is not an exhaustive exposition of phase behavior. We concentrate on the aspects of phase behavior most pertinent to EOR. (For more complete treatments of phase behavior, see Francis, 1963; Sage and Lacey, 1939; and Standing, 1977.)

4-1 PHASE BEHAVIOR OF PURE COMPONENTS

In this section, we discuss the phase behavior of pure components in terms of pressure–temperature (P-T) and pressure–molar-volume diagrams.

Definitions

A *system* is a specified amount of material to be studied. In other chapters, the word *system* refers to the permeable medium, including the fluid with the pore space. In this chapter, the word refers only to the fluids. With this definition, a system can be described by one or more *properties*, any of several attributes of the system that can be measured. This definition implies a quantitative nature to physical properties—that is, they can be assigned a numerical value.

Properties are of two types: *extensive properties*, those dependent on the amount of mass in the system (the mass itself, volume, enthalpy, internal energy, and so on) and *intensive properties*, those independent of the amount of mass (temperature, pressure, density, specific volume, specific enthalpy, phase composition, and so on). Many times we designate intensive quantity by the modifier *specific* (quality per unit mass) or by molar (quantity per unit mole). Thermodynamic laws and physical properties are usually expressed in terms of intensive properties. The most important intensive properties in this chapter are

$$\begin{aligned}\rho &= \text{the density, mass per volume (or g/cm}^3 \text{ in practical SI)} \\ \bar{V} &= \text{the specific volume, volume per mass (or the reciprocal of } \rho \text{)} \\ \bar{V}_M &= \text{the specific molar volume, volume per amount (or m}^3/\text{kg-mole in SI)} \\ \rho_M &= \text{the molar density, moles per volume (or the reciprocal of } \bar{V}_M \text{)}\end{aligned}$$

Often the standard density of a fluid is given as the specific gravity, where

$$\gamma = \begin{cases} \frac{\rho}{\rho_{\text{water}}} & \text{for liquids} \\ \frac{\rho}{\rho_{\text{air}}} & \text{for gases} \end{cases} \quad (4.1-1)$$

All densities in Eq. (4.1-1) are evaluated at standard conditions of 273 K and approximately 0.1 MPa. The petroleum literature uses other standards (60°F and 14.7 psia).

In all discussions of phase behavior, it is important to understand the difference between a component and a phase. A *phase* is a homogeneous region of matter. Homogeneous means it is possible to move from any point in the region to any other without detecting a discontinuous change in a property. Such a change occurs when the point crosses an *interface*, and thereby the system consists of more than one phase. The three basic types of phases are gas, liquid, and solid, but of the last two, there can be more than one type.

A *component* is any identifiable chemical entity. This definition is broad enough to distinguish among all types of chemical isomers or even among chemical species that are different only by the substitution of a radioactively tagged element. Examples are H₂O, CH₄, C₄H₁₀, Na⁺, Ca²⁺, and CO₃²⁻. Natural systems contain many components, and we are commonly forced to combine several components into *pseudocomponents* to facilitate phase behavior representation and subsequent calculations.

The relationship among the number of components N_C , number of phases N_P , number of chemical reactions N_R , and “degrees of freedom” N_F of the system is given by the Gibbs phase rule:

$$N_F = N_C - N_P + 2 - N_R \quad (4.1-2)$$

In many textbooks, the number of components is defined to be $N_C - N_R$, the total number of chemical species minus the chemical reactions involving them, or the number of independent species. The resulting N_F is the same. The +2 in Eq. (4.1-2) accounts for the intensive properties temperature and pressure. If one or both of these properties is specified, the equation must be reduced accordingly.

The meaning of N_C and N_P in Eq. (4.1-2) is clear enough, but N_F invariably requires some amplification. The degrees of freedom in the phase rule is the number of independent *intensive* thermodynamic variables that must be fixed to specify the thermodynamic state of all properties of the system. Intensive thermodynamic variables include phase compositions (ω_{ij} in Chap. 2) as opposed to overall compositions or volume fractions (W_i and S_j in Chap. 2), which are not thermodynamic properties. The phase rule does not itself specify the values of the N_F variables, nor does it identify the variables; it merely gives the number required.

Intuitively, we expect a relationship among the three intensive properties, temperature, pressure, and molar volume, for a pure component. Using density, molar density, or specific volume in place of the molar volume would mean no loss of generality. However, in two dimensions it is difficult to completely represent this relationship, but we can easily plot any two of these variables.

Pressure–Temperature Diagrams

Figure 4-1 shows a schematic P-T plot for a pure component. The lines on the diagram represent temperatures and pressures where phase transitions occur. These lines or phase boundaries separate the diagram into regions in which the system is

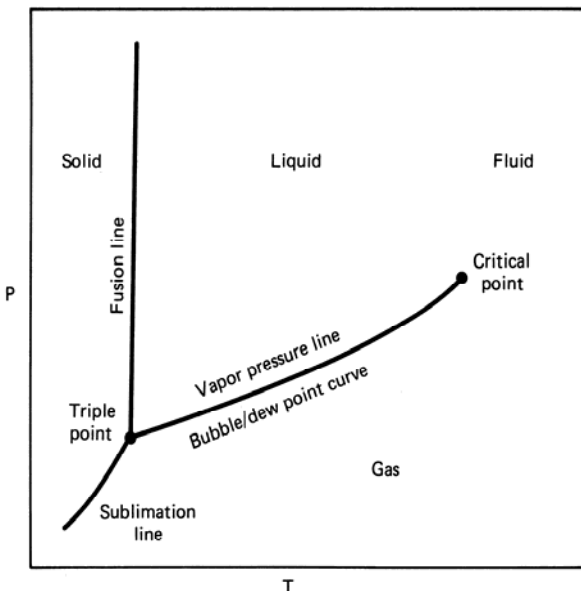


Figure 4-1 Pure component PT diagram (constant composition)

single phase. Specifically, the phase boundary separating the solid and liquid phases is the *fusion*, or melting, curve, that between the solid and gas phases is the *sublimation* curve, and that between the liquid and vapor phases is the *vapor pressure* curve. Based on our definition of a phase, a discontinuous change in system properties will occur when any phase boundary is crossed.

The phase transitions we refer to in this chapter are those of fluids in thermodynamic equilibrium. Thus it is possible for a fluid in a particular phase to momentarily exist at a P-T coordinate corresponding to another phase. But this condition is not permanent since the material would eventually convert to the appropriate stable equilibrium state.

From the phase rule we know that when two phases coexist, N_F equals 1. This can happen for a pure component only on the phase boundaries since a curve has one degree of freedom. By the same argument, three phases can coexist at only a single point in P-T space since $N_F = 0$ for this condition. This single point is a *triple point*, shown in Fig. 4-1 as the point where the three phase boundaries intersect. Other triple points such as three solids may also exist. For pure components, the phase rule says no more than three phases can form at any temperature and pressure.

Each phase boundary terminates at a *critical point*. The most interesting of these is the critical point at the termination of the vapor pressure curve. The coordinates of the critical point on a P-T plot are the critical temperature T_c and critical pressure P_c , respectively. The formal definition of P_c is the pressure above which a liquid cannot be vaporized into a gas regardless of the temperature. The definition of T_c is the temperature above which a gas cannot be condensed into a liquid regardless of the pressure. At the critical point, gas and liquid properties are identical. Obviously, the region above the critical point represents a transition from a liquid to gas state without a discontinuous change in properties. Since this region is neither clearly a liquid nor a gas, it is sometimes called the supercritical *fluid* region. The exact definition of the fluid region is arbitrary: Most texts take it to be the region to the right of the critical temperature ($T > T_c$) though it would seem that defining it to be the region to the right *and* above the critical point ($T > T_c$ and $P > P_c$) would be more consistent with the behavior of mixtures.

The behavior shown in Fig. 4-1 for a pure component is qualitatively correct though less detailed than what can be observed. There can exist, in fact, more than one triple point where solid–solid–liquid equilibria are observed. Water is a familiar example of a pure component that has this behavior. Remarkably, observations of multiple gas phases for pure components have also been reported (Schneider, 1970). Such nuances are not the concern of this text, which emphasizes gas–liquid and liquid–liquid equilibria. In fact, in all further discussions of phase behavior, we ignore triple points and solid-phase equilibria. Even with these things omitted, the P-T diagrams in this chapter are only qualitatively correct since the critical point and the vapor pressure curve vary greatly among components. Figure 7-2 shows some quantitative comparisons.

Critical phenomena do play an important role in the properties of EOR fluids. If a laboratory pressure cell contains a pure component on its vapor pressure curve

(Fig. 4-1), the pure component exists in two phases (gas and liquid) at this point, and the cell pressure is P_v . Thus the cell will contain two regions of distinctly different properties. One of these properties being the density, one phase will segregate to the top of the cell, and the other to the bottom. The phases will most likely have different light transmittance properties so that one phase, usually the upper or light phase, will be clear, whereas the other phase, the lower or heavy phase, will be translucent or dark.

We can simultaneously adjust the heat transferred to the cell so that the relative volumes of each phase remain constant, and both the temperature and pressure of the cell increase if the fluid remains on the vapor pressure curve. For most of the travel from the original point to the critical point, no change occurs in the condition of the material in the cell. But the properties of the individual phases are approaching each other. In some region near the critical point, the light phase would become darker, and the heavy phase lighter. Very near the critical point, the interface between the phases, which was sharp at the original temperature and pressure, will become blurred and may even appear to take on a finite thickness. At the critical point, these trends will continue until there is no longer a distinction between phases—that is, two phases have ceased to exist. If we continue on an extension of the vapor pressure curve, there would be a single-fluid phase and gradual changes in properties.

Pressure–Molar-Volume Diagram

A way of representing how the discontinuity in intensive properties between phases vanishes at the critical point is the pressure–molar-volume diagram. Figure 4-2 compares such a diagram with the corresponding P-T diagram. Both schematic plots show *isotherms*, changes in pressure from a high pressure P_1 to a lower pressure P_2 , at four constant temperatures, T_1 through T_4 .

At conditions $(P, T)_1$, the pure component is a single-phase liquid. As pressure decreases at constant temperature, the molar volume increases but only slightly since liquids are relatively incompressible. At $P = P_v(T_1)$, the molar volume increases discontinuously from some small value to a much larger value as the material changes from a single-liquid to a single-gas phase. Since the change takes place at constant temperature and pressure, this vaporization appears as a horizontal line in Fig. 4-2(b). Subsequent pressure lowering again causes the molar volume to increase, now at a much faster rate since the compressibility of the gas phase is much greater than that of the liquid phase. The endpoints of the horizontal segment of the pressure–molar-volume plot represent two coexisting phases in equilibrium with each other at the same temperature and pressure. The liquid and vapor phases are said to be *saturated* at $P = P_v(T_1)$.

At a higher temperature T_2 , the behavior is qualitatively the same. The isotherm starts at a slightly higher molar volume, the vaporization at $P = P_v(T_2)$ is at a higher pressure, and the discontinuous change from saturated liquid to saturated vapor \bar{V}_M is not as large as at T_1 . Clearly, these trends continue as the isotherm

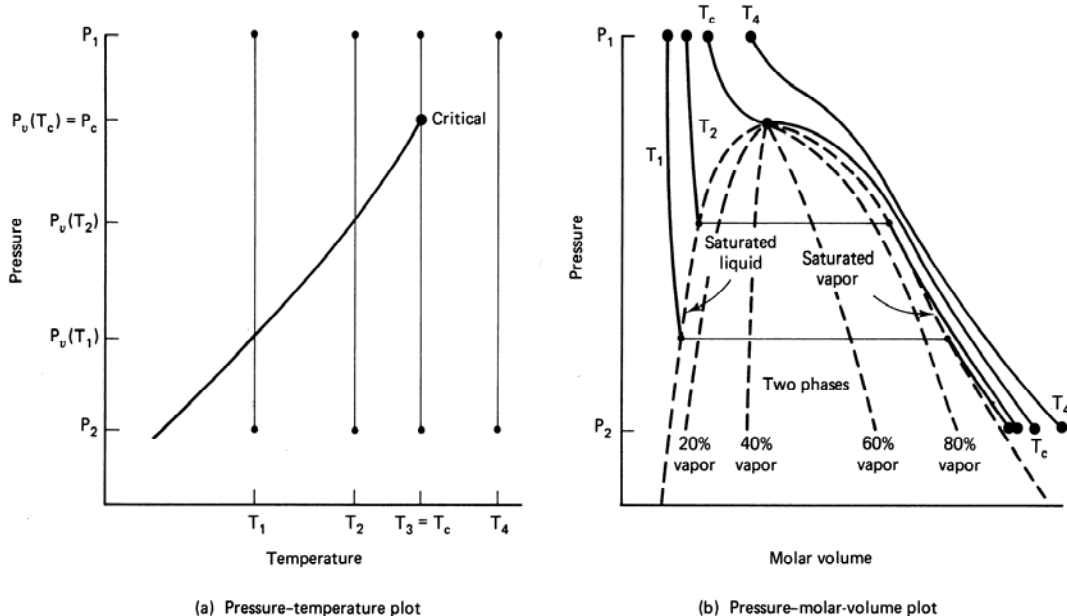


Figure 4-2 Schematic pressure–temperature and pressure–molar-volume diagrams

temperature approaches $T_3 = T_c$. All isotherms on the pressure–molar-volume plot are continuously nonincreasing functions with discontinuous first derivatives at the vapor pressure line.

At the critical temperature, the two phases become identical, and the saturated liquid and gas molar volumes coincide. Since this temperature is only infinitesimally higher than one at which there would still be distinguishable liquid and gas phases, the isotherm at $T = T_c$, the critical isotherm, continuously decreases with continuous first derivatives. At the critical point $P = P_c$, the critical isotherm must have zero slope and zero curvature, or

$$\left(\frac{\partial P}{\partial \bar{V}_M} \right)_{T_c, P_c} = \left(\frac{\partial^2 P}{\partial \bar{V}_M^2} \right)_{T_c, P_c} = 0 \quad (4.1-3)$$

These *critical constraints* follow from the physical argument given above and can also be derived by requiring a minimum in the Gibbs free energy at the critical point (Denbigh, 1968).

At isotherm temperatures above the critical temperature, $T = T_4$ in Fig. 4-2, the isotherm is monotonically decreasing with continuous first derivatives but without points of zero slope or curvature.

The endpoints of all the horizontal line segments below the critical points in the pressure–molar-volume plot define a two-phase envelope as in Fig. 4-2(b). Though rarely done, it is also possible to show lines of constant relative amounts of liquid and gas within the two-phase envelope. These *quality* lines (dotted lines in Fig. 4-2b) must converge to the critical point. The two-phase envelope on a pressure–

molar-volume plot for a pure component, which projects onto a line in a P-T diagram, is not the same as the two-phase envelope on a P-T diagram for mixtures. Both Figs. 4-2(a) and 4-2(b) are merely individual planar representations of the three-dimensional relation among temperature, pressure, and molar volume. Figure 4-3 illustrates the three-dimensional character of this relation for water.

Finally, though we illustrate the phase envelope of a pure component on a pressure–molar-volume diagram, discontinuities in properties below the critical point are present in all other intensive properties except temperature and pressure (see Fig. 11-3, the pressure–enthalpy diagram for water).

4-2 PHASE BEHAVIOR OF MIXTURES

Because the purpose of EOR is to recover crude oil, an unrefined product, we need not deal with the phase behavior of pure components except as an aid to understanding mixtures. Since the phase behavior of hydrocarbon mixtures is so complex, in this and the next section, we simply compare the phase behavior of mixtures to pure components and introduce pressure–composition (P-z) and ternary diagrams.

Pressure–Temperature Diagrams

For a multicomponent mixture, $N_F > 2$ when two phases are present. Therefore, two (or more) phases can coexist in a planar region in P-T space, compared to the single component case, where two phases coexist only along a line in P-T space. Mixtures have two phases in a region, or *envelope*, in P-T space (Fig. 4-4).

Consider, along with this figure, a change in pressure from P_1 to P_5 at constant temperature T_2 . The phase envelope is fixed for constant overall composition (ω_i or z_i). Since the indicated change is usually brought about by changing the volume of a pressure cell at constant composition and temperature, the process is frequently called a *constant composition* expansion.

From P_1 to P_3 , the material in the cell is a single-liquid phase. At P_3 , a small amount of vapor phase begins to form. The upper boundary of the phase envelope passing through this point is the *bubble point curve*, and the y coordinate at this point is the *bubble point pressure* at the fixed temperature. From P_3 to P_5 , successively, more gas forms as the liquid phase vaporizes. This vaporization takes place over a finite pressure range in contrast to the behavior of a pure component. Continuing the constant composition expansion to pressures lower than P_5 would result in eventually reaching a pressure where the liquid phase would disappear, appearing only as drops in the cell just before this point. The pressure the liquid vanishes at is the *dew point pressure* at the fixed temperature, and the lower boundary of the phase envelope is the *dew point curve*.

For a pure component (Fig. 4-1), the dew and bubble point curves coincide.

Within the two-phase envelope, there exist quality lines that as before, indicate constant relative amounts of liquid and vapor. The composition of the liquid

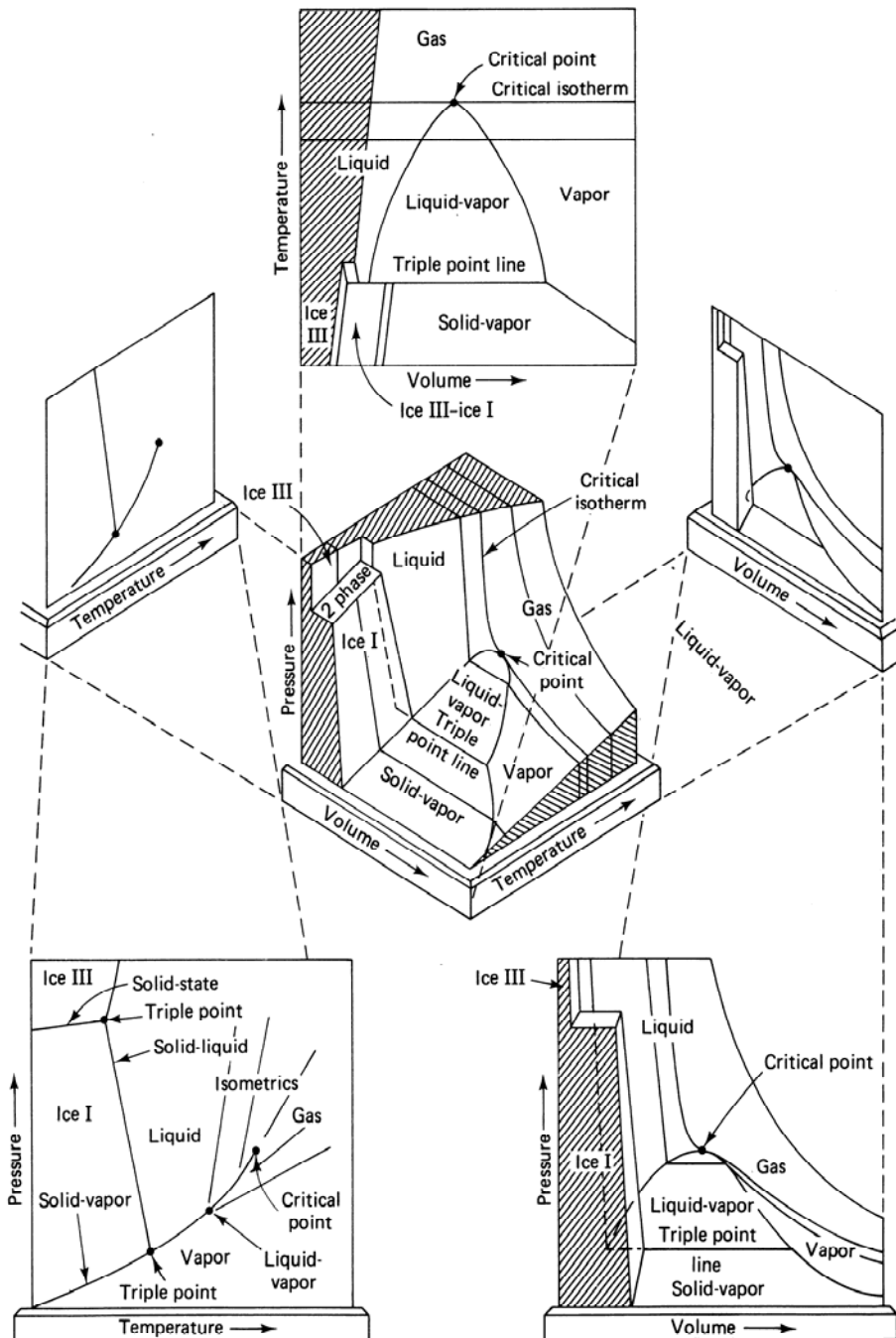


Figure 4-3 Schematic pressure-specific volume–temperature surface and projections (from Himmelblau, 1982)

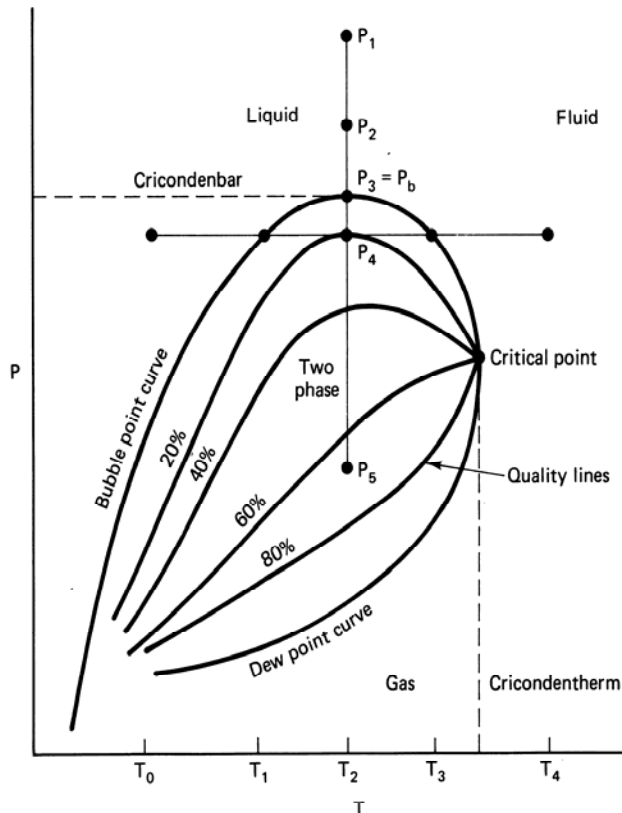


Figure 4-4 Schematic pressure-temperature diagram for hydrocarbon mixtures (constant composition)

and gas phases is different at each point within the envelope, and both change continuously as the pressure decreases.

Phase compositions are not shown on the P-T plot. But we do know that the liquid and gas phases are saturated with respect to each other in the two-phase envelope. Hence at any T and P within the envelope, the liquid phase is at its bubble point, and the gas phase at its dew point. The quality lines converge to a common point at the critical point of the mixture though this point does not, in general, occur at extreme values of the temperature and pressure on the phase envelope boundary. The maximum pressure on the phase envelope boundary is the *cricondenbar*, the pressure above which a liquid cannot be vaporized. The maximum temperature on the phase envelope is the *cricondentherm*, the temperature above which a gas cannot be condensed. These definitions are the same as for the critical point in pure component systems; hence the best definition of the critical point for mixtures is the temperature and pressure at which the two phases become identical.

For mixtures, there exists, in general, a pressure range between the cricondenbar and P_c and between the cricondentherm and T_c where *retrograde* behavior can occur. A horizontal constant pressure line in Fig. 4-4 at $P = P_4$ begins in the liquid region at T_0 and ends in the fluid region at T_4 . As temperature is increased, gas begins to form at the bubble point temperature T_1 and increases in amount from

then on. But at T_2 , the amount of gas begins to decrease, and the gas phase vanishes entirely at a second bubble point T_3 . From T_2 to T_3 , the behavior is contrary to intuition—a gas phase disappearing as temperature increases—and the phenomenon is called retrograde vaporization.

Retrograde behavior does not occur over the entire range between the two bubble point temperatures but only over the range from T_2 to T_3 . By performing the above thought experiment at several pressures, one can show that retrograde behavior occurs only over a region bounded by the bubble point curve on the right and a curve connecting the points of zero slope on the quality lines on the left (McCain, 1973).

Though not possible in the P-T diagram in Fig. 4-4, retrograde phenomena are also observed for changes in pressure at constant temperature. This case, which is of more interest to a reservoir engineer, happens when the cricondentherm is larger than T_c and the constant temperature is between these extremes. This type of retrograde behavior is a prominent feature of many hydrocarbon reservoirs, but it impacts little on EOR.

We do not discuss the pressure–molar-volume behavior of hydrocarbon mixtures in detail. The main differences between the behavior of pure components and mixtures is that the discontinuous changes in \bar{V}_M do not occur at constant P , and the critical point no longer occurs at the top of the two-phase region (see Exercise 4B). These differences cause interesting variations in the shape of pressure–molar-volume diagrams for mixtures but, again, are not directly relevant to EOR.

Since EOR processes are highly composition dependent, the behavior of the P-T envelope as the overall composition of the mixture changes is highly important. Consider the dilution of a crude oil M_4 with a more volatile pure component A as shown in Fig. 4-5. As the overall mole fraction of A increases, the phase envelope migrates toward the vertical axis, increasing the size of the gas region. Simultaneously, the phase envelope shrinks as it approaches the vapor pressure curve of the pure component A . There are, of course, an infinite number of mixtures (Fig. 4-5 shows only three) of the crude oil with A . Each mixture has its respective critical point in P-T space, which also migrates to the critical point of the pure component on a critical locus. The overall composition of a mixture at a critical point is the *critical mixture* at that temperature and pressure.

Pressure–Composition Diagrams

The phase behavior of the dilution in Fig. 4-5 on a plot of mole fraction of component A versus pressure at fixed temperature shows composition information directly. Such a plot is a *pressure composition*, or P-z, plot. The P-z plot for the sequence of mixtures in Fig. 4-5 is shown in Fig. 4-6. Since the P-T diagram in Fig. 4-5 shows only three mixtures and does not show quality lines, phase envelope boundaries are represented at relatively few points in Fig. 4-6 (see Exercise 4C).

Starting at some high pressure in Fig. 4-5 and following a line of constant temperature as pressure is reduced produces a dew point curve for mixture M_1 at

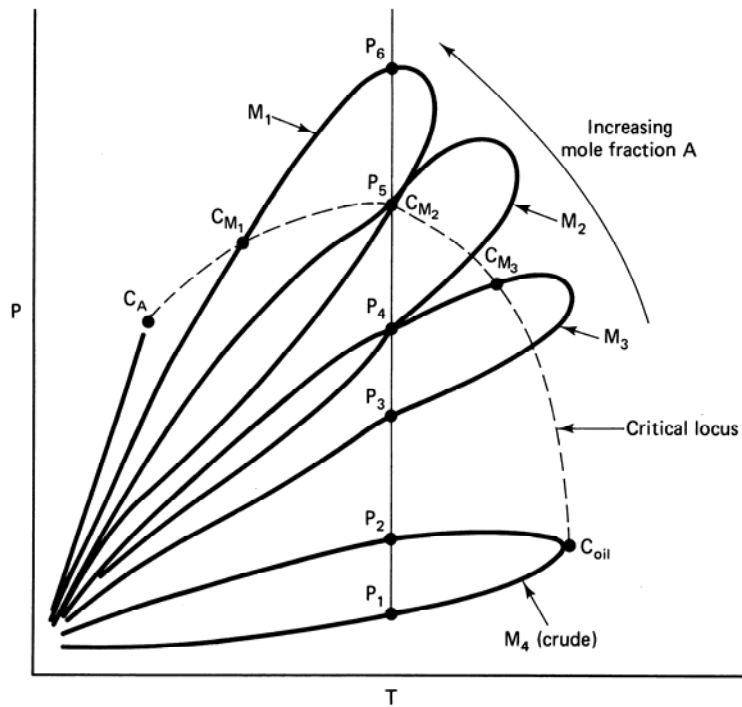


Figure 4-5 Schematic dilution of a crude oil by a more volatile pure component

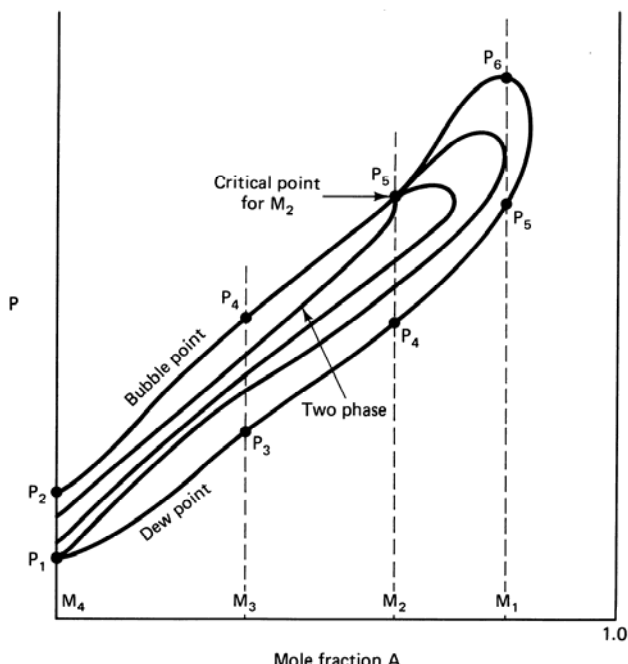


Figure 4-6 The pressure-composition plot for the dilution in Fig. 4-5

pressure P_6 . Since this mixture is rich in component A , this point plots nearest the right vertical axis in Fig. 4-6 at the pressure coordinate P_6 . Continuing down the constant temperature line, at P_5 the critical point for mixture M_2 is encountered (mixture M_2 is the critical composition at this temperature and pressure). But this point is also a second dew point for mixture M_1 ; hence P_5 plots at the same vertical coordinate for both mixtures in Fig. 4-6 but with different horizontal coordinates. At P_4 there is a bubble point for mixture M_3 and a dew point for M_2 . These points again define the corresponding phase boundaries of the P-z plot in Fig. 4-6. The process continues to successively lower pressures in the same manner. Each pressure below the critical is simultaneously a bubble point and a dew point pressure for mixtures of different overall compositions. The pressures P_2 and P_1 are the bubble and dew point pressures of the undiluted crude oil. The two-phase envelope in Fig. 4-6 does not intersect the right vertical axis since the fixed temperature is above the critical temperature of the pure component A . The diagram shows the closure of the two-phase envelope as well as a few quality lines.

Since the entire P-z diagram is at constant temperature, we cannot represent the phase behavior at another temperature without showing several diagrams. More important, the composition plotted on the horizontal axis of the P-z plot is the overall composition, not either of the phase compositions. Thus horizontal lines do not connect equilibrium mixtures. Such *tie lines* do exist but are, in general, oriented on a horizontal line in a hyperspace whose coordinates are the phase compositions. However, for binary mixtures, the tie lines are in the plane of the P-z plot, and the critical point is necessarily located at the top of the two-phase region. Finally, though Fig. 4-6 is schematic, it bears qualitative similarity to the actual P-z diagrams shown in Figs. 7-10 through 7-12.

4-3 TERNARY DIAGRAMS

On a P-z plot, we sacrifice a degree of freedom (temperature) to obtain compositional information. But the diagrams can show only the composition of one component, and this representation is often insufficient for the multitude of compositions that can form in an EOR displacement. A plot that represents more composition information is the *ternary diagram*.

Definitions

Imagine a mixture, at fixed temperature and pressure, consisting of three components 1, 2, and 3. The components may be pure components. But more commonly in EOR, they are pseudocomponents, consisting of several pure components. The composition of the mixture will be a point on a plot of the mole fraction of component 3 versus that of component 2. In fact, this entire two-dimensional space is made up of points that represent the component concentrations of all possible mixtures.

We need to plot the concentrations of only two of the components since the

concentration of the third may always be obtained by subtracting the sum of the mole fractions of components 2 and 3 from 1. This means all possible compositions will plot into a right triangle whose hypotenuse is a line from the 1.0 on the y axis to the 1.0 on the x axis. Though ternary diagrams are on occasion shown this way (see Fig. 7-15), they are most commonly plotted so that the right triangle is shifted to an equilateral triangle, as in Fig. 4-7.

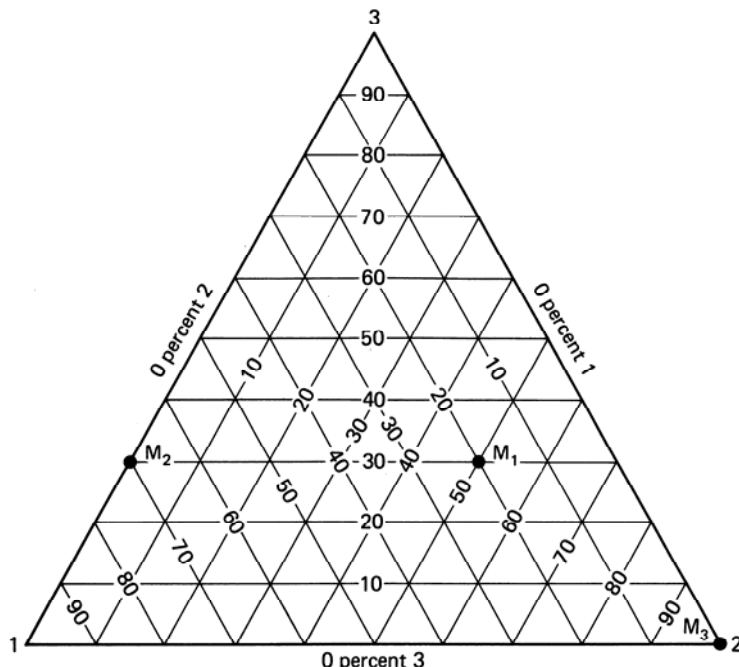


Figure 4-7 Ternary Diagram

All possible ternary compositions fall on the interior of the equilateral triangle; the boundaries of the triangle represent binary mixtures (the component at the apex opposite to the particular side is absent), and the apexes represent pure components. Thus in Fig. 4-7, point M_1 is a mixture having 20%, 50%, and 30% components 1, 2, and 3, respectively; point M_2 is a binary mixture of 70% component 1 and 30% component 3, and point M_3 is 100% component 2. Representing the compositions in this manner is possible for any concentration variable (mole fraction, volume fraction, mass fraction) that sums to a constant.

Ternary diagrams are extremely useful tools in EOR because they can simultaneously represent phase and overall compositions as well as relative amounts. The correspondence of the P-T diagram to the ternary diagram in Figs. 4-8 and 4-9 compares to the P-z diagram in Figs. 4-5 and 4-6. Here we consider a ternary system consisting of components 1, 2, and 3, and consider the dilution of mixtures having constant ratios of components 2 and 3 by component 1. Each dilution represents a line corresponding to a fixed 2 : 3 ratio on the ternary in Fig. 4-9.

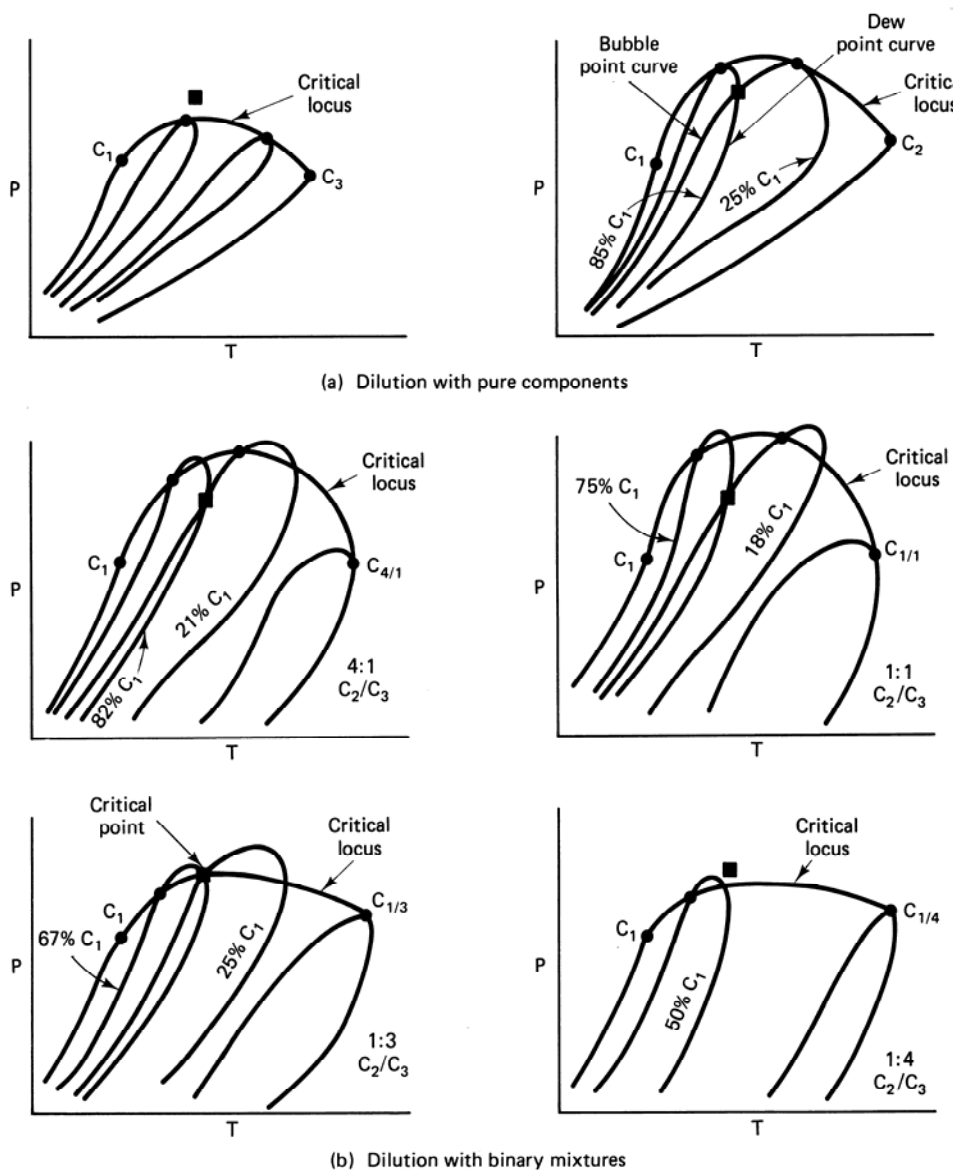


Figure 4-8 Schematic evolution of P-T diagram in three component systems

We want to follow the formation and disappearance of phases on the ternary diagram at the fixed temperature and pressure indicated by the box in Fig. 4-8. For the dilution of component 3 by component 1, the reference temperature and pressure is above the critical locus in the upper left-hand panel (Fig. 4-8a). Thus the C_1-C_3 axis of the ternary indicates no phase changes. The C_1-C_2 binary dilution in the upper right-hand panel (Fig. 4-8a) does encounter phase changes, and in fact, the reference temperature and pressure is a bubble point for a mixture of 25% C_1 and a dew point for a mixture of 85% C_1 . These phase transitions are shown on the C_1-C_2 axis on the

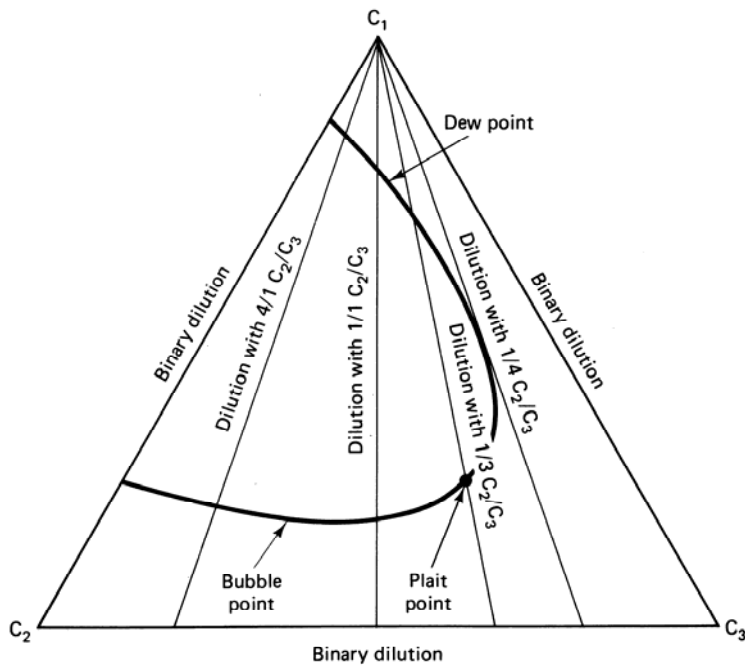


Figure 4-9 Schematic ternary diagram of dilutions in Fig. 4-8

ternary. The dilution indicated in the middle left-hand panel (Fig. 4-8b) shows phase transitions at 82% and 21%, respectively, which are also plotted on the ternary. For the dilution of the 1 : 3 mixture, the critical locus passes through the fixed temperature and pressure, and this composition, 25% C_1 , is the critical composition of the ternary mixture. This composition is indicated on the ternary diagram in Fig. 4-9 as a *plait* point after the more common designation of the critical mixture in liquid–liquid phase equilibria. At the fixed temperature and pressure, there can exist a second phase transition—a dew point at 67% C_1 —at the same temperature and pressure. After making several dilution passes through the ternary diagram, the points where there are phase transitions define a closed curve in Fig. 4-9. This curve, the *binodal* curve, separates regions of one- and two-phase behavior. Within the region enclosed by the binodal curve, two phases exist, and outside this region, all components are in a single phase.

Phase Compositions

One useful but potentially confusing feature of ternary diagrams is that it is possible to represent the composition of the phases as well as the overall composition on the same diagram. Consider an overall composition C_i on the inside of the binodal curve in Fig. 4-10

$$C_i = C_{i1}S_1 + C_{i2}S_2, \quad i=1, 2, 3 \quad (4.3-1)$$

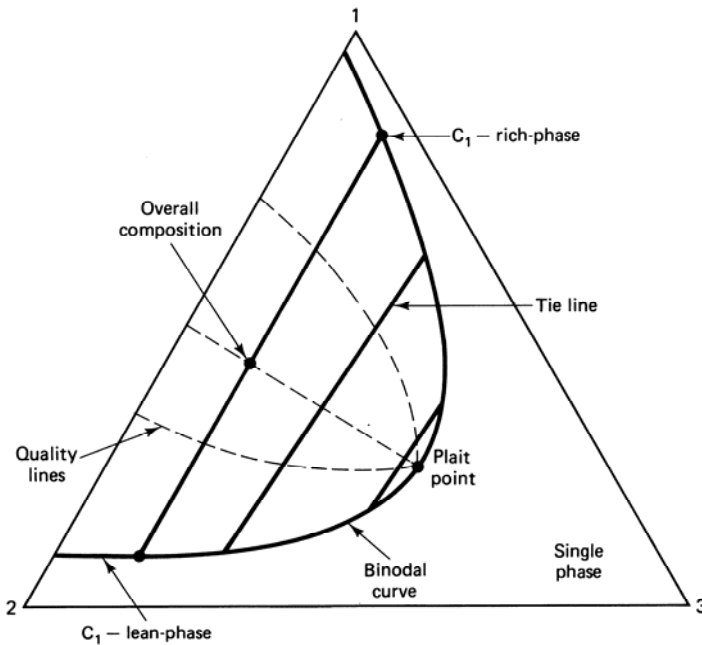


Figure 4-10 Two-phase ternary equilibria

where C_{ij} is the concentration of component i in phase j , and S_j is the relative amount of phase j . By convention, we take phase 1 to be the C_1 -rich phase and phase 2 to be the C_1 -lean phase. Since $S_1 + S_2 = 1$, we can eliminate S_1 from two of the equations in Eq. (4.3-1) to give

$$S_2 = \frac{C_3 - C_{31}}{C_{32} - C_{31}} = \frac{C_1 - C_{11}}{C_{12} - C_{11}} \quad (4.3-2)$$

This equation says a line through the composition of phase 1 and the overall composition has the same slope as a line passing through the composition of phase 2 and the overall composition. Both lines, therefore, are merely segments of the same straight line that passes through both phase compositions and the overall composition. The intersection of these *tie lines* with the binodal curve gives the phase compositions shown in Fig. 4-10. The entire region within the binodal curve can be filled with an infinite number of these tie lines, which must vanish as the plait point is approached since all phase compositions are equal at this point. Of course, there are no tie lines in the single-phase region.

Further, Eq. (4.3-2) implies, by a similar triangle argument, that the length of the line segment between C_i and C_{il} divided by the length of the segment between C_{i2} and C_{11} is the relative amount S_2 . This, of course, is the well-known *lever rule*, which can also be derived for S_1 . By holding S_2 constant and allowing C_i to vary, we can construct quality lines, as indicated in Fig. 4-10, which must also converge to the plait point as do the tie lines.

Tie lines are graphical representations of the equilibrium relations (Eq. 2.2-11). Assuming, for the moment, the apexes of the ternary diagram represent true components, the phase rule predicts there will be $N_F = 1$ degrees of freedom for mixtures within the binodal curve since temperature and pressure are already specified. Thus it is sufficient to specify one concentration in either phase to completely specify the state of the mixture. A single coordinate of any point on the binodal curve gives both phase compositions if the tie lines are known. This exercise does not determine the relative amounts of the phases present since these are not state variables. Nor does specifying a single coordinate of the overall concentration suffice since these, in general, do not lie on the binodal curve. Of course, it is possible to calculate the phase compositions and the relative amounts from equilibrium relations, but these must be supplemented in “flash calculations” by additional mass balance relations to give the amounts of each phase.

Three-Phase Behavior

When three phases form, there are no degrees of freedom ($N_F = 0$). The state of the system is entirely determined. It follows from this that three-phase regions are represented on ternary diagrams as smaller subtriangles embedded within the larger ternary triangle (Fig. 4-11). Since no tie lines are in three-phase regions, the apexes or *invariant points* of the subtriangle give the phase compositions of any overall composition within that subtriangle. The graphical construction indicated in Fig. 4-11 gives the relative amounts of the three phases present (see Hougé et al., 1966, and Exercise 4D).

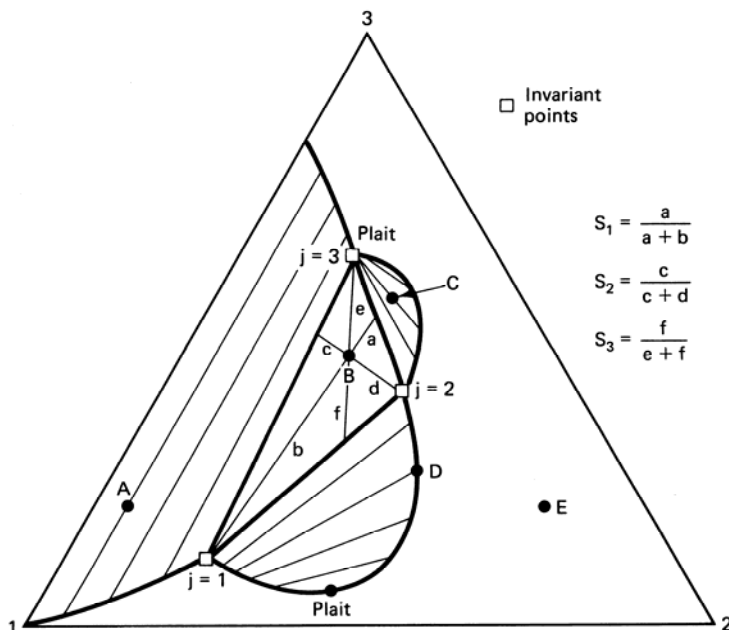


Figure 4-11 Three-phase diagram example (from Lake, 1984)

A point on a nonapex side of the subtriangle may be regarded as being simultaneously in the three-phase region or in a two-phase region; thus the subtriangle must always be bounded on a nonapex side by a two-phase region for which the side of the subtriangle is a tie line of the adjoining two-phase region. By the same argument, the apexes of the subtriangle must adjoin, at least in some nonzero region, a single-phase region. To be sure, the adjoining two-phase regions can be quite small (see Fig. 9-6).

Thus points *A* and *C* in Fig. 4-11 are two-phase mixtures, point *B* is three phase, and points *D* and *E* are single phase, though point *D* is saturated with respect to phase 1. (For more detail on the geometric and thermodynamic restrictions of ternary equilibria, see Francis, 1963.)

4-4 QUANTITATIVE REPRESENTATION OF TWO-PHASE EQUILIBRIA

Several mathematical relations describe the qualitative representations in the previous section. The most common are those based on (1) equilibrium flash vaporization ratios, (2) equations of state, and (3) a variety of empirical relations. In this section, we concentrate only on those two-phase equilibria aspects directly related to EOR. Three-phase equilibria calculations are discussed elsewhere in the literature (Mehra et al., 1980; Risnes and Dalen, 1982; Peng and Robinson, 1976) and in Chap. 9, which covers three-phase equilibria for micellar systems.

Equilibrium Flash Vaporization Ratios

If we let x_i and y_i be the mole fractions of component *i* in a liquid and in contact with a vapor phase, the equilibrium *flash vaporization ratio* for component *i* is defined by

$$K_i = \frac{y_i}{x_i}, \quad i = 1, \dots, N_C \quad (4.4-1)$$

This quantity is universally known as the *K*-value for component *i*.

At low pressures, the *K*-values are readily related to the mixture temperature and pressure. The partial pressure of component *i* in a low-pressure gas phase is $y_i P$ from Dalton's law of additive pressures. The partial pressure of component *i* in the vapor above an ideal liquid phase is $x_i P_{vi}$ from Raoult's law, where P_{vi} is the pure component vapor pressure of component *i* (see Figs. 4-1 and 7-2). At equilibrium for this special case, the partial pressures of component *i* calculated by either means must be equal; hence

$$K_i = \frac{y_i}{x_i} = \frac{P_{vi}}{P}, \quad i = 1, \dots, N_C \quad (4.4-2)$$

Equation (4.4-2) says at low pressures, a plot of the equilibrium *K*-value for a particular component at a fixed temperature will be a straight line of slope -1 on a

log–log plot. Under these conditions, the K -value itself may be estimated from pure component vapor pressure data.

At higher pressures, where the assumptions behind Dalton's and Raoult's laws are inaccurate, the K -values are functions of overall composition. The additional composition information, usually based on the liquid-phase composition, can be incorporated into a *convergence pressure*, which is then correlated to the K -values. Convergence pressure correlations are usually presented in graphical form (*GPSA Data Book*, 1983) or as equations. The introduction of a composition variable directly into the K -value functions adds considerable complexity to the flash procedure.

The flash calculation proceeds as follows: Let z_i be the overall mole fraction of component i in the mixture (analogous to ω_i , the overall mass fraction in Chap. 2). Then

$$z_i = n_L x_i + n_V y_i, \quad i = 1, \dots, N_C \quad (4.4-3)$$

where n_L and n_V are the relative molar amounts of the liquid and gas phases, respectively. Since all quantities in Eq. (4.4-3) are relative, they are subject to the following constraints

$$\sum_{i=1}^{N_C} x_i = \sum_{i=1}^{N_C} y_i = \sum_{i=1}^{N_C} z_i = n_L + n_V = 1 \quad (4.4-4)$$

Eliminating n_L from Eq. (4.4-3) with this equation, and substituting the definition (Eq. 4.4-1) for y_i , yields the following for the liquid-phase composition:

$$x_i = \frac{z_i}{1 + (K_i - 1)n_V}, \quad i = 1, \dots, N_C \quad (4.4-5)$$

But these concentrations must also sum to 1.

$$\sum_{i=1}^{N_C} \frac{z_i}{1 + (K_i - 1)n_V} = 1 \quad (4.4-6a)$$

Equation (4.4-6a) is a single polynomial expression for n_V , with K_i and z_i known, that must be solved by trial and error. The equation itself is not unique since we could have eliminated n_V and x_i from Eq. (4.4-3) to give the entirely equivalent result

$$\sum_{i=1}^{N_C} \frac{z_i}{1 + \left(\frac{1}{K_i} - 1\right)n_L} = 1 \quad (4.4-6b)$$

The usual flash procedure is to calculate n_V or n_L by trial and error, and then use Eqs. (4.4-1) and (4.4-5) to calculate the phase concentrations.

Alternatively, Eqs. (4.4-6a) and (4.4-6b) can be used to calculate quality lines in a P-T diagram by specifying n_V or n_L and then performing trial-and-error solutions

for pressure at various fixed temperatures. Two special cases of the above procedure follow directly. The bubble point curve for a mixture ($n_L = 1$) is given implicitly from Eq. (4.4-6b) as

$$1 = \sum_{i=1}^{N_C} z_i K_i \quad (4.4-7a)$$

and the dew point curve ($n_V = 1$) from Eq. (4.4-6a) as

$$1 = \sum_{i=1}^{N_C} \frac{z_i}{K_i} \quad (4.4-7b)$$

These equations suggest the necessity of doing a flash calculation. Because the K -values increase as temperature increases, a mixture of overall composition z_i at fixed temperature and pressure will be two phase only if

$$\sum_{i=1}^{N_C} z_i K_i > 1 \quad \text{and} \quad \sum_{i=1}^{N_C} \frac{z_i}{K_i} > 1 \quad (4.4-8)$$

If the first inequality in Eq. (4.4-8) is violated, the mixture is a single-phase liquid; if the second is violated, the mixture is a single-phase gas.

Equations of State

Though the K -value approach is easily the most common representation of two-phase equilibria, it suffers from a lack of generality and may result in inaccuracies particularly near the convergence pressure. In recent years, the trend has been toward equation of state (EOS) representations since these are potentially able to work near the critical point and yield internally consistent densities and molar volumes. (For more details on EOS and its underlying thermodynamic principles, see Smith and van Ness, 1975, and Denbigh, 1968.)

Pure components. An EOS is any mathematical relationship among the three intensive properties molar volume, temperature, and pressure. Usually, the relation is written in a pressure-explicit form $P = f(\bar{V}_M, T)$, and the most elementary form is the ideal gas equation

$$P = \frac{RT}{\bar{V}_M} \quad (4.4-9)$$

This equation applies only to gases at low pressure. Equation (4.4-9) can be corrected to apply to real gases by introducing a correction factor z , the *compressibility factor*

$$P = \frac{zRT}{\bar{V}_M} \quad (4.4-10)$$

The compressibility factor is itself a function of temperature and pressure that is given in many sources (see McCain, 1973, for example). Since Eq. (4.4-10) is

actually a definition of the compressibility factor, the equation can also be applied to fluids and liquids though the latter is rarely done. Given the relation between z and T and P , Eq. (4.4-10) could predict volumetric behavior for all T and P .

Consider the pressure–molar-volume behavior of a pure component as shown in Fig. 4-2. Figure 4-12 also shows this type of plot with two isotherms T_1 and T_2 , both below the critical temperature. Equation (4.4-9) is the equation of a hyperbola on this plot that matches the experimental isotherm well at low pressure or high molar volume. The ideal gas law fails badly in the liquid region, particularly for pressure predictions, since it predicts a zero asymptote on the molar volume axis. This is equivalent to saying the component molecules themselves have no intrinsic volume even at the highest pressure, which is, of course, a basic hypothesis in the derivation of the ideal gas law from statistical mechanics.

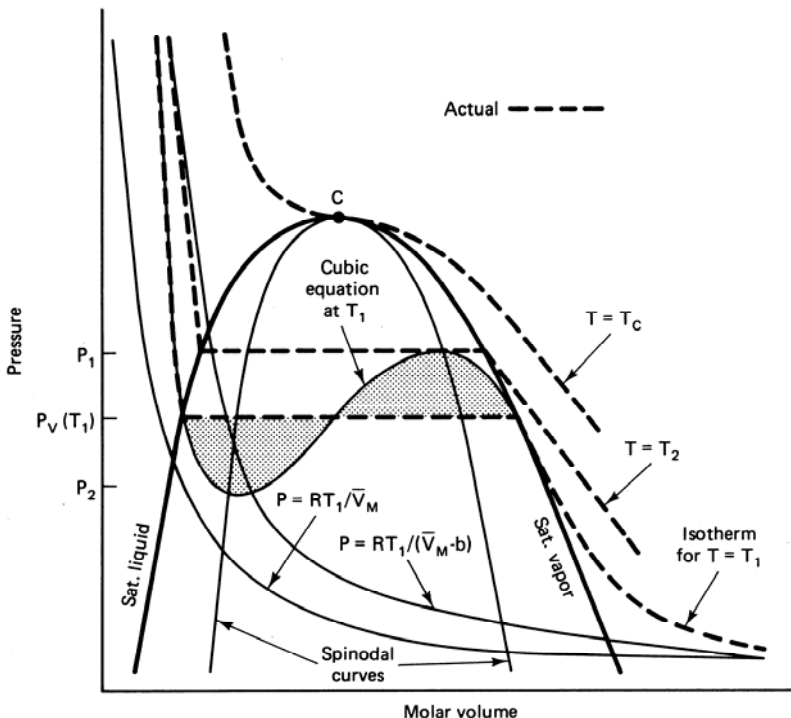


Figure 4-12 General features of cubic equations of state

To introduce a nonzero asymptote, we try an equation of the form

$$P = \frac{RT}{(\bar{V}_M - b)} \quad (4.4-11)$$

where b is now the asymptotic value of \bar{V}_M as pressure increases. Figure 4-12 shows this equation can be made to match the liquid molar volumes reasonably well at high

pressures. The value of b , the intrinsic molecular volume, is usually so small that Eq. (4.4-11) still provides a good estimate at low pressures.

But Eq. (4.4-11) still fails for temperature and pressure combinations that are fairly close to the pure component vapor pressure curve. To predict the molar volume up to and including the vapor pressure curve requires a function of the form

$$P = \frac{RT}{(\bar{V}_M - b)} - f(T, \bar{V}_M) \quad (4.4-12)$$

where the term $f(T, \bar{V}_M)$ is specific to the particular EOS. Equation (4.4-12) is frequently interpreted as a sum of forces, the first term being the force that will not allow the molecules to be compressed to zero volume (repulsive force), and the second being the force due to the intermolecular attraction among molecules.

A practical EOS must be accurate, internally consistent near the critical point, and relatively simple. Moreover, since we are to use it to predict vapor–liquid equilibria, it must predict both liquid and gas properties.

For pure components, there can exist two values of molar volume at a particular temperature and pressure; hence Eq. (4.4-12) must have at least two real roots at this point. Moreover, since P is a monotonically decreasing function of \bar{V}_M regardless of the fluid-phase identity, f must be at least second order in \bar{V}_M so that the entire function (Eq. 4.4-12) must be at least cubic in molar volume. Cubic EOS, therefore, are the simplest form that satisfy the three criteria mentioned. Though there have been more than 100 EOS proposed in the technical literature, many of which are quite complicated and have more thermodynamic rigor, we discuss only cubic EOS since these seem to be the most commonly used class of equations in EOR.

In the vicinity of the vapor pressure curve (pressures between P_1 and P_2 at temperature T_1 in Fig. 4-12), there are three real roots to the cubic EOS. The vapor pressure P_v corresponding to T_1 is the y -coordinate value that causes the shaded areas above and below P_v to have equal areas (Abbott and van Ness, 1972). For pressures above P_v , only the smallest root has physical significance and corresponds to \bar{V}_M of a compressed liquid; at pressures below P_v , the largest root corresponds to \bar{V}_M of a superheated vapor. At the vapor pressure, both the smallest and largest roots have physical significance corresponding to the saturated liquid and vapor molar volumes, respectively. The intermediate root has no physical significance.

As the critical point is approached, all three roots converge to the value of \bar{V}_M at the critical point \bar{V}_{Mc} . For temperatures above T_c , cubic equations have only one real root, that of the molar volume of a fluid. For the critical isotherm itself, there is also only one real root, and the critical constraints Eq. (4.1-3) are satisfied at the critical pressure.

Within the two-phase region on the pressure–molar-volume plot, the quadratic curves defined by $(\partial P / \partial \bar{V}_M)_T = 0$ for $P < P_c$ are the *spinodal curves*. They represent the maximum degree of supersaturation with respect to the particular phase transition. Thus theoretically at least, we could lower the pressure on a single compressed liquid phase at T_1 to P_2 without changing phase. The liquid between P_v and P_2 is supersaturated with respect to the vapor phase. A phase transition must

occur beyond this pressure since the partial derivative $(\partial P / \partial \bar{V}_M)_T$ is constrained to be negative on thermodynamic and physical grounds. Similarly, a vapor phase at pressure P_1 could be supercooled down to only temperature T_2 without causing a phase change, and the vapor at P_1 and T_2 is supersaturated with respect to the liquid phase. These are metastable states that will change to stable states on perturbation.

The above discussion gives the properties of any general cubic EOS. The particular form of such equations, of course, can take a wide variety of forms. Abbott (1973) gives the general form

$$P = \frac{RT}{(\bar{V}_M - b)} - \frac{\theta(\bar{V}_M - \eta)}{(\bar{V}_M - b)(\bar{V}_M^2 + \delta\bar{V}_M + \varepsilon)} \quad (4.4-13)$$

where the parameters θ , η , δ , and ε are given in Table 4-1 for nine specific equations of state. Equation (4.4-13) is, perhaps, not the most general form of the cubic equations available (Martin, 1979), but it does include most of the commonly accepted equations used in predicting the phase behavior of EOR fluids.

Abbott's original work (1973) contains complete references on each of the equations in Table 4-1. Thus far, only two of these equations have seen extensive use in predicting EOR phase behavior: the Soave modification (1972) of the Redlich-Kwong equation (RKS) and the Peng-Robinson (1976) equation (PR). We discuss these two equations here.

Except for the Clausius equation, all the equations in Table 4-1 are two-parameter equations. The value of these parameters may be chosen to force the equation to make internally consistent predictions in the vicinity of the critical point for pure components. Thus the values of the parameters come from enforcing the critical constraints (Eq. 4.1-3) and from evaluating the original equation at the critical point. Since there are three equations, the procedure also specifies a specific value of the critical molar volume \bar{V}_M or critical z -factor z_c in addition to a and b .

It is somewhat easier, though entirely equivalent, to use the procedure of Martin and Hou (1955) to determine the parameters a and b . Expressing the RKS equation in the z -factor form will eliminate \bar{V}_M between Eq. (4.4-10) and the RKS equation. By applying Descartes' rule of roots to this equation, there is either one or

**TABLE 4-1 CLASSIFICATION OF SOME CUBIC EQUATIONS OF STATE
(FROM ABBOTT, 1978)**

Equation	θ	η	δ	ε
van der Waals (1873)	a	b	0	0
Berthelot (1900)	a/T	b	0	0
Clausius (1880)	a/T	b	$2c$	c^2
Redlich-Kwong (1949)	$a/T^{1/2}$	b	b	0
Wilson (1964)*	$\theta_w(T)$	b	b	0
Peng-Robinson (1976)	$\theta_{PR}(T)$	b	$2b$	$-b^2$
Lee-Erbar-Edmister (1973)	$\theta_{LEE}(T)$	(T)	b	0

*Similarly, Barner et al. (1966) and Soave (1972)

three positive and no negative real roots. The z -factor equation evaluated at the critical point must have only one real root; hence

$$(z - z_c)^3 = z^3 - 3z_c z^2 + 3z_c^2 z - z_c^3 = 0 \quad (4.4-14)$$

This equation is identically equal to the form in Table 4-2; hence equating coefficients, we immediately have $z_c = 1/3$ and

$$3z_c^2 = A - B - B^2 \quad (4.4-15a)$$

$$z_c^3 = AB \quad (4.4-15b)$$

Eliminating A from these equations gives the cubic form

$$27B^3 + 27B^2 + 9B = 1 \quad (4.4-16)$$

Moreover, using Descartes' rule, it follows that this equation has only one real positive root, which may be solved for directly to give $B = (2^{1/3} - 1)/3 = 0.08664$. Solving for A from Eq. (4.4-15b) gives $A = (9(2^{1/3} - 1))^{-1} = 0.4247$. Using the definitions for A and B gives the forms in Table 4-2 for a and b .

Clearly, the above procedure is valid for any a and b that are a function of temperature only. To match experimental vapor pressure data to subcritical temperatures, the a given by this procedure is multiplied by a factor α_i , a function of temperature that reduces to unity at the critical temperature. The factor α_i is also component specific through its dependence on the acentric factor ω_i . Acentric factors roughly express the deviation of the shape of a molecule from a sphere and are available in extensive tabulations (Reid et al., 1977).

Mixtures. The true test and practical utility of any EOS is in its prediction of mixture properties. For mixtures, many of the arguments advanced above in conjunction with Fig. 4-12 do not apply. In particular, the critical constraints are no longer satisfied at the critical point since this point is no longer at the top of the two-phase envelope.

To account for mixture behavior, the pure component parameters a_i and b_i come from various mixing rules, as shown in Table 4-2. The inclusion of the component index in Table 4-2 means the parameters used in the definitions of these quantities— T_{ci} , P_{ci} , and ω_i —are those for the pure component i .

The most general form of the mixing rules incorporates another parameter, the *binary interaction coefficient* δ_{ij} into the RKS and PR equations, which accounts for molecular interactions between two unlike molecules. By definition δ_{ij} is zero when i and j represent the same component, small when i and j represent components that do not differ greatly (for example, if i and j were both alkanes), and large when i and j represent components that have substantially different properties. Ideally, the δ_{ij} are both temperature and pressure independent (Zudkevitch and Joffe, 1970), depending only on the identities of components i and j . Though the interaction coefficients are considerably less available than acentric factors, literature tabulations are becoming more common (Yarborough, 1978; Whitson, 1982; Prausnitz et al., 1980).

TABLE 4-2 COMPARISON OF THE RKS AND PR EQUATIONS OF STATE (FROM NGHIEM AND AZIZ, 1979)

	RKS	PR
Equation	$P = \frac{RT}{\bar{V} - b} - \frac{a}{\bar{V}_M (\bar{V}_M + b)}$	$P = \frac{RT}{\bar{V}_M - b} - \frac{a}{\bar{V}_M^2 + 2b\bar{V}_M - b^2}$
z -factor	$z^3 - z^2 + z(A - B - B^2) - AB = 0$ $A = \frac{aP}{(RT)^2}$	$z^3 - (1-B)z^2 + (A - 3B^2 - 2B)z - (AB - B^3 - B^2) = 0$ $B = \frac{bP}{RT}$
Pure component i	$a_i = \frac{0.42747R^2T_{ci}^{2.5}\alpha_i}{P_{ci}}, z_c = 0.333$ let $a = a_i$ $b = b_i$ $m_i = 0.480 + 1.57\omega_i - 0.176\omega_i^2$	$a_i = \frac{0.45724R^2T_{ci}^{2.5}\alpha_i}{P_{ci}}, z_c = 0.307$ $b_i = \frac{0.07780RT_{ci}}{P_{ci}}$ $m_i = 0.37464 + 1.54226\omega_i - 0.26992\omega_i^2$ $\alpha_i = \left[1 + m_i \left[1 - \left(\frac{T}{T_{ci}} \right)^{1/2} \right] \right]^2$
Mixture	$a_m = \sum_{ij} x_i x_j a_{ij}, b_m = \sum_i x_i b_i$ let $a = a_m$ $b = b_m$	$a_{ij} = (1 - \delta_{ij}) (a_i a_j)^{1/2}$
Pure component fugacity use z^L for f^L z^V for f^V	$\ln \frac{f_i}{P} = z - 1 - \ln(z - B) - \frac{A}{B}$ $\ln \left[\frac{z + B}{z} \right]$	$\ln \frac{f_i}{P} = z - 1 - \ln(z - B) - \frac{A}{2\sqrt{2}B}$ $\ln \left[\frac{z + 2.414B}{z - 0.414B} \right]$
Fugacity of component i use z^L and x_i for f_i^L z^V and y_i for f_i^V	$\ln \left(\frac{f_i}{P x_i} \right) = \frac{b_i}{b} (z - 1) - \ln(z - B) -$ $\frac{A}{B} \left(\frac{2 \sum_j x_j a_{ij}}{a} - \frac{b_i}{b} \right) \ln \left(\frac{z + B}{z} \right)$	$\ln \left(\frac{f_i}{x_i P} \right) = \frac{b_i}{b} (z - 1) - \ln(z - B) -$ $\frac{A}{2\sqrt{2}B} \left(\frac{2 \sum_j x_j a_{ij}}{a} - \frac{b_i}{b} \right) \ln \left(\frac{z + 2.414B}{z - 0.414B} \right)$

Flash calculations. To calculate vapor–liquid equilibria for mixtures from the RKS equation, an expression for the fugacity of a component i in a mixture is needed. This is most conveniently done by introducing a *fugacity coefficient* of component i defined as

$$\phi_i = \frac{f_i}{x_i P} \quad (4.4-17)$$

In Eq. (4.4-17), and all subsequent equations in this section, the composition variable may be either the liquid-phase mole fraction x_i , if calculating the fugacity coefficient of component i in the liquid phase, or the vapor-phase mole fraction y_i , if calculating the fugacity coefficient in the vapor phase. Following the arguments presented in standard texts (Smith and van Ness, 1975), the fugacity coefficient is, for a mixture,

$$\ln \phi_i = \int_{\bar{V}_M}^{\infty} \left[\left(\frac{\partial(nz)}{\partial n_i} \right)_{T,V,n} - 1 \right] \frac{d\bar{V}_M}{\bar{V}_M} - \ln z \quad (4.4-18a)$$

and, for a pure component,

$$\ln \phi = \int_{\bar{V}_M}^{\infty} (z-1) \frac{d\bar{V}_M}{\bar{V}_M} + z - 1 - \ln z \quad (4.4-18b)$$

Equation (4.4-18b) is a special case of Eq. (4.4-18a) as one of the x_i becomes unity. The partial derivative in the integral of Eq. (4.4-18a) is taken at constant temperature and total volume V , where n is the total number of moles in the mixture, and n_i is the total number of moles of species i in the phase. Clearly,

$$V = n\bar{V}_M, \quad n = \sum_{i=1}^{N_C} n_i, \quad \text{and} \quad x_i = n_i / n.$$

The fugacity coefficient definition (Eq. 4.4-18a) also can be written in a variety of equivalent forms (Smith and van Ness, 1975; Coats, 1980). To evaluate the integral in Eq. (4.4-18a), it is convenient to express z in an explicit form

$$z = \frac{\bar{V}_M}{\bar{V}_M - b} - \frac{a}{RT(\bar{V}_M + b)} \quad (4.4-19)$$

After multiplying Eq. (4.4-19) by n and introducing the mixing rules for a and b from Table 4-2, the resulting expression may be differentiated with respect to n_i . After some algebra, this gives

$$\left(\frac{\partial(nz)}{\partial n_i} \right)_{T,V,n} = \frac{\bar{V}_M}{\bar{V}_M - b} - \frac{\bar{V}_M b_i}{(\bar{V}_M - b_m)^2} - \frac{1}{RT} \left(\frac{\sum_j x_j a_{ij}}{\bar{V}_M + b_m} - \frac{ab_i}{(\bar{V}_M + b_m)^2} \right) \quad (4.4-20)$$

Equation (4.4-20) is explicit in \bar{V}_M which, when substituted into Eq. (4.4-18a) and integrated, leads to the closed-form expression given in Table 4-2. Similar procedures may be used on the PR equation (see Exercise 4F).

The actual calculation of vapor–liquid equilibria follows from two general procedures based on the EOS approach. From Eqs. (4.4-1) and (4.4-17), the equilibrium K -values become

$$K_i = \frac{\phi_i^L}{\phi_i^V}, \quad i = 1, \dots, N_C \quad (4.4-21)$$

since the component fugacities are equal at equilibrium. Thus based on an initial estimate of the K_i , a flash calculation, as described above, will obtain the vapor and liquid compositions from Eq. (4.4-5), the K -value definition, and the K_i calculated from Eq. (4.4-21). If the beginning and initial K -value estimates agree, the calculated compositions are the correct values; if they do not agree, new values of the K_i must be estimated and the entire procedure repeated until the K -values do not change. Since the flash calculation is itself a trial-and-error procedure, this procedure is somewhat analogous to the convergence pressure approach we already described.

The second approach to calculating vapor–liquid equilibria from EOS is to directly use the equilibrium constraints. Thus the equations

$$f_i^L = f_i^V, \quad i = 1, \dots, N_C \quad (4.4-22a)$$

may be regarded as a set of N_C independent simultaneous nonlinear equations in either x_i or y_i (but not both since x_i and y_i are related through the K -values) that may be linearized, solved as a system of simultaneous linear equations, and iterated until the phase compositions do not change. Either way the calculation is fairly convoluted, so it is not surprising that many variations of the procedure exist (Fussell and Fussell, 1979; Mehra et al., 1980).

Equation (4.4-22a) is easily generalized to the condition for equilibrium among any number of phases N_P

$$f_{ij} = f_{ik}, \quad i = 1, \dots, N_C; \quad j, k = 1, \dots, N_P \quad (4.4-22b)$$

Empirical Representations

There are three common empirical representations of phase behavior. All are used primarily for liquid–liquid equilibria.

Hand's rule. Hand (1939) gave a fairly simple representation of two-phase equilibria that has proved useful for some EOR systems (Pope and Nelson, 1978; Young and Stephenson, 1982). The procedure is based on the empirical observation that certain ratios of equilibrium phase concentrations are straight lines on log–log or *Hand plots*.

In this section, the concentration variable C_{ij} is the volume fraction of component i ($i = 1, 2$, or 3) in phase j ($j = 1$ or 2). Using volume fractions has become conventional in the Hand representation since these are convenient in liquid–liquid equilibria.

Figure 4-13 shows the one- and two-phase regions on the ternary diagram and its correspondence to the Hand plot. The line segments AP and PB represent the binodal curve portions for phase 1 and 2, respectively, and curve CP represents the distribution curve of the indicated components between the two phases. The ratios on the distribution curve are analogous to, but entirely different from, the definitions of the K -values given above. The equilibria relations based on the Hand plot are

$$\frac{C_{3j}}{C_{2j}} = A_H \left(\frac{C_{3j}}{C_{1j}} \right)^{B_H}, \quad j = 1, 2 \quad (4.4-23)$$

$$\frac{C_{32}}{C_{22}} = E_H \left(\frac{C_{31}}{C_{11}} \right)^{F_H} \quad (4.4-24)$$

where A_H, B_H, E_H, F_H are empirical parameters. Equation (4.4-23) represents the binodal curve, and Eq. (4.4-24) represents the distribution curve. In this form, these equations require the binodal curve to enter the corresponding apex of the ternary diagram. A simple modification overcomes this restriction (see Exercise 4G).

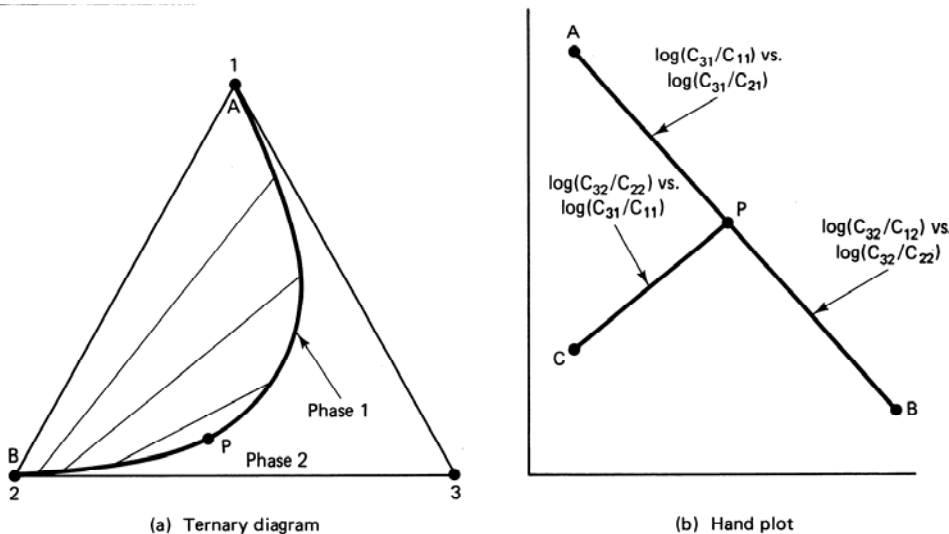


Figure 4-13 Correspondence between ternary diagram and Hand plot

Within the two-phase region of the binodal curve, there are six unknowns, the C_{ij} phase concentrations and five equations, three from Eqs. (4.4-23) and (4.4-24) and two consistency constraints

$$\sum_{i=1}^3 C_{ij} = 1, \quad j = 1, 2 \quad (4.4-25)$$

Thus there is $N_F = 1$ degree of freedom as required by the phase rule since temperature and pressure are fixed for ternary equilibria.

A flash calculation using the Hand procedure solves for the relative amounts of the two phases. This introduces two additional variables, S_1 and S_2 , into the calculation, but there are now three additional equations, the mass balance Eq. (4.3-1) with the overall concentrations C_i known and $S_1 + S_2 = 1$. As in all the phase equilibria flash calculations, the procedure is trial and error though for certain special cases, phase concentrations follow from direct calculation. The iterative procedure is to first pick a phase concentration (say, C_{32}), calculate all the other phase concentrations from Eqs. (4.4-23) through (4.4-25), and then substitute these into the tie line Eq. (4.3-2). If this equation is satisfied, convergence has been attained; if it is not satisfied, a new C_{32} must be picked and the procedure repeated until either C_{32} does not change or Eq. (4.3-2) is satisfied.

Two other empirical representations of the distribution of components between phases are of interest: the conjugate curve and the tie line extension curve. Both require separate representations of the binodal curve, as in Eq. (4.4-23).

Conjugate curve. The conjugate curve is a curve in ternary space whose coordinates define the ends of the tie lines. Thus for phases 1 and 2, the conjugate curve would be of the form

$$C_{11} = f(C_{22}) \quad (4.4-26)$$

Figure 4-14 shows the projections of the coordinates of this curve onto the binodal curve. The Hand distribution curve is of the form shown in Eq. (4.4-26). The conjugate curve must pass through the plait point.

Tie line extension curve. The tie line extension curve is another curve $C_3^0 = f(C_2^0)$ in ternary space that passes through the plait point, at which point it is tangent to the binodal curve (Fig. 4-15a). The two-phase tie lines are extensions of tangents from this curve through the binodal curve. Thus equations of the tie lines are given by straight lines having the equation

$$C_{3j} - f(C_2^0) = f'|_{C_2^0} (C_{2j} - C_2^0), \quad j=1 \text{ or } 2 \quad (4.4-27a)$$

where $f'|_{C_2^0}$ is the slope of the tie line extension curve evaluated at the coordinate C_2^0 . The tie lines follow from Eq. (4.4-27a), the equation of the extension curve, and the equation for the binodal curve.

A useful special case of the tie line extension curve occurs when all tie lines extend to a common point, as in Fig. 4-15(b). We need specify only the coordinates of this common point to define the equation for the tie lines

$$C_{3j} - C_3^0 = \eta (C_{2j} - C_2^0), \quad j=1 \text{ or } 2 \quad (4.4-27b)$$

where η is the slope of the tie line. Note that if $C_3^0 > 0$, the selectivity of the components for the two phases can reverse near the base of the ternary. The representation is extremely simple because it requires only two values: any two of the

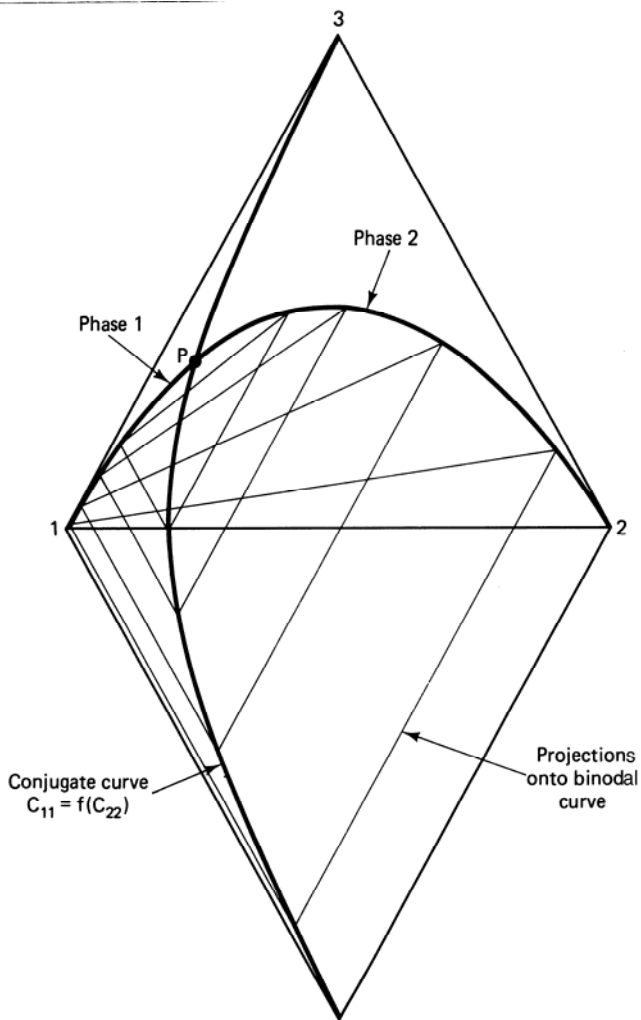


Figure 4-14 Schematic representation of a conjugate curve

coordinates C_i^0 or, alternatively, any of the plait point coordinates and one of the C_i^0 since the tie lines must be tangent to the binodal curve there.

This representation is far less general than either Eq. (4.4-24), (4.4-26), or (4.4-27). But experimental accuracy is often not enough to warrant more complicated equations. Moreover, the form (Eq. 4.4-27b) is extremely convenient for calculating the flow behavior of two-phase mixtures; we use it extensively in Chaps. 7 and 9.

4-5 CONCLUDING REMARKS

Multiple representations of phase behavior are clear evidence that no single method is sufficient. In most cases we find ourselves compromising between accuracy and mathematical ease in the resulting calculation. Our goal here is the exposition of the

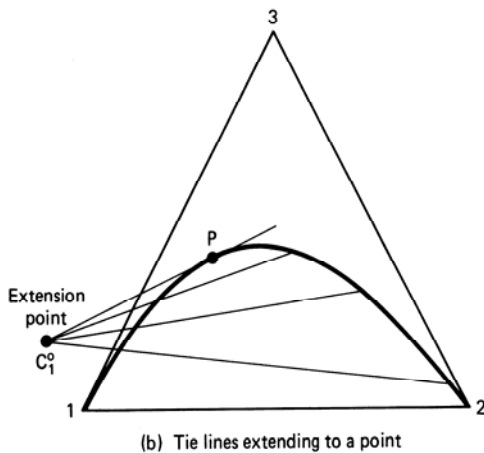
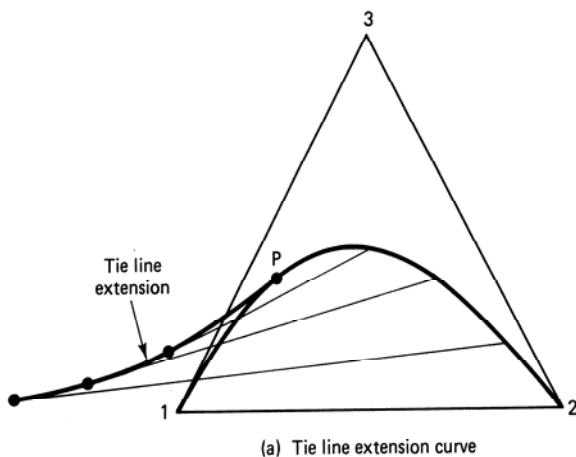


Figure 4-15 Tie line extension representation of phase behavior

underlying principles of EOR phenomena; hence we emphasize phase behavior representations which lend themselves to visual or graphical analysis in later calculations—as long as the representations themselves are qualitatively correct. The important points to grasp in this chapter, then, are graphical representations in Sec. 4-3, particularly as related to the ternary diagram; the physical meaning of tie lines and binodal curves; and the component distribution expressed by Eqs. (4.4-23), (4.4-24), and (4.4-27b).

EXERCISES

- 4A.** *Pure Component Phase Behavior.* Sketch the following for a pure component:
- Lines of constant pressure on a temperature–molar-volume plot
 - Lines of constant temperature on a density–pressure plot
 - Lines of constant molar volume on a temperature–pressure plot

- 4B.** *Paths on a Pressure–Volume Plot.* Indicate the paths AA' , BB' , and DD' , shown on the pressure–specific-volume plot in Fig. 4B, on the corresponding pressure–temperature plot.

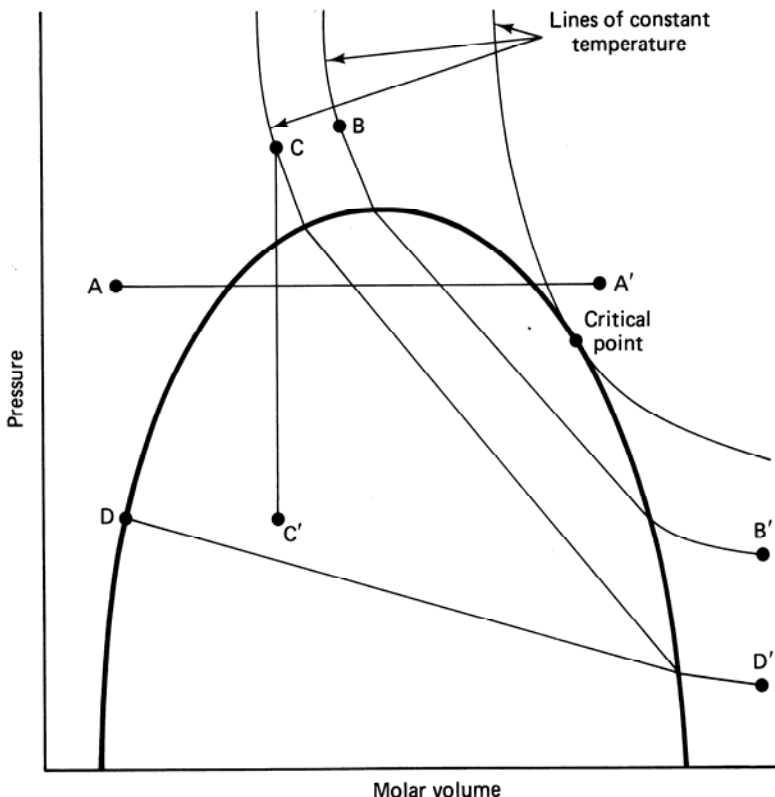


Figure 4B Pressure–specific-volume plot for Exercise 4B

- 4C.** *Migration of P-T Envelope.* Figure 4C shows the hypothetical change in the pressure–temperature envelope of a crude oil as it is diluted with a more volatile component (CO_2). The quality lines within each envelope are in volume percent. For this data, sketch the pressure–composition diagram at 340 K and 359 K (152°F and 180°F). These temperatures are the critical temperatures for the 40% and 20% CO_2 mixtures. Include as many quality lines as possible.
- 4D.** *Lever Rule Application.* Consider the three-component system represented in Fig. 4-11.
- Estimate the relative amounts of each phase present at overall compositions A , C , D , and E .
 - Derive the expressions (indicated on the figure) for the relative amounts of each phase present at the three-phase overall composition.
 - Estimate the relative amounts of each phase present at B .
- 4E.** *Parameters for RKS and RP Equations of State*
- Derive the parameters a and b for the RKS equation using the critical constraints and the original equation given in Table 4-1.
 - Derive the parameters a and b for the PR equation using the procedure of Martin and Hou (1955). Compare your results to Table 4-2.

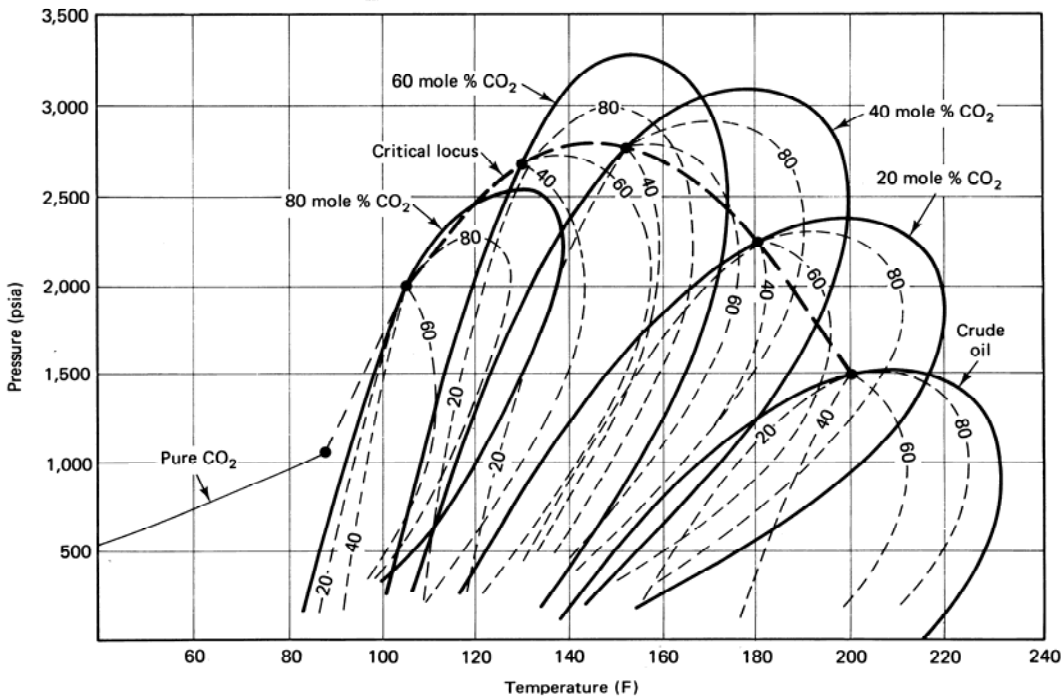


Figure 4C Change in crude oil pressure–temperature diagram with dilution by CO_2

- 4F.** *Fugacity Coefficient from an Equation of State*
- Derive the expressions for the fugacity coefficient starting with Eq. (4.4-18a) for the PR equation.
 - Show for both the PR and RKS equations that the fugacity coefficient for a mixture approaches that of a pure component as one of the x_i approaches 1.
- 4G.** *Partially Soluble Binaries (Welch, 1982).* For cases when the partially soluble binaries on a ternary plot have some mutually soluble region, the Hand representation may be altered as

$$\frac{C'_{3j}}{C'_{2j}} = A_H \left(\frac{C'_{3j}}{C'_{1j}} \right)^{B_H}, \quad j = 1, 2 \quad (4G-1)$$

and

$$\frac{C'_{32}}{C'_{22}} = E_H \left(\frac{C'_{31}}{C'_{11}} \right)^{F_H} \quad (4G-2)$$

where the C_{1j} are normalized concentrations

$$C'_{1j} = \frac{C_{1j} - C_{1L}}{C_{1U} - C_{1L}} \quad (4G-3)$$

$$C'_{2j} = \frac{C_{2j} - (1 - C_{1U})}{C_{1U} - C_{1L}} \quad (4G-4)$$

$$C'_{3j} = \frac{C_{3j}}{C_{1U} - C_{1L}} \quad (4G-5)$$

C_{1U} and C_{1L} are the upper and lower solubility limits of the 1-2 binary. Take $B_H = -1$ and $F_H = 1$ in the following.

- (a) Derive an expression for A_H in terms of the true maximum height of the binodal curve $C_1 - C_2$. Show that the binodal curve takes value $C_{3\max}$ when $C'_1 = C'_2$ (symmetrical in normalized concentrations).
- (b) Express E_H as a function of A_H and the component 1 coordinate of the plait point (C_{1p}). The A_H and E_H in parts (a) and (b) will also be a function of C_{1U} and C_{1L} .
- (c) Plot the binodal curve and the two representative tie lines for $C_{1U} = 0.9$, $C_{1L} = 0.2$, $C_{3\max} = 0.5$, and $C_{1p} = 0.3$.

- 4H.** *Using the Hand Representations.* The following data were collected from a three-component system at fixed temperature and pressure.

Phase 1		Phase 2	
Component 1	Component 2	Component 1	Component 2
0.45	0.31	0.015	0.91
0.34	0.40	0.020	0.89
0.25	0.48	0.030	0.85
0.15	0.60	0.040	0.82

The concentrations are in volume fractions.

- (a) On a ternary diagram, plot as many tie lines as possible, and sketch in the binodal curve.
 - (b) Make a Hand plot from the data, and determine the parameters A_H , B_H , E_H , and F_H .
 - (c) Estimate the coordinates of the plait point from the plot in part (b).
- 4I.** *Application of Conjugate Curve.* Consider the ternary diagram in Fig. 41 for a three-component system. The binodal curve is the solid line, and the conjugate curve the dotted line.
- (a) Sketch in three representative tie lines.
 - (b) For the overall composition, marked as A , give the equilibrium phase compositions and the relative amounts of both phases.
 - (c) Plot the two-phase equilibria on a Hand plot.
 - (d) If the Hand equations are appropriate, determine the parameters A_H , B_H , E_H , and F_H .

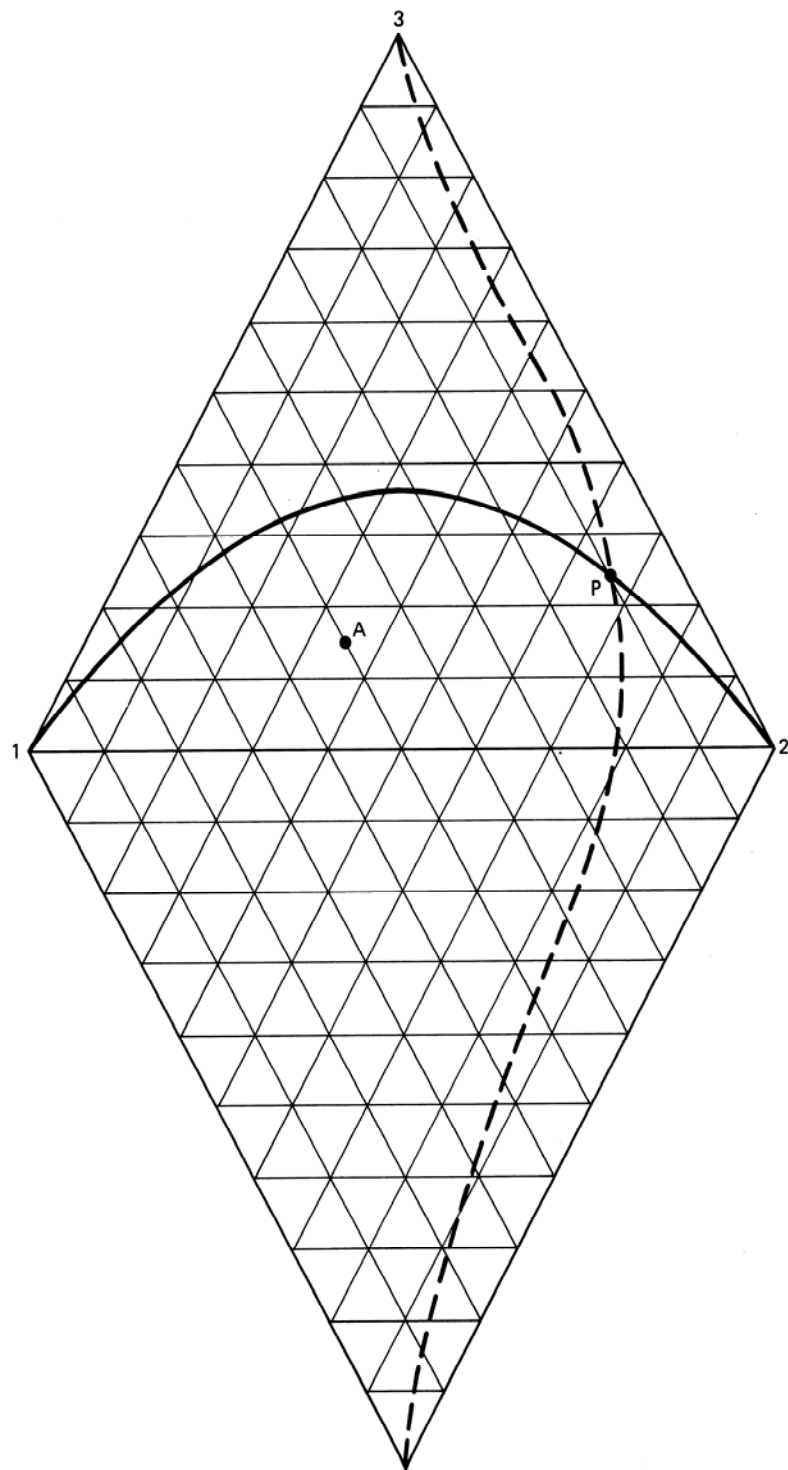


Figure 4I Diagram for Exercise 4I

5

Displacement Efficiency

The definitions for recovery, displacement, and sweep efficiencies in Eq. (2.5-5) apply to an arbitrary chemical component, but they are almost exclusively applied to oil and gas displacement. Since displacement efficiency and sweep efficiency are multiplied by each other, they are equally important to the magnitude of the recovery efficiency and, hence, the oil recovery. In Chap. 6, we discuss volumetric sweep efficiency; in this chapter, we present fundamental concepts in displacement efficiency.

For the most part, we restrict our discussion to oil displacement efficiency based on solutions to the fractional flow Eq. (2.4-3). We apply these equations to displacements in one-dimensional, homogeneous, isotropic permeable media. Thus, the results apply most realistically to displacements in laboratory floods, the traditional means of experimentally determining displacement efficiency. These results do not, of course, estimate recovery efficiency for three-dimensional, nonlinear flows without correcting for volumetric sweep efficiency and without correcting the displacement efficiency to account for differences in scale.

5-1 DEFINITIONS

If we assume constant oil density, the definition of displacement efficiency for oil becomes

$$E_D = \frac{\text{Amount of oil displaced}}{\text{Amount of oil contacted by displacing agent}} \quad (5.1-1)$$

E_D is bounded between 0 and 1. The rate at which E_D approaches 1 is strongly affected by the initial conditions, the displacing agent, and the amount of displacing agent. Fluid, rock, and fluid–rock properties also affect E_D . If the displacement is such that the displacing agent will contact all the oil initially present in the medium, the volumetric sweep efficiency will be unity, and E_D becomes the recovery efficiency E_R .

From Eq. (2.5-4) then,

$$E_D = 1 - \frac{\bar{S}_2}{\bar{S}_{2I}} \quad (5.1-2)$$

for an incompressible, single-component oil phase flowing in an incompressible permeable medium. Equation (5.1-2) says E_D is proportional to the average oil saturation in the medium. For cases where the oil may occur in more than one phase, or where more than oil can exist in the hydrocarbon phase, we must use the general definition (Eq. 2.5-5b).

5-2 IMMISCIBLE DISPLACEMENT

Virtually all of our understanding about EOR displacements begins with an understanding of the displacement of one fluid by an immiscible second fluid. The specific case of water displacing oil was first solved by Buckley and Leverett (1942) and later broadened by Welge (1952). In this section, we develop the Buckley-Leverett theory in a manner much like the original paper and several subsequent references (Collins, 1976; Craig, 1971; Dake, 1978).

For the isothermal flow of oil and water in two immiscible, incompressible phases in a one-dimensional permeable medium, the mass conservation equations of Table 2-2 reduce to

$$\phi \frac{\partial S_1}{\partial t} + u \frac{\partial f_1}{\partial x} = 0 \quad (5.2-1)$$

for flow in the positive x direction, as we discussed in Chap. 2. In this equation, f_1 is the fractional flow of water,

$$f_1 = \frac{u_1}{u} = \frac{\lambda_{r1}}{\lambda_{r1} + \lambda_{r2}} \left(1 - \frac{k \lambda_2 \Delta \rho g \sin \alpha}{u} \right) \quad (5.2-2)$$

in the absence of capillary pressure. In Eq. (5.2-2), α is the dip angle defined to be positive when measured in the counterclockwise direction from the horizontal, and $\Delta \rho = \rho_1 - \rho_2$ is the density difference between the water and oil phases.

The choice of S_1 as the dependent variable in Eq. (5.2-1) is largely a matter of convention; we could easily have chosen S_2 since $S_2 + S_1 = 1$, and $f_2 + f_1 = 1$. An important point is that in the absence of capillary pressure, f_1 is uniquely determined as a function of S_1 only through the relative permeability relations $\lambda_{r1} = k_{r1}/\mu_1$ and

$\lambda_{r2} = k_{r2} / \mu_2$ discussed in Sec. 3-3. In fact, since the shape of the f_1 - S_1 curve proves to be the main factor in determining the character of the displacement, we digress briefly to discuss how flow conditions affect this curve.

Fractional Flow Curves

If we introduce the exponential form of the oil–water relative permeability curves (Eq. 3.3-4) into Eq. (5.2-2), we obtain

$$f_1 = \frac{1 - N_g^0 (1 - S)^{n_2} \sin \alpha}{1 + \frac{(1 - S)^{n_2}}{M^0 S^{n_1}}} \quad (5.2-3a)$$

where

$$S = \frac{S_1 - S_{1r}}{1 - S_{2r} - S_{1r}} = \text{Reduced water saturation} \quad (5.2-3b)$$

and

$$M^0 = \frac{k_{r1}^0 \mu_2}{\mu_1 k_{r2}^0} = \text{Endpoint water–oil mobility ratio} \quad (5.2-3c)$$

$$N_g^0 = \frac{k k_{r2}^0 \Delta \rho g}{\mu_2 u} = \text{Gravity number} \quad (5.2-3d)$$

N_g^0 is the ratio of gravity to viscous pressure gradients based on the endpoint oil relative permeability. In the form of Eq. (5.2-3a), f_1 depends parametrically on M^0 , N_g^0 , α , and the shape of the relative permeability curves (n_1 and n_2). The f_1 - S_1 curve is sensitive to all these factors, but usually M^0 and N_g^0 are most important. Figure 5-1 shows f_1 - S_1 curves for various values of M^0 and $N_g^0 \sin \alpha$ with the other parameters fixed ($S_{1r} = 0.2$, $S_{2r} = 0.2$, $n_1 = n_2 = 2$). The S-shaped curves have an inflection point that varies with M^0 and $N_g^0 \sin \alpha$. The curvature of all curves generally becomes more negative as M^0 increases or $N_g^0 \sin \alpha$ decreases. The curves where f_1 is less than 0 or greater than 1 are physically correct. This circumstance indicates a flow where gravity forces are so strong that flow in the negative x direction occurs (water flows in the negative x direction for $f_1 < 0$). In Sec. 3-3, we showed that shifting the wettability of the permeable medium from water wet to oil wet caused k_{r1}^0 to increase and k_{r2}^0 to decrease. Thus for constant phase viscosities, making the medium more oil wet is qualitatively equivalent to increasing M^0 . But for fixed relative permeability curves, the effect of increasing μ_1 or decreasing μ_2 is to decrease M^0 .

Buckley-Leverett Solution

Returning now to Eq. (5.2-1), to calculate E_D , we seek solutions $S_1(x, t)$ subject to the initial and boundary conditions

$$S_1(x, 0) = S_{1I}, \quad x \geq 0 \quad (5.2-4a)$$

$$S_1(0, t) = S_{1J}, \quad t \geq 0 \quad (5.2-4b)$$

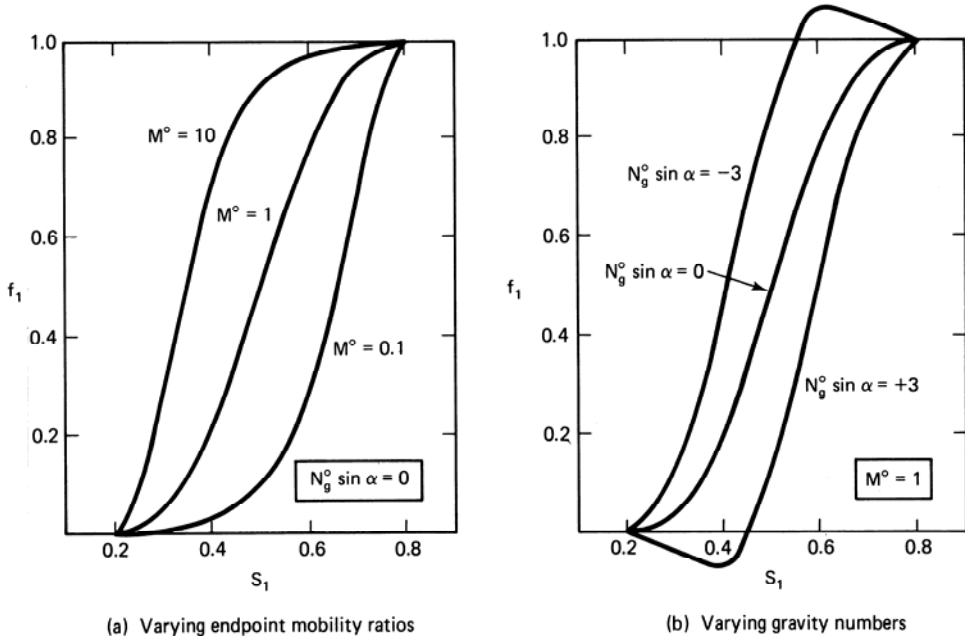


Figure 5-1 Fractional flow curves for $m = n = 2$ and $S_{1r} = S_{2r} = 0.2$

In core floods, a specified fractional flow is usually imposed on the inflow ($x = 0$) so that we may replace Eq. (5.2-4b) with

$$f_1(0, t) = f_1(S_1(0, t)) = f_{1J} = f_1(S_{1J}), \quad t \geq 0 \quad (5.2-4c)$$

This equation shows that f_1 is a function of x and t only through its dependence on S_1 . The definition used in a given instance depends on the particular application. The conditions (Eqs. 5.2-4) also have a convenient geometrical interpretation in xt space because at the point $t = x = 0$, all values of S_1 between S_{1I} and S_{1J} exist. The Buckley-Leverett problem is usually posed with S_{1I} and S_{1J} taken to be S_{1r} and $1 - S_{2r}$, respectively.

For greater generality, we render Eqs. (5.2-1) and (5.2-4) into the following dimensionless forms:

$$\left(\frac{\partial S_1}{\partial t_D} \right) + \left(\frac{df_1}{dS_1} \right) \left(\frac{\partial S_1}{\partial x_D} \right) = 0 \quad (5.2-5a)$$

$$S_1(x_D, 0) = S_{1I}, \quad x_D \geq 0 \quad (5.2-5b)$$

$$S_1(0, t_D) = S_{1J}, \quad t_D \geq 0 \quad (5.2-5c)$$

where the dimensionless variables x_D and t_D are

$$x_D = \frac{x}{L} = \text{Dimensionless position} \quad (5.2-6a)$$

$$t_D = \int_0^t \frac{udt}{\phi L} = \text{Dimensionless time} \quad (5.2-6b)$$

L is the total macroscopic permeable medium dimension in the x direction. In these equations, u may be a function of time but not of position because of the assumption of incompressibility. Moreover, df_i/dS_1 is a total derivative since f_i is a function of S_1 only. Introducing dimensionless variables reduces the number of parameters in the problem from four (ϕ , u , S_{1I} , and S_{1J}) in Eqs. (5.2-1) and (5.2-4) to two (S_{1I} and S_{1J}). We could further reduce the number by redefining the dependent variable S_1 (see Exercise 5A).

The dimensionless time t_D can also be expressed as

$$t_D = \int_0^t \frac{Audit}{\phi AL} = \int_0^t \frac{qdt}{V_p} \quad (5.2-7)$$

where A is the cross-sectional area of the one-dimensional medium in the direction perpendicular to the x axis, q is the volumetric flow rate, and V_p is the pore volume. t_D is the total volume of fluid injected up to time t divided by the total pore volume of the medium. In principle, V_p is well defined even for a highly irregular geometry so that t_D is a scaling variable in virtually any application. In fact, t_D is the fundamental variable used to scale from the laboratory to the field. It has been used with a wide variety of definitions for the reference volume V_p (see Table 5-1). Numerical values of t_D are frequently given as “fraction of a pore volume,” or simply “pore volume”; thus it is easy to confuse with V_p , the actual pore volume, which has units of L^3 (t_D , of course, has no units).

We seek solution to Eqs. (5.2-5) in the form $S_1(x_D, t_D)$. S_1 may be written as a total differential

$$dS_1 = \left(\frac{\partial S_1}{\partial x_D} \right)_{t_D} dx_D + \left(\frac{\partial S_1}{\partial t_D} \right)_{x_D} dt_D \quad (5.2-8)$$

TABLE 5-1 TABULATION OF VARIOUS DEFINITIONS FOR DIMENSIONLESS TIME

Reference volume	Usage
Area \times length \times porosity	Core floods
Area \times thickness \times porosity ($A\phi h = V_p$ = total pore volume)	General
$V_p \times$ volumetric sweep efficiency ($V_p \times E_v$ = floodable pore volume = V_{PF})	Micellar polymer floods
$V_{PF} \times \Delta S_2$ = movable pore volume	Waterfloods
$V_{PF} \times S_{2I}$ = hydrocarbon pore volume (HCPV)	Miscible floods
Note: $t_D = \frac{\text{Total volume of fluid injected}}{\text{Reference volume}}$ } consistent units	

from which follows that the velocity v_{S_1} of a point with constant saturation S_1 in $x_D t_D$ space is

$$\left(\frac{dx_D}{dt_D} \right)_{S_1} = - \frac{(\partial S_1 / \partial t_D)_{x_D}}{(\partial S_1 / \partial x_D)_{t_D}} \equiv v_{S_1} \quad (5.2-9)$$

v_{S_1} is the “specific” velocity of the saturation S_1 because it has been normalized by the bulk fluid interstitial velocity u/ϕ . It is dimensionless. You can see this by converting Eq. (5.2-9) back to dimensional quantities using the definitions (Eqs. 5.2-6).

Eliminating either of the derivatives in Eq. (5.2-9) by Eq. (5.2-5a) gives

$$v_{S_1} = \frac{df_1}{dS_1} = f'_1 \quad (5.2-10)$$

This equation says the specific velocity of a constant saturation S_1 is equal to the derivative of the fractional flow curve at that saturation. In dimensional form, Eq. (5.2-10) is the Buckley-Leverett equation. Since all saturations between S_{1I} and S_{1J} are initially at the origin in $x_D t_D$ space, and v_{S_1} is defined with S_1 constant, the position of any saturation $S_{1I} \leq S_1 \leq S_{1J}$ at a given t_D is

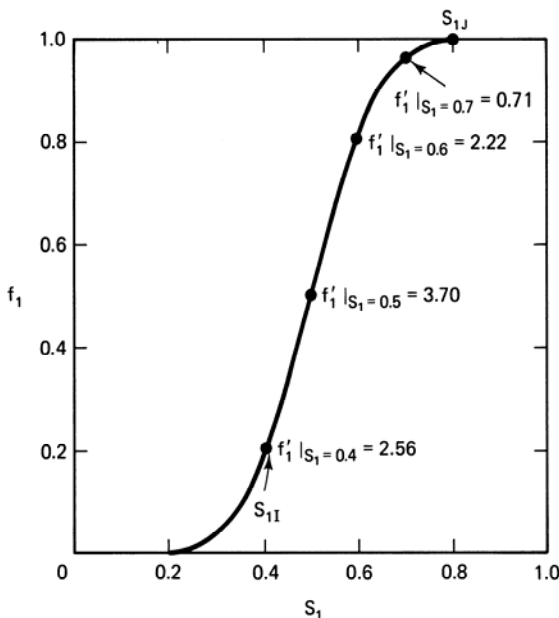
$$x_D |_{S_1} = \frac{df_1}{dS_1} \Big|_{S_1} t_D = f'_1(S_1) t_D \quad (5.2-11)$$

where we include evaluation symbols to help clarify the subsequent development. Equation (5.2-11) is the solution to the one-dimensional water-displacing-oil problem; by selecting several S_1 ’s between S_{1I} and S_{1J} , we can construct $S_1(x_D, t_D)$. Figure 5-2(a) shows the procedure for one of the fractional flow curves of Fig. 5-1. Except for relatively simple cases (see Exercise 5E), the relation (Eq. 5.2-11) generally cannot be solved explicitly for $S_1(x_D, t_D)$.

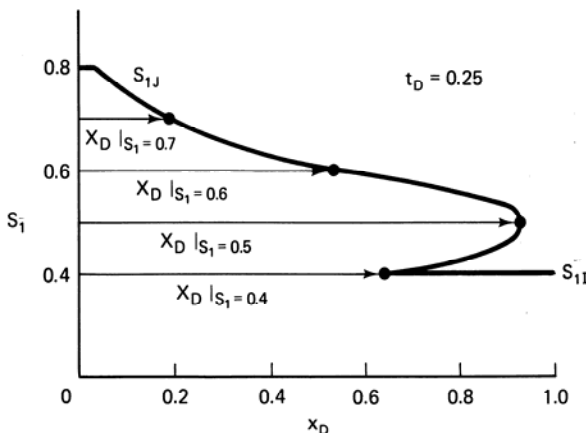
Shock Formation

Figure 5-2(a) also shows a disconcerting tendency for an S-shaped f_1 - S_1 curve to generate solutions that have three values of S_1 at the same x_D and t_D . In Fig. 5-2(b), this occurs for $0.64 < x_D < 0.94$. Of course, such triple values are nonphysical though they are entirely valid mathematically. The triple values are the result of the saturation velocity v_{S_1} increasing over some saturation region ($S_{1I} < S_1 < S'_1$ in Fig. 5-2) as S_1 changes from its initial (downstream) value to the final (upstream) value.

We eliminate the triple value region by invoking the formation of *shocks*, discontinuous changes in a physical quantity such as pressure (as in the case of sonic booms), concentration, or in this case, saturation. Shocks are characteristic features of hyperbolic equations, a class of which are the dissipation-free conservation equations. Strictly speaking, shocks are not present in nature since some dissipation (dispersion, diffusion, capillary pressure, compressibility, and thermal conductivity) is always present, which militates against their formation. When such effects are present, the shocks are smeared or spread out around the shock front position, but the position of the shock is unaltered. Despite this restriction, shocks play a central role



(a) Slopes of a fractional flow curve

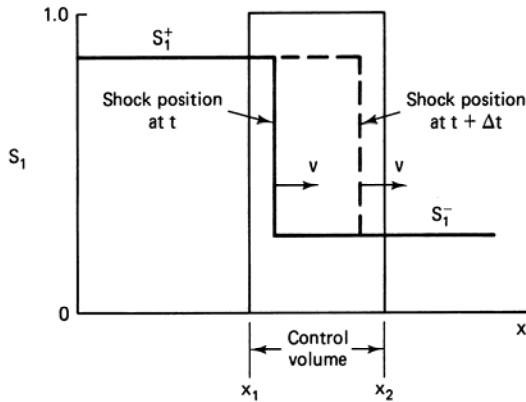


(b) Corresponding saturation profile

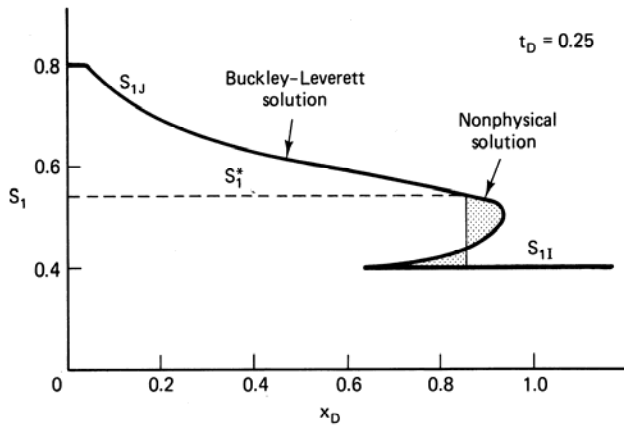
Figure 5-2 Buckley-Leverett construction of $S_1(x_D, t_D)$

in fractional flow theory, where dissipative effects are neglected, and describe many actual flows to a good approximation.

To calculate the velocity and magnitude of the shock, we recast the differential equations of this chapter into difference equations. This we do generally in Sec. 5-4; here we restrict ourselves to the water-displacing-oil problem already begun. Paradoxically, we find that calculations are considerably easier when shocks form. Figure 5-3(a) shows a water saturation shock moving from left to right. The water saturation ahead of the shock is S_1^- (downstream direction), and that behind



(a) Schematic of material balance around shock



(b) Saturation profile for fractional flow curve of Fig. 5-2(a)

Figure 5-3 Water saturation profiles with shocks

the shock is \$S_1^+\$ (upstream direction). The quantity \$\Delta S_1 = S_1^+ - S_1^-\$ is the saturation jump across the shock. A cumulative water balance on a control volume that contains the shock in the time interval \$\Delta t\$ is

$$\begin{aligned} \left(\text{Volume water present at } t + \Delta t \right) - \left(\text{Volume water present at } t \right) &= \left(\text{Volume water in during } \Delta t \right) - \left(\text{Volume water out during } \Delta t \right) \\ [(v(t + \Delta t) - x_1)S_1^+ + (x_2 - v(t + \Delta t))S_1^-]A\phi &= [f_1(S_1^+) - f_1(S_1^-)] \int_t^{t + \Delta t} q dt \end{aligned}$$

After some cancellation, we obtain a specific shock velocity

$$v_{\Delta S_1} = \frac{f_1(S_1^+) - f_1(S_1^-)}{S_1^+ - S_1^-} \equiv \frac{\Delta f_1}{\Delta S_1} \quad (5.2-12)$$

To incorporate shock formation into the water-displacing-oil problem, consider a saturation profile containing a triple value over some region and containing a single value elsewhere (Fig. 5-3b). In general, some saturation S_1^* will mark the end of the continuous water saturation region and the beginning of a shock. This saturation must simultaneously satisfy Eqs. (5.2-10) and (5.2-12); Eq. (5.2-12) gives velocities of S_1 greater than S_1^* , and Eq. (5.2-10) gives velocities of S_1 less than S_1^* . Equating Eqs. (5.2-10) and (5.2-12) yields the following equation for S_1^* :

$$f'_1|_{S_1^*} = \frac{f_1(S_1^*) - f_1(S_{1I})}{S_1^* - S_{1I}} \quad (5.2-13)$$

where we have taken $S_1^- = S_{1I}$ in Eq. (5.2-12). Equation (5.2-13) lends itself to a graphical solution since

$$f_1 - f_1(S_{1I}) = m(S_1 - S_{1I}) \quad (5.2-14)$$

is the equation of a straight line of slope m passing through the point (f_{1I}, S_{1I}) on the fractional flow plot. If $m = f'_1|_{S_1^*}$, then m is the slope of the fractional flow plot at S_1^* . Comparing Eq. (5.2-14) to Eq. (5.2-13), S_1^* is at the tangent to the fractional flow curve of a straight line passing through the point (f_{1I}, S_{1I}) . Figure 5-4 schematically illustrates this construction. The slope of this straight line is the specific shock

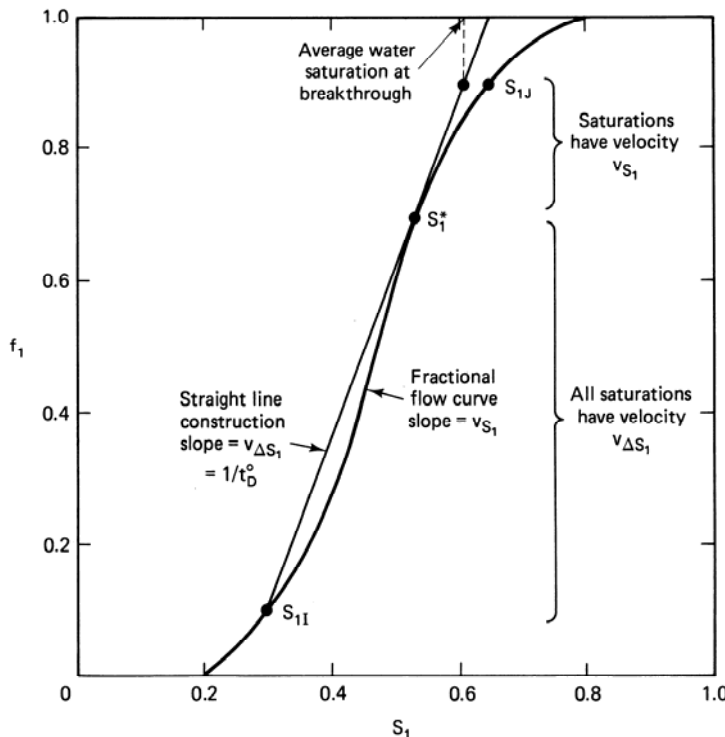


Figure 5-4 Schematic illustration of shock construction

velocity. The shock itself is a discontinuous change in saturation from S_{1I} to S_1^* at $x_D = v_{\Delta S_1} t_D$ as Fig. 5-3(b) illustrates. The saturation S_1^* is not the same as S_1^- (Fig. 5-2), the saturation having the largest v_{S_1} . S_1^* is the saturation whose position requires the net area between the mathematical solution and the physical solution (shaded region in Fig. 5-3b) to be zero. This requires the shock to preserve the material balance. With this construction, all saturation velocities are monotonically (though not continuously) decreasing in the upstream direction. Figure 5-3(b) illustrates the results of the entire construction. The resulting saturation profile is sometimes called the leaky piston profile.

Wave Classification

Before further developing this theory and its applications to EOR, we define a few more terms used in subsequent discussions. These definitions are important to the interpretation of x_D-t_D plots that graphically present the solution $S_1(x_D, t_D)$.

We have been discussing how to calculate water saturation as a function of position and time for water–oil displacements. A plot of saturation, or concentration, versus time at fixed position is a saturation *history*. If the fixed position in such a plot is at the outflow end of the permeable medium, it is an *effluent history*. Plots of saturation versus position at fixed time are saturation *profiles*. Figure 5-2(b) is a water saturation profile. Changes in saturation with time and position are saturation *waves*. Thus the previous development estimates the rate of propagation of waves through a permeable medium.

An important and unifying aspect of our understanding of EOR displacements is the study and characterization of the number and types of waves they form. Depending on their spreading characters, waves may be classified into four categories.

1. A wave that becomes more diffuse on propagation is a nonsharpening, rarified, or *spreading* wave. When these waves occur, the rate of spreading is usually much larger than that caused by dissipation.
2. A wave that becomes less diffuse on propagation is a *sharpening* wave. In the absence of dissipation, these waves will become shocks even if the initial saturation profile is diffuse. When dissipation is present, these waves will asymptotically approach a *constant pattern* condition (see Sec. 5-3).
3. A wave that has both spreading and sharpening character is *mixed*. The Buckley-Leverett water saturation wave of Fig. 5-2(b) is mixed, being a sharpening wave for $S_{1I} < S_1 < S_1^*$ and a spreading wave for $S_1^* < S_1 < S_{1J}$.
4. A wave that neither spreads nor sharpens on propagation is *indifferent*. In the absence of dissipation, indifferent waves appear as shocks.

This behavior may be summarized by defining a dimensionless mixing or transition zone Δx_D . This is the fraction of the total system length that lies between arbitrary saturation limits at a given time. We take the saturation limits to be 0.1 and

0.9 of the span between the initial and injected saturations

$$\Delta x_D(t_D) = x_D|_{S_{0,1}} - x_D|_{S_{0,9}} \quad (5.2-15a)$$

where

$$S_{0,1} = 0.1(S_{1,I} - S_{1,I}) + S_{1,I} \quad (5.2-15b)$$

$$S_{0,9} = 0.9(S_{1,I} - S_{1,I}) + S_{1,I} \quad (5.2-15c)$$

The exact value of the limits is unimportant to the behavior of the mixing zone. The wave classification, which may be restated as Δx_D , increases with time for spreading waves, decreases for sharpening waves, and either increases or decreases for mixed waves depending on whether the shock portion of the wave exceeds the saturations used to define Δx_D . The mixing zone concept has general use in classifying mixing phenomena in a wide variety of displacements.

The final definition concerning the Buckley-Leverett development is the *time-distance diagram*. These diagrams are plots of x_D versus t_D on which appear lines of constant saturation. Figure 5-5 shows a time-distance diagram for the water-oil displacement in Figs. 5-3(b) and 5-4. The constant saturation curves are straight lines with slope given by v_{S_1} from Eq. (5.2-9). Similarly, shocks are the bold straight lines with slope given by Eq. (5.2-12). The region having varying saturation is shaded. Regions of constant saturation are adjacent to the waves and have no saturation lines. Time-distance diagrams are very convenient since they subsume both profiles and histories.

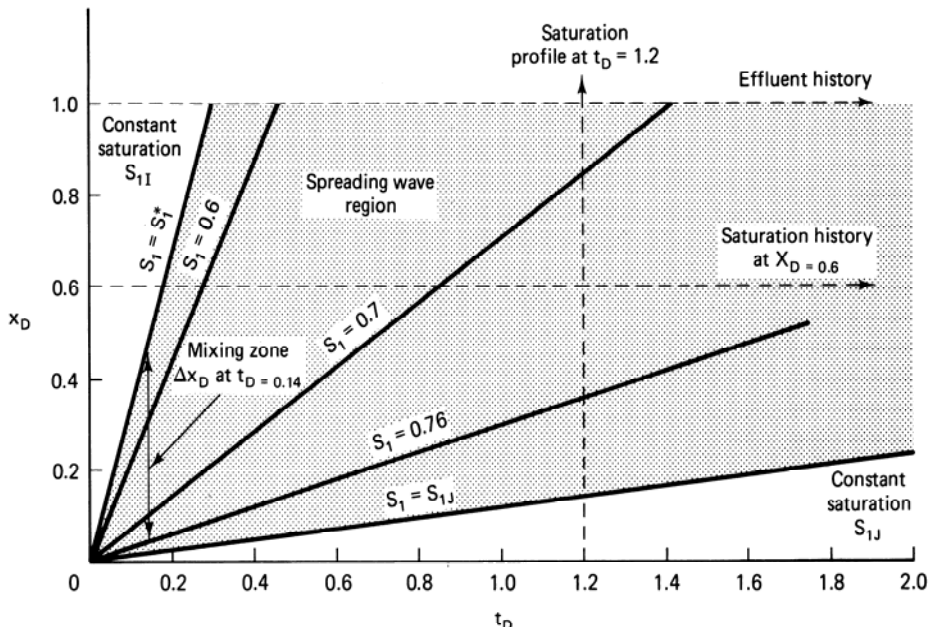


Figure 5-5 Time-distance diagram for displacement of Figs. 5-3(b) and 5-4

From the definition of effluent history, the shock portion of the water–oil displacement arrives at $x_D = 1$ when

$$t_D^0 = \frac{S_1^* - S_{1I}}{f_1^* - f_{1I}} \quad (5.2-16a)$$

from Eqs. (5.2-12) and (5.2-13). The *breakthrough time* t_D^0 is an important event in the displacement; for values $t_D > t_D^0$, we are producing some of the water being injected. The obvious inefficiency of this should suggest that we would like to conduct the displacement so that t_D^0 is as large as possible; that is, we would like to enhance the shock-forming character of the displacement. For $t_D > t_D^0$, the water saturation at the outflow end is given implicitly by

$$f'_1|_{x_D=1} = \frac{1}{t_D} \quad (5.2-16b)$$

from Eq. (5.2-10). In laboratory floods, it is usually more direct to measure $f_1|_{x_D=1}$, the water “cut,” than the saturation at the effluent end. The water and oil cuts ($1 - f_1|_{x_D=1}$) are functions of only time from Eq. (5.2-16b).

Average Saturations

In the displacement efficiency, we must have some way to calculate average saturations since, from Eq. (5.1-2), these appear in the definition of E_D . These averages are provided by the Welge integration procedure (Welge, 1952). Consider the saturation profile in Fig. 5-3(b) at fixed t_D , and let x_{D1} be any dimensionless position at or behind the shock front position, $x_{D1} \leq v_{\Delta S_1} t_D$. The average water saturation behind x_{D1} is

$$\hat{S}_1(t_D) = \frac{1}{x_{D1}} \int_0^{x_{D1}} S_1 dx_D \quad (5.2-17)$$

Equation (5.2-17) may be integrated by parts

$$\hat{S}_1 = \frac{1}{x_{D1}} \left((x_D S_1)|_0^{x_{D1}} - \int_{S_{1I}}^{S_{11}} x_D dS_1 \right) \quad (5.2-18)$$

where $S_{11} = S_1|_{x_{D1}}$. Since x_{D1} is in the spreading portion of the saturation wave, the x_D integrand may be substituted by Eq. (5.2-11)

$$\hat{S}_1 = S_{11} - \frac{1}{x_{D1}} \int_{S_{1I}}^{S_{11}} t_D f'_1 dS_1 \quad (5.2-19)$$

which may be readily integrated (recall t_D is fixed) to

$$\hat{S}_1 = S_{11} - \frac{t_D}{x_D} (f_{11} - f_{1I}) \quad (5.2-20)$$

Equation (5.2-20) relates the average water saturation behind x_{D1} to the fractional flow and saturation at that point. t_D may be replaced by Eq. (5.2-11) at this point to give

$$\hat{S}_1 = S_{11} - \frac{(f_{11} - f_{1J})}{f'_{11}} \quad (5.2-21)$$

Equation (5.2-21) is the final form of the Welge integration.

The most common use of this procedure is to let $x_{D1} = 1$ after water breakthrough ($t_D \geq t_D^0$), at which point $\hat{S}_1 = \bar{S}_1$, and f_{11} becomes the water cut. Thus the water saturation at the outflow end may be calculated from Eq. (5.2-20) as

$$S_1|_{x_D=1} = \bar{S}_1 - t_D(f_{1J} - f_1|_{x_D=1}) \quad (5.2-22)$$

If we know the water cut and average water saturation from direct measurement, simultaneously applying Eqs. (5.2-16) and (5.2-22) provides a way of estimating fractional flow curves ($f_1|_{x_D=1}$ versus $S_1|_{x_D=1}$ or f_{11} versus S_{11}) from experimental data.

The average water saturation follows from Eq. (5.2-21) for \bar{S}_1 with the f_1 - S_1 curve known. This equation may be rearranged to give

$$f_1|_{x_D=1} - f_{1J} = f'_1|_{x_D=1} (S_1|_{x_D=1} - \bar{S}_1) \quad (5.2-23)$$

Thus \bar{S}_1 at any $t_D \geq t_D^0$ is given by the extension of a straight line tangent to the fractional flow curve at $(f_1, S_1)|_{x_D=1}$ to intersect with the y coordinate at $f_1 = f_{1J}$. The dimensionless time required to bring this point to $x_D = 1$ is the reciprocal slope of this line from Eq. (5.2-16). Figure 5-4 shows the graphical procedure for this. From the \bar{S}_1 thus determined, $\bar{S}_2 = 1 - \bar{S}_1$ may be used in the definition (Eq. 5.1-2) to calculate E_D .

The above construction and Eqs. (5.2-22) and (5.2-23) apply only to dimensionless times after breakthrough. Before breakthrough the average water saturation is

$$\bar{S}_1 = S_{1I} + t_D(f_{1J} - f_{1I}), \quad t_D < t_D^0 \quad (5.2-24)$$

by applying the overall water material balance (Eq. 2.5-2) to this special case. Equations (5.2-22) and (5.2-24) are identical except for the value used for the effluent water cut.

We are now ready to demonstrate the effect of endpoint mobility ratio M^0 , relative permeability, and $N_g^0 \sin \alpha$ on oil displacement efficiency. Figure 5-6 schematically shows the effect of these parameters for displacements with $f_{1I} = 0$ and $f_{1J} = 1$. Figure 5-6 shows, from top to bottom, plots of E_D versus t_D , water saturation profiles at various t_D , and the fractional flow curve that would give the indicated behavior. From left to right, the figures show oil displacement behavior for decreasing M^0 , increasing $N_g^0 \sin \alpha$, and increasing water wetness through shifts in the relative permeability curves. Figure 5-6 represents three of the four types of waves—spreading, mixed, and sharpening. Several important conclusions follow directly from Fig. 5-6.

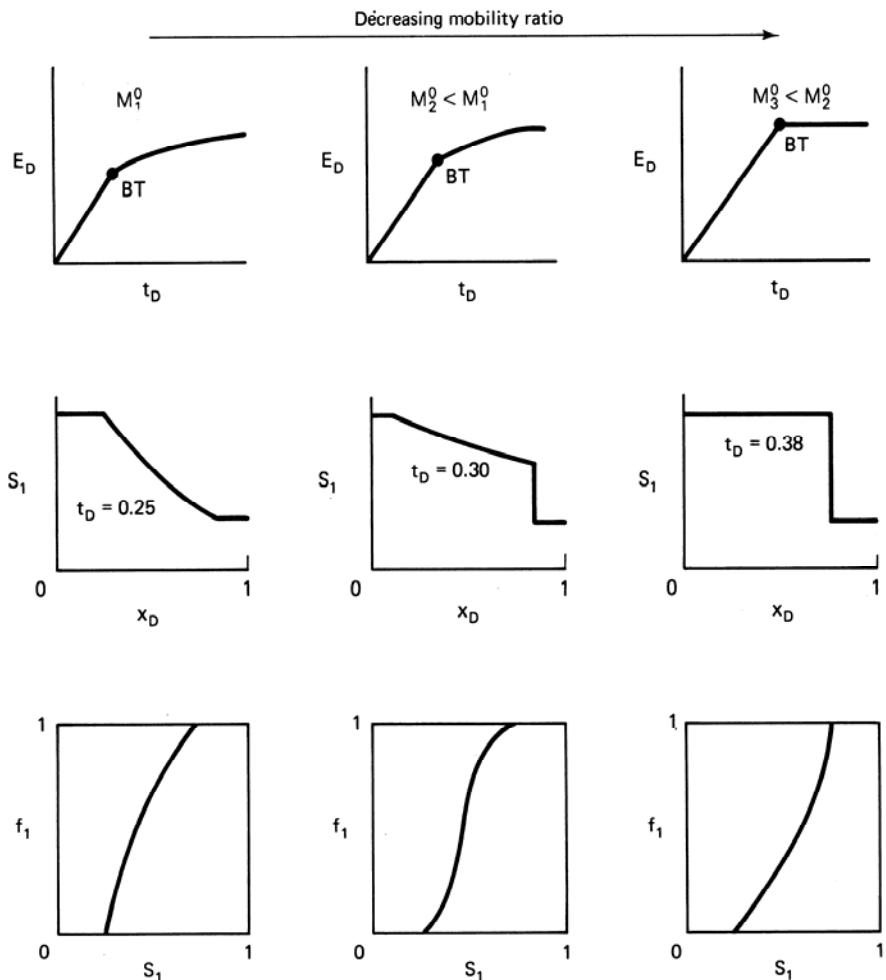


Figure 5-6 Schematic illustration of effect of mobility ratio on displacement efficiency

1. Any change that increases the size of the shock portion of the water saturation wave also increases E_D at any given t_D . These changes also delay water breakthrough and decrease the time over which the permeable medium is simultaneously producing two phases.
2. Decreasing M^0 , increasing $N_g^0 \sin \alpha$, and increasing water wetness improve E_D . Of these three, M^0 is usually the only one we can have any impact on. In Chap. 6, we see that decreasing mobility ratio also increases vertical and areal sweep efficiency; hence decreasing the mobility ratio improves oil recovery in at least three ways. EOR processes that rely, partly or totally, on lowering the mobility ratio between the displacing and displaced fluids are said to be based on the *mobility ratio concept* of oil recovery. Figure 5-6 shows that when the water saturation wave becomes a complete shock, no

advantage is to be gained on E_D by further lowering M^0 . Finally, there is no unique value of M^0 at which the wave changes from spreading to sharpening since the displacement is affected also by the shape of the relative permeability curves.

3. However low M^0 might be, the ultimate displacement efficiency

$$E_D^\infty = \frac{(S_{2I} - S_{2r})}{S_{2I}}$$

is limited by the presence of a residual oil saturation. EOR methods that intend to recover residual oil must rely on something other than the mobility ratio concept, such as displacing with miscible agents (see Sec. 5-5 and Chap. 7) or lowering the water–oil interfacial tension (see Chap. 9).

Besides M^0 , at least two other mobility ratios are in common use. The average mobility ratio \bar{M} , defined as

$$\bar{M} = \frac{(\lambda_{r1} + \lambda_{r2})|_{S_i=\bar{S}_i}}{(\lambda_{r1} + \lambda_{r2})|_{S_i=S_{1I}}} \quad (5.2-25a)$$

is the ratio of total relative mobility at the average water saturation behind the shock front to the same quantity evaluated at the initial water saturation. \bar{M} is commonly used to correlate the areal sweep efficiency curves (see Chap. 6). The shock front mobility ratio M_{sh} is

$$M_{sh} = \frac{(\lambda_{r1} + \lambda_{r2})|_{S_i=S_i^*}}{(\lambda_{r1} + \lambda_{r2})|_{S_i=S_{1I}}} \quad (5.2-25b)$$

M_{sh} is the quantity that controls the formation of viscous fingers. For pistonlike displacements, all three definitions are the same.

The most general definition of mobility ratio is actually the ratio of pressure gradients ahead of and behind a displacing front. The above definitions, depending on the character of the displacing front, follow from this for the case of incompressible flow (spatially independent volumetric flow rate). For compressible flows or flows of condensing fluids, the general definition is more appropriate (see Chap. 11 and Exercise 5J).

5-3 DISSIPATION IN IMMISCIBLE DISPLACEMENTS

In this section, we discuss two common dissipative effects in one-dimensional flows: capillary pressure and fluid compressibility. Both phenomena are dissipative; they cause mixing zones to grow faster than or differently from a dissipation-free flow. Both phenomena also bring additional effects.

Capillary Pressure

We do not present a closed-form solution to the water conservation equation. But we can qualitatively illustrate the effect of capillary pressure on a water–oil displacement

and can give, through scaling arguments, quantitative guidelines on when it might be important. For incompressible fluids and with capillary pressure P_c included, the water material balance (Eq. 5.2-1) still applies, but the water fractional flow (Eq. 5.2-2) becomes (see Exercise 5F)

$$f_1(S_1) = \frac{\lambda_{r1}}{\lambda_{r1} + \lambda_{r2}} \left(1 - \frac{k\lambda_{r2}\Delta\rho g \sin \alpha}{u} \right) + \frac{k\lambda_{r1}(\partial P_c / \partial x)}{(1 + \lambda_{r1} / \lambda_{r2})u} \quad (5.3-1)$$

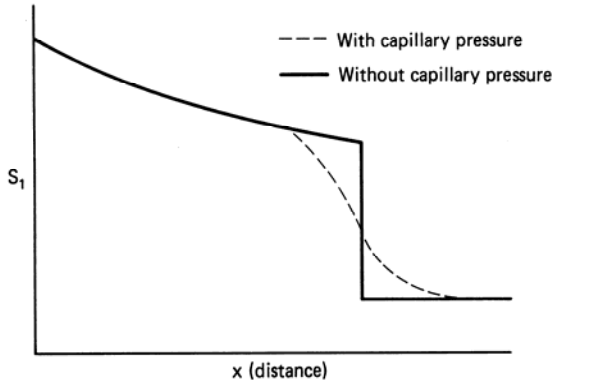
The first term on the right side of Eq. (5.3-1) is simply the water fractional flow in the absence of capillary pressure (Eq. 5.2-2); thus many of the conclusions about displacements with $P_c = 0$, though somewhat modified, carry over to displacements with capillary pressure. The second right term in Eq. (5.3-1) is the contribution of P_c to the water fractional flow. Including the capillary pressure term causes the character of Eq. (5.2-1) to change from hyperbolic to parabolic, a general result of dissipative effects because of the spatial P_c derivative.

The capillary pressure in Eq. (5.3-1) is the phase pressure difference between two continuous oil and water phases (see Sec. 3-2). The derivative $\partial P_c / \partial x = (dP_c / dS_1) \cdot (\partial S_1 / \partial x)$ has a positive sign for displacements in both oil-wet or water-wet media since dP_c / dS_1 is negative for both cases (see Fig. 3-5), and $\partial S_1 / \partial x$ is also negative. Therefore, for waterfloods, capillary pressure increases the water fractional flow at a given water saturation. This augmentation is particularly important in regions having large saturation gradients, that is, around shock fronts predicted by the Buckley-Leverett theory. In an oil displacement of water, P_c causes a smaller water fractional flow since $\partial S_1 / \partial x > 0$.

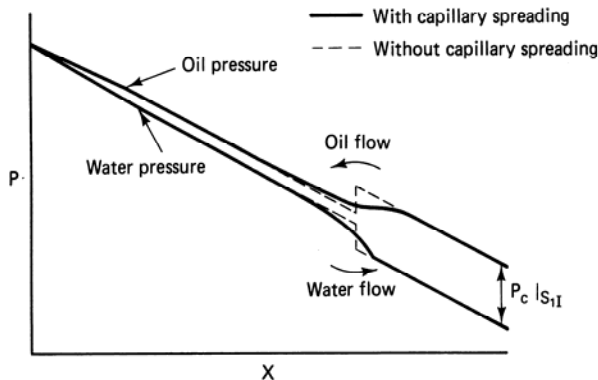
The effect of P_c on a one-dimensional displacement is to spread out the water saturation wave, particularly around shocks; Fig. 5-7, which illustrates how this comes about, is a simulated water saturation and pressure profile for a one-dimensional waterflood in a water-wet medium. Figure 5-7(a) shows water saturation profiles with and without capillary pressure; Fig. 5-7(b) shows the corresponding pressure profiles. Both panels are at the same t_D . The dotted phase pressures in Fig. 5-7(b) are those that would be present if the shock remained in the water saturation profile. Of course, representing shock waves with $P_c \neq 0$ is not correct, but such a portrayal presents the driving force for capillary mixing.

Ahead of the front (downstream), the difference between the oil and water phase pressures is constant and equal to the capillary pressure at S_{1J} . At the front, the phase pressures change rapidly. But behind the front (upstream), the difference between the oil and water phase pressures declines to the value at $S_1 = S_{1J}$. Compare these comments to Figs. 5-7(a) and 3-5. There is now a local pressure gradient at the shock that causes oil to flow upstream (countercurrent imbibition) and water to flow downstream faster than under the influence of viscous forces only. The resulting local mixing causes the shock to spread (Fig. 5-7a) and the pressure discontinuity to disappear. Behind the front, in the spreading portion of the water saturation wave, the effect of capillary pressure is small.

Capillary pressure will be small if the system length L is large. Consider the



(a) Water saturation profiles



(b) Water and oil phase pressure profiles

Figure 5-7 Saturation and pressure profiles under longitudinal capillary imbibition (Yokoyama, 1981)

dimensionless water conservation equation with Eq. (5.3-1) substituted and $\alpha = 0$

$$\frac{\partial S_1}{\partial t_D} + \frac{\partial}{\partial x_D} \left(\frac{1}{1 + \frac{\lambda_{r2}}{\lambda_{r1}}} \right) + \frac{\partial}{\partial x_D} \left(\frac{k \lambda_{r1}}{uL \left(1 + \frac{\lambda_{r1}}{\lambda_{r2}} \right)} \frac{\partial P_c}{\partial x_D} \right) = 0 \quad (5.3-2)$$

The last term on the left side of this equation is nonlinear in S_1 and thus difficult to estimate. Using the Leverett j -function expression (Eq. 3.2-2), we can write Eq. (5.3-2) as

$$\frac{\partial S_1}{\partial t_D} + \frac{\partial}{\partial x_D} \left(\frac{1}{1 + \frac{\lambda_{r2}}{\lambda_{r1}}} \right) - \frac{1}{N_{RL}} \frac{\partial}{\partial x_D} \left(g(S_1) \frac{\partial S_1}{\partial x_D} \right) = 0 \quad (5.3-3)$$

where g is a positive dimensionless function of water saturation

$$g(S_1) = - \left(\frac{1}{1 + \frac{\lambda_{r2}}{\lambda_{r1}}} \right) \left(\frac{S_1 - S_{1r}}{1 - S_{2r} - S_{1r}} \right)^{n_1} \frac{dj}{dS_1} \quad (5.3-4)$$

and N_{RL} , the Rapoport and Leas number, is a dimensionless constant first implied by these authors (1953) to indicate when capillary pressure effects will be important.

$$N_{RL} = \left(\frac{\phi}{k} \right)^{1/2} \frac{\mu_1 u L}{k_{r1}^0 \phi \sigma_{12} \cos \theta} \quad (5.3-5)$$

Figure 5-8 is a plot of fractional oil recovery at water breakthrough versus $\mu_1 v L$ (recall $v = u/\phi$) from the experimental work of Rapoport and Leas. Since the $S_{1L} = 0$ in their cores, the vertical axis in Fig. 5-8 is the breakthrough displacement efficiency, E_D^0 . As $\mu_1 v L$ increases, E_D^0 increases to a maximum of 0.58. For larger $\mu_1 v L$, E_D^0 is constant at the value predicted by the Buckley-Leverett theory.

Rapoport and Leas did not plot their results against the more general N_{RL} ; however, using the given $k = 0.439 \text{ } \mu\text{m}^2$ and $\phi = 0.24$, and taking $k_{r1}^0 \sigma_{12} \cos \theta = 1 \text{ mN/m}$ (typical for water-wet media), P_c will not affect a one-dimensional water-oil

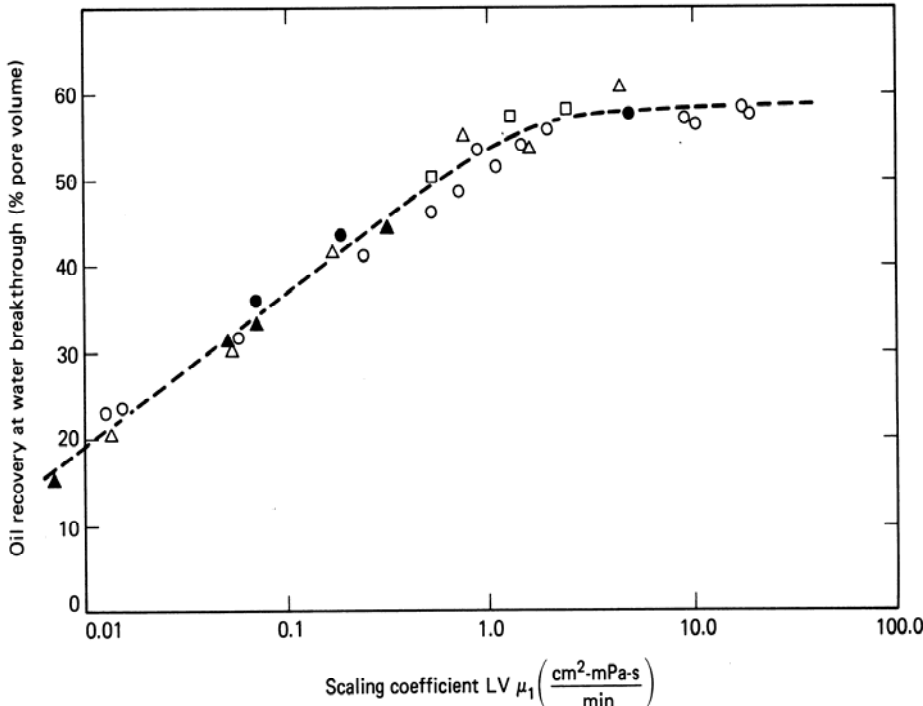


Figure 5-8 Relation between oil recovery at breakthrough and scaling coefficient in dry-filmed alumdum cores with no connate water. Different symbols represent varying core lengths and oil viscosities. (From Rapoport and Leas, 1953)

displacement if N_{RL} is greater than about 3. Because of the length appearing in the numerator of Eq. (5.3-5), P_c will affect the displacement front to a much greater degree in laboratory floods than in field-scale displacements because of the large disparity in L .

Of course, on a microscopic scale, capillary forces are important in determining the amount of trapped or residual oil in either laboratory or field displacements. In Sec. 3-3, we saw that the S_{2r} depended on a local viscous-to-capillary-force ratio, the capillary number N_{vc} . A common form of capillary number $N_{vc} = v\mu_1/k_r^0\sigma_{12}\cos\theta$ is embedded in the definition of N_{RL}

$$N_{RL} = \left(\frac{\phi}{k} \right)^{1/2} LN_{vc} \quad (5.3-6)$$

The factor, $L(\phi/k)^{1/2}$, is a measure of the ratio of the macroscopic permeable medium dimension to a characteristic rock dimension. Therefore, N_{vc} and N_{RL} are expressing the same physical idea—capillary-to-viscous-force ratios—but at different scales.

Recall that if N_{vc} is less than about 10^{-5} , the residual phase saturations are roughly constant. For well-sorted media, we can then put limits on N_{RL} so that capillary forces, on any scale, do not affect the displacement

$$3 < N_{RL} < 10^{-5} L \left(\frac{\phi}{k} \right)^{1/2} \quad (5.3-7)$$

(no dissipation) (constant residual
 saturations)

For large L , this is an extremely wide range and accounts for the common neglect of all capillary forces in one-dimensional displacement calculations. For laboratory scale, it may not be possible to satisfy both requirements.

N_{RL} may be expressed in more direct ways. From Eq. (5.3-5), we can substitute Darcy's law for water evaluated at $S_1 = 1 - S_{2r}$ for $v = u/\phi$ to obtain

$$N'_{RL} = \left(\frac{\phi}{k} \right)^{1/2} \frac{\Delta P_1}{\sigma_{12} \cos\theta} \quad (5.3-8)$$

where ΔP_1 is the pressure drop across the permeable medium measured through the water phase. The terms containing permeability and interfacial tension may be expressed in terms of the Leverett j -function to give yet another approximation to N_{RL}

$$N''_{RL} = \frac{\Delta P_1}{\Delta P_c} \quad (5.3-9)$$

where ΔP_c is the change in capillary pressure between the initial and final water saturation states. Equation (5.3-9) is a direct comparison of viscous to capillary pressure drops and is the least rigorous, but most direct, of all the measures.

For small N_{RL} , capillary pressure will cause shock waves to spread out. Though there is a parallel between dispersion in miscible displacements (see Sec. 5-5) and P_c effects in immiscible displacements, the analogy does not carry over to mixing zone growth. We show in Sec. 5-5 that dispersive mixing zones grow in proportion to the square root of time. Capillary pressure generally causes mixing zones to grow exponentially to some asymptotic limit where it proceeds, without further growth, in simple translation. How this comes about may be qualitatively explained by considering: a water saturation wave that would be a shock over the entire possible Saturation range, as in the right column in Fig. 5-6, where we neglected P_c effects. As we have seen, P_c effects cause such a wave to spread, but there is still a strong tendency for the wave to sharpen because of the convex-upward shape of the fractional flow curve. These two effects tend to balance each other, causing the wave to approach an asymptotic limit. The existence of such a limit further restricts the importance of capillary pressure as a mixing mechanism in one dimension. Asymptotic or “stabilized” mixing zones in one-dimensional laboratory waterfloods have been noted by several authors (Bail and Marsden, 1957).

No discussion of how capillary pressure influences a one-dimensional displacement is complete without some mention of the capillary end effect. This effect occurs when there is a discontinuity in the capillary pressure curve as, for example, when the one-dimensional permeable medium consists of two homogeneous media of differing permeabilities arranged in series. But it most commonly occurs at the end of a laboratory core where the flowing phases pass from a permeable to a nonpermeable region. The saturation behavior at the plane of discontinuity is considerably different from that predicted by the Buckley-Leverett theory.

Consider the water saturation and pressure profiles of a waterflood in a water-wet medium shown in Fig. 5-9. Capillary forces are such that they cannot be neglected. Figure 5-9(a) shows the instant that water arrives at the outflow end ($x = L$), and Fig. 5-9(b) shows some time later. On the right of the outflow end, there is no permeable medium. This region has a capillary pressure curve that is zero everywhere except at $S_1 = 0$, where all values of capillary pressure exist. The oil and water phase pressures must be continuous at $x = L$; hence the water saturation for $x > L$ is constrained to be zero because there is a nonzero phase pressure difference. This, in turn, implies water cannot flow across the outflow end of the medium until the capillary pressure just inside the system vanishes. With no production at $x = L$, but with continual water transport to the outflow end, the water saturation must build up at $x = L$ until $P_c = 0$ ($S_1 = 1 - S_{2r}$) at this plane. Hence the capillary end effect causes a delay in water production and a distortion of the water saturation at $x = L$ compared to that predicted by the Buckley-Leverett theory (Fig. 5-9b).

This delay can cause considerable error in applying the Welge integration procedure (Eq. 5.2-22). The capillary end effect has been observed experimentally by Kyte and Rapoport (1958) and in simulations by Douglas et al. (1958). Figure 5-10 reproduces data reflecting the capillary end effect.

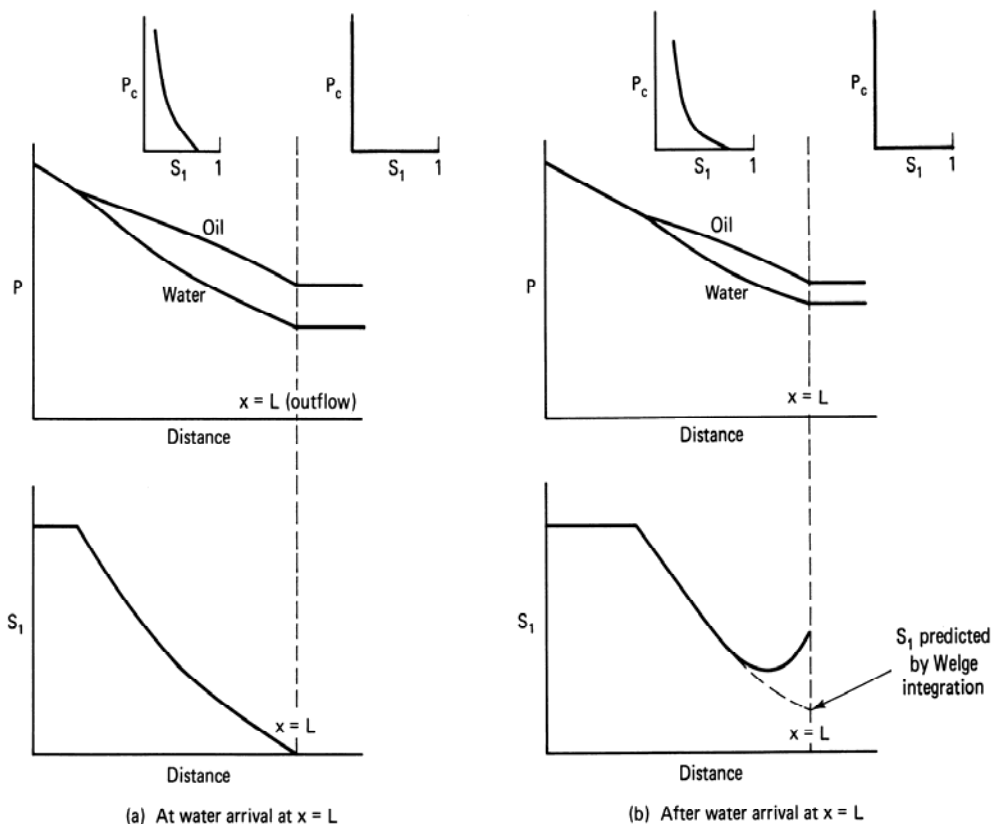


Figure 5-9 Schematic of the capillary end effect

To eliminate the capillary end effect, laboratory floods have been run at high velocities and with long lengths (both increase N_{RL}) or by placing a second permeable material at the outflow end to ensure good capillary contact.

Fluid Compressibility

A second dissipative effect is fluid compressibility. Figure 5-11 shows water saturation profiles for two waterfloods having compressible oil and incompressible water (Fig. 5-11a) and compressible water and incompressible oil (Fig. 5-11b). The completely incompressible Buckley-Leverett case is shown for comparison. These results are from computer simulations that were at constant water injection rate (Fig. 5-11a) and constant oil production rate (Fig. 5-11b). We present the results as the product of compressibility and total pressure drop ΔP (neglecting capillary forces) since this quantity determines the appropriateness of the small compressibility fluid assumption in well test analysis. For $c_i \Delta P$ products of 0.01 or less, the effect of fluid compressibility is negligible; the smearing of the shock fronts for the $c_i \Delta P = 1.25 \times 10^{-3}$ runs is because of numerical dispersion, which is an artificial dissipative effect.

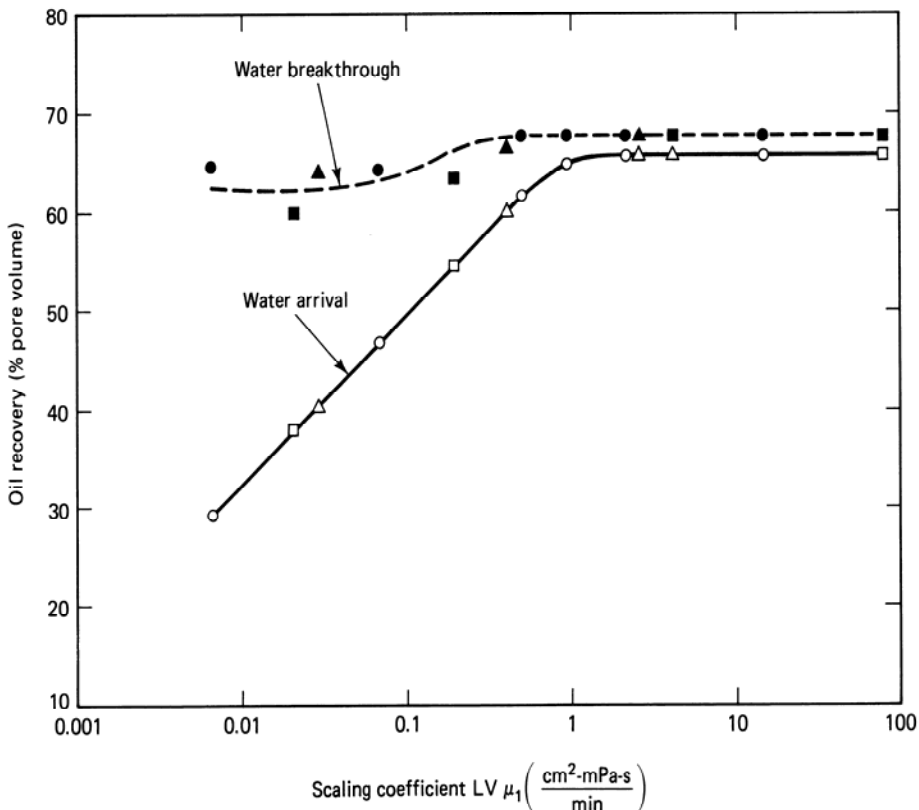
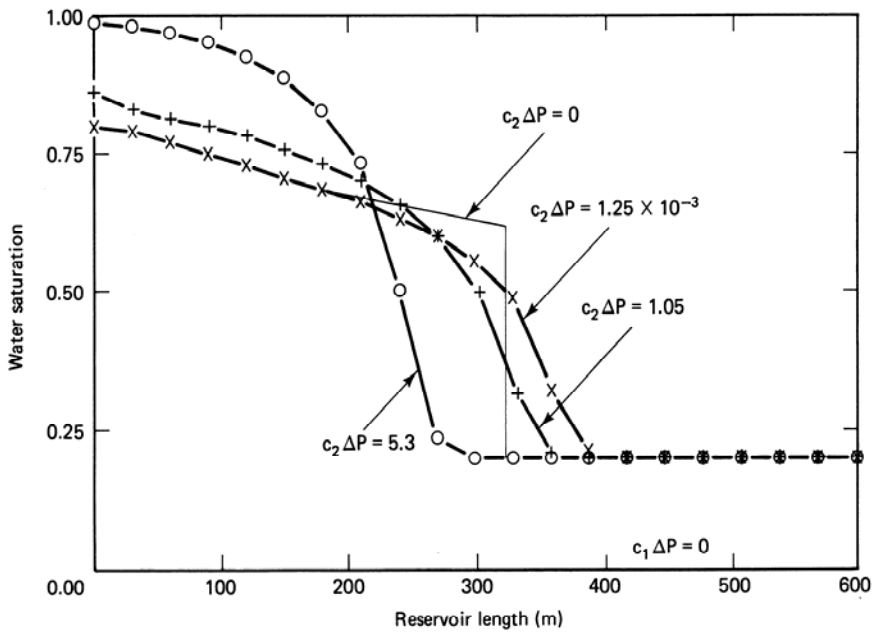


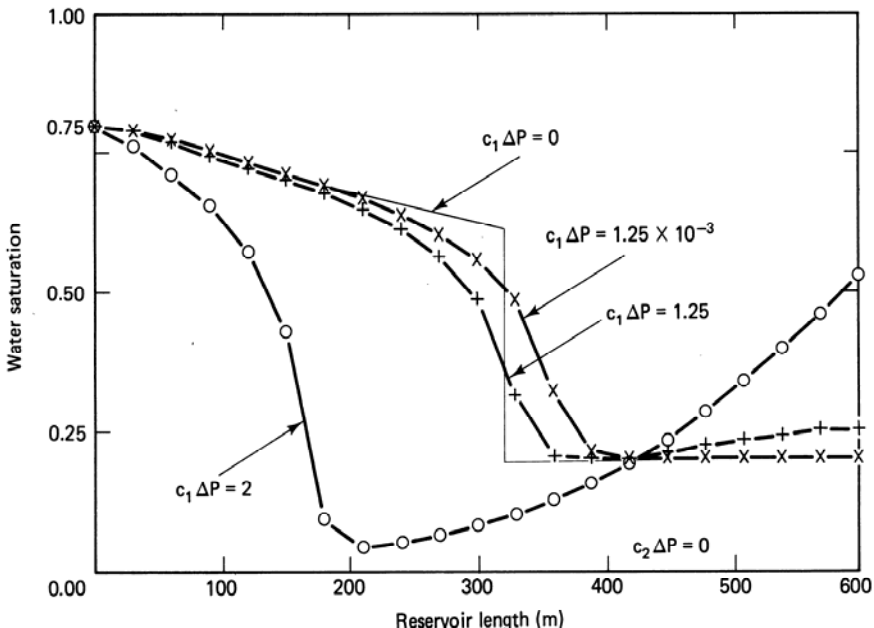
Figure 5-10 Correlation of waterflood test data in strongly water-wet alumdum cores (from Kyte and Rapoport, 1985)

The $c_i\Delta P$ products shown in Fig. 5-11 are, of course, unrealistically high; we have selected these values merely to emphasize the effect of compressibility.

The effect of either oil or water compressibility is to spread out the Buckley-Leverett shock front in addition to the spreading caused by numerical dispersion but the effect does not become pronounced until $c_i\Delta P$ is 1 or more. However, we would expect displacements in which both fluids are compressible to experience a combined dissipative effect with greater spreading. In Fig. 5-11(a), the water saturation exceeds $1 - S_{2r}$ at the inflow end. At higher pressure, oil compression below its residual occurs. Similarly, in Fig. 5-11(b), the water saturation exceeds S_{1r} at the effluent end because, at the reduced pressure, the water will expand. These effects are characteristics of the particular conditions the runs were made under. If we had held the production pressure constant and not allowed phase saturations to decrease below their respective residuals, neither effect would be present. Still, we can see from Fig. 5-11 that the effect of compressibility is qualitatively similar to that of capillary pressure; a spreading of the shock fronts occurs but with a smaller effect on the saturation "tail."



(a) Compressible oil, incompressible water



(b) Compressible water, incompressible oil

Figure 5-11 Water saturation profiles for one-dimensional water-displacing-oil floods at $t = 200$ days (adapted from Samizo, 1982)

5-4 IDEAL MISCIBLE DISPLACEMENTS

Two components are mutually miscible if they mix in all proportions without an interface forming between them. The definition is translated into the fluid flow equations by allowing a phase to be composed of several components they are mutually miscible within.

In this section, we discuss isothermal miscible displacements using fractional flow theory and with one or more phases present. Our presentation considers ideal miscible displacements with components that do not change the properties of the phases they are formed in (see Chap. 7 for more complicated displacements).

Concentration Velocities

Many of the concepts in Sec. 5-2 readily generalize to miscible displacements. We write a one-dimensional conservation equation for $i = 1, \dots, N_c$ components as

$$\phi \frac{\partial}{\partial t} \left(\sum_{j=1}^{N_p} S_j C_{ij} + \left(\frac{1-\phi}{\phi} \right) C_{is} \right) + u \frac{\partial}{\partial x} \left(\sum_{j=1}^{N_p} f_j C_{ij} \right) = 0, \\ i = 1, \dots, N_c \quad (5.4-1)$$

Equation (5.4-1) is a special case of Eq. (2.4-10) with dispersion neglected. f_j is the fractional flow of phase j , given by Eq. (2.4-2) with capillary pressure neglected, and C_{ij} and C_{is} are the phase concentrations of component i in phase j and on the solid, respectively. Of course, the assumptions associated with Eq. (2.4-10)—constant porosity, incompressible fluids, and ideal mixing—also apply. In nondimensional form, Eq. (5.4-1) becomes

$$\frac{\partial}{\partial t_D} (C_i + C'_{is}) + \frac{\partial F_i}{\partial x_D} = 0, \quad i = 1, \dots, N_c \quad (5.4-2)$$

where

$$C_i = \text{Overall fluid phase concentration of species } i \\ = \sum_{j=1}^{N_p} S_j C_{ij} \quad (5.4-3a)$$

$$C'_{is} = \text{Solid phase concentration of } i \text{ on a pore volume basis} \\ = C_{is} \left(\frac{1-\phi}{\phi} \right) \quad (5.4-3b)$$

$$F_i = \text{Overall flux of species } i \\ = \sum_{j=1}^{N_p} f_j C_{ij} \quad (5.4-3c)$$

The transform accomplished by Eq. (5.4-3b) changes the solid phase concentration from a solid volume basis (C_{is} is amount i on solid/volume solid) to a pore volume

basis (C'_{is} is amount i on solid/pore volume). Thus C_i and C'_{is} are directly comparable and may be used together in later work without the need to manipulate units. The definition of overall flux is from Hirasaki (1981) and Helfferich (1981).

In principle, the fluxes F_i are functions of the C_i for $i = 1, \dots, N_C$, and we may carry over many of the definitions, particularly those of saturation velocity, directly from Sec. 5-2. In practice, however, the relations $F_i = F_i(C_1, C_2, \dots, C_{N_C})$ are extremely convoluted. We discuss this in more detail later, but we can give a summary of this relation here.

With C_i known, the C_{ij} and S_j may be calculated from phase equilibrium relations. The exact nature of the “flash” calculation depends on the nature of the phase -behavior (see Sec. 4-4 and Chaps. 7 and 9). With the S_j and C_{ij} known, the phase relative permeabilities $k_{rj} = k_{rj}(S_j, C_{ij})$ and viscosities $\mu_j = \mu_j(C_{ij})$ may be calculated from petrophysical relations (see Sec. 3-3). From these follow the relative mobilities $\lambda_{rj} = k_{rj}/\mu_j$, which lead directly to the f_j from Eq. (2.4-2). If the phase densities are also required (if, for example, the permeable medium is not horizontal), they follow from $\rho_j = \rho_j(C_{ij})$ (Eq. 2.2-12). With the f_j and C_{ij} known F_i follows from Eq. (5.4-3c). If needed, $C'_{is} = C'_{is}(C_{ij})$ may be calculated also from the adsorption isotherm (see Chaps. 8 and 9).

Despite this complexity, we can write Eq. (5.4-2) as

$$\left(1 + \left(\frac{\partial C'_{is}}{\partial C_i}\right)_{x_D}\right) \frac{\partial C_i}{\partial t_D} + \left(\frac{\partial F_i}{\partial C_i}\right)_{t_D} \frac{\partial C_i}{\partial x_D} = 0, \quad i = 1, \dots, N_C \quad (5.4-4)$$

The partial derivatives $(\partial C'_{is} / \partial C_i)_{x_D}$ and $(\partial F_i / \partial C_i)_{t_D}$ in Eq. (5.4-4) follow from the chain rule. These derivatives are not the same as $(\partial C'_{is} / \partial C_j)_{C_{mxj}}$, which are in the definition of the total differential. The latter derivatives may be calculated directly from $C'_{is} = C'_{is}(C_{ij})$ and $F_i = F_i(C_i)$, whereas the former derivatives require knowledge of $C_i = C_i(x_D, t_D)$, which are solutions. Therefore, Eq. (5.4-4) is of little use except to allow the definition of specific concentration velocity v_{C_i}

$$v_{C_i} = \frac{(\partial F_i / \partial C_i)_{t_D}}{1 + (\partial C'_{is} / \partial C_i)_{x_D}}, \quad i = 1, \dots, N_C \quad (5.4-5a)$$

by analogy with Eq. (5.2-10). The definition of the specific shock velocity v_{AC_i} is

$$v_{AC_i} = \frac{(\Delta F_i / \Delta C_i)}{1 + (\Delta C'_{is} / \Delta C_i)} \quad (5.4-5b)$$

Without additional constraints, the definitions (Eqs. 5.4-5a and 5.4-5b) impart no new information. But for the water-oil case of Sec. 5-2, they reduce to $C_i = S_1$, $F_i = f_1$, and $C'_{is} = 0$, giving

$$v_{C_i} = v_{S_1} = \left(\frac{\partial f_1}{\partial S_1}\right)_{t_D} = \frac{df_1}{dS_1} = f'_1(S_1) \quad (5.4-6)$$

The last equality is possible because f_1 is a function of S_1 only; hence $f'_1 = (\partial F_1 / \partial S_1)_{t_D} = (\partial F_1 / \partial S_1)_{x_D}$. Certainly for more complicated cases, this simplification

is not possible; still, many of the displacements of interest may be solved with the coherent or simple wave theory that we discuss in Sec. 5-5. We now discuss other particularly simple special cases of miscible displacements.

Tracers in Two-Phase Flow

The simplest case we consider is the miscible displacement in single-phase flow of component 2 by component 1. For this case, f_j and S_j are zero for all j except 1. For this particular j , f_j and S_j are unity. If component 1 does not adsorb, the concentration velocity becomes

$$v_{C_1} = 1 \quad (5.4-7)$$

from either Eq. (5.4-5a) or (5.4-5b). This seemingly trivial result has two important consequences.

1. The dimensional velocity of component 1 is equal to the bulk fluid velocity, meaning the dimensionless breakthrough time t_D^0 for component 1 is also unity. From Eq. (5.2-7), we may estimate the pore volume of the medium by knowing the cumulative fluid injected when breakthrough occurs (see Exercise 5K). Components that travel at the bulk fluid velocity are “conservative” tracers for this reason.
2. The specific concentration velocity is independent of C_1 , meaning waves caused by conservative tracers are indifferent, which is generally true for ideal miscible displacements.

Most EOR displacements are only partially miscible. To illustrate a partially miscible displacement, we now consider a displacement of oil–water mixture at water saturation $S_{1,I}$ by another at a water fractional flow $f_{1,J} = f_1(S_{1,J})$. We wish to distinguish between the initial and injected oil and water, so let's suppose the injected fluids contain conservative tracers. The oil-miscible tracer is completely immiscible in water, and the water-miscible tracer is similarly immiscible in oil. The process is now the displacement of an oil–water mixture by a tagged oil–water mixture. To keep this simple, we assume the tracers do not affect the fractional flow functions at all. The specific velocity of the tagged water-resident water wave is

$$v_{1'} = \frac{\partial(C_{11}f_1)}{\partial(C_{11}S_1)} = \frac{f_1}{S_1} \quad (5.4-8a)$$

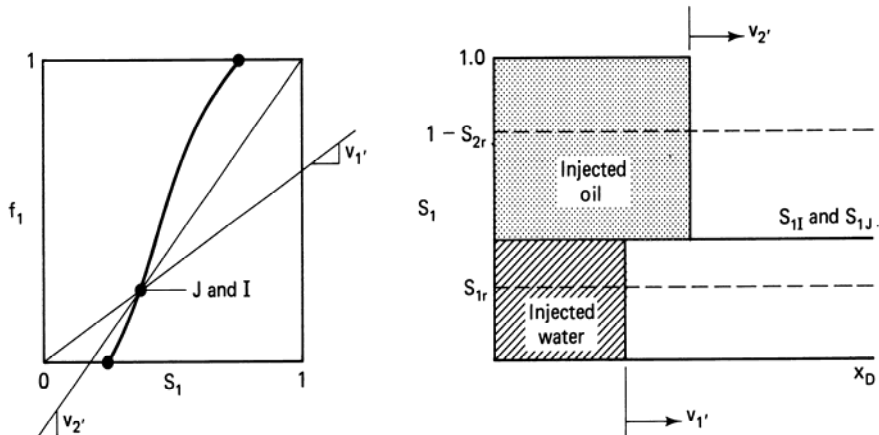
from Eq. (5.4-5a), where C_{11} is the water tracer concentration. Similarly, the specific velocity of the tagged oil is

$$v_{2'} = \frac{f_2}{S_2} = \frac{1-f_1}{1-S_1} \quad (5.4-8b)$$

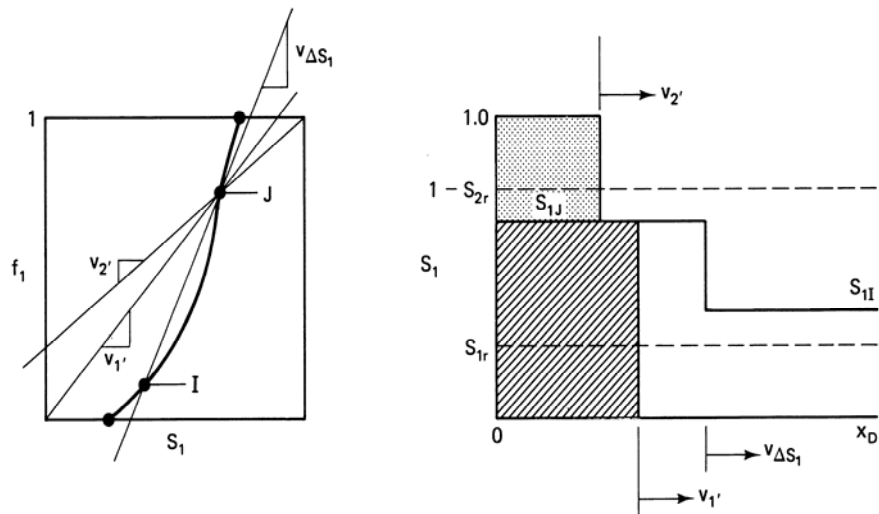
$v_{1'}$ and $v_{2'}$ are both independent of tracer concentration; hence the miscible tagged water and oil waves are indifferent. Of course, since neither of the tracers affects f_1 ,

the saturation velocity of the water—tagged or untagged—is given by Eq. (5.2-10) or Eq. (5.2-12). The values of f_1 and S_1 in Eq. (5.4-8) are determined by the character of the oil–water wave.

Figure 5-12 illustrates some of the cases that can occur for this displacement. On each plot, the fractional flow curve is on the left, and a saturation-concentration profile is on the right. In case A, $S_{1I} = S_{1J}$ and the specific velocities are the slopes of straight lines passing through $(0, 0)$ and $(f_1, S_1)_J$ and $(1, 1)$ and $(f_1, S_1)_J$, respectively, from Eqs. (5.4-8a) and (5.4-8b). $v_2' > v_1'$, and the tagged oil wave leads the tagged water wave.

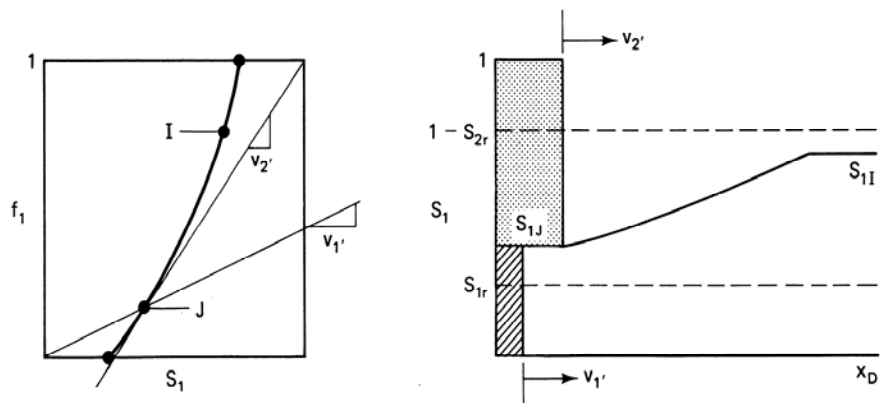


(a) Case A

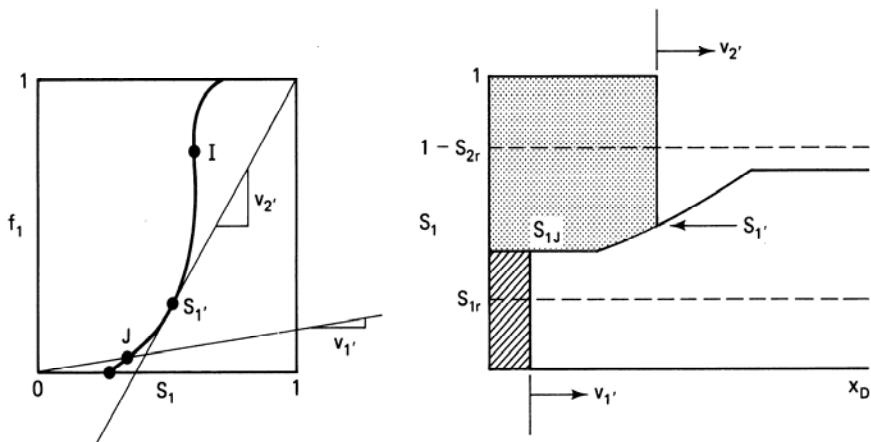


(b) Case B

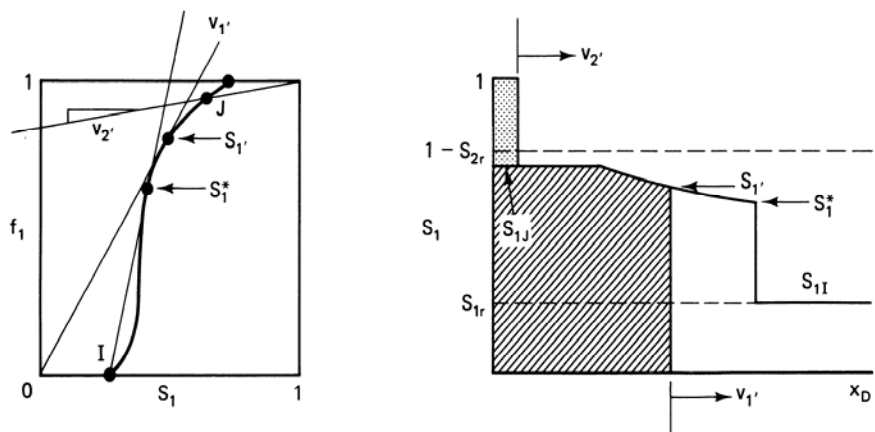
Figure 5-12 Illustration of various partially miscible displacements



(c) Case C



(d) Case D



(e) Case E

Figure 5-12 Continued.

In case B, $S_{1J} > S_{1I}$, and the f_1 curve is such that the oil–water wave is a shock. Both tagged waves lag the oil–water wave. The region between the tagged water and oil–water waves contains a “bank” of resident water that will be produced before the injected water breakthrough. Breakthrough of a resident water bank in this manner has been observed experimentally (Brown, 1957) though dispersion tends to be large in such displacements (see Fig. 5-18).

Case C illustrates a spreading water–oil wave with $v_{2'} > v_{1'}$ but with all tagged concentration waves having a smaller velocity than the smallest saturation velocity at S_{1J} .

Case D is the same as case C with the fractional flow curve more convex upward. This shape causes the oil–water wave to spread more and the tagged oil front to fall somewhere in the spreading portion of the oil–water wave. The saturation, $S_{1'}$, whose velocity is the same as the tagged oil wave, is given by

$$v_{2'} = \frac{1 - f_1(S_{1'})}{1 - S_{1'}} = \left(\frac{df_1}{dS_1} \right)_{S_{1'}} \quad (5.4-9)$$

The line whose slope is $v_{2'}$ does not pass through S_{1J} , as it did in all previous cases. This is because a line through $(1, 1)$ and $(S_{1'}, f_1)$ would have a second intersection point with the fractional flow curve. The tagged oil front would then travel with two different water saturations—a physical impossibility.

Case E, the traditional Buckley-Leverett problem, is the inverse of case D where the tagged water front is now traveling in the spreading zone region. The oil–water displacement in case E is mixed, whereas in case D, it is spreading.

The important points in Fig. 5-12 are as follows:

1. As postulated, neither the tagged oil nor the tagged water causes deviation in the water–oil displacement character. When banks of resident fluids form, they do so within their respective phases.
2. One can easily imagine the tagged oil to be a hydrocarbon of less value than the oil. The tracer fronts now take on added significance since these miscible fronts are now displacing the resident oil. The resident oil, in turn, is completely displaced. Thus the ultimate E_D for these idealized displacements is 1.0. This maximum efficiency occurs without interfacial tension lowering, changes in wettability, or mobility reduction.

Of course, we have not as yet discovered a fluid that is simultaneously cheaper than and miscible with crude oil and that does not drastically change the hydrocarbon transport properties. These changes can return the ultimate displacement efficiency to something less than 1; still, the idea of displacing with miscible fluids, or those that will develop miscibility, is the central concept of Chap. 7.

5-5 DISSIPATION IN MISCELLY DISPLACEMENTS

Because miscible waves are ideally indifferent, they are also susceptible to dissipation. By far the most prominent of the dissipative effects in miscible displacements are dispersion and viscous fingering. The latter is a two-dimensional effect, so we postpone our discussion of it to Chaps. 6 and 7. In this section, we discuss the effects of dispersion on a miscible front.

The Error Function Solution

Consider now the isothermal miscible displacement of a component by another it is completely miscible with in a one-dimensional, homogeneous permeable medium. The convection-diffusion (CD) equation (Eq. 2.4-7) describes the conservation of the displacing component with mass concentration C ,

$$\phi \frac{\partial C}{\partial t} + u \frac{\partial C}{\partial x} - \phi K_l \frac{\partial^2 C}{\partial x^2} = 0 \quad (5.5-1)$$

Equation (5.5-1) also assumes incompressible fluid and rock, ideal mixing, and a single phase at unit saturation. The following development is valid if other phases are present (Delshad, 1981) and as long as all fractional flows and saturations are constant (see Exercise 5M). K_l is the longitudinal dispersion coefficient. In dimensionless terms, Eq. (5.5-1) becomes

$$\frac{\partial C}{\partial t_D} + \frac{\partial C}{\partial x_D} - \frac{1}{N_{Pe}} \frac{\partial^2 C}{\partial x_D^2} = 0 \quad (5.5-2)$$

which is solved with the following boundary and initial conditions on $C(x_D, t_D)$:

$$C(x_D, 0) = C_I, \quad x_D \geq 0 \quad (5.5-3a)$$

$$C(x_D \rightarrow \infty, t_D) = C_I, \quad t_D \geq 0 \quad (5.5-3b)$$

$$C(0, t_D) = C_J, \quad t_D \geq 0 \quad (5.5-3b)$$

where C_I and C_J are the initial and injected compositions, respectively. In Eq. (5.5-2), N_{Pe} , the Peclet number, is defined as

$$N_{Pe} = \frac{uL}{\phi K_l} \quad (5.5-4)$$

which is the ratio of convective to dispersive transport. N_{Pe} is the analogue of N_{RL} for immiscible displacements as seen by comparing Eqs. (5.3-3) and (5.5-2). This displacement must take place at constant u unlike Eqs. (5.2-6b). The equation and boundary conditions contain three independent parameters, C_I , C_J , and N_{Pe} , but the problem may be restated with only N_{Pe} as a parameter by defining a dimensionless

concentration CD

$$C_D = \frac{C - C_I}{C_J - C_I} \quad (5.5-5)$$

With this definition, the equation and boundary conditions become

$$\frac{\partial C_D}{\partial t_D} + \frac{\partial C_D}{\partial x_D} - \frac{1}{N_{Pe}} \frac{\partial^2 C_D}{\partial x_D^2} = 0 \quad (5.5-6)$$

$$C_D(x_D, 0) = 0, \quad x_D \geq 0 \quad (5.5-7a)$$

$$C_D(x_D \rightarrow \infty, t_D) = 0, \quad t_D \geq 0 \quad (5.5-7b)$$

$$C_D(0, t_D) = 0, \quad t_D \geq 0 \quad (5.5-7c)$$

We have replaced the original boundary condition at $x_D = 0$ (Eq. 5.5-3c) with one at $x_D \rightarrow -\infty$ (Eq. 5.5-7c). This is an approximation to simplify the following derivation of an analytic solution. The approximate solution thus obtained will be valid, strictly speaking, for large t_D or large N_{Pe} where the influence of the inlet boundary appears as though it were a great distance from the displacing front. In practice, the resulting approximate analytic solution accurately describes single-phase displacements for all but extreme cases.

The first step in deriving $C_D(x_D, t_D)$ is to transform Eqs. (5.5-6) and (5.5-7) to a moving coordinate system x'_D where $x'_D = x_D - t_D$. This may be done by regarding C_D as a function of x_D and t_D where a differential change in C_D caused by differential changes in x_D and t_D is

$$dC_D = \left(\frac{\partial C_D}{\partial t_D} \right)_{x_D} dt_D + \left(\frac{\partial C_D}{\partial x_D} \right)_{t_D} dx_D \quad (5.5-8a)$$

But regarded as a function of x'_D and t_D , dC_D is

$$dC_D = \left(\frac{\partial C_D}{\partial t_D} \right)_{x'_D} dt_D + \left(\frac{\partial C_D}{\partial x'_D} \right)_{t_D} dx'_D \quad (5.5-8b)$$

Differential changes in variables are equal regardless of the coordinate system they are viewed in. The right-hand sides of Eqs. (5.5-8a) and (5.5-8b) are therefore equal. But x'_D is a known function of x_D and t_D , from which

$$dx'_D = dx_D - dt_D \quad (5.5-9)$$

When dx'_D is replaced in the above equality, we have

$$\begin{aligned} & \left[\left(\frac{\partial C_D}{\partial x_D} \right)_{t_D} - \left(\frac{\partial C_D}{\partial x'_D} \right)_{t_D} \right] dx_D \\ & + \left[\left(\frac{\partial C_D}{\partial t_D} \right)_{x_D} - \left(\frac{\partial C_D}{\partial t_D} \right)_{x'_D} + \left(\left(\frac{\partial C_D}{\partial x'_D} \right)_{t_D} \right) \right] dt_D = 0 \end{aligned} \quad (5.5-10)$$

Since x_D and t_D are independent variables, dx_D and dt_D are not linearly related; hence the terms in brackets in Eq. (5.5-10) are zero, giving

$$\left(\frac{\partial C_D}{\partial x_D} \right)_{t_D} = \left(\frac{\partial C_D}{\partial x'_D} \right)_{t_D} \quad (5.5-11a)$$

$$\left(\frac{\partial C_D}{\partial t_D} \right)_{x_D} = \left(\frac{\partial C_D}{\partial t_D} \right)_{x'_D} - \left(\left(\frac{\partial C_D}{\partial x'_D} \right)_{t_D} \right) \quad (5.5-11b)$$

When these are substituted into Eq. (5.5-6), we have

$$\left(\frac{\partial C_D}{\partial x_D} \right)_{x'_D} - \frac{1}{N_{Pe}} \frac{\partial^2 C_D}{\partial (x'_D)^2} = 0 \quad (5.5-12)$$

and the boundary conditions retain the form of Eq. (5.5-7) thanks to the replacement of the inlet boundary condition at $x_D = 0$ with one at $x_D \rightarrow -\infty$.

Equation (5.5-12) is now the heat conduction equation whose solution may be obtained by the method of combination of variables (Bird et al., 1960). To do this, we define yet another dimensionless variable $\eta = x'_D / 2\sqrt{t_D / N_{Pe}}$, with which the governing equations and boundary conditions may be transformed into

$$2\eta \frac{dC_D}{d\eta} + \frac{d^2C_D}{d\eta^2} = 0 \quad (5.5-13a)$$

$$C_D(\eta \rightarrow \infty) = 0 \quad (5.5-13b)$$

$$C_D(\eta \rightarrow -\infty) = 1 \quad (5.5-13c)$$

As required for the successful transformation of a partial to an ordinary differential equation, the conditions (Eqs. 5.5-7a and 5.5-7b) collapse into the single condition (Eq. 5.5-13b). The transformation to an ordinary differential equation is sometimes called Boltzmann's transformation. Equations (5.5-13) may be separated and integrated twice to give

$$C_D = \frac{1}{2} \left(1 - \frac{2}{\sqrt{\pi}} \int_0^\eta e^{-u^2} du \right) \quad (5.5-14)$$

The product times the integral on the right side of Eq. (5.5-14) is the error function, a widely tabulated integral (see Table 5-2 and Fig. 5-13), and abbreviated with the symbol $\text{erf}(\eta)$. By substituting the definitions for η and x'_D , we have the final form for the approximate analytic solution.

$$C_D = \frac{1}{2} \left[1 - \text{erf} \left(\frac{x_D - t_D}{2\sqrt{\frac{t_D}{N_{Pe}}}} \right) \right] = \frac{1}{2} \text{erfc} \left(\frac{x_D - t_D}{2\sqrt{\frac{t_D}{N_{Pe}}}} \right) \quad (5.5-15)$$

TABLE 5-2 TABULATED VALUES OF ERF (x) (FROM JAHNKE AND EMDE, 1945)

x	0	1	2	3	4	5	6	7	8	9	d
0.0	0.0	000	113	226	338	451	564	676	789	901	*013
1	0.1	125	236	348	459	569	680	790	900	*009	*118
2	0.2	227	335	443	550	657	763	869	974	*079	*183
3	0.3	286	389	491	593	694	794	89	992	*090	*187
4	0.4	284	380	475	569	662	755	847	937	*027	*117
5	0.5	205	292	379	465	549	633	716	798	879	959
6	0.6	039	117	194	270	346	420	494	566	638	708
7		778	847	914	981	*047	*112	*175	*128	*300	*361
8	0.7	421	480	538	595	651	707	761	814	867	918
9		969	*019	*068	*116	*163	*209	*254	*299	*342	*385
1.0	0.8	427	468	508	548	586	624	661	698	733	768
1		802	835	868	900	931	961	991	*020	*048	*076
2	0.9	103	130	155	181	205	229	252	275	297	319
3		340	361	381	400	419	438	456	473	490	507
4	0.95	23	39	54	69	83	97	*11	*24	*37	*49
5	0.96	61	73	84	95	*06	*16	*26	*36	*45	*55
6	0.97	63	72	80	88	96	*04	*11	*18	*25	*32
7	0.98	38	44	50	56	61	67	72	77	82	86
8		91	95	99	*03	*07	*11	*15	*18	*22	*25
9	0.99	28	31	34	37	39	72	44	47	49	51
2.0	0.995	32	52	72	91	*09	*26	*42	*59	*73	*88
1	0.997	02	15	28	41	53	64	75	95	95	*05
2	0.998	14	22	31	39	46	54	61	67	74	80
3		86	91	97	*02	*06	*11	*15	*20	*24	*28
4	0.999	31	35	38	41	44	47	50	52	55	57
5		59	61	63	65	67	69	71	72	74	75
6		76	78	79	80	81	82	83	84	85	86
7		87	87	88	89	89	90	91	91	92	92
8	0.9999	25	19	33	37	41	44	48	51	54	56
9		59	61	64	66	68	70	72	73	75	77

where erfc denotes the complementary error function. The exact analytic solution as derived by Laplace transforms is (Marle, 1981)

$$C_D = \frac{1}{2} \text{erfc} \left(\frac{x_D - t_D}{2\sqrt{\frac{t_D}{N_{pe}}}} \right) + \frac{e^{x_D N_{pe}}}{2} \text{erfc} \left(\frac{x_D + t_D}{2\sqrt{\frac{t_D}{N_{pe}}}} \right) \quad (5.5-16)$$

The second term in Eq. (5.5-16) approaches zero exponentially as x_D and N_{pe} grow.

Figure 5-14 shows concentration profiles of C_D versus x_D with t_D and N_{pe} varying. As N_{pe} increases, the concentration profile approaches the step function at $x_D = t_D$ suggested by Eq. (5.4-7). In fact, the concentration profile given by Eq. (5.5-15)

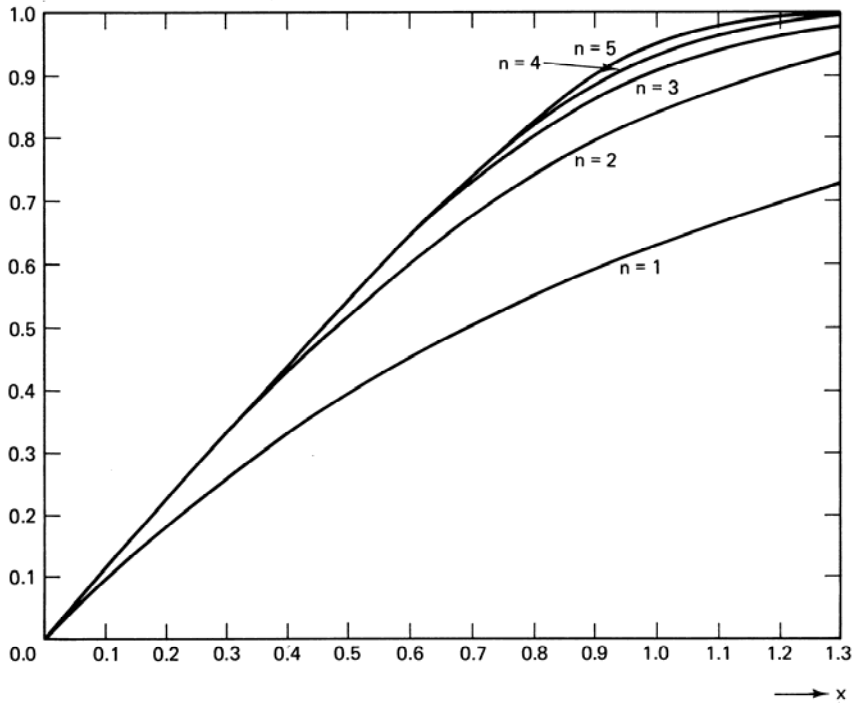


Figure 5-13 The function $En(x) = \frac{1}{n!} \int_0^{x^n} e^{-v} v^{(1/n)-1} dv$, where $n = 2$ is the error function (from Jahnke and Emde, 1945)

is symmetric and centered on this point. The complete solution (Eq. 5.5-16) is not symmetric, but as we noted, this effect is small. Dispersion, therefore, does not affect the rate of wave propagation, but it does affect the degree of mixing in the wave.

The displacement efficiency for the displaced component is

$$E_D = \bar{C}_D = \int_0^1 C_D(x_D, t_D) dx = \left(\frac{\sqrt{t_D}}{N_{Pe}} \right) \left[ierfc\left(\frac{-\sqrt{t_D N_{Pe}}}{2} \right) - ierfc\left(\frac{1-t_D}{2\sqrt{\frac{t_D}{N_{Pe}}}} \right) \right] \quad (5.5-17)$$

where $ierfc(x) = \int_x^\infty erfc(\xi) d\xi$ is the integral complementary error function also tabulated (Carslaw and Jaeger, 1959). Figure 5-15 plots E_D versus t_D for various N_{Pe} . E_D decreases at fixed t_D as dispersion increases. Since miscible displacements do not have residual phase saturations, E_D approaches 1 as t_D increases. Figures 5-14 and 5-15 indicate a stronger effect of N_{Pe} on concentration profiles than on displacement

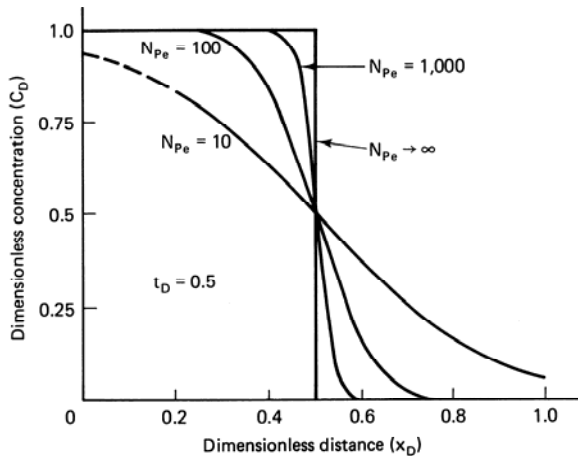
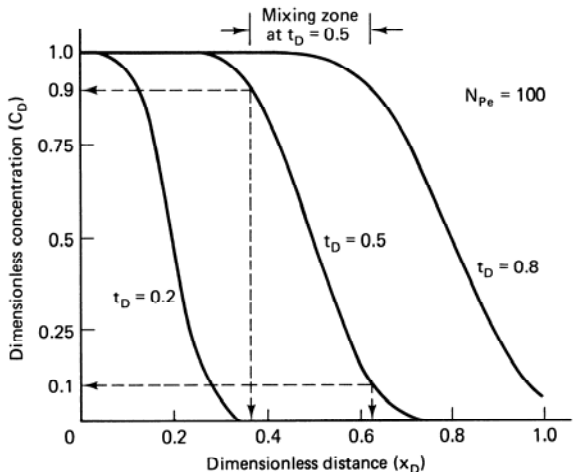


Figure 5-14 Dimensionless concentration profiles

efficiency; hence concerns about the detrimental effect of dispersion on recovery are usually limited to slugs. This topic we defer to Sec. 7-6.

The dimensionless mixing zone, the distance between the distances where $C_D = 0.1$ and $C_D = 0.9$, follows from Eq. (5.5-15),

$$\Delta x_D = x_D|_{C_D=0.1} - x_D|_{C_D=0.9} = 3.625 \sqrt{\frac{t_D}{N_{Pe}}} \quad (5.5-18)$$

To arrive at this, invert Eq. (5.5-15) for $x_D|_{C_D=0.1}$ to yield

$$x_D|_{C_D=0.1} = t_D + 2 \sqrt{\frac{t_D}{N_{Pe}}} \operatorname{erf}^{-1}(0.8)$$

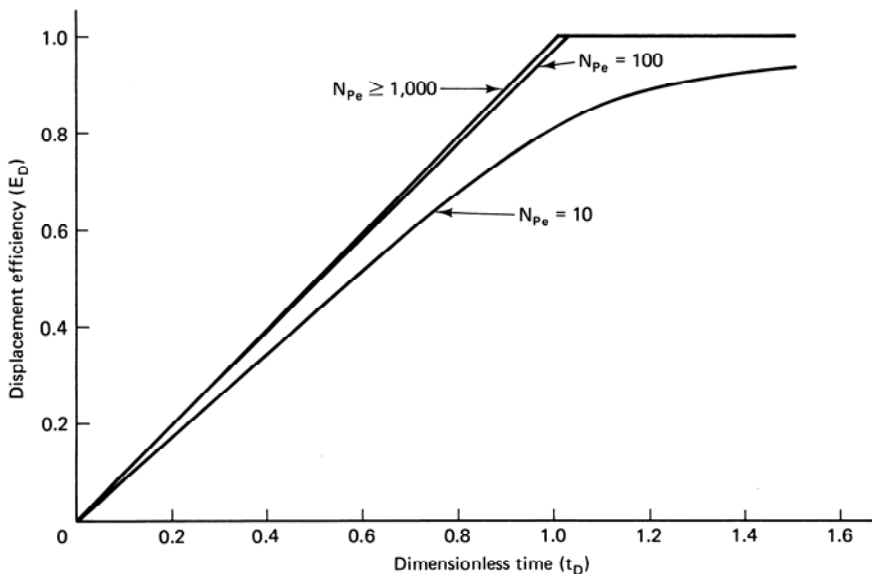


Figure 5-15 Displacement efficiency for one-dimensional miscible displacements

A similar procedure yields $x_D|_{C_D=0.9}$, and these substituted into the definition for Δx_D give Eq. (5.5-18). Equation (5.5-18) shows that dispersive mixing zones grow in proportion to the square root of time. Immiscible mixing zones grow in proportion to time. The growth suggested by Eq. (5.5-18) is generally slower than that for an immiscible mixing zone, particularly if N_{Pe} is large. This slow growth is a partial justification for neglecting dispersion in modeling semimiscible displacements compared to fractional flow effects.

Δx_D is also useful to compare laboratory to field mixing zone lengths. An immiscible mixing zone contains no free parameters if dissipation is small. Therefore, if we conduct a laboratory immiscible flood under conditions as nearly identical to a field prototype as possible (displacement in native or restored state cores, at reservoir temperature and pressure, using actual reservoir fluids), the laboratory Δx_D will be the same as in the field.

In miscible displacements, we are generally unable to make N_{Pe} equal between the laboratory and the field. Moreover N_{Pe} is usually smaller in the laboratory; thus Δx_D usually will be larger in the laboratory than in the field. Of course, the dimensional mixing zone length, $\Delta x_D L$, will always be greater in the field because L is much greater. Why we are unable to match N_{Pe} is derived from the following discussion of dispersion coefficients.

Dispersivity

Bear (1972) suggests “hydrodynamic” dispersion is “the macroscopic outcome of the actual movements of the individual tracer particles through the pores and various physical and -chemical phenomena that take place within the pores.” This movement

can arise from a variety of causes. In this text, *dispersion* is the mixing of two miscible fluids caused by diffusion, local velocity gradients (as between a pore wall and a pore center), locally heterogeneous streamline lengths, and mechanical mixing in pore bodies. Gravity tonguing and viscous fingering are two-dimensional effects that we discuss in Chap. 6. Here we summarize experimental findings on dispersion coefficients and some qualitative reasons for these observations.

For one-dimensional flow, the longitudinal dispersion coefficient K_l is given by

$$\frac{K_l}{D_0} = C_1 + C_2 \left(\frac{|v| D_p}{D_0} \right)^\beta \quad (5.5-19)$$

where C_1 , C_2 , and β are properties of the permeable medium and the flow regime. D_0 is the effective binary molecular diffusion coefficient between the miscible displacing and displaced fluids. D_p is an average particle diameter.

For very slow flows, the second term in Eq. (5.5-19) is negligible, and K_l is proportional to D_0 . This case is analogous to a slow displacement in a wide channel where mixing is due entirely to molecular diffusion. The constant C_1 has been found to be $1/\phi F$, where F is the electrical formation resistivity factor (Pirson, 1983) to account for the presence of the stationary phase.

For faster displacements, the second term in Eq. (5.5-19) becomes significant. Deans (1963) has shown that well-stirred tanks in series give mixing zones that can be described by dispersion coefficients proportional to velocity. Here, mixing is the result of the highly irregular flow paths in the REV, which cause fluids to mix completely as they are produced from each cell. Diffusion, of course, is negligible if the fluids are well mixed.

An alternate, two-dimensional interpretation, including diffusion in this flow regime, is the theory of Taylor (1953), whereby the flow channels are visualized as having lateral dimensions much smaller than the longitudinal dimensions. For this idealization, diffusion equalizes concentration gradients in the lateral direction giving rise to an “effective” diffusion coefficient. Mixing is now the result of transverse diffusion and variations in velocity caused by the no-slip condition at the pore wall. Taylor’s theory predicts dispersion coefficients proportional to velocity squared.

Experimentally, it is found (Perkins and Johnston, 1963) that $\beta = 1$ to 1.25 in Eq. (5.5-19); hence it seems the local mixing interpretation is closer to the mark than Taylor’s theory.

This local mixing flow regime is where most EOR processes will occur. In fact, if the interstitial velocity is greater than about 3 cm/day, the local mixing term in Eq. (5.5-19) dominates the first term, and we can write

$$K_l = \frac{D_0}{\phi F} + C_2 \left(\frac{|v| D_p}{D_0} \right)^\beta D_0 \cong \alpha_l |v| \quad (5.5-20)$$

This does not imply that diffusion is categorically negligible in miscible flow. Several phenomena involve flow around stagnant regions (for example, dead-end pores, water blocked pores, or adjacent nonflowing zones) where diffusion rates are

important even in regimes that would otherwise be well described by Eq. (5.5-20). α_l in Eq. (5.5-20) is the longitudinal *dispersivity* of the permeable medium (Eq. 2.2-14), a measure of the local heterogeneity scale. Bear (1970) classifies α_l as one of the fundamental properties of the medium. For the local mixing flow regime, α_l is a more fundamental measure of dispersion than K_l .

Figure 5-16 shows the three flow regimes from Perkins and Johnston (1963). Similar data is in Bear (1970) and in several references of Perkins and Johnston.

The form of Eq. (5.5-20) is particularly convenient as the Peclet number (Eq. 5.5-4), and the dimensionless concentration balance (Eq. 5.5-2) now become independent of velocity

$$N_{Pe} = \frac{L}{\alpha_l} \quad (5.5-21)$$

Therefore, the dimensionless mixing zone is directly related to α_l through Eq. (5.5-18). In fact, α_l/L can be crudely regarded as the dimensionless mixing zone length.

Suppose we try to design a laboratory displacement that has the same dimensionless mixing zone length as a field prototype. Then we must have

$$\left(\frac{\alpha_l}{L} \right)_{\text{field}} = \left(\frac{\alpha_l}{L} \right)_{\text{lab}} \quad (5.5-22)$$

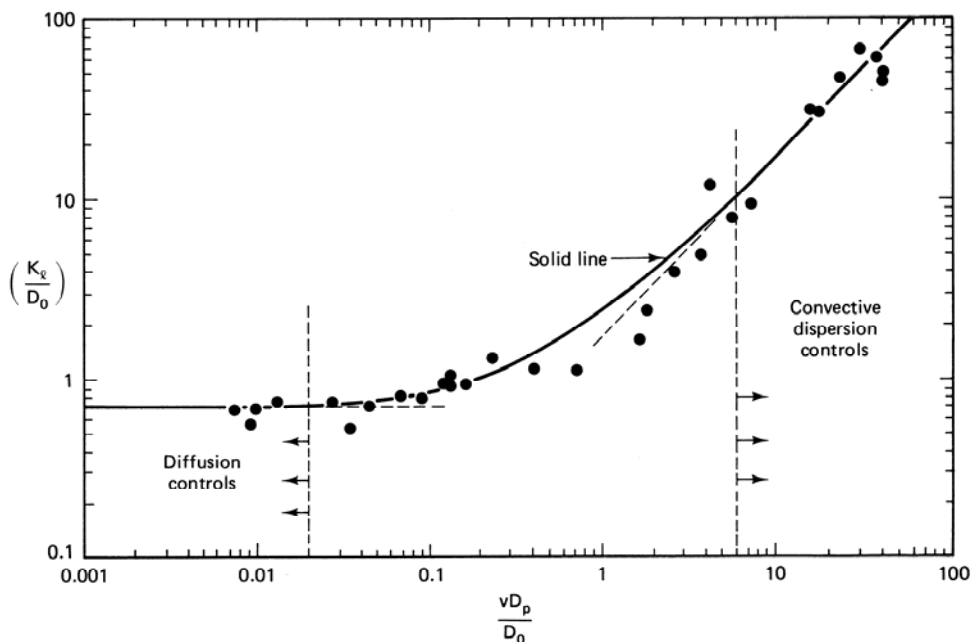


Figure 5-16 Longitudinal dispersion coefficients in permeable media flow (from Perkins and Johnson, 1963)

Equation (5.5-22) clearly cannot be satisfied if the laboratory and field dispersivities are assumed equal.

To enforce the equality in Eq. (5.5-22), we must have laboratory and field values of α_l . Laboratory-measured α_l 's are available through correlations or experiments. They are generally a few centimeters or less depending on the core material. The estimated field-measured values of α_l are far less certain. A good summary of field-measured dispersivities is shown in Fig. 5-17. This figure shows field-measured α_l 's for several formation types plotted against the length scale it was measured over. On the log-log scale, there is clearly considerable variation in α_l at

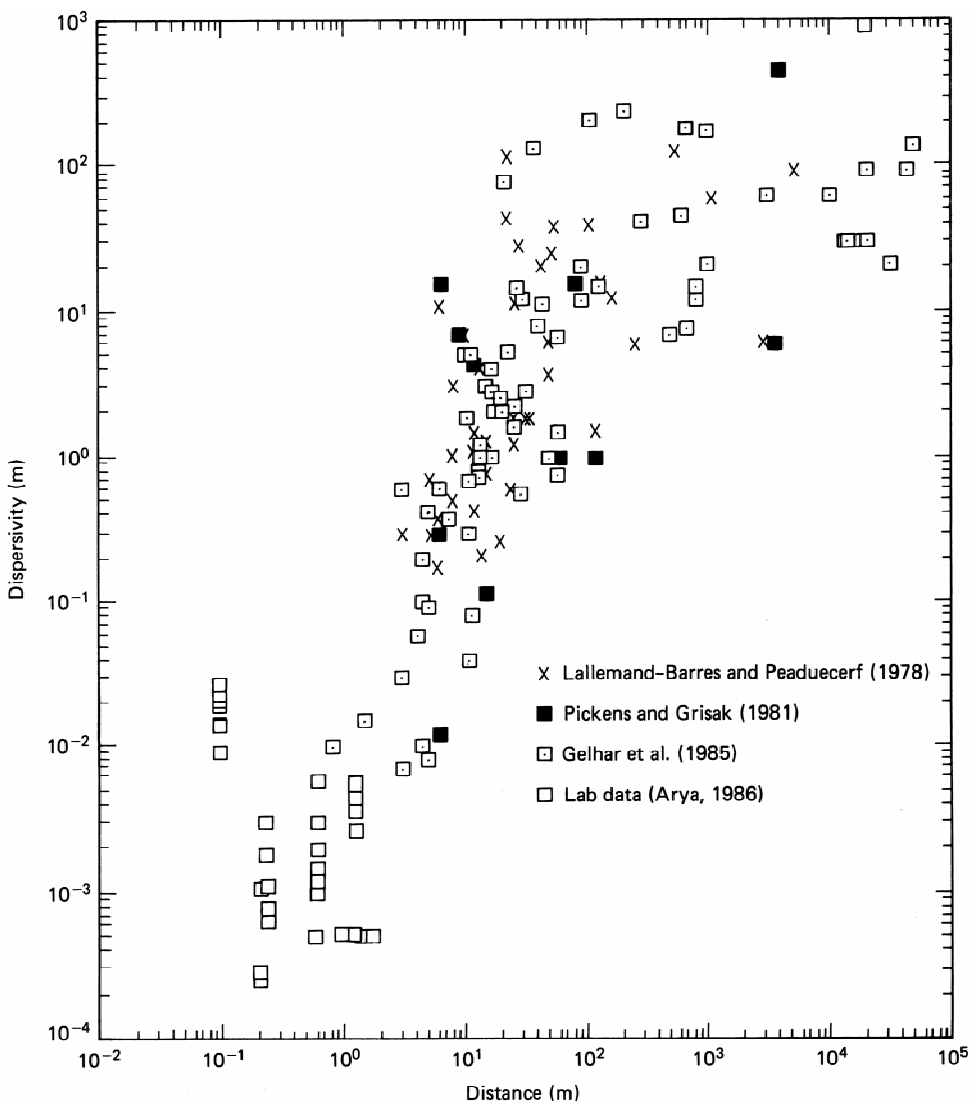


Figure 5-17 Field and laboratory measured dispersivities (from Arya et al., 1988)

the same length, and even for the same formation, even though there is little or no correlation with the latter.

Despite the scatter, there is a clear trend of increasing α_l with measurement distance. We can explain this increase qualitatively by saying the scale of heterogeneity captured by a given measurement increases as the volume sampled increases. Quantitatively, the phenomenon is the subject of active research (Gelhar et al., 1979; Dagan, 1984) because of the complicated interplay between heterogeneity, local dispersion coefficients, diffusion, and other permeable media properties that combine to make α_l length dependent.

Figure 5-17 points out the interesting and significant behavior of α_l as system macroscopic length increases. But even on a local scale, the behavior of longitudinal dispersivity is not well known when multiple phases are flowing. Figure 5-18 gives experimental data showing how the intraphase dispersivity changes as the phase saturation changes. The data in this figure are for constant saturation flow of micellar fluids for which the more general definition of K_l (Eq. 2.2-14) is appropriate. Figure 5-18 shows that aqueous phase dispersivity can increase by more than a factor of 10 as the aqueous phase saturation decreases. (This dispersivity increases as the effective heterogeneity increases, but now the “heterogeneity” must be related to the

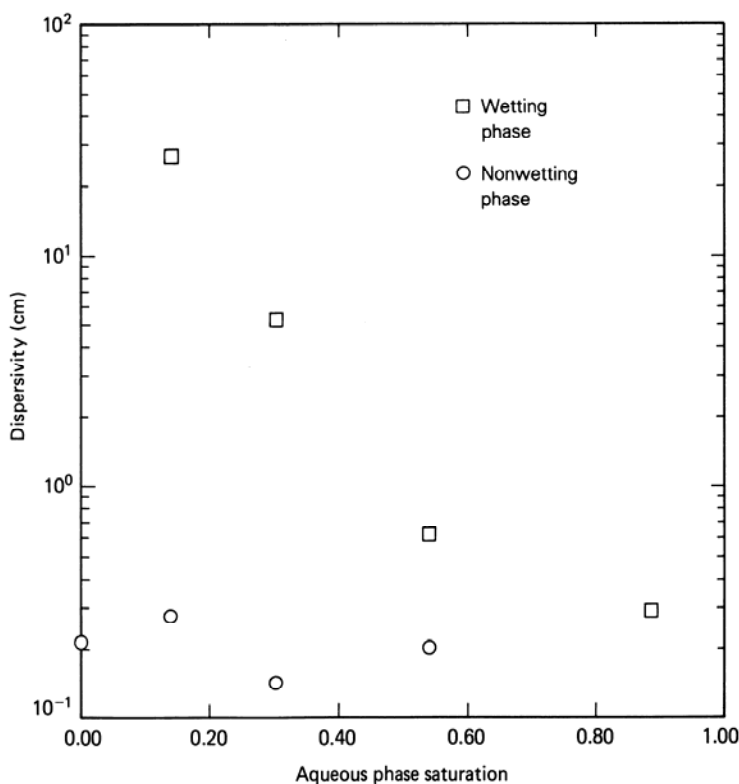


Figure 5-18 Dispersivities for constant saturation miscible flows (from MacAllister, 1982)

characteristics of the flowing fluids.) It is likely that wetting conditions play a large role in the α_l increase since no such changes in α_l were observed for the nonwetting phase in Fig. 5-18.

We summarize the most important points about the effects of dispersion on one-dimensional miscible flow as follows:

1. Dispersion controls the rate of mixing of two fluids but does not affect wave velocity.
2. Dispersive mixing zones can grow no faster than in proportion to the square root of time.
3. The fluid velocity of most EOR processes is such that the flow is in the local mixing flow regime where the dispersion coefficient is proportional to the interstitial velocity. The proportionality constant is the longitudinal dispersivity α_l .
4. α_l is a measure of the heterogeneity of the permeable medium and varies with phase saturation and the measurement scale.
4. Neglecting dispersion in field-scale displacements is not proper because dispersivity appears to increase with travel distance.

5-6 GENERALIZATION OF FRACTIONAL FLOW THEORY

In this section, we present the mathematical formalities to broaden the fractional flow theories of Secs. 5-2 and 5-4 to multiple component, multiphase flow. As in those sections, we neglect dissipative effects and restrict the equations to one-dimensional flow. Our presentation is based on a subset of the method of characteristics (MOC) solution technique known as simple wave theory, or coherence theory. (For more careful mathematical detail, see Courant and Friedrichs, 1948; Helfferich and Klein, 1970; and Jeffrey and Taniuti, 1964.)

The fundamental principle in the MOC is to solve partial differential equations (PDEs) by first converting them to a set of ordinary differential equations (ODEs) that may then be integrated simultaneously. This set of ODEs can rarely be integrated in closed form, but there is a large class of permeable media flow problems for which the integrations will appear in a general form. To illustrate these ideas, we consider first a single PDE and then pairs of PDEs in the dependent variables u and v . The theory may be generalized to more than two PDEs, but in practice, the procedures become cumbersome.

One Dependent Variable

Consider the following partial differential equation for $u(x, t)$

$$L(u) = Au_t + Bu_x + E = 0 \quad (5.6-1)$$

where A , B , and E are known functions of u , x , and t . The operator $L(u)$ is linear in the derivatives of u . The notation u_x and u_t means partial differentiation with respect to x and t holding the other variable constant. We want solutions to Eq. (5.6-1) in the form $u(x, t)$ subject to the appropriate initial and boundary conditions. In the MOC, we seek these solutions in the form $u(s)$, where s is a parameter along a curve C in xt -space such that $x = x(s)$ and $t = t(s)$. We may, therefore, write the total derivative of u with respect to s as

$$u_s = t_s u_t + x_s u_x \quad (5.6-2)$$

Equation (5.6-2) is a mixture of total derivatives u_s , t_s , and x_s and partial derivatives u_t and u_x . However, we use the same notation for both types of derivatives since the type of derivative should be clear from the usage. Comparing Eqs. (5.6-1) and (5.6-2) leads to

$$t_s = A \quad (5.6-3a)$$

$$x_s = B \quad (5.6-3b)$$

$$u_s = -E \quad (5.6-3c)$$

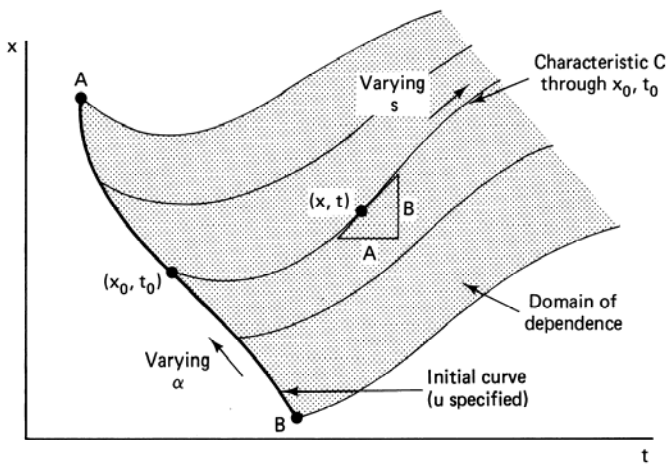
Equations (5.6-3), which imply the operator $L(u)$ is a directed derivative along C , are a set of three ODEs that may be integrated from an initial curve, as shown in Fig. 5-19(a), to give a characteristic curve C in xt space along which u varies as given by the integration of Eq. (5.6-3c).

The various integrations are possible only if C is nowhere tangent to the initial curve. Figure 5-19(a) schematically shows the integration of these equations for a curve C that begins at the point (x_0, t_0) on the initial curve. We could take other points on the initial curve and thereby cover the shaded *domain of dependence* in Fig. 5-19(a) defined by the characteristics through the points A and B on ends of the initial curve. If α is a parameter along the initial curve, the solution to Eqs. (5.6-3) is $t = t(s, \alpha)$, $x = x(s, \alpha)$, and $u = u(s, \alpha)$. s and α are the coordinates of a natural, generally curved, coordinate system for Eq. (5.6-1). Since α , in effect, determines which curve C passes through the point (x, t) , at which the value of u is desired, the characteristics for Eq. (5.6-1) are a one-parameter (α) family of curves, and α is a label for this one-parameter family. An important observation is that at every point (x, t) in the shaded region in Fig. 5-19(a), the slope of the characteristic curve is given by

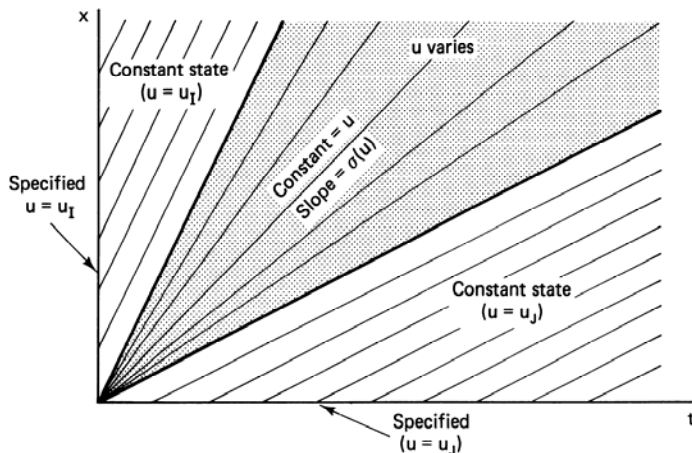
$$\frac{x_s}{t_s} = \frac{dx}{dt} \Big|_C = \frac{B}{A} = \sigma(u, x, t) \quad (5.6-4)$$

σ is the *characteristic direction* at a given (x, t) . Equation (5.6-4) implies it will generally be unnecessary to determine $t = t(s, \alpha)$ and $x = x(s, \alpha)$ since $t = t(x, \alpha)$ will follow directly from Eqs. (5.6-4) and (5.6-3c).

Consider now a special case of Eq. (5.6-1) where $E = 0$, and A and B are functions of u only. The initial data are a curve that coincides with the x axis, where



(a) Characteristic construction for general one dependent variable problem



(b) Characteristic construction for one variable simple wave

Figure 5-19 Domains of dependence for one-variable hyperbolic equations

$u = u_I$ and then coincides with the t axis, where $u = u_J$. Thus the boundary ($x = 0$) and initial ($t = 0$) data are uniform except for a step change at the origin where all values of u between u_I and u_J exist. It follows immediately from Eqs. (5.6-3c) and (5.6-4) that u is constant along the characteristics C , which are themselves straight lines. Figure 5-19(b) shows the characteristics for this case. In regions adjacent to the x and t axes, the characteristics are parallel with slopes $\sigma(u_I)$ and $\sigma(u_J)$, respectively. These regions are constant-state regions since the dependent variable u is constant therein. The shaded region in Fig. 5-19(b) is a fanlike region where σ changes continuously between the limits imposed by the constant-state regions. Each ray emanating from

the origin carries a particular constant σ from the infinite numbers of u 's between u_I and u_J , and each has a slope σ evaluated at that u . Therefore, the shaded region in Fig. 5-19(a) is a wave since, in any noncharacteristic direction, u is changing.

From Fig. 5-19(b), the characteristics cannot cross, but there is nothing that requires σ to decrease monotonically, as in the case shown. When σ does not decrease monotonically, a mathematically valid solution exists that leads to the formation of shock waves, u being a physical variable.

Finally, the characteristic direction σ may clearly be interpreted as a velocity (if x and t are distance and time) and written as

$$\sigma = \frac{dx}{dt} \Big|_C = \frac{dx}{dt} \Big|_u \quad (5.6-5)$$

With the appropriate forms for A , B , t , and x , Eq. (5.6-5) becomes the Buckley-Leverett equation (Eq. 5.2-10) for water displacing oil in a permeable medium as we discussed in Sec. 5-2. Note the similarity between Figs. 5-5 and 5-19(b).

Two Dependent Variables

Let us consider now a pair of PDEs in the dependent variables $u(x, t)$ and $v(x, t)$

$$L_1(u, v) = A_1 u_t + B_1 u_x + C_1 v_t + D_1 v_x + E_1 = 0 \quad (5.6-6a)$$

$$L_2(u, v) = A_2 u_t + B_2 u_x + C_2 v_t + D_2 v_x + E_2 = 0 \quad (5.6-6b)$$

Initially, we consider the most general case of the coefficients A – E being functions of x , t , u , and v . The first pair of terms in the linear operators L_1 and L_2 may be regarded as directed derivatives of u and v . From the total derivative of du and dv , there are four such directions ($A_1 u_t + B_1 u_x$, $C_1 v_t + D_1 v_x$, and so on) for each PDE. But to transform the pair to a set of ODEs, we seek a curve in (x, t) space where $u = u(s)$, $v = v(s)$, $x = x(s)$, and $t = t(s)$. We, therefore, seek a combination $L = \lambda_1 L_1 + \lambda_2 L_2$ so that L is a linear function of total derivatives u_s and v_s . As before, s is a parameter along such a curve. For solutions to the equations, the operator L must be equal to zero, hence

$$L = (A_1 \lambda_1 + A_2 \lambda_2) u_t + (B_1 \lambda_1 + B_2 \lambda_2) u_x + (C_1 \lambda_1 + C_2 \lambda_2) v_t + (D_1 \lambda_1 + D_2 \lambda_2) v_x + (E_1 \lambda_1 + E_2 \lambda_2) = 0 \quad (5.6-7)$$

For the directed derivatives of u and v to be colinear, it is necessary that

$$\frac{x_s}{t_s} = \sigma = \frac{B_1 \lambda_1 + B_2 \lambda_2}{A_1 \lambda_1 + A_2 \lambda_2} = \frac{D_1 \lambda_1 + D_2 \lambda_2}{C_1 \lambda_1 + C_2 \lambda_2} \quad (5.6-8)$$

be obtained from the total derivative for each dependent variable. The two equations

in Eq. (5.6-8) may be written as

$$(A_1 x_s - B_1 t_s) \lambda_1 + (A_2 x_s - B_2 t_s) \lambda_2 = 0 \quad (5.6-9a)$$

$$(C_1 x_s - D_1 t_s) \lambda_1 + (C_2 x_s - D_2 t_s) \lambda_2 = 0 \quad (5.6-9b)$$

For nonzero λ_1 and λ_2 , the determinant of the coefficient matrix must be zero; hence

$$\begin{aligned} (A_1 C_2 - A_2 C_1) \sigma^2 + (A_2 D_1 - D_2 A_1 + C_1 B_2 - C_2 B_1) \sigma \\ + (B_1 D_2 - D_1 B_2) = 0 \end{aligned} \quad (5.6-10)$$

where we have substituted the characteristic direction σ from Eq. (5.6-8). Immediately, it is apparent that there are, in general, two characteristic directions, not one as in the analogous expression (Eq. 5.6-4) for the one variable problem. Whether or not these directions are real for all (x, t) depends on the form of the coefficients. For permeable media flow problems, σ is real in at least some, and usually all, of the domain (x, t) . This, in fact, is the definition of hyperbolic PDEs. Further, the roots in Eq. (5.6-10) are generally distinct. Let σ^+ designate the larger root and σ^- the smaller of Eq. (5.6-10). Clearly, the corresponding characteristic curves, C^+ and C^- , cover the domain of dependence in (x, t) since the slope of C^+ is everywhere larger than the slope of C^- . Figure 5-20 shows these curves. The shaded domain of dependence is bounded for the two dependent variable problem by the fast σ^+ characteristic through B and the slow σ^- characteristic through A .

Each point in the domain of dependence is on the intersection of an σ^+ and σ^- characteristic. The coordinates of a point may then be located as a distance s along a particular characteristic having label α ; that is, $x = x(s, \alpha)$, and $t = t(s, \alpha)$. Alternatively, the coordinates may also be located by giving the labels of both characteristics passing through it, or $x = x(\alpha, \beta)$ and $t = t(\alpha, \beta)$, where β is now the label of the other characteristic. The notion of labels is somewhat confusing since α and β can take on the same numerical values on the initial curve; however, in the interior of the domain of influence, they are distinct.

The characteristic curves cannot be obtained, in general, unless it is known how u and v change along the characteristic directions. This may be obtained by replacing the coefficients of u_x and v_x in Eq. (5.6-7) by the numerators in Eq. (5.6-8)

$$(A_1 \lambda_1 + A_2 \lambda_2) u_s + (C_1 \lambda_1 + C_2 \lambda_2) v_s + (E_1 \lambda_1 + E_2 \lambda_2) t_s = 0 \quad (5.6-11a)$$

where we have rearranged with $u_s = u_x x_s + u_t t_s$, and so on. A similar procedure on u_t and v_t gives

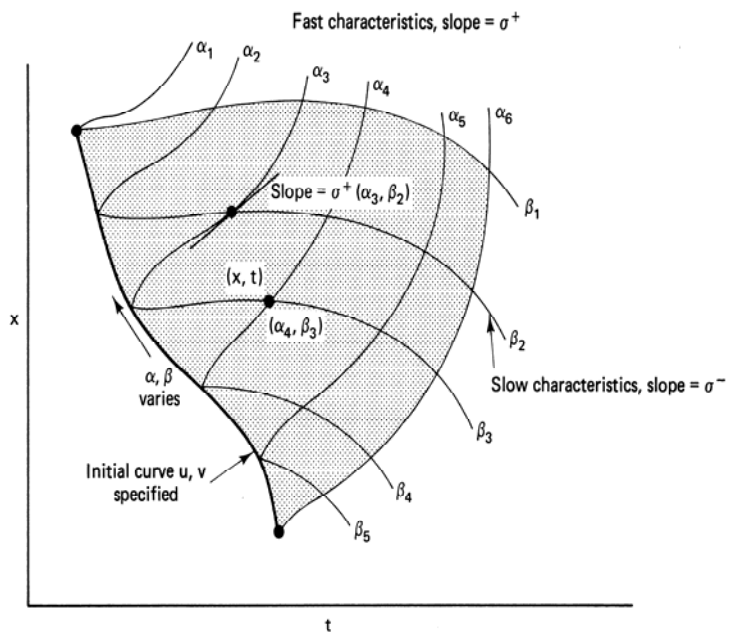
$$(B_1 \lambda_1 + B_2 \lambda_2) u_s + (D_1 \lambda_1 + D_2 \lambda_2) v_s + (E_1 \lambda_1 + E_2 \lambda_2) x_s = 0 \quad (5.6-11b)$$

These equations rearranged are

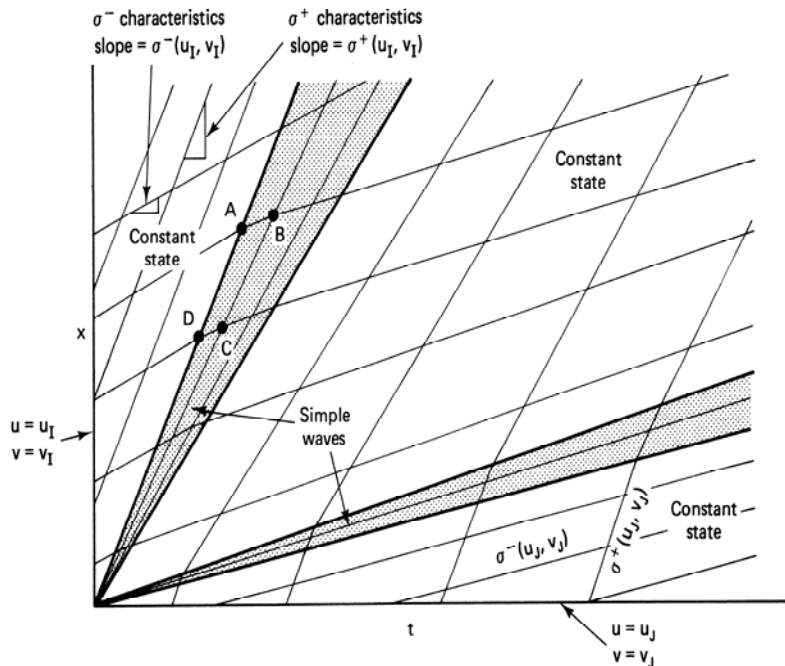
$$(A_1 u_s + C_1 v_s + E_1 x_s) \lambda_1 + (A_2 u_s + C_2 v_s + E_2 t_s) \lambda_2 = 0 \quad (5.6-12a)$$

$$(B_1 u_s + D_1 v_s + E_1 x_s) \lambda_1 + (B_2 u_s + D_2 v_s + E_2 t_s) \lambda_2 = 0 \quad (5.6-12b)$$

Again, for nontrivial λ_1 and λ_2 , the determinant of the coefficient matrix must be zero, and again, the characteristic equation has two real, distinct roots for u_s or v_s .



(a) Characteristics for general two-variable problem



(b) Characteristics for two-variable centered simple wave

Figure 5-20 Domains dependence for two-variable hyperbolic equations

The roots to these equations form, along with the two roots to Eq. (5.6-10), four ODEs that may be integrated simultaneously for u , v , x , and t from an initial curve.

Rather than expound further on this, let's consider the special case where E_1 and $E_2 = 0$, and the remaining coefficients are functions of u and v only. Such equations are said to be *reducible*. The characteristic directions from Eq. (5.6-10) are a known function of u and v only. Further, along each characteristic curve, there is a relation between u and v given by

$$(B_2 A_1 - B_1 A_2) \frac{du}{dv} = (B_1 C_2 - C_1 B_2) + \sigma^\pm (C_1 A_2 - A_1 C_2) \quad (5.6-13)$$

from the determinant of the singular matrix formed by Eqs. (5.6-9a) and (5.6-12a). There are three equivalent forms to this equation, but the important point is that u and v are related to each other along the C^\pm curves in $x-t$ space since all the coefficients in Eq. (5.6-13) are known functions of u and v . The $u-v$ plot that contains the above solution is said to be the image, or hodograph, space and the function $u = u(v)$ for C^+ is the image curve Γ^+ or C^+ , as is $u = u(v)$ for Γ^- the image curve for C^- . In this text, we call the $u-v$ space the *composition path diagram*, and the Γ^+ and Γ^- curves the *composition paths*.

Besides the restriction to reducible PDEs, let's now consider the special case of $u = u_I$ and $v = v_I$ being specified on the x axis, and $u = u_J$ and $v = v_J$ being specified on the t axis. As before, this means that all (u, v) values between $(u, v)_I$ and $(u, v)_J$ exist at the origin. Also as before, there are regions of constant state adjacent to both axes where the characteristic directions, and hence, the labels α and β are constant. But unlike before, there are now two fan-shaped regions (Fig. 5-20b) where first the fast or α characteristics change slope, and then the β characteristics change. The regions cannot overlap, or there would be finite regions where $\sigma^+ < \sigma^-$. This fact causes the creation of a new constant-state region (u, v) between the fans that is, in general, different from either $(u, v)_I$ or $(u, v)_J$. Within the fan-shaped regions, the α and β characteristics cannot both be straight, or else these would be constant-state regions. But one of the characteristic directions must be straight in each region (σ^+ in the first shaded region in Fig. 5-20(b), and σ^- in the second). This is so because two points A and D on the boundary have the same (u, v) values since they can be regarded as being in the constant-state region. This must be true of all other rays in the fan-shaped region, for example, that passing through C and B . Otherwise, the ray would be curved (from Eq. 5.6-10) and would ultimately intersect either of the constant-state regions. It follows, then, that all points on the straight-line characteristic carry the same (u, v) value. Since $(u, v)_A = (u, v)_D$ and $(u, v)_B = (u, v)_C$, it follows that $\sigma_B^- = \sigma_C^-$ and the slope of the α characteristics is the same on all the σ^+ characteristics. This means the $u = u(v)$ relationship defined by Eq. (5.6-13) is the same on any slow characteristic in the region. Thus $(du/dv)_\sigma^-$ and $(du/dv)_\sigma^+$ uniquely determine the variations in u and v in the respective fan-shaped regions. The function $u = u(v)$ is always calculated based on the curved characteristic.

The above concepts apply generally to reducible sets of PDEs in any number of N dependent variables. Stated concisely, the observations are

1. Adjacent to any constant-state region, there is a region having at least one straight line characteristic. The second region is a *simple wave* region.
2. Within a simple wave region, the dependent variables are related to each other through a set of ODEs.
3. For boundary and initial conditions that are uniform except for a step change at the origin, the entire (x, t) domain consists of alternating constant-state and simple wave regions. The simple waves in this case are *centered* simple waves.

Coherence

The information on reducible equations may be restated with more physical insight by referring to simple waves in the terminology of *coherent* waves (Helfferich and Klein, 1970). Since (u, v) is constant on a straight-line characteristic in a simple or coherent wave region, and since σ is a function of u and v only, it follows that

$$\left. \frac{dx}{dt} \right|_u = \left. \frac{dx}{dt} \right|_v \quad (5.6-14a)$$

or for u_1, \dots, u_N dependent variables

$$\left. \frac{dx}{dt} \right|_{u_1} = \left. \frac{dx}{dt} \right|_{u_2}, \dots, = \left. \frac{dx}{dt} \right|_{u_N} \quad (5.6-14b)$$

Equation (5.6-14b) states that the velocity of constant values of the dependent variables is the same—the coherence condition. As we illustrate in Sec. 5-7, the coherence method of calculating simple waves is more direct than using MOC. Equation (5.6-14b) implies, further, that there can be no more than N waves.

5-7 APPLICATION TO THREE-PHASE FLOW

In this section, we apply the results of the coherence theory by calculating the displacement efficiencies for a three-phase water ($i = 1$), oil ($i = 2$), gas ($i = 3$) flow problem. We assume away dissipative effects—capillary pressure and pressure-dependent fluid properties—and restrict the fluids to be single pseudocomponent phases. The assumption of an incompressible gas phase is, of course, realistic only if

$$c_3 \Delta P \approx \frac{\Delta P}{P} \quad (5.7-1)$$

is small. This condition is not met in general although for flows in high permeability media $c_3 \Delta P$ can be fairly small, particularly considering that gas viscosity is also

small. But even if $c_3\Delta P$ is large, we have seen from Sec. 5-3 that fluid compressibility causes waves to spread and does not affect wave velocity.

Subject to the above restrictions, the species conservation Eq. (5.4-1) becomes

$$\frac{\partial S_j}{\partial t_D} + \frac{\partial f_j}{\partial x_D} = 0, \quad j = 1 \text{ or } 2 \quad (5.7-2)$$

in dimensionless form, where for a horizontal reservoir

$$f_j = \left(\frac{\lambda_{rj}}{\sum_{m=1}^3 \lambda_{rm}} \right) \quad (5.7-3)$$

The relative mobilities in Eq. (5.7-3) are known functions of S_1 and S_2 . Only two independent saturations are in this example, since $S_1 + S_2 + S_3 = 1$, which we arbitrarily take to be the water and oil saturations. Equation (5.7-3) implies that the fractional flows are known functions of S_1 and S_2 .

From Eq. (5.4-5), the specific velocity of a constant saturation S_j is

$$v_{S_j} = \left(\frac{\partial f_j}{\partial S_j} \right)_{t_D}, \quad j = 1 \text{ or } 2 \quad (5.7-4a)$$

if the wave is nonsharpening and

$$v_{\Delta S_j} = \frac{\Delta f_j}{\Delta S_j}, \quad j = 1 \text{ or } 2 \quad (5.7-4b)$$

if the wave is a shock. We cannot take the derivative in Eq. (5.7-4a) without knowing the solution to the problem $S_j(x_D, t_D)$. The results of the previous section carry over to this problem with $A_1 = 1$, $B_1 = f_{11}$, $D_1 = f_{12}$, $B_2 = f_{21}$, $C_2 = 1$, $D_2 = f_{22}$, $A_2 = C_1 = 0$, $E_1 = E_2 = 0$. For brevity, we have adopted the convention that $f_{12} = (\partial f_1 / \partial S_2)S_1$, and so on. B_1 , B_2 , C_1 , and C_2 are known functions of S_1 and S_2 —though perhaps very complicated—but we can calculate them without knowing the solution $S_1(x_D, t_D)$ and $S_2(x_D, t_D)$.

Let's now let the initial saturations in the medium be uniform at (S_1, S_2) , and impose at $x_D = 0$ the saturations $(S_1, S_2)_J$. From Sec. 5-6, we know the coherence condition applies at all points in the domain where

$$\frac{df_1}{dS_1} = \frac{df_2}{dS_2} = \sigma \quad (5.7-5)$$

from Eqs. (5.6-14b) and (5.7-4a). The derivatives in Eq. (5.7-5) are total derivatives since the coherence condition implies the existence of a relation $S_2 = S_2(S_1)$ in saturation space. We expand the derivatives in Eq. (5.7-5) and write the two equations in matrix form as

$$\begin{pmatrix} f_{11} & f_{12} \\ f_{21} & f_{22} \end{pmatrix} \begin{pmatrix} dS_1 \\ dS_2 \end{pmatrix} = \sigma \begin{pmatrix} dS_1 \\ dS_2 \end{pmatrix} \quad (5.7-6)$$

To solve for $S_2(S_1)$, we first solve this equation for the eigenvalues, σ^\pm

$$\sigma^\pm = \frac{1}{2} \{(f_{22} + f_{11}) \pm [\{(f_{22} + f_{11})^2 + 4f_{21}f_{12}\}]^{1/2}\} \quad (5.7-7)$$

Both roots to Eq. (5.7-7) are real, $\sigma^+ > \sigma^-$, and both are known functions of S_1 and S_2 . Recall that the σ^\pm are saturation velocities. Solving for dS_1 and dS_2 in Eq. (5.7-6) gives

$$\frac{dS_1}{dS_2} = \frac{\sigma^\pm - f_{11}}{f_{12}} \quad (5.7-8)$$

Equations (5.7-7) and (5.7-8) are the special cases of Eqs. (5.6-10) and (5.6-13). Equation (5.7-8) is an ordinary differential equation whose integration gives the function $S_2(S_1)$. There are two such functions corresponding to σ^+ and σ^- . The velocity of any saturation along $S_2(S_1)$ is given by σ^+ and σ^- depending on whichever is physically realistic.

The above procedure could perhaps be made clearer by addressing a particular problem. Consider an oil–gas–water mixture being displaced by water. To make the problem simple, we take the relative permeabilities to be

$$k_{rj} = \frac{S_j - S_{jr}}{1 - S_{1r} - S_{2r} - S_{3r}}, \quad j = 1 \text{ or } 2 \quad (5.7-9)$$

and let $S_{1r} = S_{2r} = S_{3r} = 0.1$. Equation (5.7-9) is not a realistic three-phase relative permeability function (see Exercise 5N), but it is sufficient for illustration. We further take $\mu_1 = 1 \text{ mPa-s}$, $\mu_2 = 5 \text{ mPa-s}$, and $\mu_3 = 0.01 \text{ mPa-s}$, and consider the initial conditions to be $S_{2I} = 0.45$, and $S_{1I} = 0.1$. Therefore, the medium is initially at residual water saturation with equal volumes of oil and gas. We are to displace this mixture with water, that is $S_{1J} = 0.8$ and $S_{2J} = 0.1$. This procedure corresponds to a waterflood initiated well into the primary production phase.

Figure 5-21 shows the functions $S_2(S_1)$ obtained by numerically integrating Eq. (5.7-8) with the indicated physical relations. The plot is on a triangular diagram to emphasize the relation $S_1 + S_2 + S_3 = 1$. The integration of Eq. (5.7-8) for various initial values of S_1 and S_2 produces two families of curves corresponding to σ^+ and σ^- , which are the image curves σ^+ and σ^- (light lines in Fig. 5-21) referred to previously. Since $\sigma^+ > \sigma^-$, the image curves nowhere coincide, and further, to every point in the saturation diagram, there are associated two velocities σ^+ and σ^- . The two families of curves we call the saturation *paths* after Helfferich (1981). The particular paths that pass from the initial to the injected condition are the saturation *routes* (bold lines in Fig. 5-21). Though we henceforth restrict our attention to the saturation routes, Fig. 5-21 gives a rapid visual perspective for any displacement having arbitrary initial and injected conditions.

In moving from the initial to injected conditions, there are two alternative saturation routes: (1) a σ^- segment going from the initial conditions to the upper apex of the three-phase flow region and then a σ^+ segment on the gas–water boundary to the injected condition and (2) a σ^+ segment from the initial conditions to $(S_1, S_2) =$

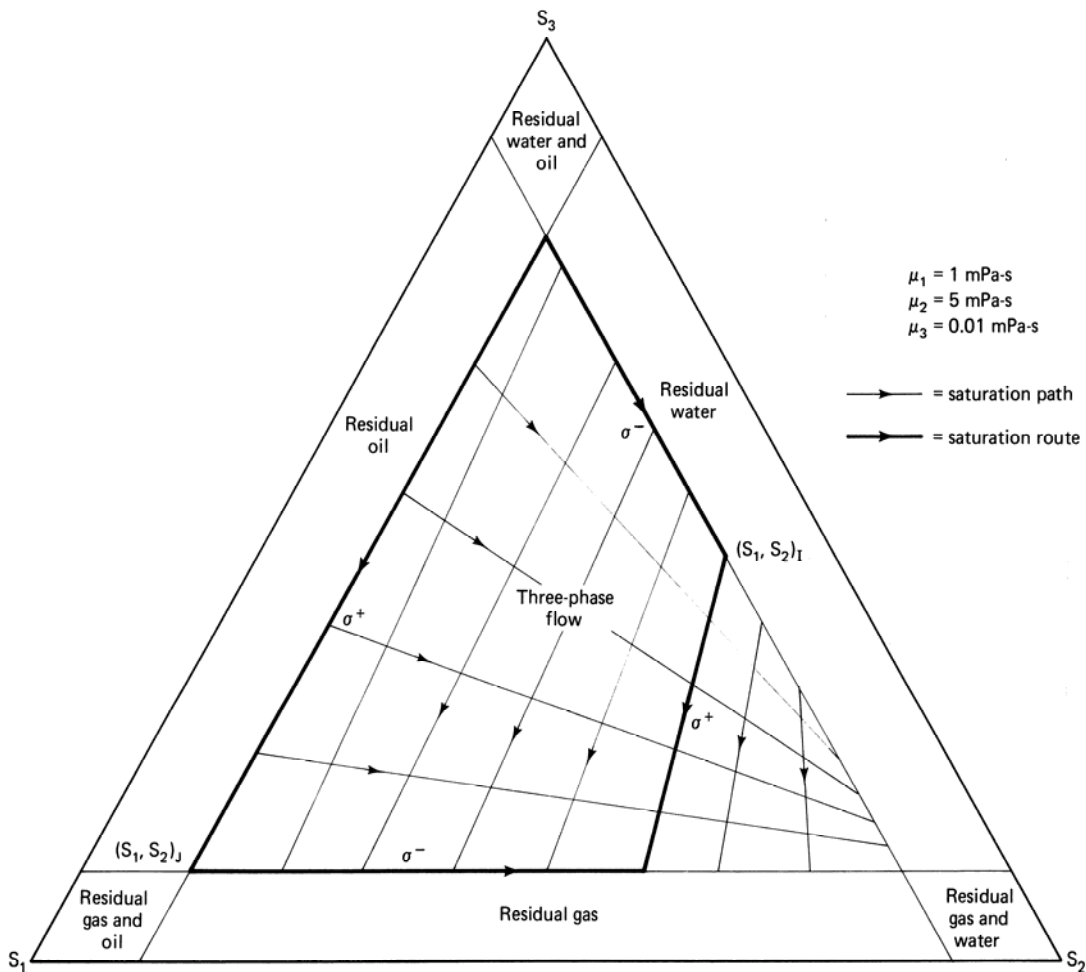
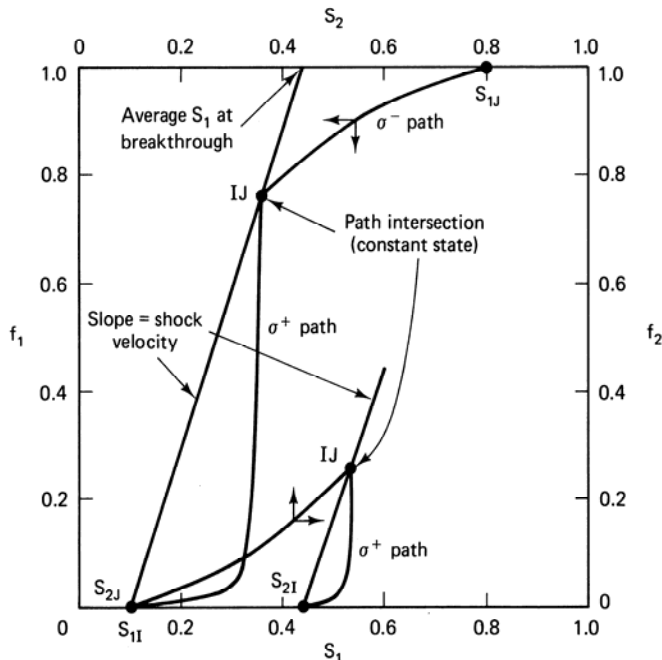


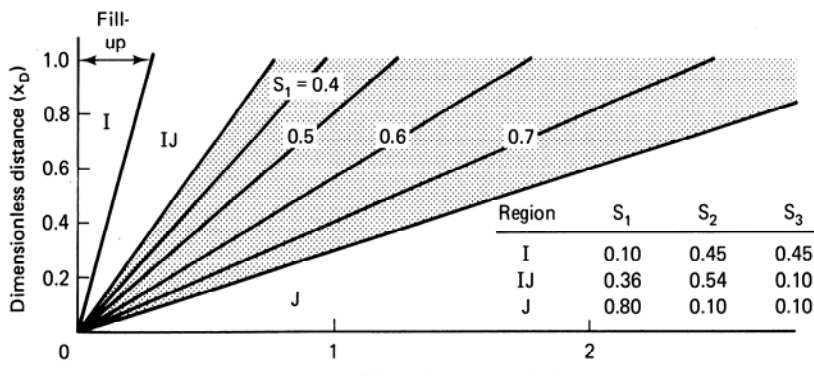
Figure 5-21 Three-phase flow saturation paths

(0.36, 0.54) followed by a σ^- segment along the oil–water boundary to the injected conditions. Both routes are mathematically valid solutions to the problem; in fact, an infinite number of mathematical solutions correspond to a route that arbitrarily switches from al to a paths in going from $(S_1, S_2)_I$ to $(S_1, S_2)_J$. From the Buckley-Leverett problem in Sec. (5-2), we know that saturation velocities must decrease monotonically (though not continuously) in the upstream direction. The only physical solution for the problem is route (2) because $\sigma^+ > \sigma^-$ forces this to be the only possible route where σ decreases monotonically from $(S_1, S_2)_I$ to $(S_1, S_2)_J$.

Within a route segment, the saturation velocities must decrease monotonically in the upstream direction also. This condition is not met on the σ^+ route segment (the arrows on the saturation routes indicate the direction of increasing saturation velocity). Such behavior indicates the wave is a shock, and we can find the shock velocity by a procedure entirely analogous to that used in Sec. (5-2). Figure 5-22(a)



(a) Flux-saturation diagram



(b) Time-distance diagram

Figure 5-22 Diagrams for three-phase flow example

plots the oil and water fluxes (f_1, f_2) versus (S_1, S_2) along the composition route. The shock construction is exactly as suggested in Fig. 5-4, and may be performed on either the f_1 - S_1 curve or the f_2 - S_2 curve. Equation (5.7-5) guarantees this equivalence. The only real difference between the three-phase and two-phase flow problems at this point is the existence of the constant-state region at IJ . The time-distance diagram for the displacement is in Fig. 5-22(b), which should be compared to Figs. 5-5 and 5-20(b).

Despite the simplified nature of the relative permeability curves used in this example, Fig. 5-22 illustrates that the most important feature of three-phase oil–gas–water flow is the extremely small gas viscosity. This viscosity causes the oil fractional flow to be small initially and to delay the appearance of an appreciable amount of oil at the outflow end until $t_D = 0.28$. This delay, or “fill-up,” time is an omnipresent feature of waterfloods begun with appreciable amounts of free gas in the medium (Caudle, 1968). A fill-up period occurs because of the very large gas mobility, not as the result of gas compressibility or redissolution. The last two effects would serve to reduce the fill-up time. A second consequence of the small gas viscosity is no simultaneous three-phase flow occurs in the medium. In fact, by assuming an oil–water mixture banks up the free gas, it is possible to repeat the results in Figs. 5-21 and 5-22 with much less effort (see Exercise 5O). A final consequence of the small gas viscosity is this behavior is qualitatively accurate regardless of the relative permeability functions used.

We end this section by discussing the displacement efficiency of the three-phase flow problem. There is now a displacement efficiency for both oil and gas for which we need average saturations for the definition (Eq. 5.1-2). Considering the fractional flux-saturation curve in Fig. 5-22(a), the average saturations follow from a procedure directly analogous to the Welge procedure in Sec. 5-2.

$$\bar{S}_j = S_j|_{x_D=1} - t_D(f_j|_{x_D=1} - f_{j,j}), \quad j=1, 2, \text{ or } 3 \quad (5.7-10)$$

where $t_D = (df_j/dS_j)^{-1}$ is the reciprocal slope of the f_j-S_j curve evaluated at $x_D = 1$. Figure 5-22(a) shows the average water saturation at water breakthrough, and Fig. 5-23 shows the displacement efficiencies for this example. Once again E_D is limited by the residual phase saturations, oil production is delayed for a fill-up period, and

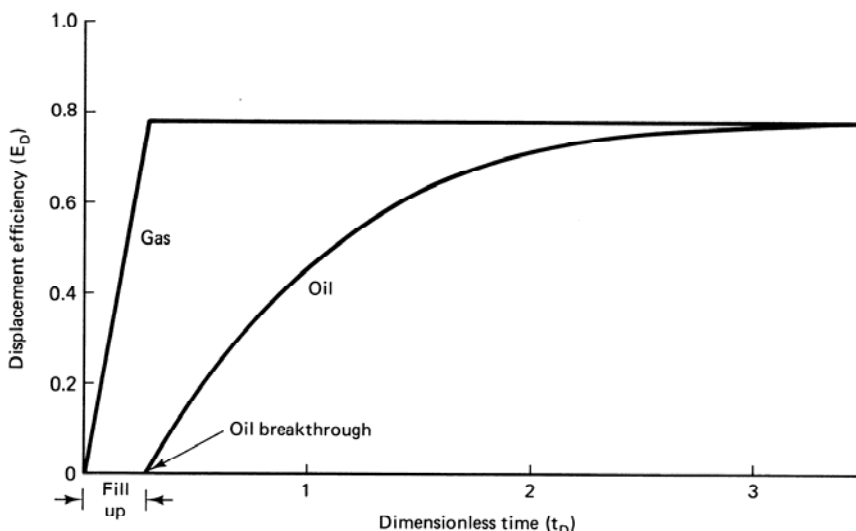


Figure 5-23 Displacement efficiencies for three-phase flow problem

the oil displacement efficiency is determined by the water–oil relative permeabilities and viscosities.

This example demonstrates the strength of simple wave theory. In later chapters, we return to these procedures for specific EOR applications.

5-8 CONCLUDING REMARKS

Any oil recovery calculation of a field-scale displacement based solely on the procedures discussed in this chapter will seriously overestimate the actual recovery: Such one-dimensional calculations neglect volumetric sweep issues which are at least as important as displacement efficiency. Nevertheless, the fractional flow calculations are important in establishing a framework for advancing our study. The items important in establishing this framework are the Buckley-Leverett theory and its generalization in Sec. 5-7, the ideas of coherent waves and their representations, and the notion of the ideal miscible displacement.

EXERCISES

- 5A.** *Parameter-Free Statement.* Show that Eqs. (5.2-5) can be reduced to a parameter-free statement by defining and introducing a reduced saturation S_D , where

$$S_D = \frac{S_1 - S_{1I}}{S_{1J} - S_{1I}} \quad (5A-1)$$

- 5B.** *Radial Form of Water Material Balance*

- (a) Show that the one-dimensional water conservation Eq. (5.2-1) for incompressible flow in radial geometry is

$$\phi \frac{\partial S_1}{\partial t} + \frac{q}{2\pi H_t r} \left(\frac{\partial f_1}{\partial r} \right) = 0 \quad (5B-1)$$

where q is the volumetric flow rate, H_t the medium thickness, and f_1 is the same as Eq. (5.2-2).

- (b) If we let $r_D = (r/R)^2$ and $t_D = \int_0^t qdt / \pi\phi H_t R^2 = \int_0^t qdt / V_p$, show that Eq. (5B-1) becomes identical to the linear Eq. (5.2-5a).

- 5C.** *Buckley-Leverett Application.* Calculate effluent histories (water cut $f_1|_{x_D=1}$ versus t) for water ($\mu_l = 1$ mPa-s) displacing oil given the following experimental data (Chang et. al., 1978):

S_1	k_{r1}	k_{r2}
0.40	0.00	0.36
0.45	0.005	0.26
0.50	0.009	0.14
0.55	0.02	0.08
0.60	0.035	0.036
0.65	0.050	0.020
0.70	0.080	0.00

Use three values of oil viscosity: $\mu_2 = 1, 5$, and 50 mPa-s. For $\mu_2 = 5$ mPa-s, calculate the endpoint, shock, and average saturation mobility ratios. The dip angle is zero.

- 5D.** *Gravity and Fractional Flow Theory.* For the exponential relative permeability functions of Eq. (3.3-4), plot water saturation profiles at $t_D = 0.3$ for dip angles of $\alpha = 0^\circ, 30^\circ$, and -30° . Additional data are $S_{1r} = S_{2r} = 0.2$, $n_1 = 1$, $n_2 = 2$, $k_{r1}^0 = 0.1$, $k_{r2}^0 = 0.8$, $\mu_1 = 1$ mPa-s, $\mu_2 = 10$ mPa-s, $k = 0.5 \mu\text{m}^2$, $\Delta\rho = 0.2 \text{ g/cm}^3$, and $\mu = 0.6 \text{ cm/day}$.

- 5E.** *Buckley-Leverett Theory with Straight Line Relative Permeabilities.* Use straight line exponential relative permeability functions with zero residual phase saturations in the following ($n_1 = n_2 = 1$, $S_{1r} = S_{2r} = 0$ in the exponential relative permeability functions). Also take $f_{1I} = 0$ and $f_{1J} = 1$.

- (a) Show that the sign of $(1 - M^0 + M^0 N_g^0 \sin \alpha)$ uniquely determines the character (spreading, indifferent, sharpening) of the water saturation wave.
- (b) For the spreading wave case— $(1 - M^0 + M^0 N_g^0 \sin \alpha) < 0$ —Eq. (5.2-10) may be inverted explicitly for $S_1(x_D, t_D)$. Derive this expression in terms of the quadratic formula.
- (c) Use the equation in part (b) to show that for $\alpha = 0$ the water saturation function is given by

$$S_1(x_D, t_D) = \begin{cases} 0, & \frac{x_D}{t_D} > M^0 \\ \frac{\left(\frac{t_D M^0}{x_D}\right)^{1/2} - 1}{M^0 - 1}, & \frac{1}{M^0} \leq \frac{x_D}{t_D} \leq M^0 \\ 1, & \frac{x_D}{t_D} < \frac{1}{M^0} \end{cases} \quad (5E-1)$$

- (d) Use Eq. (5E-1) to derive an expression for the average water saturation $\bar{S}(t_D)$ and the displacement efficiency $E_D(t_D)$.

- 5F.** *Water Fractional Flow with Capillary Pressure.* Derive the expression for water fractional flow including capillary pressure (Eq. 5.3-1).

- 5G.** *Analytic Relative Permeability Ratios (Ershaghi and Omoregie, 1978).* Over intermediate water saturation ranges, the oil–water relative permeability ratio plots approximately as a straight line on a semilog scale, using

$$\frac{k_{r2}}{k_{r1}} = A e^{-BS_1} \quad (5G-1)$$

where A and B are positive constants. Using the Buckley-Leverett theory, show that a plot of the product of oil and water cuts is a straight line with slope $1/B$ when plotted against $1/t_D$. The dip angle is zero.

- 5H.** *Fractional Flow with Two Inflections.* For the fractional flow curve of Fig. 5H, construct plots of fractional flow versus dimensionless distance at breakthrough for saturation $S_1 = 1$ displacing $S_1 = 0$, and $S_1 = 0$ displacing $S_1 = 1$.

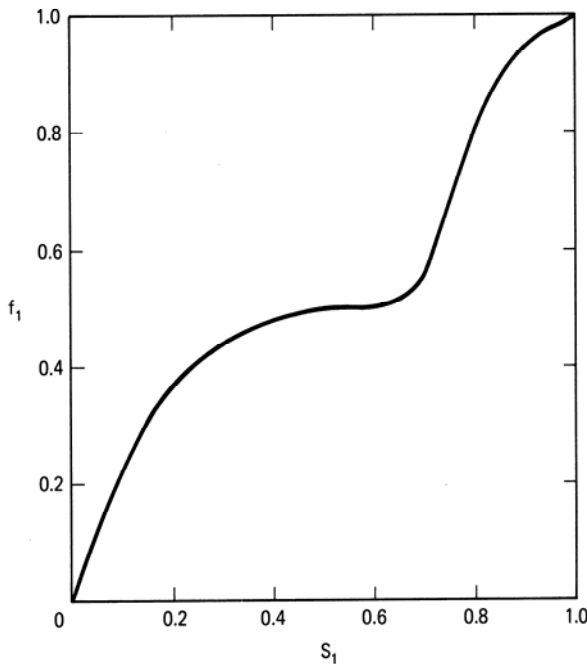


Figure 5H Fractional flow curve for Exercise 5H

- 5I.** *The Reversibility of Dispersion and Fractional Flow.* Fluid 2 is to be partially displaced by fluid 1 in a one-dimensional permeable medium. Fluid 1 is injected until just before it is produced, and then the flow is reversed (that is, fluid 2 is *injected* at the effluent end). In all that follows, take the initial (*I*) condition to be 100% fluid 2 flowing and the injected (*J*) condition to be 100% fluid 1.
- (a) Sketch two time-distance diagrams for this case using fractional flow curves like those on the extreme right and left of Fig. 5-6.
 - (b) If fluids 1 and 2 are completely miscible with identical viscosities and mix only by dispersion, use Eq. (5.5-18) to sketch the time-distance diagram.
 - (c) Based on the results of parts (a) and (b), what can you conclude about the mixing caused by fractional flow compared to that caused by dispersion?
 - (d) If fluids 1 and 2 are water and oil and a fractional flow curve like that on the middle panel of Fig. 5-6 applies, calculate and plot the time-distance diagram.
- 5J.** *Mobility Ratio for Compressible Flow.* Consider the pistonlike displacement of fluid 2 by fluid 1 in the x direction. Use the general definition of mobility ratio (pressure gradient ahead of front divided by pressure gradient behind front) in the following:
- (a) Show that the mobility ratio becomes the endpoint mobility ratio if the volumetric flowrate uA is not a function of x (fluids are incompressible).
 - (b) If the mass flux ρuA is not a function of x , on the other hand, show that the mobility ratio becomes

$$M_v = \frac{k_{r1}^o v_2}{k_{r2}^o v_1} \quad (5J-1)$$

where $v = \mu/\rho$ is the kinematic viscosity.

- (c) Calculate both M^0 and M_v for the following conditions: $\rho_1 = \text{mg}/\text{cm}^3$, $\mu_1 = 1 \text{ }\mu\text{Pa-s}$, $\rho_2 = 0.8 \text{ g}/\text{cm}^3$, $\mu_2 = 2 \text{ mPa-s}$, $k_{r1}^o = 0.1$ and $k_{r2}^o = 1.0$.

- 5K.** *Using Tracer Data.* Consider a one-dimensional permeable medium containing oil at a uniform residual saturation S_{2r} , and through which is flowing 100% water at a constant rate. At $t = 0$, a second water stream is introduced at the inlet that contains two ideal (nondispersing and nonabsorbing) tracers. Tracer 1 remains only in the water phase, but tracer 2 partitions into the residual oil phase with a partition coefficient of 2. The partition coefficient is the ratio of the concentration of tracer 2 in the oil phase to that in the water phase $K_{21}^2 = C_{22}/C_{21}$. Tracer 1 breaks through after three hours, and tracer 2 after six hours. If the volumetric injection rate is 1 cm³/min, calculate the pore volume and S_{2r} .
- 5L.** *Laboratory Estimation of Dispersivity.* Dispersivity may be estimated from laboratory, first-contact miscible displacements with the following development:
- Show from Eq. (5.5-15) that a plot of $(1 - t_D)/\sqrt{t_D}$ versus $\text{erf}^{-1}(1 - 2C_e)$ will yield a straight line with slope $2N_{pe}^{-1/2}$. Here C_e is the effluent concentration ($C_D|_{x_D=1}$)
 - Estimate the pore volume, dispersion coefficient, and dispersivity from the following experimental data:

Volume produced (cm ³)	Effluent concentration
60	0.010
65	0.015
70	0.037
80	0.066
90	0.300
100	0.502
110	0.685
120	0.820
130	0.906
140	0.988
150	0.997

The interstitial velocity is 20 cm/day, and the length is 0.5m. Note that $\text{erf}^{-1}(1 - 2x)$ is the probability axis (x axis) on probability paper.

- 5M.** *Tracers in Two-Phase Flow.* Consider a permeable medium flowing oil and water at constant oil fractional flow (case A in Fig. 5-12). Show that if a tracer with partition coefficient defined as in Exercise 5K is introduced at $t_D = 0$, the conservation equation for the tracer concentration C in the aqueous phase is (Delshad, 1981)

$$\frac{\partial C}{\partial t_D} + \frac{\partial C}{\partial x_D} - \frac{\bar{K}}{v_T L} \frac{\partial^2 C}{\partial x_D^2} = 0 \quad (5M-1)$$

where

$$t_D = t \frac{v_T}{L} \quad (5M-2)$$

$$v_T = \frac{q}{A\phi} \frac{f_1 + K_{21}f_2}{S_1 + K_{21}S_2} \quad (5M-3)$$

$$\bar{K} = \frac{S_1 K_{l1} + K_{21} S_2 K_{l2}}{S_1 + K_{21} S_2} \quad (5M-4)$$

K_{l1} and K_{l2} are the longitudinal dispersion coefficients for the tracer in the oil and water phases. Take $(q/A\phi)$ to be constant.

5N. *Three-Phase Coherence Calculation.* A more realistic three-phase relative permeability for oil, gas, and water is

$$k_{r1} = k_{r1}^0 \left(\frac{S_1 - S_{1r}}{1 - S_{1r} - S_{2r}} \right)^{n_1} \quad (5N-1)$$

$$k_{r3} = k_{r3}^0 \left(\frac{1 - S_1 - S_2 - S_{3r}}{1 - S_{1r} - S_{3r}} \right)^{n_3} \quad (5N-2)$$

$$k_{r2} = k_{r2}^0 \left\{ \left(\frac{k_{r21}}{k_{r2}^0} + k_{r1} \right) \left(\frac{k_{r23}}{k_{r2}^0} + k_{r3} \right) - (k_{r1} + k_{r3}) \right\} \quad (5N-3)$$

where

$$k_{r21} = k_{r2}^0 \left(\frac{1 - S_1 - S_{2r1}}{1 - S_{2r1} - S_{1r}} \right)^{n_{21}} \quad (5N-4)$$

$$k_{r23} = k_{r2}^0 \left(\frac{S_2 + S_1 - (S_{2r3} + S_{1r})}{1 - (S_{2r3} + S_{1r}) - S_{3r}} \right)^{n_{23}} \quad (5N-5)$$

These are modifications of the Stone relative permeability model (1970).

In Eqs. (5N-1) through (5N-5)

n_{21} = Oil relative permeability exponent in water–oil system

n_{23} = Oil relative permeability exponent in gas–oil system

S_{2r1} = Residual oil saturation in water–oil system

S_{2r3} = Residual oil saturation in gas–oil system

Calculate and plot the following:

- (a) Lines of constant k_{r1} , k_{r2} , k_{r3} , in the triangular composition space, S_1 , S_2 , and S_3 .
- (b) The composition paths and a waterflood composition route for initial saturations of 0.5, 0.3, and 0.2 for oil, gas, and water.
- (c) The wave positions in a dimensionless time–distance diagram.

Use the following data:

$$\begin{array}{lll} \mu_1 = 1 \text{ mPa-s} & \mu_2 = 2 \text{ mPa-s} & \mu_3 = 0.01 \text{ mPa-s} \\ S_{2r1} = 0.3 & k_{r2}^0 = 0.6 & n_{21} = 1.5 \\ S_{2r3} = 0.05 & k_{r1}^0 = 0.3 & n_{23} = 2 \\ S_{1r} = 0.2 & k_{r3}^0 = 0.7 & n_1 = 3 \\ S_{3r} = 0.05 & \alpha = 0 & n_3 = 2.5 \end{array}$$

This problem requires a numerical solution.

5O. *Simplified Three-Phase Fractional Flow.* Rework part (c) of Exercise 5N by assuming the displacement becomes a shock wave from the initial conditions to a region of

simultaneous two-phase oil-water flow followed by a wave of undetermined character to the injected conditions. The velocity of the first wave is given by

$$v_{AS_1} = \frac{f_{3I}}{S_{3I} - S_{3r}} = \frac{f_{1I} - f_1^+}{S_{1I} - S_1^+} = \frac{f_{2I} - f_2^+}{S_{2I} - S_2^+} \quad (5O-1)$$

where f_1^+ and f_2^+ are the water fractional flow and saturation behind the shock. The velocity of the second wave is then given by the Buckley-Leverett construction. Plot an effluent history of oil and water cuts to demonstrate the fill-up phenomenon.

- 5P.** *Method of Characteristics for Reducible Equations.* Consider the following pair of partial differential equations for $u(x, t)$ and $v(x, t)$

$$\frac{\partial u}{\partial t} + \frac{\partial(u^2 v)}{\partial x} = 0 \quad (5P-1)$$

$$\frac{\partial u}{\partial t} + \frac{\partial v^2}{\partial x} = 0 \quad (5P-2)$$

where both u and v are less than or equal to 1.

- (a) Write these equations in the “canonical” form of Eqs. (5.6-6). Are these reducible? Why or why not?
 - (b) Write the coherence requirement for Eqs. (5P-1) and (5P-2). Use this to develop an expression for σ , the composition velocity along the characteristic directions.
 - (c) Use σ to develop an expression for $u = u(v)$ along both characteristic directions.
 - (d) If the boundary data are specified along a line $u = 1$ plot the “composition” path grid (u, v space) for $u < 1$ and $v < 1$.
 - (e) On the plot of part (d) show the “composition” route for $(u, v)_J = (0.6, 0.2)$ displacing $(u, v)_I = (1, 1)$. Treat u and v as physical variables so that the composition velocity must decrease monotonically from I to J . Plot the time (t) – distance (x) diagram for this “displacement” where $t > 0$ and $1 > x > 0$.
 - (f) Based on this problem and what you know about the ideal miscible displacement, discuss why the constructions in Fig. 5-12 can be done without the procedures in parts (a) through (e).
- 5Q.** *Gravity Segregation and Fractional Flow.* Consider the homogeneous, one-dimensional permeable medium shown in Fig. 5Q for which all the fractional flow assumptions apply. Both ends of the medium are sealed. For $t < 0$, the medium contains a completely saturated water zone above a saturated oil zone ($0 < \varepsilon < 1$). At $t = 0$, the more dense water is allowed to flow downward while the less dense oil flows upward. This results in a complete reversal of the oil and water zones after a sufficiently long time. Figure 5Q also shows the long-time condition of the medium.
- (a) Show that there is no bulk flow ($u = 0$) at any point in the medium.
 - (b) Derive a water conservation equation for this special case from the general equations in Chap. 2. Give also the boundary conditions needed to solve this equation for $S_1(x, t)$.
 - (c) Make the equation of part (b) dimensionless by introducing appropriate scaling factors.
 - (d) Derive a dimensionless water flux (analogous to a fractional flow) by eliminating the water pressure gradient from the equation of part (c). The absence of bulk flow does *not* eliminate pressure gradients (Martin, 1958).

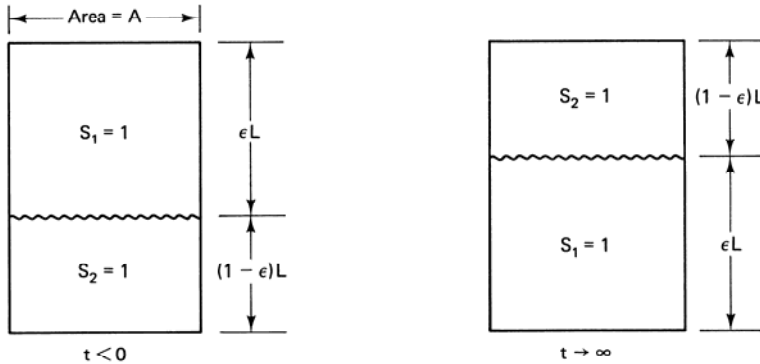


Figure 5Q Gravity segregation with fractional flow

- (e) For the following values, plot the dimensionless water flux of part (d) versus water saturation.

$$\begin{array}{ll} k_{r1} = 0.1 S_1^4 & k_{r2} = .8(1-S_1)^2 \\ \mu_1 = 1 \text{ mPa-s} & \mu_2 = 5 \text{ mPa-s} \end{array}$$

- (f) Based on the curve of part (e) and $\varepsilon = 0.6$, construct the time-distance diagram showing the progress to complete gravity segregation of the water and oil zones. Estimate the dimensionless time this occurs at.

- 5R.** *An Alternate Derivation of the Characteristic Equations.* Consider the following reducible equations for $u(x, t)$ and $v(x, t)$:

$$\begin{aligned} A_1 u_t + B_1 u_x + C_1 v_t + D_1 v_x &= 0 \\ A_2 u_t + B_2 u_x + C_2 v_t + D_2 v_x &= 0 \end{aligned} \quad (5R-1)$$

- (a) Suppose that u and v are functions of the combined variable $\sigma = x/t$. Show that Eq. (5R-1) can be written as

$$\begin{pmatrix} B_1 - \sigma A_1 & D_1 - \sigma C_1 \\ B_2 - \sigma A_2 & D_2 - \sigma C_2 \end{pmatrix} \begin{pmatrix} u' \\ v' \end{pmatrix} = 0 \quad (5R-2)$$

where $u' = du/d\sigma$, and so on.

- (b) For a nontrivial solution, the determinant of the coefficient matrix of Eq. (5R-2) must be zero. Show that this gives the characteristic directions given by Eq. (5.6-10).
- (c) Again, for a nontrivial solution, the determinant of the augmented matrix (matrix with the solution vector substituted for a column) must also be zero. Show that if we replace the second column, this operation yields the following relation between u and v :

$$\frac{du}{dv} = \frac{B_1 - \sigma^\pm A_1}{B_2 - \sigma^\pm A_2} \quad (5R-3)$$

Solutions that can be expressed in terms of (x/t) are said to be *self-similar*.

6

Volumetric Sweep Efficiency

Typical values of residual oil and connate water saturations indicate ultimate displacement efficiency should normally be between 50% and 80% of the contacted oil in a waterflood. This range is substantially higher than the 30% average recovery efficiency observed in waterfloods; it is also higher than recovery efficiency in most EOR projects (see Sec. 1-4). Of course, the reason displacement efficiency is higher than the recovery efficiency is that not all the oil is contacted by the displacing agent. This effect is present in the oil recovery Eq. (2.5-5) where the displacement efficiency is multiplied by the volumetric sweep efficiency E_V . Based on these approximate figures, the volumetric sweep efficiency is between 40% and 60% for a waterflood. For many EOR processes, it can be much smaller, and for others, effecting a large E_V is a primary design objective.

In this chapter, we provide both an overview of volumetric sweep efficiency and techniques to combine areal, vertical, and displacement sweep to arrive at a recovery efficiency. We deal almost exclusively with the immiscible water–oil displacement since this literature on recovery efficiency is well established and many of the more important features also carry over to EOR. In later chapters, we discuss the volumetric sweep efficiency of specific EOR processes. To further distinguish between volumetric and displacement sweep efficiency, we usually deal with indifferent or self-sharpening displacements in which dispersive effects are small. For these cases, the calculation techniques are equally valid whether the displacement is miscible or immiscible since there is no simultaneous flow of components.

6-1 DEFINITIONS

Based on the overall material balance of Sec. 2-5, the cumulative mass of oil recovered is

$$N_{p2} = V_b \bar{W}_{2I} E_{R2}$$

from Eq. (2.5-3) with no oil injection. We wish to convert this equation to a more standard form by the following transformations: Eliminate the recovery efficiency E_{R2} through Eq. (2.5-5a), and replace \bar{W}_{2I} with $\phi(\rho_2 S_2 \omega_{22})_I$, which assumes oil is in only the liquid oleic phase. This gives

$$N_{p2} = V_b \phi(\rho_2 S_2 \omega_2)_I E_D E_V$$

Next, eliminate $(\rho_2 \omega_{22})_I$ with the oil formation volume factor definition Eq. (2D-5), and let $V_b \phi = V_p$, the pore volume, and $N_p = N_{p2} / \rho_2^o$, the oil production in standard volumes. These substitutions yield

$$N_p = \frac{E_D E_V S_{2I} V_p}{B_{2I}} \quad (6.1-1)$$

In Eq. (6.1-1), E_D is the displacement sweep efficiency defined in Eq. (5.1-1), and E_V is the volumetric sweep efficiency defined as

$$E_V = \frac{\text{Volumes of oil contacted by displacing agent}}{\text{Volumes of oil originally in place}} \quad (6.1-2)$$

The term $(\frac{S_{2I} V_p}{B_{2I}})$ represents the oil in place at the start of the displacement in standard volumes. We have also dropped the subscript $i = 2$ because all efficiencies in this chapter refer to oil recovery.

The volumetric sweep efficiency can be decomposed into the product of an areal sweep efficiency and a vertical sweep efficiency

$$E_V = E_A E_I \quad (6.1-3)$$

The definition of the areal sweep efficiency is

$$E_A = \frac{\text{Area contacted by displacing agent}}{\text{Total area}} \quad (6.1-4)$$

Figure 6-1(a) shows a schematic of a highly idealized pistonlike displacement in a four-layer areally homogeneous reservoir. Figure 6-1(b) is an areal view of Figure 6-1(a). Based on the definition of Eq. (6.1-4), E_A is the doubly cross-hatched area (at t_2) divided by the singly cross-hatched area. The vertical sweep efficiency,

$$E_I = \frac{\text{Cross-sectional area contacted by displacing agent}}{\text{Total cross-sectional area}} \quad (6.1-5)$$

is also similarly defined in Fig. 6-1 (a) at a particular time.

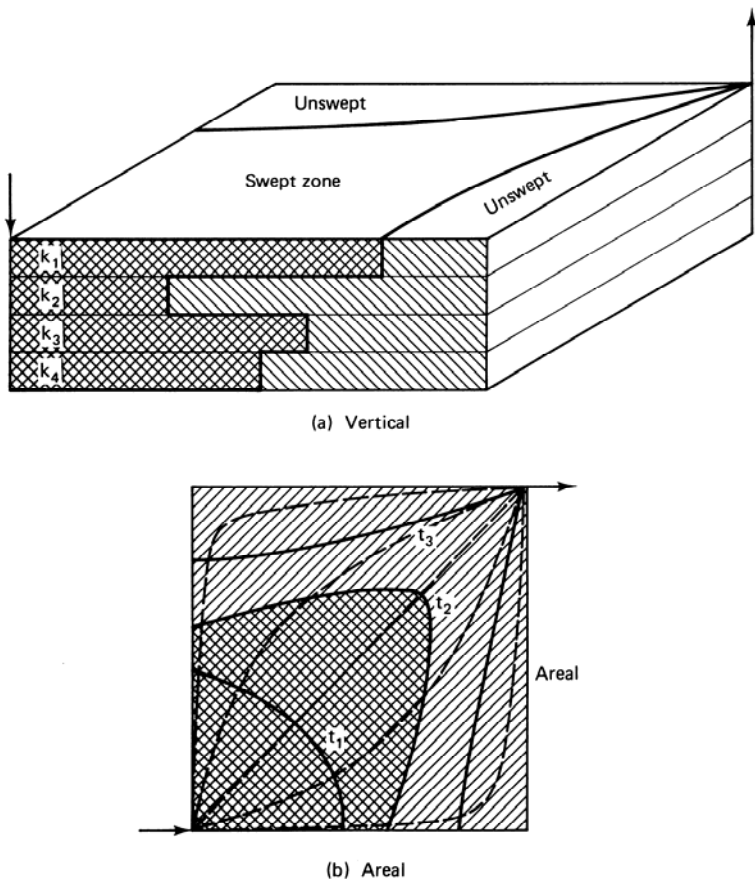


Figure 6-1 Sweep efficiency schematic

The definitions of Eqs. (6.1-3) through (6.1-5) have several subtle difficulties. Both areal and vertical sweep efficiency are ratios of areas; therefore, their product E_V must be a ratio of areas squared. This observation contradicts the definition of Eq. (6.1-2) which says E_V must be a ratio of lengths cubed. The redundant dimension in either Eq. (6.1-4) or (6.1-5) is the dimension parallel to the displacement direction. This direction is nonlinear and varies with both position and time. Thus the decomposition Eq. (6.1-3) transforms E_V into a product of two plane flows.

A second consequence of the redundant dimension in E_V is that both E_A and E_I depend on each other. Note from Fig. 6-1 that E_A depends on vertical position. Similarly, though not so obviously, E_I will be different from the cross section shown for each cross section between the injector and producer. If we restrict ourselves to cross sections defined by pathlines between the injector and producer (dotted lines in Fig. 6-1b), E_I will be the same for each cross section if it can be expressed in a dimensionless form independent of rate. But for the general case, E_I is a function of rate and will be different for each cross section. As we see in Sec. 6-7, the practical consequence of this observation is that neither the areal nor the vertical sweep

efficiency in Eq. (6.1-3) can be evaluated at the same time for which the volumetric sweep efficiency is desired.

To use Eq. (6.1-1), even with the above complications, we must have independent estimates of E_A and E_V . For certain very special cases—confined displacements in areally homogeneous regular patterns with no or very good vertical communication—these are available to us through correlation (see Sec. 6-2) or calculation (see Secs. 6-3 through 6-5). When these conditions are not met, E_V must be estimated through scaled laboratory experiments or numerical simulation. In the latter case, though certainly possible to obtain sweep efficiency estimates, the oil recovery itself may be obtained directly, and Eq. (6.1-1) is unnecessary. Still, the equation provides a better understanding of sweep efficiency concepts and the factors necessary to maximize E_V than does simulation alone.

6-2 AREAL SWEEP EFFICIENCY

Though areal sweep efficiency may be determined through simulation or by analytical methods (Morel-Seytoux, 1966), the most common source of areal sweep efficiency data is from displacements in scaled physical models. Figures 6-2 through

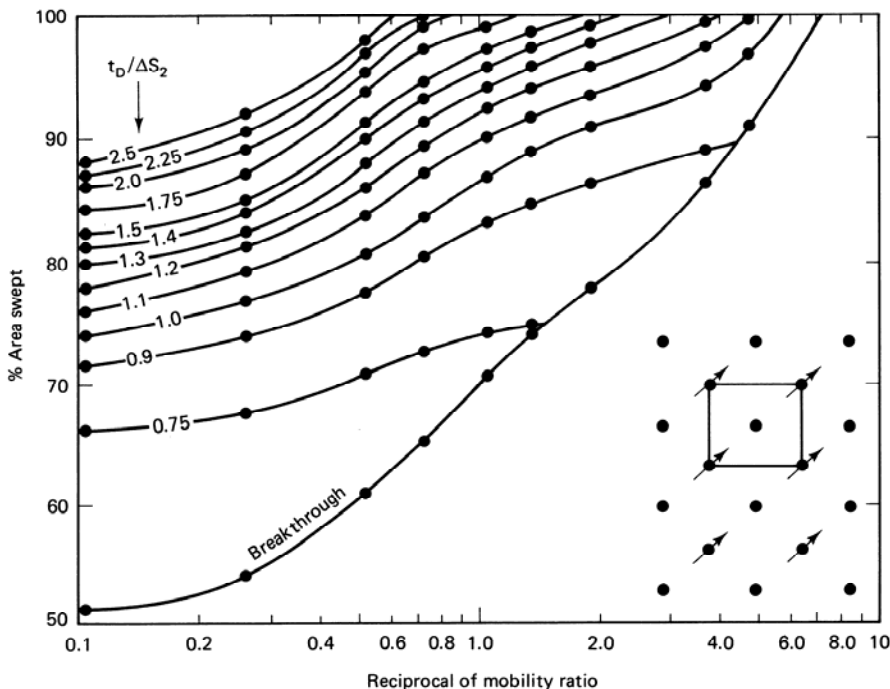


Figure 6-2 Areal sweep efficiency for a confined five-spot pattern (from Dyes et al., 1954)

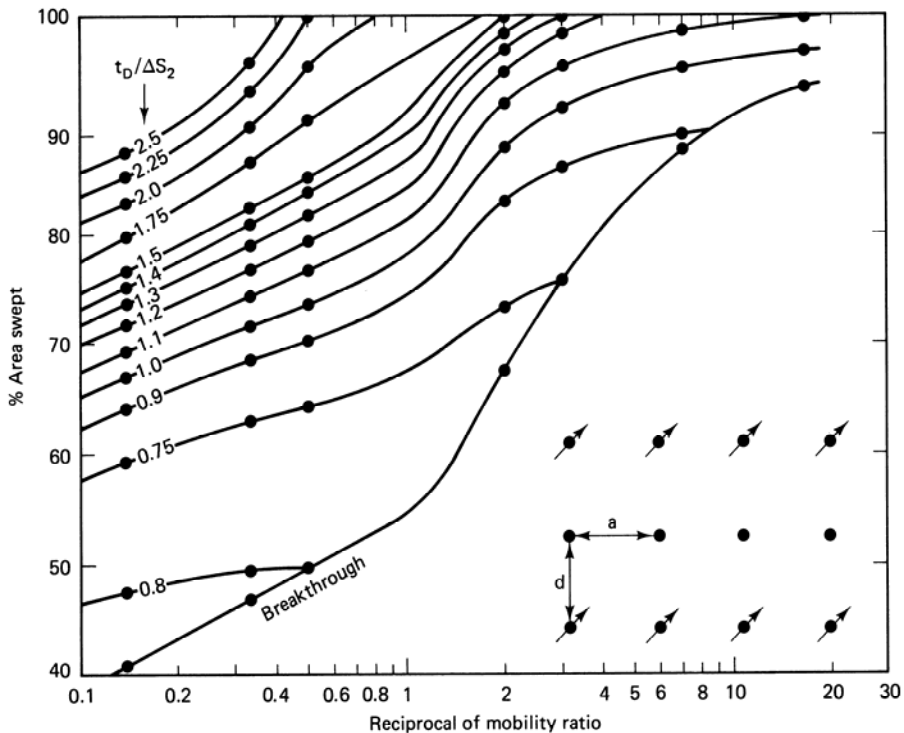


Figure 6-3 Areal sweep efficiency for a confined direct line drive pattern, $d/a = 1$ (from Dyes et al., 1954)

6-4 present three of these areal sweep “correlations” from the work of Dyes et al. (1954) for three different regular well patterns. Several more of these correlations are in the work of Craig (1971), and an extensive bibliography of areal sweep efficiency is given by Claridge (1972). For the patterns shown in the lower right-hand corner, Figs. 6-2 through 6-4 plot E_A on the y axis versus the reciprocal mobility ratio on the x axis with time as a parameter. Since mobility ratio and pattern type are fixed for a given displacement, time is actually the dependent variable. The dimensionless time in Figs. 6-2 through 6-4 is cumulative displaceable pore volumes of displacing agent injected. Since time is the dependent variable in these correlations, a more direct representation would be a plot of E_A versus dimensionless time at fixed mobility ratio and pattern type (see Exercise 6A). You should remember that these correlations are for pistonlike displacements in regular, homogeneous, confined patterns. When the well patterns are unconfined, the reference area in Eq. (6.1-4) can be much larger, and E_A smaller. Based on an extensive survey of the available correlations for spreading displacements, Craig (1971) determined that the appropriate mobility ratio for the areal sweep correlations is the average saturation mobility ratio \bar{M} given by Eq. (5.2-25a).

From the correlations, E_A increases with increasing time, or throughput, and decreasing mobility ratio. At a fixed mobility ratio, E_A is equal to the displaceable

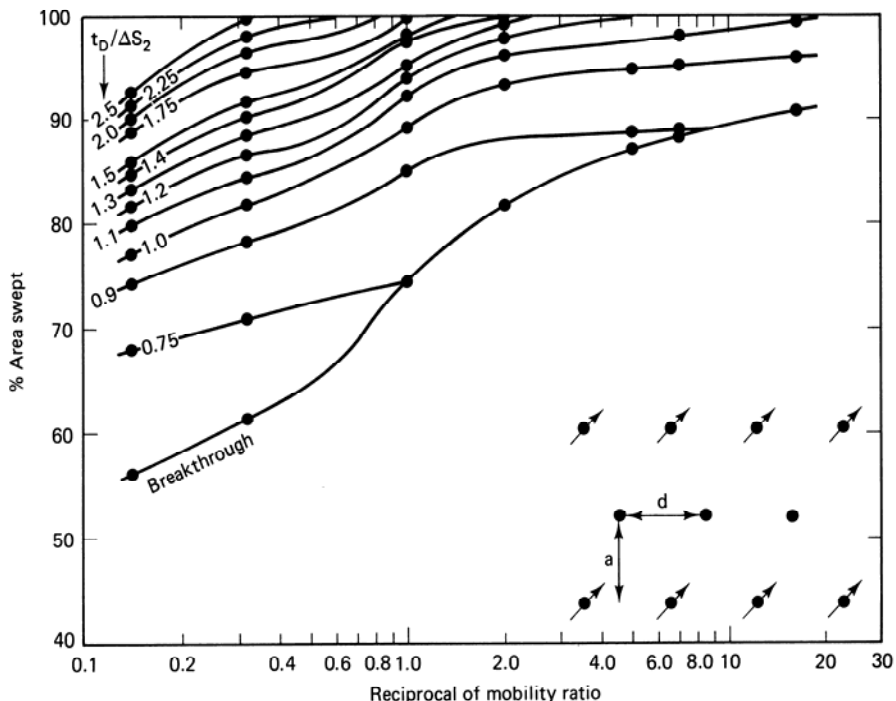


Figure 6-4 Areal sweep efficiency for a staggered line drive pattern, $d/a = 1$ (from Dyes et al., 1954)

pore volumes injected until breakthrough and then given by the indicated curves in Figs. 6-2 through 6-4 thereafter. E_A also increases as the pattern type more closely approaches linear flow, but this sensitivity is not great for the more common patterns. The decrease in E_A with increasing \bar{M} is in the same direction as the change in displacement efficiency with mobility ratio discussed in Sec. 5-2; thus large mobility ratios are detrimental to both areal and displacement sweep.

6-3 MEASURES OF HETEROGENEITY

Considering the manner reservoirs are deposited in and the complex diagenetic changes that occur thereafter, it should not be surprising that no reservoir is homogeneous. This does not imply all reservoirs are dominated by their heterogeneity since in many cases, one mechanism is so strong that it completely overshadows all others. For example, gravity can be so pronounced in a high-permeability reservoir that it may be considered homogeneous to good approximation.

Nevertheless, heterogeneity is always present in reservoirs, is the most difficult feature to define, and usually has the largest effect on vertical sweep efficiency. Therefore, before we explore vertical sweep efficiency, we discuss the most common measures of heterogeneity and their limitations.

Definitions

The three principal forms of nonidealities in reservoirs are anisotropies, nonuniformities, and heterogeneities. These terms can be applied to any property but usually describe permeability, porosity, and occasionally, relative permeability. An *anisotropic* property varies with the direction of measurement and, hence, has intrinsic tensorial character (see Sec. 2-2). Following Greenkorn and Kessler (1969), the definitions of nonuniformity and heterogeneity are closely related (Fig. 6-5). A homogeneous, uniform property is represented on a frequency distribution plot as a single delta function (spike), and a heterogeneous, uniform property by a finite number of these functions. A homogeneous, nonuniform property cannot be represented by a finite number of delta functions but can be a continuous function having only one peak. A heterogeneous, nonuniform property is represented by a continuous distribution function having two or more peaks. Most laboratory displacements are homogeneous and nonuniform. Most calculation techniques assume the reservoir is uniform and heterogeneous. Actual nonuniformities are frequently “averaged” out by capillary pressure or dispersion.

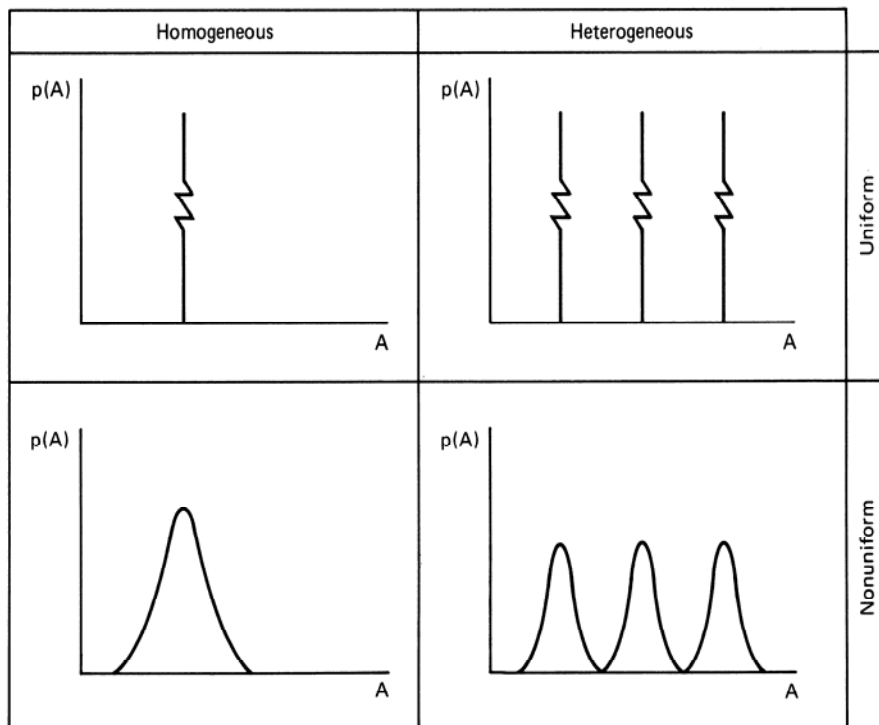


Figure 6-5 Probability distribution functions for parameter A (from Greenkorn and Kessler, 1965)

Flow and Storage Capacity

Since permeability can change several factors of 10 within a short distance in a reservoir, whereas porosity changes by only a few percent over the same scale, it is common to view the reservoir as homogeneous with respect to porosity and heterogeneous with respect to permeability. Although most of the traditional measures of heterogeneity adopt this convention it is not necessary and can even lead to occasional errors. In the following discussion, we include porosity variations in the definitions; the more traditional definitions can be recovered by letting porosity and thicknesses be constant.

Imagine an ensemble of N_L permeable media elements each having different permeability k_l , thickness h_l , and porosities ϕ_l . The elements are arranged as resistances parallel to flow. From Darcy's law, the interstitial velocity of the single-phase flow of a conservative tracer is proportional to the ratio of permeability to porosity $r_l = k_l/\phi_l$. Thus if r_l is a random variable, we can rearrange the elements in order of decreasing r_l (this is equivalent to arranging in order of decreasing fluid velocity), and we can define a cumulative flow capacity at a given cross section as

$$F_n = \sum_{l=1}^n \frac{k_l h_l}{H_t \bar{k}} \quad (6.3-1a)$$

where H_t is the total thickness,

$$H_t = \sum_{l=1}^{N_L} h_l \quad (6.3-1b)$$

The average quantities are defined as

$$\bar{k} = \frac{1}{H_t} \sum_{l=1}^{N_L} (kh)_l \quad (6.3-1c)$$

and similarly for porosity. A cumulative storage capacity follows in a similar fashion

$$C_n = \sum_{l=1}^n \frac{\phi_l h_l}{H_t \bar{\phi}} \quad (6.3-1d)$$

The physical interpretation of F_n is that if the N_L elements are arranged in parallel, F_n is the fraction of total flow of velocity r_n or faster. C_n is the volume fraction of these elements. A plot of F_n versus C_n yields the curve shown in Fig. 6-6(a); if N_L becomes very large, the ensemble approaches the continuous distribution shown in Fig. 6-6(b). We designate the continuous distribution by F and C without subscripts. From the definitions F , C , and r , the slope of either curve at any C is the interstitial velocity at that point divided by the average interstitial velocity of the whole ensemble

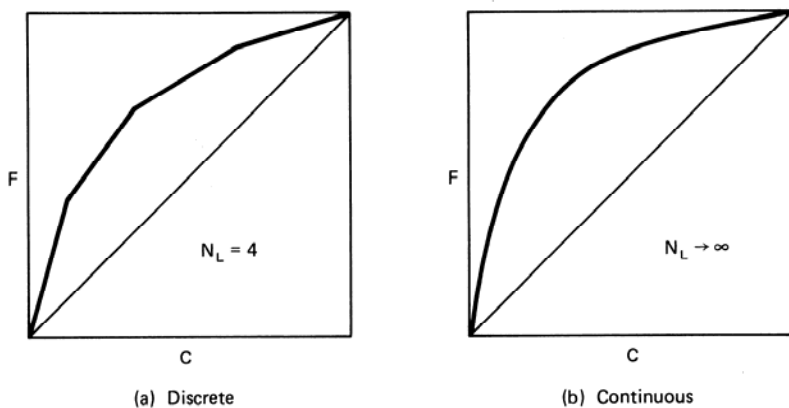


Figure 6-6 Schematic of discrete and continuous flow-storage capacity plots

$$\frac{dF}{dC} = F' = \begin{cases} \frac{r_n}{\bar{r}} & \text{(discrete)} \\ \frac{r}{\bar{r}} & \text{(continuous)} \end{cases} \quad (6.3-2)$$

Because the elements were rearranged, the slope is monotonically decreasing and, from the definitions, $F_n = C_n = 1$, when $n = N_L$.

Measures of Heterogeneity

A common measure of reservoir heterogeneity is the Lorenz coefficient L_c , defined as the area between the F - C curve and a 45° line (homogeneous F - C curve) and normalized by 0.5,

$$L_c = 2 \left\{ \int_0^1 F dC - \frac{1}{2} \right\} \quad (6.3-3)$$

for the continuous curve. The Lorenz coefficient varies between 0 (homogeneous) and 1 (infinitely heterogeneous). A second, perhaps more common, measure that lies between the same limits is the Dykstra-Parsons (1950) coefficient V_{DP} .

$$V_{DP} = \frac{(F')_{C=0.5} - (F')_{C=0.841}}{(F')_{C=0.5}} \quad (6.3-4)$$

Both L_c and V_{DP} are independent of the particular form of the k/ϕ distribution, and both rely on the rearrangement of this ratio. As originally defined, V_{DP} is actually taken from a straight line fit to the $k-\phi$ data plotted on a log-probability scale. This procedure introduces a nonuniqueness (two different distributions having the same V_{DP}) into V_{DP} when the data are not lognormal (Jensen and Lake, 1986). For lognormal data, Eq. (6.3-4) is unique.

To relate F to C , we assume the permeability assembly is lognormally distributed; hence the relationship between cumulative frequency Λ and r is (Aithison and Brown, 1957)

$$\Lambda = \frac{1}{2} \left[1 - \operatorname{erf} \left\{ \frac{\ln \left(\frac{r}{\hat{r}} \right)}{\sqrt{2v_{LN}}} \right\} \right] \quad (6.3-5)$$

where \hat{r} is the geometric or log-mean of the distribution, and v_{LN} is the variance of the distribution. The relationship between \hat{r} and \bar{r} is given by

$$\bar{r} = \hat{r} e^{(v_{LN}/2)} \quad (6.3-6)$$

If we identify Λ with the storage capacity C and use Eqs. (6.3-2), (6.3-5), and (6.3-6), we obtain

$$C = \frac{1}{2} \left[1 - \operatorname{erf} \left\{ \frac{\ln(e^{v_{LN}/2} F')}{\sqrt{2v_{LN}}} \right\} \right] \quad (6.3-7)$$

Equation (6.3-7) may be solved for F' and then integrated subject to the boundary condition $F = C = 0$,

$$F = \int_0^C \exp \left\{ \frac{v_{LN}}{2} + \sqrt{2v_{LN}} \operatorname{erf}^{-1}(1-2\xi) \right\} d\xi \quad (6.3-8)$$

We integrate Eq. (6.3-8) numerically to give the F - C curve for fixed V_{LN} . Figure 6-7, which uses V_{DP} instead of v_{LN} , shows the results of such an integration where the

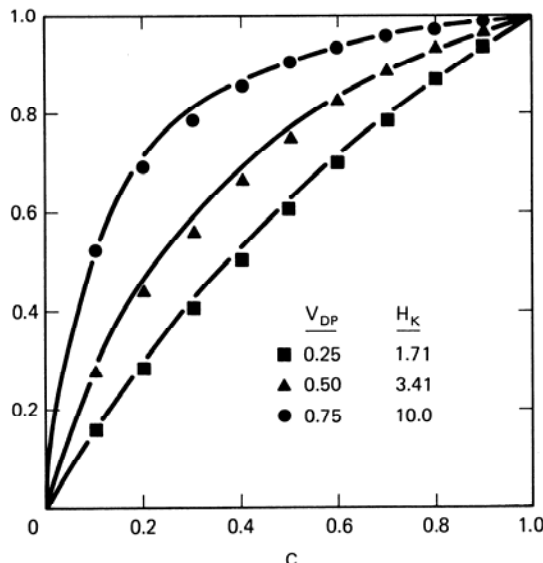


Figure 6-7 Flow-capacity-storage-capacity curves (from Paul et al., 1982)

filled points are the results of the integration. It follows from Eqs. (6.3-4) and (6.3-5) that

$$V_{DP} = 1 - e^{-\sqrt{v_{LN}}} \quad (6.3-9)$$

and, further, that the relationship among Lorenz and Dykstra-Parsons coefficients and v_{LN} is

$$L_c = \operatorname{erf}\left(\frac{\sqrt{v_{LN}}}{2}\right) = \operatorname{erf}\left(\frac{-\ln(1-V_{DP})}{2}\right) \quad (6.3-10)$$

Note from Eq. (6.3-10) that L_c and V_{DP} are bounded, whereas v_{LN} is not.

Considering the three heterogeneity measures in Eq. (6.3-10), it must seem odd to propose a fourth, but none of the measures discussed so far directly relates to flow in permeable media. To ameliorate this, Koval (1963) proposed a heterogeneity factor H_K as a fourth measure of heterogeneity. H_K is defined by

$$H_K = \frac{1-C}{C} \cdot \frac{F}{1-F} \quad (6.3-11)$$

Equation (6.3-11) follows from observing the similarity between a homogeneous media fractional flow curve having straight-line relative permeabilities and zero residual phase saturations, and the points generated in Fig. 6-7. In fact, the solid lines in Fig. 6-7 are calculated from Eq. (6.3-11), with H_K adjusted to fit the calculated points. Hence there is a unique correspondence between V_{DP} and H_K , which is shown in Fig. 6-8 as the filled points. From Eqs. (6.3-8) and (6.3-11), it follows that $H_K \rightarrow \infty$

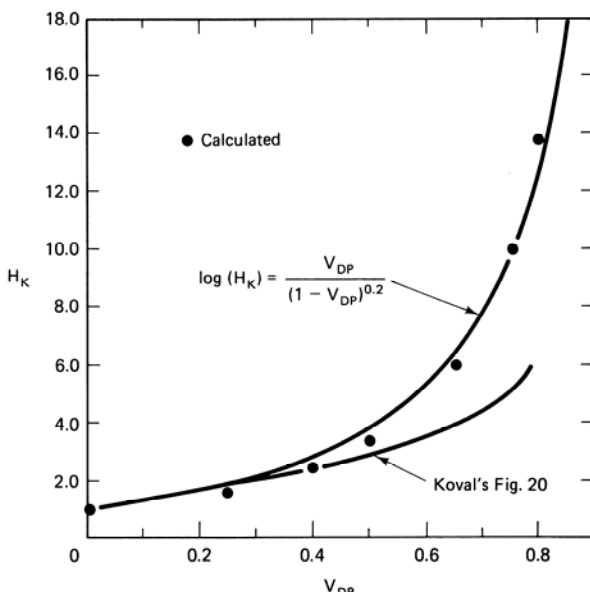


Figure 6-8 Relation between effective mobility ratio and heterogeneity (from Paul et al., 1982)

as $V_{DP} \rightarrow 1$ (infinitely heterogeneous) and $H_K \rightarrow 1$ as $V_{DP} \rightarrow 0$. Between these limits, the relation between V_{DP} and H_K is given by the following empirical fit to points in Fig. 6-8:

$$\log(H_K) = \frac{V_{DP}}{(1-V_{DP})^{0.2}} \quad (6.3-12)$$

which is also shown in Fig. 6-8.

Using the $F-C$ curve in Eq. (6.3-11), the vertical sweep efficiency of a unit mobility ratio displacement may be calculated by the one-dimensional theory in Sec. 5-2 (see Exercise 5E).

Table 6-1 shows various statistical information from several producing formations. V_{DP} varies between 0.65 and 0.89 for these formations. This rather tight range corresponds to the range in Fig. 6-7 where H_K begins to be an exceedingly strong function of V_{DP} . Since E_I decreases with increasing H_K , displacements in most reservoirs should be affected by heterogeneity. Table 6-1 also shows the areal V_{DP} based on the distribution of the average well permeabilities. In only three of the entries shown are the areal variations larger than the vertical variations. This, plus the lack of sensitivity of E_I to heterogeneous permeabilities arranged in series, partly accounts for the popularity of the stratified, or "layer-cake," model for reservoirs. We use the layer-cake model (uniform and heterogeneous) in the next two sections to calculate E_I . Finally, Table 6-1 shows the number of wells in each formation whose core plug permeabilities most closely conform to the normal, lognormal, and exponential distributions. As you can see, the wells are usually lognormal though there are significant exceptions (see Jensen et al., 1987). If the permeabilities are distributed normally, the procedure for calculating V_{DP} and L_c is still correct, but the form of the distribution function (Eq. 6.3-5) changes (see Exercise 6B).

None of the measures of heterogeneity given above are entirely satisfactory for predicting displacement performance. Since all the measures capture both heterogeneities and nonuniformities, there is a persistent, and largely ignored, question about how to use them in displacement calculations. It seems reasonable that nonuniformities would alter values of the permeable media properties such as dispersivity and capillary pressure; however, the scale of the nonuniformity is different between the field and laboratory measurements, and there is little to suggest how labmeasured properties can be changed to reflect these nonuniformities. For this reason, nonuniformities are usually ignored, and displacement calculations are based on uniformly heterogeneous permeable media models. A second reason for the inadequacies in the heterogeneity measures is that for many reservoirs it is inappropriate to treat permeability and porosity as independent variables. Correlations exist between permeability and porosity (bivariate correlations), and these variables themselves can have spatial structure (autocorrelation). When such structure does exist, the displacement response of a rearranged ensemble of layers will not be the same as that of the original distribution of layers. Determining when structure exists, and separating it from the random stochastic component, are tasks usually left to the geological interpretation in current practice.

TABLE 6-1 TYPICAL VALUES OF VERTICAL AND AREAL DYKSTRA-PARSONS COEFFICIENTS
(ADAPTED FROM LAMBERT, 1981)

			Number of wells studied*	Lognormal	Exponential	\bar{k}	$\bar{\phi}$	$(V_{DP})_{\text{areal}}$	\bar{V}_{DP}
1	El Dorado	Admire	262	35	42	370.14	0.2538	0.484	0.697
2	Keystone	Cardium	67	61	5	15.15	0.1063	0.752	0.653
3	Garrington	Meanville B	38	35	2	5.73	0.1124	0.671	0.822
4	Madison	Bartlesville	36	10	10	29.95	0.1790	0.238	0.823
5	Pembina	Cardium	16	13	0	273.64	0.1220	0.837	0.894
		Belly River	17	15	0	12.66	0.1623	0.687	0.814
6	Hamilton Dome	Tensleep	33	11	10	98.24	0.1430	0.501	0.694
7	Rozet	Muddy	33	25	3	43.14	0.1708	0.457	0.846
8	Salt Creek	2nd Wall Creek	30	8	6	59.08	0.1843	0.495	0.851
9	Kitty	Muddy	20	19	0	11.74	0.0871	0.795	0.731
10	E. Salt Creek	2nd Wall Creek	5	3	2	35.71	0.1660	0.124	0.840
		Lakota	7	6	0	38.01	0.1540	0.424	0.899
11	Dixie West	Tradewater	16	5	3	129.13	0.1880	0.202	0.598
12	Burke Ranch	Dakota	14	6	3	23.18	0.1191	0.625	0.663
13	Oklahoma City	Prue	14	6	4	15.90	0.1368	0.473	0.683
14	Gas Draw	Muddy	14	6	0	71.61	0.1572	0.615	0.899
15	Recluse	Muddy	12	9	0	74.93	0.1437	0.591	0.855
16	W. Moorcroft	Muddy	8	6	0	201.39	0.2150	0.973	0.833
17	S. Rozet	Minnelusa	8	7	1	135.86	0.1283	0.443	0.861
18	Ute	Muddy	8	2	2	62.14	0.1790	0.752	0.758
19	Riverton Dome	Tensleep	7	2	0	2.68	0.0480	0.474	0.729
20	Carson-Hamm	Minnelusa	7	2	3	160.36	0.1624	0.465	0.722
21	N.W. Sumatra	Heath	6	0	2	124.98	0.1285	0.254	0.890
22	Pitchfork	Tensleep	5	1	4	91.54	0.1410	0.229	0.728
		Phosphoria	6	4	1	18.16	0.1430	0.544	0.833
	Total		689	297	102				

* Difference between lognormal and exponential represents number of normally distributed wells

6-4 DISPLACEMENTS WITH NO VERTICAL COMMUNICATION

In this section, we illustrate the effects of mobility ratio and heterogeneity for noncommunicating reservoirs. We treat pistonlike displacements of oil ($i = 2$) by water ($i = 1$) in uniformly heterogeneous, horizontal layer-cake models (see Exercise 6C). Further, we do not allow permeability or transmissibility in the vertical direction, a condition that could apply in actual practice if the reservoir contains impermeable and continuous shale breaks in the total interval. The reservoir now consists of an ensemble of one-dimensional elements arranged in parallel. Since there is no vertical communication, we can rearrange the layers in decreasing k/ϕ , as in Sec. 6-3. We also ignore dissipative effects to derive the noncommunication displacement model first proposed by Dykstra and Parsons (1950).

Subject to the above assumptions, the vertical sweep efficiency of the reservoir is

$$E_I = \frac{\sum_{l=1}^n (\phi h)_l + \sum_{l=1}^{N_L} (\phi h x_D)_l}{\bar{\phi} H_t} \quad (6.4-1)$$

where x_{Dl} is the dimensionless front position (x_d/L) between the displacing fluid (water) and the displaced fluid (oil). The index n denotes the layer that has just broken through to the producer at a particular dimensionless time t_D

$$t_D = \frac{\int_0^t q dt}{H_t W L \bar{\phi}} = \frac{\sum_{l=1}^{N_L} (\phi h x_D)_l}{\bar{\phi} H_t} \quad (6.4-2)$$

where x_{Dl} for $l > n$ is greater than 1, W is the width of the cross section, and L is the length.

Two Layers

First, let's consider the case of a reservoir having only two layers ($N_L = 2$) as shown in Fig. 6-9 with water saturation change $\Delta S = S_{1I} - S_{1I}$. The $k/\phi\Delta S$ for the upper or fast layer is greater than that for the lower or slow layer. The front position in each layer may be determined from Darcy's law

$$\frac{dx_{fl}}{dt} = v_l = -\left(\frac{k}{\phi\Delta S}\right)_l \lambda_{re_l} \frac{\Delta P}{L}, \quad l = 1, 2 \quad (6.4-3)$$

where v_l is the interstitial x velocity in layer l , and λ_{re_l} is the effective relative mobility in layer l defined by

$$\lambda_{re_l} = \begin{cases} \left[\frac{x_{Dl}}{\lambda_{r1}^0} + \frac{(1-x_{Dl})}{\lambda_{r2}^0} \right]^{-1} & \text{for } x_{Dl} < 1 \\ \lambda_{r1}^0 & \text{for } x_{Dl} > 1 \end{cases} \quad (6.4-4)$$

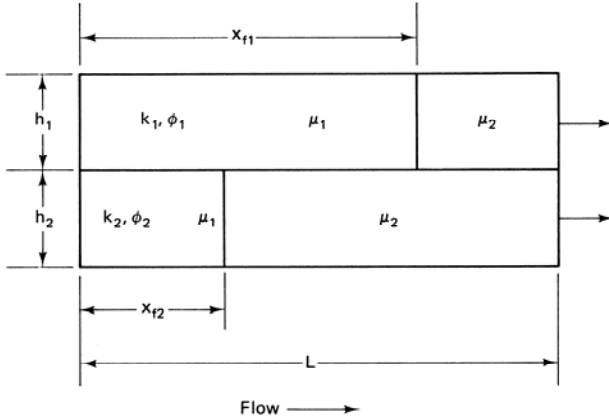


Figure 6-9 Schematic illustration of heterogeneous reservoir for Dystra-Parsons model

Taking the ratio of the interstitial velocities in the two layers will eliminate time and the pressure drop since both layers experience the same ΔP . This equality implies communication in the wells even though there is no communication elsewhere. Because ΔP cancels, the calculation is valid whether the displacement is at constant rate or constant ΔP . Thus before breakthrough ($x_{D1} < 1$), we have

$$\frac{dx_{D1}}{dx_{D2}} = r_{12} \frac{x_{D2} + M^0(1 - x_{D2})}{x_{D1} + M^0(1 - x_{D1})} \quad (6.4-5a)$$

where r_{12} , the heterogeneity contrast ($k_1\phi_2\Delta S_2/k_2\phi_1\Delta S_1$), is greater than 1. After breakthrough ($x_{D1} > 1$), the same quantity is

$$\frac{dx_{D1}}{dx_{D2}} = r_{12}(x_{D2} + M^0(1 - x_{D2})) \quad (6.4-5b)$$

In both equations, M^0 is the endpoint mobility ratio defined in Eq. (5.2-3c). Before breakthrough x_{D1} and x_{D2} are less than 1, we can integrate Eq. (6.4-5a) subject to the boundary condition that $x_{D1} = 0$ when $x_{D2} = 0$ to give

$$\frac{1 - M^0}{2} x_{D1}^2 + M^0 x_{D1} = r_{12} \left(\frac{1 - M^0}{2} x_{D2}^2 + M^0 x_{D2} \right) \quad (6.4-6)$$

The front position in the lower layer at breakthrough x_{D2}^2 follows from Eq. (6.4-6) by setting $x_{D1} = 1$

$$x_{D2}^0 = \frac{\left\{ (M^0)^2 + \frac{1 - (M^0)^2}{r_{12}} \right\}^{1/2} - M^0}{1 - M^0} \quad (6.4-7a)$$

After breakthrough, the front in the upper layer (outside the reservoir) is given by integrating Eq. (6.4-5b) with the boundary condition $x_{D2} = x_{D2}^0$ when $x_{D1} = 1$.

$$x_{D1} = 1 + r_{12} \left[\frac{1 - M^0}{2} (x_{D2}^2 - (x_{D2}^0)^2) + M^0 (x_{D2} - x_{D2}^0) \right] \quad (6.4-7b)$$

The front “position” in the upper layer at complete sweepout is given by Eq. (6.4-7b) with $x_{D2} = 1$

$$x_{D1} = 1 + (r_{12} - 1) \left(\frac{1 + M^0}{2} \right) \quad (6.4-7c)$$

For fixed values of the mobility ratio, and heterogeneity contrast, E_I at a given dimensionless cumulative injection may be obtained by substituting the front positions calculated from Eqs. (6.4-6) and (6.4-7) in the definitions (Eqs. 6.4-1 and 6.4-2). Figure 6-10 shows the results of this procedure for three values of M^0 and two values of the permeability contrast.

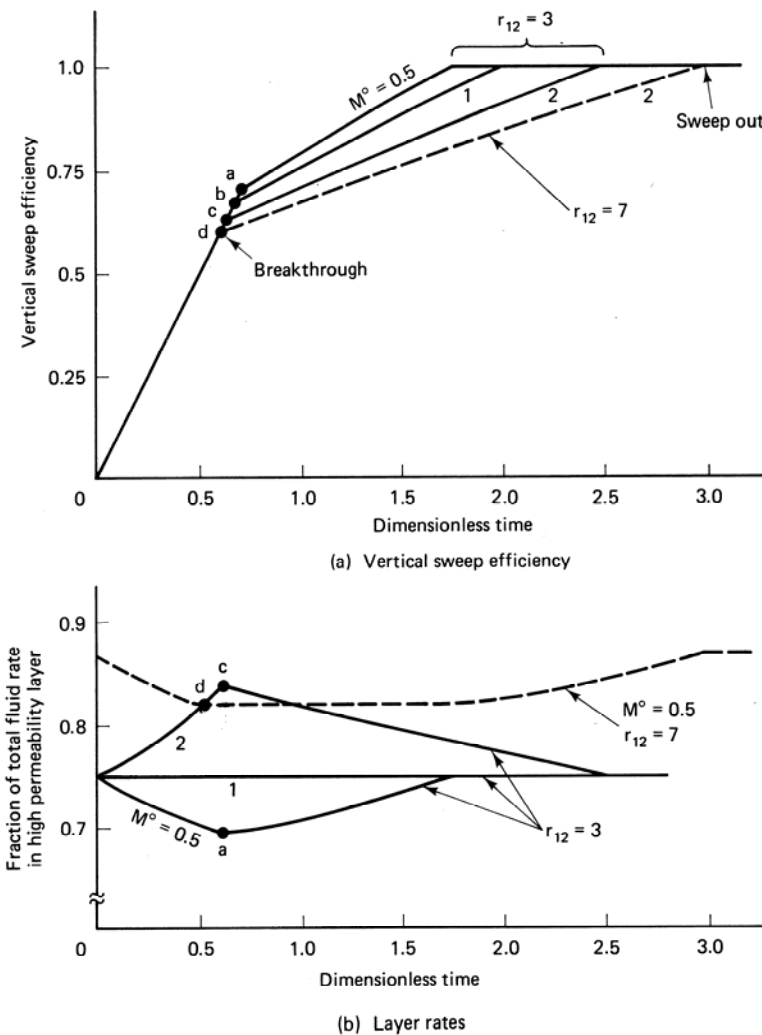


Figure 6-10 Two-layer Dykstra-Parsons calculation

For increasing permeability contrast E_I decreases (Fig. 6-10a). A decreasing M^0 improves, and an increasing M^0 worsens E_I , just as similar changes do for the areal and displacement sweep efficiencies. Fig. 6-10(b) plots the ratio of the volumetric flow rate into layer 1 to the total flow rate as a function of t_D . This follows from Eqs. (6.4-6) and (6.4-7)

$$\frac{q_1}{q_1 + q_2} = \frac{(\phi h \Delta S v)_1}{(\phi h \Delta S v)_1 + (\phi h \Delta S v)_2} = \frac{1}{1 + \frac{(kh)_2}{(kh)_1} \left[\frac{M^0 + x_{D1}(1 - M^0)}{M^0 + x_{D2}(1 - M^0)} \right]} \quad (6.4-8)$$

Equation (6.4-8) shows the reason for the changes in E_I . For $M^0 < 1$, the fast layer is filling up with a low mobility fluid faster than the slow layer. Thus the fast layer resistance to flow is increasing faster than the slow layer resistance, causing the fast layer flow rate to decrease. For $M^0 > 1$, the situation is exactly reversed. Of course, for $M^0 = 1$, there are no changes in mobility, and the ratio of fast layer rate to total rate stays constant. Mobility ratio can have an effect on E_I even if there is no vertical communication. This effect has qualitatively the same trend as the areal and displacement sweep.

N_L Layers

The above results may be readily generalized to an ensemble of N_L layers. First, we generalize the heterogeneity contrast to be between any two layers l and n

$$r_{nl} = \left(\frac{k}{\phi \Delta S} \right)_n \left(\frac{\phi \Delta S}{k} \right)_l \quad (6.4-9)$$

At a particular time, if n is the number of the layer breaking through, the front position in all the faster layers is given by

$$x_{Dl} = 1 + (r_{ln} - 1) \left(\frac{1 + M^0}{2} \right), \quad l = 1, \dots, n \quad (6.4-10a)$$

from Eq. (6.4-7c). Similarly, the position in all the slower layers is

$$x_{Dl} = \frac{\left\{ (M^0)^2 + \frac{1 - (M^0)^2}{r_{nl}} \right\}^{1/2} - M^0}{1 - M^0}, \quad l = n + 1, \dots, N_L \quad (6.4-10b)$$

from Eq. (6.4-7a). By letting n take on values between 1 and N_L , calculating all N_L front positions, and substituting these into Eqs. (6.4-1) and (6.4-2), we can construct a plot of E_I versus t_D (see Exercise 6D). The E_I - t_D plot follows from this by connecting these points by straight-line segments. That this procedure is not rigorous may be seen from Fig. 6-10, where the curves between breakthrough and sweepout are slightly curved. But if N_L is large, the error introduced by this procedure will be small. The procedure may be easily modified to calculate E_I in an ensemble having the continuous F - C distribution discussed in Sec. 6-3. Using the water-oil ratio

$$\text{WOR} = \frac{\sum_{l=1}^n q_l}{\sum_{l=n+1}^{N_L} q_l} \quad (6.4-11)$$

as the time variable in place of t_D , Johnson (1956) has presented the vertical sweep efficiency as a function of V_{DP} and M^0 in graphical form.

6-5 Vertical Equilibrium

A useful procedure for making general oil recovery calculations is to invoke the assumption of *vertical equilibrium* (VE) across the cross section of the reservoir the displacement is taking place in. When VE applies, it is possible to combine vertical and displacement sweep efficiencies into a pseudodisplacement sweep, which then may be estimated by the one-dimensional theory of Sec. 5-2. This combination means recovery efficiency E_R becomes

$$E_R = E_A E_I E_D = E_A \tilde{E}_D \quad (6.5-1)$$

where \tilde{E}_D is the *pseudodisplacement* sweep efficiency. Of course, the areal sweep efficiency E_A must still be estimated and used in Eq. (6.5-1). We discuss how to combine E_A and \tilde{E}_D in Sec. 6-7. Another consequence of the VE assumption is this represents a state of maximum transverse fluid movement, or crossflow. Thus calculations based on VE are useful in estimating the tendency of crossflow to affect displacements when compared to the noncrossflowing calculations of Sec. 6-4.

The VE Assumption

Formally, vertical equilibrium is a condition where the sum of all the fluid flow driving forces in the direction perpendicular to the direction of bulk fluid flow is zero. We see this condition is more nearly met by flow in reservoirs having large aspect ratios (length to thickness) and good vertical communication. Moreover, Sec. 6-6 shows that several classical displacement calculations in the petroleum literature are, in fact, subsets of the more general theory of vertical equilibrium.

To derive a general VE theory, we restrict ourselves to incompressible, immiscible displacements of oil by water and derive the water saturation profile in the transverse direction (z direction) at a fixed cross section (x position). For the assumptions listed above, the conservation Eq. (2D-1) for water becomes in x - z coordinates,

$$\phi \frac{\partial S_1}{\partial t} + \frac{\partial u_{x1}}{\partial x} + \frac{\partial u_{z1}}{\partial z} = 0 \quad (6.5-2)$$

If we introduce Darcy's law (Eq. 2.2-5) into Eq. (6.5-2) and scale the independent variables x and z as

$$x_D = \frac{x}{L}, \quad z_D = \frac{z}{H_t} \quad (6.5-3)$$

Eq. (6.5-2) becomes

$$\begin{aligned} \phi \left(\frac{L^2}{k} \right) \frac{\partial S_1}{\partial t} - \frac{\partial}{\partial x_D} \left(\lambda_{r1} \left(\frac{\partial P_1}{\partial x_D} + L \rho_1 g \sin \alpha \right) \right) \\ - \left(\frac{L^2}{H_t^2 k} \right) \frac{\partial}{\partial z_D} \left(k_z \lambda_{r1} \left(\frac{\partial P_1}{\partial z_D} + H_t \rho_1 g \cos \alpha \right) \right) = 0 \end{aligned} \quad (6.5-4)$$

The terms in this equation represent water accumulation, x -direction flow, and z -direction flow, respectively (see Fig. 6-11). We assume flow in the z direction is finite; therefore, if the group L^2 / kH_t^2 large, it follows that the term it multiplies must be small. This means the z -direction water flux is a function of x only, or

$$k_z \lambda_{r1} \left(\frac{\partial P_1}{\partial z} + \rho_1 g \cos \alpha \right) = f(x) \quad (6.5-5)$$

Since the water flux in the z direction is finite, if k_z is large, Eq. (6.5-5) implies

$$\frac{\partial P_1}{\partial z} = -\rho_1 g \cos \alpha \quad (6.5-6)$$

Clearly, the above reasoning breaks down at water saturations near the irreducible water saturation where λ_{r1} is zero. But it is true that the saturation range where Eq. (6.5-6) breaks down is precisely the range where the analogous equation for the oil phase is most relevant. Therefore, the arguments leading to Eq. (6.5-6) should be valid in some average sense when applied to both the water and oil phases.

Assuming the group L^2 / kH_t^2 large is reasonable for many practical cases. But assuming k_z is large strains credibility since for most naturally occurring media k_z is less than k . For permeable media having dispersed shale barriers, k_z can be much smaller than k .

The requirements of large L^2 / kH_t^2 and k_z may be combined into a single requirement that the effective length-to-thickness ratio

$$R_L = \frac{L}{H_t} \left(\frac{\bar{k}_z}{\bar{k}} \right)^{1/2} \quad (6.5-7a)$$

be large. In Eq. (6.5-7a), the permeabilities are an arithmetic average for

$$\bar{k} = \frac{1}{H_t} \int_0^{H_t} k dz \quad (6.5-7b)$$

and a harmonic average for k_z

$$\bar{k}_z = \frac{H_t}{\int_0^{H_t} \frac{dz}{k_z}} \quad (6.5-7c)$$

A displacement actually approaches VE asymptotically as R_L becomes large. Based on numerical solution (Zapata, 1981) and analytic solutions (Lake and Zapata, 1987), an R_L greater than 10 is sufficient to ensure that the z -direction sweep efficiency is reasonably well described by VE. You may easily verify that R_L can be large for a wide variety of reservoirs. For example, for a 16.2 hm² (40-acre) spacing of five-spot patterns, the injector-producer distance is 285 m (933 ft). If we take this to be L , then for $H_t = 6.1$ m (20 ft) and $\bar{k}_z = 0.1 \bar{k}$, we have $R_L = 14.8$, which is large enough for VE to be a good approximation. By taking the \bar{k} to be a harmonic average over the reservoir interval, it is clear the $\bar{k}_z = R_L = 0$ if there are one or more impermeable barriers (for example, continuous shale layers) within the interval H_t . Clearly, the VE assumption will not apply in this case. But the pseudodisplacement sweep efficiency of the intervals between the barriers may be estimated based on VE, and the combined response of all such intervals may be estimated by the communicating methods of Sec. 6-4.

R_L may be regarded as a ratio of a characteristic time for fluid to cross the reservoir in the x direction to that in the z direction. If R_L is large, saturation or pressure fluctuations in the z direction decay much faster than those in the x direction. Therefore, we neglect the z -direction perturbations. Thus when we say that the VE assumption applies or that the subject reservoir is in vertical equilibrium, we are saying, for the bulk of the reservoir, z -direction fluctuations are negligible. Arguments based on the decay time of perturbations were originally advanced by G. I. Taylor for flow in capillary tubes (Lake and Hirasaki, 1981).

For large R_L , the P_1 profile in the z direction is given by Eq. (6.5-6) for most of the cross sections in the reservoir. This procedure applies equally well to the oil phase, giving

$$\frac{\partial P_1}{\partial z} + \rho_1 g \cos \alpha = 0 = \frac{\partial P_2}{\partial z} + \rho_2 g \cos \alpha \quad (6.5-8)$$

When the definition for oil–water capillary pressure $P_c = P_2 - P_1$ is introduced into this equation, we have

$$\frac{\partial P_c}{\partial z} = -(\rho_1 - \rho_2)g \cos \alpha \equiv -\Delta \rho g \cos \alpha \quad (6.5-9)$$

Equation (6.5-9) implicitly describes the water saturation profile in the z direction since P_c is a known function of water saturation. But this saturation distribution is just what would be observed in the transition zone between oil and water under static conditions. Compare Eqs. (6.5-9) and (2A-1), noting the z and P_c increase in the opposite directions. Hence the z -direction saturation profile given by Eq. (6.5-9) is identical to that predicted by assuming no flow in the z direction.

We stated that VE is a condition that causes maximum crossflow of fluids, so it is surprising, to say the least, that the same equation describes the saturation profile under conditions of zero and maximum z -direction flow. The situation is analogous to heat conduction in metal rod where the driving force for heat transfer is a temperature gradient along the axis of the rod (Coats et al., 1971). If the thermal

conductivity of the rod is not zero and no heat flows along the rod, the temperature difference between the ends of the rod is zero. But if heat flows at a fixed finite rate along the rod, and the thermal conductivity of the rod is large, the temperature difference is again small. The latter case is analogous to the VE flow in the z direction of Fig. 6-11 where, since the thermal conductivity is large, the heat transfer rate is maximum; the former case is the analogue to hydrostatic equilibrium.

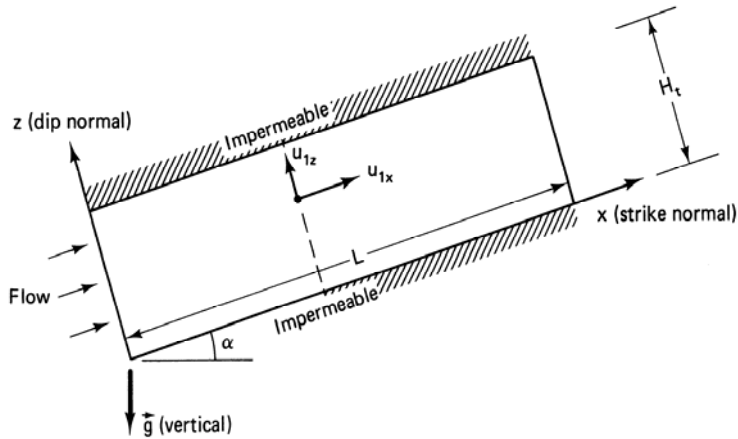


Figure 6-11 Schematic cross-section for vertical equilibrium procedure

Displacement Classification

One of the consequences of VE is a classification of displacements according to degree of segregation. Let S_1^+ be some water saturation slightly below $1 - S_{2r}$, and S_1^- slightly above S_{1r} . We can define a capillary transition zone thickness z_{CTZ} as the z -direction distance over which the water saturation changes between these two limits. From Eq. (6.5-9) and Fig. 6-12, this is

$$z_{CTZ} \equiv z \left| \frac{P_c}{S_1^+} - \frac{P_c}{S_1^-} \right| = \frac{\Delta \rho g \cos \alpha}{\left| \frac{P_c}{S_1^-} - \frac{P_c}{S_1^+} \right|} \quad (6.5-10)$$

We have made the integration of Eq. (6.5-9) assuming the capillary-pressure–water-saturation relation applies throughout z_{CTZ} . In general, the capillary transition zone defined by Eq. (6.5-10) is not the same as that existing at the original water–oil contact, down structure to the left in Fig. 6-11. The idea of the capillary transition zone in a VE reservoir allows the definition of two broad classes of displacements (Dake, 1978). If $z_{CTZ} \gg H_t$, the water saturation profiles in the z direction are essentially flat, and the flow is said to be *diffuse*. If $z_{CTZ} \ll H_t$, the capillary transition zone is small with respect to the reservoir thickness, and the flow is *segregated*. These definitions suggest ideas similar to the definitions of sharpening and spreading waves in Sec. 5-2 except that the latter definitions apply to cross-sectional averaged

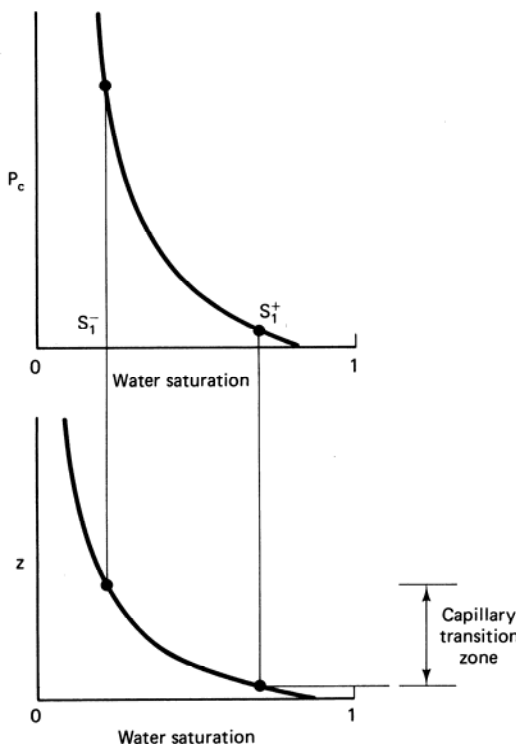


Figure 6-12 Schematic of capillary transition zone

saturation waves. The mixing or transition zones in Sec. 5-2 were in the x direction only and were largely caused by chromatographic effects inherent in the permeable medium oil–water fractional flow curves. The capillary transition zone defined by Eq. (6.5-10) is in the z direction and defined by the capillary-pressure–water-saturation relation, the dip angle, and the density difference.

Saturation Profile

Let's now consider the integration of Eq. (6.5-9) at the three different cross sections A , B , and C in Fig. 6-13. In this figure, flow is from right to left for ease of illustration. We take S_{1A} , S_{1B} , and S_{1C} to be the water saturations at the bottom ($z = 0$) of the reservoir at the indicated cross sections $x = x_A$, x_B , and x_C . Because of the direction of flow, and because the initial water saturation is near the irreducible value $S_{1A} > S_{1B} > S_{1C}$. The water saturation profile at each of these cross sections is given implicitly from Eq. (6.5-9)

$$P_c(S_1(x_k, z)) = P_c(S_{1k}) + \Delta\rho g z \cos\alpha, \quad k = A, B, \text{ or } C \quad (6.5-11)$$

We do not, at this point, know the x -direction position of the $z = 0$ water saturations, which we indirectly determine below. But we can schematically sketch in lines connecting constant values of S_1 , as indicated in Fig. 6-13. For positive values of the

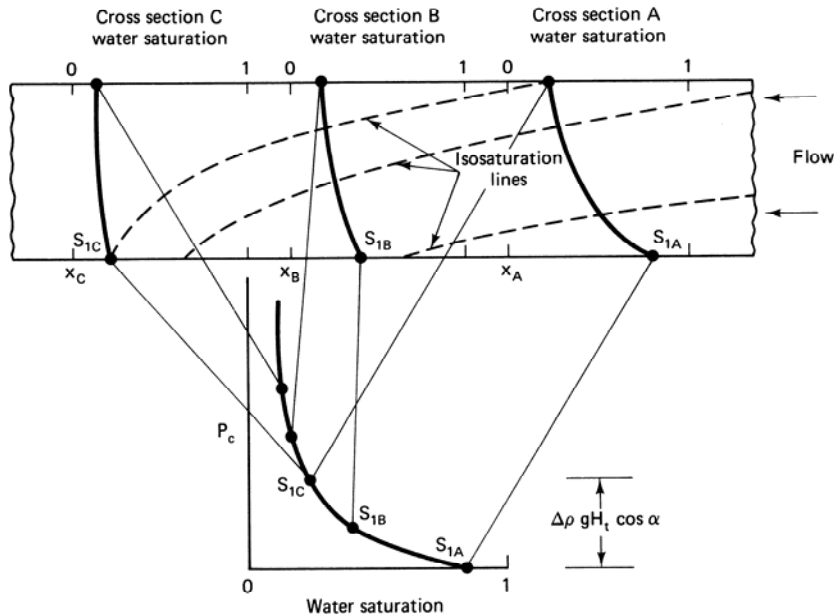


Figure 6-13 Schematic of z -direction water saturation profiles at various cross sections

density difference, the usual case, the isosaturation lines suggest an underrunning of the oil by the injected water. This underrunning, or gravity tongue, is a persistent feature of reservoirs in which gravity forces are strong. Tonguing occurs even in reservoirs that have no dip $\cos \alpha = 1$ ($D_z = -z$). The extent of the tonguing is greatly influenced by the shape of the capillary pressure curve. In Sec. 6-6, we discuss a special case of the VE theory in which capillary forces are negligible, and the gravity tonguing occurs as segregated flow.

Pseudoproperties

To use the z -direction S_1 profile, we must convert the original two-dimensional Eq. (6.5-2) to an equivalent one-dimensional equation. Let's integrate Eq. (6.5-2) over the interval thickness H_t and divide the equation by H_t

$$\frac{1}{H_t} \int_0^{H_t} \frac{\partial S_1}{\partial t} dz + \frac{1}{H_t} \int_0^{H_t} \frac{\partial u_{x1}}{\partial x} dz + \frac{1}{H_t} \int_0^{H_t} \frac{\partial u_{z1}}{\partial z} dz = 0 \quad (6.5-12)$$

Since H_t is a constant, the integration and differentiation in the first term commutes, and Eq. (6.5-12) becomes

$$\bar{\phi} \frac{\partial \bar{S}_1}{\partial t} + \frac{\partial \bar{u}_{x1}}{\partial x} = 0 \quad (6.5-13)$$

Terms involving z -direction water flux do not appear in Eq. (6.5-13) since all fluxes

vanish at the upper and lower impermeable boundaries of the reservoir. In Eq. (6.5-13), the averages are

$$\bar{S}_1 = \frac{1}{H_t \bar{\phi}} \int_0^{H_t} \phi S_1 dz \quad (6.5-14a)$$

$$\bar{\phi} = \frac{1}{H_t} \int_0^{H_t} \phi dz, \quad \bar{u}_{1x} = \frac{1}{H_t} \int_0^{H_t} u_{x1} dz \quad (6.5-14b)$$

In these definitions, and in those that follow, all averages are arithmetic averages except the water saturation, which is weighted by the porosity. Introducing the definitions for dimensionless independent variables

$$x_D = \frac{x}{L}, \quad t_D = \int_0^t \frac{\bar{u}_x dt}{\bar{\phi} L} \quad (6.5-15)$$

into Eq. (6.5-13) yields,

$$\frac{\partial \bar{S}_1}{\partial t_D} + \frac{\partial \bar{f}_1}{\partial x_D} = 0 \quad (6.5-16)$$

where $\bar{u}_x = \bar{u}_{x1} + \bar{u}_{x2}$, and $\bar{f}_1 = \bar{u}_{x1}/\bar{u}_x$ is a cross-sectional averaged water fractional flow function. Eq. (6.5-16) is identical to Eq. (5.2-5a) and can be solved in the same manner as the Buckley-Leverett and Welge integration procedures once we define \bar{f}_1 in terms of \bar{S}_1 .

Consider the cross-sectional averaged total flux multiplied by H_t with Darcy's law substituted for the local flux

$$H_t \bar{u}_x = - \int_0^{H_t} k \lambda_{r2} \left(\frac{\partial P_2}{\partial x} + \rho_2 g \sin \alpha \right) dz - \int_0^{H_t} k \lambda_{r1} \left(\frac{\partial P_1}{\partial x} + \rho_1 g \sin \alpha \right) dz \quad (6.5-17)$$

We can express the x -direction oil phase pressure gradient in terms of the water phase pressure gradient and factor to give

$$H_t \bar{u}_x = - \int_0^{H_t} k (\lambda_{r2} + \lambda_{r1}) \frac{\partial P_1}{\partial x} dz - \int_0^{H_t} k \lambda_{r2} \frac{\partial P_c}{\partial x} dz - g \sin \alpha \int_0^{H_t} k (\lambda_{r2} \rho_2 + \lambda_{r1} \rho_1) dz \quad (6.5-18)$$

But from Eq. (6.5-6), it follows that

$$\frac{\partial^2 P_1}{\partial x \partial z} = \frac{\partial^2 P_1}{\partial z \partial x} = \frac{\partial}{\partial z} \left(\frac{\partial P_1}{\partial x} \right) = 0$$

hence under VE, the water phase pressure gradient in the x direction is independent of z , as are both $\partial P_2/\partial x$ and $\partial P_c/\partial x$. All gradients may be factored from the integrations and solved for as

$$-\frac{\partial P_1}{\partial x} = \frac{H_t \bar{u}_x + \left(\frac{\partial P_c}{\partial x} \right) \int_0^{H_t} \lambda_{r2} k dz + g \sin \alpha \int_0^{H_t} k (\lambda_{r2} \rho_2 + \lambda_{r1} \rho_1) dz}{\int_0^{H_t} k (\lambda_{r2} + \lambda_{r1}) dz} \quad (6.5-19)$$

The pressure gradient of Eq. (6.5-19) substituted into the averaged water flux

$$H_t \bar{u}_{x1} = \left(-\frac{\partial P_1}{\partial x} \right) \int_0^{H_t} k \lambda_{r1} dz - g \sin \alpha \int_0^{H_t} k \lambda_{r1} \rho_1 dz \quad (6.5-20)$$

gives

$$\bar{f}_1 = \frac{\bar{u}_{x1}}{\bar{u}_x} = \frac{(\bar{k} \lambda_{r1})}{\bar{k} (\lambda_{r1} + \lambda_{r2})} \left\{ 1 + \frac{(\bar{k} \lambda_{r2})}{\bar{u}_x} \left(\frac{\partial P_c}{\partial x} \right) - \frac{(\bar{k} \lambda_{r2}) \Delta \rho g \sin \alpha}{\bar{u}_x} \right\} \quad (6.5-21)$$

Comparing this equation with Eq. (5.3-1) suggests the following definitions for *pseudorelative permeabilities*

$$\tilde{k}_{r1} = \frac{1}{H_t \bar{k}} \int_0^{H_t} k k_{r1} dz \quad (6.5-22a)$$

$$\tilde{k}_{r2} = \frac{1}{H_t \bar{k}} \int_0^{H_t} k k_{r2} dz \quad (6.5-22b)$$

The capillary pressure in Eq. (6.5-21) is the capillary-pressure–water-saturation relation for any z position in the reservoir. It does not matter which z position since $\partial P_c / \partial x$ is equal at all z positions. From this, it does not follow that the capillary-pressure–water-saturation relation is the same in all z positions since these can vary with permeability. The capillary pressure in Eq. (6.5-21) is often regarded as a pseudofunction, even though it is an actual local curve, since it must be a function of \bar{S}_1 .

To use the one-dimensional theory of Sec. 5-2 on these equations, we must neglect the x -direction capillary pressure term in Eq. (6.5-21). This omission is not equivalent to neglecting capillary pressure entirely since the capillary pressure in the z direction determines, in part, the z -direction saturation profile. Though it seems inconsistent to maintain capillary pressure in the z direction and neglect it in the x direction, one can show by scaling arguments similar to those used in Sec. 5-3 that when the conditions for VE apply, z -direction effects are far more important than x -direction effects (Yokayama and Lake, 1981).

The procedure for calculating pseudorelative permeability curves (\tilde{k}_{r1} and \tilde{k}_{r2} versus \bar{S}_1) is as follows:

1. Select a water saturation at the bottom of the reservoir S_{1k} .
2. Determine the z -direction water saturation profile $S_1(x_k, z)$ at cross section k using Eq. (6.5-11) and the capillary-pressure–water-saturation relation.

3. Calculate the average water saturation at cross section k , $\bar{S}_1(x_k)$, from Eq. (6.5-14a) and from the z -direction porosity profile.
4. Calculate the pseudorelative permeabilities corresponding to \bar{S}_{1k} from Eq. (6.5-22) and the z -direction permeability profile.

Steps 1–4 give a single point on the pseudorelative permeability curve. To construct the entire curve, we repeat the procedure with different values of S_{1k} . The procedure gives all possible water saturation profiles and average water saturations for the reservoir (see Fig. 6-13) though it does not give the x positions of these quantities, which come from solving the one-dimensional Eq. (6.5-13). Though the averaging procedure is fairly straightforward, most of the integrations in it must be evaluated numerically in the absence of analytic functions for the capillary pressure and relative permeability curves (see Exercise 6F).

Once the pseudorelative permeabilities are constructed, the pseudodisplacement sweep efficiency \tilde{E}_D follows from Eqs. (5.1-2) and (5.2-24) with the appropriately averaged quantities appearing in place of the local quantities.

You should appreciate the generality of the VE approach, for we now have a means for calculating and combining displacement E_D and vertical E_I sweep efficiencies with little more trouble than calculating the displacement sweep alone, VE can greatly simplify oil recovery calculations in desktop procedures and numerical simulations (Coats et al., 1971); however, the entire procedure is restricted to reservoirs having a large R_L .

The generalized VE approach for EOR processes has yet to be worked out. (For miscible flow, see Lake and Hirasaki, 1981.)

6-6 SPECIAL CASES OF VERTICAL EQUILIBRIUM

Though the VE procedure in Sec. 6-5 is quite general, being restricted to reservoirs having constant properties in the x direction and a large R_L , several VE flows are special cases. Since these cases are useful in understanding many EOR processes, in this section we review them and show how they follow from the general theory.

Homogeneous with Large Transition Zone

In this case, k and ϕ are both constant in the reservoir, and $z_{CTZ} \gg H_t$. From the procedure given above, the saturation profile in the z direction will be essentially flat, and the saturation at the reservoir bottom will not differ much from the average saturation. In this case, the pseudorelative permeabilities \tilde{k}_{rj} become the local (or REV) relative permeabilities k_{rj} . Large z_{CTZ} would be the rule in most of the longer laboratory core floods. In the shorter core experiments, VE is usually not a good assumption, but S_1 may still be uniform in a cross section since the S_1 profile has not had much time to distort.

Homogeneous, Uniform with No Transition Zone

Easily the most celebrated of the VE theories is the theory of gravity tonguing, or underrunning, originally proposed by Dietz (1953). This theory was first proposed as an alternative to the Buckley-Leverett theory, but it is actually a special case of the VE theory because a finite time is required for the conditions underlying the theory to apply. Since the publication of the original Dietz paper, the theory has been applied to gravity overrunning by a miscible gas process (Hawthorne, 1960), and other work has been published describing the approach to VE conditions (Crane et al., 1963). In this section, we restrict ourselves to the water-displacing-oil case though the overrunning case can be similarly developed.

The key assumption in the Dietz theory is the absence of a transition zone, or $z_{CTZ} = 0$. This condition can be accurate only for conditions where the capillary pressure is small (well-sorted or high-permeability media). The sharp transition zone or macroscopic interface resulting from this condition suggests the theory is applicable to any displacement where simultaneous flow of more than one component or phase is absent at any point in the reservoir. If P_c is identically zero, Eq. (6.5-8) cannot be satisfied at any point in the reservoir since the oil and water densities are not, in general, equal. The resolution of this is to let Eq. (6.5-6) apply to zones flowing water and to let the analogous equation for oil apply to zones flowing oil. Figure 6-14 shows the relevant cross section and these zones.

At any cross section containing the tongue, the average water saturation from Eq. (6.5-14a) is

$$\bar{S}_1 = \frac{1}{H_t} [b(1 - S_{2r}) + S_{1r}(H_t - b)] \quad (6.6-1)$$

and the pseudorelative permeability functions from Eq. (6.5-22) are

$$\tilde{k}_{r1} = k_{r1}^o \left(\frac{b}{H_t} \right) \quad (6.6-2a)$$

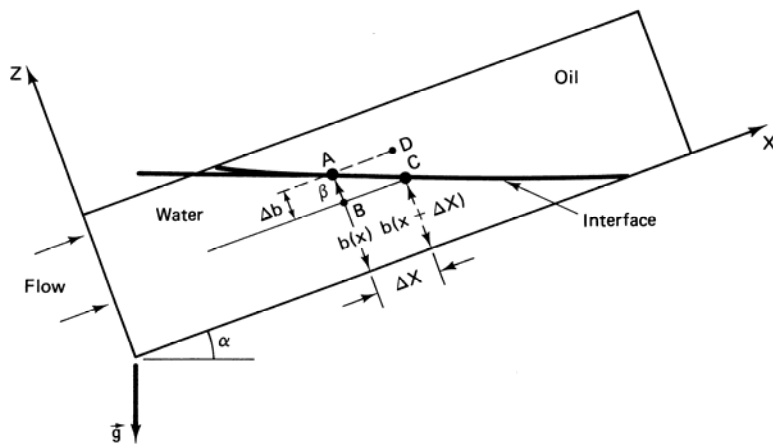


Figure 6-14 Schematic cross section of a water tongue

$$\tilde{k}_{r2} = k_{r2}^o \left(\frac{H_t - b}{H_t} \right) \quad (6.6-2b)$$

The interface height b may be eliminated between Eqs. (6.6-1) and (6.6-2) to give

$$\tilde{k}_{r1} = k_{r1}^o \left(\frac{\bar{S}_1 - S_{1r}}{1 - S_{1r} - S_{2r}} \right), \quad \tilde{k}_{r2} = k_{r2}^o \left(\frac{1 - S_{2r} - \bar{S}_1}{1 - S_{1r} - S_{2r}} \right) \quad (6.6-3)$$

Thus the pseudorelative permeabilities are straight-line functions of the average water saturation.

We can also derive the tilt angle β of the oil–water interface. Consider the rectangle $ABCD$ of height Δb and width Δx shown in Fig. 6-14. The dimensions Δx and Δb are small (we pass to zero limit below) so that the interface between points A and C is the diagonal of the rectangle. Along the BC side of the rectangle, the x -direction water flux is

$$u_{x1} = -\frac{kk_{r1}^o}{\mu_1} \left(\frac{P_C - P_B}{\Delta x} + \rho_1 g \sin \alpha \right) \quad (6.6-4a)$$

and along the AD side, the x -direction oil flux is

$$u_{x2} = -\frac{kk_{r2}^o}{\mu_2} \left(\frac{P_D - P_A}{\Delta x} + \rho_2 g \sin \alpha \right) \quad (6.6-4b)$$

In the limit of $\Delta x \rightarrow 0$, these two fluxes approach a common value u_x since there can be no accumulation at the interface. Further, the pressures at A and B , and at D and C , are related because of the VE conditions (Eq. 6.5-8)

$$P_B - P_A = \rho_1 g \Delta b \cos \alpha, \quad P_C - P_D = \rho_2 g \Delta b \cos \alpha \quad (6.6-5)$$

The four equations (Eqs. 6.6-4 and 6.6-5) may be combined to eliminate the four pressures. This procedure gives

$$\tan \beta = \frac{(u_{x1} - u_{x2} M^o) \mu_1}{(kk_{r1}^o \Delta \rho g) \cos \alpha} + \tan \alpha \quad (6.6-6)$$

The tangent of the tilt angle is defined as

$$\tan \beta = + \lim_{\Delta x \rightarrow 0} \frac{\Delta b}{\Delta x} \quad (6.6-7)$$

β is defined to be positive and can take on the entire range of values between 0° and 90° . If β is greater than 90° , the tongue is overrunning, and this procedure must be repeated with the displacing fluid above the resident fluid.

For $\beta > 0$ —that is, the interface is not parallel to the x axis—the interface reaches a stabilized shape where β is independent of both time and z position. This limit is not an automatic consequence of VE, but the time interval between the onset of the VE conditions and the attainment of the stabilized interface shape appears to be small (Crane et al., 1963). When this steady-state tilt angle β_s is reached, the x -direction fluxes u_{x1} and u_{x2} become independent of z and equal to the cross-sectional

average flux \bar{u}_x . Equation (6.6-6) then becomes

$$\tan \beta_s = \frac{1 - M^0}{M^0 N_g^0 \cos \alpha} + \tan \alpha \quad (6.6-8)$$

where N_g^0 and M^0 are gravity numbers and mobility ratios defined in Eq. (5.2-3).

Equation (6.6-8) approaches the correct limits of an interface perpendicular to the x direction for $N_g^0 = 0$ (no tonguing) and of a horizontal interface for $M^0 \rightarrow 1$. In the case of a stable gravity tongue, the cross-sectional average water saturation profile approaches a “constant pattern” mixing zone, whereas the directly analogous case of a one-dimensional displacement with straight-line relative permeabilities approaches a shock front. This is a consequence of the finite length of time required for the VE conditions to apply in the tonguing case.

For $\beta < 0$, the interface completely underruns the oil and is said to be unstable. The condition for stability is, from Eq. (6.6-8),

$$M^0 - 1 < M^0 N_g^0 \sin \alpha \quad (6.6-9)$$

The equality form of Eq. (6.6-9) naturally leads to definitions of a critical endpoint mobility ratio $M_c^0 = M^0 |_{\beta_s=0}$

$$M_c^0 = \frac{1}{1 - N_g^0 \sin \alpha} \quad (6.6-10a)$$

and of a critical flux or rate $u_c = u_x |_{\beta_s=0}$

$$u_c = \frac{\Delta \rho g k k_{r1}^0}{\mu_1 (M^0 - 1)} \sin \alpha \quad (6.6-10b)$$

The conditions to prevent complete underrunning of the oil by the water are $u_x < u_c$ or $M^0 < M_c^0$. Equation (6.6-10a) indicates gravity stabilization is possible even when $M^0 > 1$. Equation (6.6-10b), in particular, is used in estimating the flooding rates in gravity-stabilized miscible displacements.

Layered, Uniform Horizontal Media with $P_c = z_{CTZ} = 0$

For this case of the permeable medium consisting of N_L layers, each of contrasting thickness h_l , permeability k_l , and porosity, ϕ_l , the integrals in the definitions (Eqs. 6.5-14 and 6.5-22) become finite sums

$$\tilde{k}_{rj} = \frac{1}{H_l \bar{k}} \sum_{l=1}^{N_L} (k h k_{rj})_l, \quad j = 1 \text{ or } 2 \quad (6.6-11a)$$

$$\bar{S}_1 = \frac{1}{H_l \bar{\phi}} \sum_{l=1}^{N_L} (\phi h S_1)_l \quad (6.6-11b)$$

The definitions (Eqs. 6.6-11a and 6.6-11b) are valid regardless of the ordering of the layers; hence we assume, without loss of generality, they are ordered with decreasing velocity as in Sec. 6-3.

Since neither gravity nor capillary pressure is present, Eq. (6.5-8) is trivially satisfied, and there is no constraint on the saturations in the z direction. To resolve this, Hearn (1971) assumed segregated flow within a layer, as in Fig. 6-15(a). The definitions become

$$\tilde{k}_{r1} = \frac{1}{H_t \bar{k}} \sum_{l=n+1}^{N_L} (khk_{r1}^0)_l, \quad \tilde{k}_{r2} = \frac{1}{H_t \bar{k}} \sum_{l=1}^{N_L} (khk_{r2}^0)_l \quad (6.6-12a)$$

$$\bar{S}_1 = \frac{1}{H_t \bar{\phi}} \left\{ \sum_{l=1}^{N_L} (\phi h(1 - S_{2r})_l + \sum_{l=n+1}^{N_L} (\phi h S_{1r})_l \right\} \quad (6.6-12b)$$

where n is the number of the slowest layer (smallest k/ϕ) flowing water at a given cross section. Thus the average water saturation and pseudorelative permeabilities are parametrically functions of n and can be regarded as functions of each other in this way.

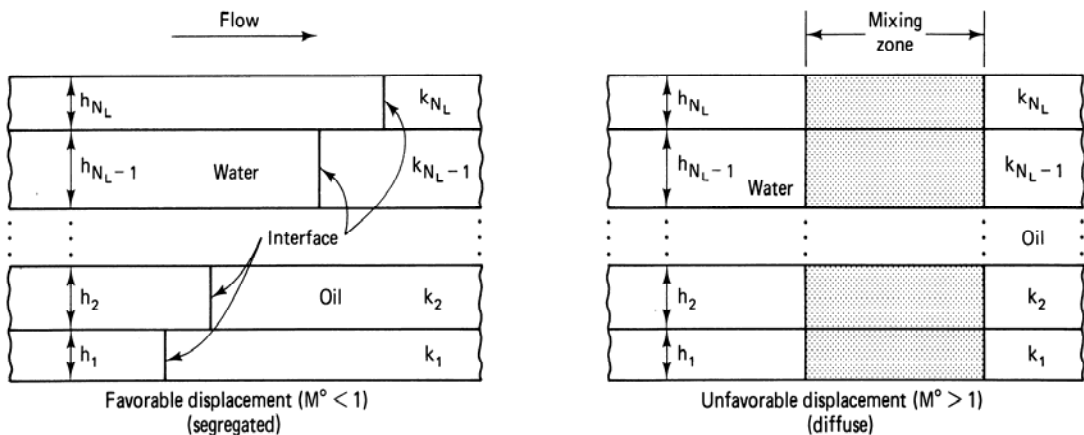


Figure 6-15 Schematic cross section of VE in stratified reservoir with no capillary and gravity effects

Based on arguments related to the direction of flow caused by the viscous pressure driving forces, Zapata and Lake (1981) have shown that assuming segregated flow within a layer is correct when the displacement is favorable $M^0 < 1$. In fact, if VE holds, it is possible for the M^0 to be so low that the effect of the heterogeneities is entirely suppressed (see Exercise 6E). But when the displacement is unfavorable, the viscous forces cause a mixing zone to develop between the front in the fastest layer and that in the slowest layer (Fig. 6-15b). This mixing zone causes the vertical sweep efficiency to be actually greater than the corresponding segregated flow case since the mixing zone attenuates the unfavorable mobility ratio. That diffuse flow can occur in VE displacements in the absence of capillary pressure is a major revelation in the understanding of these processes. The implication is clear that such crossflow might be a source of mixing in all unstable flows.

Stratified, Uniform with $\Delta P = 0$ and Constant Mobility

Here, there are no gravity forces to counteract the z -direction imbibition, and the z -direction water saturation profile is uniform within each layer. But because of the variable properties in the z direction, the $P_c - S_1$ function changes. Figure 6-16(a) illustrates this change for the four-layer medium shown. From Eq. (6.5-9), the capillary pressure (not the capillary pressure function) is a constant through any cross section. As indicated in Fig. 6-16, if the constant is known, this specifies the water saturation in each layer at that cross section. Because the mobility is constant, the x -direction viscous pressure gradient is independent of both position and time. For this case, the average water saturation and pseudorelative permeability curves are given by Eq. (6.6-11), but each of the water saturations S_{ll} are determined by the relation $P_c = \text{constant}$ and the $P_c - S_1$ relation. Again, the average water saturation and pseudorelative permeabilities are parametrically related through this constant. This procedure yields an immiscible mixing zone between the most advanced and the least advanced front, as shown in Fig. 6-16(b).

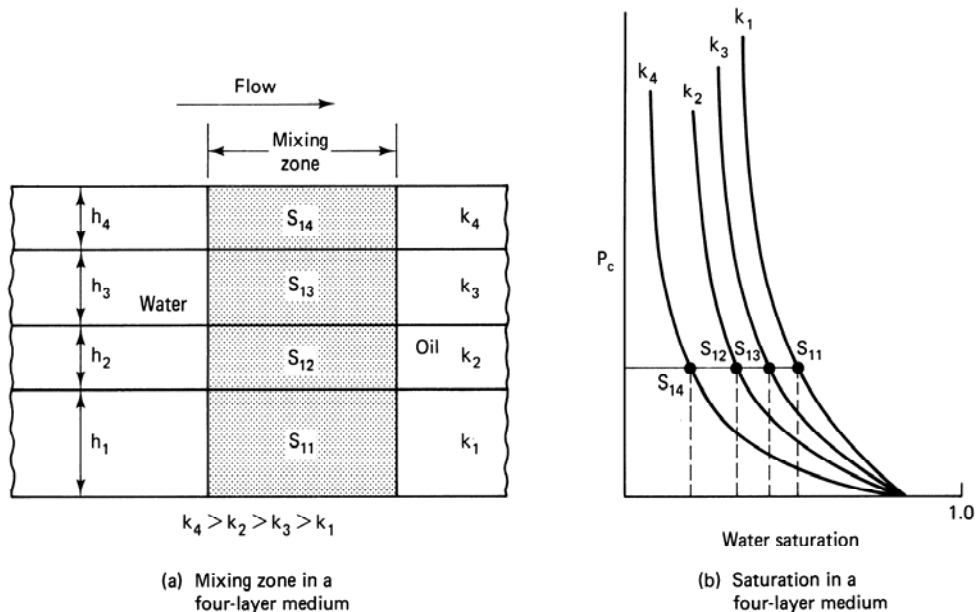


Figure 6-16 Schematic of stratified cross section with no gravity and viscous forces

6-7 COMBINING SWEEP EFFICIENCIES

In this section, we seek to provide an estimate of the recovery efficiency $E_R = E_D E_V$, from Eq. (2.5-5), as a function of dimensionless time by combining vertical, areal, and displacement sweeps. As we mentioned in Sec. 6-1, this procedure is complicated because all three sweep efficiencies depend on one another, and all must

be evaluated at times different from that at which the recovery efficiency is desired. If the reservoir is layered and noncommunicating, we could, of course, calculate the areal sweep efficiency of each layer and then average the ϕh of each layer times its areal sweep to obtain the volumetric sweep efficiency. The procedure we describe here includes this method as a special case, but it is valid for combining all types of sweep efficiency curves, not just those for layer-cake models.

Our procedure is based on the idea of apparent pore volumes first presented by Claridge (1972). We assume we have independently determined curves for E_A , E_I , and E_D as functions of t_D . For E_D , it is more convenient to work in the average water saturations \bar{S}_1 , but there is no loss of generality since the two are related through Eq. (5.1-2). Here, we are restricted to sweep efficiency functions that depend on dimensionless time, heterogeneity, capillary pressure, and so on but that do not depend explicitly on rate or fluid velocity.

Combining Areal and Vertical Sweep

The definition for volumetric sweep efficiency is repeated here as $E_V = E_A E_I$. From Fig. 6-1 (or Fig. 6-17), E_A depends on the z position in the reservoir, and E_I on a particular cross section between the injector and producer. Rather than directly determining these positions, we seek to determine that value of the dimensionless time argument at which the respective values of E_A and E_V will give average values. Therefore, we can rewrite Eq. (6.1-3) as

$$E_V(t_D) = E_A(t_{DA})E_I(t_{DI}) \quad (6.7-1)$$

where t_{DA} and t_{DI} are dimensionless times based on the apparent pore volumes for areal and vertical sweep, respectively.

Figure 6-17(a) schematically shows the positions of a pistonlike displacement at or after breakthrough. Imagine that the shaded volumes have no porosity or permeability, then the volumetric sweep efficiency is equal to the vertical sweep efficiency. The ultimate volume to be swept out, for this rather oddly shaped reservoir then, at infinite throughput is the unshaded or apparent pore volume. But this is just the E_A times the total pore volume; hence the dimensionless time for E_I is

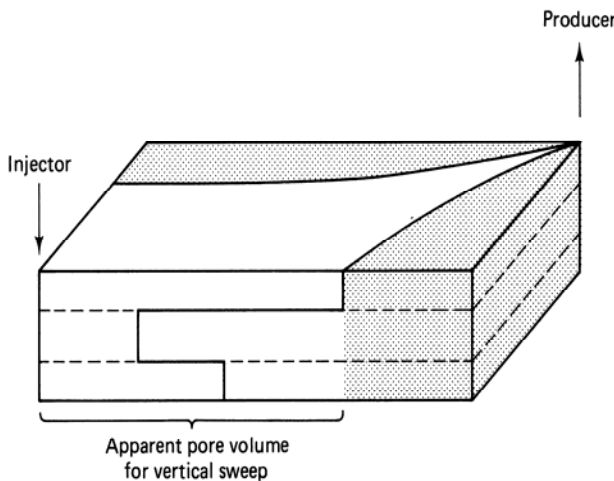
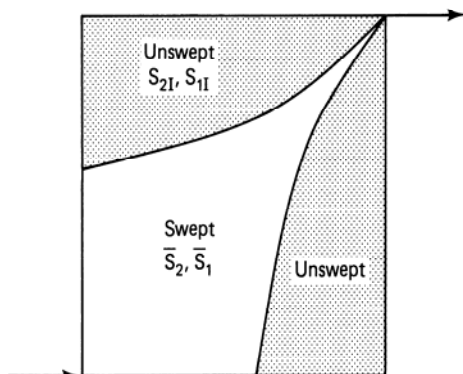
$$t_{DI} = \frac{t_D}{E_A} \quad (6.7-2a)$$

By a similar argument, though it is much more difficult to show parallel cross sections, the dimensionless time for the E_A is

$$t_{DA} = \frac{t_D}{E_I} \quad (6.7-2b)$$

The equation for the volumetric sweep may be written in combined form as

$$E_V = E_A \left(\frac{t_D}{E_I} \right) \cdot E_I \left(\frac{t_D}{E_A} \right) \quad (6.7-3)$$

(a) Schematic showing the reference volume for t_{DI} 

(b) Schematic showing swept and unswept volumes

Figure 6-17 Schematics for combining sweep efficiencies

Since E_A and E_I appear as both multiplications and in the arguments, constructing a volumetric sweep function requires a trial-and-error procedure.

1. Determine the cumulative injection at breakthrough t_D^0 . This is just the product of E_A and E_I at their respective breakthrough values, E_A^0 and E_I^0 .
2. Pick some t_D after breakthrough t_D^0 .
3. Select a trial E_I .
4. Calculate the areal sweep efficiency from $E_A = E_A(t_D/E_I)$.
5. Calculate the vertical sweep from $E_I = E_I(t_D/E_A)$ using E_A .

If E_I agrees with that assumed in step 3, $E_A \cdot E_I$ is the volumetric sweep efficiency at t_D . If E_I is different from step 3, select a new trial E_I , and return to step 4.

Experience has shown that the procedure converges within two to three iterations for typical E_A and E_I functions using direct substitution. By repeating the procedure for several values of t_D , a volumetric sweep efficiency curve may be calculated (see Exercise 6H).

Combining Pseudodisplacement and Areal Sweep

The pseudodisplacement sweep efficiency \tilde{E}_D may be determined from the VE theory of Sec. 6-5. The recovery efficiency follows from this as

$$E_R = \tilde{E}_D(t_{DA})E_A(t_{DD}) \quad (6.7-4)$$

where t_{DA} and t_{DD} are the dimensionless times based on the apparent pore volumes appropriate for the particular sweep efficiency.

Combining a displacement and areal sweep in the manner described here is again a generalization of the procedure proposed by Claridge (1972) and is repeated in Chap. 7 for a miscible flood. The dimensionless time for \tilde{E}_D is the same as Eq. (6.7-2a), but for E_A , we must view the displacement differently. Consider Fig. 6.17(b), which shows an areal view of a displacement divided into a swept and an unswept region. The unswept region contains oil and water saturations at the values present at the initiation ($S_1, S_2)_I$ of the displacement. We identify the saturations \bar{S}_1, \bar{S}_2 in the swept region with the cross-sectional averaged saturations determined from \tilde{E}_D

$$\bar{S}_1 = S_{1I} + \tilde{E}_D(1 - S_{1I}) \quad (6.7-5)$$

At a particular time, the pore volume available to flow for a pistonlike displacement whose front occupies the same position as that shown in Fig. 6-17(b) is the water volume in the swept region. (Another way of viewing this is to suppose the oil saturation \bar{S}_2 is part of the immobile phase.) Therefore, the dimensionless time for E_A is now

$$t_{DD} = \frac{t_D}{\bar{S}_1} \quad (6.7-6)$$

The procedure for calculating the recovery efficiency is similar to that given above.

1. Calculate the cumulative injection at breakthrough t_D^o . This is equal to the product of the breakthrough values of \tilde{E}_D and E_A .
2. Pick some t_D after breakthrough t_D^o .
3. Select a trial \tilde{E}_D , and calculate \bar{S}_1 from Eq. (6.7-6).
4. Calculate the areal sweep efficiency from $E_A = E_A(t_D/\bar{S}_1)$.
5. Calculate the pseudodisplacement sweep from $\tilde{E}_D = \tilde{E}_D(t_D/E_A)$.

If the \tilde{E}_D agrees with that in step 3, the recovery efficiency is the product of \tilde{E}_D and E_A . If \tilde{E}_D does not agree, return to step 3 with a new trial value.

Combining Vertical, Areal, and Displacement Sweep Efficiencies

If all three efficiencies are independently available, the above procedure may easily be generalized as

$$E_R(t_D) = E_A \left(\frac{t_D}{E_I \bar{S}_1} \right) E_I \left(\frac{t_D}{E_A \bar{S}_1} \right) E_D \left(\frac{t_D}{E_V} \right) \quad (6.7-7)$$

The procedure now requires a two-level trial and error, which is equivalent to first combining E_A and E_I and then combining E_V and E_D . The final result in Eq. (6.7-7) is independent of the order the combinations are carried out in.

As a conclusion to this section, we remind you of the limitations inherent in these procedures. First, we must have independently specified functions of E_A , E_I , and E_D , and these functions must be independent of explicit rate dependence. If a rate dependence is present, the function E_I will depend on the particular pathline it was evaluated on. Perhaps we could evaluate on a pathline having a fluid velocity representative of the entire pattern (this is commonly tried), but there is considerable uncertainty about what this representative value is even in the most well-defined displacements. Recall that, particularly in the VE approaches, the dependence of the sweep efficiencies on rate may not be particularly evident (for example, the Dietz theory is strongly rate dependent, but this is not evident from the general VE approach when capillary pressure becomes small). Further recall that independent specifications of each of the three efficiencies are available through relatively idealized calculations (see Secs. 6-4 through 6-6) for extremes in certain physical properties or through physical models. When any of the above conditions are seriously violated—and their violation significantly affects the results—one must resort to numerical simulation, from which the oil recovery could be directly calculated.

A second more subtle, and perhaps more serious, limitation of the combined sweep efficiency approach deals with scaling. Scaling simply means any of the sweep efficiencies, however determined, must themselves be adjusted for the considerably different scale between the laboratory experiment or analytical calculation and the field application. For example, few of the independent determinations of E_D or E_I account for the nonuniformities surely present in a field displacement.

A classical example of this scale effect involves applying E_D to a viscously unstable field-scale displacement. Much theoretical and experimental work has gone into showing that the size of the instabilities formed, and indeed, whether they propagate or not, is a function of the characteristic lengths of the laboratory experiment or calculation. Thus unless the scaling is such that both effects are the same in the laboratory and in the field (a sometimes impossible task), the lab-derived E_D will be too optimistic. We cover the subject of viscous instabilities in the next section.

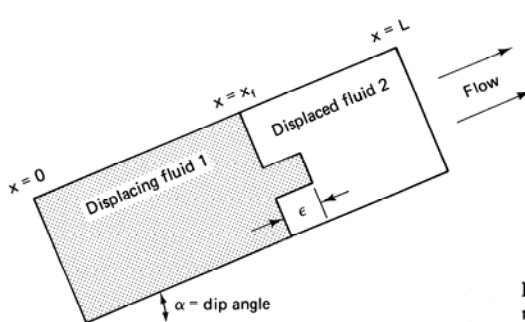
6-8 INSTABILITY PHENOMENA

No EOR process is free from some sort of instability. Hence substantial effort has gone into minimizing or preventing instabilities (using polymer to drive surfactants and alkaline agents, or foaming agents to drive CO_2 and steam) and into predicting the oil recovery if fingering is inevitable. We discuss predicting the results of a fingering process in Chap. 7 in connection with solvent flooding where instability phenomena have received the most attention. In this section, we deal with the formation of fingers.

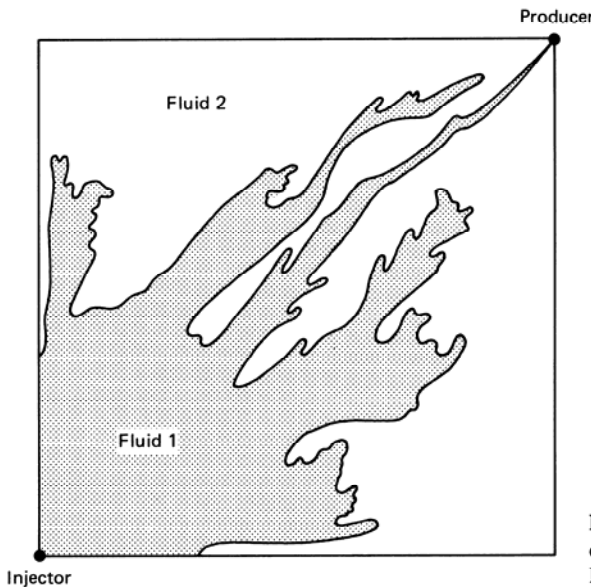
We use the term *fingering* to describe the bypassing of a resident fluid by a displacing agent in a homogeneous, nonuniform medium. The actual bypassing region is a finger. This definition encompasses instabilities caused by both viscous forces (viscous fingers) and gravity forces (gravity fingers) but does not include bypassing by permeability heterogeneities. This definition is a little more rigid than that used in the literature, but we believe the inherent distinction is useful because fingering can be prevented from displacements, whereas bypassing caused by heterogeneities cannot (though it can be reduced). In this section, we deal with isothermal flows; in Chap. 11, we discuss the stability of a nonisothermal displacement.

A Necessary Condition for Stability

In keeping with the notion that fingering is a general phenomenon, consider the incompressible, dissipation-free displacement of fluid 2 by fluid 1 in a dipping reservoir, as shown in Fig. 6-18. This figure is a cross section of a displacement, but fingering can occur in either the vertical or areal sense. There is no z -direction communication in this problem. We also consider a perturbation of length ϵ of the displacement front (caused, perhaps, by an isolated nonuniformity in the permeability field), and strive to determine the conditions under which $\epsilon(t)$ will grow or decay as a function of time. The actual fingering phenomenon is, of course, much more random and chaotic than that shown in Fig. 6-18, as evidenced by an areal view of a fingering displacement in a quarter five-spot model shown in Fig. 6-19. Nevertheless, the



Fi **Figure 6-18** Viscous fingering
m schematic



Fi **Figure 6-19** Viscous fingering in a
qu quarter five-spot model, $M^0 = 17$ (from
H Habermann, 1960)

simple geometry of Fig. 6-18 is tractable to mathematical analysis and yields insights into the more complex situations.

To solve for the conditions ε will grow or decay under, we proceed by the moving boundary technique discussed by Collins (1976). In the region behind the displacing fluid front, $x < x_f$, the conservation of fluid 1 gives

$$\frac{\partial u_{sj}}{\partial x} = 0 \quad (6.8-1)$$

where $j = 1$ for $x < x_f$, and $j = 2$ for $x > x_f$. The accumulation terms in both equations are zero since there is no change in concentration in the respective regions. For the same reason, when we substitute Darcy's law into these equations, they become

$$\frac{\partial}{\partial x} \left(\frac{\partial P_j}{\partial x} + \rho_j g \sin \alpha \right) = 0, \quad j = 1 \text{ or } 2 \quad (6.8-2)$$

The solutions to Eq. (6.8-2) will be of the form

$$P_j = (s_j - \rho_j g \sin \alpha)x + b_j, \quad j = 1 \text{ or } 2 \quad (6.8-3)$$

where a_j and b_j are integration constants to be determined with appropriate boundary conditions. If P_0 and P_L are the pressures at the reservoir inlet and outlet, respectively, then b_j can be determined as

$$b_1 = P_0 \quad (6.8-4a)$$

$$b_2 = P_L - (a_2 - \rho_2 g \sin \alpha)L \quad (6.8-4b)$$

Using these relations, and requiring continuous x velocities across the front

$$u_{x1}|_{x=x_f} = u_{x2}|_{x=x_f} = u_x \quad (6.8-5)$$

gives, once again using Darcy's law,

$$M^0 a_1 = a_2 \quad (6.8-6)$$

Equation (6.8-6) determines a_1 , for we must have continuity of pressure at x_f in the absence of capillary pressure

$$P_1|_{x_f} = P_2|_{x_f} \quad (6.8-7)$$

Inserting Eq. (6.8-3) into Eq. (6.8-7) and using Eqs. (6.8-4) and (6.8-6), yields

$$a_1 = \frac{-\Delta P + \rho_2 g \sin \alpha (L - x_f) + \rho_1 g \sin \alpha x_f}{M^0 L + (1 - M^0)x_f} \quad (6.8-8)$$

where $\Delta P = P_0 - P_L$ is the overall pressure drop. The rate of frontal advance is from Darcy's law

$$\frac{dx_f}{dt} = \frac{u_x|_{x_f}}{\phi \Delta S} = \frac{k \lambda_{r1}}{\phi \Delta S} \frac{\Delta P + g \sin \alpha [\Delta \rho (L - x_f) - \rho_1 L]}{M^0 L + (1 - M^0)x_f} \quad (6.8-9)$$

Equation (6.8-9) applies to any point on the displacement front. We could have equally well developed an expression for a point on the perturbation front

$$\frac{d(x_f + \varepsilon)}{dt} = \frac{k \lambda_{r1}}{\phi \Delta S} \frac{\Delta P + g \sin \alpha [\Delta \rho (L - x_f - \varepsilon) - \rho_1 L]}{M^0 L + (1 - M^0)(x_f + \varepsilon)} \quad (6.8-10)$$

Equation (6.8-10) is identical to Eq. (6.8-9) except $x_f + \varepsilon$ has replaced x_f everywhere. The rate of change of the perturbation is

$$\frac{d\varepsilon}{dt} = \frac{d(x_f + \varepsilon)}{dt} - \frac{dx_f}{dt} = \dot{\varepsilon} \quad (6.8-11)$$

which yields, when Eqs. (6.8-9) and (6.8-10) are substituted,

$$\dot{\varepsilon} = -\frac{k \lambda_{r1}}{\phi \Delta S} \frac{\Delta P (1 - M^0) + L g \Delta \rho \sin \alpha - L g \rho_1 (1 - M^0) \sin \alpha}{[M^0 L + (1 - M^0)x_f]^2} \varepsilon \quad (6.8-12)$$

In Eq. (6.8-12), we have assumed $\varepsilon \ll x_f$ with the corresponding simplification. Equation (6.8-12) could be integrated, but for our purpose it is sufficient to investigate only the sign of $\dot{\varepsilon}$. The perturbation will grow if $\dot{\varepsilon} > 0$, will remain constant if $\dot{\varepsilon} = 0$, and will decay if $\dot{\varepsilon} < 0$. From the equality of these three choices, we find the condition of neutral stability as

$$-(\Delta P)_c = \frac{L \Delta \rho g \sin \alpha}{1 - M^0} - L g \rho_1 \sin \alpha \quad (6.8-13)$$

where $(\Delta P)_c$ is a critical pressure drop. The superficial velocity corresponding to this is the *critical rate* u_c

$$u_c \equiv -k\lambda_{r1}^o \left[\frac{-(\Delta P)}{L} + \rho_l g \sin \alpha \right] = \frac{k\lambda_{r1}^o \Delta \rho g \sin \alpha}{M^0 - 1} \quad (6.8-14)$$

Using the critical rate, the conditions for finger growth may be restated

$$u_x \begin{cases} > u_c & (\text{unstable}) \\ = u_c & (\text{neutral}) \\ < u_c & (\text{stable}) \end{cases} \quad (6.8-15)$$

where we have also used Darcy's law to express u_x in these inequalities.

Note the similarity between Eq. (6.8-14) and Eq. (6.6-10b), the corresponding critical rate for gravity tonguing. Analogous expressions can be worked out for almost any segregated flow conditions, so this similarity should not be regarded as merely fortuitous. But the differences in the two flows should be kept in mind. The critical rate in Eq. (6.8-14) is based on an unstable displacement in a reservoir having no z -direction communication; that in Eq. (6.6-10b) is the consequence of a VE displacement in a reservoir with very good communication.

To further investigate the stability issue, let's write the condition for stability (finger decay) as

$$(M^0 - 1)u_x < k\lambda_{r1}^o \Delta \rho g \sin \alpha \quad (6.8-16)$$

The superficial velocity u_x in this inequality is always positive, but the density difference can be negative (less dense fluid displacing more dense), as can the dip angle (displacing down dip). Of course, M^0 can take on only positive values though over quite a large range. Table 6-2 shows typical signs of M^0 and $\Delta \rho$ for various EOR processes. Immediately it follows from Eq. (6.8-16) that the condition for stability in a horizontal reservoir is simply $M^0 < 1$. This condition is used universally throughout the EOR literature to describe a stable displacement, particularly in laboratory floods, though the more general Eq. (6.8-16) is actually the most appropriate form (Hill, 1952).

TABLE 6-2 TYPICAL VALUES FOR MIBILITY RATIOS AND DENSITY DIFFERENCES BY PROCESS TYPE

	$M^0 < 1$	$M^0 > 1$
$\Delta \rho > 0$	Waterflood	Waterflood
	Polymer flood	Polymer flood
	Micellar polymer	
$\Delta \rho < 0$	Foam	Steam

Considering the signs possible for α and $\Delta \rho$, we can divide the stability possibilities into four cases, as Table 6-3 shows. Case 1 is unconditionally stable regardless of the values of $\Delta \rho g \sin \alpha$ and M^0 as $\Delta \rho g \sin \alpha$ is positive, and $M^0 < 1$. Similarly, if $\Delta \rho g \sin \alpha < 0$ and $M^0 > 1$, case 4, the displacement is unconditionally

TABLE 6-3 POSSIBLE CASES FOR A STABLE DISPLACEMENT

Case			
1	$M^0 < 1$	$\Delta\rho g \sin \alpha > 0$	Stable
2	$M^0 > 1$	$\Delta\rho g \sin \alpha > 0$	Conditionally stable (type I)
3	$M^0 < 1$	$\Delta\rho g \sin \alpha < 0$	Conditionally stable (type II)
4	$M^0 > 1$	$\Delta\rho g \sin \alpha < 0$	Unstable ^a

^a Infinite lateral boundaries

Note: Write stability criterion as $(M^0 - 1)u_x < k\lambda_{r1}^0 \Delta\rho g \sin \alpha$. For $\alpha = 0$ (no dip), the stability criterion becomes $M^0 < 1$.

unstable. The more interesting cases are 2 and 3, which we call type I and type II conditional stability.

For type I stability, if we divide through Eq. (6.8-16) by the positive quantity $(M^0 - 1)$, the stability criterion is written for u_x as in Fig. 6-20. The criterion is an upper bound for u_x and a plot of sweep efficiency (vertical, areal, or volumetric) versus the dimensionless rate u_D

$$u_D = \frac{u_x(M^0 - 1)}{k\lambda_{r1}^0 \Delta\rho g \sin \alpha} \quad (6.8-17)$$

shows that E_V remains essentially constant until $u_D = 1$ and then decreases thereafter. Since increasing the displacement velocity causes the instability to form, we see that viscous forces destabilize the displacement ($u_D > 1$), whereas gravity forces tend to stabilize the displacement ($u_D < 1$). The resulting instability is a *viscous instability* or *finger*. For type II conditional stability, a similar plot (Fig. 6-21) shows sweep efficiency decreasing for decreasing u_D , beginning a precipitous decline at $u_D = 1$. This is because the stability criterion is now a lower bound since $(M^0 - 1)$ is now negative. For type II conditional stability, viscous forces stabilize the displacement,

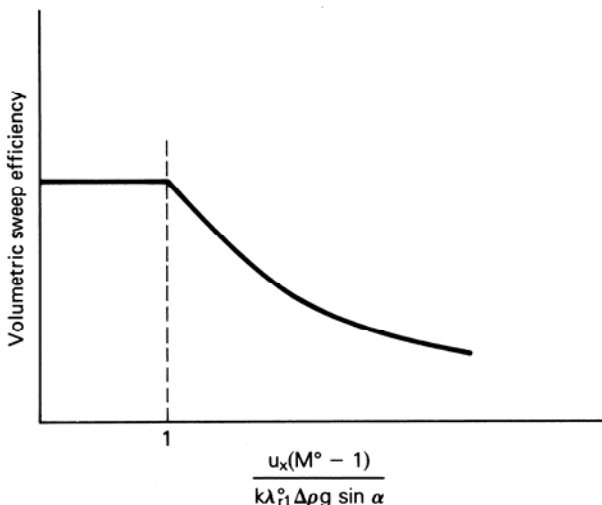


Figure 6-20 Type I conditional stability

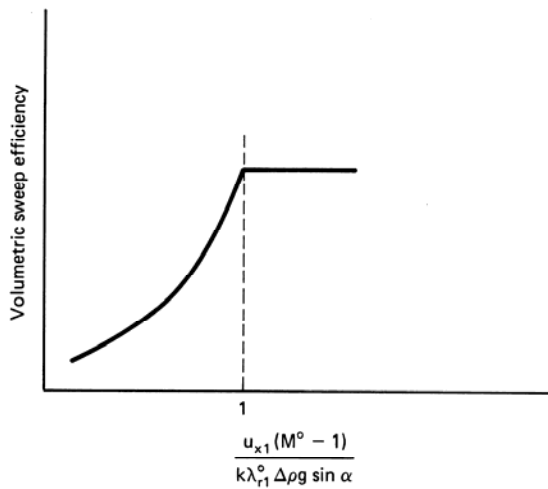


Figure 6-21 Type II conditional stability

and gravity forces destabilize. The resulting instability is a gravity instability.

For certain values of the parameters, then, both types of displacements are or can be made stable. The conditional stability is most useful in determining a maximum rate in a dipping displacement where $M^0 > 1$. But usually, this rate is below that required for economic oil production. For type II stability, a larger rate is required, but in practice, this situation is not commonly encountered.

Critical Wavelength

Whereas $u_x < u_c$ is a necessary and sufficient condition for stability, the condition $u_x > u_c$ is, unfortunately, a necessary condition only for instability. This condition is because dissipative effects in flows in media of limited lateral extent tend to suppress fingering. This effect means fingering may be abnormally suppressed in laboratory displacements compared to the same displacement under field conditions. One may legitimately wonder, then, about the purpose of doing laboratory experiments on unstable displacements when this scale effect is not considered.

To investigate this scale effect, we reproduce an argument based on linear stability analysis originally given by Chouke et al. (1959) and then by Gardner and Ypma (1982).

Based on a linear stability analysis of a downward secondary miscible displacement of oil by a less viscous and less dense solvent in a homogeneous, uniform medium, the critical wavelength λ_c of an unstable miscible displacement is

$$\lambda_c = 4\pi \frac{M^0 + 1}{M^0 - 1} \left(\frac{K_l}{u_x - u_c} \right) \quad (6.8-18)$$

where the dispersion coefficient K_l is taken to be isotropic. Since the displacement is unstable, we must have $M^0 > 1$ and $u_x > u_c$ so that λ_c is always positive.

The analogous expression for an initially sharp immiscible displacement was also determined by Chouke et al. (1959) and reproduced in greater detail by Peters (1979)

$$\lambda_c = \frac{C}{3} \left[\frac{k \lambda_r^0 \sigma_{12}}{(M^0 - 1)(u_x - u_c)} \right]^{1/2} \quad (6.8-19)$$

The constant C in Eq. (6.8-19) is called Chouke's constant by Peters, who also determined values $C = 25$ for immiscible displacements with no residual water initially present, and $C = 190$ with irreducible water present. Clearly, the critical wavelength is greater with irreducible water initially present, but the reason for this stabilizing effect is not well understood.

The necessary and sufficient conditions for a type I instability to form based on this analysis are now

$$M^0 > 1 \quad \text{or} \quad u_x > u_c \quad \text{and} \quad \lambda_c < (H_t)_{\max} \quad (6.8-20)$$

where $(H_t)_{\max}$ is the maximum lateral extent of the permeable medium. One may readily show (see Exercise 61) that λ_c is of the order of a few centimeters for typical conditions. Thus, if fingering is desired in a displacement, one must take special precautions that conditions (Eq. 6.8-20) are met. This usually means running displacements at excessively high rates, compared to field rates, or in systems having at least one large transverse dimension. Such a system is the Hele Shaw cell, in which the displacement of Fig. 6-19 is occurring. But if the intent is to suppress fingering, systems having very small transverse dimensions, such as the slim tube experiments we discuss in Chap. 7, are preferable.

Three things are important about both the derivation of critical velocity and wavelength. First, neither says anything about how fingers propagate once they are formed. A finger forms, bifurcates into two branches, one of these dominates (or shields) the other, and the dominant one then bifurcates again to repeat the process (Homsy, 1987). If continued indefinitely, a single finger with numerous appendages representing the bifurcations will result. Figure 6-19 suggests the bifurcation through the various levels of fingers each superimposed on the next larger scale. The smallest scale corresponds to the critical wavelength.

Second, both the critical wavelength and velocity derivations depended on the perturbation being small. It is impossible to say from this what the response to a large perturbation would be, and we can be assured that such large perturbations do exist. Thus Eq. (6.8-20) should also be regarded as only necessary conditions.

Finally, the issues of fingering and heterogeneity cannot be rigorously separated. After all, heterogeneity caused the perturbation in Fig. 6-16 even though we proceeded as though the reservoir was homogeneous. The merging of the fingering and heterogeneity issues is one of the most interesting topics in EOR research; in Chap. 7, we discuss some primitive attempts at this merging.

6-9 SUMMARY

That volumetric sweep efficiency is a complex issue accounts for the scarcity of treatment in this text compared to displacement efficiency. Three factors account for this complexity: a strong dependency on operational issues, nonlinear and irregular geometries, and the difficulty in capturing realistic heterogeneities. Numerical simulators can handle all three of these issues to some extent even though some questions remain about how to represent heterogeneity in simulation models.

There is little in the behavior of the volumetric sweep efficiency of actual reservoir displacements that cannot be at least qualitatively understood through the material we present here. Examples of such behavior are reservoirs with high-permeability thief zones that behave essentially as a two-layer medium, generally high-permeability reservoirs dominated by gravity that conform well to the Dietz theory, low-permeability reservoirs in which crossflow tends to be unimportant, and high-permeability reservoirs with large well spacing that tend to the VE limit rather quickly.

Above all, the recognition of bypassing—through channeling, viscous fingering, gravity segregation, or some combination of these—is important, for this seems to occur in a good many waterfloods and EOR projects.

EXERCISES

- 6A.** *Using Areal Sweep Correlations.* Use the areal sweep efficiency correlations for a confined five-spot in this exercise.
- (a) Plot areal sweep efficiency E_A versus dimensionless time t_D for a mobility ratio of 6.5.
 - (b) If the pattern pore volume is 10^6 m^3 , and the average injection rate is $500 \text{ m}^3/\text{D}$, plot cumulative oil recovery (SCM) versus time (months or years). Assume the displacement is pistonlike, vertical sweep is 1, and the pore volume given above is movable. The residual water and oil saturations are 0.2 and 0.3, respectively.
- 6B.** *Heterogeneity Measures of Normal Distributions.* As Table 6-1 shows, permeability often is distributed normally rather than lognormally. When this happens, the cumulative frequency distribution function (Eq. 6.3-5) becomes

$$\Lambda = \frac{1}{2} \left\{ 1 - \operatorname{erf} \left[\frac{r - \bar{r}}{\sqrt{2v_N}} \right] \right\} \quad (6B-1)$$

where \bar{r} is the average permeability–porosity ratio, and v_N is the variance of the normal distribution. Using Eqs. (6B-1), (6.3-3), and (6.3-4), derive formulas for the Lorenz and Dykstra–Parsons coefficients in terms of v_N .

- 6C.** *Vertical Sweep Efficiency in a Two-Layer Reservoir*
- (a) Derive Eq. (6.4-4) for flow in layer l in a horizontal reservoir.
 - (b) Calculate and plot the vertical sweep efficiency E_l and the fraction of total flow going into the high velocity layer for a two-layer horizontal reservoir with $k_1 = 2k_2$, $\phi_1 = \phi_2$, $\Delta S_1 = \Delta S_2$, and $h_1 = 3h_2$. Take $M^0 = 0.5$.

- 6D.** *Vertical Sweep Efficiency in a Noncommunicating Reservoir.* For a reservoir having no vertical communication, calculate and plot the vertical sweep efficiency versus dimensionless cumulative water injected for the following five-layer cross section:

$h_l(\text{m})$	ϕ_l	$k_l(\mu\text{m}^2)$
5	0.2	0.100
10	0.22	0.195
2	0.23	0.560
15	0.19	0.055
4	0.15	0.023

The endpoint mobility ratio is 0.5.

- 6E.** *Vertical Equilibrium for Continuous Layers.* For a reservoir for which the VE Hearn model applies with $M^0 < 1$ and $\alpha = 0$,
- (a) Show that if the permeability distribution is continuous, the cross-sectional averaged water fractional flow may be written as

$$\bar{f}_1 = \left(1 + \frac{(1-C)}{H_K M^0 C} \right)^{-1} \quad (6E-1)$$

where H_K is the Koval heterogeneity factor (Fig. 6-8).

- (b) Recalculate and plot the vertical sweep efficiency for the two-layer model of part (b) in Exercise 6C. Use $M^0 = 0.5$.
- (c) In a two-layer horizontal reservoir, show that the effects of the heterogeneity contrast may be completely suppressed (that is, the fronts travel at equal velocities in both layers) if

$$M^0 < \frac{k_2}{k_1} \frac{\phi_1}{\phi_2} \quad (6E-2)$$

where 1 and 2 represent the high and low velocity layers, respectively.

- 6F.** *Calculating Pseudorelative Permeabilities.* For the discrete permeability–porosity data of Exercise 6D,
- (a) Calculate and plot the pseudorelative permeabilities for a waterflood in a horizontal reservoir using the VE Hearn model.
 - (b) Calculate and plot the vertical sweep efficiency for this flood.
 - (c) Repeat part (a) for a nonzero capillary pressure function given by

$$P_c = \sigma_{12} \left(\frac{\phi}{k} \right)^{1/2} \cos \theta (1 - S)^4 \quad (6F-1)$$

where σ_{12} is the oil–water interfacial tension, θ is the contact angle, and

$$S = \frac{S_1 - S_{1r}}{1 - S_{1r} - S_{2r}} \quad (6F-2)$$

- (d) Calculate and plot the vertical sweep efficiency for part (c).

Additional data for this problem are $\Delta\rho = 0$, $S_{1r} = S_{2r} = 0.2$, $\mu_1 = 1 \text{ mPa}\cdot\text{s}$, $\mu_2 = 10$

mPa-s, $k_{r1}^o = 0.05$, $k_{r2}^o = 0.9$, and the relative permeability curves are given as

$$k_{r1} = k_{r1}^o S^2, \quad k_{r2} = k_{r2}^o (1 - S) \quad (6F-3)$$

- 6G.** *Deriving Pseudorelative Permeabilities.* The water–oil capillary-pressure–water-saturation function often may be represented as

$$P_c = K \left(\frac{1}{S^2} - 1 \right) \quad (6G-1)$$

where K is a constant, and S is the reduced saturation (Eq. 6F-2). If the VE assumptions apply and the reservoir is homogeneous,

- (a) Derive the water saturation profile in the dip normal or z direction in terms of a water saturation at the bottom of the reservoir (S_{1B} or S_B).
- (b) Derive an expression for the average water saturation as a function of S_{1B} or S_B .
- (c) If the local (laboratory-measured) relative permeabilities are approximated by Eq. (6F-3), show that the oil and water pseudorelative permeabilities expressed in terms of the average saturation of part (b) are

$$\tilde{k}_{r1} = \frac{k_{r1}^o}{N_g^o} \ln \left\{ 1 + \frac{N_g^o \bar{S}^2}{\left(1 - \frac{N_g^o \bar{S}^2}{4} \right)^2} \right\}, \quad \tilde{k}_{r2} = k_{r2}^o (1 - \bar{S})$$

where

$$N_g^o = \frac{\Delta \rho g \cos \alpha H_t}{K}$$

- (d) For $N_g^o = 1$ and $M^o = 4$, calculate and plot the pseudodisplacement sweep efficiency versus dimensionless time. The dip angle of the reservoir is zero.
- 6H.** *Combining Sweep Efficiencies.* The vertical sweep efficiency curve for a pistonlike displacement is shown in Fig. 6H. Combine this curve with the areal sweep efficiency curve of Exercise 6A to give the volumetric sweep efficiency curve.
- 6L. Viscous Fingering Calculations**
- (a) Calculate the critical rate for a miscible displacement having the following properties:

$$k = 0.12 \mu\text{m}^2$$

$$M^o = 50$$

$$\text{Oil-solvent density difference} = -0.8 \text{ g/cm}^3$$

$$\text{Solvent mobility} = 10 (\text{mPa-s})^{-1}$$

$$\text{Dip angle} = -10^\circ$$

- (b) If the superficial velocity in the above displacement is $0.8 \mu\text{m/s}$, calculate the critical wavelength from stability theory. Take the dispersion coefficient to be $10^{-5} \text{ cm}^2/\text{s}$.

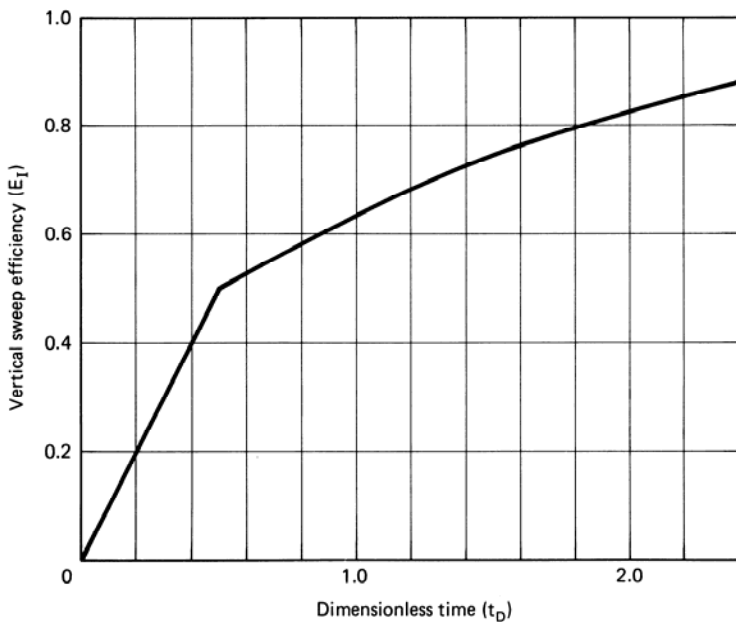


Figure 6H Vertical sweep efficiency function for Exercise 6H

7

Solvent Methods

One of the earliest methods for producing additional oil is through the use of solvents to extract the oil from the permeable media. In the early 1960s, interest centered on injecting liquified petroleum gas (LPG) in small “slugs” and then displacing the LPG by a dry “chase” gas. This process became economically less attractive as the value of the solvent increased. In the late 1970s, interest in solvent methods resurged because of an increased oil price and more confidence in the ability to estimate oil recovery. During this period, the leading solvent became carbon dioxide though several other fluids were used also (Stalkup, 1985).

Two fluids that mix together in all proportions within a single-fluid phase are *miscible*. Therefore, miscible agents would mix in all proportions with the oil to be displaced. But most practical miscible agents exhibit only partial miscibility toward the crude oil itself, so we use the term *solvent* flooding in this text. Many solvents, of course, will become miscible with crude under the right conditions, but all solvents of commercial interest are immiscible to an aqueous phase.

Solvent flooding refers to those EOR techniques whose main oil recovering function is because of extraction, dissolution, vaporization, solubilization, condensation, or some other phase behavior change involving the crude. These methods have other, sometimes very important, oil recovery mechanisms (viscosity reduction, oil swelling, solution gas drive), but the primary mechanism must be extraction.

This oil extraction can be brought about by many fluids: organic alcohols, ketones, refined hydrocarbons, condensed petroleum gas (LPG), natural gas and liquified natural gas (LNG), carbon dioxide, air, nitrogen, exhaust gas, flue gas, and

others. In this chapter, we emphasize miscible flooding with gaseous solvents CO_2 , CH_4 , and N_2 , but you should remember there are many potential agents.

7-1 GENERAL DISCUSSION OF SOLVENT FLOODING

Considering the wide variety of solvents, process types, and reservoirs, our discussion must ignore one or more interesting variations. Thus in this section, we discuss CO_2 solvent flooding, and later, we indicate more general aspects of solvent flooding.

Figure 7-1 shows an idealized vertical cross section between an injection and production well. By far the most common application of solvent methods is in a displacement mode as shown, but injection and production through the same wells have been reported (Monger and Coma, 1986). Solvent injection commences into a reservoir in some stage of depletion, most commonly at residual oil or true tertiary conditions. Most solvent floods are in reservoirs containing light crudes (less than 3 mPa-s oil viscosity) though there are exceptions (Goodrich, 1980). The solvent may be introduced continuously in undiluted form, alternated with water in the water-alternating-gas (WAG) process as in Fig. 7-1, or even injected simultaneously with water through paired injection wells. Water is injected with the solvent in this fashion to reduce the usually unfavorable mobility ratio between the solvent and the oil. Carbon dioxide, in particular, can be injected dissolved in water in a distinctly immiscible fashion that recovers oil through swelling and viscosity reduction (Martin, 1951).

If the solvent is completely (first-contact) miscible with the oil, the process has a very high ultimate displacement efficiency since there can be no residual phases (see Sec. 5-4). If the solvent is only partially miscible with the crude, the total composition in the mixing zone (miscible zone in Fig. 7-1) between the solvent and the oil can change to generate or develop miscibility in situ. Regardless of whether the displacement is developed or first-contact miscible, the solvent must immiscibly displace any mobile water present with the resident fluids.

The economics of the process usually dictates that the solvent cannot be injected indefinitely. Therefore, a finite amount or *slug* of solvent is usually followed by a *chase* fluid whose function is to drive the solvent toward the production wells. This chase fluid— N_2 , air, water, and dry natural gas seem to be the most common choices—may not itself be a good solvent. But it is selected to be compatible with the solvent and because it is available in large quantities. The similarity between the chase fluid in solvent flooding and the mobility buffer drive in micellar-polymer flooding is evident in Figs. 7-1 and 9-1.

Though the process shown in Fig. 7-1 appears relatively simple, the displacement efficiency and volumetric sweep efficiency are quite complex. In Secs. 7-6 and 7-8, we apply the theory of Chaps. 5 and 6 to solvent flooding, but first we must discuss selected physical properties of solvents and solvent-crude oil systems.

CARBON DIOXIDE FLOODING

This method is a miscible displacement process applicable to many reservoirs. A CO₂ slug followed by alternate water and CO₂ injections (WAG) is usually the most feasible method.

Viscosity of oil is reduced providing more efficient miscible displacement.

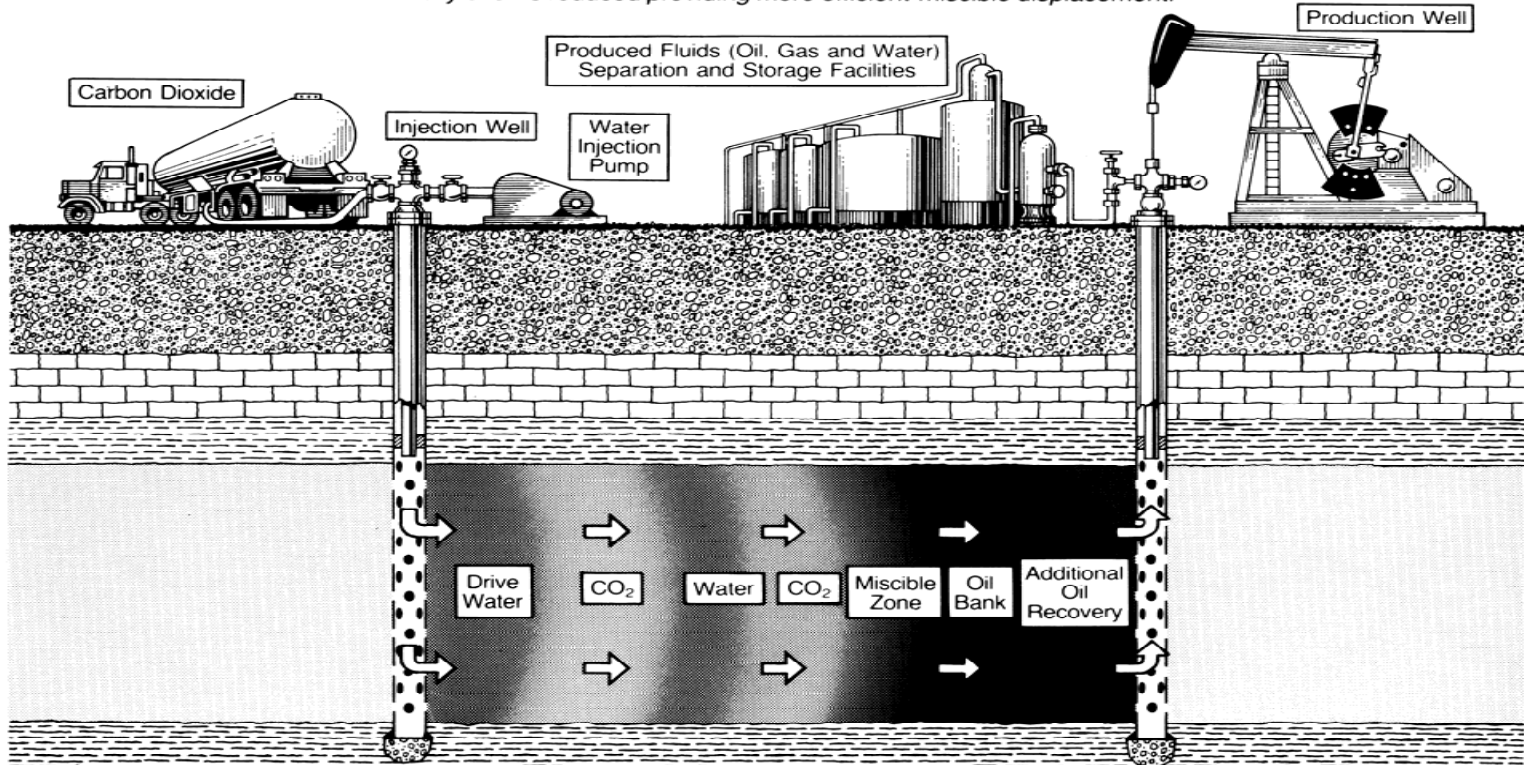


Figure 7-1 Schematic of a solvent flooding process (drawing by Joe Lindley, U.S. Department of Energy, Bartlesville, Okla.)

7-2 SOLVENT PROPERTIES

Figure 7-2 shows phase behavior data (P-T diagram) for various pure components and air. For each curve, the line connecting the triple and critical points is the vapor pressure curve; the extension below the triple point is the sublimation curve (see Sec. 4-1). The fusion curve is not shown. The pressure-temperature plot for air is really an envelope, but its molecular weight distribution is so narrow that it appears as a line in Fig. 7-2. Flue gas is also a mixture of nitrogen, carbon monoxide, and carbon dioxide with a similarly narrow molecular weight distribution; its P-T curve would fall near the nitrogen curve in Fig. 7-2.

The critical pressures for most components fall within a relatively narrow range of 3.4–6.8 MPa (500–1,000 psia), but critical temperatures vary over a much wider range. The critical temperatures of most components increase with increasing molecular weight. Carbon dioxide (molecular weight, $M_w = 44$) is an exception to this trend with a critical temperature of 304 K (87.8°F), which is closer to the critical temperature of ethane ($M_w = 30$) than to propane ($M_w = 44$). (See Vukalovich and Altunin (1968) for a massive compilation of CO₂ properties.) Most reservoir applications would be in the temperature range of 294–394 K (70–250°F) and at pressures greater than 6.8 MPa (1,000 psia); hence air, N₂, and dry natural gas will all be supercritical fluids at reservoir conditions. Solvents such as LPG, in the molecular weight range of butane or heavier, will be liquids. Carbon dioxide will usually be a supercritical fluid since most reservoir temperatures are above the critical temperature. The proximity to its critical temperature gives CO₂ more liquidlike properties than the lighter solvents.

Figures 7-3 and 7-4 give compressibilities factors for air and carbon dioxide, respectively. From these the fluid density ρ_3 can be calculated

$$\rho_3 = \frac{PM_w}{zRT} \quad (7.2-1)$$

The formation volume factor at any temperature and pressure B_3 , a specific molar volume, also follows

$$B_3 = z \frac{P_s}{P} \frac{T}{T_s} \quad (7.2-2)$$

In Eq. (7.2-2), T_s and P_s are the standard temperature and pressure, respectively. All fluids become more liquidlike, at a fixed temperature and pressure, as the molecular weight increases. The anomalous behavior of CO₂ is again manifest by comparing its density and formation volume factor to that of air. For CO₂ at 339 K (150°F) and 17 MPa (2,500 psia), $\rho_3 = 0.69 \text{ g/cm}^3$, and $B_3 = 2.69 \text{ dm}^3/\text{SCM}$. The values for air at the same temperature and pressure are $\rho_3 = 0.16 \text{ g/cm}^3$, and $B_3 = 7.31 \text{ dm}^3/\text{SCM}$. The CO₂ density is much closer to a typical light oil density than is the air density; hence CO₂ is much less prone to gravity segregation during a displacement than is air. Usually, gravity segregation in a CO₂ flood is more likely where the water saturation is high since CO₂ tends to segregate more from water than oil.

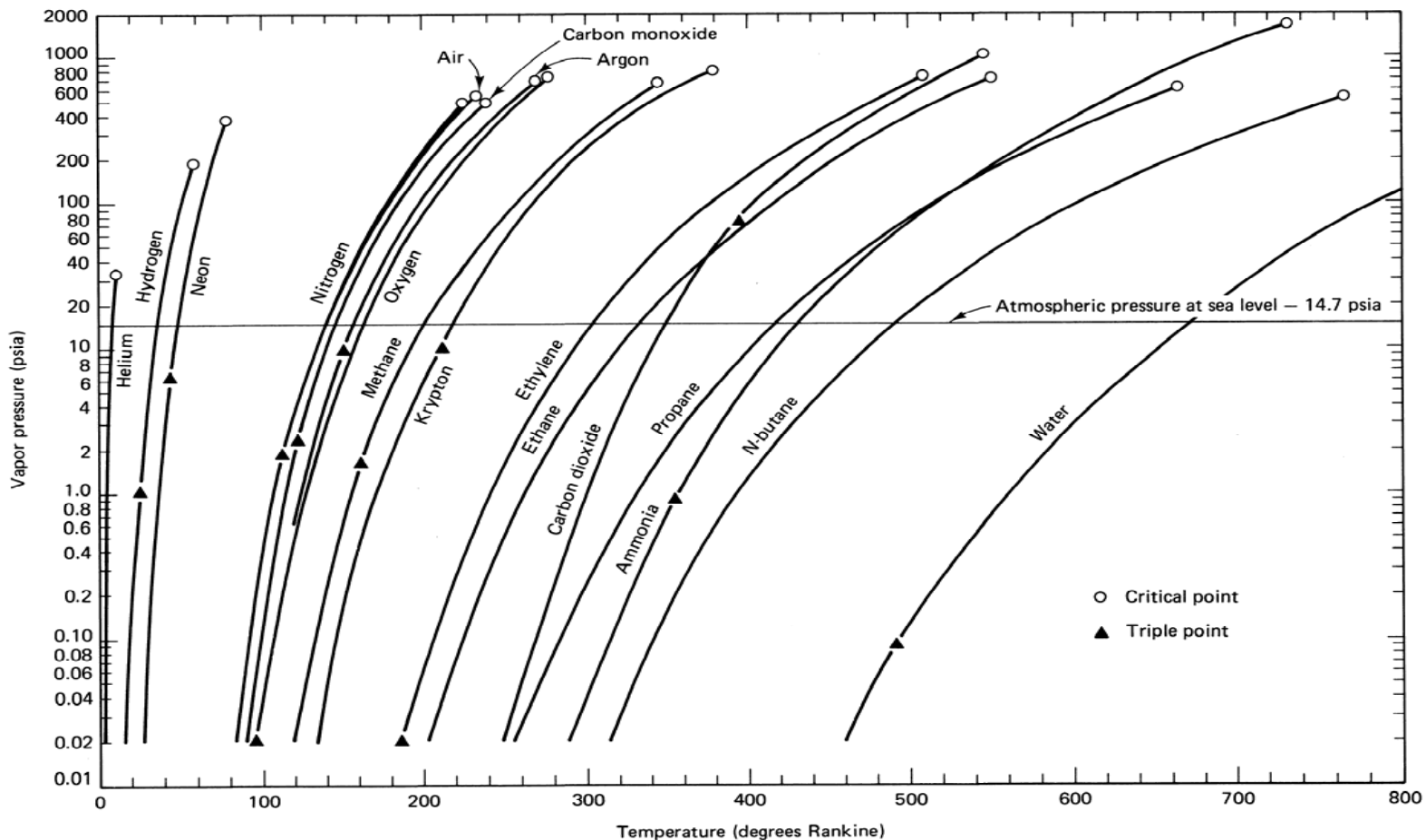


Figure 7-2 Vapor pressure curves for various substances (from Gibbs, 1971)

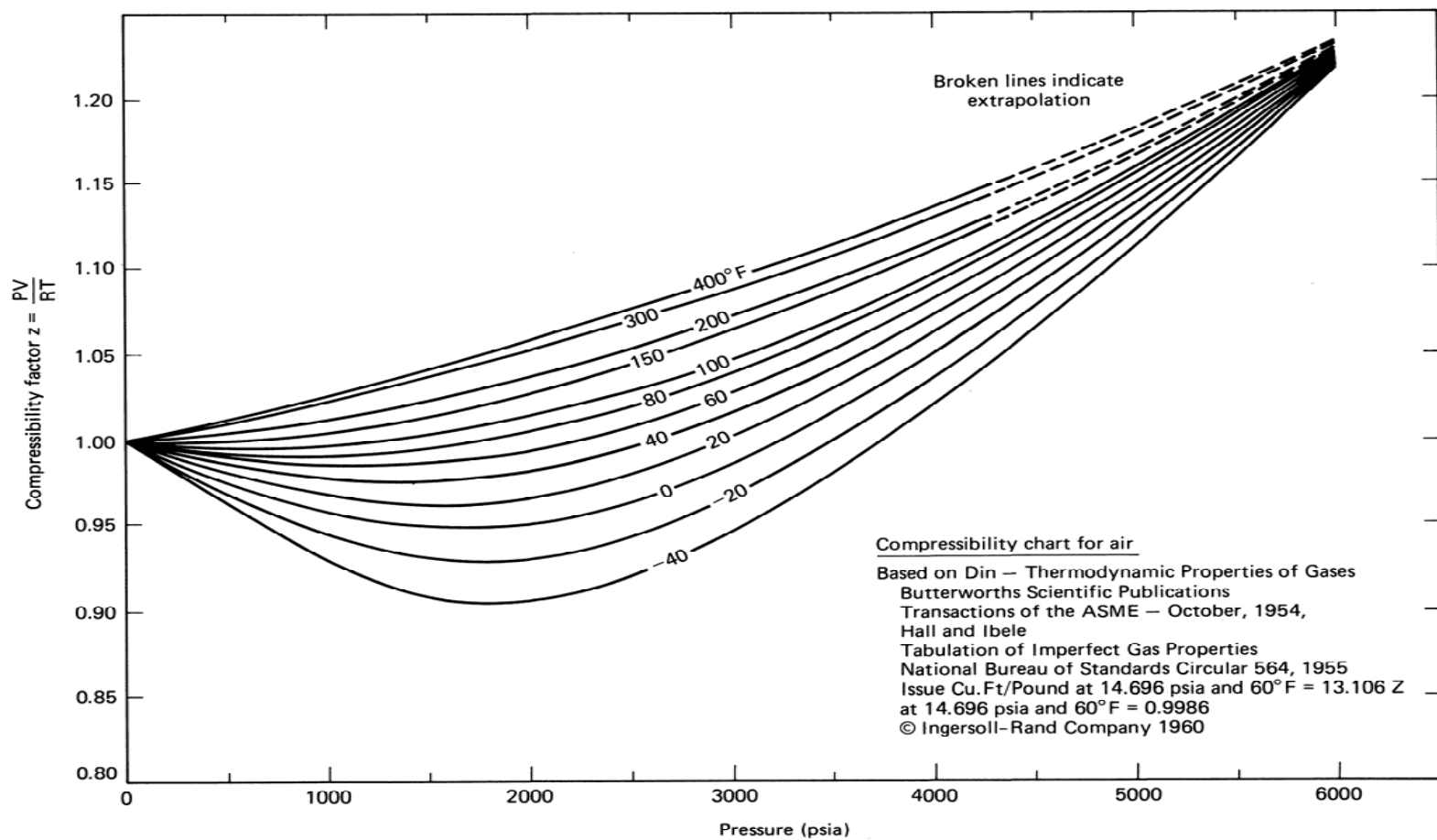


Figure 7-3 Compressibility chart for air (from Gibbs, 1971)

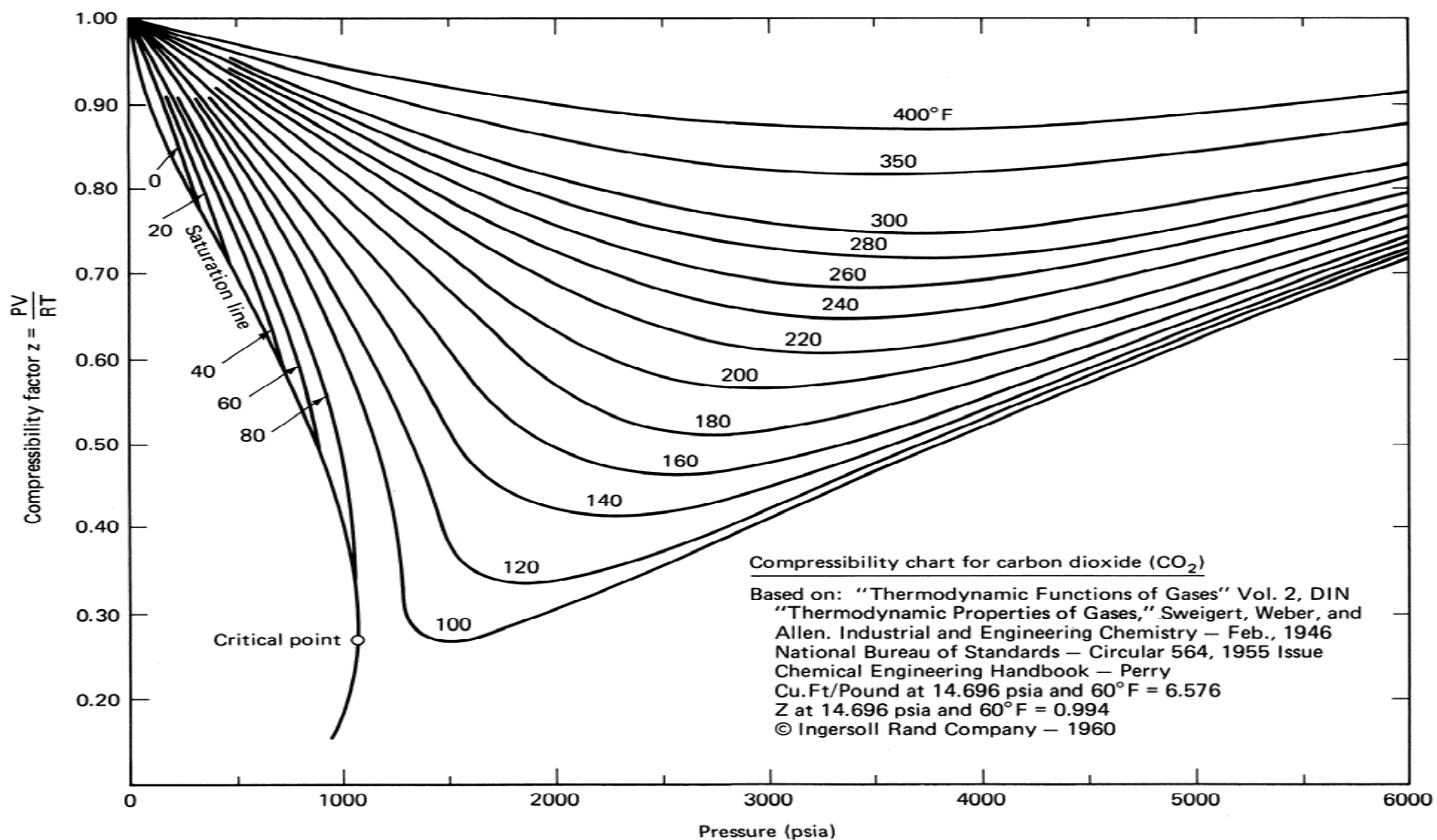


Figure 7-4 Compressibility chart for carbon dioxide (CO₂) (from Gibbs, 1971)

From the formation volume factors, 370 SCM of CO₂ is required to fill one cubic meter of reservoir volume, whereas only 140 SCM air is required at the same temperature and pressure. Thus about three times as many moles (recall that B_3 is a specific molar volume) of CO₂ are required to fill the same reservoir volume as air.

Figures 7-5 and 7-6 give the viscosities of a natural gas mixture and pure CO₂. Over the pressure and temperature range shown, which includes the conditions of interest in EOR, the viscosities of natural gas, and CH₄, air, flue gas, and N₂ are about the same. But the CO₂ viscosity is generally two or three times higher. Relative to a hydrocarbon liquid or water viscosity, the values are still low, so there should be no appreciable difference in the ease of injection of these solvents. However, the CO₂—crude-oil mobility ratio will be two or three times smaller than the other light solvents; hence volumetric sweep efficiency will generally be better for CO₂. (For the correlations for other solvents and solvent mixtures, see McCain, 1973; Reid et al., 1977; and Gas Processors Suppliers Association, 1973.)

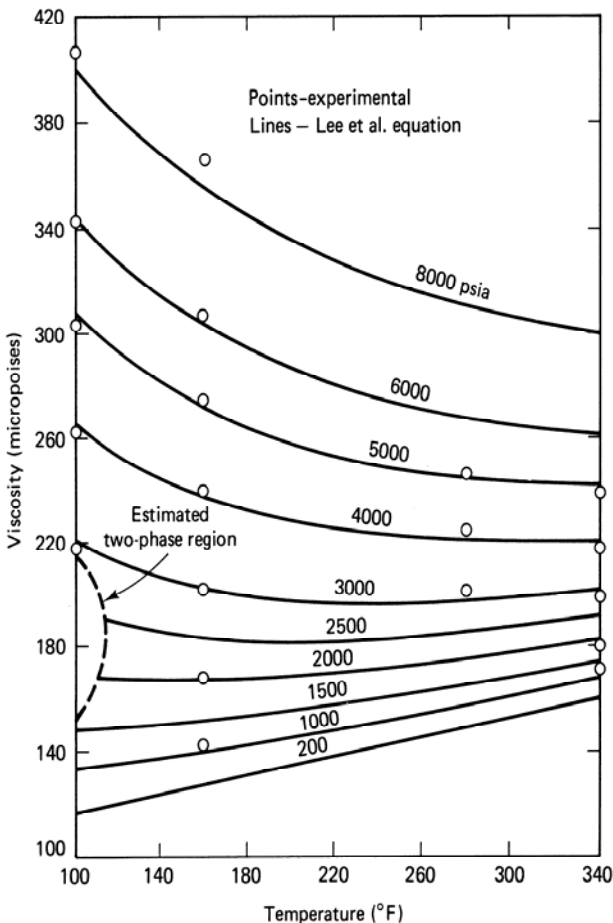


Figure 7-5 Viscosity of a natural gas sample (from Lee et al., 1966)

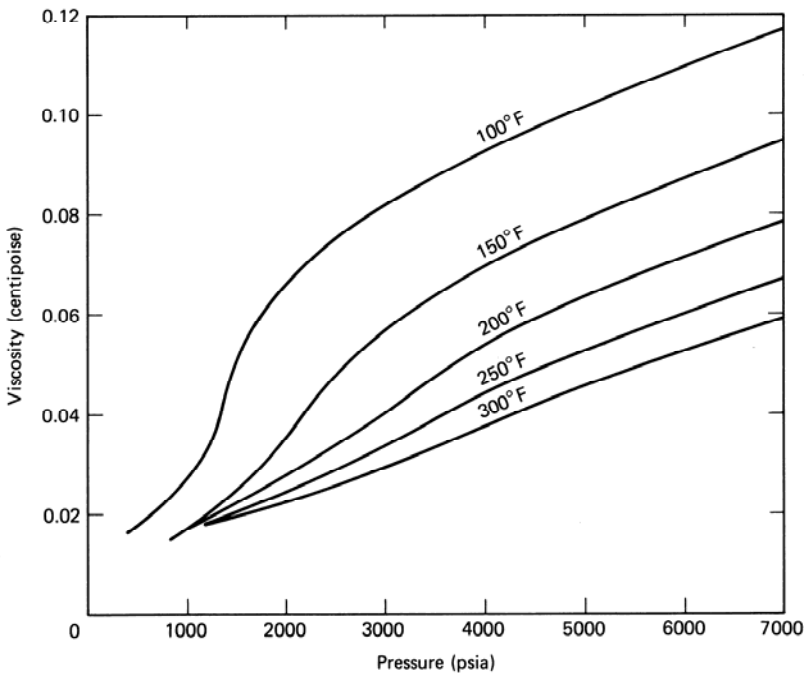


Figure 7-6 Viscosity of carbon dioxide as a function of pressure at various temperatures (from Goodrich, 1980)

7-3 SOLVENT-CRUDE-OIL PROPERTIES

In Secs. 4-1 and 4-2, we discussed general aspects of phase behavior for pure components and mixtures. In this section, we give specific features of solvent-crude phase behavior necessary for the development in later sections.

Figures 7-7 and 7-8 show pressure-composition (P-z) diagrams for two different solvent-crude systems. Recall that these diagrams are plots, at constant temperature, of pressure versus the overall mole percent of solvent in contact with a crude oil. These plots show the number and types of phases and the volume percent liquid. Figure 7-7 is for the recombined Wasson crude oil at 105°F (314 K), and Fig. 7-8 is for the Weeks Island "S" Sand crude at 225°F (381 K). Other diagrams are reported elsewhere (Turek et al., 1980; Orr and Jensen, 1982). The data in Figs. 7-7 and 7-8 represent behavior typical of low- and high-temperature systems. Recall that no water is present during the phase behavior measurements. For mixtures, the mole percent can represent both phase and overall concentrations.

The P-z diagrams have the same general form regardless of the temperature. The left vertical axis gives the phase behavior of the CO₂-free crude; thus the bubble point of the recombined Wasson crude at 314 K (105°F) is 6.81 MPa (1,000 psia) from Fig. 7-7. The right vertical axis similarly gives pure CO₂ properties, which will

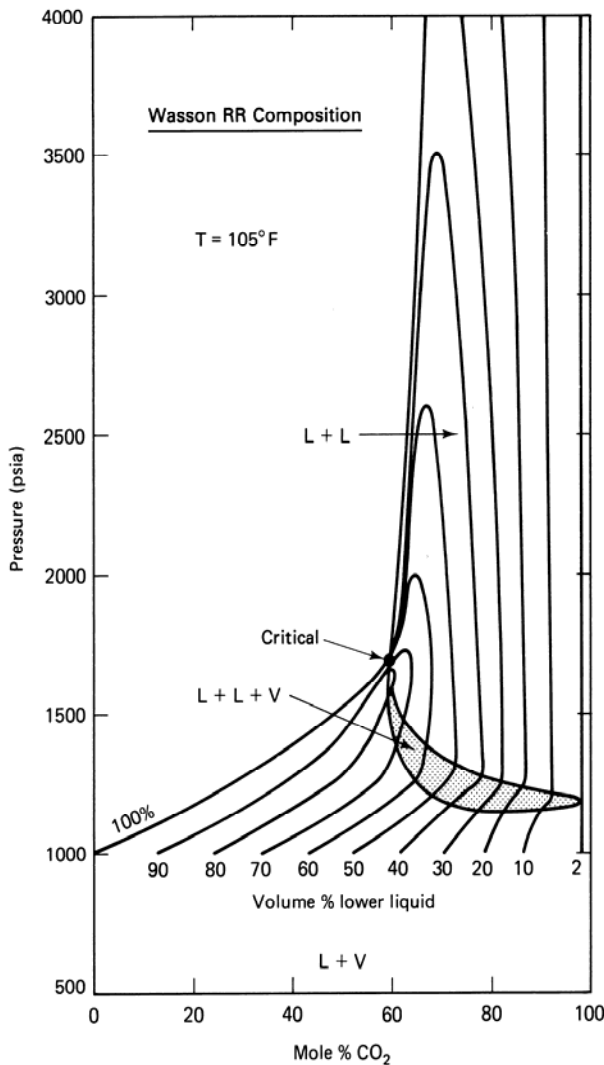


Figure 7-7 P-z diagram for recombined Wasson crude, CO_2 system (from Gardner et al., 1981)

be a single-phase fluid for Figs. 7-7 and 7-8 since both are above the CO_2 critical temperature. At low pressures and for all CO_2 concentrations, except very near the right axis, the mixture is two-phase liquid and vapor. The liquid volume quality lines are also shown. At high pressures and low CO_2 concentration, the mixture is single phase. At about 60% CO_2 , a critical point exists through which pass two single-phase boundaries. The CO_2 composition at this point is the critical composition for the fixed temperature and indicated pressure. The phase boundary line below the critical point is a bubble point curve, and that above is a dew point curve. Thus the upper left corner of the P-z diagram is a supercritical fluid region. The system could form a liquid phase as the light component increases in concentration at a constant pressure greater than the critical. This change is a type of retrograde behavior.

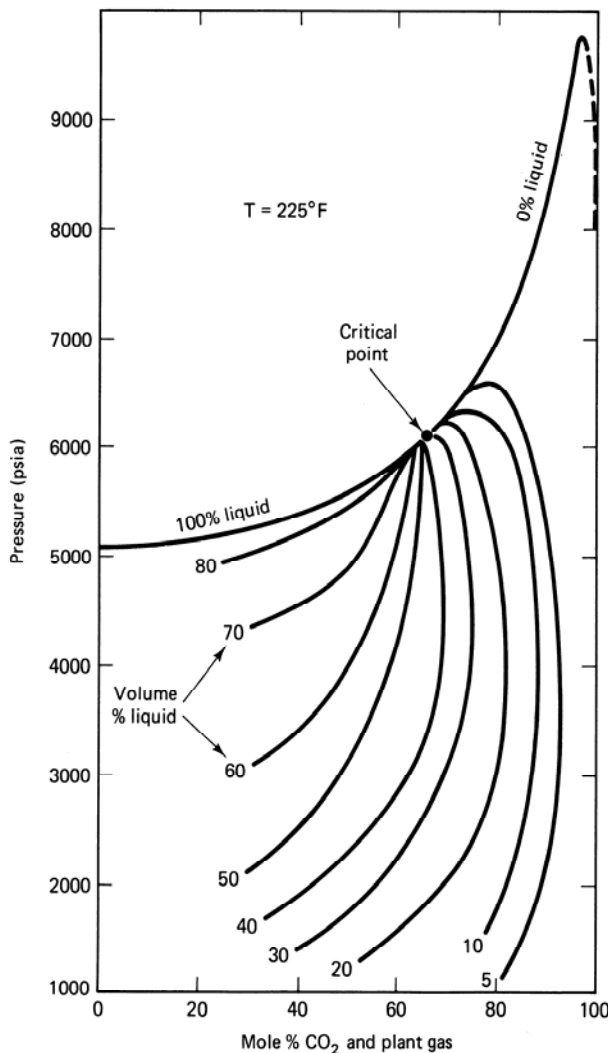


Figure 7-8 Phase envelope for Weeks Island "S" Sand crude and 95% CO_2 , 5% plant gas at 225°F (from Perry, 1978)

Though few P-z diagrams are for solvents other than CO_2 in the literature, it appears, based on the N_2 -crude-oil data in Fig. 7-9, that the above qualitative character applies to other solvents as well. The critical pressure for the N_2 solvent mixture in Fig. 7-9 is much larger (off the scale) than either of the critical pressures of the CO_2 systems in Figs. 7-7 and 7-8.

The main difference between the low- and high-temperature phase behavior is the presence, in Fig. 7-7, of a small three-phase region just below and to the right of the critical point. These phases are two liquids—a light or upper phase and a heavy or lower phase—and a vapor phase. Such behavior has generally not been observed at high temperatures (Fig. 7-8) (Turek et al., 1980). Moreover, at low temperatures, a small amount of solid precipitate can exist over some composition and pressure ranges. The precipitate is composed mainly of asphaltenes, the *n*-heptane insoluble

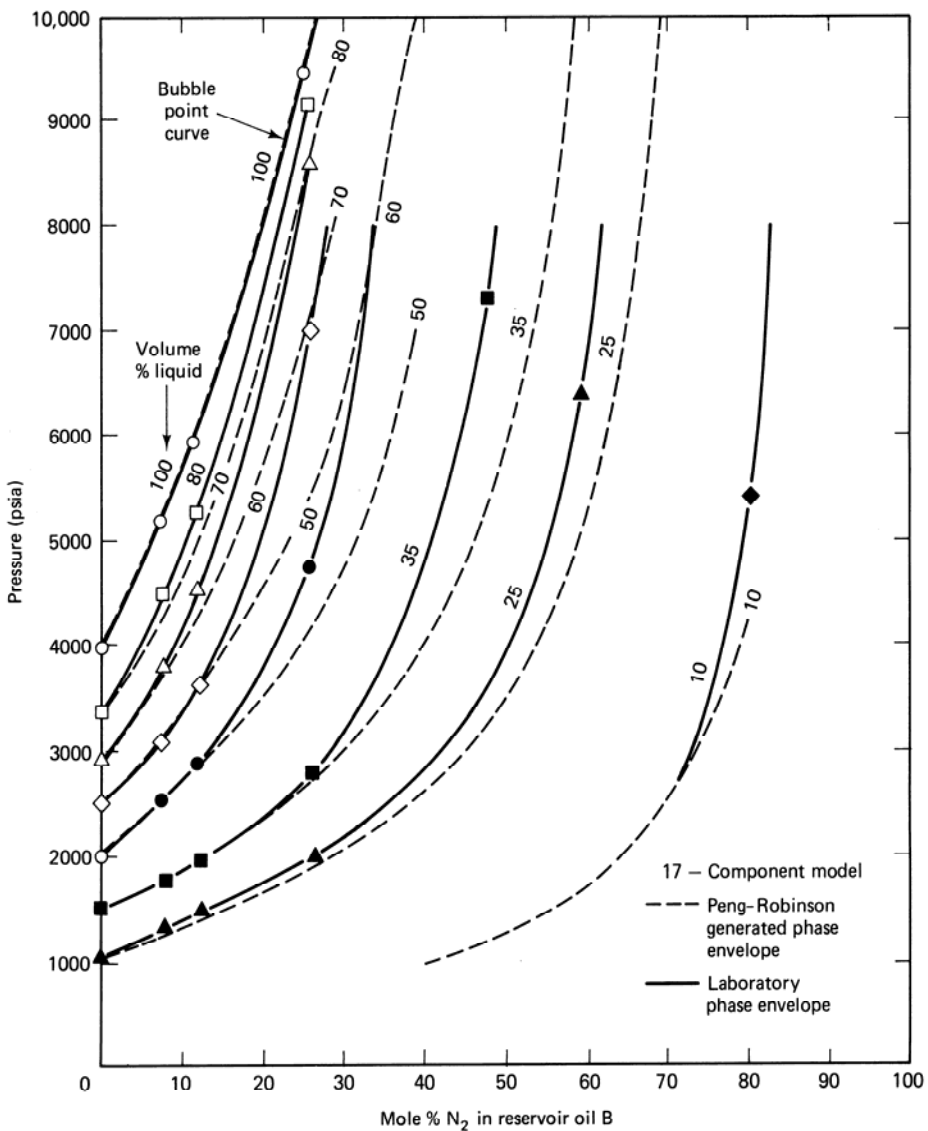


Figure 7-9 Pz diagram for reservoir fluid B-nitrogen system at 164°F (347 K)
(from Hong, 1982)

fraction of crude oil (Hirshberg et al., 1982). The region of precipitate formation may overlap the three-phase region. This behavior offers a complication to the displacement process and may even present operational problems since the solid precipitate can cause formation plugging.

Consider now a displacement of a crude by a pure solvent in a permeable medium at some time before solvent breakthrough. The conditions at the injection end of the medium plot on the right vertical axis of the P-z diagram, and those at the production end plot on the left axis at some lower pressure. Conditions in the medium

between these extremes are *not* represented on the P-z diagram since the relative amounts of each hydrocarbon component do not remain constant during a displacement, as they do in the PVT measurements of Figs. 7-7 through 7-9. Therefore, the diagrams are not particularly useful for displacement classification, which is based on the ternary diagrams we describe next. Still, one can see qualitatively from these diagrams that completely miscible displacements—those that are a single phase for all solvent concentrations—would require high reservoir pressures, in excess of 66.7 MPa (9,800 psia) for the data in Fig. 7-8.

Ternary diagrams are more useful in classifying solvent floods because they impart more compositional information than do P-z diagrams. Figures 7-10 through 7-12 show representations of these. On these diagrams the solvent–crude mixture is represented by three components; a light component on the top apex, an intermediate crude fraction on the right apex, and a heavy crude fraction on the left apex. The exact split between intermediate and heavy crude components is immaterial to the general features of the phase equilibria or to the miscibility classification. In Figs. 7-10 and 7-11, the split is between the C_6 and C_7 molecular weight fractions. Therefore,

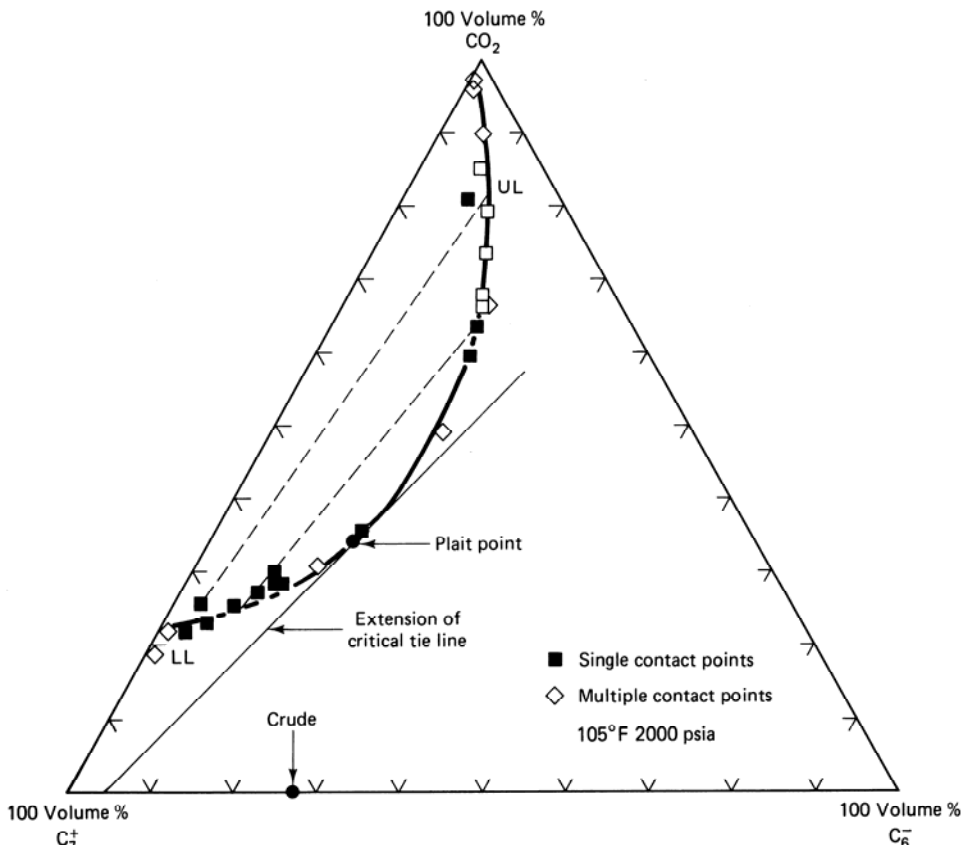


Figure 7-10 Ternary equilibria for CO_2 -recombined Wasson crude mixture (Gardner et al., 1981)

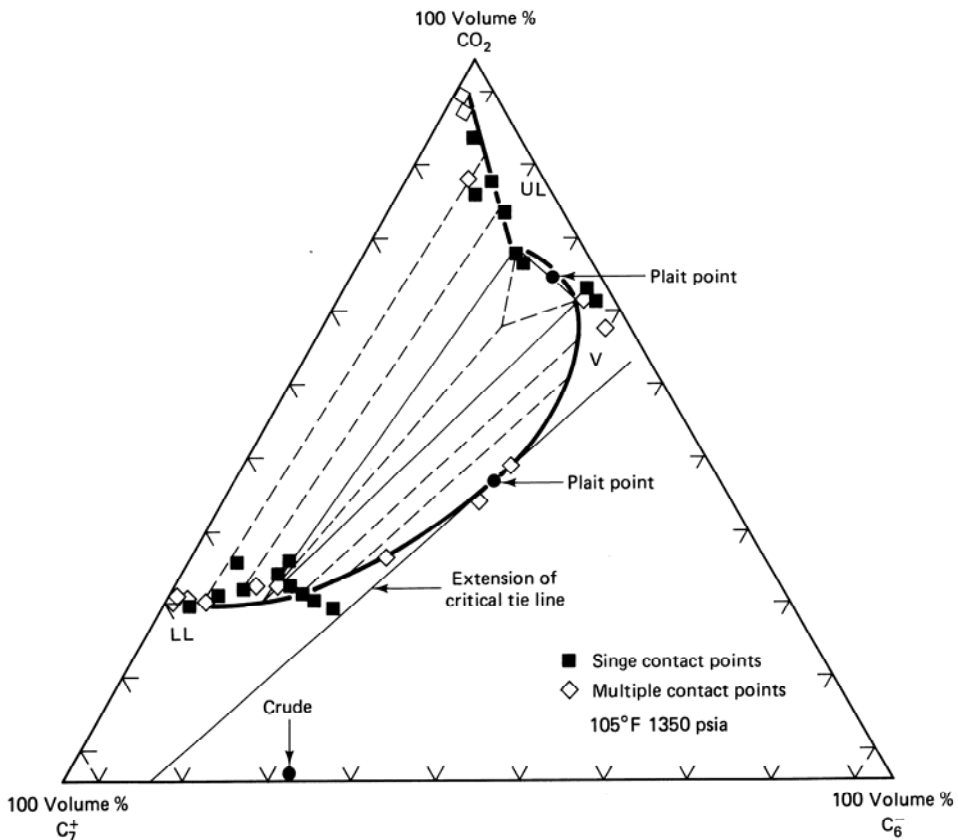


Figure 7-11 Ternary equilibria for CO_2 -recombined Wasson crude system (from Gardner et al., 1981)

none of the corners of these ternaries are pure components, hence the designation pseudocomponents. As before, no water is on the diagrams. In addition to those given here, ternary diagrams are in the literature in several other sources: for alcohol solvents (Holm and Csaszar, 1965; Taber and Meyer, 1965), for natural gas solvents (Rowe, 1967), for CO_2 (Metcalfe and Yarborough, 1978; Orr et al., 1981; Orr and Silva, 1982), for N_2 solvents (Ahmed et al., 1981), and for mixtures of CO_2 , SO_2 , and CH_4 (Sazegh, 1981).

A good example of CO_2 -crude-oil equilibria is shown in Fig. 7-10 for the recombined Wasson crude (compare Figs. 7-10 and 7-11 with Fig. 7-8, the P-z diagram for the same mixture). In these solvent-crude systems, the phase equilibria is strongly dependent on reservoir temperature and pressure (recall that the ternary is at constant T and P). Typically, though, the pressure is larger than the cricondenbar of the light-intermediate component pseudobinary; hence these two components are miscible in all proportions. The pressure is smaller than that of the light-heavy binary, and there is a region of limited miscibility or two-phase behavior along the

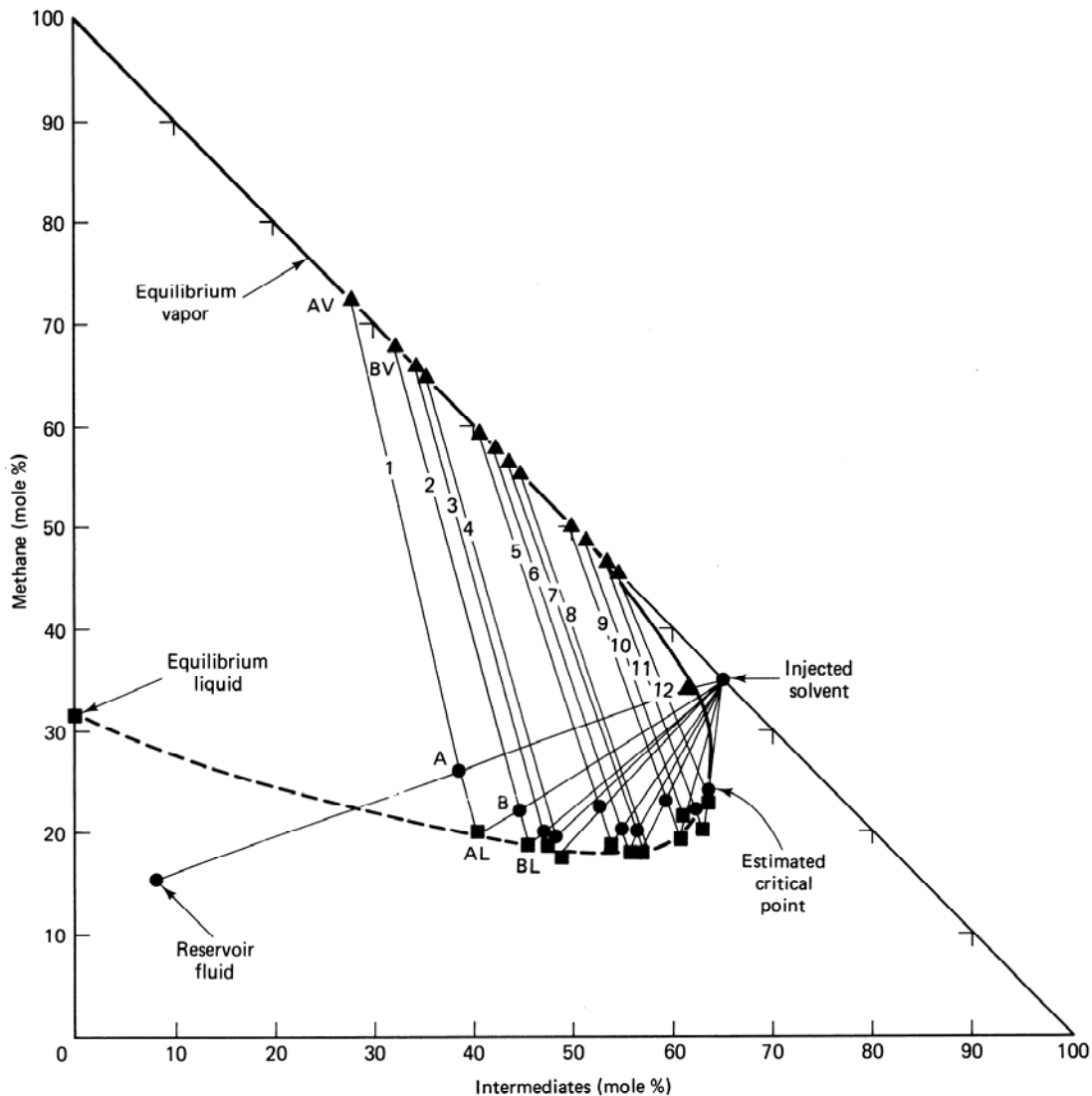


Figure 7-12 Methan–crude oil ternary phase behavior (from Benham et al., 1961)

light–heavy axis. This region of two-phase behavior extends into the interior of the ternary and is bounded by a binodal curve (see Sec. 4-3). Within the binodal curve, there are tie lines whose ends represent the composition of the equilibrium phases. These shrink to a plait point where the properties of the two phases are indistinguishable. The plait point is the critical mixture at this temperature and pressure.

Of great importance in what follows is the critical tie line, the fictitious tie line tangent to the binodal curve at the plait point. The critical tie line is the limiting case of the actual tie lines as the plait point is approached. As pressure increases, the two-phase region shrinks—that is, light–heavy miscibility increases. No general

statement is possible about the effect of temperature though the two-phase region generally increases with increasing temperature. For low pressure and low temperature, a three-phase region can intrude into the two-phase region (Fig. 7-11).

These general characteristics apply for solvents other than CO₂ (Fig. 7-12). The composition of the reservoir crude can be placed on the ternary, as can the composition of the solvent. In doing this, we are neglecting the pressure change that is, of course, an essential ingredient in making the fluids flow in the reservoir. Even with this approximation, all compositions in the solvent-crude mixing zone do not lie on a straight line connecting the initial and injected. This is because the composition changes are affected by the phase behavior. In fact, these changes are the basis for the classification of solvent displacements that we give in the next few paragraphs (Hutchinson and Braun, 1961).

We represent a one-dimensional displacement of a crude by a solvent on the schematic ternary diagram in Fig. 7-13. The crude is in the interior of the ternary, indicating some of the light component is present initially in the crude. If a straight-line *dilution path* between the solvent and the crude does not intersect the two-phase

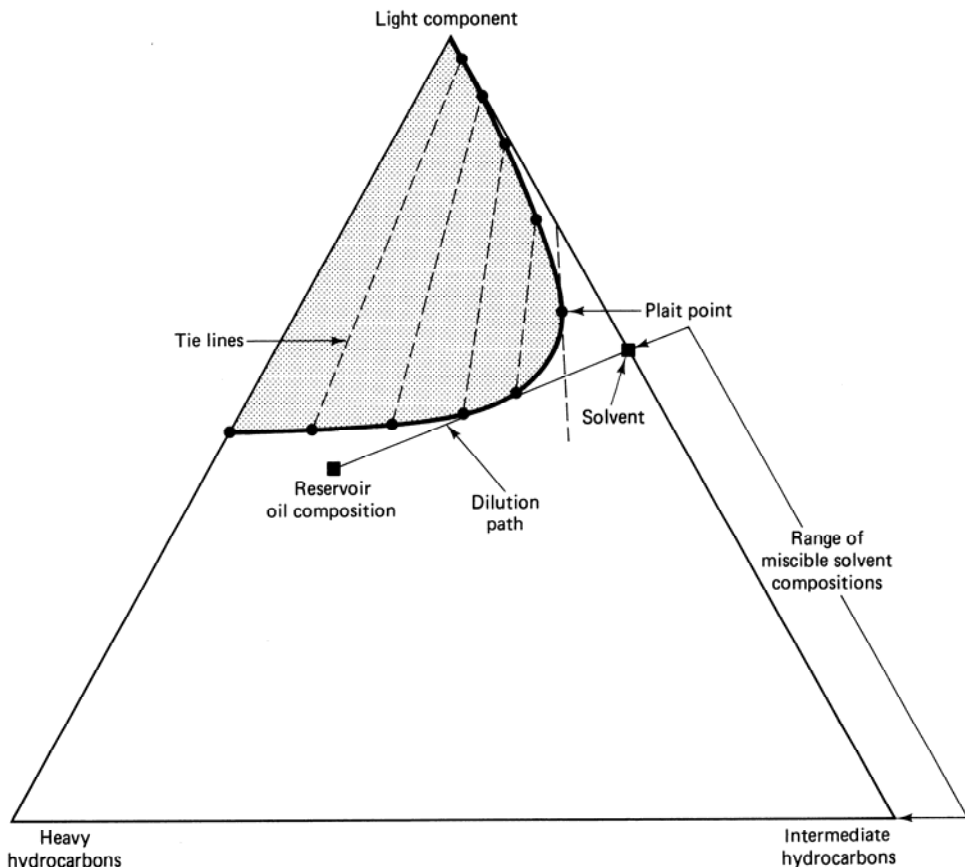


Figure 7-13 Schematic of the first-contact miscible process

region, the displacement will consist of a single hydrocarbon phase that changes in composition from crude to undiluted solvent through the solvent oil mixing zone. The dilution path is linear (see Sec. 7-6) since the only mechanism for mixing is dispersion, there being no water or fractional flow effects associated with the single hydrocarbon phase. A displacement that occurs entirely within one hydrocarbon phase is *first-contact miscible*. There is a range of solvent compositions that will be first-contact miscible with the crude at this temperature and pressure.

Suppose the solvent consists entirely of the light component (Fig. 7-14). The displacement is not first-contact miscible since the dilution path passes through the two-phase region. Imagine a series of well-mixed cells that represent the permeable medium in a one-dimensional displacement. The first cell initially contains crude to which we add an amount of solvent so that the overall composition is given by M_1 . The mixture will split into two phases, a gas G_1 and a liquid L_1 , determined by the equilibrium tie lines. The gas G_1 will have a much higher mobility than L_1 , and this phase moves preferentially into the second mixing cell to form mixture M_2 . Liquid L_1 remains behind to mix with more pure solvent. In the second cell mixture, M_2 splits into gas G_2 and liquid L_2 , G_2 flows into the third cell to form mixture M_3 , and so

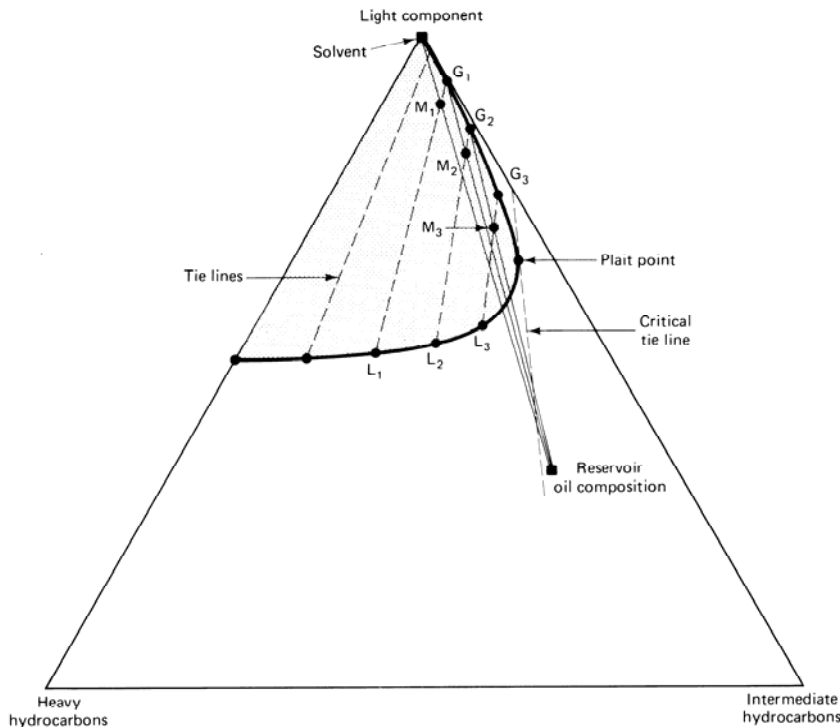


Figure 7-14 Schematic of the vaporizing gas drive process (adapted from Stalkup, 1983)

forth. At some cell beyond the third (for this diagram), the gas phase will no longer form two phases on mixing with the crude. From this point forward, all compositions in the displacement will be on a straight dilution path between the crude and a point tangent to the binodal curve. The displacement will be first-contact miscible with a solvent composition given by the point of tangency. The process has *developed miscibility* since the solvent has been enriched in intermediate components to be miscible with the crude. Since the intermediate components are vaporized from the crude, the process is a *vaporizing gas drive*. Miscibility will develop in this process as long as the injected solvent and crude are on opposite sides of the critical tie line.

Suppose the crude and solvent compositions are again on opposite sides of the critical tie line but reversed from the vaporizing gas drive (Fig. 7-15). In the first mixing cell, the overall composition M_1 splits into gas G_1 and liquid L_1 . Gas G_1 moves on to the next mixing cell as before, and liquid L_1 mixes with fresh solvent to form mixture M_2 . Liquid L_2 mixes with fresh solvent, and so forth. Thus in the first mixing cell, this mixing process will ultimately result in a single-phase mixture.

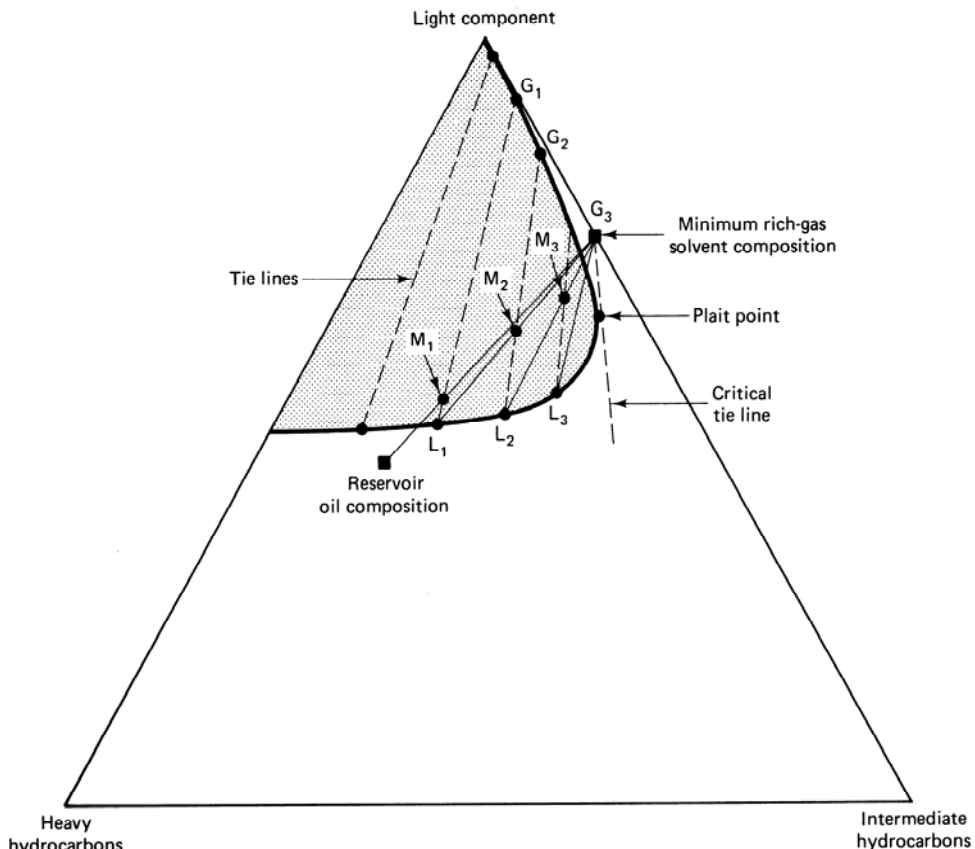


Figure 7-15 Schematic of the rich-gas drive process (adapted from Stalkup, 1983)

Since the gas phase has already passed through the first cell, the miscibility now develops at the rear of the solvent-crude mixing zone as a consequence of the enrichment of the liquid phase in intermediate components there. The front of the mixing zone is a region of immiscible flow owing to the continual contacting of the gas phases G_1 , G_2 , and so on, with the crude (this is also true at the rear of the mixing zone in the vaporizing gas drive). The process in Fig. 7-15 is the *rich gas drive* process since intermediates were added to enrich the injected solvent. Since these intermediates condense into the liquid phase, the process is sometimes called a *condensing gas drive*. Figure 7-12 shows that more than twelve contacts are necessary to develop miscibility in an actual system.

Figure 7-16 shows a schematic of an immiscible displacement. The crude and solvent are in single-phase regions, but both are on the two-phase side of the critical tie line. Now the initial mixture M_1 in the first mixing cell will form gas G_1 , which will flow forward to form mixture M_2 , and so forth. This gas is being enriched in intermediate components at the leading edge (forward contacts) of the solvent-crude mixing zone as in a vaporizing gas drive. But the enrichment cannot proceed beyond the gas-phase composition given by the tie line whose extension passes

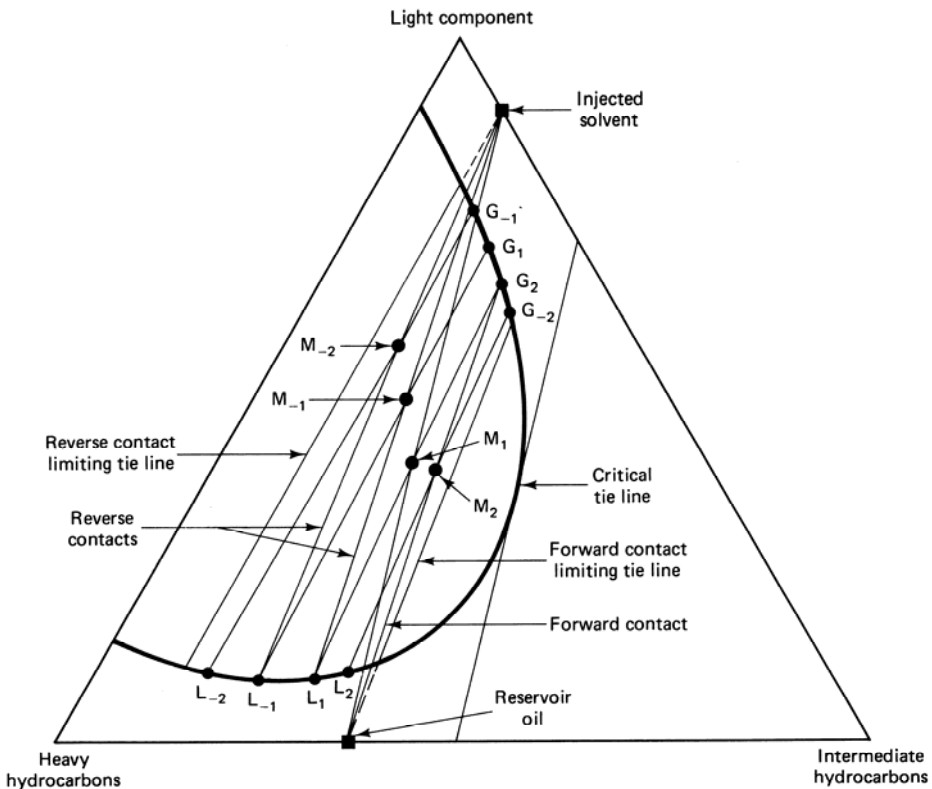


Figure 7-16 Schematic of an immiscible displacement

through the composition crude. At the forward contacts, there will be an immiscible displacement of the crude by a mixture on the limiting tie line. Back at the first mixing cell, liquid L_1 mixes with solvent to form mixture M_{-1} , just as in the condensing gas drive. The displacement is immiscible here since a single-phase solvent is displacing a two-phase mixture. The liquid phase becomes progressively stripped of intermediates (L_{-1} , L_{-2} and so on) until it reaches another limiting tie line. The displacement is entirely immiscible, then, at both the forward and reverse contacts. The intermediate components are in a gas phase near the production end of the permeable medium, and in a liquid phase at the injection end. An immiscible flood entirely devoid of injected intermediates is a *dry* gas flood.

Figure 7-17 summarizes the classification of solvent displacements. A dilution path (I_2-J_3) that does not pass through the two-phase region is a first-contact miscible displacement. A dilution path entirely on the two-phase side of the critical tie line constitutes immiscible displacement (I_1-J_1). When initial and injected compositions are on opposite sides of the critical tie line, the displacement is either a

Dilution path	Type
---------------	------

I_1-J_1	Immiscible
I_1-J_2	Multiple contact (developed) Miscibility (rich gas)
I_2-J_1	Multiple contact (developed) Miscibility (vaporizing gas)
I_2-J_3	First-contact miscible

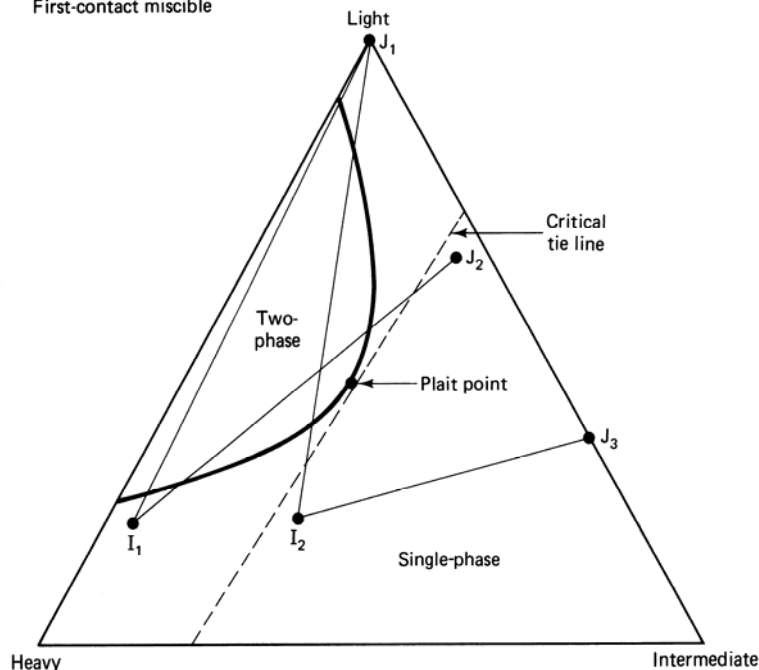


Figure 7-17 Summary of miscibility and developed miscibility

vaporizing gas drive (I_2-J_1) or a condensing gas drive (I_1-J_2). The last two cases are developed or multiple-contact miscible displacement.

At the conditions shown in Fig. 7-10, CO_2 displaces oil as a vaporizing gas drive. At comparable conditions (Figs. 7-12 and 7-18), N_2 and CH_4 are usually an immiscible solvent. The CH_4 in Fig. 7-12 can be converted into a condensing gas drive by adding about 35 mole % intermediates.

The solvent flooding classifications given here are corroborated by simple wave theory (see Sec. 7-7) and experimental results. Figure 7-19 shows the effluent history of three CO_2 floods in a Berea core. The oil in this displacement was a mixture of 25 mole % C_1 , 30 mole % C_4 , and 45 mole % C_{10} . The three runs were at 10.2 MPa (1,500 psia) (run 4), an immiscible displacement; 12.9 MPa (1,900 psia) (run 5), a first-contact miscible displacement; and 11.6 MPa (1,700 psia) (run 6), a vaporizing gas drive. The temperature was 344 K (160°F) for all runs.

The effluent histories in Fig. 7-19 are plots of C_1 , C_4 , and C_{10} concentrations, normalized by their initial values, versus the hydrocarbon pore volumes (HCPV) of CO_2 injected (see Table 5-1). If the dilution path between the oil and the solvent were a straight line, the normalized concentration of all displaced components would be identical. They are identical in the first-contact miscible run 5. The vaporizing gas drive run 6 shows that the normalized concentrations of the heavy component C_{10} declines slightly before the C_4 curve declines (Fig. 7-19b). (The run 6 composition at

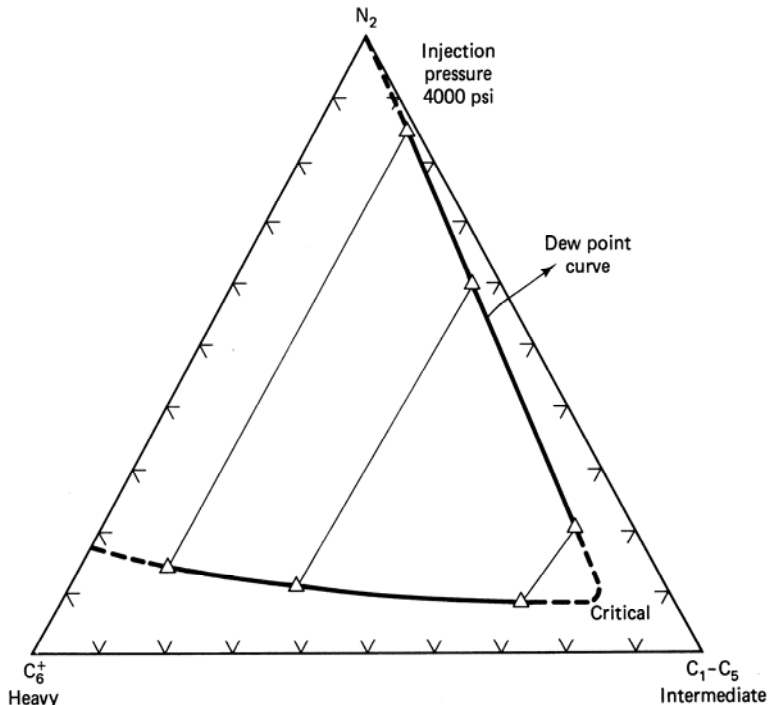


Figure 7-18 Ternary equilibria for N_2 -crude-oil mixture (from Ahmed et al., 1981)

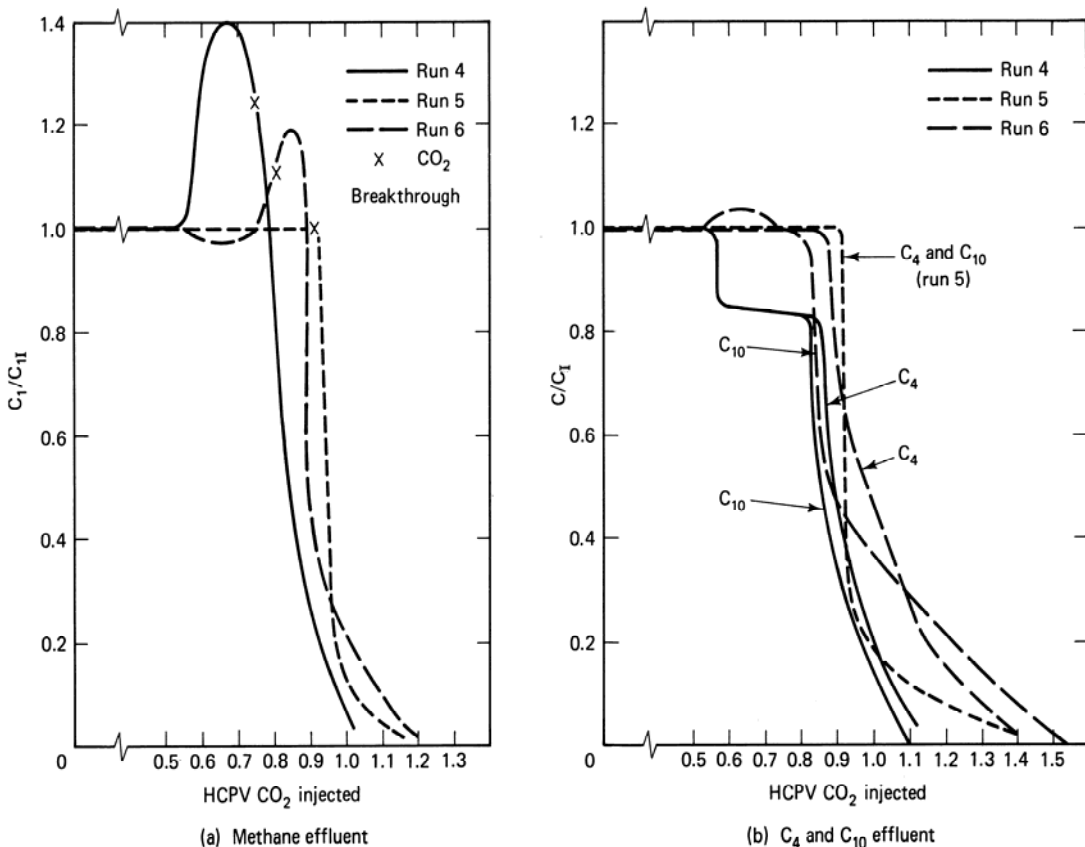


Figure 7-19 Effluent histories from laboratory displacement run 4 immiscible, run 5 first-contact miscible, run 6 multiple-contact miscible (from Metcalfe and Yarborough, 1978)

0.9 HCPV is relatively rich in C_4 .) In addition, the light components C_1 go through a maximum at about the same point (Fig. 7-19a). The C_1 maximum is even more pronounced in the immiscible displacement probably because the fluids can now be saturated with respect to C_1 . A similar effect should occur in a condensing gas drive process though the enrichment will now occur at the rear of the mixing zone.

The immiscible displacement and vaporizing gas drive process are similar; however, the oil recovery (displacement efficiency) in the immiscible run (80%) was considerably smaller than that for either the first-contact (97%) or the vaporizing gas drive run (90%). Developed miscibility displacements can give oil recoveries approaching first-contact miscible displacements; immiscible processes are usually much poorer.

Immiscible displacements have merit since pressure requirements are not large, the solvents are usually less expensive, and they can recover some oil. The principal recovery mechanisms for immiscible solvents are (1) a limited amount of vaporization and extraction, (2) oil viscosity reduction, (3) oil swelling, (4) solution gas drive during pressure decline, and (5) interfacial tension lowering. All immiscible

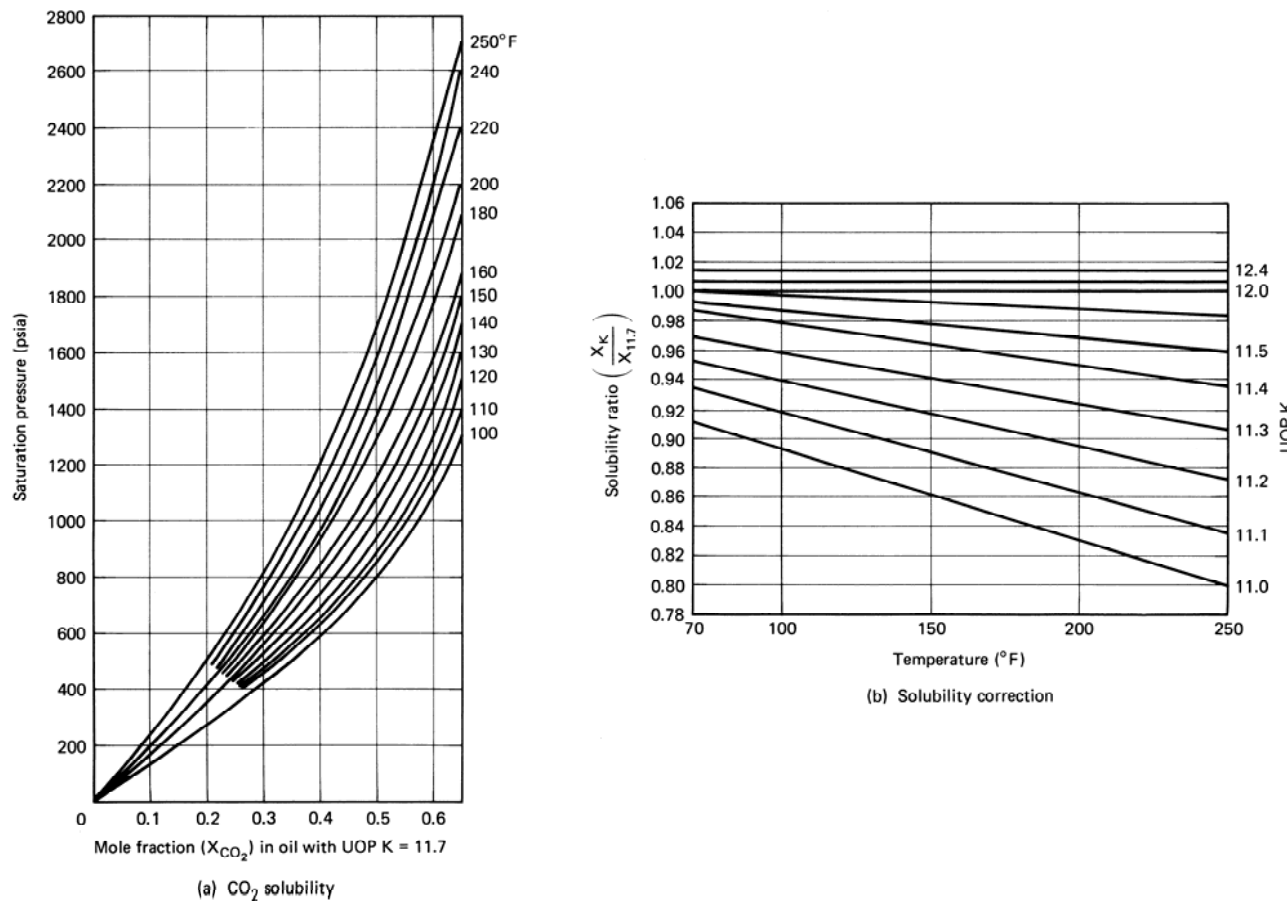


Figure 7-20 Solubility (mole fraction) of carbon dioxide in oils as a function of UOP number (from Simon and Graue, 1965)

displacements recover oil in this manner though the data showing these effects are most complete on CO₂-immiscible displacements (Simon and Graue, 1965).

Figures 7-20 through 7-22 show experimental data that emphasize immiscible recovery mechanisms 1–3. Figure 7-20(a) shows the solubility of CO₂ in oil versus temperature and saturation pressure for a crude with a Universal Oil

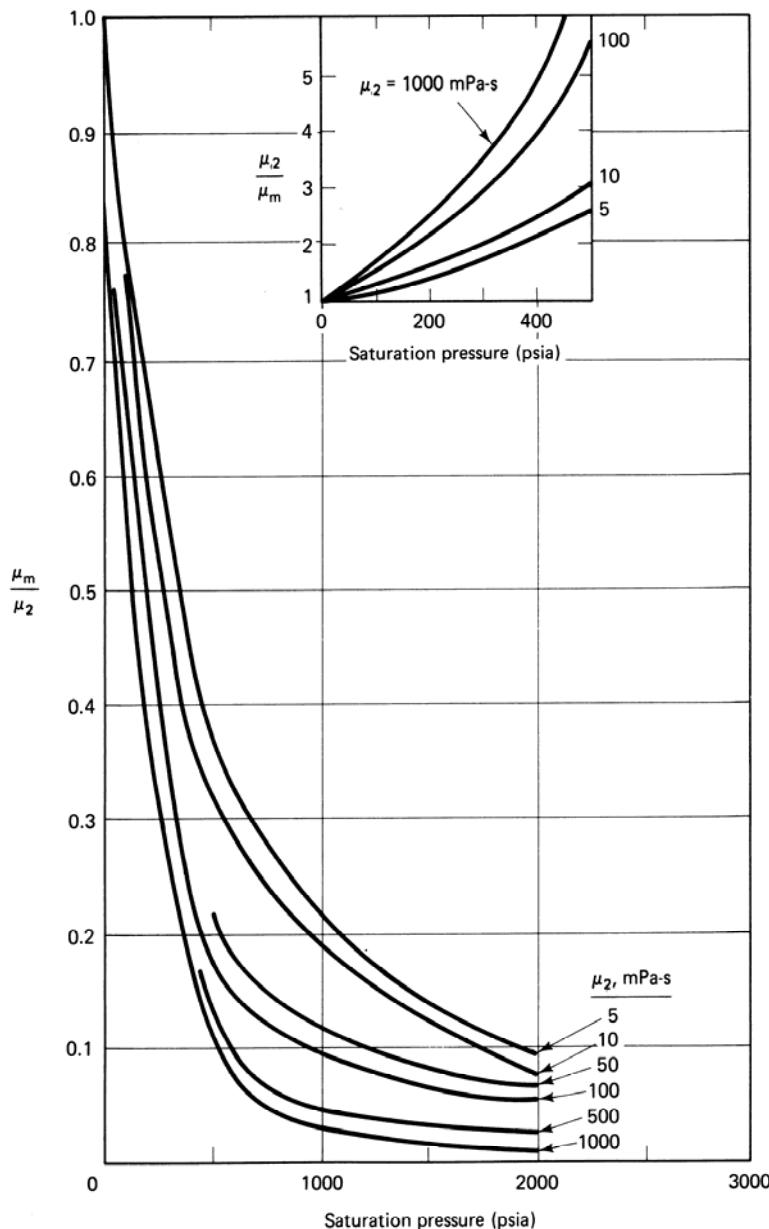


Figure 7-21 Viscosity correlation charts for carbon-dioxide–oil mixtures (from Simon and Graue, 1965)

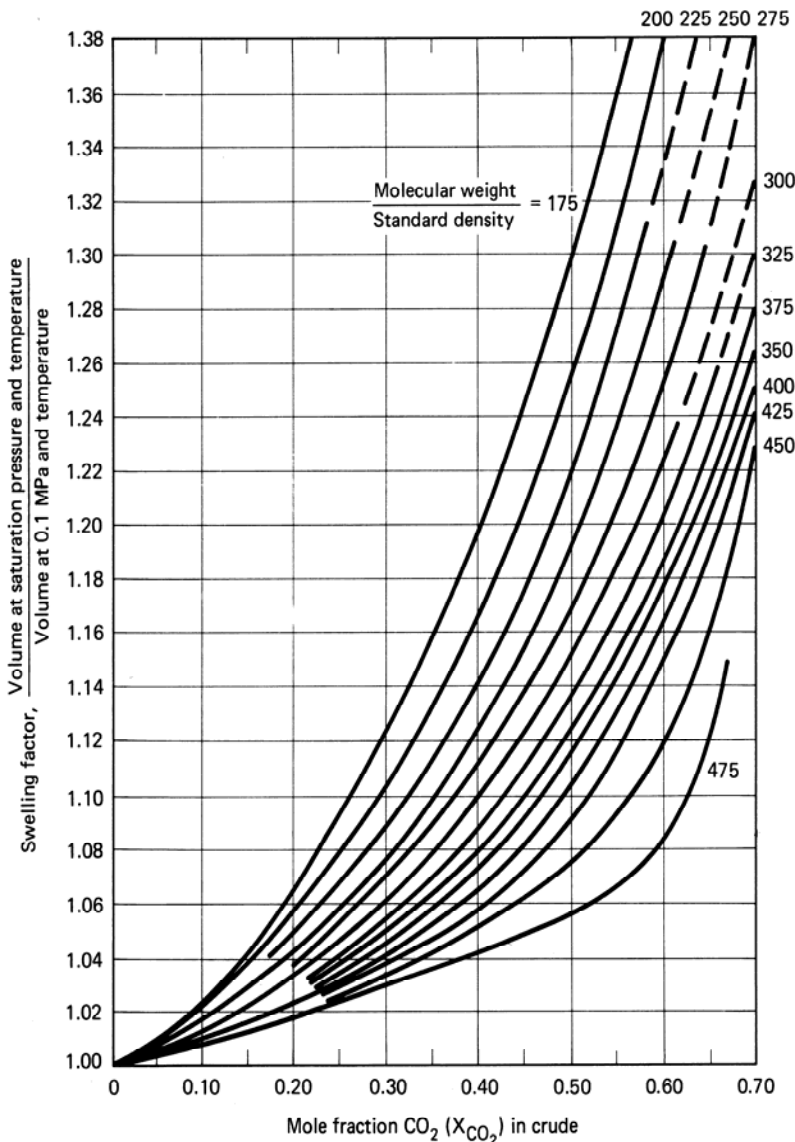


Figure 7-22 Swelling of oil as a function of mole fraction of dissolved carbon dioxide (from Simon and Graue, 1965)

Characterization factor (K) of 11.7. This factor is the ratio of the cube root of the average boiling point in degrees R to the specific gravity. It can be related to API gravity and viscosity (Watson et al., 1935). The saturation pressure is the bubble point pressure; hence Fig. 7-20(a) is giving the maximum solubility of CO_2 at the indicated temperature and pressure. Figure 7-20(b) corrects the solubility data to other characterization factors. Figure 7-21 gives the viscosity ratio of a CO_2 -swollen crude (μ_m in this figure) to the CO_2 -free crude (μ_0) as a function of pressure. For

moderate saturation pressures, the viscosity reduction is pronounced, particularly for large crude viscosities.

Figure 7-22 illustrates the oil swelling mechanism by giving crude swelling factors correlated with ratios of molecular weight to standard density (g/cm^3). Similar data on the swelling of crude by N_2 are given by Vogel and Yarborough (1980).

Figures 7-20 through 7-22 are complementary. Let's estimate the CO_2 solubility, oil viscosity reduction, and swelling factor for a crude oil at 389 K (150°F) and 8.2 MPa (1,200 psia). Recall that we are calculating the properties of a liquid hydrocarbon phase immiscible with CO_2 . Therefore, the overall CO_2 mole fraction must be large enough to be in the two-phase region of the ternary diagram. The relevant physical properties of the crude are as follows: molecular weight = 130, UOP characterization factor K = 11.8, specific gravity = 0.70, normal boiling point = 311 K (100°F), and viscosity = 5 mPa-s. This gives a CO_2 solubility of 55 mole % from Fig. 7-20. This solubility causes the oil viscosity to decrease to 1 mPa-s from Fig. 7-21, and the oil to swell by about 33% from Fig. 7-22. (For additional data on the properties of crude containing immiscible solvents, see Holm, 1961; de Nevers, 1964; Holm and Josendal, 1974; and Tumasyn et al., 1969.)

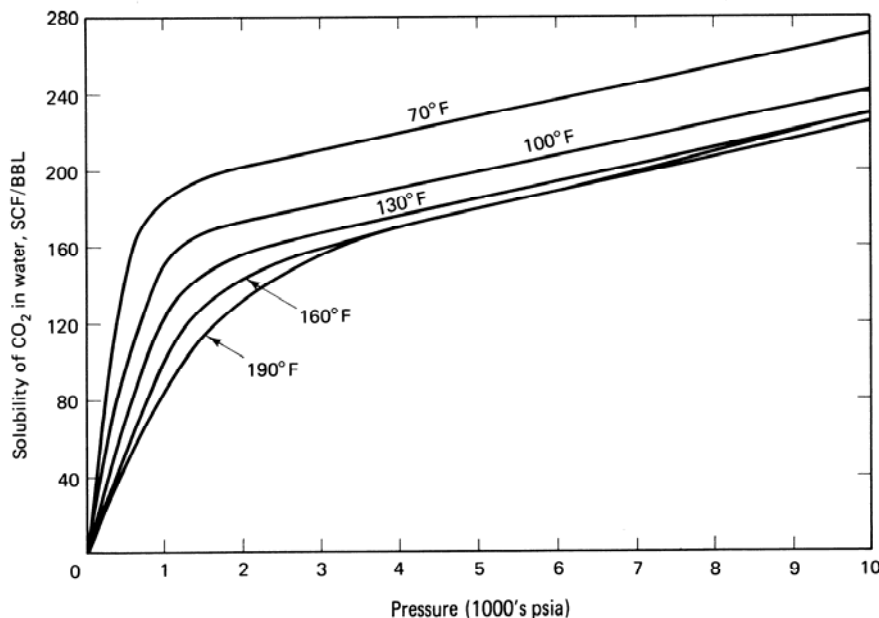


Figure 7-23 Solubility of carbon dioxide in water (from Crawford et al., 1963)

7-4 SOLVENT-WATER PROPERTIES

The solubility of CO_2 in water is a function of temperature, pressure, and water salinity (McRee, 1977). Figure 7-23 shows this solubility as a solution gas–water ratio. The data in Fig. 7-23 give the maximum CO_2 solubility at the indicated

tempeature and pressure; hence the horizontal axis is actually saturation pressure. The data are entirely equivalent to the data in Fig. 7-21(a) for CO₂-oil mixtures. The solution gas-water ratio may be readily converted into mole fraction.

Carbon dioxide is the only solvent with appreciable solubility in water over EOR temperature and pressure ranges (Culberson and McKetta, 1951). The CO₂ increases the viscosity of water slightly (Tumasyn et al., 1969) and decreases the density (Parkinson and de Nevers, 1969). This density change has been shown (Welch, 1982) to be less than that predicted by ideal solution theory. Neither the change in viscosity nor the change in density is likely to affect oil recovery very much.

7-5 SOLVENT PHASE BEHAVIOR EXPERIMENTS

Solvent phase behavior does not solely determine the character of a solvent flood, but it is of such fundamental importance that we devote a section to some of the common experiments used to measure phase behavior. This discussion leads naturally to the most frequently reported characteristic of solvent phase behavior—minimum miscibility pressure.

Single Contact

In a single-contact experiment, a known amount of solvent is charged into a transparent pressure cell containing a known amount of crude oil. After equilibrium is established at the desired temperature and pressure, a small amount of each phase is withdrawn. The phase compositions represent the ends of an equilibrium tie line. Only the composition of one phase need be measured since the composition of the other phase can be calculated from material balance. Single-contact experiments are useful for measuring P-z diagrams since the pressure can be changed, at fixed overall composition, by changing the cell volume. If the experiment is repeated for various amounts of solvent, the single-contact experiment traces a dilution path on a ternary diagram between the solvent and crude.

Multiple Contact

The multiple-contact experiment duplicates the process described in Sec. 7-3 under miscible process classification. In it (Fig. 7-24), known amounts of solvent and crude are charged to a transparent pressure cell as in the single-contact experiment, but after equilibration, the upper phase is decanted and mixed in a second cell with fresh crude. The lower phase in the cell is similarly mixed with fresh solvent. The upper phase is repeatedly decanted in this manner to simulate, discretely, the mixing that would take place at the forward contacts of the solvent-crude mixing zone. The successive mixings with the lower phase are the reverse contacts. All contacts are at a fixed temperature and pressure.

From Fig. 7-24, the multiple-contact experiment for Fig. 7-10, the solvent

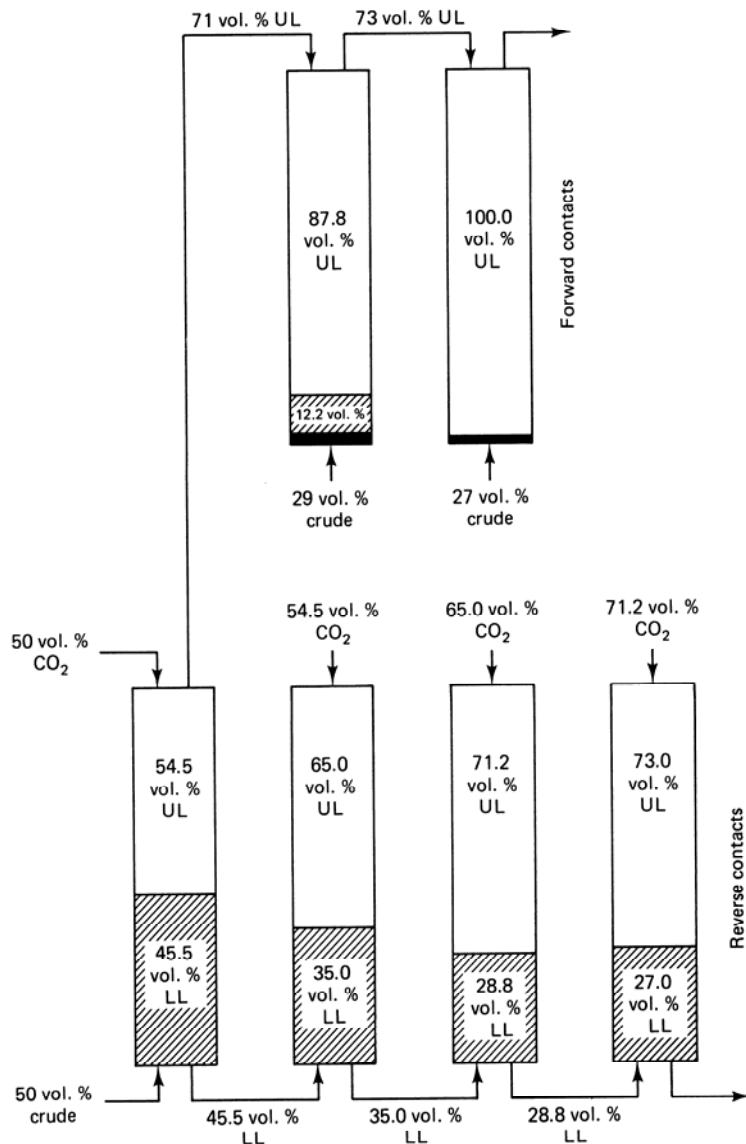


Figure 7-24 Multiple-contact experiment in 105°F (2,000 psia) (from Gardner et al., 1981)

enrichment in the forward contacts or the crude enrichment in the reverse contacts can cause one of the phases to disappear. This is exactly what is predicted by the arguments used in the process classification section: A single phase cell in the forward contacts indicates a vaporizing gas drive; in the reverse contacts, a condensing gas drive; and two or more phases in all contacts, an immiscible process. If the original cell is single phase for all combinations of solvent and crude oil, the process is first-contact miscible.

The experiment depends somewhat on the initial charges to the first cell, so the results are no more than indications of process classification. If phase compositions are measured at every step, the binodal curve and tie lines on a ternary diagram are established. Agreement between single- and multiple-contact experiments, as in Fig. 7-10, substantiates the pseudocomponent representation of the multicomponent equilibria.

Both single- and multiple-contact experiments place a premium on visual observations, but with careful selection of the initial volumes, these experiments are convenient ways to determine complete ternary equilibria data. Orr and Silva (1982) have proposed a method to measure phase behavior through continuous contacting.

Slim Tube

Filling the gap between the above static measurements and core floods are the *slim tube* experiments. These experiments are crude displacements by solvent, in the absence of water, at fixed temperature. The permeable medium consists of beads or unconsolidated sands packed in tubes of very thin cross section and, frequently, large length. The displacements are run with a fixed pressure at the one end of the system, and because the permeability of the medium is large, pressure gradients are negligible. Table 7-1 shows characteristics of selected slim tube experiments.

The overriding feature of slim tube experiments is the large aspect ratio (length-to-diameter ratio). This is intended to suppress viscous fingering since the long length means there is sufficient time during the displacement for all perturbations to be suppressed by transverse dispersion. Small wavelength perturbations will not form at all since the tube diameter is smaller than the critical wavelength (see See. 6-8).

The slim tube experiment, then, is designed to provide an unambiguous measure of solvent displacement efficiency. But because of both the highly artificial nature of the permeable medium and the experimental conditions (no water), this is not a realistic displacement efficiency. The results are best regarded as a dynamic measure of phase behavior properties.

Minimum Miscibility Pressure

Although effluent compositions can be monitored during a slim tube displacement, by far the most common information derived from the experiments is the *minimum miscibility pressure* (MMP). Since solvent miscibility increases with pressure, ultimate oil recovery should also increase with pressure. This, in fact, happens, but there is a pressure above which a further pressure increase causes only a minimal increase in oil recovery. The pressure at which oil recovery levels out is the MMP, or minimum *dynamic* miscibility pressure. MMP is variously defined as

- The pressure at which the oil recovery at $t_D = 1.2$ PV of CO_2 injected was equal to or very near the maximum final recovery obtained in a series of tests (Yellig and Metcalfe, 1980)

TABLE 7-1 CHARACTERISTICS OF SLIM TUBE DISPLACEMENT EXPERIMENTS (ADAPTED FROM ORR ET AL., 1982)

Author(s)*	Length (meters)	ID (cm)	Geometry	Packing (mesh)	Permeability (μm^2)	Porosity (%)	Rate (cm/hr)	$\frac{K_t \phi}{\mu\text{L}}$
Rutherford (1962)	1.5	1.98	Vertical tube	50–70 mesh Ottawa sand	24	35	37	0.2
Yarborough and Smith (1970)	6.7	0.46	Flat coil	No. 16 AGS	2.74		66	11.9
Holm and Josendal (1974)	14.6	0.59		No. 60 Crystal sand			3.81	109.1
Holm and Josendal (1982)	25.6			No. 60 Crystal sand	20	39	101–254	12.5
Huang and Tracht (1974)	15.8	0.59	Coil					14.9
Yellig and Metcalfe (1980)	6.1	1.65			1.78	43	4.7	4.8
Peterson (1978)	12.2	0.64 OD	Flat coil	160–200 mesh sand	2.5		5.2–10.2	33.4
Wang and Locke (1980)	17.1	0.64		60–65 mesh sand	19			58.1
Orr and Taber (1981)	18.0	0.62	Spiral coil	80–100 mesh	13	35	381	12.3
Gardner, Orr, and Patel (1981)	12.2	0.64	Spiral coil	170–200 mesh glass beads	5.8	37	42	13.5
Sigmund et al. (1979)	6.1	0.46	Flat coil	230–270 mesh glass beads	1.4	37	32 64	15.0
	17.9	0.78		140 mesh	5	42		

* References in Orr et al.

- The pressure that causes 80% oil recovery at CO_2 breakthrough and 94% recovery at a gas-to-oil ratio of 40,000 SCF/stb (Holm and Josendal, 1974)
- The pressure that causes 90% oil recovery at $t_D = 1.2$ HCPV of CO_2 injected (Williams et al., 1980)

Others (Perry, 1978; Yellig and Metcalfe, 1980) emphasize the qualitative nature of the miscibility pressure determination. The importance of the exact definition is unknown; all definitions show the same trends in correlations.

The results of slim tube experiments are giving the minimum pressure necessary for the displacement to develop miscibility. Thus the MMP corresponds to the pressure at which the critical tie line passes through the crude composition. This pressure is considerably less than that required for complete or first-contact miscibility (compare the MMP plots with the P-z diagrams). This is the origin of the plateau on the oil-recovery-pressure plot: Any further pressure increase does not increase oil recovery since above the MMP the displacement will tend from developed to first-contact miscibility. These observations are also supported by compositional measurements wherein the properties (viscosity, density, and composition) of phases produced below the MMP become closer to one another as the MMP is approached.

The CO_2 MMP is determined by temperature, pressure, solvent purity, and molecular weight of the heavy fraction of the reservoir crude. Generally, the MMP increases with temperature and heavy fraction molecular weight. Holm and Josendal (1974 and 1982) note that the development of miscibility for CO_2 solvents is the result of extracting hydrocarbon components into a CO_2 -rich phase. Therefore, at a given temperature and crude composition, sufficient compression must be applied to the solvent to promote solvency with the crude. This solvency is manifest by the CO_2 density at the temperature of the test. Figure 7-25(a) shows the CO_2 density required to develop miscibility at a given temperature with the C_5-C_{30} percent of the C_5^+ crude fraction. The CO_2 density can be connected to MMP through Fig. 7-4 or Fig. 7-25(b). CO_2 MMP is affected by the type of hydrocarbons (aromatic or paraffinic) in the crude but to a lesser degree than by temperature and CO_2 density (Monger, 1985).

Several works have presented determinations of MMP for impure CO_2 . Figure 7-26 shows the results of the effects of N_2 , CH_4 , H_2S and $\text{H}_2\text{S}-\text{CH}_4$ mixtures on the CO_2 MMP. Methane and particularly nitrogen increase the CO_2 MMP, whereas H_2S decreases it. Whether an impurity increases or decreases the MMP depends on whether the solvency of the solvent has been enhanced. Solvency is improved (MMP decreases) if CO_2 is diluted with an impurity whose critical temperature is more than that of CO_2 . Solvency deteriorates (MMP increases) if CO_2 is diluted with an impurity with a critical temperature less than CO_2 . Compare the trends in Fig 7-26 with the critical temperatures in Fig. 7-2.

The above idea of solvency can be used to estimate the MMP of an impure CO_2 solvent. Sebastian et al. (1984) have correlated the diluted CO_2 MMP by the following:

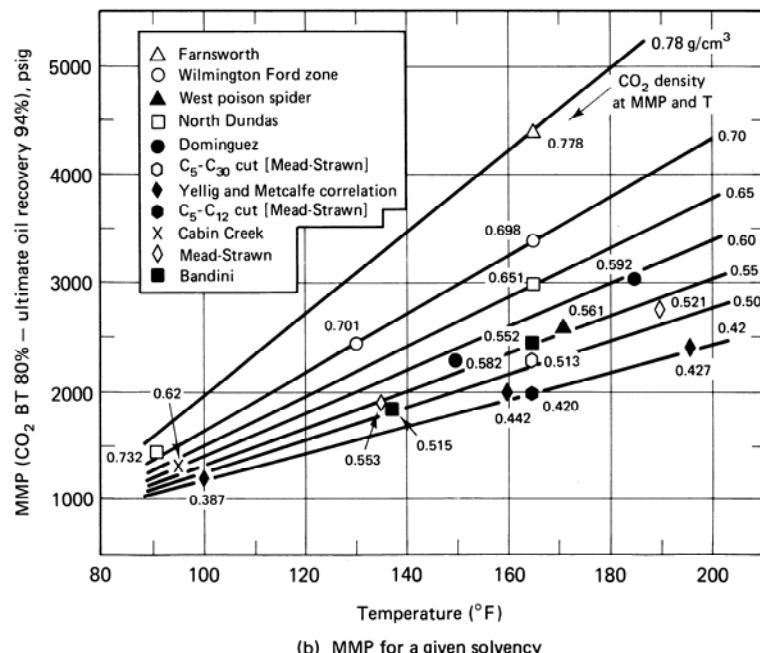
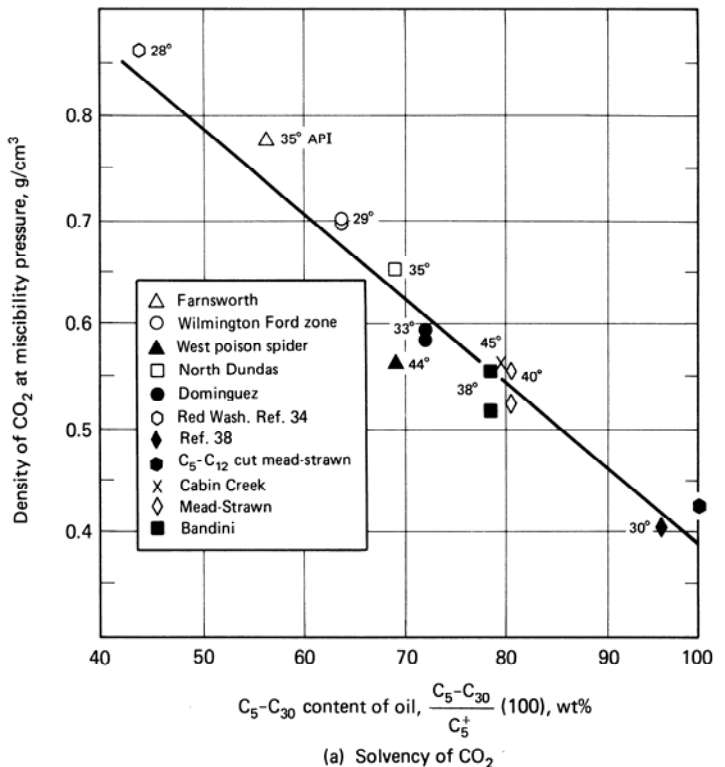


Figure 7-25 Density of CO_2 required for miscible displacement of various oils at 90° to 190°F (from Holm and Josendal, 1982)

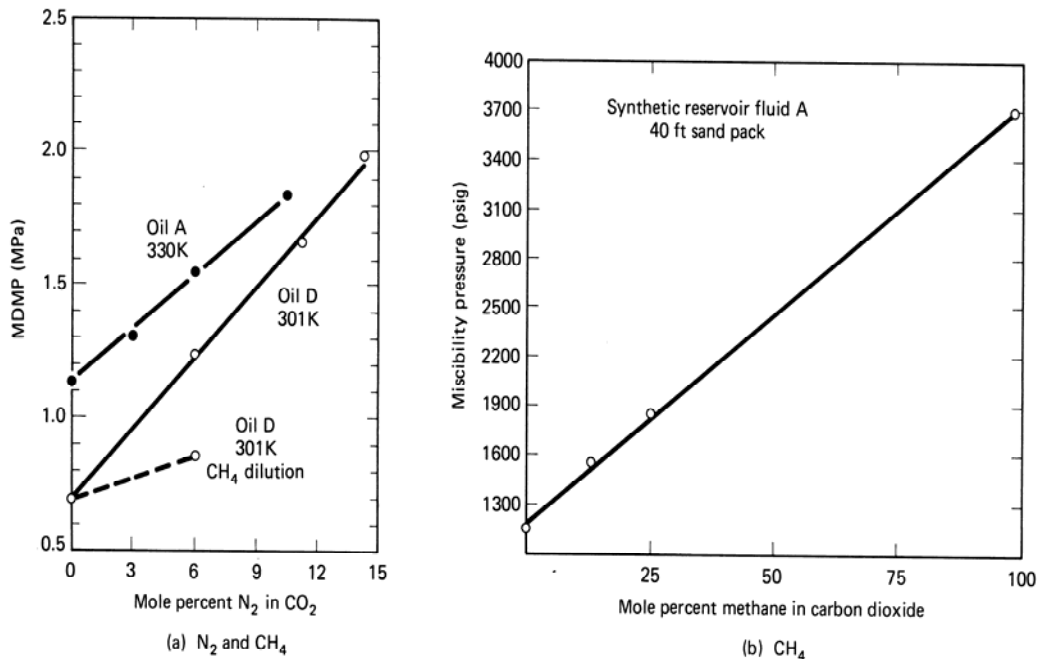


Figure 7-26 Effect of impurities on CO_2 minimum miscibility pressure (from Johnson and Pollin, 1981; Whitehead et al., 1980; Metcalfe, 1981)

$$\frac{P_{MM}}{(P_{MM})_{CO_2}} = 1.0 - (2.13 \times 10^{-2})(T_{pc} - T_c) + (2.51 \times 10^{-4})(T_{pc} - T_c)^2 - (2.35 \times 10^{-7})(T_{pc} - T_c)^3 \quad (7.5-1)$$

where $T_{pc} = \sum_i T_{ci}y_i$ is the pseudocritical temperature of the mixture, and y_i is the mole fraction of species i in the solvent. The denominator of the left side of Eq. (7.5-1) can be estimated from Fig. 7-25. (For other correlations, see Johnson and Pollin, 1981.) No MMP correlation is especially accurate; errors as much as 0.34 MPa (50 psia) are common.

Minimum Enrichment Correlations

For a dry gas process, slim tube results will give an estimate of the amount of intermediates that must be added to develop miscibility in a condensing gas drive. Such experiments were precursors to the MMP experiments (Benham et al., 1961). The oil recovery plot would consist of several experiments each with a successively richer injected solvent but each at constant pressure. When the solvent composition coincided with the tie line extension (through the reverse contacts), oil recovery would cease to increase as the solvent becomes richer in intermediates.

Figure 7-27 is one of 12 plots from Benham et al. (1961) that shows the maximum methane concentration permissible in an LPG solvent that will develop miscibility with the subject crude. These authors correlated the maximum dilution (or

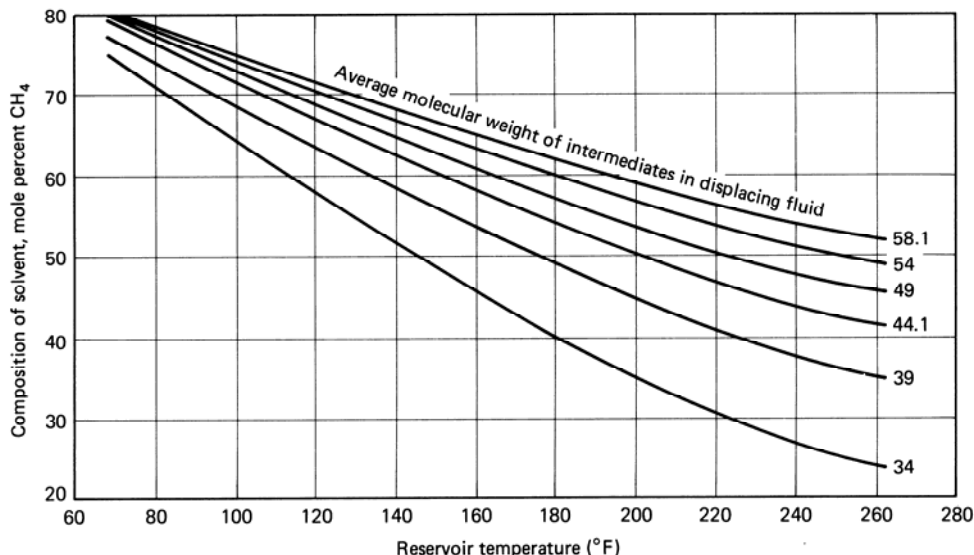


Figure 7-27 Maximum methane dilution in LPG solvent for developed miscibility at 2,500 psia and for a reservoir fluid whose C_5^+ component molecular weight is 240 (from Benham et al., 1961)

minimum enrichment) with temperature, pressure, molecular weight of the intermediate component in the solvent, and molecular weight of the C_5^+ fraction in the crude. The minimum dilution increases with decreasing C_5^+ molecular weight, pressure, and temperature, and it increases with increasing intermediate molecular weight.

Each of these trends follows from the trends in the phase behavior and the position of the crude and solvent on the ternary diagram. And each may be quantitatively established on true ternaries with accurate thermodynamic properties. But the pseudocomponent representation of more than three components on a ternary is not rigorous, and this leads to some difficulty in quantitatively predicting both the minimum dilution and the MMP on actual systems.

7-6 DISPERSION AND SLUG PROCESSES

In the next few sections, we look in detail at how a miscible solvent behaves during oil displacement. You should remember that first-contact and developed miscibility solvent behave very much alike.

Dilution Paths

The concentration of species i in a first-contact miscible displacement is from Eq. (5.5-15)

$$C_i = C_{iI} + \frac{(C_{iJ} - C_{iI})}{2} \left[1 - \text{erf} \left(\frac{x_D - t_D}{2\sqrt{\frac{t_D}{N_{pe}}}} \right) \right] \quad (7.6-1)$$

For this equation to be valid, we cannot have viscous fingering, layering, or gravity tonguing; hence it is restricted to constant viscosity and density floods in one-dimensional media. In Eq. (7.6-1), x_D is the dimensionless length, t_D the dimensionless time in fractional pore volumes, N_{pe} the Peclet number, and the subscripts I and J refer to initial and injected conditions, respectively.

If we let the component subscript i refer to the light, intermediate, and heavy pseudocomponents of Sec. 7-3, we can easily show from Eq. (7.6-1) that dilution paths are straight lines on a pseudoternary diagram. Eliminating the term in brackets among the three equations gives

$$\frac{C_1 - C_{1I}}{C_{1J} - C_{1I}} = \frac{C_2 - C_{2I}}{C_{2J} - C_{2I}} = \frac{C_3 - C_{3I}}{C_{3J} - C_{3I}} \quad (7.6-2)$$

The C_i in Eq. (7.6-2) lie on a straight line in composition space; hence the dilution path of Sec. 7-3 is linear.

Superposition

Solvents are usually too expensive to be injected continuously. Thus a typical displacement consists of a finite amount or slug of solvent followed by a less expensive chase fluid. The concentration of a slug follows from Eq. (7.6-1) and the principle of *superposition*. This principle applies to linear partial differential equations, which Eq. (7.6-1) is an approximate solution to. We can, in fact, derive the concentration response of an infinite number of step changes in the influent concentration (see Exercise 7C), but we restrict our discussion here to the case of a single solvent slug displaced by a chase fluid.

Let I , J , and K denote the concentrations of species i in the original fluid, the slug, and the chase fluids, respectively. Superposition states that the sum of individual solutions to a linear differential equation is also a solution to the equation. This seems easy enough to do in practice, but we must take care in selecting the boundary conditions of the individual solutions to give the correct composite solution. Figure 7-28 shows the influent or imposed boundary conditions of the single front problem

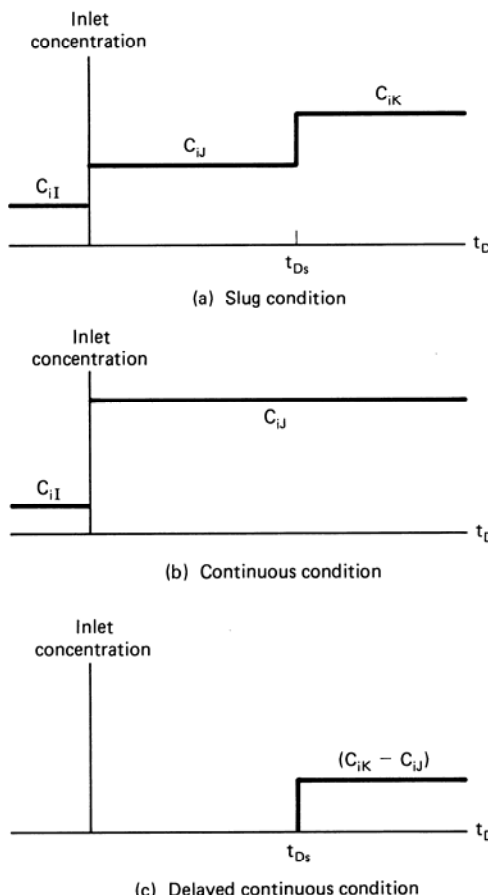


Figure 7-28 Schematic of influent boundary conditions for slugs

(Fig. 7-28b) and that of the composite solution (Fig. 7-28c). The composite solution gives $C_i(x_D, t_D)$ for the imposed conditions in Fig. 7-28(a), simply the sum of the solutions to the conditions in Figs. 7-28(b) and 7-28(c), respectively. The solution to the imposed conditions in Fig. 7-28(b) is Eq. (7.6-1), and that of the imposed condition in Fig. 7-28(c) is

$$C_i = \frac{(C_{iK} - C_{iI})}{2} \left[1 - \operatorname{erf} \left(\frac{x_D - (t_D - t_{Ds})}{2 \sqrt{\frac{(t_D - t_{Ds})}{N_{Pe}}}} \right) \right] \quad (7.6-3)$$

By superposition $C_i(x_D, t_D)$ for the influent condition in Fig. 7-28(a) is the sum of Eqs. (7.6-1) and (7.6-3)

$$\begin{aligned} C_i = & \frac{C_{iI} + C_{iK}}{2} + \left(\frac{C_{iJ} - C_{iI}}{2} \right) \operatorname{erf} \left(\frac{x_D - t_D}{2 \sqrt{\frac{t_D}{N_{Pe}}}} \right) \\ & + \left(\frac{C_{iJ} - C_{iK}}{2} \right) \operatorname{erf} \left(\frac{x_D - (t_D - t_{Ds})}{2 \sqrt{\frac{t_D - t_{Ds}}{N_{Pe}}}} \right), \quad t_D > t_{Ds} \end{aligned} \quad (7.6-4)$$

Equation (7.6-4) is valid for any value of the injected concentrations.

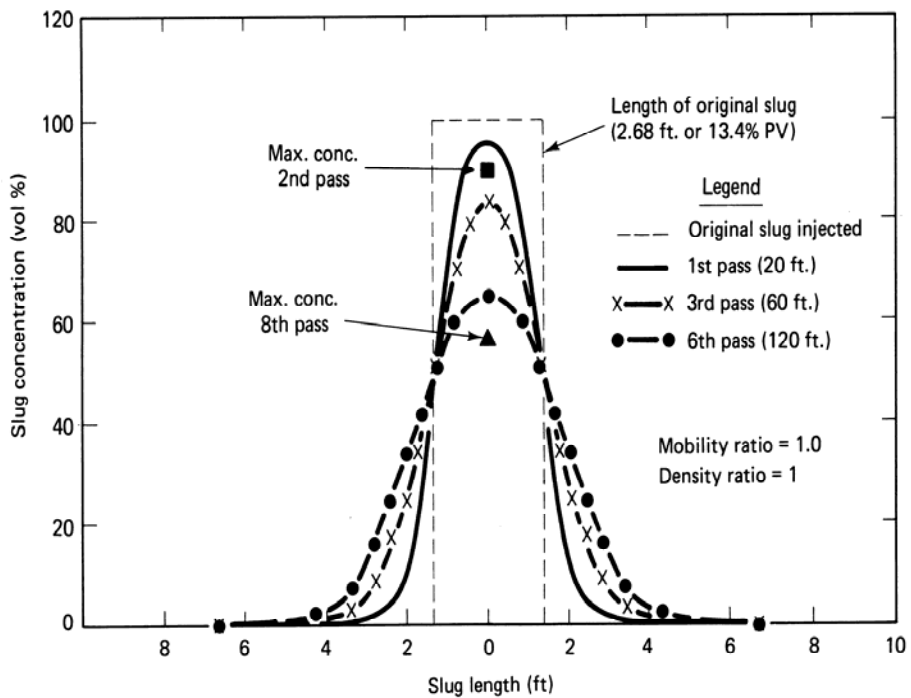
Frequently, we are interested in the concentration of the solvent at the midpoint between $x_D = t_D$ and $x_D = t_D - t_{Ds}$. Evaluating Eq. (7.6-4) at $x_D = t_D - t_{Ds}/2$ yields this midpoint concentration \bar{C}_i

$$\bar{C}_i = \frac{C_{iI} + C_{iK}}{2} \left[1 - \operatorname{erf} \left(\frac{t_{Ds}}{4 \sqrt{\frac{t_D}{N_{Pe}}}} \right) \right] + C_{iJ} \operatorname{erf} \left(\frac{t_{Ds}}{4 \sqrt{\frac{t_D}{N_{Pe}}}} \right) \quad (7.6-5)$$

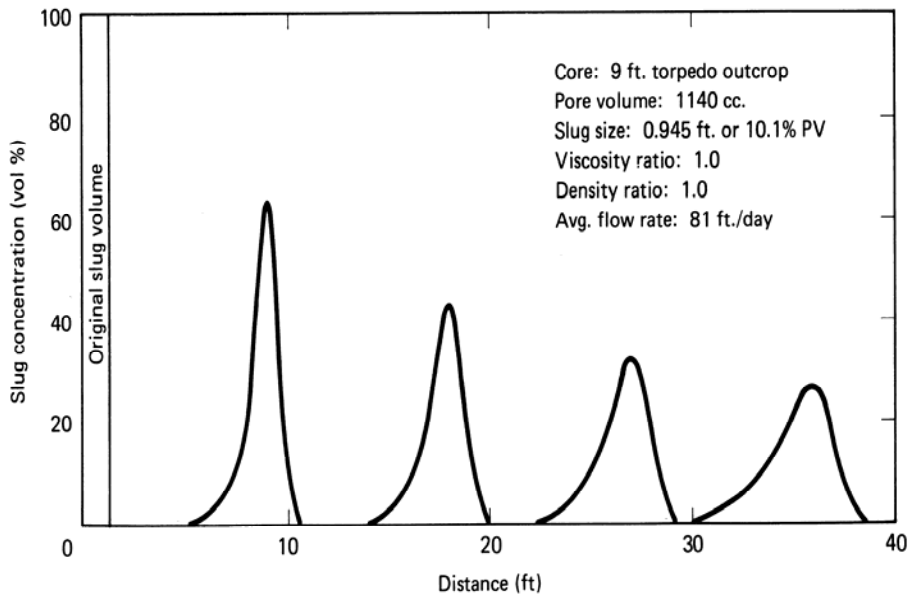
This equation is valid only for relatively small t_{Ds} where the difference between the square roots of t_D and $t_D - t_{Ds}$ in the denominator of the error function argument is not large. If $C_{iJ} > C_{iI}$ and $C_{iJ} > C_{iK}$, the midpoint concentration is usually called the *peak* concentration. For $C_{iI} = C_{iK} = 0$, the peak concentration falls with increasing time according to

$$\bar{C}_i = C_{iJ} \operatorname{erf} \left(\frac{t_{Ds}}{4 \sqrt{\frac{t_D}{N_{Pe}}}} \right) \quad (7.6-6)$$

The error function may be replaced by its argument for small values of the argument. In this event, the peak concentration falls in inverse proportion to the square root of time. Since $x_D = t_D - t_{Ds}/2$ at the peak concentration, this is equivalent to \bar{C}_i falling in proportion to the inverse square root of the distance traveled.



(a) Slug concentration profiles normalized to slug midpoint



(b) Slug concentration profiles at various times

Figure 7-29 Miscible slug concentration profiles for matched viscosity and density displacements (from Koch and Slobod, 1956)

The peak concentration falling below C_{iJ} is the consequence of -overlapping front and rear mixing zones. Figure 7-29 shows experimental concentration profiles from a miscible slug displacement at different throughputs. Figure 7-29(a) has the concentration profiles normalized to the midpoint position $x_D = t_D - t_{Ds}/2$ on the horizontal axis. The areas under all curves are the same (material balance is preserved), but the peak concentration falls as the number of passes (travel distance) increases. The unnormalized profiles in Fig. 7-29(b) show that the peak concentration falls approximately as the inverse square root of t_D in experimental floods.

The midpoint concentrations also trace a straight line in the pseudoternary diagram since the error function arguments in Eq. (7.6-5) may be eliminated to give

$$\frac{\bar{C}_1 - \frac{C_{1K} + C_{1I}}{2}}{C_{1J} - \frac{C_{1K} + C_{1I}}{2}} = \frac{\bar{C}_2 - \frac{C_{2K} + C_{2I}}{2}}{C_{2J} - \frac{C_{2K} + C_{2I}}{2}} = \frac{\bar{C}_3 - \frac{C_{3K} + C_{3I}}{2}}{C_{3J} - \frac{C_{3K} + C_{3I}}{2}} \quad (7.6-7)$$

This equation says that as time increases, the midpoint concentration traces a straight line between the injected slug concentration C_{iJ} and the average concentration of the

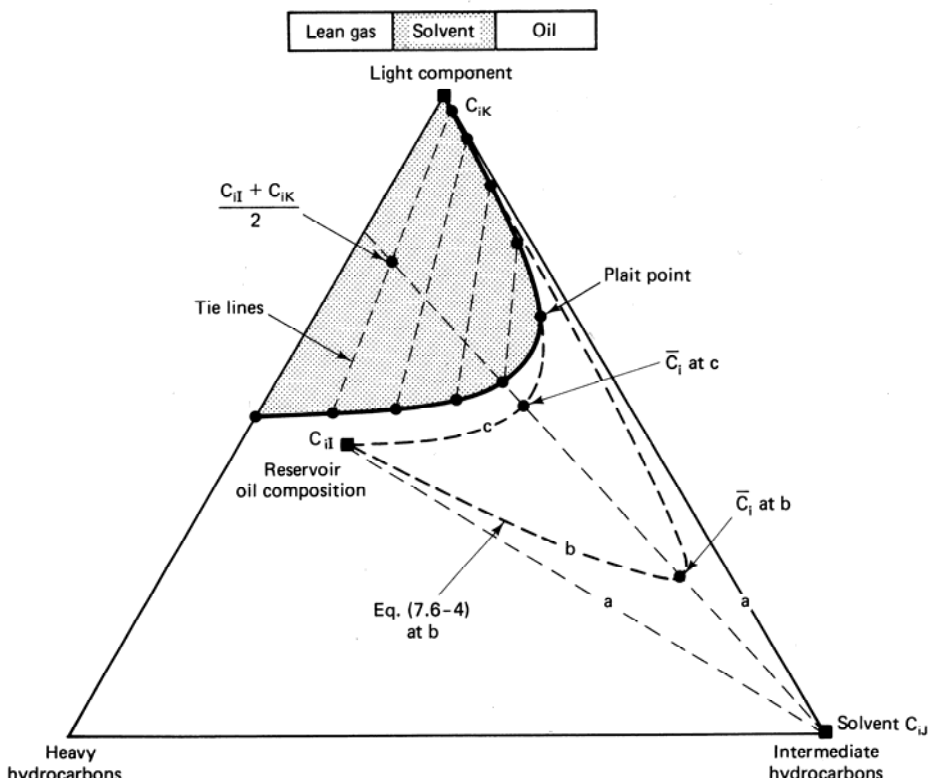


Figure 7-30 Dilution of solvent slug by mixing (from Stalkup, 1983)

fluids ahead of and behind the slug. The midpoint concentrations at successive times a , b , and c are shown in Fig. 7-30, as are the dilution paths given by Eq. (7.6-4). The dilution paths become straight line segments from C_{iJ} to \bar{C}_i and then from \bar{C}_i to C_{iK} for t_{Ds} small. These considerations are valid only so long as the entire dilution path stays in the single-phase region of the diagram. It is not necessary for \bar{C}_i to fall into the two-phase region for the displacement to lose first-contact miscibility (see Exercise 7E).

7-7 TWO-PHASE FLOW IN SOLVENT FLOODS

Two or more phases are all too common in solvent floods. When this happens, the dispersion theory of Sec. 7-6 does not apply. But general conclusions about such displacements are still possible based on the coherent or simple wave theory first introduced in Sec. 5-6. This theory neglects dissipative effects of any kind; hence we omit dispersion in the following discussion and restrict our treatment to centered simple waves (see Sec. 5-4 for definitions).

We treat two cases of two-phase flow in miscible displacements: (1) solvent floods in the absence of an aqueous phase and (2) first-contact miscible displacements in the presence of an aqueous phase. In both cases, fluid displacement takes place in a one-dimensional permeable medium at constant temperature and with incompressible fluids and solid.

Solvent Floods in the Absence of an Aqueous Phase

In this section, we give a theoretical base for the classifications of Sec. 7-3. Consider a three-component system consisting of an intermediate hydrocarbon ($i = 2$), a light hydrocarbon ($i = 3$), and a heavy hydrocarbon that can form no more than two phases at constant temperature and pressure. As we discussed in Sec. 4-3, the overall concentrations C_i , the phase concentrations C_{ij} , and the saturations S_j ($j = 2$ or 3) can be conveniently represented on ternary diagrams.

The topology within the two-phase region is important for this problem. Figure 7-31 shows a ternary diagram with a two-phase region exaggerated to point out certain landmarks. Within the two-phase region is a family of quality lines that do not intersect and converge at the plait point. The binodal curve itself is a quality line. There are also lines denoting the residual saturations of the two phases. These lines do not, in general, coincide with quality lines since residual saturations must decrease as the plait point is approached (see Sec. 3-4). This decrease is because the interfacial tension between the two phases must vanish at the plait point. Along each tie line, there exists a curve relating the fractional flow of one of the phases to its saturation. Three of these curves, along tie lines $A-A'$, $B-B'$ and $C-C'$, are in the upper left insert to Fig. 7-31. The shape of the fractional flow curves is not determined by the phase behavior alone, but the curves become straighter (more miscible-like) with smaller residual phases along tie lines near the plait point. Because phase compositions are

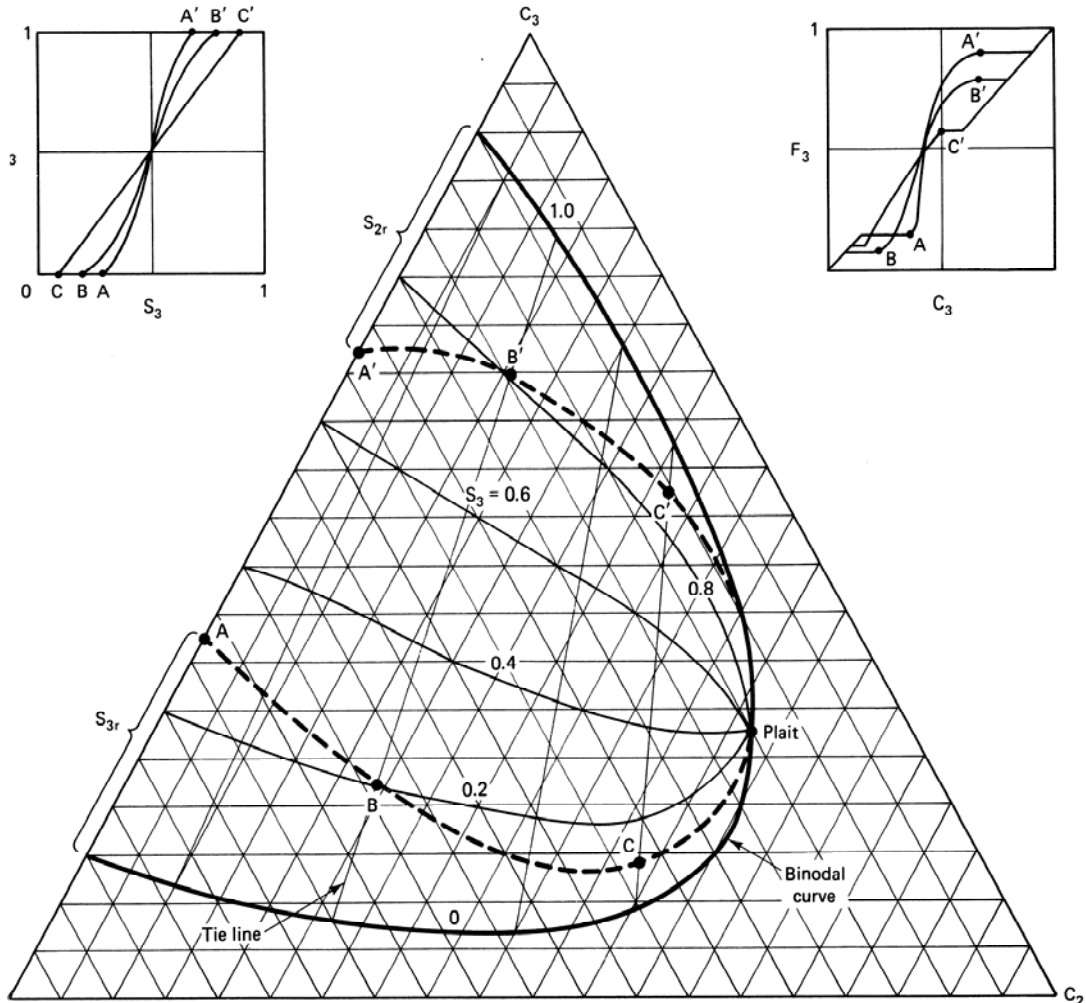


Figure 7-31 Landmarks on a two-phase ternary

constant along tie lines, the C_{ij} , S_j and f_i can be converted to fractional flux and overall concentration through Eqs. (5.4-3). The upper right insert of Fig. 7-31 shows an F_3-C_3 along the three tie lines.

This ternary system has only two independent components, which we arbitrarily take to be C_2 and C_3 . The coherence condition (Eqs. 5.4-5 and 5.6-14) for this case becomes

$$v_{C_2} = \frac{dF_2}{dC_2} = \frac{dF_3}{dC_3} = v_{C_3} \quad (7.7-1)$$

Using the condition $f_2 + f_3 = 1$, and the definitions for overall flux and concentration (Eqs. 5.4-3a and 5.4-3c), Eq. (7.7-1) can be rewritten as (Helfferich, 1982)

$$\begin{aligned} v_{C_2} &= \frac{f_2(dC_{22} - dC_{23}) + dC_{23} + (C_{22} - C_{23})df_2}{S_2(dC_{22} - dC_{23}) + dC_{23} + (C_{22} - C_{23})dS_2} \\ &= \frac{f_2(dC_{32} - dC_{33}) + dC_{33} + (C_{32} - C_{33})df_2}{S_2(dC_{32} - dC_{33}) + dC_{33} + (C_{32} - C_{33})dS_2} = v_{C_3} \end{aligned} \quad (7.7-2)$$

The curve in the ternary composition space that a displacement follows (the composition route) is quite complex, but certain segments (composition paths) are readily apparent from Eq. (7.7-2).

1. Unit velocity paths. These occur along any direction in the single-phase region (all directions are coherent) or along the binodal curve. In both cases, $f_2 = S_2 = 1$ or $f_3 = S_3 = 1$, depending on the side of the plait point, and the composition velocity is

$$v_{C_2} = v_{C_3} = 1 \quad (7.7-3)$$

Equation (7.7-3) is the same result as Eq. (5.4-7).

Within the two-phase region is an *equivelocity* path where $f_2 = S_2$. This path is the intersection of a straight line through $f_2 = S_2 = 0$ and $f_2 = S_2 = 1$ and the family of fractional curves (Fig. 7-31). It converges to the plait point, but it does not, in general, coincide with a quality line.

2. Tie line paths. On tie lines in the two-phase region, $dC_{ij} = 0$. This also satisfies Eq. (7.7-2). On these paths, the concentration velocities are

$$v_{C_i} = \frac{df_2}{dS_2}, \quad i = 2, 3 \quad (7.7-4)$$

Equation (7.7-4) is the same as the saturation velocity in the Buckley-Leverett theory (Eq. 5.2-10).

Two other types of paths are not so easily derived. Both follow from integrating the composition path curve

$$\frac{dC_2}{dC_3} = \frac{v_C^\pm - F_{22}}{F_{23}} \quad (7.7-5a)$$

where the composition velocity is

$$v_C^\pm = \frac{1}{2} \left\{ (F_{22} + F_{33}) \pm [(F_{33} - F_{22})^2 + 4F_{23}F_{32}]^{1/2} \right\} \quad (7.7-5b)$$

and

$$F_{22} = \left(\frac{\partial F_2}{\partial C_2} \right)_{C_3}$$

and so on.

3. Singular curves. Along these curves, the velocity of the fast and slow paths is equal. The curves follow from setting the discriminant of Eq. (7.7-5b) equal

to zero. Singular curves are composition paths since they can be generated from Eq. (7.7-5a) as long as $F_{23} \neq 0$.

4. Non-tie line paths. Within the two-phase region, there are also composition paths whose trajectories are not readily apparent from the above equations. Figure 7-32 shows each of these paths.

If the tie lines extend to a common point, the concentration velocity along the non-tie line paths is constant (Cere and Zanotti, 1985). The phase equilibria is now represented by Eq. (4.4-27b), which we repeat for this special case

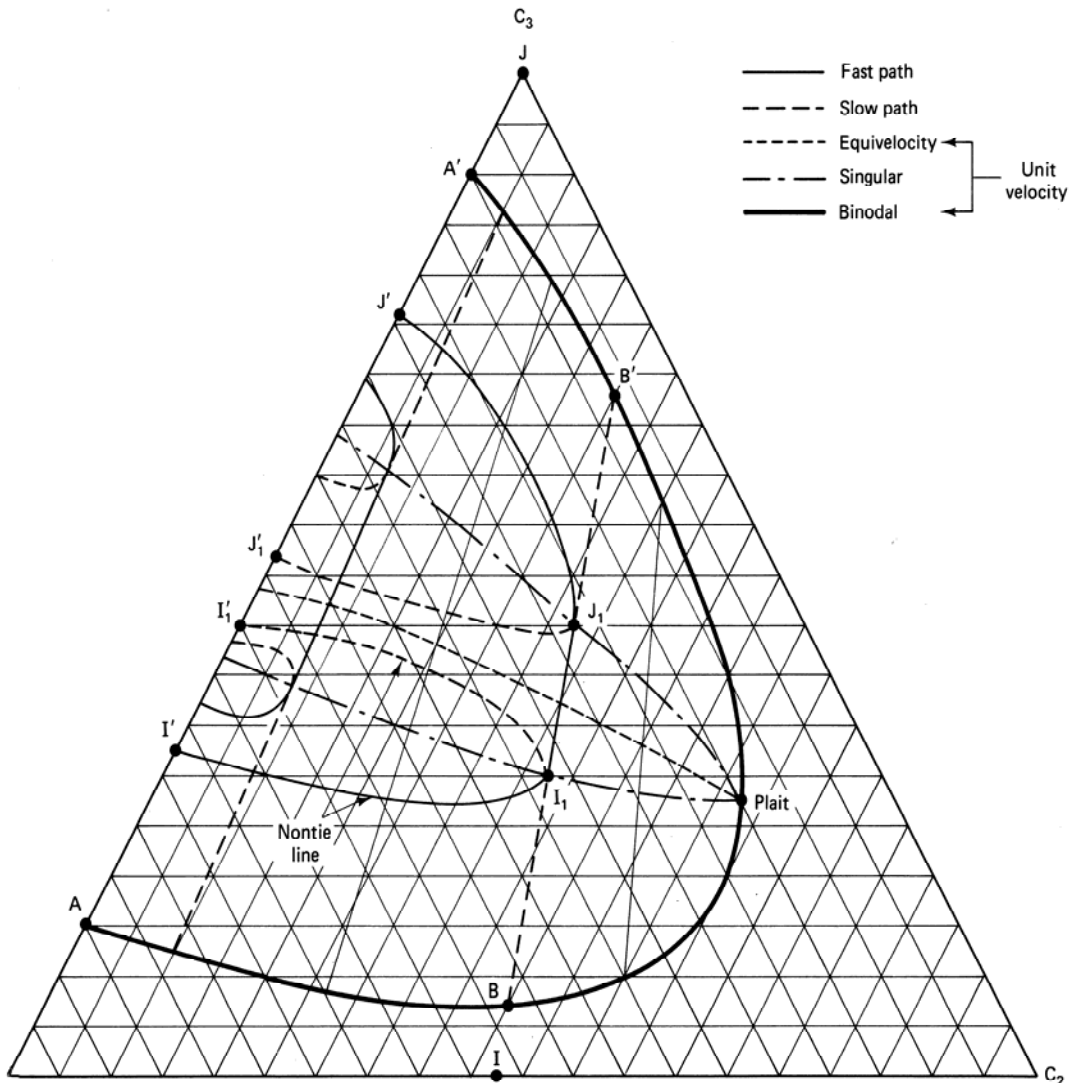


Figure 7-32 Composition path in two-phase ternary equilibria

$$C_{3j} - C_3^0 = \eta(C_{2j} - C_2^0), \quad j = 2 \text{ or } 3 \quad (7.7-6)$$

A particular tie line is represented by a particular value of η . If we introduce the definitions for overall flux and concentration into the coherence condition Eq. (7.7-1), we have

$$\frac{dF_2}{dC_2} = \frac{d(C_{22}f_2 + C_{23}f_3)}{d(C_{22}S_2 + C_{23}S_3)} = \frac{d(C_{32}f_2 + C_{33}f_3)}{d(C_{32}S_2 + C_{33}S_3)} = \frac{dF_3}{dC_3} \quad (7.7-7)$$

We can substitute Eq. (7.7-6) into the third term to give, after some rearrangement and identification,

$$\frac{dF_2}{dC_2} = \frac{d\eta(F_2 - C_2^0) + \eta dF_2}{d\eta(C_2 - C_2^0) + \eta dC_2} \quad (7.7-8)$$

Our task is to find the combination of variables that makes this equation an identity.

Immediately we see that the equivelocity and tie line paths are returned from Eq. (7.7-8), for the conditions $F_2 = C_2^0 = C_2$ and $d\eta = 0$ clearly satisfy the equation. But the existence of both paths is more general than this since it follows from Eq. (7.7-2).

The non-tie line paths are defined by the following equations:

$$\begin{aligned} dF_2 &= d\eta(F_2 - C_2^0) + \eta dF_2 \\ dC_2 &= d\eta(C_2 - C_2^0) + \eta dC_2 \end{aligned} \quad (7.7-9)$$

Eliminating η between these two equations gives an ordinary differential equation relating F_2 and C_2 along the non-tie line path

$$\frac{dF_2}{dC_2} = \frac{F_2 - C_2^0}{C_2 - C_2^0} \quad (7.7-10)$$

Integrating this equation yields a linear relation between F_2 and C_2

$$F_2 - C_2^0 = I_c(C - C_2^0) \quad (7.7-11a)$$

where I_c is an integration constant independent of either F_2 and C_2 . Immediately it follows from Eqs. (7.7-11a) and (7.7-1) that the velocity along the non-tie line path is constant and that the constant velocity is, in fact, the integration constant. The path itself is given by the linear relation

$$F_i - C_i^0 = v_c(C_i - C_i^0), \quad i = 2, 3 \quad (7.7-11b)$$

Since the above development applies for either independent species, we drop the subscript on v_c .

As Fig. 7-32 shows, the entire two-phase region is covered with a net of non-tie line paths along each of which the velocity is constant. Some of these paths cross the tie line paths, but others merge continuously with it at a point where the velocity along both paths is equal. The curve defining the locus of these intersection points is given by

$$\left(\frac{dF_2}{dC_2} \right)_{\text{tie line}} = \left(\frac{F_2 - C_2^0}{C_2 - C_2^0} \right)_{\text{nontie line}} \quad (7.7-12)$$

from Eqs. (7.7-4) and (7.7-11b). This curve is the singular curve discussed above wherein the discriminant of Eq. (7.7-5b) vanishes.

Figure 7-33 shows two fractional flux curves going from points J to I along the lines $A-A'$ and $B-B'$. These were selected because they are on tie lines that extend to the points J and I , respectively. The curves consist of three segments: a portion of unit slope corresponding to the single-phase regions in Fig. 7-32, horizontal portions corresponding to single-phase flow in the presence of another residual phase, and a curved portion corresponding to two-phase flow. The curve with the more compressed curved portion corresponds to the tie line nearest the plait point.

Figure 7-33 also shows the construction for the singular point as suggested by Eq. (7.7-12). Since the slope of a tie line path is the coherent velocity, the tie line

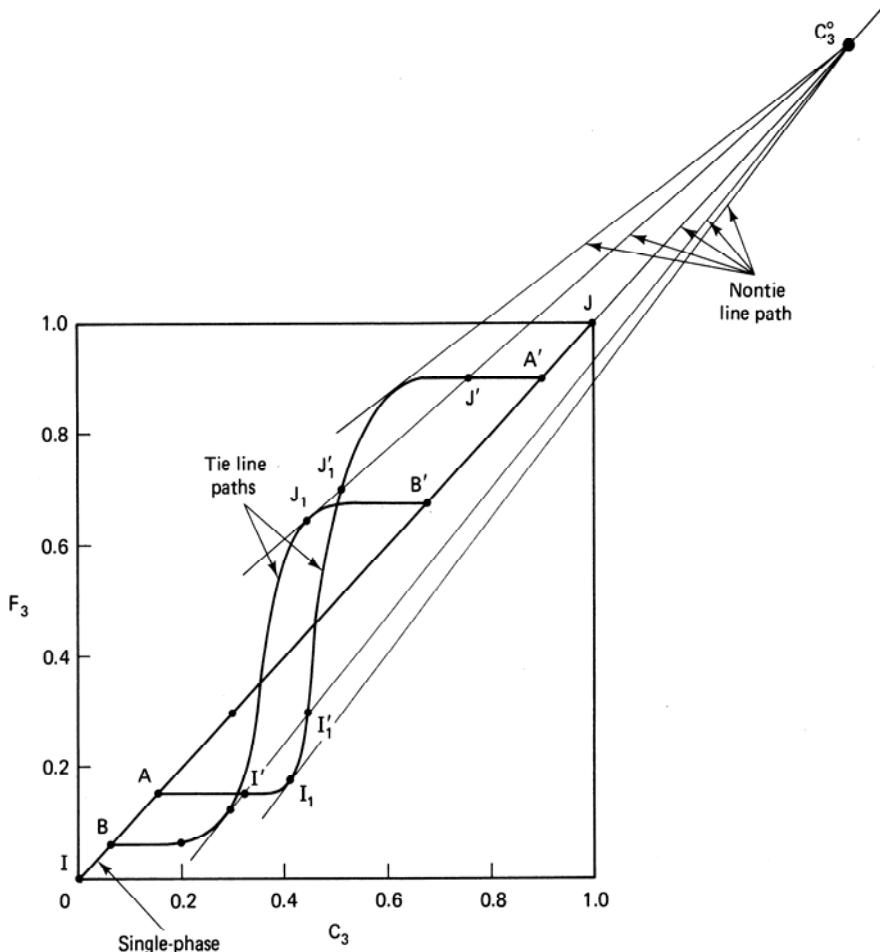


Figure 7-33 Fractional flux curves for Fig. 7-32

paths are slow outside the singular point intersections, and fast within the intersections. Understanding how a given tie line path can be both fast and slow is important for what follows.

You should compare both the above constructions with those in Fig. 5-12(d). Just as there are a variety of possibilities in Fig. 5-12, because of the variety of fractional flow shapes, so there are several possible behaviors for the singular curves. For example, a fractional curve without an inflection (Fig. 5-12a) will have one singular curve that coincides with a residual phase saturation curve.

We use the curves in Fig. 7-33 to select the only physically possible composition routes in Fig. 7-32. Before doing this, we remind you of the principles established in Sec. 5-6 for centered simple waves.

1. The composition route must stay on the composition path segments in the ternary diagram.
2. The composition velocity must decrease monotonically in the upstream direction. (This rule is actually a special case of the more general statement that all concentrations must be single valued.)
3. The correct composition route must be insensitive to infinitesimal perturbations in concentration. (This rule was not needed in Chap. 5, but it is here.)

We build the composition path from I to J in three segments, each of which must satisfy these rules.

Consider first the displacement of J_1 by J . There are an infinite number of paths between J and J_1 , but we consider only the two extreme routes $J \rightarrow J' \rightarrow J_1$ and $J \rightarrow B' \rightarrow J_1$. The second path is nonphysical because it involves a fast segment (in the single-phase region) upstream of the slow segment between B' and J_1 . We could resolve this by putting a shock directly from J to J_1 but this would no longer follow the composition paths. Route $J \rightarrow J' \rightarrow J_1$ also contains fast paths upstream of slow paths, but the resulting resolution into shocks (Fig. 7-34a) remains on the composition paths. In fact, this is the only route between the two extremes we discuss here that remains so because the switch from one tie line to the other, J to J_1 , takes place along a non-tie line path.

We see that the general use of non-tie line paths is to switch between tie lines. Figure 7-34(b) shows a composition profile for this displacement. The displacement shocks across the residual phase 2 saturation, causing complete recovery of this phase. This recovery, which takes place in the absence of lowered interfacial tension and developed miscibility, occurs because phase 2 dissolves into the injected phase J . Dissolution waves are normally inefficient since their propagation velocity is slow (Fig. 7-34).

These comments also apply to the path from I'_1 to I . Of the two extreme routes, $I'_1 \rightarrow I_1 \rightarrow I$ and $I'_1 \rightarrow A \rightarrow I$, only the latter yields a route along which the shock resolutions will remain on the composition path segments. Figure 7-35 shows the construction and corresponding profiles.

By comparing the routes $J \rightarrow J_1$ and $I'_1 \rightarrow I$, we see both entry and exit from

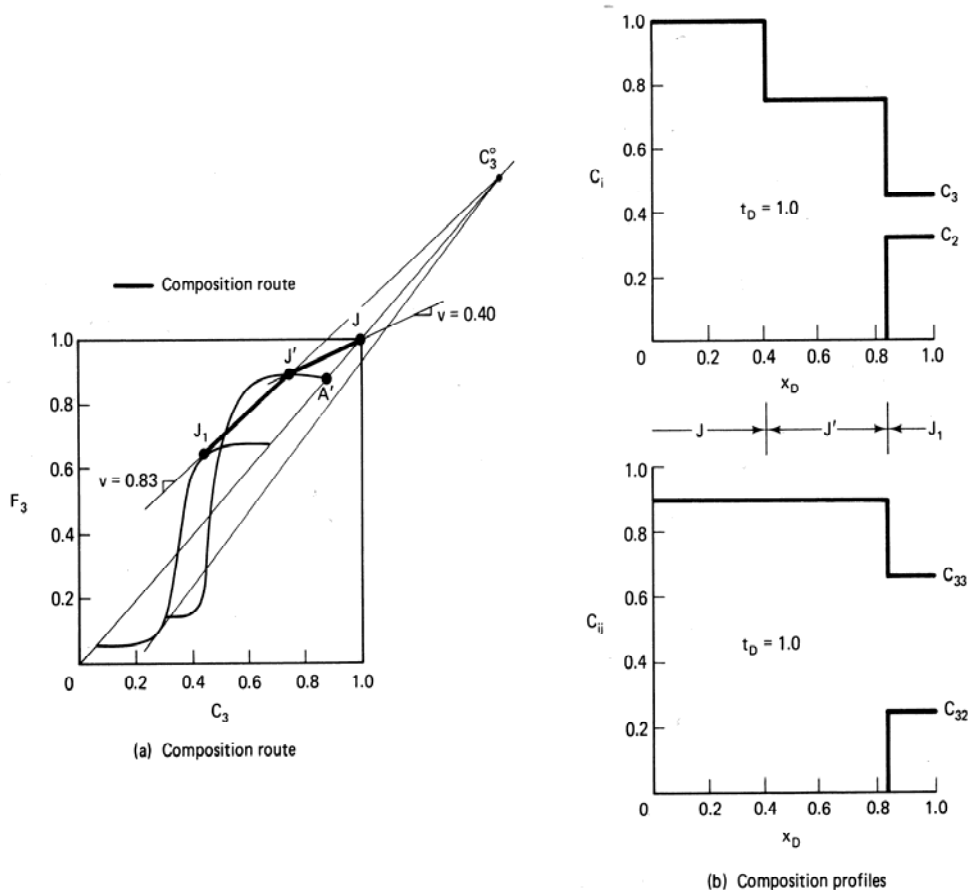


Figure 7-34 Composition route and profiles for displacement $J \rightarrow I_1$

a two-phase region take place along tie line extensions. Further, both entry and exit contain slow shocks, which are the direct result of the slow segments of the fractional flux curves. If I'_1 were above the equivelocity curve in Fig. 7-35(a), the route would follow a fast shock along the tie line nearest the plait point.

The third segment, J_1 to I_1 , follows a single tie line path whose velocity is given by the Buckley-Leverett construction (Fig. 7-36) from Eq. (7.7-4).

In a sense, the above constructions, particularly I'_1 to I , are misleading when applied to the entire displacement from I to J because the rules for centered simple waves must apply globally rather than individually to segments. To see this, consider the four possible composition routes from J to I : $J \rightarrow J' \rightarrow J_1 \rightarrow I$, $J \rightarrow J'_1 \rightarrow J_1 \rightarrow I$, $J \rightarrow I'_1 \rightarrow I_1 \rightarrow I$, and $J \rightarrow J'' \rightarrow J_1 \rightarrow I$. After you carefully consider each case, with shock segments interspersed, the requirement of a monotonically increasing concentration velocity forces you to see the only correct choice is $J \rightarrow J' \rightarrow J_1 \rightarrow I$. The immiscible displacement $J \rightarrow I$ will consist of two shock segments between which is a small spreading wave; these are sketched schematically in Fig. 7-37a.

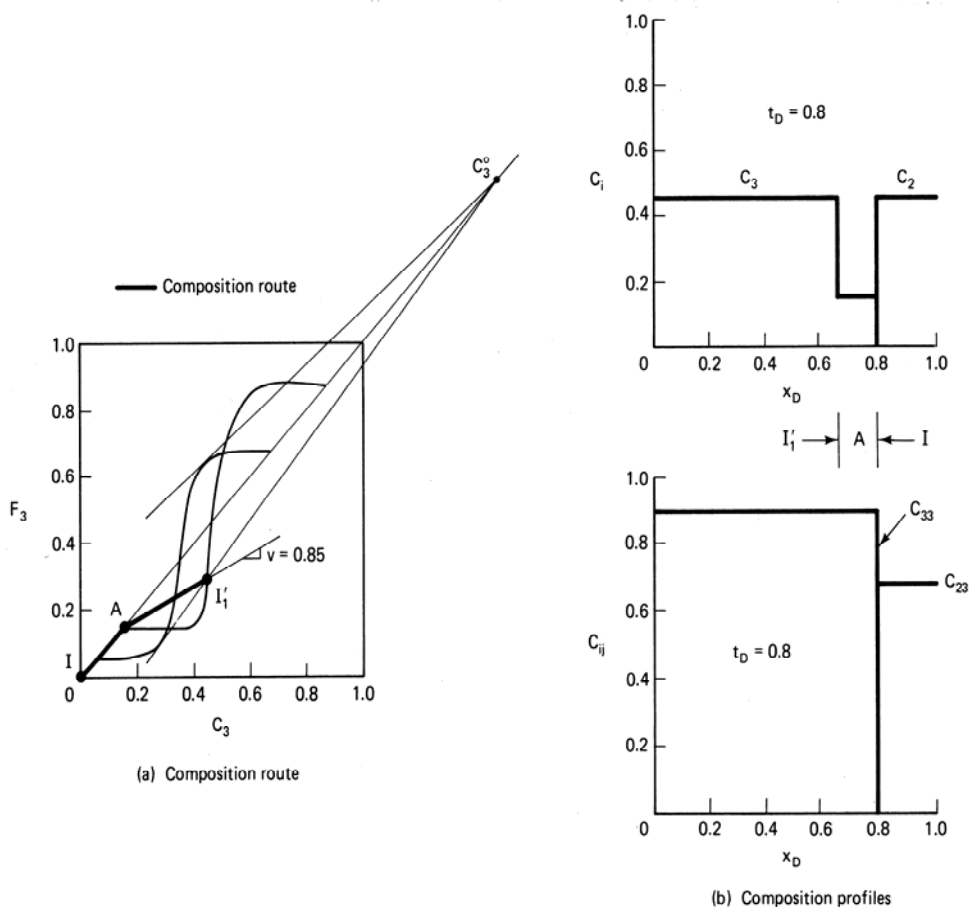


Figure 7-35 Composition route and profiles for displacement $I'_1 \rightarrow I$

As in all MOC problems, an infinite number of mathematical solutions exist, but by assumption, only one physical solution exists. Finding the physical solution involves trial and error according to the following procedure:

1. Locate a tentative composition route between the injected and initial conditions on the fractional flux diagram. This route consists of segments that conform to the paths we discussed above.
2. Resolve all physical inconsistencies along the tentative route with shocks. In doing this, assume the differential and integral composition routes are the same.
3. Discard any tentative solution in which the shock resolution leads to a route that does not follow the composition path sequence. When this happens, return to step 1 with another tentative route. The correct solution is usually clear after a few trials.

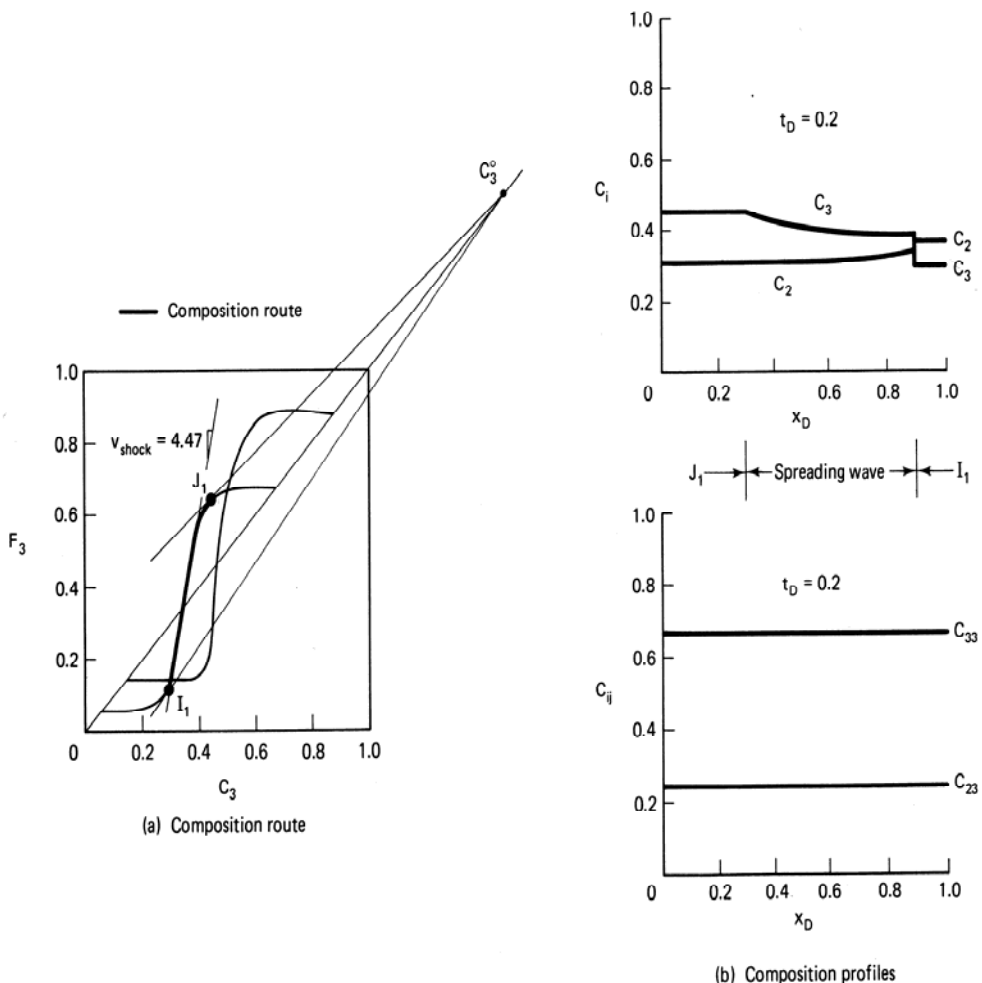


Figure 7-36 Composition route and profiles for displacement $I_1 \rightarrow I'$

These rules enable us to sketch the composition routes for the three types of displacements (Fig. 7-37). The composition route of the immiscible displacements (Fig. 7-37a) both enters and exits the two-phase region on tie line extensions. The entering segment is an extremely slow shock (a solubilization wave), which is the consequence of the residual phase saturations. If the system includes more than three true components—that is, at least one apex was a pseudocomponent—the displacement would not revert to single-phase behavior as suggested by Fig. 7-37(a) (Gardner and Ypma, 1982). Compare Fig. 7-37(a) to Fig. 7-16.

The vaporizing gas drive process (Fig. 7-37b) shows a composition route that approaches the binodal curve on a tie line extension and then follows the binodal curve until it reaches a point on a straight line tangent to the initial composition. Compare Fig. 7-37(b) to Fig. 7-14.

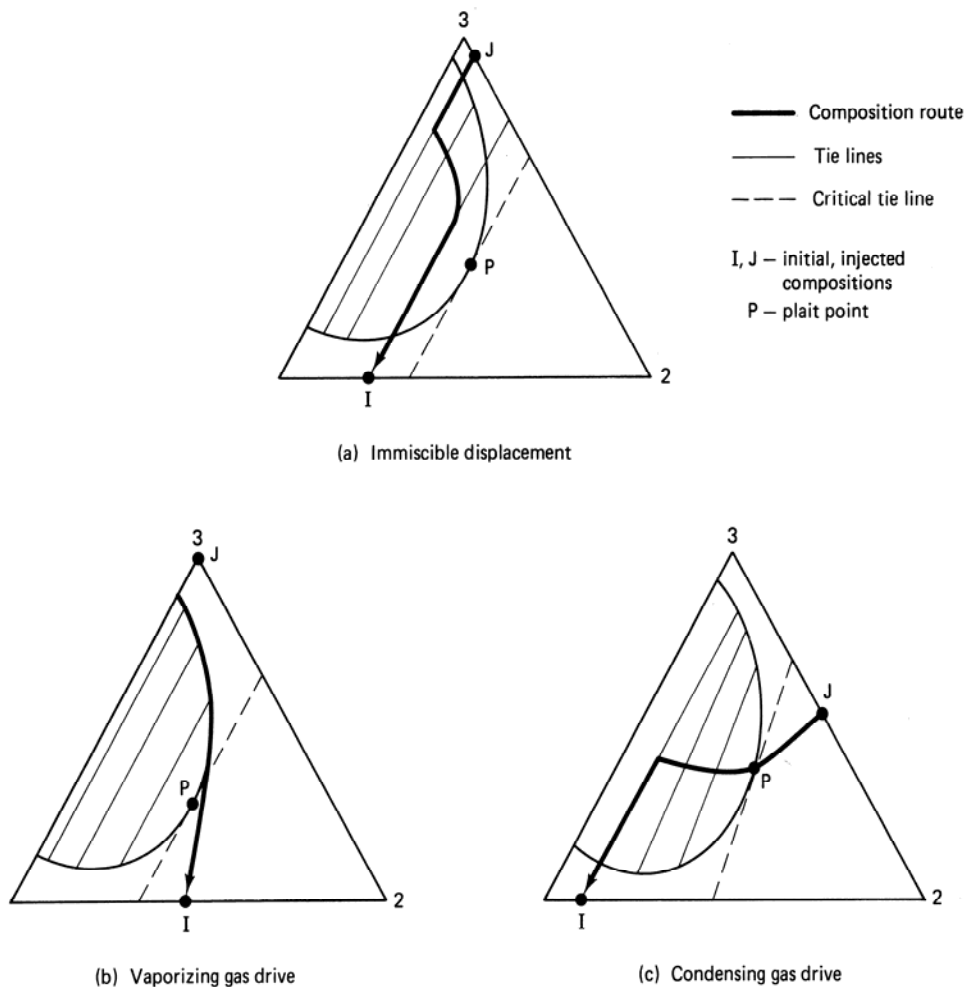


Figure 7-37 Composition routes for immiscible and developed miscibility processes

In the condensing gas drive process (Fig. 7-37c), the composition route enters the two-phase region through the plait point (Hutchinson and Braun, 1961), follows the equivelocity path, and then exits from the two-phase region on a tie line extension. The route definitely passes through the two-phase region, but it does so as a shock since the concentration velocity on the equivelocity curve is unity, and the tie line extension segment is a shock. Compare Fig. 7-37(c) to Fig. 7-15. Auxiette and Chaperon (1981) give an experimental investigation of these processes.

Both developed miscibility cases will appear as a first-contact displacement in the absence of dissipation. The similarity between developed and first-contact displacements justifies using first-contact approximations on all the developed miscibility displacements we discuss below.

First-Contact Miscible Displacements in the Presence of an Aqueous Phase

Water does not affect hydrocarbon phase behavior, and the water solubility of most solvents is small. But the inevitable presence of an aqueous phase can affect displacement behavior through fractional flow effects. In this section, we investigate the effects of an aqueous phase on a first-contact miscible displacement. Although the treatment here can be given formally, as was that discussed above, we present instead an entirely equivalent, but more direct, approach based on fractional flow curves.

To do this, we assume incompressible fluids and rock, no dissipative effects, and solvent–water relative permeabilities are the same as oil–water relative permeabilities. Thus a water–solvent fractional flow f_1^s differs from a water–oil fractional flow f_1 only by the difference between the use of solvent and oil viscosities and densities. Figure 7-38 shows both the f_1 and f_1^s curves based on relative permeabilities from Dickey et al. (1972). Because the relative permeabilities do not change, residual phase saturations of both the aqueous and oleic phases are invariant. The initial condition I in the one-dimensional displacement is uniform with water cut f_{1I} .

We take an arbitrary injection condition J to be comprised of some pre-specified proportion of solvent and water f_{1J}^s given on the solvent–water curve. Injecting water and solvent together in the so-called water-alternating-gas (WAG) process is commonly used in solvent floods. The solvent–water mixture has better volumetric sweep efficiency and is less prone to viscous fingering than solvent alone (Caudle and Dyes, 1958). The volumetric flow rate ratio of water to solvent in the injected fluid is the *WAG ratio* W_R , given by

$$f_{1J}^s = \frac{W_R}{1 + W_R} \quad (7.7-13)$$

In Eq. (7.7-13) and hereafter, we assume no solubility of solvent ($i = 3$) or oil ($i = 2$) in the aqueous ($i = j = 1$) phase, and we assume no solubility of water in the hydrocarbon ($j = 2$) phase.

In an actual WAG process, the water and solvent are usually injected in alternate slugs so that the cumulative volumes of solvent and water really define the WAG ratio rather than Eq. (7.7-13). The differences in displacement behavior caused by simultaneous injection rather than alternating injection have been investigated by Welch (1982).

Since the displacement is first-contact miscible, the wave between the injected solvent and the oil is indifferent. Hence the oil–solvent wave velocity is

$$v_3 = \frac{1 - f_{1J}^s}{1 - S_{1J}} \quad (7.7-14)$$

from Eq. (5.4-5b). Equation (7.7-14) neglects solvent adsorption. v_3 can also be written in terms of the change in water saturation change across the solvent–oil front

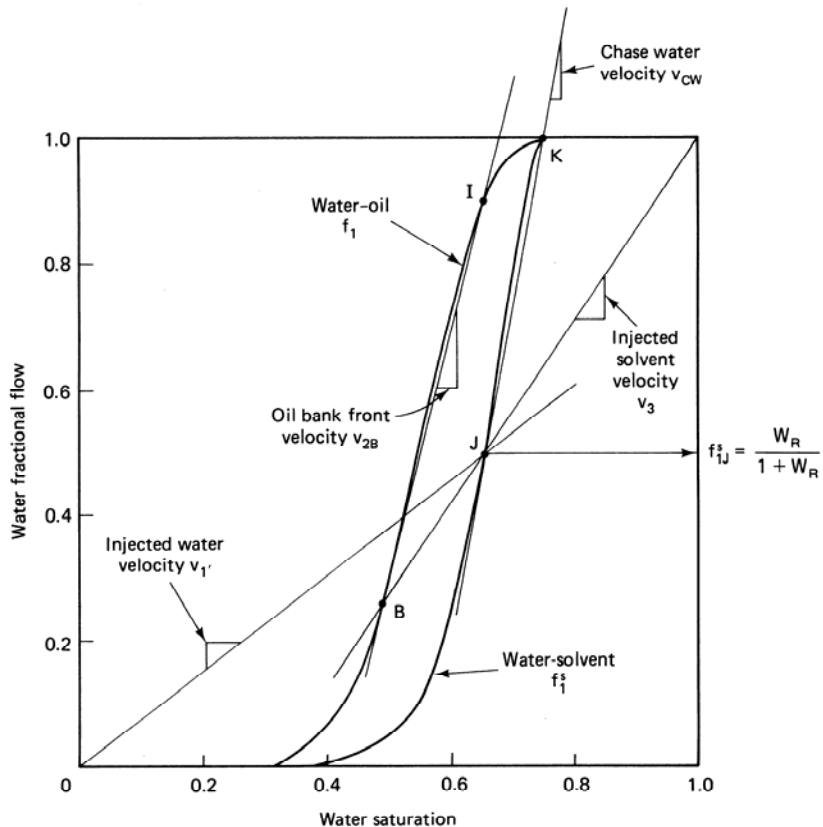


Figure 7-38 Schematic fractional flow construction for first-contact miscible displacements in the presence of an aqueous phase

$$v_3 = \frac{f_{1J}^s - f_{1B}}{S_{1J} - S_{1B}} \quad (7.7-15)$$

Equation (7.7-14) is the equation of a straight line from the upper right-hand corner of the fractional flow plot through the injected conditions (Fig. 7-38). Equating Eq. (7.7-14) to Eq. (7.7-15) says if this line is continued, its intersection with the water-oil fractional flow curve will give the water and oil saturation and fractional flow in the region ahead of the solvent-oil wave. Since $1 - f_{1B}$ is larger than $1 - f_{1I}$, the displaced oil forms a region of high oil saturation or *oil bank* ahead of the solvent-water front.

The leading edge of this oil bank flows with specific velocity v_{2B} given by

$$v_{2B} = \frac{f_{1I} - f_{1B}}{S_{1I} - S_{1B}} \quad (7.7-16)$$

also from Eq. (5.4-5b). This is the equation of a straight line from the initial condi-

tions I to the oil bank, point B in Fig. 7-38. Since the injected water miscibly displaces the resident water, the specific velocity of the displaced water wave v_1' is the straight line from the lower left corner of the fractional flow plot to the injected conditions (compare the lines for v_1' and v_3 with case B in Fig. 5-12).

The velocity of the connate water banked up by the injected water is

$$v_{l'} = \frac{f_{1J}^s}{S_{1J}} \quad (7.7-17)$$

which is also shown in Figs. 7.38 and 7.39. The water ahead of this wave is banked-up connate water which, for a secondary solvent flood ($f_{1I} = 0$), constitutes a waterflood ahead of the solvent front. Caudle and Dyes (1958) verified experimentally that injecting at a WAG ratio so that the banked-up connate water does not propagate faster than the solvent resulted in optimal oil recovery.

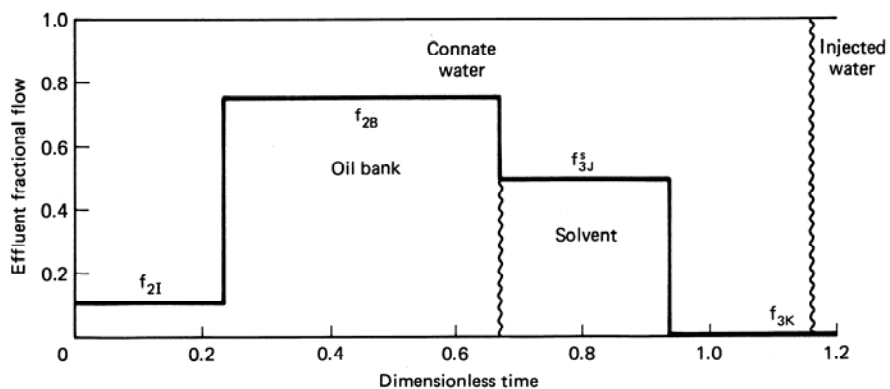
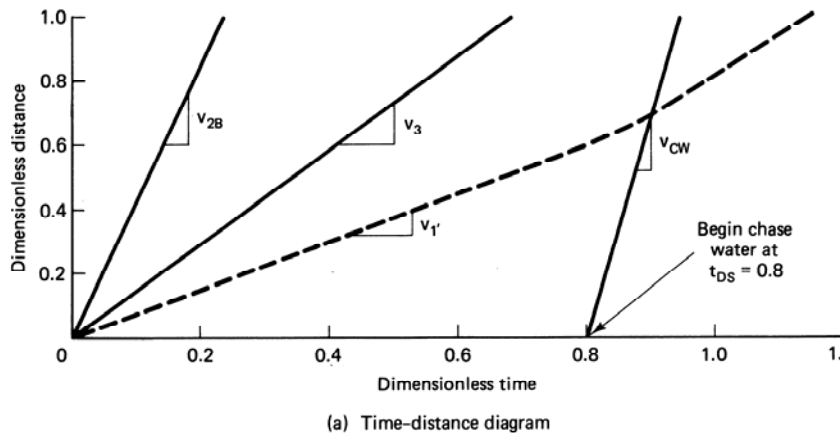


Figure 7-39 Time-distance diagram and effluent history plot for the displacement

It is also possible to treat slug behavior with fractional flow theory. Suppose after injecting at condition J for some dimensionless time t_{Ds} , we follow with chase water at condition K on the diagram. Since the slope of the solvent–water fractional flow curve is monotonically decreasing from K to J , this displacement front is a shock with specific velocity

$$v_{cw} = \frac{1 - f_{1J}^s}{1 - S_{2r} - S_{1J}} \quad (7.7-18)$$

whose straight-line construction is also shown in Fig. 7-38. If the chase fluid were to be a second gas having the same properties as and first-contact miscible with the solvent, the velocity of the chase-fluid–solvent front would be given by the slope of the f_1^s - S_1 curve since the slope of this curve is monotonically increasing from $S_1 = S_{1r}$ to the injected conditions.

Figure 7-39 shows the time–distance diagram and effluent history for the displacement in Fig. 7-38. We have taken $t_{Ds} = 0.8$ to avoid interference between the oil-bank–solvent and the solvent–chase water waves. In the effluent history plot, the miscible displacement fronts are designated by a wavy line.

Several general observations follow from these plots. First, the ultimate oil recovery is complete—that is, the final condition in the system is zero oil saturation. Of course, this is the natural consequence of first-contact miscible displacements where no residual phases are allowed. Second, oil production ceases when solvent breaks through. The moderately early solvent breakthrough is the consequence of the pore space inaccessible to the solvent caused by the presence of irreducible water: With no water present, the solvent slug always breaks through near $t_D = 1$. Based on hydrocarbon pore volumes ($1 - S_{1r}$), the solvent in Fig. 7-39 breaks through at $t_D = 0.96$ HCPV, which is much more in line with dispersion theory. Finally, the amount of solvent produced (0.14 PV) is considerably less than the amount injected (0.4 PV). This reduction is the consequence of trapping of the hydrocarbon-miscible solvent by the chase water. If the solvent slug size t_{Ds} were less than about 0.6, the chase-water–solvent front would have overtaken the solvent–oil-bank front and trapped some oil. Such an observation suggests a procedure whereby we could select the minimum solvent slug size ($t_{Ds} = 0.53$ in Fig. 7-39) that effects complete oil recovery.

7-8 SOLVENT FLOODS WITH VISCOUS FINGERING

Unfortunately, first-contact miscible displacements actually behave considerably differently than that shown in Fig. 7-38. Figure 7-40 shows the experimental results of a developed miscible displacement in a Berea core in which oil initially at residual conditions is displaced by a CO_2 solvent in a $W_R = 0$ displacement. The deviation of this displacement from a straight-line composition route in the ternary diagram was small. In the experimental displacement, the water cut was initially 1.0 and decreased to about 0.15 at $t_D = 0.15$. The water cut remained essentially constant until about

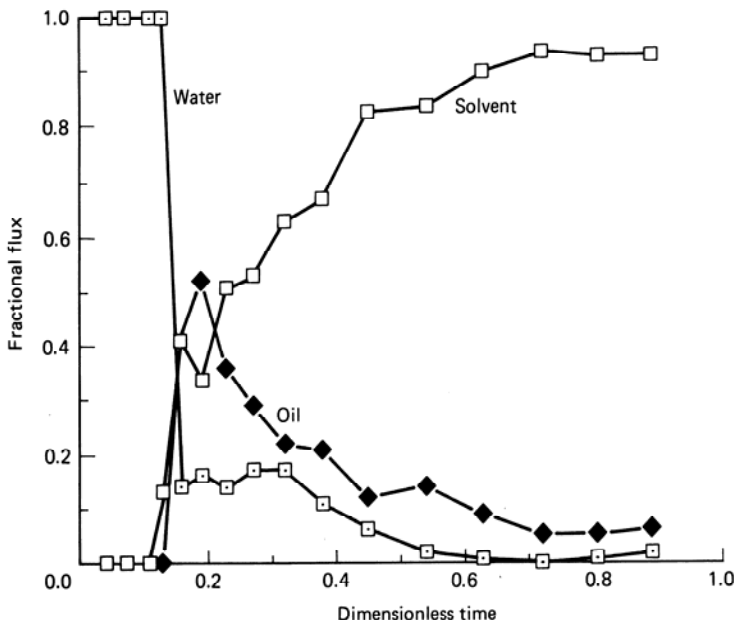


Figure 7-40 Effluent history of a carbon dioxide flood (from Whitehead et al., 1981)

$t_D = 0.33$, at which point, it decreased gradually to 0. But when the water cut originally fell to $t_D = 0.14$, both oil and solvent broke through. This leaves a remaining oil saturation of about 0.25 at termination. It is unclear if 100% oil recovery would have been obtained had the experiment been continued. Several pore volumes of solvent injection would have been required, however.

The primary cause of the simultaneous oil and solvent breakthrough and prolonged oil recovery in experimental displacements is viscous fingering. In Sec. 6-8, we concluded that miscible displacements with typical solvents were always unstable, barring a gravity stabilization or a boundary effect, because the solvent–oil mobility ratio is greater than 1. Here we give descriptions of the character of simultaneous oil and solvent flow after the onset of fingering.

Heuristic Models

Because of the chaotic nature of viscous fingering, a rigorous mathematical theory is not possible. The behavior of a fingering displacement may be estimated by various heuristic theories, including (1) a modification of fractional flow theory (Koval, 1963), (2) rate-controlled mass transfer between solvent and oil fingers (Dougherty, 1963), (3) defining a suitably weighted mixture viscosity (Todd and Longstaff, 1972), (4) accounting for mixing in fingers directly (Fayers, 1984), and (5) defining a composition-dependent dispersion coefficient (Young, 1986).

In this section, we deal exclusively with the Koval theory; we leave the others as an exercise. By excluding the others, we do not imply the Koval approach is

superior since all involve empirical parameters that must be determined by history matching. However, the Koval theory is in common use, and it fits naturally into our fractional flow theme.

The mixing zone length (the dimensionless distance between prespecified values of a cross-sectionally averaged concentration profile) of a fingering displacement, in the absence of boundary effects, grows in proportion to time. This observation prompted Koval to instigate a fractional flow theory for viscous fingering. If viscous fingers initiate and propagate, their growth in horizontal plane flow would look something like the cross section in Fig. 7-41, where the oil and solvent are in segregated flow. The displacement is first-contact miscible, with no dissipation, and without water present. If dissipation can vertically smear the fingers, the mixing zone will grow in proportion to the square root of time, as in dispersion theory. This growth can be quite small if longitudinal dispersion is small or the system length is large (Hall and Geffen, 1965).

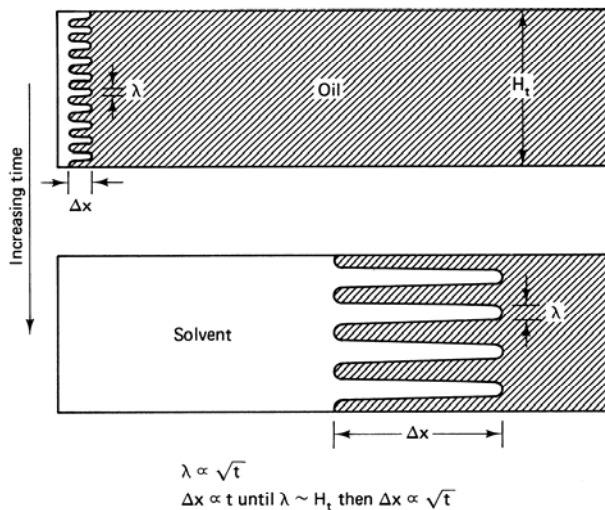


Figure 7-41 Idealization of viscous finger propagation (from Gardner and Ypma, 1982)

With these qualifications, the volumetric flow rate of solvent across a vertical plane within the mixing zone is

$$q_3 = -\frac{A_3 k}{\mu_3} \left(\frac{\partial P}{\partial x} \right) \quad (7.8-1a)$$

and that of oil is

$$q_2 = -\frac{A_2 k}{\mu_2} \left(\frac{\partial P}{\partial x} \right) \quad (7.8-1b)$$

where A_3 and A_2 are cross-sectional areas of oil and solvent. There are no relative permeabilities or capillary pressures in these equations since the displacement is first-contact miscible. These equations assume a horizontal displacement. The fractional flow of solvent in the oleic phase across the same vertical plane is

$$f_{32} = \frac{q_3}{q_3 + q_2}$$

by definition, which, when Eq. (7.8-1) is substituted, yields

$$f_{32} = \frac{A_3 / \mu_3}{A_3 / \mu_3 + A_2 / \mu_2} \quad (7.8-2)$$

Equation (7.8-2) assumes the x -direction pressure gradients are equal in the oil and solvent fingers. Because the displacement is in plane flow, the oil and solvent cross-sectional areas are proportional to average concentrations, or

$$f_{32} = \left(1 + \frac{1}{v} \left(\frac{1 - \bar{C}_{32}}{\bar{C}_{32}} \right) \right)^{-1} \quad (7.8-3)$$

where v is the oil–solvent viscosity ratio, and \bar{C}_{32} is the average solvent concentration in the oleic phase across the cross section.

Equation (7.8-3) is a description of the segregated flow fingering in Fig. 7-41. Koval had to modify the definition of v to match experimental displacements. The final form of the solvent fractional flow is

$$f_{32} = \left(1 + \frac{1}{K_{val}} \left(\frac{1 - \bar{C}_{32}}{\bar{C}_{32}} \right) \right)^{-1} \quad (7.8-4)$$

where K_{val} is the Koval factor.

Koval Corrections

The Koval factor modifies the viscosity ratio to account for local heterogeneity and transverse mixing in the following fashion:

$$K_{val} = H_K \cdot E \quad (7.8-5)$$

The parameter E changes the viscosity ratio to account for local mixing

$$E = (0.78 + 0.22v^{1/4})^4 \quad (7.8-6)$$

The consequence of Eq. (7.8-6) is that the numerical value of E is usually smaller than that of v . That is, the effect of fingering is not as severe as it appears from the original viscosity ratio. The 0.22 and 0.78 factors in Eq. (7.8-8) seem to imply the solvent fingers contain, on the average, 22% oil, which causes the viscosity ratio attenuation through the quarter-power mixing rule. In fact, Koval eschewed this interpretation by remarking that the numerical factors were simply to improve the agreement with experimental results. This would seem to restrict Eq. (7.8-6) to the exact class of experiments reported by Koval. Remarkably, Claridge (1980) has shown that the 0.22–0.78 factors accurately describe fingering displacements over large ranges of transverse dispersion. Very likely the finger dilution is being caused by viscous crossflow since the mechanism is consistent with linear mixing zone growth (Waggoner and Lake, 1987).

The heterogeneity factor H_K corrects the reduced viscosity ratio for the local heterogeneity of the medium. Selecting the correct value for H_K is the most subjective feature of the Koval theory. In Fig. 6-8, the heterogeneity factor was calculated from the Dykstra-Parsons coefficient. It has also been correlated with the longitudinal Peclet number (Gardner and Ypma, 1982).

The fractional flow expression (Eq. 7.8-4) is the same as the water fractional flow in a waterflood where the oil and water have straight-line relative permeabilities. For such a case (see Exercise 5E), the Buckley-Leverett equation (Eq. 5.2-10) may be integrated analytically to give the following expression for effluent fractional flow:

$$f_{32} |_{x_D=1} = \begin{cases} 0, & t_D < 1 - \frac{1}{K_{val}} \\ \frac{K_{val} - \left(\frac{K_{val}}{t_D} \right)^{1/2}}{K_{val} - 1}, & \frac{1}{K_{val}} < t_D < K_{val} \\ 1, & K_{val} < t_D \end{cases} \quad (7.8-7)$$

The oil fractional flow is $1 - f_{32} |_{x_D=1}$. This equation has been compared to experimental data in the original Koval paper and elsewhere (Claridge, 1980; Gardner and Ypma, 1982).

Koval with Mobile Water

The Koval theory applies to first-contact miscible displacements in the absence of flowing water. The theory may be readily generalized to fingering first-contact miscible displacements with water present by modifying the overall flux and concentration definitions (see Sec. 5-4). The overall flux for oil and solvent becomes

$$F_2 = (1 - f_{32})f_2 \quad (7.8-8a)$$

$$F_3 = f_{32}f_2 \quad (7.8-8b)$$

where f_1 and f_2 are the actual water and hydrocarbon fractional flow functions, and f_{32} is given by Eq. (7.8-4). To be consistent with Eq. (7.8-6), the hydrocarbon phase viscosity in both f_1 and f_2 is given by the quarter-power mixing rule.

The overall concentrations of the oil and solvent are

$$C_2 = (1 - \bar{C}_{32})S_2 \quad (7.8-9a)$$

$$C_3 = \bar{C}_{32}S_2 \quad (7.8-9b)$$

The water concentration is simply S_1 because there is no solvent solubility in the water phase. Equations (7.8-8) and (7.8-9), substituted into the conservation equations for oil and solvent, may then be solved by the simple wave procedure discussed in Sec. 5-7 for the oil-gas-water problem.

Figure 7-42 shows the effluent fluxes for four displacements using this procedure. Figure 7-42(a) is for a non-WAG secondary flood, which is simply the results of the original theory (Eq. 7.8-7). Figure 7-42(b) is for a tertiary non-WAG

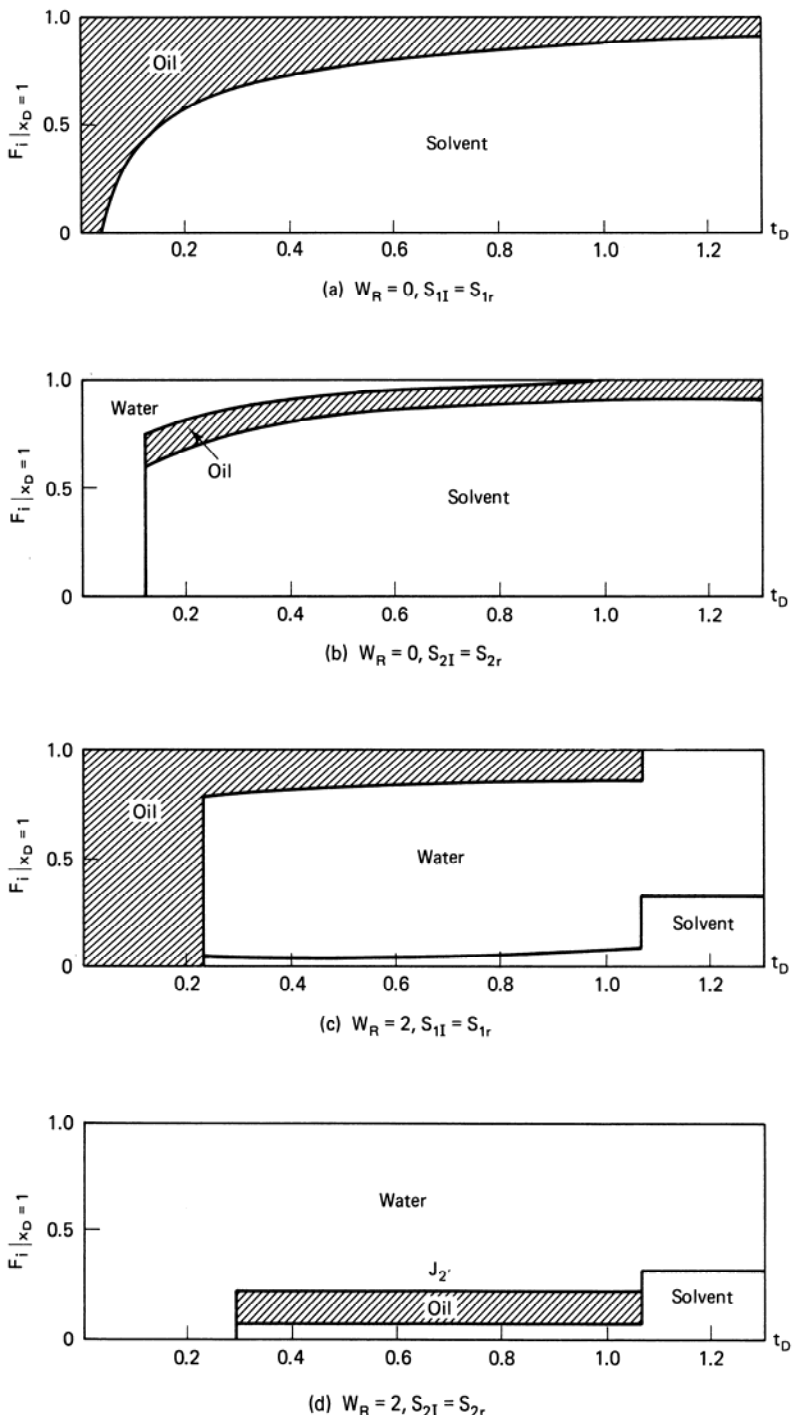


Figure 7-42 Effluent histories for four fingering cases

displacement. Figures 7-42(c) and 7-42(d) are for secondary and tertiary WAG displacements ($W_R = 2$). The oil and water relative permeabilities in Figs. 7-39 and 7-42 are the same so that comparing Fig. 7-39 and Fig. 7-42(d) should reveal the effect of fingering on a first-contact miscible displacement with water present.

For both cases, the oil is produced as a bank of constant cut. But the bank oil cut is smaller for the fingering displacement, and the oil breakthrough and complete sweepout times are later. In the fingering case, oil and solvent break through together though the solvent is at low cut. By comparing Figs. 7-42(a) and 7-42(c) and Figs. 7-42(b) and 7-42(d), we see that, regardless of the initial conditions, the WAG procedure delays solvent breakthrough and hastens complete oil recovery.

Based on the comparisons in Fig. 7-42, it appears that WAG is universally better than injecting solvent alone, particularly when the solvent efficiency is considered. However, the presence of an initial mobile water saturation causes a residual oil saturation to even a first-contact displacement (see Sec. 7-9), and it is possible that the WAG process will cause this also.

Other methods besides WAG to improve mobility control in miscible flooding include the use of polymers (Heller et al., 1984) and foams. To date only foams have been extensively investigated, and since foams are envisioned to drive a variety of EOR processes, we delay their discussion until Chap. 10, where they more naturally fit after micellar-polymer flooding.

7-9 SOLVENT FLOODING RESIDUAL OIL SATURATION

A residual oil saturation in solvent flooding can come about by two broad phenomena: (1) a local heterogeneity (dead-end pores) in the permeable medium and (2) an interaction of dispersion or viscous fingering with the phase behavior. The former phenomenon occurs in first-contact miscible displacements, and the latter in developed miscible flood.

The definition of residual oil in a miscible flood (a paradoxical quantity) is slightly different from that in a waterflood. In a waterflood, residual oil is left behind as capillary-trapped globs, and no amount of throughput will displace this oil without some imposed change in the local capillary number. In a first-contact or developed miscible flood, all the oil, even that “trapped” by whatever mechanism, will eventually be recovered through extraction if enough solvent is injected. By residual oil in a miscible flood, then, we mean that quantity of oil left behind a solvent flood at some practical extreme of oil cut, oil rate, water–oil ratio, or gas–oil ratio (the data in Fig. 7-40 are up to a gas–oil ratio of about 550 SCM/SCM). Admittedly, this lacks the precision of the waterflood definition, but from the practical view of recovering oil economically, this distinction is not serious. By this definition, oil severely bypassed by a viscous finger is residual oil. Since we discussed capillary-trapped residual oil earlier in Sec. 3.4, we discuss other causes here.

Local Heterogeneity

To investigate the effects of local heterogeneity on trapped oil saturation, researchers have conducted experiments in laboratory cores on first-contact miscible displacements (Raimondi and Torcaso, 1964; Stalkup, 1970; Shelton and Schneider, 1975; Spence and Watkins, 1980). In these experiments, viscous fingering was suppressed by gravity stabilization or by matching the viscosity and density of the displacing and displaced fluids.

The miscible flood residual oil was found to depend on several things, the most important of which is the presence of a high mobile water saturation. A sample of this experimental data (Fig. 7-43) plots trapped oil saturation S_{2r}' , normalized by the waterflood residual oil saturation, versus the steady-state flowing water saturation. The normalized trapped oil saturations approach unity at high water saturations in these data and are close to zero for water saturations less than 50%. The steepness of the curves and the magnitudes of the residual saturations at high water saturation are of concern in displacements where a high water saturation is present (tertiary floods or WAG floods). The data in Fig. 7-43 were from displacements in strongly water-wet media. In oil-wet or intermediate-wet media, the trapping is not nearly as pronounced. Thus the trapped oil saturation has been correlated with capillary pressure curve hysteresis (Shelton and Schneider, 1975), a fractional relative permeability ratio (Raimondi and Torcaso, 1964), and

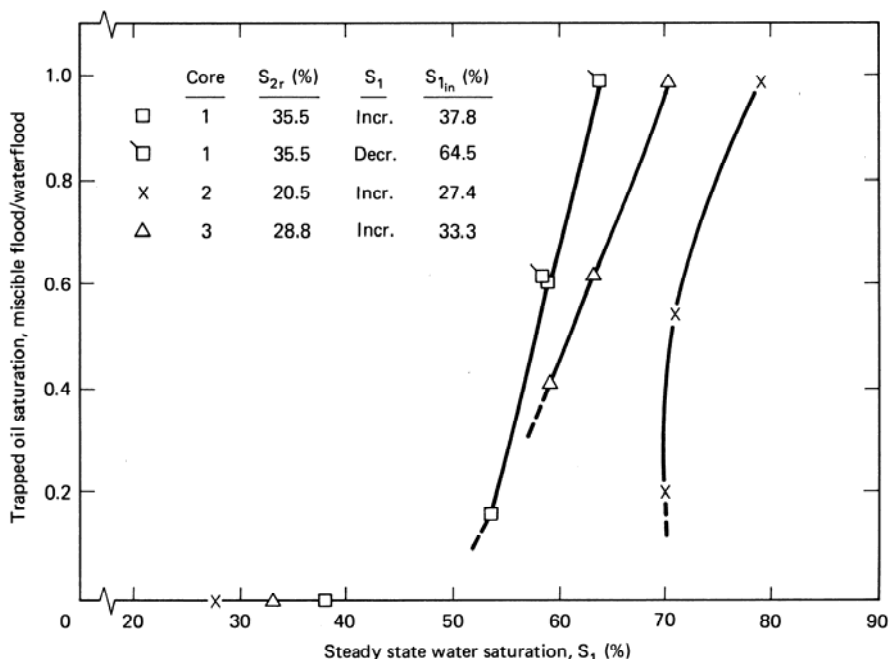


Figure 7-43 Oil trapped on imbibition as a function of water saturation (from Raimondi and Torcaso, 1964)

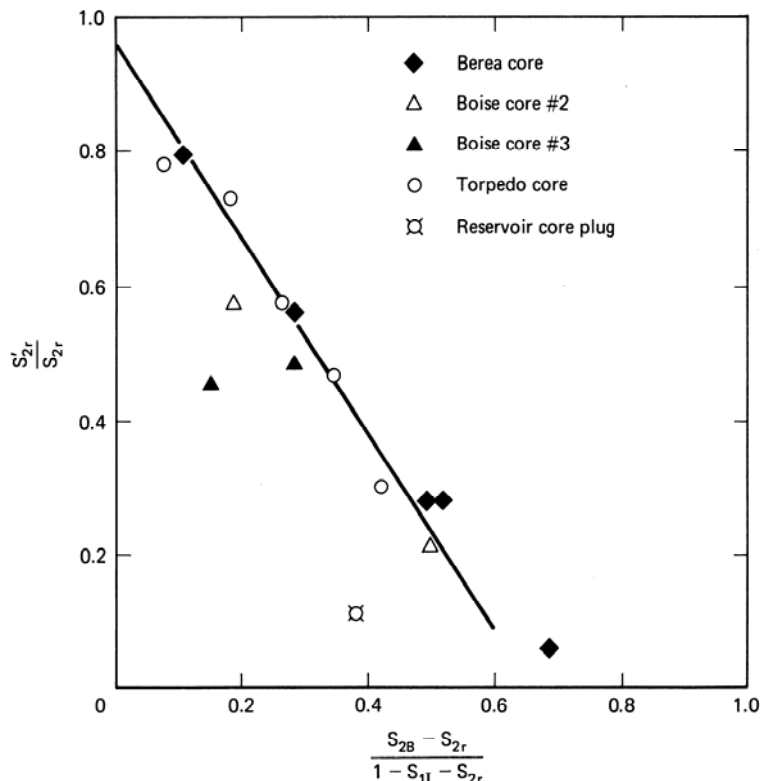


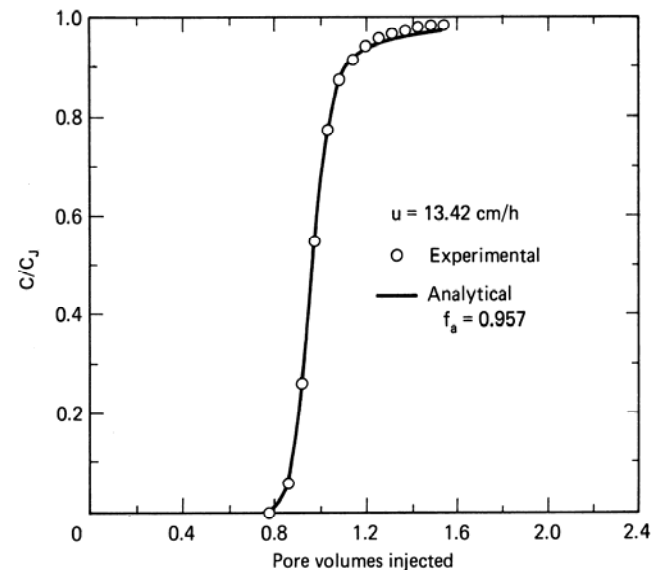
Figure 7-44 Influence of oil bank and residual oil saturation on the total stagnant hydrocarbon saturation (from Stalkup, 1970)

dimensionless oil bank saturation (Stalkup, 1970). Figure 7-44 shows the correlation of trapped or stagnant oil saturation with dimensionless oil bank saturation. S_{2B} is the oil bank saturation determined from the graphical construction in Fig. 7-39 and should contain corrections for the wettability of the medium since wettability is contained in the fractional flow curves. The oil bank saturation should contain corrections for injected water since the WAG ratio also affects the construction.

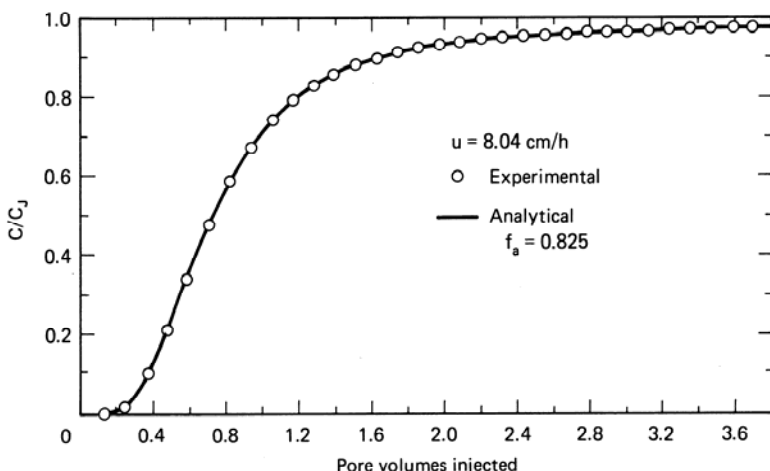
The most common interpretation for the effect of mobile water in miscible flood trapped oil saturation is that on a microscopic basis the water shields, or blocks, the solvent from contacting the oil. This explanation also qualitatively accounts for the effect of wettability since the oil and water phases are, depending on the wettability, differently distributed in the medium. In water-wet media, oil is contained in the large pores mostly away from the rock surfaces. The water phase is far more connected compared to the oil phase and thus could serve as a shield to oil originally present in pores not in the main flow channels. For oil-wet media, the phase distribution is reversed—the oil phase is the more continuous, and water is a less effective shield.

The interpretation of water blocking stagnant pores is somewhat like the dead-end pore model used to explain the behavior of water-free, first-contact

displacements. The capacitance or dead-end pore model was originally proposed to explain the concentration “tail” observed in the breakthrough curves of first-contact, stable miscible displacements. This tail is more pronounced in carbonates than in sandstones (Fig. 7-45) because the pore structure of a typical carbonate is more heterogeneous (Spence and Watkins, 1980). Mathematical solutions fit the breakthrough curves well (Fig. 7-45) even though the physical interpretation of the parameters in the dead-end pore model has been questioned (Coats and Smith, 1964).



(a) Sandstone media



(b) Carbonate media

Figure 7-45 Typical breakthrough curves (from Spence and Watkins, 1980)

The dead-end pore model also qualitatively explains other features of first-contact miscible flood trapping, so we summarize the mathematical theory here.

Consider a stable, first-contact miscible displacement, in the absence of water, flowing in a permeable medium where a fraction f_a of the pore space is available to flow and a fraction $(1 - f_a)$ is stagnant. Solvent can flow from or into the stagnant or dead-end pores only by diffusion, represented by a mass-transfer coefficient k_m . The conservation equation for solvent becomes in the absence of dispersion

$$\begin{aligned}\phi f_a \frac{\partial C_{32}}{\partial t} + u \frac{\partial C_{32}}{\partial x} &= -k_m (C_{32} - C_{3s}) \\ (1 - f_a) \frac{\partial C_{32}}{\partial t} &= k_m (C_{32} - C_{3s})\end{aligned}\quad (7.9-1)$$

where C_{32} and C_{3s} are the solvent concentrations in the flowing and dead-end pores. With dimensionless distance and time, these equations become

$$\begin{aligned}f_a \frac{\partial C_{32}}{\partial t_D} + \frac{\partial C_{32}}{\partial x} &= -N_{Da} (C_{32} - C_{3s}) \\ (1 - f_a) \frac{\partial C_{32}}{\partial t_D} &= N_{Da} (C_{32} - C_{3s})\end{aligned}\quad (7.9-2)$$

where $N_{Da} = k_m L \phi / u$ is the *Damkohler number*, a dimensionless quantity that is a ratio of the rates of diffusion from the dead-end pores to the bulk fluid flow. Equation (7.9-2) is a two-parameter (f_a and N_{Da}) representation of flow without dispersion. Deans (1963) gives the analytic solution to Eq. (7.9-2) subject to a step change in influent solvent concentration

$$\frac{C_{32}}{C_{eJ}} = \begin{cases} 0, & Z \leq 0 \\ 1 - e^{-Z} \int_0^Y e^{-\xi} - I_0(2\sqrt{\xi Z}) d\xi, & Z \geq 0 \end{cases} \quad (7.9-3)$$

where $Z = N_{Da}(t_D - x_D f_a) / (1 - f_a)$, $Y = N_{Da} x_D$, and I_0 is the modified Bessel function of the first kind, zero order. Equation (7.9-3) says the solvent concentration changes abruptly from zero to $C_{32}/C_{eJ} = e^{-Y}$ at $Z = 0$.

The solvent effluent history (at $x_D = 1$) is from Eq. (7.9-3)

$$\frac{C_{32}}{C_{eJ}} = \begin{cases} 0, & t_D \leq f_a \\ 1 - e^{-Z} \int_0^{N_{Da}} e^{-\xi} - I_0(2\sqrt{\xi Z}) d\xi, & t_D \geq f_a \end{cases} \quad (7.9-4)$$

Figure 7-46 plots Eq. (7.9-4) for fixed f_a and various N_{Da} . For very small N_{Da} , the breakthrough curve behaves normally with the pore space contracted by $(1 - f_a)$. For this case, the miscible flood trapped oil saturation would simply be $(1 - f_a)$ times the oil saturation in the dead-end pores since the solvent cannot enter the stagnant pores. But for very large N_{Da} , the effect of the stagnant pore space vanishes since mass transfer to and from the flowing fraction is rapid. In this extreme, the trapped oil saturation should vanish.

These observations partly explain the dependence of miscible flood trapped

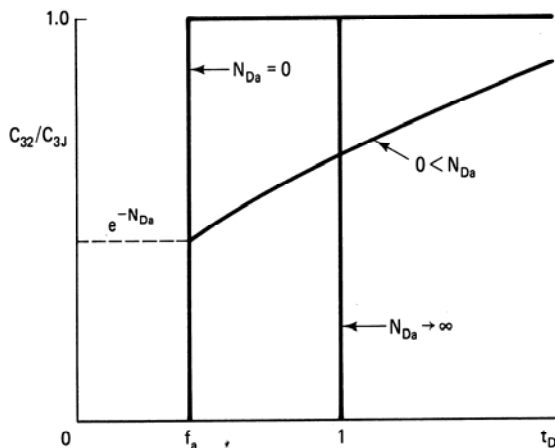


Figure 7-46 Effluent solvent concentration for fixed flowing fraction f_a and various N_{Da} ; no dispersion

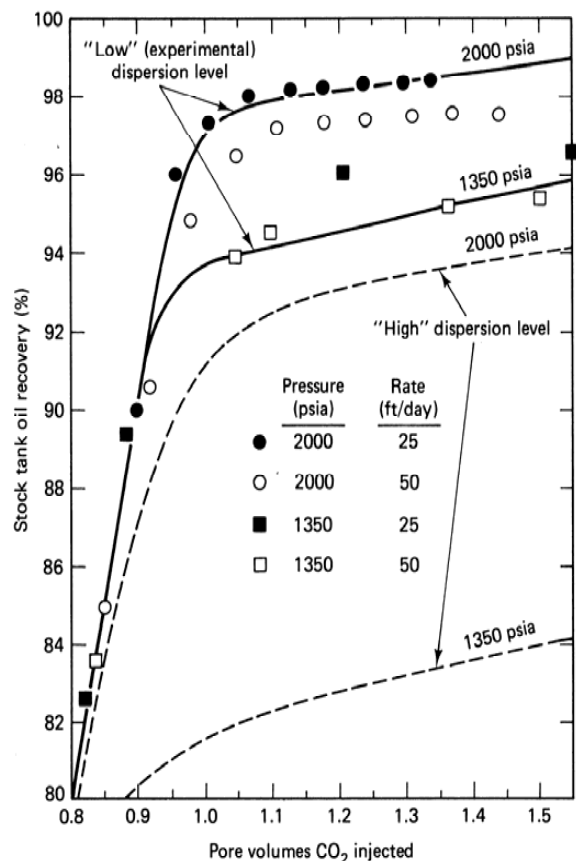
oil saturation on velocity and system length. As suggested by the definition of the Damkohler number, the trapped oil saturation should decrease with decreasing velocity and increasing system length. At field-scale conditions, large length and small velocity, the Damkohler number is usually much larger than in a laboratory experiment. Thus laboratory experiments may be overestimating miscible flood trapped oil saturation.

Including dispersion in Eq. (7.9-1) requires a numerical solution (Coats and Smith, 1964). Of course, the solutions so obtained fit experimental data better than Eq. (7.9-4) but do not alter the general conclusions.

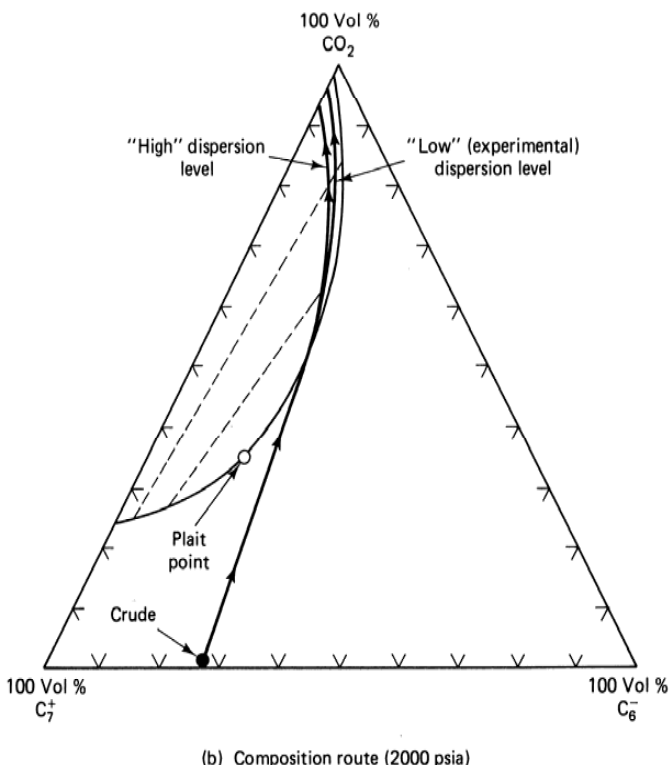
The effect of water blocking is difficult to see from the preceding mathematics. For conceptual clarity, it is best to separate the water-blocking and dead-end pore effects by dividing the permeable medium pore space into flowing, isolated, and dendritic fractions (Salter and Mohanty, 1982). The flowing pore space is the fraction through which a phase flows into and from at least one pore throat. The dendritic fraction is connected to the flowing fraction through a mass transfer coefficient as above but does not exhibit flow itself. The isolated fraction of a phase is completely surrounded by the other phase through which no diffusion can occur. The amounts and properties of all fractions are functions of the phase saturations, the wettability of the medium, and the saturation history. Generally, the isolated and dendritic fractions vanish as the nonwetting phase saturation increases. But these two nonflowing fractions can occupy most of the total pore space at low nonwetting phase saturations.

Phase Behavior Interference

When the miscibility of a displacement is developed, the analysis is considerably complicated because, besides the water-blocking effect, a solvent flood can now trap oil by interactions with the phase behavior. Fig. 7-47 gives results from a combined experimental and theoretical study of Gardner et al. (1981) that shows the results of CO_2 displacements at two different pressure and dispersion levels. At both pressures,



(a) Experimental effluent histories



(b) Composition route (2000 psia)

Figure 7-47 Results of CO_2 displacements at two different pressure and dispersion levels (from Gardner et al., 1981)

the displacements are vaporizing gas drives. Still, the lower pressure gives a measurably lower oil recovery than the higher pressure. The effect is relatively insensitive to rate, and there was no mobile water, indicating the lower recovery is caused by something more than the dead-end pore effect.

Figure 7-47(b) shows the composition route for the 13.6 MPa (2,000 psia) displacement in Fig. 7-47(a). Dispersion causes the composition route for this developed miscibility displacement to enter the two-phase region (compare this to the no-dispersion extreme in Fig. 7-37b). This intrusion will lower oil recovery because the trapped phase saturations within the two-phase region are large, the interfacial tension between the two hydrocarbon phases being large. Though the effect of dispersion on the experimental data ("low" dispersion level) is relatively minor, the simulated effect at the high dispersion level is pronounced.

The displacements in Fig. 7-47 were gravity stabilized so that it would be proper to ignore viscous fingering. That this phenomenon also contributes to the trapped oil saturation in an unstable displacement is demonstrated by the work of Gardner and Ypma (1982). Figure 7-48 shows literature data on trapped miscible oil saturation plotted versus residence ($L\phi/u$) time for several secondary CO_2 floods. The decrease in trapped oil saturation with residence time is very much like the decrease associated with increasing N_{Da} in the first-contact miscible floods discussed earlier. But the displacements in Fig. 7-48 were generally not stable, and there was no mobile water present.

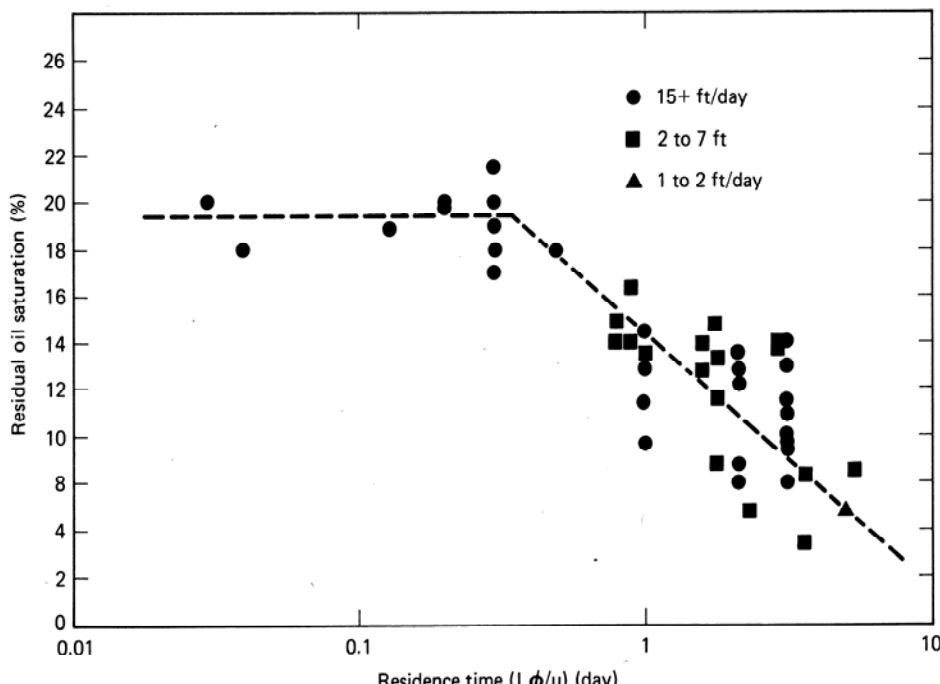


Figure 7-48 Literature data on trapped miscible flood oil saturation versus residence time (from Gardner and Ypma, 1982)

Gardner and Ypma interpret the large residual oil saturations at small residence times to be the consequence of a synergistic effect between the phase behavior and viscous fingering. They argue that in the longitudinal direction at the tip of the viscous finger, miscibility between the solvent and crude oil develops much like that shown in Fig. 7-37b. In the transverse direction, mixing takes place because of transverse dispersion and, perhaps, viscous crossflow. As we have seen, mixing due to dispersion causes straight-line dilution paths on pseudoternary diagrams (see Fig. 7-13). Such mixing does not cause developed miscibility unless very long residence times or very high transverse dispersion is allowed. Thus oil is first swept out by the longitudinal movement of a finger, the tip of which contains the light-enriched CO₂ solvent, and then reflows back into the finger from the transverse direction into a region of pure CO₂. Since CO₂ and crude are not first-contact miscible, multiple phases form in the finger, and trapping occurs. In fact, in simulations, it was observed that the trapped oil was actually present in highest amounts in the regions where the solvent fingers had passed because of this resaturation and phase behavior effect. Though this seems paradoxical—that the largest remaining oil saturation is where the solvent has swept—the contention is supported by correlating the data in Fig. 7-48 against a transverse dispersion group, reproducing this correlation with simulation, and finally, matching the effluent history of laboratory floods with the simulation results. Interestingly, the composition routes of zones both inside and outside the fingers passed well into the interior of the two-phase region of the ternary. When transverse dispersion is large, the transverse

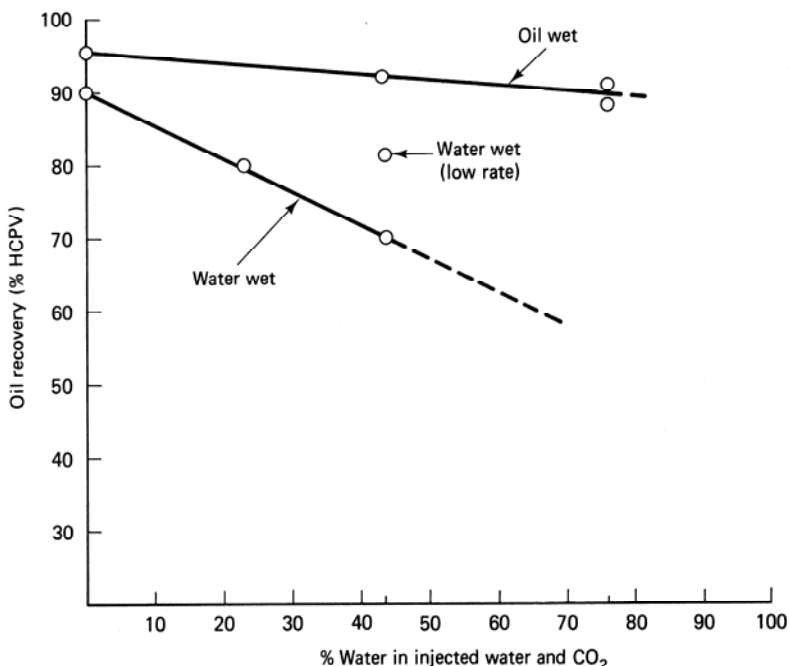


Figure 7-49 Oil recovery versus injected water fraction for tertiary CO₂ displacements in water-wet and oil-wet media (Tiffin and Yellig, 1982)

mixing takes place before the solvent fingers have emptied of the displacing mixture, and trapped oil saturation goes down.

Undoubtedly, the interaction with phase behavior, dispersion, and viscous fingering all play a part in understanding these complex phenomena. Still, it seems persuasive that the wettability of the medium plays a central role, particularly since there seems to be a wettability effect in even the most complicated developed miscible, unstable, displacements (Fig. 7-49).

7-10 ESTIMATING FIELD RECOVERY

In this section, we combine the effects of areal sweep efficiency and displacement efficiency.

Assume we have a plot of average solvent and oil concentration versus dimensionless time in a one-dimensional displacement. This can be from an overall material balance of a laboratory experiment or from the fractional flow calculation in Secs. 7-7 and 7-8. Figure 7-52 shows the average concentrations from the experimental data in Fig. 7-40. The solid lines are the fractional flow solution.

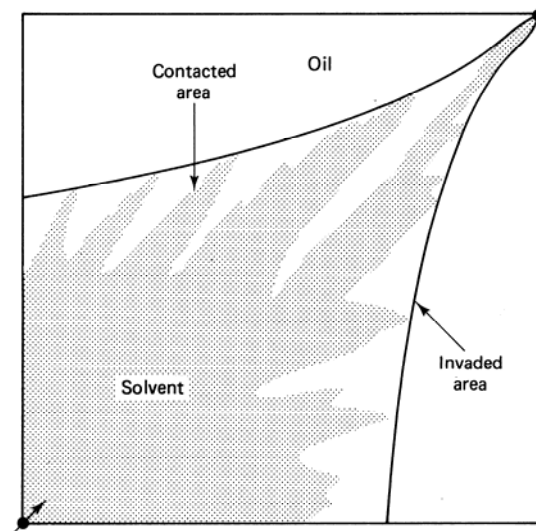


Figure 7-50 Schematic illustration of contacted and invaded area in quarter 5-spot pattern

In this section, we illustrate the correction of this data for areal sweep efficiency only. The procedure for correcting for vertical sweep is similar except we must now use a volumetric sweep efficiency function rather than an areal sweep efficiency function. The correction based on areal sweep would also be correct if the average concentration curves are corrected for vertical sweep, that is, were they averaged over a cross section using pseudofunctions.

Since we are explicitly including viscous fingering in the average concentration function, it is important *not* to include it in the areal sweep correlation also. Claridge anticipated this event by defining an “invaded area” sweep efficiency

as shown in Fig. 7-51. He determined that the areal sweep correlation of Caudle and Witte (1959) most nearly approximated the invaded area sweep and derived equations to describe it for flow in a confined five-spot. He also gave a procedure for combining areal and displacement sweep for secondary, non-WAG displacements. Our procedure is a generalization of Claridge's to first-contact floods of arbitrary WAG ratios and arbitrary initial conditions.

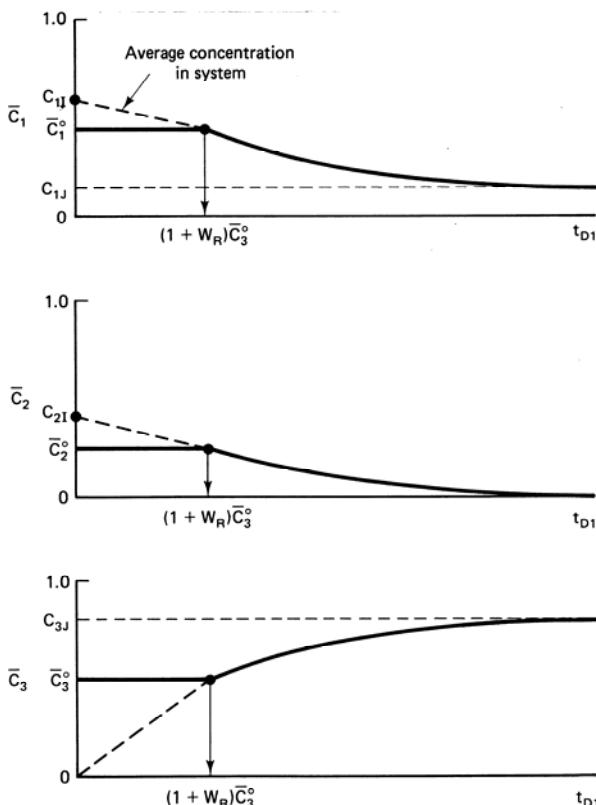


Figure 7-51 Schematic of the behavior of average concentrations

The invaded area is defined by a curve connecting the extreme tips of the viscous fingers (Fig. 7-50) and given by the product of E_A , the invaded areal sweep efficiency, and the pattern area. E_A as a function of dimensionless time and mobility ratio is given in Claridge's paper; it is not repeated here though it could be given graphically for a particular case. In Fig. 7-50, the contacted area is that actually occupied by the solvent fingers.

Central to the procedure is the idea of average concentrations behind the front. We define these to be the average concentrations in the invaded zone

$$\bar{C}_i = \frac{\text{Volume of component } i \text{ in invaded zone}}{\text{Volume of invaded zone}} \quad (7.10-1)$$

The average concentrations in the contacted area are $(C_1, C_2, C_3)_j$, the injected concentrations. The \bar{C}_i are equal to the average concentration functions after breakthrough; before this, they are constant and equal to their breakthrough value \bar{C}_i^0 (see Fig. 7-52).

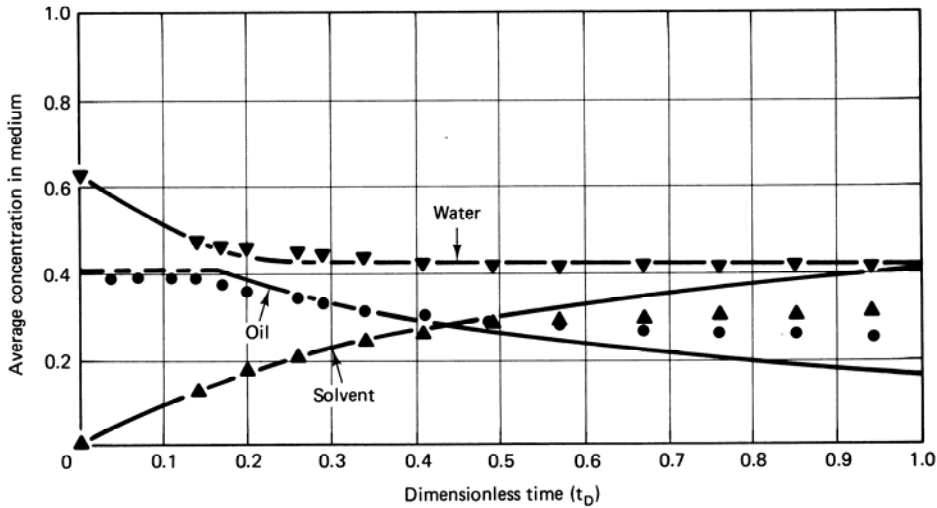


Figure 7-52 Average concentration from the experimental displacement in Fig. 7-40

Since E_A and \bar{C}_i are both known functions of time, the cumulative production of component i is

$$N_{pi} = \int_0^t F_{ij} q dt - V_p E_A (\bar{C}_i - \bar{C}_{ij}), \quad i = 1, 2, 3 \quad (7.10-2)$$

from an overall material balance (Eq. 2.5-2). In Eq. (7.10-2), q is the injection-production rate, V_p is the total pore volume, and t is time. All volumes in this equation are in reservoir volumes. For oil, in particular, we can write

$$N_{p2D} = E_A \left(1 - \frac{\bar{C}_2}{\bar{C}_{2I}} \right) \quad (7.10-3)$$

where N_{p2D} is the cumulative oil produced expressed as a fraction of oil in place at the start of solvent injection ($N_p/V_p C_{2I}$). To express oil recovery as a fraction of original (at discovery) oil in place, Eq. (7.10-3) should be multiplied by the ratio of C_{2I} to $(1 - S_{1r})$, the original oil saturation.

We begin here to use t_{D1} as the time variable for the C_i , and t_{D2} for E_A since, in general, neither function depends explicitly on the actual dimensionless time t_D in Eq. (7.10-3). We relate t_{D1} , t_{D2} , and t_D to one another below.

Breakthrough occurs at $t_{D1} = (1 + W_R) \bar{C}_3^0$ where \bar{C}_3^0 is the average solvent concentration behind the front at or before breakthrough. In Fig. 7-52, plotted curves show the average concentration in the one-dimensional system versus t_{D1} (dotted lines). In the following development, we do not use system average concentrations;

we show them in Fig. 7-52 for completeness. Average system concentrations and average concentrations behind the front coincide after breakthrough.

Imagine a continuous one-dimensional permeable medium with $\bar{C}_2 = \bar{C}_2(t_{D1})$ and $\bar{C}_3 = \bar{C}_3(t_{D1})$ known. An appropriate definition for t_{D1} is

$$t_{D1} = \frac{\text{Volume solvent + Water injected}}{\text{Volume invaded}} \quad (7.10-4)$$

If we identify the flow-excluded regions with the uninvaded regions in Fig. 7-51, the dimensionless time t_{D1} becomes

$$t_{D1} = \frac{t_D}{E_A} \quad (7.10-5)$$

On the other hand, consider a homogeneous five-spot pattern with $E_A = E_A(t_{D2})$ known, into which solvent and water are being simultaneously injected. If the oil and water in the invaded region are regarded as part of the rock matrix, the appropriate dimensionless time t_{D2} becomes

$$t_{D2} = \frac{\text{Volume solvent injected}}{\text{Volume solvent in invaded region}} \quad (7.10-6)$$

which may be decomposed into

$$\begin{aligned} t_{D2} &= \frac{\text{Volume solvent injected}}{\text{Volume solvent + Water injected}} \\ &\times \frac{\text{Volume solvent + Water injected}}{\text{Volume of pattern}} \\ &\times \frac{\text{Volume of pattern}}{\text{Volume solvent in invaded region}} \end{aligned} \quad (7.10-7)$$

After breakthrough, t_{D2} may be written in our terminology as

$$t_{D2} = \frac{t_D}{(1 + W_R) \bar{C}_3} \quad (7.10-8)$$

Equations (7.10-5) and (7.10-8) are the relations among the various dimensionless times. Claridge calls t_{D1} and t_{D2} the *apparent* pore volumes injected for the appropriate variable. t_D may be eliminated between Eqs. (7.10-5) and (7.10-8) to give

$$t_{D1} = \frac{t_{D2}}{E_A} (1 + W_R) \bar{C}_3 \quad (7.10-9)$$

The definitions in Eqs. (7.10-5) and (7.10-8) may be verified by observing that when breakthrough happens in an areal sense, it also happens in a one-dimensional sense. Thus at breakthrough, we have $t_{D2} = E_A$ and $\bar{C}_3 = \bar{C}_3^0$ from which it follows that $t_{D1} = (1 + W_R) \bar{C}_3^0$ from Eq. (7.10-9). Figure 7-52 shows this is indeed the correct dimensionless breakthrough time for the one-dimensional system.

The procedure to calculate the correct t_{D1} , t_{D2} , and t_D is iterative.

1. Estimate the mobility ratio \bar{M} to be used in the areal sweep correlation. We take this to be the mobility ratio based on the average concentrations behind the front at breakthrough

$$\bar{M} = \frac{(\lambda_{rt})_{\bar{C}_i^0}}{(\lambda_{rt})_{\bar{C}_u}} \quad (7.10-10a)$$

This requires a knowledge of the relative permeability curves. If these are not available, \bar{M} may be estimated from the one-dimensional data as

$$\bar{M} \approx \frac{(q/\Delta P)_{\text{final}}}{(q/\Delta P)_I} \quad (7.10-10b)$$

where q = total volumetric rate, and ΔP = overall pressure drop. The numerical value of \bar{M} does not change during the calculation.

2. For this value of \bar{M} , find the breakthrough areal sweep efficiency $t_{D2}^0 = E_A^0$. The dimensionless breakthrough time for the combined areal and displacement sweep is $t_D^0 = E_A^0(1 + W_R)\bar{C}_3^0$ from Eq. (7.10-8). The iterative calculations begin at t_D^0 .
3. Fix $t_D > t_{D2}^0$
4. Pick $t_{D1} > \bar{C}_3^0(1 + W_R)$.
5. Calculate $\bar{C}_3(t_{D1})$ from the one-dimensional results.
6. Calculate t_{D2} from Eq. (7.10-8).
7. Estimate $E_A(t_{D2})$ from the areal sweep correlation.
8. Calculate t_{D1} from Eq. (7.10-5).
9. Test for convergence. If the t_{D1} estimated in steps 4 and 8 differ by less than some small preset tolerance, the procedure has ~converged; if not, reestimate t_{D1} , and return to step 4.
10. Calculate cumulative oil produced from Eq. (7.10-3), and calculate the combined fraction flow of each component from

$$F_i^T = \left(1 - \frac{dE_A}{dt_{D2}}\right) F_i(t_{D1}) + \frac{dE_A}{dt_{D2}} F_{iJ} \quad (7.10-11)$$

11. Increment t_D , and return to step 3 for a later time. The entire procedure continues until t_D is larger than some preset maximum. The procedure converges in two to four iterations per step by simple direct substitution. The combined fractional flow in Eq. (7.10-11) represents contributions from the invaded zone (first term) and the uninvaded zone (second term), with all expressions being evaluated at consistent values of t_{D1} , t_{D2} , t_D . The F_i terms in Eq. (7.10-11) are from the one-dimensional curves, and the derivatives are numerically evaluated. Once $F_i^T(t_D)$ is known, we calculate component rates in standard volumes as

$$q_i = \frac{qF_i^T}{B_i}, \quad i = 1, 2, 3 \quad (7.10-12a)$$

corresponding to a real time t by inverting

$$t_D = \int_0^t \frac{q dt}{V_P} \quad (7.10-12b)$$

Figure 7-53 shows the results of the corrections for areal sweep applied to the data in Fig. 7-52. The y -axis plots cumulative oil produced as a fraction of initial oil in place at the start of solvent injection, and the x -axis plots each of the three dimensionless times. The combined areal and displacement sweep case breaks through earlier than the other two and, except for early time, is everywhere smaller. The combined fractional oil recovery at a particular dimensionless time is not simply the product of displacement and areal sweep at that time. The correct dimensionless time for consistently evaluating the latter two is given by Eqs. (7.10-5) and (7.10-8). For this particular case, Fig. 7-53 indicates the combined oil recovery is roughly equally dependent on areal and displacement sweep efficiencies.

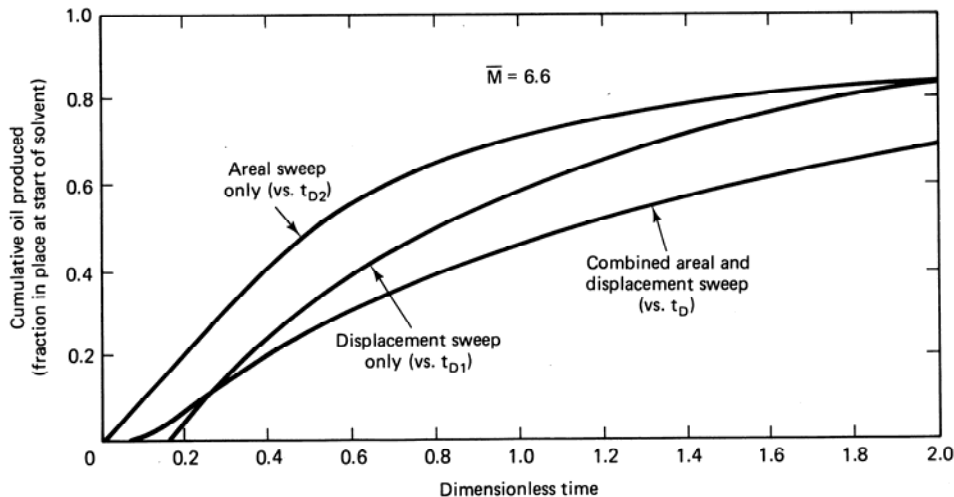


Figure 7-53 Calculated cumulative oil produced

7-11 CONCLUDING REMARKS

Solvent methods currently occupy a large fraction of implemented EOR methods. For certain classes of reservoirs—low permeability, fairly deep, and with light oil—they are clearly the method of choice. Future technology, particularly related to gravity stabilization and mobility control methods, could expand this range somewhat, but the target oil is nevertheless immense.

The topics of special importance in this chapter are the solvent flooding classifications, the usefulness of the minimum miscibility pressure correlations, and viscous fingering. The importance of viscous fingering remains largely unappreciated in large-scale displacement because of the obscuring effects of heterogeneity;

however, it is undoubtedly true that this phenomenon, perhaps in conjunction with others, accounts for the large discrepancy between lab-scale and field-scale oil recoveries. The material on dispersion and slugs and on solvent-water-oil fractional flow can form the basis for many design procedures. Of course, both topics easily lend themselves to the graphical presentation which is an essential part of this text.

EXERCISES

- 7A.** *Immiscible Solvent.* A particular crude oil has a specific gravity of 0.76, normal boiling point of 324 K (124°F), molecular weight of 210 kg/kg-mole, and viscosity of 15 mPa-s. At 8.16 MPa (1,200 psia) and 322 K (120°F), estimate
- The CO₂ solubility in the oil
 - The viscosity of the saturated CO₂-crude-oil mixture
 - The swelling factor of the mixture
 - The CO₂ water solubility, and express this as a mole fraction
- Use the Simon and Graue correlations (Figs. 7-20 through 7-22) and the water solubility correlations (Fig. 7-23).
- 7B.** *Calculating Minimum Miscibility Pressure.* An analysis of a particular separator oil is given below, including analyses at two different solution gas levels. Using the 1982 Holm and Josendal correlation (Fig. 7-25), estimate the minimum miscibility pressure (MMP) for the separator oil and the oil with 53.4 and 106.9 SCM dissolved gas/SCM dissolved oil. The reservoir temperature is 344 K (160°F).

Component	Separator oil	Weight percent	
		Oil + 53.4 SCM gas/SCM oil	Oil + 106.9 SCM gas/SCM oil
C ₁		21.3	53.0
C ₂		7.4	18.4
C ₃		6.1	15.1
C ₄		2.4	6.0
C ₅ -C ₃₀	86	54.0	6.5
C ₃₁ ⁺	41	8.8	1.1

What can you conclude about the effect of solution gas on the MMP? How would you explain this with a ternary diagram?

- 7C.** *Superposition and Multiple Slugs.* Using the principle of superposition applied to M influent step changes to a one-dimensional medium, show the composite solution to the convective-diffusion equation is

$$C_i = \frac{C_{i0} - C_{iM}}{2} - \frac{1}{2} \sum_{j=1}^M (C_{ij} - C_{ij-1}) \phi \left(t_D - \sum_{k=1}^j t_{Dk} \right) \quad (7C-1)$$

where C_{ij} = injected concentration of component i during time interval j (C_{i0} is the same as C_{i1}), and t_{Dj} = duration of interval j , and where

$$\phi(t_D) = \operatorname{erf} \left\{ \frac{x_D - t_D}{2 \sqrt{\frac{t_D}{N_{pe}}}} \right\}$$

Eq. (7C-1) is valid only for $t_D > \sum_{k=1}^j t_{Dk}$.

7D. *Dilution Paths on Ternary Diagrams.* Plot for the following:

- (a) Concentration profiles at $t_D = 0.5$ for the displacement of an oil of composition $(C_2, C_3) = (0.1, 0)$ by a small slug ($t_{Ds} = 0.1$) of composition $C_{2J} = 1.0$, which is then followed by a chase gas of composition $C_{3K} = 1.0$. Take the Peclet number to be 100.

- (b) The dilution path of the concentration profile in part (a) on a ternary diagram as in Fig. 7-30.

7E. *Rich Gas Dilution.* Based on the ternary diagram in Fig. 7E with initial oil composition $(C_2, C_3)_I = (0.1, 0)$,

- (a) Determine the minimum intermediate component concentration (C_{2J}) that may be used in a continuous mixture of dry gas and intermediate displacing fluid that will ensure developed miscibility.
- (b) Using the C_{2J} of part (a) as a lower bound, estimate the solvent slug size necessary to ensure first-contact miscibility at $t_D = 1$ for a series of C_{2J} values. Plot the total amount of intermediate injected ($C_{2J}t_{Ds}$) versus the slug size to determine an optimum. Take the Peclet number to be 1,000.

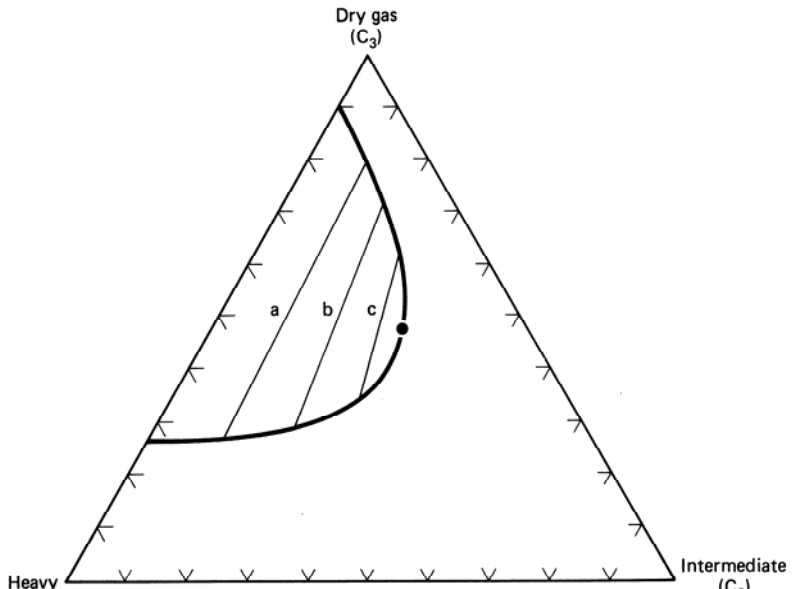


Figure 7E Ternary diagram for rich gas design problem

7F. *Fractional Flow Solution of Immiscible Displacement.* The fractional flow curves along the three tie lines in Fig. 7E are shown in Fig. 7F. The straighter curves (with the smaller residual phase saturations) are nearer to the plait point. Phase 3 is that richest in component 3.

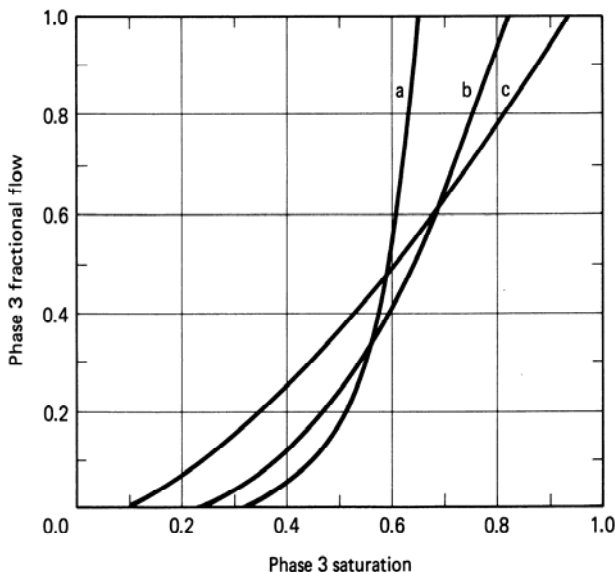


Figure 7F Fractional flow curve for Exercise 7F

- (a) On the ternary diagram, sketch residual saturation lines, the singular curve(s), the equivelocity path, and as many non-tie line paths as possible.
 - (b) Plot all the possible fractional flux curves you can. The initial oil composition is $(C_2, C_3)_I = (0.28, 0)$, and the injected solvent composition is $(C_2, C_3)_J = (0.09, 0.91)$. These compositions are on extensions of the lines farthest and nearest the plait point, respectively.
 - (c) Pick the physically possible solutions from the curves of part (b), and plot saturation and concentration profiles at $t_D = 0.8$.
- 7G.** *WAG Calculations.* Figure 7G gives representative relative permeability curves for the Slaughter Estate Unit (SEU). The water, oil, and solvent viscosities are 0.5, 0.38, and 0.037 mPa-s, respectively.
- (a) Plot the water–oil and water–solvent fractional flow curves. Assume the relative permeability curves for these pairs are the same and take $\alpha = 0$.
 - (b) Determine the optimal WAG ratio for a first-contact miscible secondary displacement in the absence of viscous fingering and dispersion.
 - (c) If the optimal WAG ratio is used, calculate the minimum solvent–water slug size (t_{Ds}) for complete displacement. The chase fluid is water.
 - (d) If the solvent–water slug size is 50% greater than that calculated in part (c), plot the time–distance diagram and effluent history for this displacement.
 - (e) Estimate the miscible flood trapped oil saturation S_{2r}^* from Fig. 7-44.
- 7H.** *Solvent Velocity with Water–Oil Solubility*
- (a) Show that by including the solvent water solubility and the solubility of the solvent in a trapped oil saturation, the solvent specific velocity (Eq. 7.7-14) becomes
- $$v_3 = \frac{1 - f_{1J}^s(1 - C_{31})}{1 - S_{1J}(1 - C_{31}) - S_{2r}'(1 - C_{32})} \quad (7H-1)$$
- where C_{31} = solvent solubility in water = $R_{31}B_3/B_1$, and C_{32} = solvent solubility in oil = $R_{32}B_3/B_2$. R_{ij} is the solubility of component i in phase j in standard volumes of i per standard volumes of j . See Fig. 7-20 and 7-23.

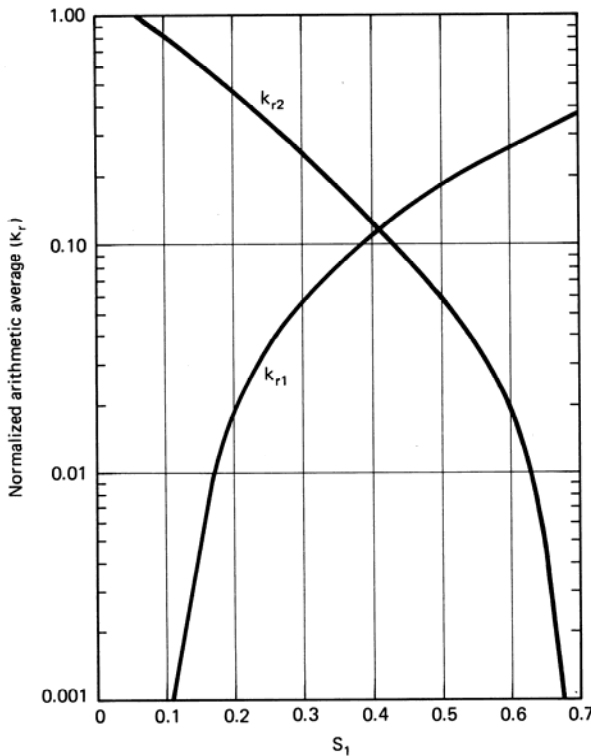


Figure 7G Slaughter Estate Unit relative permeability curves (from Ader and Stein, 1982)

- (b) Using the S_{2r} from part (e) of Exercise 7G, and taking $R_{31} = 17.8 \text{ SCM/SCM}$, $R_{32} = 214 \text{ SCM/SCM}$, $B_3 = 10^{-3} \text{ m}^3/\text{SCM}$, $B_1 = 1 \text{ m}^3/\text{SCM}$, and $B_2 = 1.2 \text{ m}^3/\text{SCM}$, repeat parts (b–d) of Exercise 7G.
- (c) Repeat parts (c) and (d) of Exercise 7G if the chase fluid is a gas having the identical properties of the solvent instead of water.
71. *Carbonated Waterflooding Fractional Flow.* One of the earlier EOR techniques is displacement by CO₂-saturated water. This technique is amenable to fractional flow analysis (de Nevers, 1964).
- (a) Show that the specific velocity of a pistonlike carbonated water front is given by

$$v_{\Delta C_3} = \frac{\frac{K_{21}^3}{K_{21}^3 - 1}}{1 - S_{2r} - \frac{K_{21}^3}{K_{21}^3 - 1}} \quad (7I-1)$$

Equation (7I-1) assumes flow behind the front is at a CO₂-saturated residual oil phase.

- (b) By matching the specific velocity of the oil bank rear to Eq. (7I-1) show the oil bank saturation and fractional flow must satisfy

$$v_{AC_3} = \frac{1 - \frac{f_1 - C_{32}}{1 - C_{32}}}{1 - \frac{S_1 - C_{32}}{1 - C_{32}}} \quad (7I-2)$$

In these equations, K_{21}^3 is the volumetric partition coefficient of CO_2 ($i = 3$) between the water ($j = 1$) and oil ($j = 2$) phases, and C_{32} is the volume fraction of CO_2 in the oil. $f_1(S_1)$ is the water fractional flow curve.

- (c) Estimate C_{32} and K_{21}^3 from Fig. 7-20 at 15 MPa and 340 K. You may assume ideal mixing in both phases.
- (d) Calculate and plot the effluent oil cut of a carbonated waterflood in a one-dimensional permeable medium with initial (uniform) oil cut of 0.1.
- (e) On the same graph, plot the effluent oil fractional flow of a noncarbonated waterflood. Finally, plot the incremental oil recovery (IOR) versus t_D .

For this problem, use the following parameters in the exponential relative permeability curves: $n_1 = n_2 = 2$, $k_{r1}^0 = 0.1$, $\phi = 0.2$, $k_{r2}^0 = 0.8$, $\mu_1 = 0.8 \text{ mPa-s}$, $\mu_2 = 5 \text{ mPa-s}$, $S_{1r} = S_{2r} = 0.2$, and $\alpha = 0$. The oil molecular weight is 200 kg/kg-mole, its density is 0.78 g/cm³, and the UOP factor is 11.2.

- 7J.** *Viscous Fingering and Displacement Efficiency.* Using the Koval theory (Eq. 7.8-7), plot the effluent history of a first-contact miscible displacement where the oil–solvent viscosity ratio is 50, and the heterogeneity factor is 5.
- 7K.** *Viscous Fingering by Mixing Parameter.* In the Todd-Longstaff (1972) representation of viscous fingering, the Koval factor K_{val} in Eq. (7.8-4) is replaced by K_{TL} where

$$K_{TL} = \frac{M_{2e}}{M_{3e}} = v^{1-\omega} \quad (7K-1)$$

where M_{2e} and M_{3e} = effective solvent and oil viscosities in the mixing zone, v = viscosity ratio, and ω = mixing parameter ($0 < \omega < 1$).

- (a) Repeat Exercise 7J with $\omega = 1/3$.
 - (b) Determine the correspondence between K_{val} and K_{TL} by setting $K_{TL} = K_{val}$ in Eq. (7.8-5) and plotting ω versus v for various H_k .
- 7L.** *Dispersion as a Normal Distribution.* One view of dispersion is that it is the result of the mixing of a large number of fluid particles along independent paths. If so, the distribution of particles should follow a normal distribution. In this exercise, we show that the equations in Sec. 7-6 reduce to such a form.

- (a) Show that Eq. (7.6-4) applied to a unit slug $C_{il} = C_{ik} = 0$ and

$$t_{Ds} C_{ij} = 1 \quad (7L-1)$$

reduces to

$$C_i = \frac{1}{2t_{Ds}} \left\{ \operatorname{erf} \left[\frac{x_D - (t_D - t_{Ds})}{2\sqrt{\frac{t_D}{N_{Pe}}}} \right] - \operatorname{erf} \left[\frac{x_D - t_D}{2\sqrt{\frac{t_D}{N_{Pe}}}} \right] \right\} \quad (7L-2)$$

for $t_D \gg t_{Ds}$.

- (b) Using the definition for the error function (Eq. 5.5-14), show that Eq. (7L-2) becomes

$$C_i = \left(\frac{N_{pe}}{4\pi t_D} \right)^{1/2} e^{-[(x_D - t_D)^2 / (4t_D / N_{pe})]} \quad (7L-3)$$

as $t_{Ds} \rightarrow 0$. Equation (7L-3) says the distribution of a large number of particles at $x_D = 0$ initially approaches a normal distribution with mean position $x_D = t_D$ and a standard deviation of $2\sqrt{t_D / N_{pe}}$.

- 7M.** *Calculating Solvent Oil Recovery.* Figure 7M shows the volumetric sweep efficiency of a tertiary solvent displacement.

- (a) Using the procedure in Sec. 7-10, estimate and plot cumulative oil recovery (fraction of oil in place at start of solvent injection) and oil cut versus dimensionless time. Use the average concentrations of Fig. 7-50.
- (b) If the oil formation volume factor is $1.2 \text{ m}^3/\text{SCM}$, the reservoir pore volume is 160 hm^3 , and the average injection rate is $80 \text{ m}^3/\text{day}$, calculate and plot the cumulative oil produced and oil rate versus time.

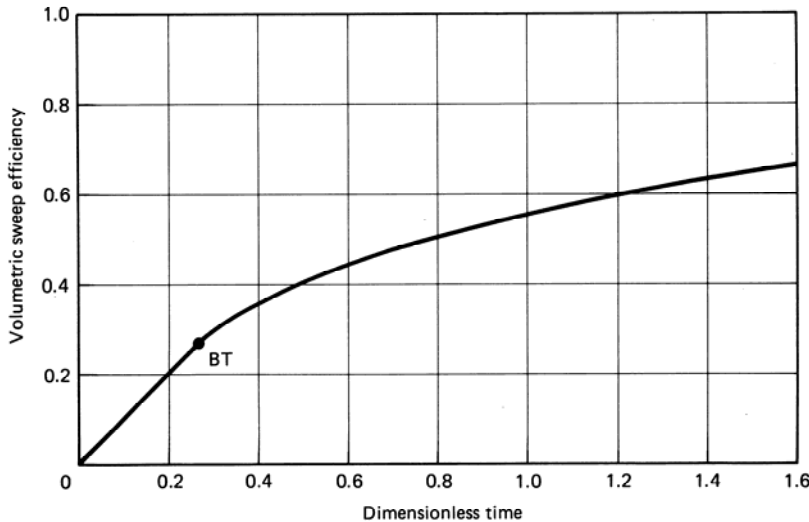


Figure 7M Volumetric sweep efficiency for miscible displacement

8

Polymer Methods

Polymer flooding consists of adding polymer to the water of a waterflood to decrease its mobility. The resulting increase in viscosity, as well as a decrease in aqueous phase permeability that occurs with some polymers, causes a lower mobility ratio. This lowering increases the efficiency of the waterflood through greater volumetric sweep efficiency and a lower swept zone oil saturation. Irreducible oil saturation does not decrease although the remaining oil saturation does, approaching S_{2r} for both waterflooding and polymer flooding. The greater recovery efficiency constitutes the economic incentive for polymer flooding when applicable. Generally, a polymer flood will be economic only when the waterflood mobility ratio is high, the reservoir heterogeneity is high, or a combination of these two occurs.

Polymers have been used in oil production in three modes.

1. As near-well treatments to improve the performance of water injectors or watered-out producers by blocking off high-conductivity zones.
2. As agents that may be cross-linked in situ to plug high-conductivity zones at depth in the reservoir (Needham et al., 1974).

These processes require that polymer be injected with an inorganic metal cation that will cross-link subsequently injected polymer molecules with ones already bound to solid surfaces.

3. As agents to lower water mobility or water–oil mobility ratio.

The first mode is not truly polymer flooding since the actual oil-displacing agent is not the polymer. Certainly most polymer EOR projects have been in the third mode, the one we emphasize here. We discussed how lowering the mobility ratio affects displacement and volumetric sweep efficiency in Chaps. 5 and 6.

CHEMICAL FLOODING (Polymer)

The method shown requires a preflush to condition the reservoir, the injection of a polymer solution for mobility control to minimize channeling, and a driving fluid (water) to move the polymer solution and resulting oil bank to production wells.

Mobility ratio is improved and flow through more permeable channels is reduced, resulting in increased volumetric sweep.

(Single 5-Spot Pattern Shown)

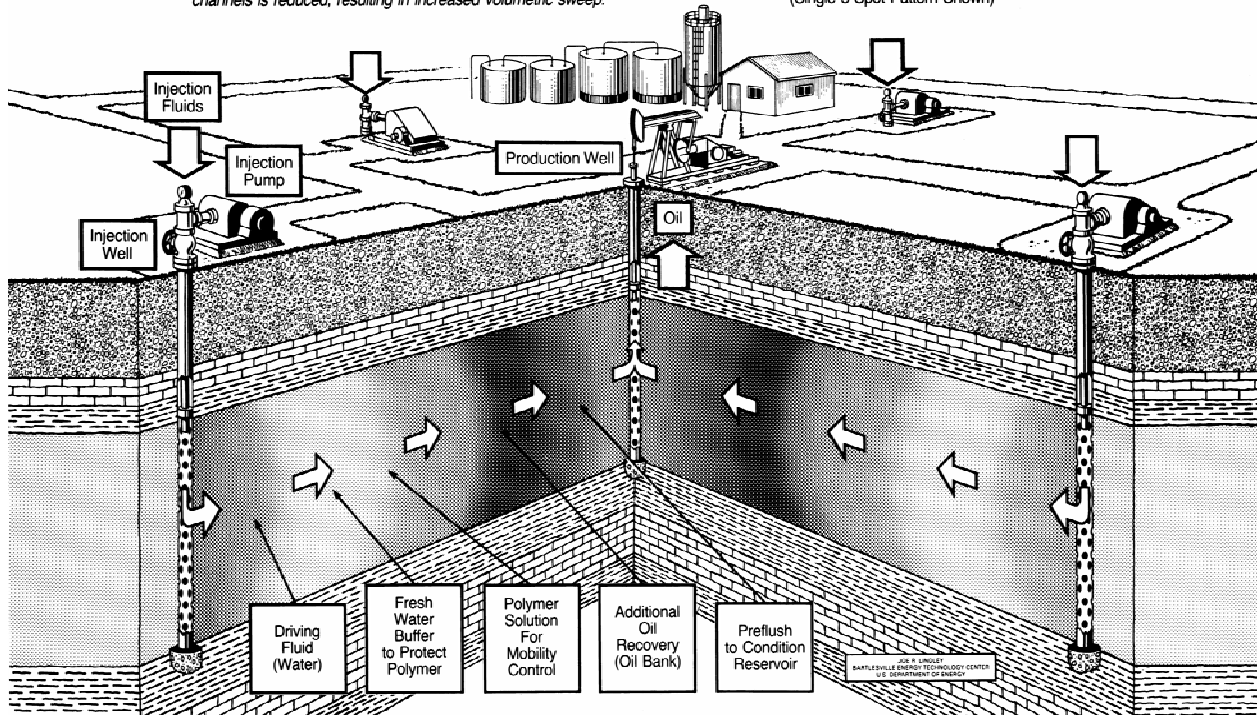


Figure 8-1 Schematic illustration of polymer flooding sequence (drawing by Joe Lindley, U.S. Department of Energy, Bartlesville, Okla.)

Figure 8-1 shows a schematic of a typical polymer flood injection sequence: a preflush usually consisting of a low-salinity brine; an oil bank; the polymer solution itself; a freshwater buffer to protect the polymer solution from backside dilution; and finally, chase or drive water. Many times the buffer contains polymer in decreasing amounts (a grading or taper) to lessen the unfavorable mobility ratio between the chase water and the polymer solution. Because of the driving nature of the process, polymer floods are always done through separate sets of injection and production wells.

Mobility is lowered in a polymer flood by injecting water that contains a high molecular weight, water-soluble polymer. Since the water is usually a dilution of an oil-field brine, interactions with salinity are important, particularly for certain classes of polymers.

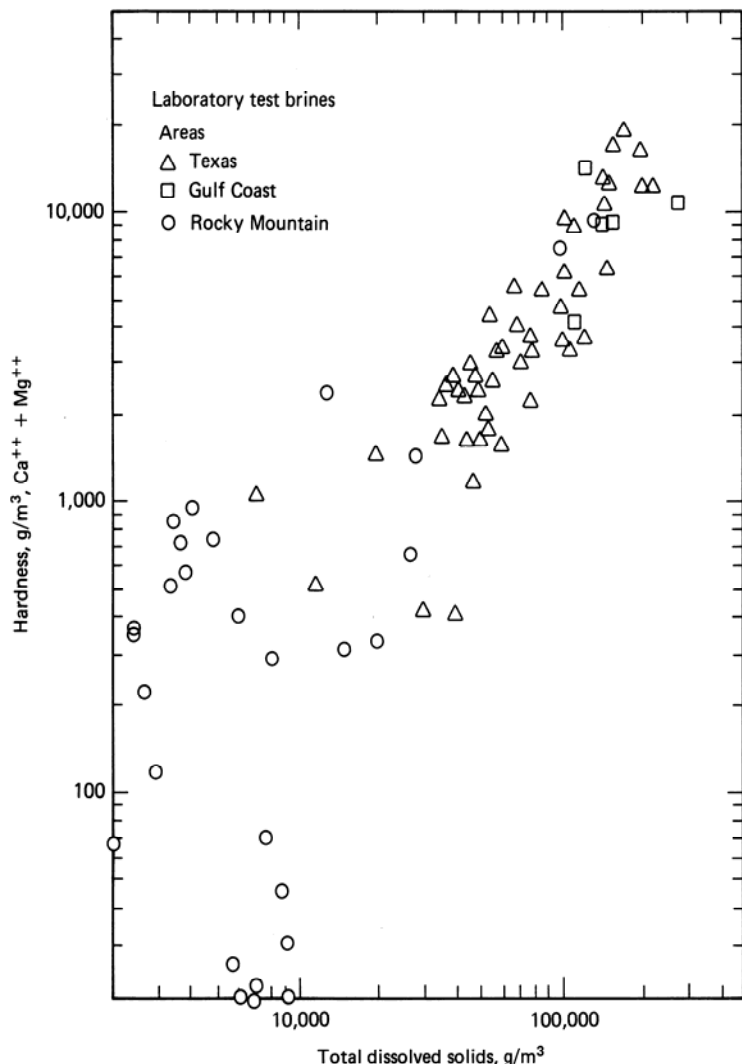


Figure 8-2 Salinities from representative oil-field brines (from Gash et al., 1981)

Salinity is the total dissolved solids (TDS) content of the aqueous phase. Figure 8-2 shows typical values. Virtually all chemical flooding properties depend on the concentrations of specific ions rather than salinity only. The aqueous phase's total divalent cation content (hardness) is usually more critical to chemical flood properties than the same TDS concentration. Figure 8-2 also shows typical brine hardnesses.

Because of the high molecular weight (1 to 3 million), only a small amount (about 500 g/m³) of polymer will bring about a substantial increase in water viscosity. Further, several types of polymers lower mobility by reducing water relative permeability in addition to increasing the water viscosity. How polymer lowers mobility, and the interactions with salinity, can be qualitatively illustrated with some discussion of polymer chemistry.

8-1 THE POLYMERS

Several polymers have been considered for polymer flooding: Xanthan gum, hydrolyzed polyacrylamide (HPAM), copolymers (a polymer consisting of two or more different types of monomers) of acrylic acid and acrylamide, copolymers of acrylamide and 2-acrylamide 2-methyl propane sulfonate (AM/AMPS), hydroxyethylcellulose (HEC), carboxymethylhydroxyethylcellulose (CMHEC), polyacrylamide (PAM), polyacrylic acid, glucan, dextran polyethylene oxide (PEO), and polyvinyl alcohol. Although only the first three have actually been used in the field, there are many potentially suitable chemicals, and some may prove to be more effective than those now used.

Nevertheless, virtually all the commercially attractive polymers fall into two generic classes: polyacrylamides and polysaccharides (biopolymers). In the remainder of this discussion, we deal with these exclusively. Figure 8-3 shows representative molecular structures.

Polyacrylamides

These are polymers whose monomeric unit is the acrylarnide molecule. As used in polymer flooding, polyacrylamides have undergone partial hydrolysis, which causes anionic (negatively charged) carboxyl groups (—COO^-) to be scattered along the backbone chain. The polymers are called partially hydrolyzed polyacrylamides (HPAM) for this reason. Typical degrees of hydrolysis are 30%–35% of the acrylamide monomers; hence the HPAM molecule is negatively charged, which accounts for many of its physical properties.

This degree of hydrolysis has been selected to optimize certain properties such as water solubility, viscosity, and retention. If hydrolysis is too small, the polymer will not be water soluble. If it is too large, its properties will be too sensitive to salinity and hardness (Shupe, 1981).

The viscosity increasing feature of HPAM lies in its large molecular weight.

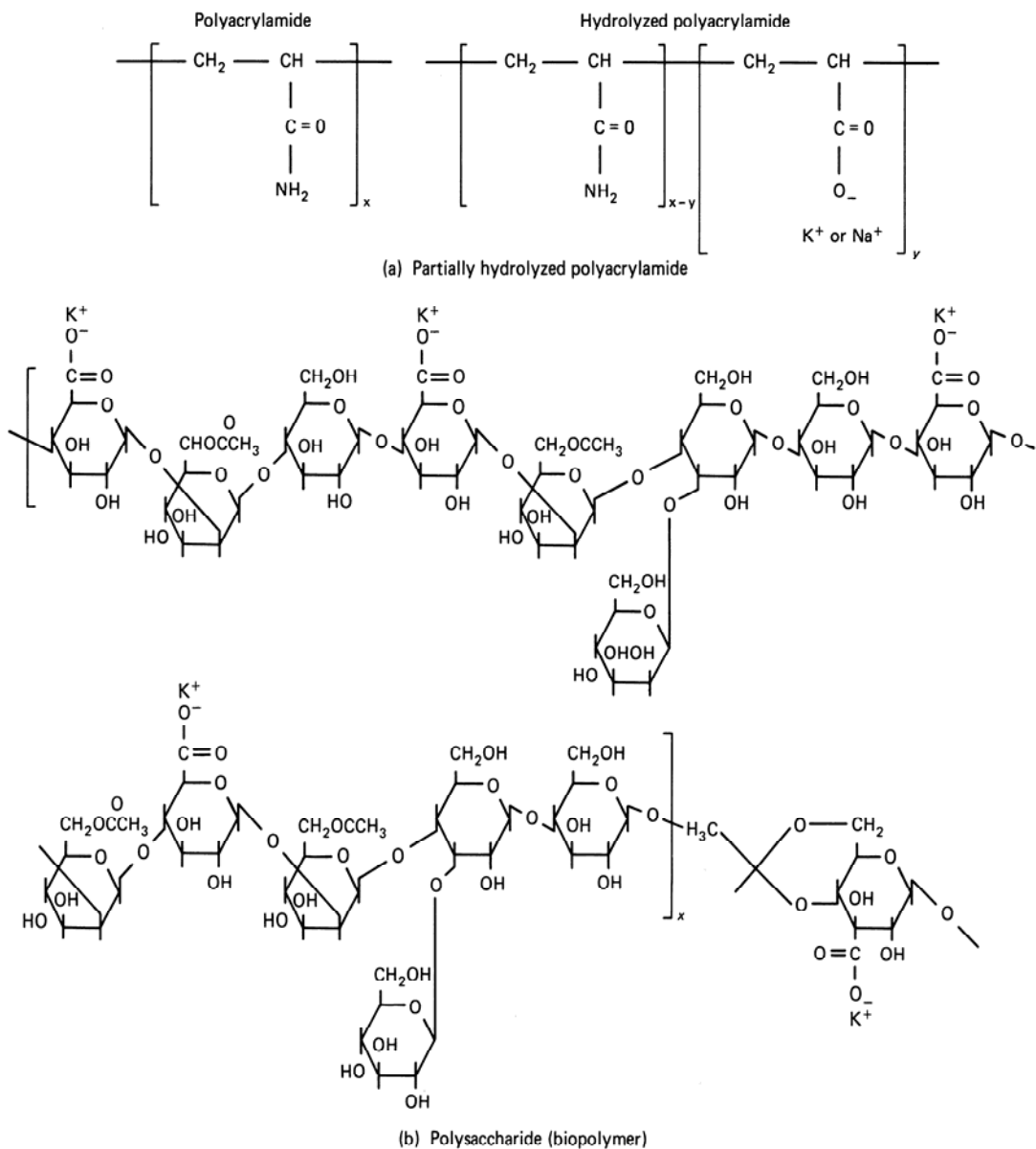


Figure 8-3 Molecular structures (from Willhite and Dominguez, 1977)

This feature is accentuated by the anionic repulsion between polymer molecules and between segments on the same molecule. The repulsion causes the molecule in solution to elongate and snag on others similarly elongated, an effect that accentuates the mobility reduction at higher concentrations.

If the brine salinity or hardness is high, this repulsion is greatly decreased through ionic shielding since the freely rotating carbon–carbon bonds (Fig. 8-3a) allow the molecule to coil up. The shielding causes a corresponding decrease in the

effectiveness of the polymer since snagging is greatly reduced. Virtually all HPAM properties show a large sensitivity to salinity and hardness, an obstacle to using HPAM in many reservoirs. On the other hand, HPAM is inexpensive and relatively resistant to bacterial attack, and it exhibits permanent permeability reduction.

Polysaccharides

These polymers are formed from the polymerization of saccharide molecules (Fig. 8-3b), a bacterial fermentation process. This process leaves substantial debris in the polymer product that must be removed before the polymer is injected (Wellington, 1980). The polymer is also susceptible to bacterial attack after it has been introduced into the reservoir. These disadvantages are offset by the insensitivity of polysaccharide properties to brine salinity and hardness.

Figure 8-3(b) shows the origin of this insensitivity. The polysaccharide molecule is relatively nonionic and, therefore, free of the ionic shielding effects of HPAM. Polysaccharides are more branched than HPAM, and the oxygen-ringed carbon bond does not rotate fully; hence the molecule increases brine viscosity by snagging and adding a more rigid structure to the solution. Polysaccharides do not exhibit permeability reduction. Molecular weights of polysaccharides are generally around 2 million.

Today, HPAM is less expensive per unit amount than polysaccharides, but when compared on a unit amount of mobility reduction, particularly at high salinities, the costs are close enough so that the preferred polymer for a given application is site specific. Historically, HPAM has been used in about 95% of the reported field polymer floods (Manning et al., 1983). Both classes of polymers tend to chemically degrade at elevated temperatures.

Polymer Forms

The above polymers take on three distinctly different physical forms: powders, broths and emulsions. Powders, the oldest of the three, can be readily transported and stored with small cost. They are difficult to mix because the first water contacting the polymer tends to form very viscous layers of hydration around the particles, which greatly slow subsequent dissolution. Broths are aqueous suspensions of about 10 wt. % polymer in water which are much easier to mix than powders. They have the disadvantage of being rather costly because of the need to transport and store large volumes of water. Broths are quite viscous so they can require special mixing facilities. In fact, it is this difficulty which limits the concentration of polymer in the broth. Emulsion polymers, the newest polymer form, contain up to 35 wt. % polymer solution, suspended through the use of a surfactant, in an oil-carrier phase. Once this water-in-oil emulsion is inverted (see Fig. 9-5), the polymer concentrate can be mixed with make-up water to the desired concentration for injection. The emulsion flows with roughly the same viscosity as the oil carrier, which can be recycled.

B-2 POLYMER PROPERTIES

In this section, we present qualitative trends, quantitative relations, and representative data on the following properties: viscosity relations, non-Newtonian effects, polymer transport, inaccessible pore volume, permeability reduction, chemical and biological degradation, and mechanical degradation.

Viscosity Relations

Figure 8-4 shows a plot of Xanflood viscosity versus polymer concentration. This type of curve has traditionally been modeled by the Flory-Huggins equation (Flory, 1953)

$$\mu'_1 = \mu_1 [1 + a_1 C_{41} + a_2 C_{41}^2 + a_3 C_{41}^3 + \dots] \quad (8.2-1)$$

where C_{41} is the polymer concentration in the aqueous phase, μ_1 is the brine (solvent) viscosity, and a_1 , a_2 , and so on are constants. In the remainder of this chapter we drop the second subscript 1 on the polymer concentration since polymer is always in an aqueous phase. The usual polymer concentration unit is g/m^3 of solution, which is approximately the same as ppm. The linear term in Eq. (8.2-1) accounts for the dilute range where the polymer molecules act independently (without entanglements). For most purposes, Eq. (8.2-1) can usually be truncated at the cubic term.

For a 1,000 g/m^3 Xanflood solution at 0.1 s^{-1} in 1 wt % NaCl brine at 24°C,

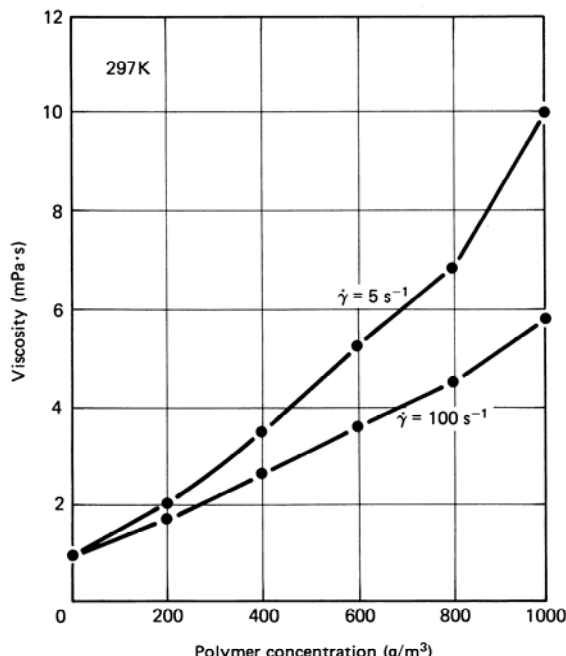


Figure 8-4 Xanflood viscosity versus concentration in 1% NaCl brine (from Tsaur, 1978)

the viscosity is 70 mPa-s (70 cp) from Fig. 8-4. Compared to the brine at the same conditions, this is a substantial increase in viscosity brought about by a relatively dilute concentration (recall that 1,000 g/m³ = 0.1 wt %). Xanflood at these conditions is an excellent thickener.

A more fundamental way of measuring the thickening power of a polymer is through its intrinsic viscosity, defined as

$$[\mu] = \lim_{C_4 \rightarrow 0} \left[\frac{\mu'_1 - \mu_1}{\mu_1 C_4} \right] \quad (8.2-2)$$

From its definition, $[\mu]$ is a measure of the polymer's intrinsic thickening power. It is insensitive to the polymer concentration. The intrinsic viscosity for the Xanflood polymer under the conditions given above is 70 dl/g, the units being equivalent to reciprocal weight percent. Intrinsic viscosity is the same as the a_1 term in Eq. (8.2-1).

For any given polymer–solvent pair, the intrinsic viscosity increases as the molecular weight of the polymer increases according to the following equation (Flory, 1953):

$$[\mu] = K' M_w^a \quad (8.2-3)$$

The exponent varies between about 0.5 and 1.5 and is higher for good solvents such as freshwater. K' is a polymer-specific constant.

The above relationships are useful for characterizing the polymer solutions. For example, the size of the polymer molecules in solution can be estimated from Flory's (1953) equation for the mean end-to-end distance

$$d_p = 8(M_w [\mu])^{1/3} \quad (8.2-4)$$

This equation, being empirical, presumes certain units; $[\mu]$ must be in dl/g, and d_p is returned in Angstroms (10^{-10} m). This measure of polymer size is useful in understanding how these very large molecules propagate through the small pore openings of rocks. The molecular weight of Xanthan gum is about 2 million. From Eq. (8.2-4), d_p is about 0.4 μm . This is the same size as many of the pore throats in a low-to-moderate permeability sandstone. As a result, we would expect to, and in fact do, observe many polymer–rock interactions.

Non-Newtonian Effects

Figure 8-5 shows polymer solution viscosity μ'_1 versus shear rate $\dot{\gamma}$ measured in a laboratory viscometer at fixed salinity. At low shear rates, μ'_1 is independent of $\dot{\gamma}$ ($\mu'_1 = 1.01$), and the solution is a Newtonian fluid. At higher $\dot{\gamma}$, μ'_1 decreases, approaching a limiting ($\mu'_1 = \mu_1^\infty$) value not much greater than the water viscosity μ_1 at some critical high shear rate. This critical shear rate is off-scale to the right in Fig. 8-5. A fluid whose viscosity decreases with increasing $\dot{\gamma}$ is *shear thinning*. The shear thinning behavior of the polymer solution is caused by the uncoiling and unsnagging

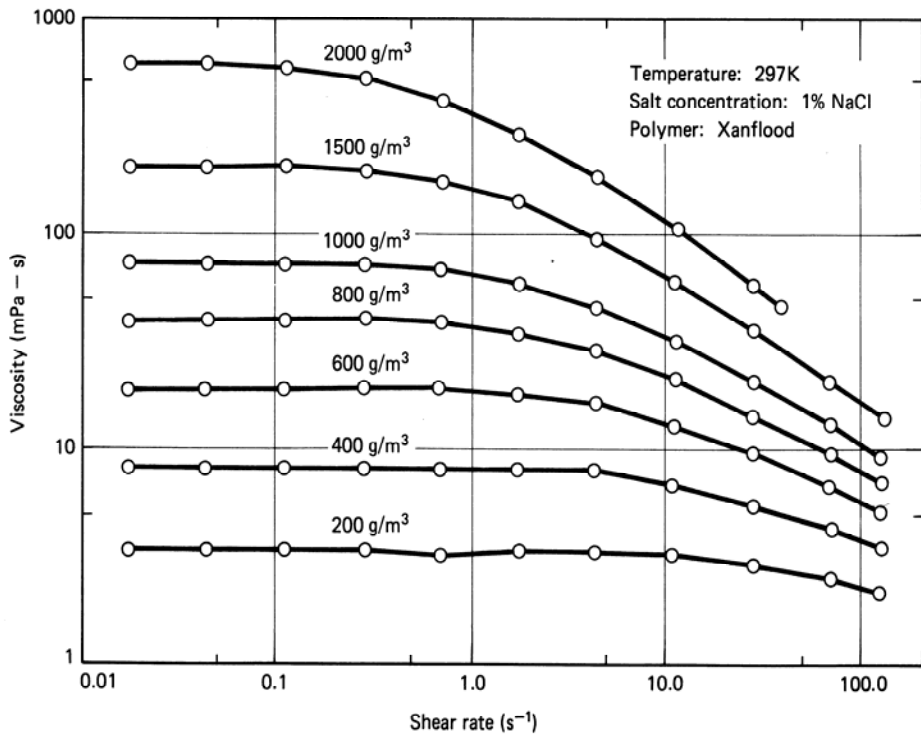


Figure 8-5 Polymer solution viscosity versus shear rate and polymer concentration (from Tsaur, 1978)

of the polymer chains when they are elongated in shear flow. Below the critical shear rate, the behavior is part reversible.

Figure 8-6 shows a viscosity–shear-rate plot at fixed polymer concentration with variable NaCl concentration for an AMPS polymer. The sensitivity of the viscosity to salinity is profound. As a rule of thumb, the polymer solution viscosity decreases a factor of 10 for every factor of 10 increase in NaCl concentration. The viscosity of HPAM polymers and HPAM derivatives are even more sensitive to hardness, but viscosities of polysaccharide solutions are relatively insensitive to both.

The behavior in Figs. 8-5 and 8-6 is favorable because, for the bulk of a reservoir's volume, $\dot{\gamma}$ is usually low (about $1\text{--}5\text{ s}^{-1}$), making it possible to attain a design mobility ratio with a minimal amount of polymer. But near the injection wells, $\dot{\gamma}$ can be quite high, which causes the polymer injectivity to be greater than that expected based on μ_1^0 . The relative magnitude of this enhanced injectivity effect can be estimated (Sec. 8-3) once quantitative definitions of shear rate in permeable media, and shear-rate–viscosity relations are given.

The relationship between polymer-solution viscosity and shear rate may be described by a *power-law* model

$$\mu'_1 = K_{pl}(\dot{\gamma})^{n_{pl}-1} \quad (8.2-5)$$

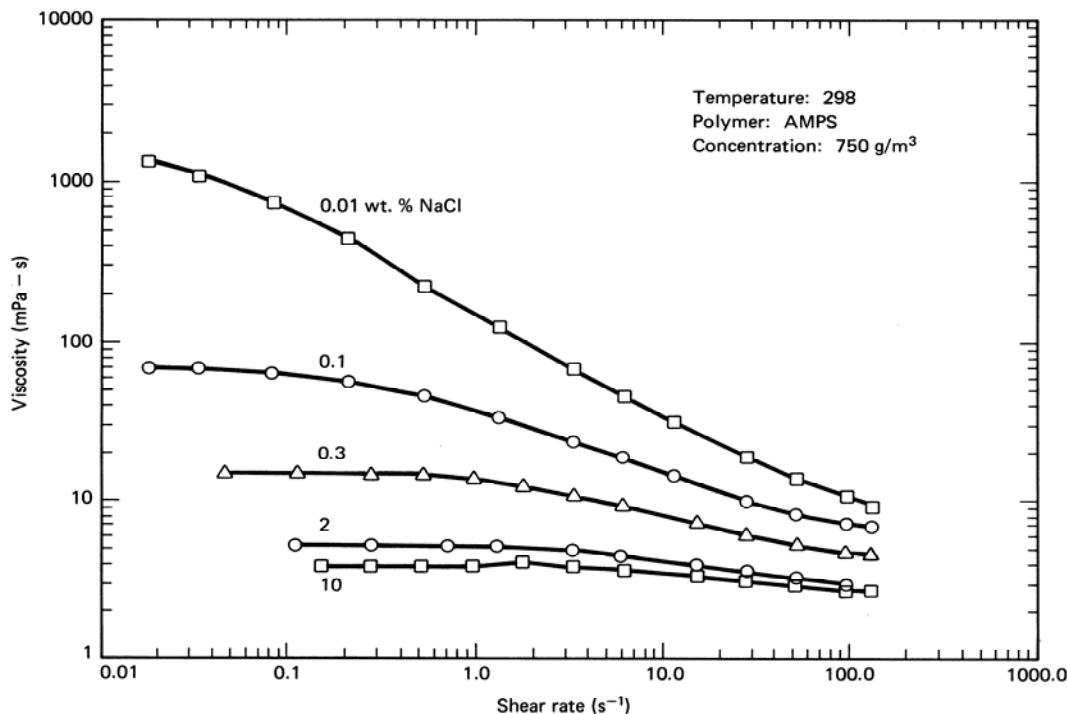


Figure 8-6 Polymer solution viscosity versus shear rate at various brine salinities (from Martin et al., 1981)

where K_{pl} and n_{pl} are the power-law coefficient and exponent, respectively. For shear thinning fluids, $0 < n_{pl} < 1$; for Newtonian fluids, $n_{pl} = 1$, and K_{pl} becomes the viscosity. $\dot{\gamma}$ is always positive. Equation (8.2-5) applies only over a limited range of shear rates: Below some low shear rate, the viscosity is constant at μ_1^0 , and above the critical shear rate, the viscosity is also constant μ_1^∞ .

The truncated nature of the power law is awkward in some calculations; hence another useful relationship is the *Meter model* (Meter and Bird, 1964)

$$\mu'_1 = \mu_1^\infty + \frac{\mu_1^0 - \mu_1^\infty}{1 + \left(\frac{\dot{\gamma}}{\dot{\gamma}_{1/2}} \right)^{n_M - 1}} \quad (8.2-6)$$

where n_M is an empirical coefficient, and $\dot{\gamma}_{1/2}$ is the shear rate at which μ'_1 is the average of μ_1^0 and μ_1^∞ . As with all polymer properties, all empirical parameters are functions of salinity, hardness, and temperature.

When applied to permeable media flow, the above general trends and equations continue to apply. μ'_1 is usually called the apparent viscosity μ_{app} and the effective shear rate $\dot{\gamma}_{eq}$ is based on capillary tube concepts, as we derived in Sec. 3-1

for Newtonian fluids. For power-law fluids, the procedure is identical (see Exercise 8B) except the beginning equation is Eq. (8.2-5). We give only the results here.

The apparent viscosity of a flowing polymer solution is

$$\mu_{app} = H_{pl} u^{n_{pl}-1} \quad (8.2-7)$$

where (Hirasaki and Pope, 1974)

$$H_{pl} = K_{pl} \left(\frac{1+3n_{pl}}{n_{pl}} \right)^{n_{pl}-1} (8k_1\phi_1)^{(1-n_{pl}/2)} \quad (8.2-8)$$

The right side of Eq. (8.2-7) is $K_{pl}\dot{\gamma}_{eq}^{n_{pl}-1}$ which yields the equivalent shear rate for flow of a power-law fluid

$$\dot{\gamma}_{eq} = \left(\frac{1+3n_{pl}}{n_{pl}} \right) \frac{u}{\sqrt{8k_1\phi_1}} \quad (8.2-9)$$

In both Eqs. (8.2-8) and (8.2-9), k_1 , the aqueous phase permeability, is the product of the phase's relative permeability and the absolute permeability. ϕ_1 , the aqueous phase porosity, is ϕS_1 .

The only difference between the equivalent shear rate and that for the Newtonian fluid (Eq. 3.1-11) is the first term on the right-hand side. This factor is a slowly varying function of n_{pl} ; hence the Newtonian shear rate affords an excellent approximation of the shear rate in non-Newtonian flow.

Even though $\dot{\gamma}_{eq}$ has units of reciprocal time, shear rate is essentially a steady-state representation since it can be realized in steady laminar flow in a tube. Thus the constitutive Eqs. (8.2-5) and (8.2-6) are representing purely viscous effects since an instantaneous change in $\dot{\gamma}_{eq}$ causes a similar change in μ'_1 . In reality, fluctuations in $\dot{\gamma}_{eq}$, or elastic effects, do affect polymer properties; these we discuss separately below.

Polymer Transport

All polymers experience retention in permeable media because of adsorption onto solid surfaces or trapping within small pores. Polymer retention varies with polymer type, molecular weight, rock composition, brine salinity, brine hardness, flow rate, and temperature. Field-measured values of retention range from 7 to 150 μg polymer/cm³ of bulk volume, with a desirable retention level being less than about 20 $\mu\text{g}/\text{cm}^3$. Retention causes the loss of polymer from solution, which can also cause the mobility control effect to be lost—a particularly pronounced effect at low polymer concentrations. Polymer retention also causes a delay in the rate of the polymer and generated oil bank propagation (see Sec. 8-4).

For more quantitative work, we represent polymer adsorption by a *Langmuir-type* isotherm

$$C_{4s} = \frac{a_4 C_4}{1 + b_4 C_4} \quad (8.2-10)$$

where C_4 and C_{4s} are the species concentrations in the aqueous and on the rock phases. The units of adsorption can take on a variety of forms, but mass of polymer per mass of rock is most common. In our notation, this is $\omega_{4s}/(1 - \omega_{4s})$, strictly speaking, but ω_{4s} is very much smaller than 1. The units conversion between $C_{4s}(\text{g/m}^3)$ and $\omega_{4s}(\mu\text{g/g-rock})$ are embedded in the constants a_4 and b_4 . The b_4 in Eq. (8.2-10) controls the curvature of the isotherm, and the ratio a_4/b_4 determines the plateau value for adsorption (Fig. 8-7).

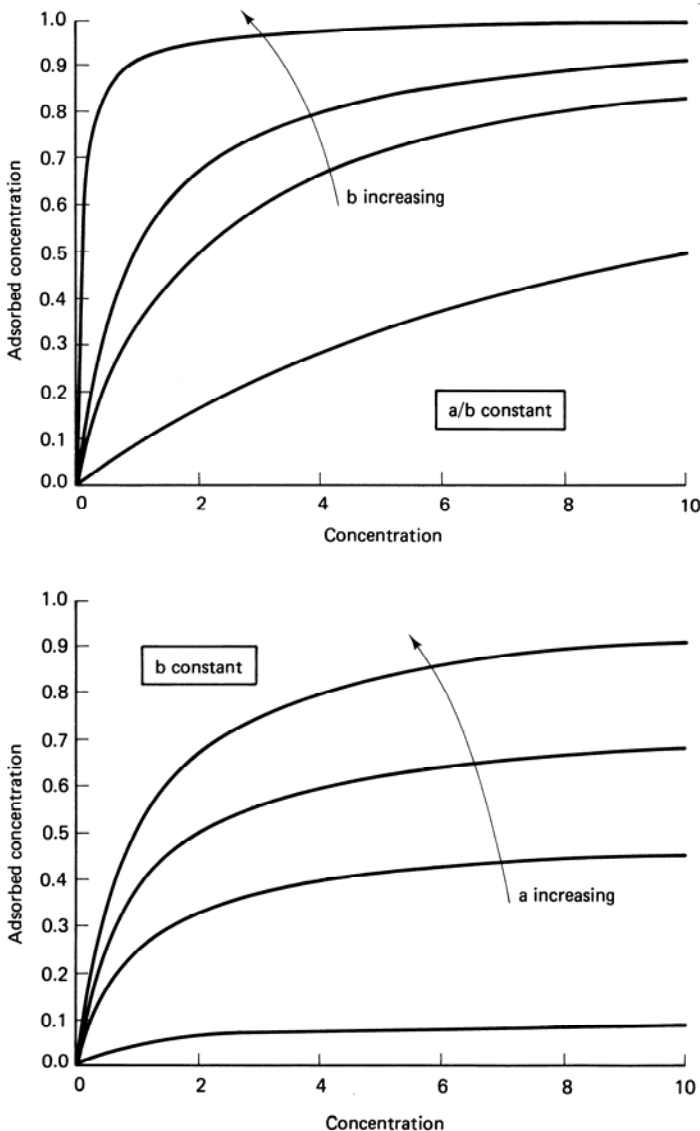


Figure 8-7 Typical Langmuir isotherm shapes

In the original Langmuir theory, the plateau adsorption corresponded to monolayer coverage of the surface by physical adsorption (see Exercise 8C). Considering the anionic character of water-soluble polymers, the adsorption is more likely to be chemical adsorption described by an exchange isotherm like Eq. (3.5-4). In fact, polymer adsorption does increase with increasing salinity and hardness but measured surface coverages are much smaller than monolayer coverage. Moreover, it is unknown if adsorption is reversible. Hence Eq. (8.2-10) and Fig. 8.7 are simply empirical representations of physical observations. (This is the origin of the term *Langmuir-type*.) Typical polymer adsorption isotherms are quite steep; that is, they attain their plateau value at very low C_4 . The values given above for polymer adsorption are referring to the plateau adsorption.

Equation (8.2-10) is a general isotherm function. The specific form depends on the units of the retention; unfortunately, no standard form exists for this. Common ways to report retention are

$$\frac{\text{Mass polymer}}{\text{Mass solid}} = \frac{\omega_{4s}}{(1 - \omega_{4s})}$$

$$\frac{\text{Mass polymer}}{\text{Surface area}} = \frac{\omega_{4s}}{a_v}$$

$$\frac{\text{Mass polymer}}{\text{Bulk volume}} = \omega_{4s} \rho_s (1 - \phi)$$

$$\frac{\text{Mass polymer}}{\text{Pore volume}} = \frac{\omega_{4s} \rho_s (1 - \phi)}{\phi} = C_{4s}$$

$$\frac{\text{Volume polymer solution}}{\text{Pore volume}} = \frac{\omega_{4s} \rho_s (1 - \phi)}{(\phi C_4)} = D_4$$

The last of these is often called the *frontal advance loss*.

Inaccessible Pore Volume

Offsetting the delay caused by retention is an acceleration of the polymer solution through the permeable medium caused by *inaccessible pore volume* (IPV). The most common explanation for IPV is that the smaller portions of the pore space will not allow polymer molecules to enter because of their size. Thus a portion of the total pore space is uninvaded or inaccessible to polymer, and accelerated polymer flow results. A second explanation of IPV is based on a wall exclusion effect whereby the polymer molecules aggregate in the center of a narrow channel (Duda et al., 1981). The polymer fluid layer near the pore wall has a lower viscosity than the fluid in the center, which causes an apparent fluid slip.

IPV depends on polymer molecular weight, medium permeability, porosity, and pore size distribution and becomes more pronounced as molecular weight increases and the ratio of permeability to porosity (characteristic pore size) decreases. In extreme cases, IPV can be 30% of the total pore space.

Permeability Reduction

For many polymers, viscosity–shear-rate data derived from a viscometer (μ' versus $\dot{\gamma}$) and those derived from a flow experiment (μ_{app} versus $\dot{\gamma}_{eq}$) will yield essentially the same curve. But for HPAM, the viscometer curve will be offset from the permeable medium curve by a significant and constant amount. The polymer evidently causes a degree of permeability reduction that reduces mobility in addition to the viscosity increase.

Actually, permeability reduction is only one of three measures in permeable media flow (Jennings et al., 1971). The *resistance factor* R_F is the ratio of the injectivity of brine to that of a single-phase polymer solution flowing under the same conditions

$$R_F = \frac{\lambda_1}{\lambda'_1} = \lambda_1 \mu_{app} = \left(\frac{k_1}{\mu_1} \right) \cdot \left(\frac{\mu'_1}{k'_1} \right) \quad (8.2-11)$$

For constant flow rate experiments, R_F is the inverse ratio of pressure drops; for constant pressure drop experiments, R_F is the ratio of flow rates. R_F is an indication of the total mobility lowering contribution of a polymer. To describe the permeability reduction effect alone, a *permeability reduction factor* R_k is defined as

$$R_k = \frac{k_1}{k'_1} = \frac{\mu_1}{\mu'_1} R_F \quad (8.2-12)$$

A final definition is the *residual resistance factor* R_{RF} , which is the mobility of a brine solution before and after (λ_{1a}) polymer injection

$$R_{RF} = \frac{\lambda_1}{\lambda_{1a}} \quad (8.2-13)$$

R_{RF} indicates the permanence of the permeability reduction effect caused by the polymer solution. It is the primary measure of the performance of a channel-blocking application of polymer solutions. For many cases, R_k and R_{RF} are nearly equal, but R_F is usually much larger than R_k because it contains both the viscosity-enhancing and the permeability-reducing effects.

The most common measure of permeability reduction is R_k , which is sensitive to polymer type, molecular weight, degree of hydrolysis, shear rate, and permeable media pore structure. Polymers that have undergone even a small amount of mechanical degradation seem to lose most of their permeability reduction effect. For this reason, qualitative tests based on screen factor devices are common to estimate polymer quality.

The screen factor device is simply two glass bulbs mounted into a glass pipette as shown in Fig. 8-8. Into the tube on the bottom of the device are inserted several fairly coarse wire screens through which the polymer solution is to drain. To use the device, a solution is sucked through the screens until the solution level is above the upper timing mark. When the solution is allowed to flow freely, the time required to pass from the upper to the lower timing mark td is recorded. The screen

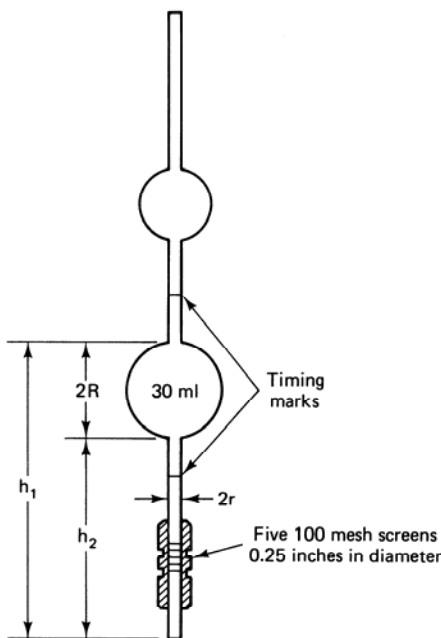


Figure 8-8 Screen factor device
(adapted from Foshee et al., 1976)

factor for the polymer solution is then defined as

$$S_F = \frac{t_d}{t_{ds}} \quad (8.2-14)$$

where t_{ds} is the similar time for the polymer-free brine.

Because of the normalization, screen factors are independent of temperature, device dimensions, and screen coarseness, and they are fairly independent of screen spacing. The screen factor is not independent of polymer concentration, but its primary intent is to measure the time-dependent portion of the polymer's solution configuration; that is, it measures the rate at which a polymer molecule returns to its steady-state flow configuration after it has been perturbed. This relaxation time is evidently very fast for the polysaccharides because they do not have a measurable screen factor even at high concentrations. HPAMs have much slower relaxation times because their screen factors can be large even at the same viscosity as a polysaccharide solution. The above explanations are consistent with the chemical properties of the two polymer groups given in Sec. 8-1 and can be used to deduce the sensitivity of screen factors to brine salinity and hardness.

Screen factors are particularly sensitive to changes in the polymer molecule itself. One definition of polymer quality is the ratio of the degraded to the undegraded screen factors. This use is important for screen factor devices, particularly in locations that prohibit more sophisticated equipment.

Another use for screen factors is as a correlator for R_F and R_{RF} (Fig. 8-9). The explanation for such a correlation is consistent with that given above on polymer

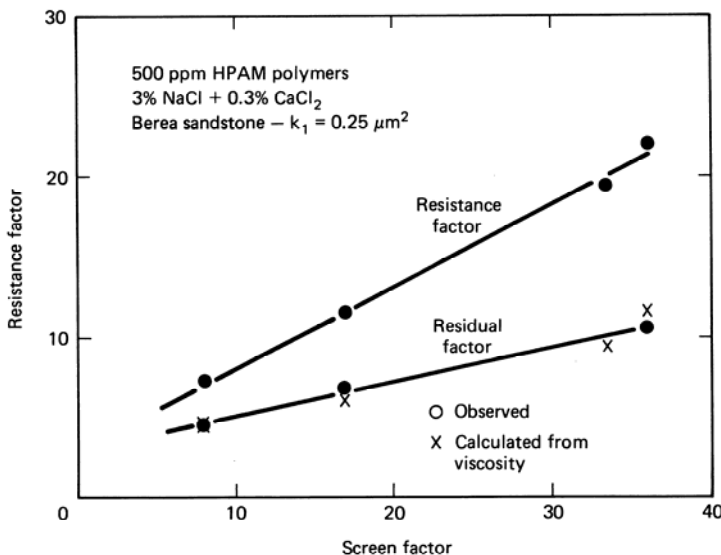


Figure 8-9 Correlation of resistance factors with screen factors (from Jennings et al., 1971)

relaxation. On a pore scale, steady flow in permeable media is actually a succession of contracting and diverging channels. The frequency with which the solution experiences these contractions, compared with the polymer relaxation time, determines the degree of permeability reduction. Such an effect also qualitatively explains the increase in viscometer viscosity at very high shear rates (Hirasaki and Pope, 1974).

The relaxation time argument cannot completely account for permeability reduction because such effects have been observed in glass capillaries. For this case, permeability reduction seems to be caused by polymer adsorption, which decreases the effective pore size (see Exercise 8E).

A reasonable question is whether permeability reduction is a desirable effect. R_k is difficult to control, being sensitive to even small deteriorations in the polymer quality. Moreover, an extremely large R_k will cause injectivity impairment. But it is possible to achieve a predesignated degree of mobility control with less polymer if $R_k > 1$. If M_T^0 is a design or target endpoint mobility ratio,

$$M_T^0 = \left(\frac{k'_1}{\mu_1^0} \right) \left(\frac{\mu_2}{k'_2} \right) = \frac{M^0|_{R_k=1}}{R_k} = \frac{M^0}{R_{RF}} \quad (8.2-15)$$

In this equation, $M^0|_{R_k=1}$ is the mobility ratio of a polymer having no permeability reduction, and M^0 is the endpoint water-oil mobility ratio. Clearly, if $R_k > 1$, the polymer viscosity μ_1^0 can be smaller than if $R_k = 1$, which indicates a given concentration of HPAM will have a lower mobility ratio than polysaccharide under conditions where both polymers have the same flowing viscosity. Note that the limiting viscosity μ_1^0 is used to estimate M^0 from Eq. (8.2-15).

Chemical and Biological Degradation

The average polymer molecular weight can be decreased, to the detriment of the overall process, by chemical, biological, or mechanical degradation. We use the term *chemical degradation* to denote any of several possible processes such as thermal oxidation, free radical substitution, hydrolysis, and biological degradation.

For a given polymer solution, there will be some temperature above which the polymer will actually thermally crack. Although not well established for most EOR polymers, this temperature is fairly high, on the order of 400 K. Since the original temperature of oil reservoirs is almost always below this limit, of more practical concern for polymer flooding is the temperature other degradation reactions occur at.

The average residence time in a reservoir is typically very long, on the order of a few years, so even slow reactions are potentially serious. Reaction rates also depend strongly on other variables such as pH or hardness. At neutral pH, degradation often will not be significant, whereas at very low or very high pH, and especially at high temperatures, it may be. In the case of HPAM, the hydrolysis will destroy the carefully selected extent of hydrolysis present in the initial product. The sensitivity to hardness will increase, and viscosity will plummet. For Xanthan gum, hydrolysis is even more serious since the polymer backbone is severed, resulting in a large decrease in viscosity.

TABLE 8-1 SELECTED BACTERICIDES AND OXYGEN SCAVENGERS (ADAPTED FROM ENHANCED OIL RECOVERY, NATIONAL PETROLEUM COUNCIL, 1984)

Bactericide	Oxygen scavengers
Commonly used	
Acrolein	Hydrazine
Formaldehyde	Sodium bisulfite
Sodium dichlorophenol	Sodium hydrosulfite
Sodium pentachlorophenol	Sulfur dioxide
Proposed or infrequent use	
Acetate salts of coco amines	
Acetate salts of coco diamines	
Acetate salts of tallow diamines	
Alkyl amino	
Alkyl dimethyl ammonium chloride	
Alkyl phosphates	
Calcium sulfate	
Coco dimethyl ammonium chloride	
Glutaraldehyde	
Paraformaldehyde	
Sodium hydroxide	
Sodium salts of phenols	
Substituted phenols	

Oxidation or free radical chemical reactions are usually considered the most serious source of degradation. Therefore, oxygen scavengers and antioxidants are often added to prevent or retard these reactions. These chemicals are strong reducing agents and have the additional advantage of reducing iron cations from the +3 to the +2 state. They, in turn, help prevent gelation, agglomeration, and other undesirable effects that can cause wellbore plugging and reduced injectivity. Wellington (1980) has found that alcohols such as isopropanol and sulfur compounds such as thiourea make good antioxidants and free radical inhibitors.

Laboratory results indicate Xanthan can be stabilized up to about 367 K, and HPAM to about 394 K. In the case of Xanthan, the results depend strongly on the precise conditions such as salinity and pH, with high salinity and pH between 7 and 9 being preferred. Obviously, one should test the particular polymer solution under the particular reservoir conditions of interest to establish the expected behavior.

Biological degradation can occur with both HPAM and polysaccharides, but is more likely with the latter. Variables affecting biological degradation include the type of bacteria in the brine, pressure, temperature, salinity, and the other chemicals present. As in waterflooding, the preventive use of biocide is highly recommended. Often too little biocide is used or it is started too late, and the ensuing problems become almost impossible to correct. Table 8-1 lists typical polymer flooding additions.

Mechanical Degradation

Mechanical degradation is potentially present under all applications. It occurs when polymer solutions are exposed to high velocity flows, which can be present in surface equipment (valves, orifices, pumps, or tubing), downhole conditions (perforations or screens), or the sand face itself. Perforated completions, particularly, are a cause for concern as large quantities of polymer solution are being forced through several small holes. For this reason, most polymer injections are done through open-hole or gravel-pack completions. Partial preshearing of the polymer solution can lessen the tendency of polymers to mechanically degrade. Because flow velocity falls off quickly with distance from an injector, little mechanical degradation occurs within the reservoir itself.

All polymers mechanically degrade under high enough flow rates. But 14PAMs are most susceptible under normal operating conditions, particularly if the salinity or hardness of the brine is high. Evidently, the ionic coupling of these anionic molecules is relatively fragile. Moreover, elongational stress is as destructive to polymer solutions as is shear stress though the two generally accompany each other. Maerker (1976) and Seright (1983) have correlated permanent viscosity loss of a polymer solution to an elongational stretch rate-length product. On a viscosity-shear-rate plot (purely shear flow), mechanical degradation usually begins at shear rates equal to or somewhat less than the minimum viscosity shear rate.

8-3 CALCULATING POLYMER FLOOD INJECTIVITY

The economic success of all EOR processes is strongly tied to project life or injection rate, but polymer flooding is particularly susceptible. In many cases, the cost of the polymer itself is secondary compared to the present value of the incremental oil. Because of its importance, many field floods are preceded by single-well injectivity tests. Here we give a simple technique for analyzing injectivity tests based on the physical properties given in the previous section.

The injectivity of a well is defined as

$$I \equiv \frac{i}{\Delta P} \quad (8.3-1)$$

where i is the volumetric injection rate into the well, and ΔP is the pressure drop between the bottom-hole flowing pressure and some reference pressure. Another useful measure is the relative injectivity

$$I_r = \frac{I}{I_1} \quad (8.3-2)$$

where I_1 is the water injectivity. I_r is an indicator of the injectivity decline to be anticipated when injecting polymer. Both I and I_r are functions of time, but the longtime limit of I_r for a Newtonian polymer solution is simply the viscosity ratio if skin effects are small. However, the ultimate I_r for an actual polymer solution can be higher than this because of shear-thinning.

We make several simplifying assumptions, many of which can be relaxed (Bondor et al., 1972). The well, of radius R_w , whose injectivity we seek, is in a horizontal, homogeneous, circular drainage area of radius R_e . The pressures at R_e and R_w are P_e and P_{wf} , respectively. P_e is constant (steady-state flow), but P_{wf} can vary with time. The fluid flowing in the reservoir is a single aqueous phase, at residual oil saturation, which is incompressible with pressure-independent rheological properties. Dispersion and polymer adsorption are negligible although the polymer can exhibit permeability reduction. The flow is one-dimensional and radial. Finally, the entire shear rate range in the reservoir lies in the power-law regime; hence Eq. (8.2-7) describes the apparent viscosity.

Subject to these assumptions, the continuity equation (Eq. 2.4-11) reduces to

$$\frac{d}{dr}(ru_r) = 0 \quad (8.3-3)$$

where u_r is the radial volumetric flux. This equation implies the volumetric rate is independent of r and equal to i since

$$i = 2\pi r H_t u_r \quad (8.3-4a)$$

Equation (8.3-4a) is a consequence of the incompressible flow assumption; however, i is not independent of time. Let us substitute Darcy's law for u_r in Eq. (8.3-4a)

$$i = -\frac{2\pi r H_t k'_1}{\mu_{app}} \frac{dP}{dr} = -\frac{2\pi r H_t k'_1}{H_{pl} u_r^{n_{pl}-1}} \frac{dP}{dr} \quad (8.3-4b)$$

from Eq. (8.2-7). This equation has been defined so that i is positive. The permeability reduction factor is introduced through Eq. (8.2-12). Eliminating u_r with Eq. (8.3-4a) yields an ordinary differential equation, which may be integrated between the arbitrary limits of P_1 at r_1 and P_2 at r_2 .

$$P_2 - P_1 = \left(\frac{i}{2\pi H_t} \right)^{n_{pl}} \frac{H_{pl} R_k}{k_1 (1 - n_{pl})} \left(r_1^{1-n_{pl}} - r_2^{1-n_{pl}} \right) \quad (8.3-5a)$$

The Newtonian flow limit, $n_{pl} = 1 = R_k$ and $H_{pl} = \mu_1$, of this equation is the familiar steady-state radial flow equation,

$$P_2 - P_1 = \frac{i \mu_1}{2\pi k_1 H_t} \ln \left(\frac{r_1}{r_2} \right) \quad (8.3-5b)$$

We now apply these equations to the polymer flood injectivity.

At some time t during the injection, the polymer front (assumed sharp) is at radial position R_p where

$$\int_0^t i dt = \pi (R_p^2 - R_w^2) H_t \phi (1 - S_{2r}) \quad (8.3-6)$$

The left side of this equation is the cumulative volume of polymer solution injected. Therefore, Eq. (8.3-5a) applies in the region $R_w < r < R_p$, and Eq. (8.3-5b) applies in the annular region $R_p < r < R_e$. With the appropriate identification of variables, we have for the second region

$$P|_{R_p} - P_e = \frac{i \mu_1}{2\pi k_1 H_t} \ln \left(\frac{R_e}{R_p} \right) \quad (8.3-7a)$$

and for the first

$$P_{wf} - P|_{R_p} = \left(\frac{i}{2\pi H_t} \right)^{n_{pl}} \frac{H_{pl}}{k_1 (1 - n_{pl}) R_k} (R_p^{1-n_{pl}} - R_w^{1-n_{pl}}) \quad (8.3-7b)$$

where $P|_{R_p}$ is the pressure at the polymer–water front. Adding these two equations gives the total pressure drop from R_w to R_e .

$$\begin{aligned} P_{wf} - P_e &= \left(\frac{i}{2\pi H_t} \right)^{n_{pl}} \frac{H_{pl} R_k}{k_1 (1 - n_{pl})} (R_p^{1-n_{pl}} - R_w^{1-n_{pl}}) \\ &\quad + \frac{i \mu_1}{2\pi k_1 H_t} \left(\ln \left(\frac{R_e}{R_p} \right) + S_w \right) \end{aligned} \quad (8.3-8)$$

where S_w the intrinsic skin factor of the well, has been introduced to account for well damage.

Equation (8.3-8) substituted into the injectivity definition (Eq. 8.3-1) gives

$$I^{-1} = \left(\frac{i}{2\pi H_t} \right)^{n_{pl}} \frac{H_{pl} R_k}{i(1-n_{pl})k_1} (R_p^{1-n_{pl}} - R_w^{1-n_{pl}}) + \frac{i\mu_l}{2\pi k_l H_t} \left(\ln \left(\frac{R_e}{R_p} \right) + S_w \right) \quad (8.3-9)$$

The water injectivity I_1 is given by Eqs. (8.3-1) and (8.3-5b), with $r_1 = R_w$ and $r_2 = R_e$. This and I , calculated from Eq. (8.3-9), yield an expression for I_r through Eq. (8.3-2). Both I and I_r relate to the cumulative polymer solution injection (or to time) through Eq. (8.3-6).

8-4 FRACTIONAL FLOW IN POLYMER FLOODS

The fractional flow treatment of polymer floods resembles the water–solvent treatment in Sec. 7-7. The only major complications are the addition of terms for polymer retention and inaccessible pore volume (IPV). In this section, we apply the usual fractional flow assumptions: one-dimensional flow, incompressible fluid and rock, and nondissipative mixing.

Single-Phase Flow

First, consider the case of a water-soluble species that is being adsorbed from solution via a Langmuir-type isotherm. The isotherm is given by Eq. (8.2-10).

Let the flow be such that species concentration C_{4J} is being displaced by concentration C_{4I} in single-phase flow where $C_{4J} > C_{4I}$. From Eq. (5.4-5a), the specific velocity of concentration C_4 is

$$v_{C_4} = \left(1 + \frac{(1-\phi)\rho_s}{\phi} \frac{d\omega_{4s}}{dC_4} \right)^{-1} = \left(1 + \frac{dC_{4s}}{dC_4} \right)^{-1}$$

From Eq. (8.2-10), the specific velocity becomes

$$v_{C_4} = \left(1 + \frac{C_4}{(1+b_4 C_4)^2} \right)^{-1} \quad (8.4-1)$$

But since $C_{4J} > C_{4I}$, we have $v_{C_4}|_J > v_{C_4}|_I$, and the displacement is a shock; if $C_{4J} < C_{4I}$ (see Exercise 8J), it would be a spreading wave. But for C_{4J} displacing C_{4I} , the front between C_{4J} and C_{4I} moves with specific velocity

$$v_{\Delta C_4} = \left(1 + \frac{(1-\phi)\rho_s}{\phi} \frac{\Delta\omega_{4s}}{\Delta C_4} \right)^{-1} = \left(1 + \frac{\Delta C_{4s}}{\Delta C_4} \right)^{-1} \quad (8.4-2)$$

from Eq. (5.4-5b). In this equation, $\Delta(\) = (\)_J - (\)_I$. If, as is usually the case for polymer floods, $C_{4I} = 0$, Eq. (8.4-2) reduces to

$$v_{\Delta C_4} = \frac{1}{1 + \frac{(1-\phi)\rho_s}{\phi} \left(\frac{\omega_{4s}}{C_4} \right)_J} = \frac{1}{1 + D_4} \quad (8.4-3)$$

where D_4 is the frontal advance loss for the polymer. It is also called the retardation factor because adsorption causes the front velocity to be lower than that of the ideal miscible displacement (see Sec. 5-4). D_4 is one of the most useful concepts in both polymer and micellar-polymer flooding because it expresses retention in pore volume units which are consistent with slug size.

Two-Phase Flow

The fractional flow treatment will consist of two phases (aqueous $j = 1$ and oleic $j = 2$) and three components (brine $i = 1$, oil $i = 2$, and polymer $i = 4$). Let the permeable medium have a uniform original water saturation of S_{1I} . We inject an oil-free polymer solution ($S_{1J} = 1 - S_{2r}$). The initial overall polymer concentration is 0, and the polymer concentration in the aqueous phase is C_{4J} . Polymer and water do not dissolve in the oil ($C_{12} = C_{42} = 0$); the oil has no solubility in the aqueous phase ($C_{21} = 0$).

Effect of IPV The aqueous phase porosity is ϕS_1 . Only a portion of this pore volume fraction, $(\phi S_1 - \phi_{IPV})$, is accessible to the polymer; hence the overall polymer concentration per unit bulk volume is

$$W_4 = (\phi S_1 - \phi_{IPV}) \rho_1 \omega_{41} + (1 - \phi) \rho_s \omega_{4s} \quad (8.4-4a)$$

Similarly, the overall water concentration is

$$W_1 = (\phi S_1 - \phi_{IPV}) \rho_1 (1 - \omega_{41}) + \phi_{IPV} \rho_1 \quad (8.4-4b)$$

since only water is present in the excluded pore volume ϕ_{IPV} . But the IPV can be easily neglected in Eq. (8.4-4b) because the polymer concentration is very small ($\omega_{41} \approx 1$). The overall oil concentration and Eqs. (8.4-4a) and (8.4-4b) sum to the porosity as required by the assumption of incompressible flow.

Oil Displacement The polymer itself alters neither the water nor the oil relative permeabilities because, as we have seen in Sec. 3-4, the apparent viscosity cannot be increased enough to change residual phase saturations. Moreover, when permeability reduction is significant, it applies over the entire saturation range but only to the wetting phase (Schneider and Owens, 1982). We may, therefore, construct a polymer-solution-oil (polymer–oil) water fractional flow curve simply by using the apparent viscosity in place of the water viscosity and dividing k_{r1} by R_k . Figure 8-10 shows both the water–oil ($f_1 - S_1$) and polymer–oil ($f_1^P - S_1$) fractional flow curves.

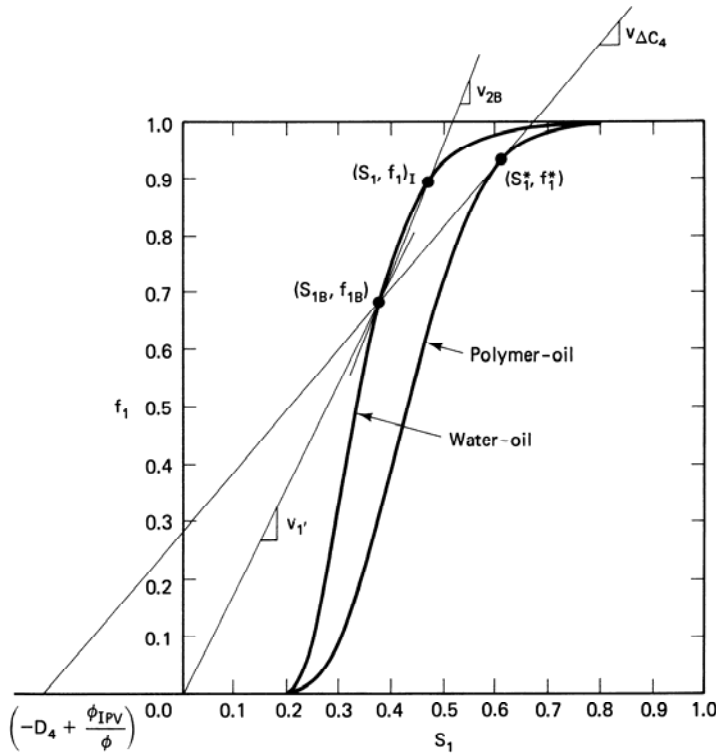


Figure 8-10 Graphical construction of polymer flooding fractional flow

Because the polymer adsorption is Langmuir-like, and because the polymer displaces the connate water miscibly, the polymer front is pistonlike and has specific velocity

$$v_{\Delta C_4} = \frac{f_1^p(S_1^*)}{S_1^* + D_4 - \phi_e} \quad (8.4-5a)$$

where D_4 is the polymer retardation factor defined in Eq. (8.4-3), and

$$\phi_e = \frac{\phi_{IPV}}{\phi} \quad (8.4-5b)$$

S_1^* and $f_1^p(S_1^*)$ are the water saturations and fractional flows at the polymer shock front. S_1^* may also be regarded as a point in the spreading portion of the mixed polymer–oil wave given by the Buckley–Leverett equation, whence from Eq. (8.4-5) we can define S_1^*

$$v_{\Delta C_4} = \frac{f_1^p(S_1^*)}{S_1^* + D_4 - \phi_e} = \left(\frac{df_1^p}{dS_1} \right)_{S_1^*} = v_{C_1} \quad (8.4-6)$$

since S_1^* is also in the shock portion of the polymer–oil wave. The Buckley–Leverett treatment in Sec. 5-2 used a similar argument.

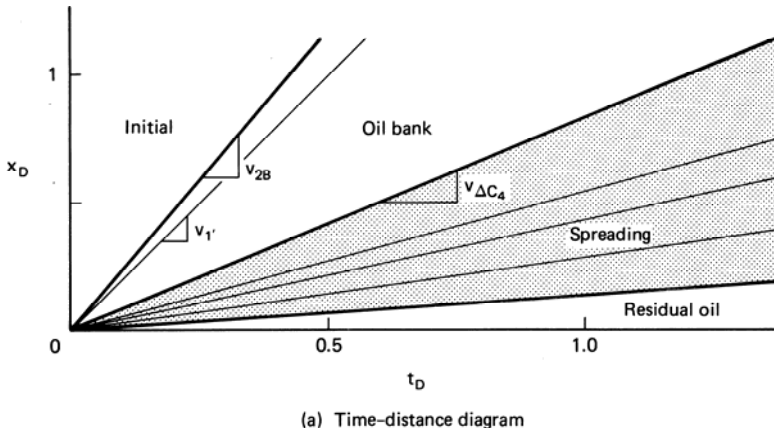
Equation (8.4-6) will also determine the oil bank saturation since S_2 will change discontinuously with velocity given by

$$v_{\Delta C_2} = \frac{f_1^P(S_1^*) - f_1(S_{1B})}{S_1^* - S_{1B}} = v_{C_1} \quad (8.4-7)$$

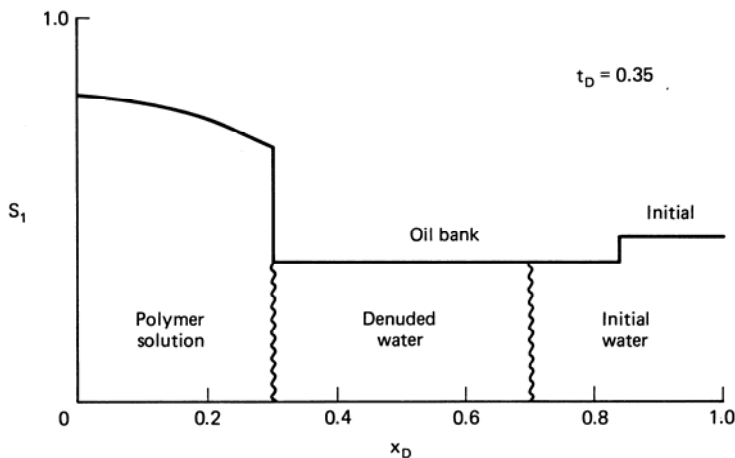
Equations (8.4-6) and (8.4-7) are particular statements of the coherence condition (Eq. 5.6-14).

As in the solvent–water treatment in Sec. 7-7, the velocity of the front of the oil (or water) bank is given by

$$v_{\Delta C_2} = \frac{f_{1B} - f_{1I}}{S_{1B} - S_{1I}} = v_{\Delta C_1} \quad (8.4-8)$$



(a) Time-distance diagram



(b) Saturation and concentration profile

Figure 8-11 Figures for the fractional flow curves in Fig. 8-10

for a pistonlike oil bank front. The construction proceeds in the same manner as in Sec. 7-7. Figure 8-11 shows the time-distance diagram and a composition profile at $t_D = 0.35$ for the construction in Fig. 8-10.

Though relatively direct, the construction in Figs. 8-10 and 8-11 has several important insights into polymer floods.

1. The oil bank breakthrough time (reciprocal of the oil bank specific velocity $v_{\Delta C_2}$) increases as S_{1I} increases, suggesting polymer floods will be more economic if they are begun at low initial water saturation. Of course, the lower S_{1I} , the higher the mobile oil saturation, also a favorable indicator for polymer floods.
2. Adsorption (large D_4) causes a delay of all fronts. D_4 can be large if the porosity is low, the retention is high, or the injected polymer concentration C_{4J} is low. Usually, C_{4J} is so low that D_4 can be high even if retention is moderate.
3. Inaccessible pore volume causes an acceleration of all fronts, exactly opposite to retention. In fact, retention and IPV can exactly cancel so that the polymer front and the denuded water front v_r (Fig. 8-10) travel at the same velocity.
4. Both D_4 and IPV influence the oil bank saturation, which in turn, influences the oil bank mobility and the desired injected polymer concentration.

8-5 ELEMENTS OF POLYMER FLOOD DESIGN

Polymer flood design is a complex subject. But most of the complexity arises from reservoir-specific aspects of a particular design. In this section, we deal in generalities that apply to all types of polymer flooding.

A polymer flood design procedure will follow these six steps.

1. Screen the candidate reservoirs. The distinction between technical and economic feasibility is important. Technical feasibility means a given reservoir can be polymer flooded regardless of the funds available. Economic feasibility means the project has a good chance of being profitable. Technical feasibility is measured by a series of binary screening parameters (see National Petroleum Council, 1984). But for polymer flooding, there are only two: the reservoir temperature should be less than about 350 K to avoid degradation, and the reservoir permeability should be greater than about $0.02 \mu\text{m}^2$ to avoid plugging. Economic feasibility can be estimated by simple hand calculations (as in the fractional flow method) or through using predictive models (Jones et al., 1984), which requires deciding how the polymer is to be used.
2. Decide on the correct mode. The choices are (a) mobility control (decrease M), (b) profile control (improve the permeability profile at the injectors or producers), or (c) some combination of both. We have not discussed profile control, but the concepts and goals are similar to polymer flooding. We want to inject an agent that will alter the permeability so that more fluid will go

into the tight rock than into the high-permeability rock. We can do this by using gels, polymers, and solids and by using selective perforation. When selective perforation is ineffective or incompletely effective, we use chemical agents or solids.

3. Select the polymer type. The requirements for EOR polymers are severe. An outline of the principal ones is as follows:
 - (a) Good thickening. This means high mobility reduction per unit cost.
 - (b) High water solubility. The polymers must have good water solubility under a wide range of conditions of temperature, electrolyte composition, and in the presence of stabilizers.
 - (c) Low retention. All polymers adsorb on reservoir rocks to various degrees. Retention may also be caused by plugging, trapping, phase separation, and other mechanisms. Low here means less than $20 \mu\text{g/g}$.
 - (d) Shear stability. During flow through permeable media, stress is applied to the polymer molecules. As we discussed, if this is excessive, they may mechanically break apart or permanently degrade, resulting in less viscosity. HPAM is especially subject to shear degradation.
 - (e) Chemical stability. Polymers, like other molecules, can chemically react, especially at high temperature and in the presence of oxygen. Antioxidants are used to prevent this.
 - (f) Biological stability. Both HPAM and polysaccharides can be degraded by bacteria, but the latter are more susceptible. Biocides are required to prevent this.
 - (g) Good transport in permeable media. This catchall includes essentially the ability to propagate the polymer through the rock intact and without excessive pressure drop or plugging. Good transport also means good injectivity and no problems with microgels, precipitates, and other debris.

Obviously, no one polymer can universally meet these requirements for all reservoir rocks. Thus we must tailor the polymer to the rock to some extent. Some general guidelines are possible for minimum standards, but the ultimate criterion must be economics.

4. Estimate the amount of polymer required. The amount, the total mass in kilograms to be injected, is the product of the slug size, the pore volume, and the average polymer concentration. Ideally, the amount would be the result of an optimization study that weights the present value of the incremental oil against the present value of the injected polymer. Each iteration of the optimization procedure requires estimating the polymer concentration in initial portion (spike) of the slug and estimating the volume of the polymer slug (spike plus rate of taper).
 - (a) Estimating the spike concentration. Suppose we have decided on a target mobility ratio that might come from simulation studies (see Chap. 6) or simply injectivity limitations. If the target mobility ratio is M_T

$$M_T = \frac{(\lambda_{rt})_{\text{polymer}}}{(\lambda_{rt})_{\text{oil bank}}} = \frac{(\lambda'_{r1} + \lambda_{r2})_{S_l^*}}{(\lambda_{r1} + \lambda_{r2})S_{1B}} \quad (8.5-1)$$

Estimating the spike concentration simply means picking the value of injected polymer concentration that gives the correct MT in this equation. The translation between apparent viscosity follows from permeability reduction factor correlations and shear rate data as in Fig. 8-4. The latter must be evaluated at a sheer rate corresponding to the median velocity in the flood—usually the low shear rate plateau. Estimating the denominator of Eq. (8.5-1), the oil bank relative mobility, is a little more difficult.

One procedure is to estimate the oil bank saturation through the graphical procedure of Sec. 8-4, and then estimate the oil bank mobility from the relative permeability curves evaluated at this saturation

$$(\lambda_{rt})_{0B} = \left(\frac{k_{r1}}{\mu_1} + \frac{k_{r2}}{\mu_2} \right) \Big|_{S_{1B}} \quad (8.5-2)$$

This procedure is iterative inasmuch as S_{1B} depends on the polymer–oil fractional flow curve. This, in turn, depends on the polymer apparent viscosity whose value we are estimating in Eq. (8.5-1). Fortunately, the dependence between S_{1B} and apparent viscosity is weak, and a trial-and-error procedure should converge rapidly.

A second procedure is to base the total mobility of the oil bank on the minimum in the total relative mobility curve (Gogarty et al., 1970). The minima in such curves do not, in general, correspond to the oil bank saturation from fractional flow theory. However, taking MT based on the minimum will yield a conservative design since the mobility ratio with the actual oil bank saturation will always be less than or equal to M_T . The method has the advantage of simplicity since it is noniterative.

Both methods require care in measuring relative permeability curves since hysteresis can render the drainage and imbibition k_r 's different (Chang et al., 1978). Such hysteresis effects are particularly difficult to reproduce when the initial water saturation begins at an intermediate value. The second method is also commonly used in micellar-polymer design (see Fig. 9-34).

- (b) Estimate the polymer slug volume. One way to do this is to simply let the slug volume be somewhat larger than the retention. Although this is the basic premise in designing a micellar slug, retention is not the dominant factor in polymer slug sizing. The major control affecting slug size is viscous fingering between the chase water and the polymer spike.

In predicting the extent of fingering, all the problems in estimating the rate of finger propagation that we discussed in Sec. 7-8 apply. Once again, we apply the Koval model, but here the effective mobility ratio must be modified to account for the polynomial mixing expressed in Eq. (8.2-1).

$$E = (1 + a_1 C_4 + a_2 C_4^2 + a_3 C_4^3 + \dots +) R_{RF} = \frac{K_{val}}{H_K} \quad (8.5-3)$$

where $C_4 = 0.22 C_{4J}$. The use of this equation, particularly the constant mixing factor 0.22, is relatively untested in polymer flooding. We have assumed complete analogy between the first-contact miscible flooding case and the unstable chase water displacement in this regard.

We use the time-distance diagram to sketch slug sizing alternatives. An obvious sizing technique is to begin chase water injection just as the polymer breaks through (Fig. 8-12a). This is excessively conservative since much full-strength polymer is produced. A second possibility is to adjust the polymer slug size so that the polymer and chase water break through simultaneously (Fig. 8-12b), leading to the following equation for slug size

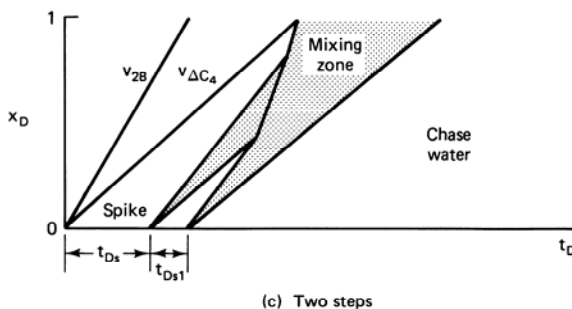
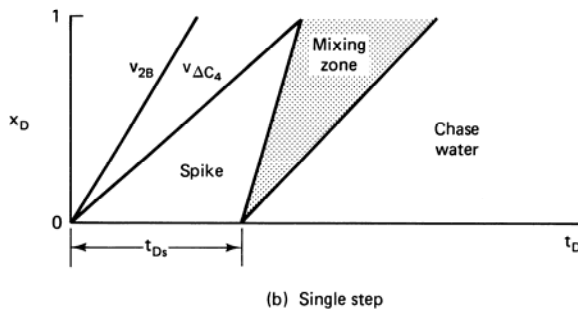
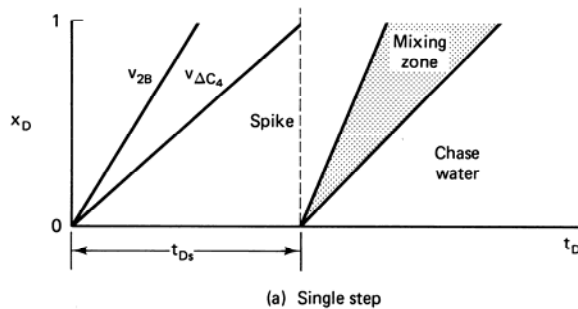


Figure 8-12 Time-distance diagrams for polymer grading

$$t_{Ds} = 1 - S_{2r} - D_4 - \frac{1 - S_{2r}}{K_{val}} \quad (8.5-4)$$

where we have taken $S_1^* = 1 - S_{2r}$, and $\phi_{IPV} = 0$. An equally viable alternative is to grade the polymer back to chase water in steps. Figure 8-12(c) shows two such steps with the size of the spike and the intermediate step adjusted so that the chase water again breaks through with the polymer. The isoconcentration lines become curved after there is wave interference.

The case in Fig. 8-12(c) uses less polymer than in Fig. 8-12(b). In fact, Claridge (1978) has shown that a continuously graded polymer drive uses the least amount of polymer. Such grading is impractical except as a limiting case to compare it to the no-grading case (Fig. 8-12b). But a succession of finite grading steps is extremely difficult to deal with theoretically because of the numerous degrees of freedom present. That is, the engineer must decide on the N number of steps, the N slug volumes, and the $N - 1$ intermediate concentrations. In practice, single-step (no-grading) polymer floods, and logarithmic grading (Mungan, 1968) are the most common procedures.

5. Design polymer injection facilities. Getting a good quality solution is, of course, important, but the cost of the injection facilities is usually small compared to well and chemical costs.

The three essential ingredients are mixing facilities, filtration, and injection equipment. The type of mixing apparatus depends on the polymer. For solid polymers, a skid-mounted solid mixer is required. Concentrates or emulsion polymers require somewhat less sophistication although the latter may require some emulsion breaking. Filtration largely depends on the success of the mixing, but ordinarily it is no more stringent than what is required by waterflooding. But if exotic and difficult filtration is required, the complexity and cost can become significant. Injection equipment is the same as that for waterflooding. All surface and downhole equipment should be modified to avoid all forms of degradation.

6. Consider the reservoir. Little is required here beyond the usual waterflood considerations such as the optimal well pattern and spacing, completion strategy, pattern allocation (balance), reservoir characterization, and allowable injection rates.

Optimal values of these quantities imply precise values that will result in the maximum rate of return on investment. Since several quantities are involved, it is usually not possible to perform optimizations on everything. Hence most of the parameters must be fixed by other considerations (such as striving for a target mobility ratio). But for the most sensitive quantities, optimization is required.

Figure 8-13 shows a schematic optimization for the amount of polymer injected. The vertical axes plot both an economic measure, such as the cumulative incremental discounted cash flow (DCF), and incremental oil

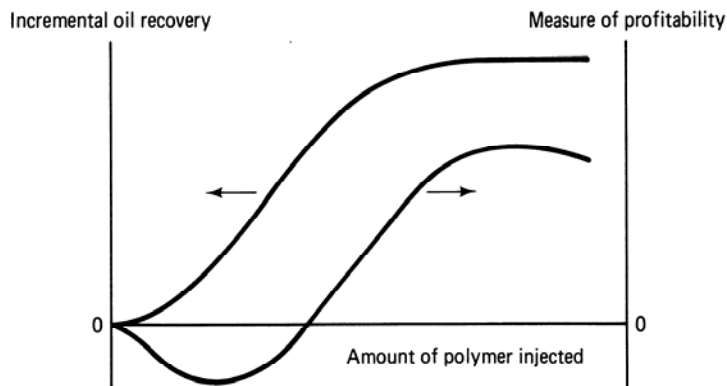


Figure 8-13 Schematic incremental oil recovered and economic trends for a mobility control flood.

recovery (IOR) versus the amount of polymer injected. The IOR curve is monotonically increasing from zero. The DCF curve begins at zero, decreases for small polymer amounts, and then rises to a maximum at substantially larger amounts. After this point, the DCF decreases monotonically. The DCF decreases initially because the entire expense of the polymer is assessed in the initial stages of a project when little incremental oil has yet been produced. This front-end loading effect is present in all EOR processes, particularly chemical floods. Such a curve is highly instructive because it counters a tendency to short-cut the amount of polymer injected if the initial economics are unfavorable. Unfortunately, many actual polymer flood applications have used less than the optimum amount of polymer.

8-6 FIELD RESULTS

The incremental oil recovery (IOR) from a polymer flood is the difference between the cumulative oil actually produced and that which would have been produced by a continuing waterflood (see Exercise 8L). Thus for a technical analysis of the project, it is important to establish a polymer flood oil rate decline and an accurate waterflood decline rate. Figure 8-14 shows the IOR for the North Burbank polymer flood.

Table 8-2 summarizes other field results on more than 250 polymer floods based on the comprehensive survey of Manning et al. (1983). The table emphasizes oil recovery data and screening parameters used for polymer flooding. Approximately one third of the reported projects are commercial or field-scale floods. The oil recovery statistics in Table 8-2 show average polymer flood recoveries of 3.56% remaining (after waterflood) oil in place and about 1 m³ of IOR for each kilogram of polymer injected with wide variations in both numbers. The large variability reflects the emerging nature of polymer flooding in the previous decades. Considering the average polymer requirement and the average costs of crude and polymer, it appears that polymer flooding should be a highly attractive

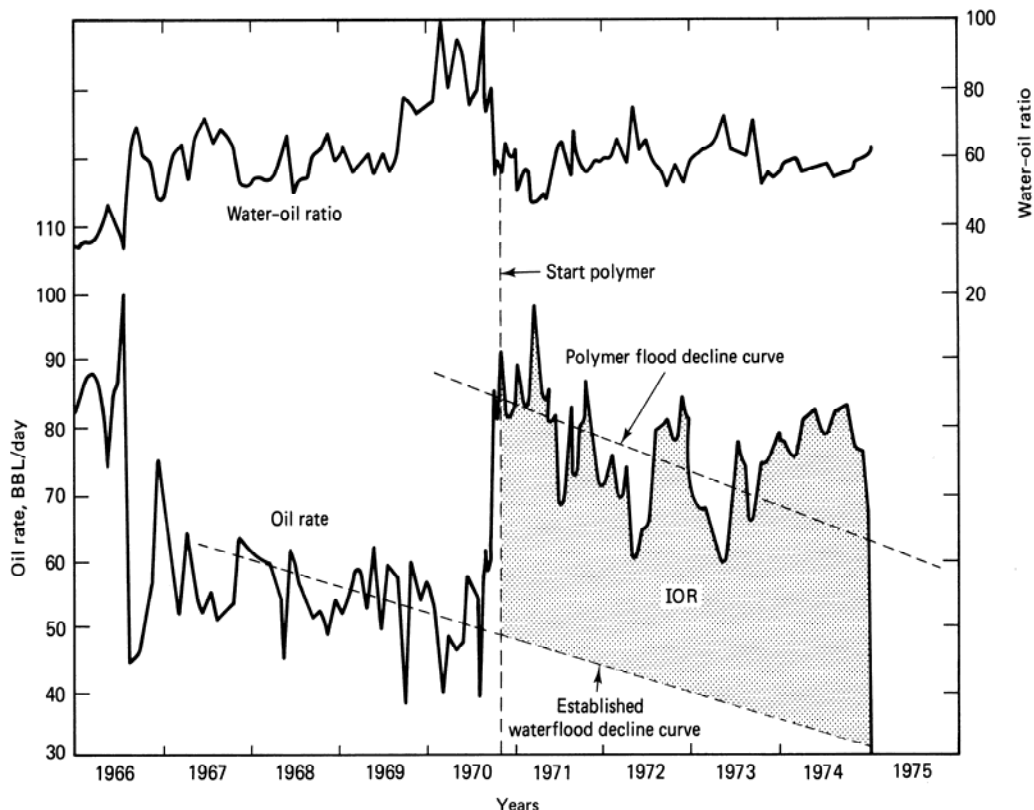


Figure 8-14 Tertiary polymer flood response from North Burbank Unit, Osage County, Okla. (from Clampitt and Reid, 1975)

EOR process. However, such costs should always be compared on a discounted basis, reflecting the time value of money. Such a comparison will decrease the apparent attractiveness of polymer flooding because of the decreased injectivity of the polymer solutions.

8-7 CONCLUDING REMARKS

In terms of the number of field projects, polymer flooding is the most common enhanced oil recovery technique in existence. The reasons for this are that, short of waterflooding, polymer flooding is the simplest technique to apply in the field and requires a relatively small capital investment. Most of the field projects have been small, however, as has the amount of oil recovered, a fact that should be expected from the treatment given in this chapter. Nevertheless, there can exist significant potential for an acceptable rate of return even when recovery is low.

The most important property covered in this chapter is the non-Newtonian behavior of polymer solutions, because such behavior impacts on the polymer

TABLE 8-2 POLYMER FLOOD STATISTICS (ADAPTED FROM MANNING, 1082)

Value standard (units)	Number projects*	Mean	Minimum	Maximum	Standard deviation
Oil recovery (% remaining OIP)	50	3.56	0	25.3	5.63
Polymer utilization (m ³ /kg polymer)	80	0.94	0	12.81	1.71
Oil recovery (m ³ /hm ³ bulk volume)	88	3.1	0	24.3	4.72
Permeability variation (fraction)	118	0.70	0.06	0.96	0.19
Mobile oil saturation (fraction)	62	0.27	0.03	0.51	0.12
Oil viscosity (mPa-s)	153	36	0.072	1,494	110.2
Resident brine salinity (kg/m ³ TDS)	10	40.4	5.0	133.0	33.4
Water-to-oil mobility Ratio (dimensionless)	87	5.86	0.1	51.8	11.05
Average polymer Concentration (g/m ³)	93	339	51	3,700	343
Temperature (K)	172	319	281	386	302
Average permeability (μm ²)	187	0.349	0.0015	7.400	0.720
Average porosity (fraction)	193	0.20	0.07	0.38	0.20

*Partial data available on most projects; includes both commercial and pilot projects

requirements through the design mobility ratio, and on the ability to accurately forecast the rate of polymer injection. Polymer injection rate determines project life which, in turn, determines the economic rate of return. Injectivity estimates along with estimates of mobile oil saturation and the likelihood that polymer will remain stable in a given application are the most important determinants in polymer flooding success.

EXERCISES

- 8A. Calculating Shear Rates.** Calculate the equivalent shear rate under the following conditions:
- In an open-hole completion (entire well cylinder open to flow) where $q = 16$ m³/day, $R_w = 7.6$ cm, and net pay $H_t = 15.25$ m.
 - In the field where the interstitial velocity is 1.77 μm/s.
 - Using the data for Xanflood at 297 K and 1% NaCl (Fig. 8-5), estimate the effective permeable medium viscosity at the above conditions for a 600 g/m³ polymer solution.

- (d) Suppose the well in part (a) is perforated with 1 cm (ID) holes over its entire net pay at a density of 4 holes/m. Assuming a uniform fluid distribution, estimate the shear rate in the perforations.
- (e) Comparing the results of parts (a) and (d), what do you conclude about the preferred completion technique in polymer flooding? Use $k_1 = 0.1 \mu\text{m}^2$, $\phi = 0.2$, and $S_1 = 1.0$ in all parts.
- 8B.** *Derivation of Power Law in Permeable Media.* Equation (8.2-9) may be derived in the same manner as Eq. (3.1-11). The procedure is as follows:
- (a) Show that a force balance on an annular element of a single-phase fluid flowing through a tube (as in Fig. 3. 1) in laminar steady-state flow is

$$\frac{1}{r} \frac{d(r\tau_{rz})}{dr} = \frac{\Delta P}{L} \quad (8B-1)$$

where τ_{rz} is the shear stress on the cylindrical face at r , and $\Delta P/L$ is the pressure gradient. This equation, when integrated, yields

$$\tau_{rz} = \frac{\Delta P}{2L} r \quad (8B-2)$$

The shear stress must be finite at $r = 0$.

- (b) The power-law expression relating shear stress to shear rate is

$$\tau_{rz} = K_{pl} \dot{\gamma}^{n_{pl}-1} \quad (8B-3)$$

where

$$\dot{\gamma} = -\frac{dv}{dr} \quad (8B-4)$$

is the shear rate. Show that combining Eqs. (8B-2) through (8B-4) leads to a differential equation whose solution is

$$v(r) = \left(\frac{\Delta P}{2LK_{pl}} \right)^{1/n_{pl}} \left(\frac{n_{pl}}{1+n_{pl}} \right) \left(R^{\frac{1+n_{pl}}{n_{pl}}} - r^{\frac{1+n_{pl}}{n_{pl}}} \right) \quad (8B-5)$$

This equation has used the no-slip condition $v(R) = 0$.

- (c) Using Eq. (8B-5), show that the shear rate at the wall of the tube depends on the average velocity as

$$\dot{\gamma}_{wall} = \frac{1+3n_{pl}}{n_{pl}} \left(\frac{\bar{v}}{R} \right) \quad (8B-6)$$

- (d) When the equivalent radius from Eq. (3.1-4) is substituted, this gives

$$\dot{\gamma}_{eq} = \left(\frac{1+3n_{pl}}{n_{pl}} \right) \frac{u}{(8k_1\phi_1)^{1/2}} \quad (8B-7)$$

With appropriate variable identifications, this equation yields Eqs. (8.2-7) and (8.2-8) when substituted into

$$\mu_{app} = \frac{\tau_{rz}}{\dot{\gamma}_{eq}} \quad (8B-8)$$

- 8C.** *Langmuir Calculations.* The Langmuir isotherm and various other insights may be derived fairly simply. Suppose a permeable medium in contact with a solution containing an adsorbing species consists of a fixed number of surface sites. A fraction ϕ of these sites is covered when the solution concentration of an adsorbing species is C .
- (a) Let the rate of adsorption be $k_f C (1 - \phi)$ and the rate of desorption be $k_r \phi$. k_f and k_r are the forward and reverse rate constants. At equilibrium, the forward and reverse reaction rates are equal. Show that the fractional surface coverage is

$$\theta = \frac{\frac{k_f}{k_r} C}{1 + \frac{k_f}{k_r} C} \quad (8C-1)$$

- (b) Show that ϕ may be related to ω_s , adsorption in mass per unit of rock mass by

$$\theta = \frac{d_p^2 N_A \rho_r}{a_v M_w} \omega_s \quad (8C-2)$$

where ρ_r is the adsorbed species density, a_v is the specific surface area of the medium, M_w is the molecular weight of the adsorbed species, and N_A is Avogadro's number. Assume the adsorbed species exists on the surface as a monolayer of cubes of diameter d_p .

- (c) If the observed polymer adsorption is 18 $\mu\text{g/g-rock}$, calculate ϕ . Take the medium to have the Berea properties tabulated in Table 3-5. You must derive the effective polymer sphere diameter from the intrinsic viscosity (Eq. 8.2-4) and the data in Fig. 8-4. The polymer molecular weight is 2 million.
- (d) What can you conclude about the nature of the adsorption of polymers from this?
- 8D.** *Complications to Langmuir Isotherm*

- (a) Suppose there is Langmuir adsorption of a single adsorbing species with a finite mass transfer rate r_{mt} between the bulk solution and the solid–fluid interface given by

$$r_{mt} = h(C - \tilde{C}) \quad (8D-1)$$

In this expression, C and \tilde{C} are the bulk and interface concentrations, and h is the specific mass transfer coefficient. Show that an isotherm relating ϕ to C has the same form as Eq. (8C-1) but with k'_f replacing k_f where

$$\frac{1}{k'_f} = \frac{1}{k_f} + \frac{1}{h} \quad (8D-2)$$

You must assume the rate of adsorption is equal to r_{mt} ,

- (b) Show that if $h \rightarrow \infty$, the isotherm approaches the expression derived in Exercise 8C.
- (c) Consider now a case where $h \rightarrow \infty$ and there are $i = 1, \dots, N_C$ adsorbing species, each competing for a fixed number of sites. Derive the Langmuir isotherm relating the adsorbed concentration of species i , ϕ_i , to its bulk concentration C_i .
- (d) Use this expression to justify the fractional coverages calculated in part (d) of Exercise 8C.

- 8E.** *Simplified Permeability Reduction.* One of the explanations for permeability reduction is that the effective pore size is decreased (or the effective grain diameter increased) because of the adsorption of a layer of polymer on the rock surface. In the following, take the medium to be comprised as spheres of diameter D_p :

- (a) Derive an expression for the permeability reduction factor R_k based on the polymer adsorbing as a uniform layer of thickness δ on the rock surface. You must use the hydraulic radius concept developed in Sec. 3-1.
- (b) Make two plots, at $\phi = 0.1$ and 0.2 , of polymer adsorption (in mg polymer/g-rock) versus R_k . Take the density of the adsorbed polymer to be 1.5 g/cm^3 and the density of the rock to be 2.5 g/cm^3 .

- 8F.** *Representation of Linear Viscoelasticity.* A powerful conceptual model of a liquid that has some elastic effects is the Maxwell model, which is the series combination of a spring and a dashpot



where F is the force sustained by the model, and ϵ_1 and ϵ_2 are the strains (dimensionless deformations). Let the spring be a linear elastic element so that

$$F = k\epsilon_1 \quad (8F-1)$$

likewise, the dashpot is a Newtonian viscous element

$$F = \mu\dot{\epsilon}_2 \quad (8F-2)$$

where k and μ are the spring constant and viscosity of the element. Because of the series arrangement, the force supported by both elements is the same; however, the total strain ϵ is

$$\epsilon = \epsilon_1 + \epsilon_2 \quad (8F-3)$$

- (a) Show that the relationship between the time behavior of the force and the strain is

$$\mu\dot{\epsilon} = \theta\dot{F} + F \quad (8F-4)$$

In this equation, $\theta = \mu/k$ is the relaxation time of the model, and $\dot{\epsilon}$ is the time derivative of ϵ .

- (b) To integrate this, we treat $\dot{\epsilon}$ as a known function of time. Show that the general solution is

$$F(t) = e^{-t/\theta} F(0) + k e^{-t/\theta} \int_0^t e^{\xi/\theta} \frac{d\epsilon}{d\xi} d\xi \quad (8F-5)$$

The next three steps complete the analogy between the Maxwell model and viscoelastic flow.

- (c) If the rate of strain is constant and the initial force of the model is zero, show that

$$F(t) = \mu\dot{\epsilon}(1 - e^{-t/\theta}) \quad (8F-6)$$

- (d) The apparent viscosity of the model is defined as $F/\dot{\epsilon}$. Show from Eq. (8F-4) that this becomes

$$\mu_{app} = \frac{\mu}{1 + \theta \frac{\dot{F}}{F}} \quad (8F-7)$$

(e) Use this equation and Eq. (8F-6) to show that

$$\mu_{app} = \frac{\mu}{1 + N_{Deb}} \quad (8F-8)$$

The quantity in the denominator of Eq. (8F-8) is the Deborah number

$$N_{Deb} = \frac{\theta}{t} \quad (8F-9)$$

This number, the ratio of relaxation time to undisturbed flow time around a rock grain, is a measure of viscoelastic effects in permeable media flow when the characteristic flow time t has been replaced by $\phi D_p / \mu$.

- 8G.** *Analysis of Screen Factor Device.* The screen factor device in Fig. 8-8 may be analyzed as a permeable medium experiencing gravity drainage. The volume V of fluid in the bulb at any height h ($h_1 > h > h_2$) is

$$V = \frac{\pi}{3} (h - h_2)(3R - h + h_2) \quad (8G-1)$$

from the bulb geometry. If we treat the screen pack as a permeable resistive element, the flux through the screens is

$$u = -\left(\frac{k \rho g h}{L \mu_{app}} \right) \quad (8G-2)$$

- (a) Since $u = -1/\pi r^2 (dV/dt)$, show from these equations that the height h is the solution to

$$\frac{dh}{dt} [(h - h_2)(2R - (h - h_2))] = \frac{r^2 \rho g k h}{\mu_{app} L} \quad (8G-3)$$

L in these equations is the height of the screen pack.

- (b) Neglecting the drainage times in the tubes above and below the lower bulb, derive an expression for the drainage time for a Newtonian fluid. The drainage time t_d is defined as

$$t_d = t|_{h=h_2} - t|_{h=h_1} \quad (8G-4)$$

- (c) Repeat part (b) with a viscoelastic fluid whose apparent viscosity is

$$\mu_{app} = \frac{H_{VE}}{1 + bu} \quad (8G-5)$$

In view of Eqs. (8G-4) and (8.2-14), show that the screen factor SF is given by

$$SF = \frac{H_{VE}}{\mu_1} + \frac{k \rho g}{\mu_1 L} bI \quad (8G-6)$$

where I is a geometric factor. From Exercise 8F, the screen factor is directly proportional to the fluid's relaxation time.

8H. Injectivity Calculation

Use the following data for the Coalinga HX sand (Tinker et al., 1976):

$$\begin{array}{ll} \phi = 0.28 & k_1 = 0.036 \mu\text{m}^2 \\ K_{pl} = 7.5 \text{ mPa-s(s)}^{n_{pl}-1} & \mu_1 = 0.64 \text{ mPa-s} \\ n_{pl} = 0.8 & H_t = 2.44 \text{ m} \\ R_k = 3 & R_w = 10 \text{ cm} \\ R_e = 284 \text{ m} & i = 30 \text{ m}^3/\text{D} \\ & S_{2r} = 0.2 \end{array}$$

- (a) Calculate the relative injectivity I_r versus cumulative polymer injected. Plot I_r versus t_D (up to $t_D = 0.5$) on linear graph paper.
- (b) Show that when $R_p = R_e$, the Newtonian polymer case ($n_{pl} = 1$) reduces to

$$I_r = \frac{\mu_1}{K_{pl}R_k} \quad (8H-1)$$

- (c) Plot the Newtonian polymer case for the HX sand on the same plot as in part (a).
- 8I. *Improvements to Injectivity Calculations.* If the shear rate range in a cylindrical reservoir is outside the power-law range, the following truncated form of Eq. (8.2-7) must be used:

$$\mu_{app} = \begin{cases} \mu_1^0, & u < u_0 \\ H_{pl}u^{n_{pl}-1}, & u_0 < u < u_\infty \\ \mu_1^\infty, & u > u_\infty \end{cases} \quad (8I-1)$$

where u_0 and u_∞ are superficial velocities which define the limits of the power law range.

- (a) Repeat the derivation in Sec. 8-3 for I and I_r using Eq. (8I-1), assuming both the maximum and minimum velocities fall outside the power-law range.
- (b) For numerical simulation, it may be more convenient to define injectivity in terms of the average reservoir pressure \bar{P} rather than P_e (Bondor et al., 1972). Rederive the expression for I defined in this manner.
- (c) For large numerical simulations, the entire non-Newtonian range of polymer behavior is confined within one grid block of the well. This being the case, the non-Newtonian effect can be effectively expressed as a time-varying skin factor in terms of an average polymer "saturation." Derive an expression for this skin factor.
- 8J. *Transport of Adsorbing Slugs.* The leading edge of a polymer slug adsorbing as a Langmuir isotherm is self-sharpening.
 - (a) Show that the rear of the slug ($C_K < C_J$) is a spreading wave.
 - (b) If the Langmuir parameters in Eq. (8.2-10) are $a = 2$ and $b = 20$, plot the time-distance diagram and effluent history of $t_{Ds} = 0.4$ slug displacement. Take $C_I = C_K = 0$ and $C_J = 1$.
 - (c) The propagation of slugs satisfies an overall material balance

$$t_{Ds} = \frac{\int_0^\infty (C + C_s) dx_D}{C_J} \quad (8J-1)$$

Use the analogy to the Welge integration in Sec. 5-2 to show that Eqs. (8.4-1) and (8.4-2) satisfy this identically. In all these calculations, take the flow to be single phase with the usual fractional flow assumptions.

- 8K.** *Asymptotic Mixing Zone Length* (Lake and Helfferich, 1978). Stabilized mixing zones occur in miscible displacements if the transported species adsorbs according to a Langmuir isotherm. The spreading caused by dispersion is balanced by the sharpening caused by adsorption. In the following, take the dimensionless material balance of an adsorbing species to be

$$\frac{\partial(C + C_s)}{\partial t D} + \frac{\partial C}{\partial x_D} - \frac{1}{N_{Pe}} \frac{\partial^2 C}{\partial x_D^2} = 0 \quad (8K-1)$$

where C and C_s are the solution and adsorbed concentrations for an adsorbing species. C is normalized so that the injected concentration is unity, $C_J = 1$, and $C_I = 0$.

- (a) Show that Eq. (8K-1) may be transformed to a moving coordinate system (x'_D, t_D) , where $x'_D = x_D - v_{AC} t_D$, and v_{AC} is the shock velocity of C . This gives

$$\frac{\partial(C + C_s)}{\partial t D} - v_{AC} \frac{\partial C_s}{\partial x'_D} + (1 - v_{AC}) \frac{\partial C}{\partial x'_D} - \frac{1}{N_{Pe}} \frac{\partial^2 C}{\partial (x'_D)^2} = 0 \quad (8K-2)$$

- (b) The displacement will asymptotically approach stabilized flow where the time derivatives in Eq. (8K-2) are zero. Show that in this limit the resulting ordinary differential equation may be integrated to give

$$\Delta x_D = \frac{1}{N_{Pe}} \int_{0.9}^{0.1} \frac{dC}{(1 - v_{AC})C - v_{AC}C_s} \quad (8K-3)$$

Equation (8K-3) uses the boundary conditions $C(+\infty) = dC(+\infty)/dx_D = 0$ and the definition of dimensionless mixing zone given in Eq. (5.2-15a).

- (c) When $C_J = 1$, it is convenient to write the Langmuir isotherm (Eq. 8.2-10) so that the plateau adsorption appears in the equation in place of the parameter a

$$C_s = \frac{(1+b)C_{sj}C}{1+bC} \quad (8K-4)$$

where C_{sj} is the maximum adsorbed concentration. Substitute Eq. (8K-4) into Eq. (8K-3), and perform the indicated integration to show that

$$\Delta x_D = \frac{1}{N_{Pe}} \left\{ \frac{1+C_{sj}}{C_{sj}} \right\} \left(1 + \frac{2}{b} \right) \ln(9) \quad (8K-5)$$

where this equation has used a form of v_{AC} consistent with Eq. (8K-4).

- (d) Take Eq. (8K-5) in the limits of $b \rightarrow \infty$, $b \rightarrow 0$, and $N_{Pe} \rightarrow \infty$, and justify each answer on physical grounds.

- 8L.** *Fractional Flow and Incremental Oil*

- (a) Calculate the polymer frontal advance lag D_4 when the maximum polymer adsorption is 38 g/m^3 (bulk volume), the injected polymer concentration is 1200 g/m^3 , and the porosity is 0.2.

- (b) Using the D_4 of part (a) and the water–oil relative permeabilities in Fig. 8L, calculate the effluent history of polymer and oil for a polymer flood with $\mu_l^0 = 30$ mPa-s. Take the oil and water viscosities to be 20 and 1 mPa-s, respectively, the dip angle to be 0, the permeability reduction factor to be 1, and the initial water saturation to be 0.4.
- (c) The technically correct way to evaluate a polymer flood is by the incremental oil recovery (IOR)

$$\text{IOR} = \left(\frac{\text{Polymer flood}}{\text{oil produced}} \right) - \left(\frac{\text{Waterflood}}{\text{oil produced}} \right) \quad (8\text{L}-1)$$

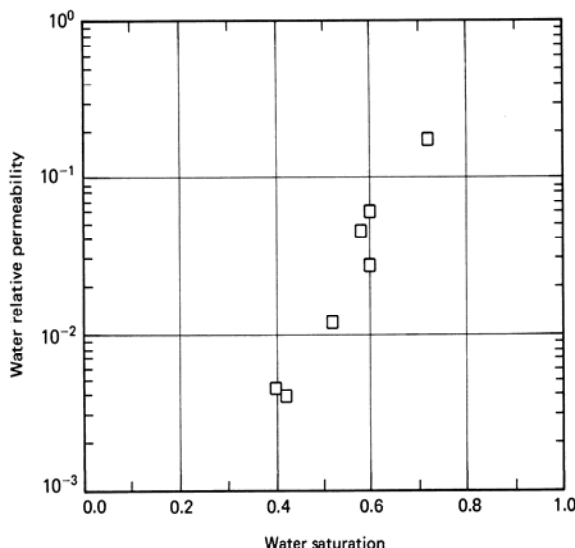
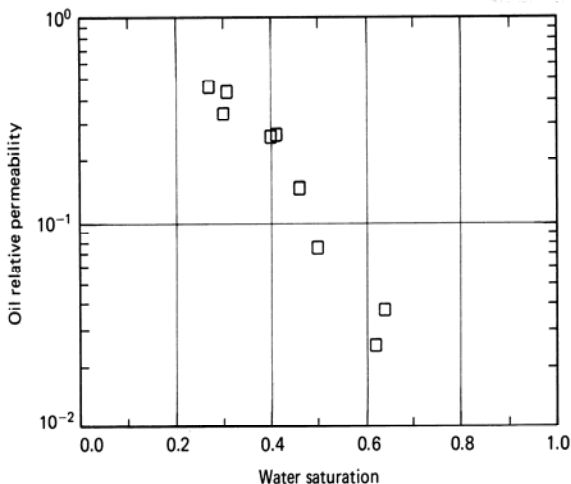


Figure 8L Relative permeabilities for Exercise 8L (from El Dorado, 1977).

Calculate and plot IOR (in SCM) versus time (years). Take the pore volume to be $1.6 \times 10^6 \text{ m}^3$, the injection rate constant at 480 SCM/day, and all formation volume factors to be $1.0 \text{ m}^3/\text{SCM}$.

- 8M.** *Fractional Flow and Slugs.* Fractional flow theory can be used to gain insight into the behavior of polymer slugs, under idealized conditions, and into the polymer utilization factor.

- (a) Assume the polymer is to be injected as a slug. If the chase water displaces the polymer as an ideal miscible displacement at residual oil saturation, show that the polymer chase water front travels with specific velocity

$$v_{CW} = \frac{1}{1 - S_{2r}} \quad (8M-1)$$

if the polymer adsorption is irreversible and excluded pore volume negligible.

- (b) Show that the polymer slug size just needed to satisfy adsorption is equal to D_4 .
(c) The data to use in the remainder of this exercise are

$$\begin{aligned} a &= 1 \text{ cm}^3/\text{g-rock} & C_{4J} &= 800 \text{ g/m}^3 \\ b &= 100 \text{ cm}^3/\text{mg} & \rho_s &= 2.65 \text{ g/cm}^3 \\ \phi &= 0.2 \end{aligned}$$

Plot the time-distance and effluent histories (oil and polymer) if the slug size used is one half that demanded by adsorption. Use the fractional flow curves and initial condition of Exercise 8L.

- 8N.** *Polymer Flood Design.* You want to design a polymer flood in a reservoir containing an oil and brine whose viscosities are 25 mPa-s and 0.38 mPa-s, respectively, at reservoir temperature of 73°C. The relative permeability curves of Fig. 8L apply, and conditions indicate the Xanflood data in Figs. 8-4 and 8-5 are satisfactory for this reservoir.

- (a) Plot the total relative mobility curves. If the desired mobility ratio is 0.7, estimate the polymer concentration required to bring this about. Use the data in Fig. 8-5, and recall that μ'_1 / μ_1 is essentially independent of temperature.
(b) Estimate the power-law parameters K_{pl} , n_{pl} , and H_{pl} for the polymer solution in part (a).
(c) The flood is to be done at a constant volumetric injection rate of 20 m³/D. Estimate and plot as a function of volume injected the bottom-hole injection pressure in MPa. Justify the shape of this curve on physical grounds.
(d) For an open-hole completion, estimate the shear rate the polymer solution will be exposed to. Does this portend mechanical degradation of the polymer?

Take the reservoir to be circular with $R_e = 950 \text{ m}$ and $P_e = 18 \text{ MPa}$. Additional properties are $k = 0.05 \text{ } \mu\text{m}^2$, $S_w = 0$, $R_w = 5 \text{ cm}$, $H_t = 42 \text{ m}$, $\phi = 0.2$, and $S_{2r} = 0.3$.

9

Micellar-Polymer Flooding

From the earliest days, it was recognized that capillary forces caused large quantities of oil to be left behind in well-swept zones of waterflooded oil reservoirs. Capillary forces are the consequence of the interfacial tension (IFT) between the oil and water phases that resists externally applied viscous forces and causes the injected and banked-up connate waters to locally bypass oil. Similarly, early efforts of enhanced oil recovery strove to displace this oil by decreasing the oil-water IFT. Though many techniques have been proposed and field tested, the predominant EOR technique for achieving low IFT is micellar-polymer (MP) flooding.

Lowering interfacial tension recovers additional oil by reducing the capillary forces that leave oil behind any immiscible displacement. This trapping is best expressed as a competition between viscous forces, which mobilize the oil, and capillary forces, which trap the oil. The local capillary number N_{vc} , the dimensionless ratio of viscous to capillary forces, determines the residual oil and water saturations through a capillary desaturation curve (CDC). Section 3-4 gives general features about the CDC and N_{vc} . In this chapter, we specialize those results to MP flooding. Recall that ultralow IFTs are required—of the order of $1 \mu\text{N}/\text{m}$ —and that these values can be attained only through highly surface-active chemicals.

9-1 THE MP PROCESS

MP flooding is any process that *injects* a surface-active agent (a surfactant) to bring about improved oil recovery. This definition eliminates alkaline flooding (see Chap. 10) where the surfactant is generated *in situ* and other EOR processes where lowering the capillary forces is not the primary means of oil recovery.

MP flooding has appeared in the technical literature under many names: detergent, surfactant, low-tension, soluble oil, microemulsion, and chemical flooding. We use the term *micellar-polymer* flooding because it is the least ambiguous (chemical flooding, for example, could describe all nonthermal EOR processes) and most comprehensive (no other name implies the polymer component). Moreover, several names imply a specific sequence and type of injected fluids as well as the specific nature of the oil-recovering MP slug itself. Though there are differences among processes, in this chapter we emphasize the similarities since they are more numerous and important.

Figure 9-1 shows an idealized version of an MP flooding sequence. The process is usually applied to tertiary floods and is always implemented in the drive mode (not cyclic or huff 'n puff). The complete process consists of the following:

Preflush. A volume of brine whose purpose is to change (usually lower) the salinity of the resident brine so that mixing with the surfactant will not cause loss of interfacial activity. Preflushes have ranged in size from 0% to 100% of the floodable pore volume (V_{pf}) of a reservoir. In some processes, a sacrificial agent is added to lessen the subsequent surfactant retention (Holm, 1982).

MP slug. This volume, ranging from 5% to 20% V_{pf} in field applications, contains the main oil-recovering agent, the primary surfactant. Several other chemicals (Fig. 9-1) are usually needed to attain the design objectives. We discuss the purpose of these chemicals in more detail later.

Mobility buffer. This fluid is a dilute solution of a water-soluble polymer whose purpose is to drive the MP slug and banked-up fluids to the production wells. All the polymer flooding technology discussed in Chap. 8 carries over to designing and implementing the mobility buffer. Thus in this chapter, we deal relatively little with the mobility buffer though there is good evidence (see Fig. 9-33) that this volume is very important to the oil recovering ability

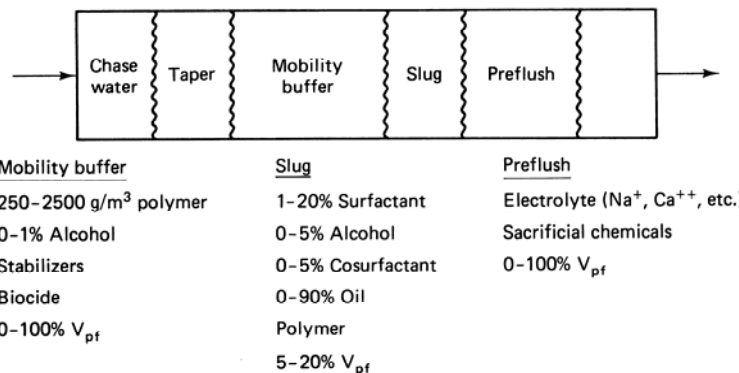


Figure 9-1 Idealized cross section of a typical micellar-polymer flood (from Lake, 1984)

of the entire sequence. The target oil for an MP flood—the residual oil—is different from that of a polymer flood—the movable oil.

Mobility buffer taper. This is a volume of brine that contains polymer, grading from that of the mobility buffer at the front end (the spike) to zero at the back. The gradual decrease in concentration mitigates the effect of the adverse mobility ratio between the mobility buffer and the chase water.

Chase water. The purpose of the chase water is simply to reduce the expense of continually injecting polymer. If the taper and mobility buffer have been designed properly, the MP slug will be produced before it is penetrated by this fluid.

9-2 THE SURFACTANTS

Since much is required of the MP surfactant, we discuss surfactant solutions here. This discussion can be no more than a précis of the voluminous literature on surfactant properties. (For more on oil-recovering surfactants, see Akstinat, 1981.)

A typical surfactant monomer is composed of a nonpolar (lyophile) portion, or *moiety*, and a polar (hydrophile) moiety; the entire monomer is sometimes called an *amphiphile* because of this dual nature. Figures 9-2(a) and 9-2(b) show the

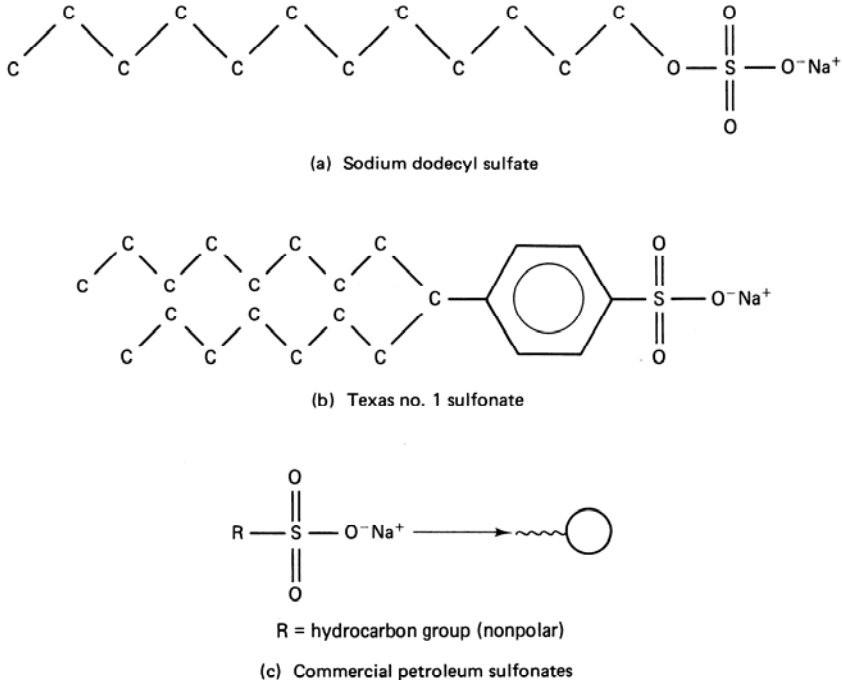


Figure 9-2 Representative surfactant molecular structures (from Lake, 1984)

molecular structure of two common surfactants and illustrate a shorthand notation for surfactant monomers: The monomer is represented by a “tadpole” symbol, with the nonpolar moiety being the tail and the polar being the head.

Surfactants are classified into four groups depending on their polar moieties, (Table 9-1).

Anionics. As required by electroneutrality, the anionic (negatively charged) surfactant molecule (distinct from monomer) is uncharged with an inorganic metal cation (usually sodium) associated with the monomer. In an aqueous solution, the molecule ionizes to free cations and the anionic monomer. Anionic surfactants are the most common in MP flooding because they are good surfactants, relatively resistant to retention, stable, and can be made relatively cheaply.

Cationics. If the polar moiety is positively charged, the surfactants are cationic. In this case, the surfactant molecule contains an inorganic anion to balance the charge. Cationic surfactants are used little in MP flooding because they are highly adsorbed by the anionic surfaces of interstitial clays.

Nonionics. A class of surfactants that have seen extensive MP use, mainly as cosurfactants but increasingly as primary surfactants, is the nonionics. These surfactants do not form ionic bonds but, when dissolved in aqueous solutions, exhibit surfactant properties by electronegativity contrasts between their constituents. Nonionics are much more tolerant of high salinities than anionics and historically have been poorer surfactants.

Amphoteric. This class of surfactants contains aspects of two or more of the other classes. For example, an amphoteric may contain both an anionic group and a nonpolar group. These surfactants have not been used in oil recovery.

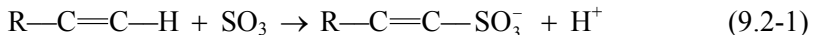
TABLE 9-1 CLASSIFICATION OF SURFACTANTS AND EXAMPLES (ADAPTED FROM AKSTINAT, 1981)

Anionics	Cationics	Nonionics	Amphoteric
			
Sulfonates	Quaternary ammonium organics, pyridinium, imidazolinium, piperidinium, and sulfononiun compounds	Alkyl-, Alkyl- aryl-, acyl-, acylamido-, acyl- aminepolyglycol, and polyol ethers	Aminocarboxylic acids
Sulfates			
Carboxylates			
Phosphates		Alkanolamides	

Within any one class, there is a huge variety of possible surfactants. Figure 9-2 shows some of this variety by illustrating differences in nonpolar molecular weight (C_{12} for the sodium dodecyl sulfate (SDS) versus C_{16} for Texas No. 1), polar moiety identity (sulfate versus sulfonate), and tail branching (straight chain for SDS versus two tails for Texas No. 1) all within the same class of anionic surfactants.

Besides these, there are variations in both the position of the polar moiety attachment and the number of polar moieties (monosulfonates versus disulfonates, for example). Even small variations can drastically change surfactant properties. For example, sulfates tend to be less thermally stable than sulfonates. (For more details on the effect of structure on surfactant properties, see Graciaa et al., 1981; Barakat et al., 1983.)

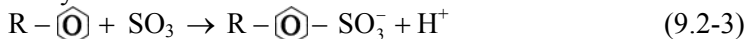
The most common primary surfactant used in MP flooding is petroleum sulfonates. These are anionic surfactants produced by sulfonating a pure organic chemical (sometimes called synthetic sulfonates), an intermediate molecular weight refinery stream, or when appropriate, even a crude oil itself. If $R-C=C-H$ represents the molecular formula of the feedstock, the sulfonation reaction proceeds as



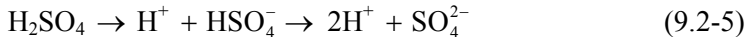
The reaction can also proceed to saturate the carbon–carbon double bond



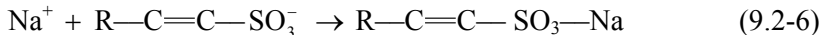
Here we adopt a shorthand notation that shows only the atoms participating in the chemical reaction. The surfactant produced in Eq. (9.2-1) is an α -olefin sulfonate, and that produced in Eq. (9.2-2) is an alkyl sulfonate. If the feedstock is aromatic, the sulfonation produces an alkyl benzene sulfonate



The sulfate in these reactions comes from bubbling SO_3 gas through the feedstock or through contact with a solvent the SO_3 is dissolved into. The sulfonation reactions (Eqs. 9.2-1 through 9.2-3) yield a highly acidic aqueous solution through the parallel reactions



The solution is subsequently restored to a neutral pH by adding a strong base, such as $NaOH$ or NH_3 , dissolved in water. This neutralization step also provides the counterion for the sulfonate; for the α -olefin sulfonate this is



If the feedstock is unrefined, a mixture of surfactant types will result. The mixture can contain a distribution of isomeric forms, molecular weights, and degrees of sulfonation (mono- versus disulfonation). The mixture is extremely difficult to characterize except through several gross properties. Table 9-2 shows some typical properties of commercial sulfonates. Typical molecular weights range from 350 to 450 kg/kg-mole, with the lower values indicating greater water solubility. In some calculations, it is better to use the surfactant equivalent weight (molecular weight divided by charge) instead of the molecular weight. Thus equivalent weight (mass per equivalent) and molecular weight are the same for monosulfonates. Some products contain impurities: unreacted oil from the sulfonation step and water from the neutralization. Part of the surfactant, as purchased, is inactive. Inasmuch as it is the

TABLE 9-2 SELECTED PROPERTIES OF A FEW COMMERCIAL ANIONIC SURFACTANTS

Company	Surfactant name	Molecular weight	Activity (wt %)	Oil (wt %)	Water (wt %)	Salt (wt %)	Type
ALCOLAC	SIPONATE DS-10	350	98.0				Sodium dodecyl benzene sulfonate
ALCOLAC	SIPONATE A168	350	70.0				
CONOCO	AES 14125		58.3	1.7			Alfonic ether sulfates
CONOCO	AES 1412A		60.0	3.0			Alfonic ether sulfates
EXXON	RL 3070	334	60.0	14.0	25.2		Alkyl aryl sodium sulfonates
EXXON	RL 3011	375	64.4	25.2	10.0		Alkyl aryl sodium sulfonates
EXXON	RL 3330	390	66.0	24.0	9.5		Alkyl aryl sodium sulfonates
EXXON	RL 3331	391	65.0	36.5	8.1		Alkyl aryl sodium sulfonates
EXXON	RL 3332	460	60.0	31.4	8.1		Alkyl aryl sodium sulfonates
EXXON	RL 2917	515	65.7	25.7	8.5		Alkyl aryl sodium sulfonates
KAO	LS 8203	330	65.0		53.0		Linear alkyl sulfonate
KAO	LS 8202	480	44.1	54.6	0.06		Linear alkyl sulfonate
LION	LEONOX E		94.0	2.0		2.0	
LION	LEONOX D	350	94.0	2.0		3.0	Alpha olefin sulfonate
LION	LION AJS-2	375	35.0				
LION	LEONOX K	570	30.0				Alfonic ether sulfates
SHELL	ENORDET AOS 310-40	317	38.0		61.0	< 1	Alcohol ethoxy sulfonate
SHELL	ENORDET LXS 370-60	375	60.1		38.0	1.9	Linear alkyl xylene sulfonates
SHELL	ENORDET LXS 395-60	395	60.0		37.4	2.6	Linear alkyl xylene sulfonates
SHELL	ENORDET LXS 420-60	417	60.6		36.6	2.8	Linear alkyl xylene sulfonates
SHELL	ENORDET 3ES-441-60	441	59.3		29.5	1.2	Linear alkyl xylene sulfonates
STEPAN	PS HMW		50.7	24.4	22.1		
STEPAN	PS MMW		53.2	18.4	26.6		
STEPAN	PS 360	360	65.8	18.9	12.4		
STEPAN	PS 420	420	56.1	13.0	28.8		
STEPAN	PS 465	464	58.7	14.9	24.2		
WITCO	TRS 40	330-350	40-43	18.0	40.0		
WITCO	TRS 10-410	315-430	61-63	33.0	4-5		
WITCO	TRS 16	440-470	61-63	32.5	4-5		
WITCO	TRS 18	490-500	61-63	32.5	4-5		

surfactant itself we are interested in, all slug concentrations should report the surfactant concentration only (100% active basis).

In the following discussion, we ignore distinctions between surfactant types by simply treating the surfactant as the tadpole structure of Fig. 9-2.

If an anionic surfactant is dissolved in an aqueous solution, the surfactant dissociates into a cation and a monomer. If the surfactant concentration is then increased, the hydrophilic moieties of the surfactant begin to associate among themselves to form aggregates or micelles containing several monomers each. A plot of surfactant monomer concentration versus total surfactant concentration (Fig. 9-3) is a curve that begins at the origin, increases monotonically with unit slope, and then levels off at the *critical micelle concentration* (CMC). Above the CMC, all further increases in surfactant concentration cause increases only in the micelle concentration. Since CMCs are typically quite small (about 10^{-5} to 10^{-4} kg-moles/m³), at nearly all concentrations practical for MP flooding, the surfactant is predominantly in the micelle form. This is the origin of the name micellar-polymer flooding. The representations of the micelles in Fig. 9-3 and elsewhere are schematic. The actual structures of the micelles are not static and can take on various forms.

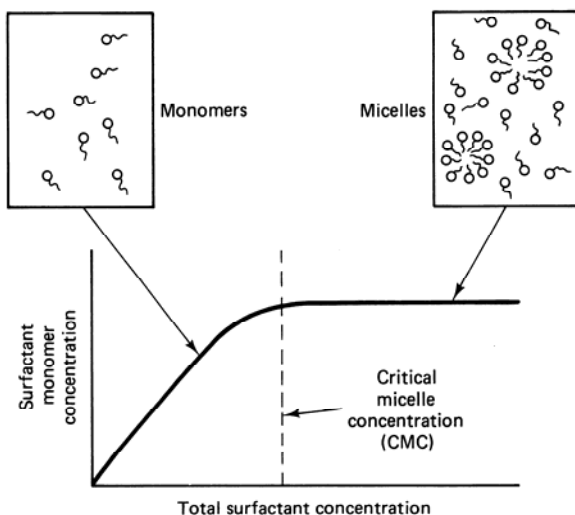


Figure 9-3 Schematic definition of the critical micelle concentration (from Lake, 1984)

When this solution contacts an oleic phase (the term *oleic phase* indicates this phase can contain more than oil), the surfactant tends to accumulate at the intervening interface. The lipophilic moiety “dissolves” in the oleic phase, and the hydrophilic in the aqueous phase. The surfactant prefers the interface to the micelle; however, only small surfactant concentrations are needed to saturate the interface. The dual nature of the surfactant is important since the accumulation at the interface causes the IFT between the two phases to lower. The IFT between the two phases is a function of the excess surfactant concentration at the interface. The excess is the

difference between the interface and bulk concentration. The interface blurs in much the same manner as do vapor–liquid interfaces near a critical point.

The surfactant itself and the attending conditions should be adjusted to maximize this effect, but this affects the solubility of the surfactant in the bulk oleic and aqueous phases. Since this solubility also impinges on the mutual solubility of brine and oil, which also affects IFTs, this discussion leads naturally to the topic of surfactant–oil–brine phase behavior. Curiously, the surfactant concentration itself plays a rather minor role in what follows compared to the temperature, brine salinity, and hardness. This is true of many micellar properties.

9-3 SURFACTANT–BRINE–OIL PHASE BEHAVIOR

Surfactant–brine–oil phase behavior is conventionally illustrated on a ternary diagram (see Sec. 4-3). By convention, the top apex of the ternary diagram represents the surfactant pseudocomponent ($i = 3$), the lower left represents brine ($i = 1$), and the lower right represents oil ($i = 2$). Table 9-3 summarizes these and other notational conventions.

TABLE 9-3 NOTATION AND COMMON UNITS FOR MP FLOODING

i	Species	Concentration unit
1	Water	Volume fraction
2	Oil	Volume fraction
3	Surfactant	Volume fraction
4	Polymer	Weight percent or g/m ³
5	Anion	meq/cm ³ -pore volume
6	Divalents	meq/cm ³ -pore volume
7	Cosurfactant	Volume fraction
8	Monovalents	meq/cm ³ -pore volume

j	Phase
1	Aqueous
2	Oleic
3	Microemulsion

MP phase behavior is strongly affected by the salinity of the brine. Consider the sequence of phase diagrams, Figs. 9-4 through 9-6, as the brine salinity is increased. The phase behavior we now describe was originally given by Winsor (1954) and adapted to MP flooding later (Healy et al., 1976; Nelson and Pope, 1978).

At low brine salinity, a typical MP surfactant will exhibit good aqueous-phase solubility and poor oil-phase solubility. Thus an overall composition near the brine–oil boundary of the ternary will split into two phases: an excess oil phase that is essentially pure oil and a (water-external) microemulsion phase that contains brine, surfactant, and some solubilized oil. The solubilized oil occurs when

globules of oil occupy the central core of the swollen micelles. The tie lines within the two-phase region have a negative slope. This type of phase environment is variously called a Winsor type I system, a lower-phase microemulsion (because it is more dense than the excess oil phase), or a type II(–) system. We adopt the type II(–) terminology here. II means no more than two phases can (not necessarily will) form, and (–) means the tie lines have negative slope (Fig. 9-4). The plait point in such a system P_R is usually located quite close to the oil apex. Any overall composition above the binodal curve is single phase.

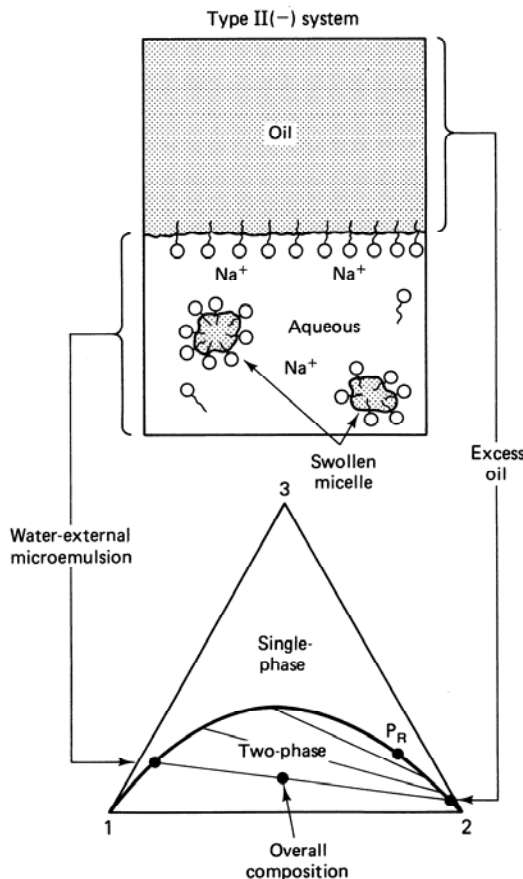


Figure 9-4 Schematic representation of the type II(–) system (from Lake, 1984)

For high brine salinities (Fig. 9-5), electrostatic forces drastically decrease the surfactant's solubility in the aqueous phase. An overall composition within the two-phase region will now split into an excess brine phase and an (*oil-external*) microemulsion phase that contains most of the surfactant and some solubilized brine. The brine is solubilized through the formation of inverted swollen micelles, with brine at their cores. The phase environment is a Winsor type II system, an upper-phase microemulsion, or a type II(+) system. The plait point P_L is now close to the brine apex.

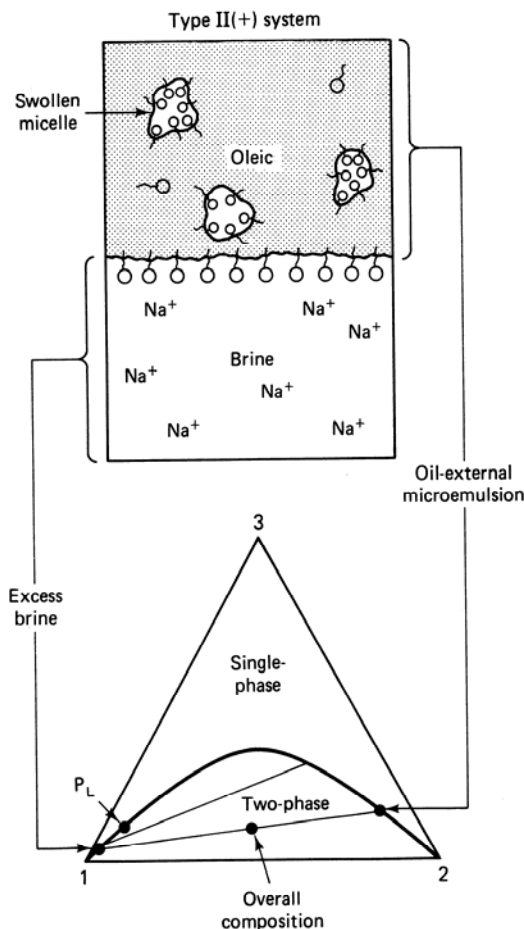


Figure 9-5 Schematic representation of high-salinity type II(+) system (from Lake, 1984)

The two extremes presented thus far are roughly mirror images: The microemulsion phase is water-continuous in the type II(−) systems and oil-continuous in type II(+) systems. The induced solubility of oil in a brine-rich phase, a type II(−) system, suggests an extraction mechanism in oil recovery. Though extraction does play some role, it is dwarfed by the IFT effect discussed below, particularly when phase behavior at intermediate salinities is considered.

At salinities between those of Figs. 9-4 and 9-5, there must be a continuous change between type II(−) and II(+) systems. The obvious change of a counterclockwise tie line rotation and corresponding plait point migration is incorrect; there is no salinity where the solubility of the surfactant in the brine- and oil-rich phases are exactly equal. But there is a range of salinities where a third surfactant-rich phase is formed (Fig. 9-6). An overall composition within the three-phase region separates into excess oil and brine phases, as in the type II(−) and II(+) environments, and into a microemulsion phase whose composition is represented by an invariant point. This environment is called a Winsor type III, a middle-phase microemulsion, or a type III system. To the upper right and left of the

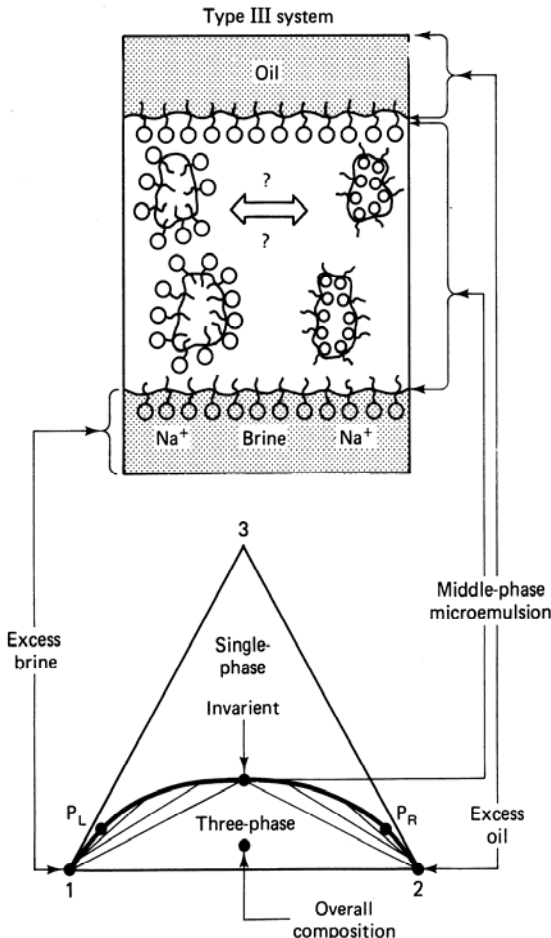


Figure 9-6 Schematic representation of optimal-salinity type III system (from Lake, 1984)

three-phase region are type II(−) and II(+) lobes wherein two phases will form as before. Below the three-phase region, there is a third two-phase region (as required by thermodynamics) whose extent is usually so small that it is neglected (Anderson et al., 1976). In the three-phase region, there are now two IFTs between the microemulsion and oil σ_{32} and the microemulsion and water σ_{31} .

Figure 9-7, a prism diagram, shows the entire progression of phase environments from type II(−) to II(+). The type III region forms through the splitting of a critical tie line that lies close to the brine–oil boundary as the salinity increases to C_{Sel} (Bennett et al., 1981). A second critical tie line also splits at C_{Sel} as salinity is decreased from a type II(+) environment. Over the type III salinity range, the invariant point M migrates from near the oil apex to near the brine apex before disappearing at the respective critical tie lines. Equally important, as the migration takes place, the surfactant concentration in the microemulsion phase goes through a minimum near where brine–oil ratio at the invariant point becomes 1.

The migration of the invariant point implies essentially unlimited solubility

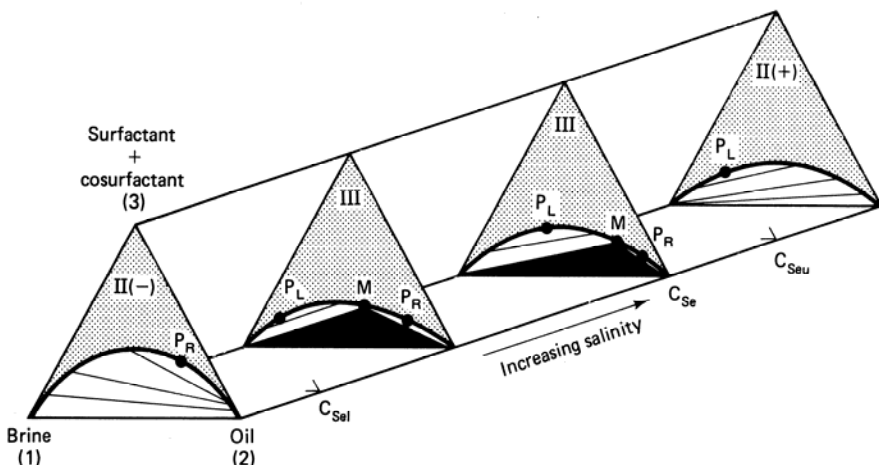


Figure 9-7 Pseudoternary or “tent” diagram representation of micellar-polymer phase behavior (from Lake, 1984)

of brine and oil in a single phase. This has generated intense research into the nature of the type III microemulsion (Scriven, 1976). The middle-phase microemulsion cannot be simultaneously oil- and water-external. Somewhere between C_{Sel} and C_{Seu} , the micelles contained therein undergo an inversion, and many phase properties (for example, electrical conductivity) abruptly change from being characteristic of the water to being characteristic of the oil. Moreover, several other properties (see Fig. 9-13) take on extreme values. Though logically appealing, the phase inversion salinity does not necessarily indicate optimal salinity.

Several variables other than brine electrolyte content can bring about the Fig. 9-7 phase environment shifts. In general, changing any condition that enhances the surfactant’s oil solubility will cause the shift from type II(–) to II(+). We discuss some of the more important below.

Surfactant Structure

In general, increasing the importance of the nonpolar end of the surfactant will increase oil solubility. Such changes include increasing the nonpolar molecular weight, decreasing the tail branching (Graciaa et al., 1981), decreasing the number of polar moieties (from disulfonates to monosulfonates), and decreasing the strength of the polar moiety.

Two common measures of the competition between the hydrophile and lipophile indicate oil solubility. The surfactant’s charge density is the number of dissociated ions per molecule divided by the molecular size. Surfactant brine solubility goes up as charge density increases. A second measure is the hydrophile-lipophile balance (HLB) number. For certain types of surfactant (for example, nonionics), the HLB number is simply related to molecular structure. But for others, the HLB number cannot be uniquely defined apart from the oil and brine it is

competing for (Shinoda and Kunieda, 1979). Though both measures have enjoyed a degree of success, they are difficult to apply to petroleum sulfonate because of the many chemical species contained therein.

Cosurfactants

One of the first uses for cosurfactants was to adjust the surfactant pseudocomponent so that the $\text{II}(-) \rightarrow \text{II}(+)$ transition occurs at different salinities. A water soluble cosurfactant (for example, tertiary amyl alcohol, a second petroleum sulfate, or *n*-butanol) also causes the surfactant to be more water soluble. Higher molecular weight alcohols cause increased oil solubility (Salter, 1977). Bourrel et al. (1978) have derived mixing rules for the properties of surfactant–cosurfactant mixtures.

Oil Properties

If the oil can be made more polar, it will act as a better solvent for the surfactant, hastening the $\text{II}(-) \rightarrow \text{II}(+)$ transition. There are several measures for this tendency. High specific gravity crudes tend to be rich in organic acids; thus surfactant oil solubility is lower in high gravity oils (Puerto and Reed, 1982). Similarly, low specific volume crudes behave in the same fashion (Nelson, 1982). Cash et al. (1976) devised a measure of oil effects on surfactant–brine–oil phase behavior by comparing the transitions observed with a crude to a refined hydrocarbon. The surfactant in all cases is Texas No. 1 (Fig. 9-2) in a NaCl brine. If the transition from the $\text{II}(-) \rightarrow \text{II}(+)$ for a crude occurs at the same salinity as the linear alkane, the alkane carbon number (ACN) of the refined oil and the equivalent alkane carbon number (EACN) of the crude are equal. Therefore, EACN is relatively easy to measure and gives an indication of the model oil to be used in formulation. The same idea can be used to categorize surfactants (Graciaa et al., 1981).

Decreasing Temperature

There is little generality in the tendency for the surfactant to dissolve in oil as temperature increases. For most anionics, higher temperatures mean more brine solubilities (Nelson and Pope, 1978). This trend is reversed for most nonionics.

Decreasing Pressure

MP phase behavior, being an all-liquid system, is relatively insensitive to pressure. But Nelson (1982) has noted a substantial pressure effect in gassy crudes. Interestingly, the trend here parallels that of the oil properties given above: As the specific volume of the oil increases (through decreased pressure), the surfactant becomes more water soluble.

Decreasing the surfactant's oil solubility will cause the reverse of these

changes. Thus Fig. 9-7 could be redrawn with any of the above variables on the base of the prism with the variable C_{Se} increasing in the direction of increased oil solubility. These observations have occupied a very great share of the MP literature. Their utility will become apparent under our discussion of IFTs in the next section.

9-4 NONIDEAL EFFECTS

In much the same manner as the ideal gas law approximates the behavior of real gases, Figs. 9-4 through 9-6 are approximations to actual MP phase behavior. Though nonidealities are significant in many instances, in this section, we mention only the most important.

1. At high surfactant concentrations or low temperatures (Scriven, 1976; Healy and Reed, 1974) or even in the presence of pure surfactants (Salter, 1983), phases other than those in Fig. 9-7 have been observed. These phases tend to be high-viscosity liquid crystals or other condensed phases. The large viscosities are detrimental to oil recovery since they can cause local viscous instabilities during a displacement or decreased injectivity. Frequently, low-to-medium molecular weight alcohols (*cosolvents*) are added to MP formulations to “melt” these undesirable viscosities. Because most alcohols are weak surfactants, the term *cosurfactant* has enjoyed popular usage for these additions, as it has for the addition of other surfactants. When the brine contains polymer, a condensed phase occurs at low surfactant concentration because of exclusion of the polymer from the microemulsion phases. Cosurfactants can be used to eliminate this polymer–surfactant incompatibility (Trushenski, 1977).
2. When cosurfactants are present, it is often inappropriate to lump all the chemicals into the surfactant apex of the prism in Fig. 9-7. If the cosurfactants do not partition with the primary surfactant during a displacement, much of the benefit from adding the chemical is lost; hence surfactant–cosurfactant separation effects are an important concern. Efforts to account for the preferential partitioning of the cosurfactant include a quaternary phase behavior representation (Salter, 1978) and a *pseudophase* theory (Hirasaki, 1982).
3. The type III salinity limits (C_{Sel} and C_{Seu}) are functions of surfactant concentration. This dependency may be visualized by tilting the vertical triangular planes in Fig. 9-7 about their bases. This is sometimes called the *dilution effect*.

One way to graphically represent the dilution effect is through the salinity requirement diagram (Fig. 9-8). This diagram is a plot of overall surfactant concentration C_3 (horizontal axis) versus the salinity (vertical axis). All other variables are held constant. Figure 9-8 represents salinity as percent dilution of a particular high salinity brine. The upper curve shows the boundary between the types II(+) and III environments or a curve of C_{Seu}

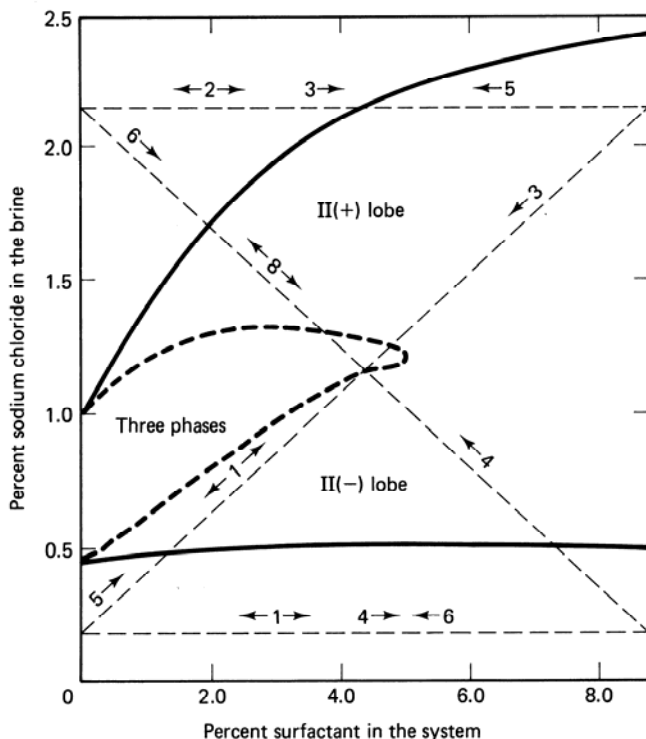


Figure 9-8 Salinity-requirement diagram (from Nelson, 1982)

versus C_3 . Similarly, the lower curve shows C_{Sel} versus C_3 ; hence the region between the two curves give the extent of the type III region as a function of C_3 . Other plots (Glover et al., 1979; Bourrel et al., 1978) plot the extent of observed three-phase behavior in a similar fashion. Figure 9-8 also shows a three-phase region within the type III region.

The MP system in Fig. 9-8 shows a type III region that decreases with salinity. For other surfactants and brines, the trend can be entirely opposite (Bourrel et al., 1978). For ideal MP phase behavior, neither C_{Seu} nor C_{Sel} should depend on C_3 —that is, the salinity requirement diagram should consist of two horizontal lines. Frequently, the behavior of soft brines will approximate this since the dilution effect is particularly pronounced when the brine contains significant quantities of divalent ions.

4. The phase behavior shifts are specific to the exact ionic composition of the brine, not simply to the total salinity. Hence just as in polymer flooding, it is insufficient to characterize the brine as merely “fresh” or in terms of its total dissolved solids content. For anionic surfactants, other anions in solution have little effect on the MP phase behavior, but cations readily cause phase environment changes. Divalent cations (calcium and magnesium are the most common) are usually 5–20 times as potent as monovalent cations (usually sodium). Divalents are usually present in oil-field brines in smaller quantities

than monovalents (Fig. 8-1), but their effect is so pronounced that it is necessary, as a minimum, to separately account for salinity—total dissolved solids—and hardness—total divalent cation concentration. Nonconstant monovalent–divalent ratios will also cause electrolyte interactions with clay minerals through cation exchange. The disproportionate effects of the salinity and hardness are accounted for by defining a weighted sum of the monovalent and divalent concentrations as an “effective” salinity C_{Se} .

The salinity effects discussed here are much less significant with nonionic surfactants where there are no ionic associations. Even for anionics, they can be greatly attenuated by adding nonionic cosurfactants. The cosurfactant monomers add into the micelle between the larger primary surfactant monomers, thus lessening the charge density of the micelle surface and making the “mixed” micelle more like a nonionic.

9-5 PHASE BEHAVIOR AND INTERFACIAL TENSION

You may be wondering what this discussion of MP phase behavior has to do with the goal of recovering oil through lowered IFT. Early MP flooding literature contains much information about the techniques of measuring IFTs and what causes them to be low (Cayias et al., 1975). IFTs depend on the types and concentration of surfactant, cosurfactant, electrolyte, oil, polymer, and temperature. However, in surely one of the most significant advances in all MP technology, all IFTs have been shown to directly correlate with the MP phase behavior. Healy and Reed (1974) originally proposed the correlation, which has been theoretically substantiated by Huh (1979) and experimentally verified by several others (for example, Glinsmann, 1979; Graciaa et al., 1981).

A practical benefit of this correlation is immediately realized: Relatively difficult measurements of IFTs can be largely supplanted by relatively easy phase behavior measurements. Indeed, in the recent literature, the behavior of IFTs has been inferred by a narrower subset of phase behavior studies based on the solubilization parameter (Bourrel et al., 1978). As important as this benefit is, a more important benefit is that the correlation logically provides a basis for MP design. We discuss design in Sec. 9-13.

To investigate further the relation between IFTs and phase behavior, let C_{23} , C_{13} , and C_{33} be the volume fractions of oil, brine, and surfactant in the microemulsion phase. According to Figs. 9-4 through 9-6, the microemulsion phase is present at all salinities; hence all three quantities are well defined and continuous. For systems containing alcohol, C_{33} is the surfactant coordinate less the cosurfactant content. Solubilization parameters between the microemulsion-oleic phases $S32$, for type II(–) and III phase behavior, and between the microemulsion-aqueous phases S_{31} for type II(+) and III are defined as

$$S_{32} = \frac{C_{23}}{C_{33}} \quad (9.5-1a)$$

$$S_{31} = \frac{C_{13}}{C_{33}} \quad (9.5-1b)$$

The interfacial tensions between the corresponding phases, σ_{32} and σ_{31} , are empirical functions only of S_{32} and S_{31} . Figure 9-9 shows a typical correlation.

Figure 9-10 shows the corresponding behavior of the solubilization parameters and IFTs in a different manner. Consider a locus at constant oil, brine, and surfactant overall concentrations in Fig. 9-7, but with a variable salinity. If nonideal effects are unimportant and the locus is at low surfactant concentration and intermediate brine–oil ratios, σ_{32} will be defined from low salinity up to C_{Sel} , and σ_{31} from C_{Sel} to high salinities. Both IFTs are the lowest in the three-phase type III region between C_{Sel} and C_{Selu} where both solubilization parameters are also large. Further, there is a precise salinity where both IFTs are equal at values low enough (about 1 $\mu\text{N}/\text{m}$) for good oil recovery. This salinity is the optimal salinity C_{Sopt} for this

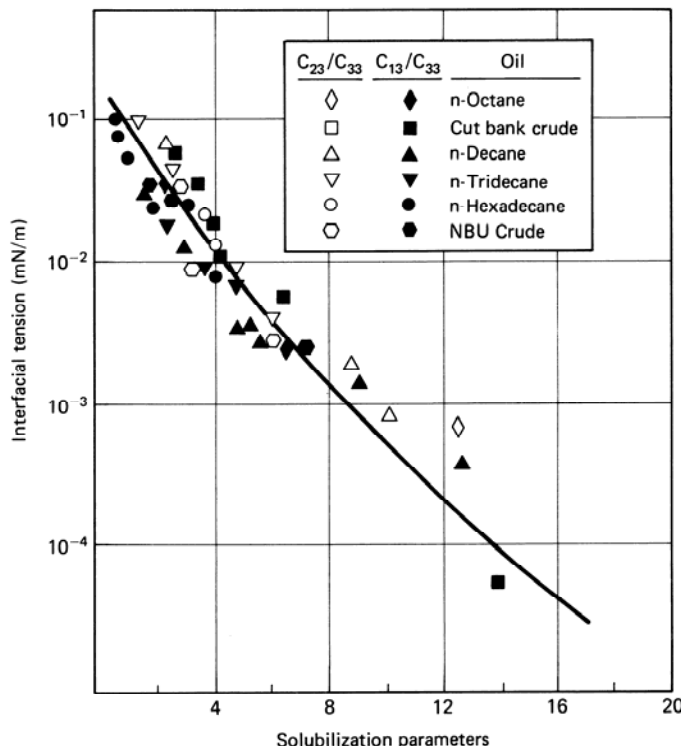


Figure 9-9 Correlation of solubilization parameters with interfacial tensions (from Glinsmann, 1979)

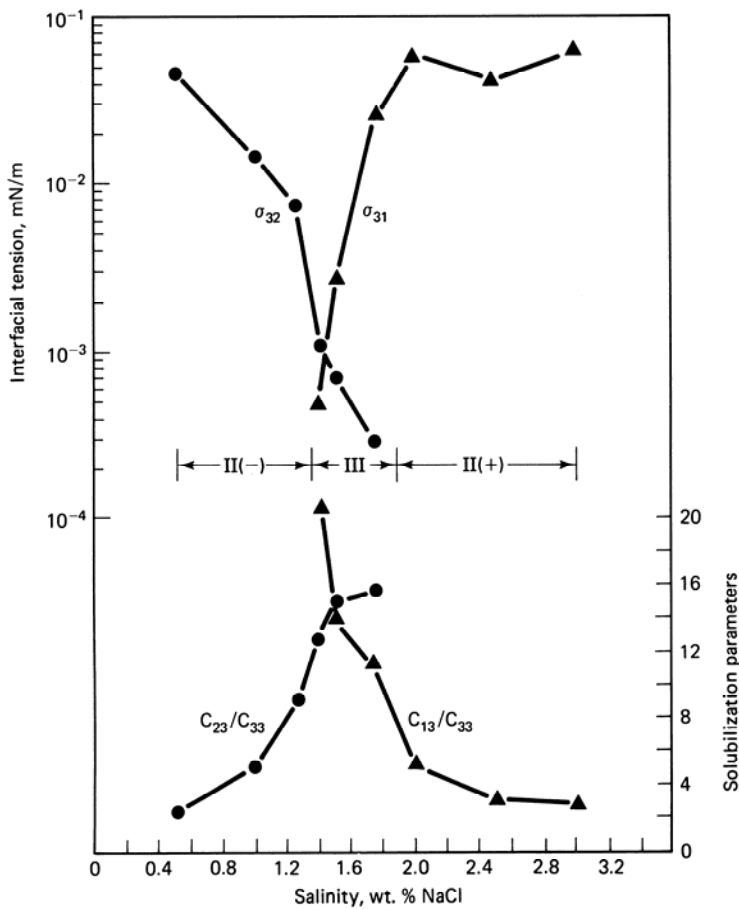


Figure 9-10 Interfacial tensions and solubilization parameters (from Reed and Healy, 1977)

particular surfactant–brine–oil combination, and the common IFT is the *optimal* IFT. Optimal salinities have been defined on the basis of equal IFTs, as in Fig. 9-10, equal solubilization ratios (Healy et al., 1976), equal contact angles (Reed and Healy, 1979), and the midpoint between C_{Seu} and C_{Sel} . Fortunately, all definitions of optimal salinity give roughly the same value.

The optimal salinity based on solubilization parameters also corresponds to the salinity where oil recovery in a core flood is a maximum. **Figure 9-11** illustrates this oil-recovery optimal salinity. The middle panel, Fig. 9-11b, shows a plot similar to the upper panel in Fig. 9-10 for a different surfactant system; the lower panel shows the oil recovery for a series of constant-salinity core floods. The optimal salinity based on solubilization parameters, IFTs, and oil recovery agree well. Since optimal phase behavior salinity is the same as maximum oil recovery salinity, clearly one of the goals of an MP design is to generate this optimal salinity in the presence of

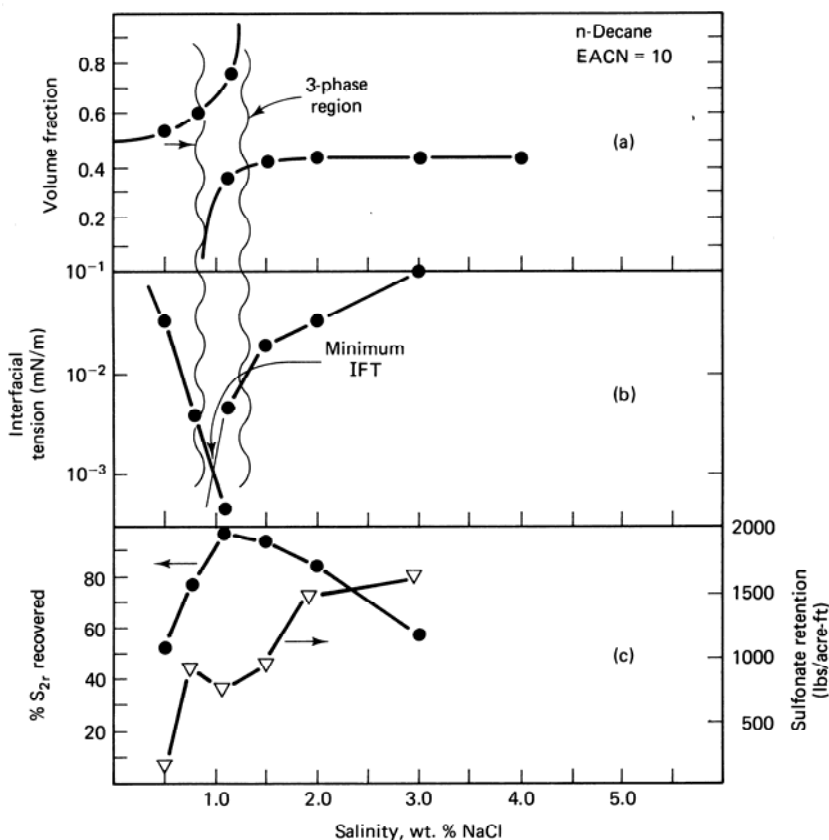


Figure 9-11 Correlation of phase volume and IFT behavior with retention and oil recovery (from Glinsmann, 1979)

the surfactant. The optimal salinity does not correspond to minimum surfactant retention (Fig. 9-11c), but this is because of competing effects as we mention below.

Because of the dilution effect mentioned above, maximum oil recovery is really where the combination of electrolyte, surfactant, and cosurfactant concentrations bring about maximum solubilization parameters. Hence one should speak of optimal *conditions* rather than optimal salinity. The optimal salinity terminology is deeply embedded within the MP literature, but it is precise only for the ideal Fig. 9-7 phase behavior. Do not confuse the optimal salinity C_{Sopt} , an intrinsic property of the oil-brine-surfactant combination, with the prevailing salinity C_{Se} , an independent variable in the MP design.

Optimal salinities can vary greatly depending on the nature of the surfactant and brine pseudocomponents. But it is dismaying that for many commercially attractive surfactants in most MP candidate reservoirs, the optimal salinity is smaller than the resident brine salinity. Optimal salinities can be raised by adding to the slug

any chemical that increases the primary surfactant's brine solubility. Adding cosurfactants to the MP slug normally increases the optimal IFT.

The notion of optimal conditions is directly connected to the phase behavior of MP systems. Even properties of MP systems apparently unrelated to phase behavior (retention, for example) are functions of salinity, cosurfactant concentration, and temperature. This observation leads to the interesting speculation that *all* MP properties (retention, phase behavior, IFT, mobilities) correlate to optimal salinity and, perhaps, to solubilization parameters.

9-6 OTHER PHASE PROPERTIES

Our understanding of MP phase behavior follows from the ternary representation of the Winsor phase behavior progression. Other representations are common, particularly to show phase properties.

A very useful phase-behavior representation is the *volume fraction diagram* (VFD) (Fig. 9-12). Imagine a point of fixed overall composition (parallel to the salinity axis) in the ternary planes in Fig 9-6. The volumes of each phase are observed and plotted as the brine salinity changes. Starting with a low salinity, the VFD shows a succession of decreasing oleic-phase volume and increasing aqueous-phase volume with some three-phase overlap in the middle. If the overall surfactant concentration is low and the brine–oil ratio (WOR) is about 1, the appearance of the lower brine phase corresponds approximately to the onset of the type III region (C_{Sel}), and the disappearance of the upper oleic phase corresponds approximately to the termination of the type III region (C_{Seu}). The salinity at which the brine and oleic phases have equal volumes is a good approximation of the optimal salinity if the surfactant and cosurfactant concentration is low enough. Compare the VFD in Fig. 9-11a to Fig. 9-12b.

Varying salinity while holding other variables constant is sometimes called a salinity scan. Varying the salinity is the most common presentation of the VFD; however, a derivative of the VFD, in which the cosurfactant concentration is varied in place of the salinity, is sometimes useful. To minimize the number of measurements, each scan can be relatively coarse (about ten measurements) and then supplemented with fill-in measurements to refine the estimate of the important events.

Of course, any phase property can be plotted in place of the phase volumes. Figure 9-13 shows the microemulsion-phase viscosity as a function of salinity. Over this range, the microemulsion phase, as defined above, is continuous and shows a viscosity maximum at a salinity near the optimal. The maximum indicates molecular ordering in the phase that seems to be the strongest at the phase inversion salinity. Such maxima can be either beneficial, if it can be used to provide mobility control in the slug, or detrimental, if it leads to excessively viscous fluids. It was to counteract the latter tendency that cosurfactants were first added to MP slugs. Over the same salinity range in Fig. 9-13, the excess phase viscosities do not change appreciably.

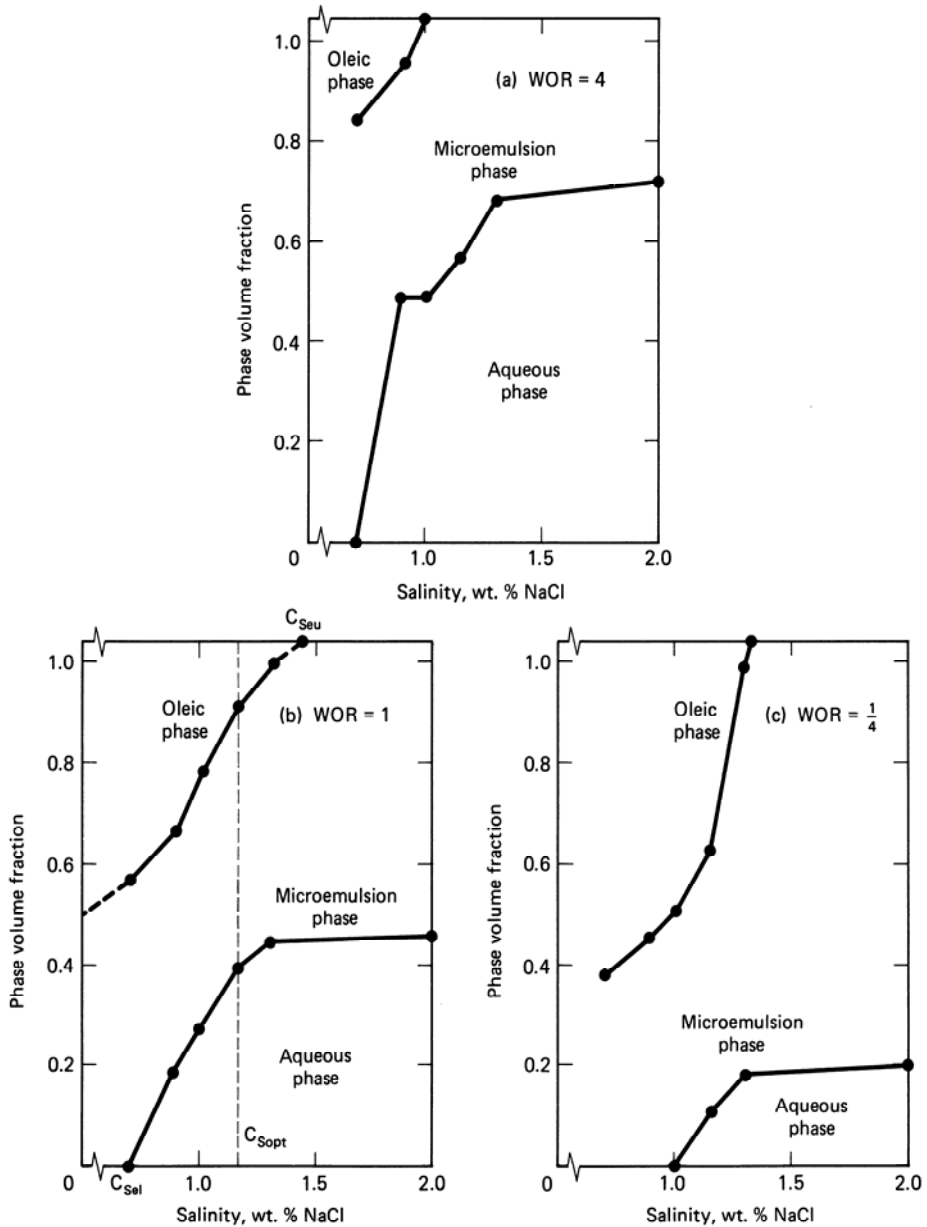


Figure 9-12 Phase volume diagrams (salinity scans) at three water–oil ratios (from Englesen, 1981)

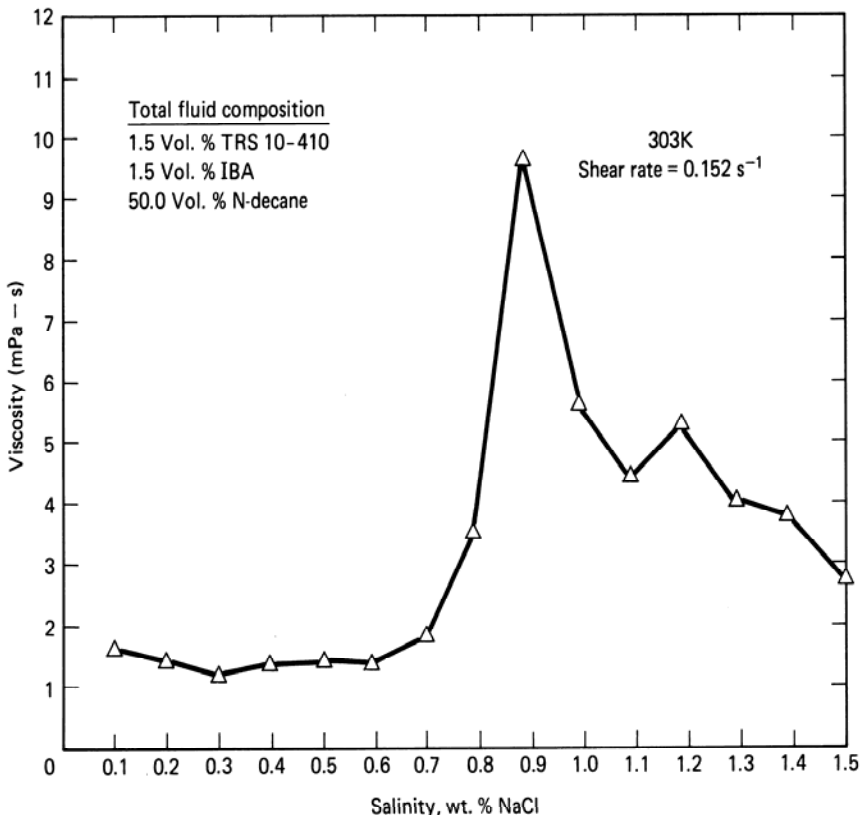


Figure 9-13 Microemulsion phase viscosity as a function of salinity (from Jones, 1981)

9-7 QUANTITATIVE REPRESENTATION OF MICELLAR PROPERTIES

Prediction of MP response rests on being able to quantitatively represent the foregoing behavior in equations. Given the complexities, many of which we have only alluded to, it is not possible to derive comprehensive representations. Here we seek to capture the major features by following these assumptions.

1. All fluids are incompressible and mix ideally.
2. Temperature does not change, and the phase behavior is insensitive to pressure. These restrictions mean phase behavior is driven only by changes in the effective salinity C_{Se} .
3. The ternary equilibria in Fig. 9-11 apply. For the moment, we neglect the nonideal effects.
4. The height of the binodal curve passes through a minimum near the optimal salinity C_{Sopt} . The minimum forces the optimal salinity based on IFT and

- phase behavior to be equal since the solubilization parameters will be a maximum at C_{Sopt} .
5. The splitting of the critical tie line as the type III system forms or disappears is so close to the ternary base that we can take the incipient invariant points to coincide with the left and right apexes at these events.

We strive for a representation that captures the basics of the MP behavior without becoming burdened with an excessive number of parameters. Such simplicity means equations are used to describe as much of the behavior as possible, and we choose these equations to have a small number of adjustable parameters. Though many of the equations are empirical, we strive to make limiting cases theoretically rigorous.

Salinity Events

We form the equations so that the adjustable parameters have physical significance on the previously described diagrams. The effective salinity corresponding to the type II(–) to III transition C_{Sel} is approximately the salinity on a VFD where the third microemulsion phase appears. C_{Seu} is where the microemulsion phase disappears. For best approximation for both quantities, use a VFD with a water–oil ratio of 1. At this water–oil ratio, the optimal salinity C_{Sopt} is the C_{Se} where the excess phases have equal volumes.

In what follows, the effective salinities are normalized by C_{Sopt} . The resulting dimensionless effective salinities

$$C_{SeD} = \frac{C_{Se}}{C_{Sopt}} \quad (9.7-1)$$

are those that control the phase behavior. Clearly, C_{SeD} can take on any positive value and is equal to 1 at optimal conditions.

Other events coming from the VFD relate to the surfactant maximum coordinate on the binodal curve at low, optimal, and high salinities. At $C_{SeD} = 1$, the surfactant coordinate of the invariant point is

$$C_{3M} = \frac{C_3}{S_3} = C_{3\max 1} \quad (9.7-2)$$

where S_3 is the volume fraction (saturation) of the microemulsion phase. The oil and brine coordinates at optimal conditions are

$$C_{1M} = C_{2M} = \frac{1 - C_{3M}}{2} \quad (9.7-3)$$

These equations assume the excess phases are free of surfactant.

At low salinity, the height of the binodal curve is

$$C_{3\max 0} = \left. \frac{C_3}{S_3} \right|_{C_{Sel}} \quad (9.7-4a)$$

and the similar quantity at high salinity is

$$C_{3\max 2} = \left. \frac{C_3}{S_3} \right|_{C_{Seu}} \quad (9.7-4b)$$

Equations (9.7-4a) and (9.7-4b) generally provide underestimations of the binodal curve heights. Figure 9-14 shows the quantities in Eqs. (9.7-2) and (9.7-4).

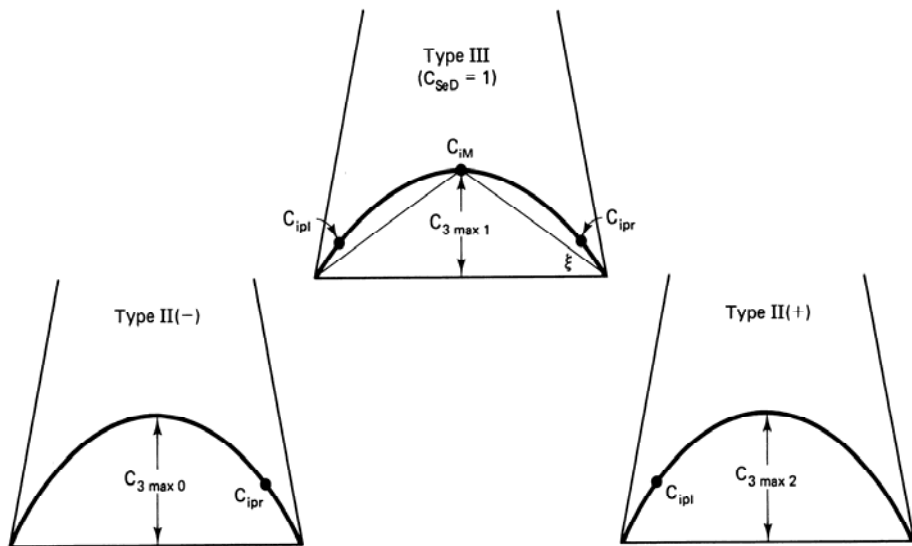


Figure 9-14 Definition of quantities for phase-behavior representation

Events not observable from the VFDs are the plait point locations. We assume the oil coordinates of the plait point vary linearly between the limits of C_{SelD} and C_{SeuD} as shown in Fig. 9-15. C_{2PL} and C_{2PR} , the left and right plait point oil coordinates, apply to the type II(−) and II(+) systems, respectively. also shows the assumed linear variation of the invariant point oil coordinate C_{2M} . The superscript * refers to low and high salinity limiting cases. Typical values of C_{2PL} and C_{2PR} are 0.05 and 0.95, respectively.

These seven parameters (C_{SelD} , C_{SeuD} , $C_{3\max 0}$, $C_{3\max 1}$, $C_{3\max 2}$, C_{2PL} , and C_{2PR}) are sufficient to define the phase behavior with a few additional assumptions.

Binodal Curve

We use the same formalism to represent the binodal curve in all phase environments. For type III, this means (Fig. 9-14) the two two-phase lobes are defined by a

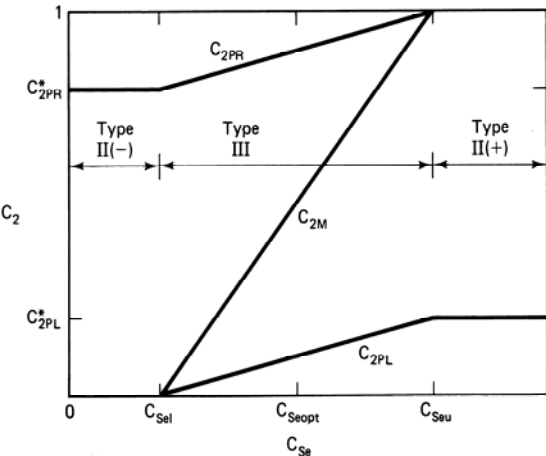


Figure 9-15 Migration of plait and invariant points with effective salinity

continuous curve. For simplicity, let the Hand representation from Eq. (4.4-23) define the binodal curve with $B_H = -1$.

$$\frac{C_{3j}}{C_{2j}} = A_H \left(\frac{C_{1j}}{C_{3j}} \right), \quad j = 1, 2, \text{ or } 3 \quad (9.7-5)$$

Equation (9.7-5) forces the binodal curve to be symmetric. Solving Eq. (9.7-5) for C_{3j} in terms of C_{2j} gives (recalling that $C_{1j} + C_{2j} + C_{3j} = 1$)

$$C_{3j} = \frac{1}{2}([(C_{2j}A_H)^2 + 4C_{2j}A_H(1 - C_{2j})]^{1/2} - C_{2j}A_H) \quad (9.7-6)$$

Since the curve is symmetric, the maximum C_{3j} occurs when $C_{2j} = C_{1j}$ or, alternatively, when $C_{2j} = (1 - C_{3j})/2$, as in Eq. (9.7-3). This substituted into Eq. (9.7-6) gives

$$A_{Hm} = \left(\frac{2C_{3\max m}}{1 - C_{3\max m}} \right)^2 \quad (9.7-7)$$

where $m = 0, 1, \text{ or } 2$ corresponding to the salinity extremes. The A_{Hm} 's are linearly interpolated as

$$\begin{aligned} A_H &= A_{H0} + (A_{H1} - A_{H0})C_{SeD}, & C_{SeD} &\leq 1 \\ A_H &= A_{H1} + (A_{H2} - A_{H1})(C_{SeD} - 1), & C_{SeD} &\geq 1 \end{aligned} \quad (9.7-8)$$

Tie Lines in Two-Phase Systems

Since the treatment for the II(+) system is identical, let us deal with the tie lines in a II(−) system only, but we use C_{2PL} instead of C_{2PR} . Again, using the Hand representation, but with $F_H = 1$, the phase distribution (Eq. 4.4-24) now becomes

$$\frac{C_{32}}{C_{22}} = E_H \left(\frac{C_{33}}{C_{13}} \right) \quad (9.7-9)$$

This equation applies at the plait point from which we have $E_H = C_{1PL}/C_{2PL} = (1 - C_{2PL} - C_{3PL})/C_{2PL}$. Since the plait point is also on the binodal curve, Eq. (9.7-6) applies to give

$$E_H = \frac{1 - C_{2PR} - \frac{1}{2}[(A_H C_{2PR})^2 + A_H C_{2PR}(1 - C_{2PR})^{1/2} - A_H C_{2PR}]}{C_{2PR}} \quad (9.7-10)$$

C_{2PR} being defined as a function of salinity, this equation and Eq. (9.7-8) give the salinity dependence of E_H .

Type III

The three-phase portion of this environment poses no difficulties since the excess phases are pure by assumption, and the composition of the microemulsion phase is given by the coordinates of the invariant point. For a given C_{SeD} , C_{2M} is fixed, and C_{3M} follows from Eq. (9.7-6).

The two-phase lobes are somewhat more trouble. Once again, we consider only the II(−) lobe since the II(+) lobe is analogous. Let's suppose the Hand representations (Eqs. 9.7-5 and 9.7-9) apply to transformed concentrations (denoted by superscript prime) where

$$C'_{2j} = C_{2j} \sec \xi \quad (9.7-11a)$$

$$C'_{3j} = C_{3j} - C_{2j} \tan \xi \quad (9.7-11b)$$

$$C'_{1j} = 1 - C'_{2j} - C'_{3j}, \quad j = 2 \text{ or } 3 \quad (9.7-11c)$$

The angle ξ in these equations is from Fig. 9-14

$$\tan \xi = \frac{C_{3M}}{C_{1M}} \quad (9.7-12a)$$

or, alternatively,

$$\sec \xi = \frac{(C_{1M}^2 + C_{3M}^2)^{1/2}}{C_{1M}} \quad (9.7-12b)$$

These relations allow the parameter E_H to be expressed in terms of the untransformed coordinates of the plait point as

$$E_H = \frac{C'_{1PR}}{C'_{2PR}} = \frac{1 - (\sec \xi - \tan \xi)C_{2PR} - C_{3PR}}{C_{2PR} \sec \xi} \quad (9.7-13)$$

When the relation between C_3 and C_2 (Eq. 9.7-6) is used, this gives E_H as a function

of salinity in the type II(–) lobe ($C_{Sel} < C_{Se} < C_{Seu}$). You can verify that these manipulations for the type III lobes merge continuously with the two-phase environments.

9-8 ADVANCED MP PHASE BEHAVIOR

For ideal surfactant–brine–oil systems, phase boundaries and optimal salinity would be independent of brine salinity. This observation means plots of phase boundaries and optimal salinity versus overall surfactant concentration—the salinity requirement diagram (SRD)—would consist of horizontal lines. Petroleum sulfonate systems generally do not manifest this type of behavior (Fig. 9-8 or Fig. 9-16); however, this nonideality can be explained by the pseudophase theory (Hirasaki, 1982; Camilleri et al., 1987). The theory also illustrates the correct measure of optima conditions, accounts for preferential partitioning of a cosurfactant among the various phases, and fits nicely into the formalism of the previous section.

Figure 9-17(b) shows a three-phase type III system with a water-external

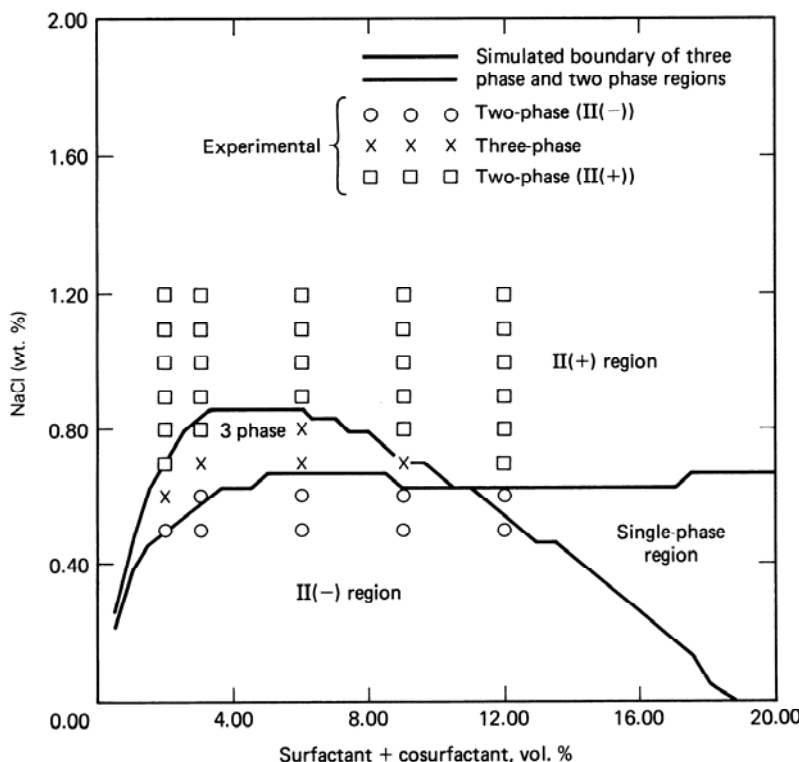


Figure 9-16 Salinity requirement diagram for brine, decane, isobutanol, TRS 10-410. Surfactant/alcohol = 1, Na/Ca = 10 (equivalents), Water–oil ratio = 1 (from Prouvost, 1984)

middle phase, and Fig. 9-17(a) shows the pseudophase representation. Since the only volume occupying components in the system are water, oil, surfactant, and cosurfactant, the system is naturally represented on a quaternary diagram (Fig. 9-17a). All charged species, except those we mention below, exist in unassociated form. The system consists of three pseudocomponents.

1. An oleic pseudocomponent consisting of the excess oil phase and the oil at the center of the swollen micelles.
2. An aqueous pseudocomponent consisting of the excess brine phase and the brine in the microemulsion. This phase contains all charged species not associated with the micelles. Both the oleic and aqueous pseudocomponents can contain cosurfactant but neither contains surfactant.
3. An interfacial pseudocomponent consisting of the surfactant, cosurfactant, and counterions associated with the micelles. Micelles containing two or more surfactant types are mixed micelles.

The theory has three separate facets: definition of effective salinity, cosurfactant partitioning, and cation association with the mixed micelles.

Definition of Effective Salinity

The phase rule (Eq. 4.1-2) states there are two ($N_C = 7$, $N_P = 3$, $N_R = 2$) degrees of freedom for an optimal surfactant system at fixed temperature and pressure. Thus there must be two variables specified to fix optimal conditions. The phase rule gives no indication of what the two degrees of freedom should be except that they should be intensive thermodynamic variables, an observation that rules out overall concentrations.

Glover et al. (1979) present experimental data that suggests the divalent cations bound to the micelles are the most direct indicator of optimality. They suggest optimal salinity decreases linearly with f_6^3 , the fraction of the total divalent cations bound to the micelles.

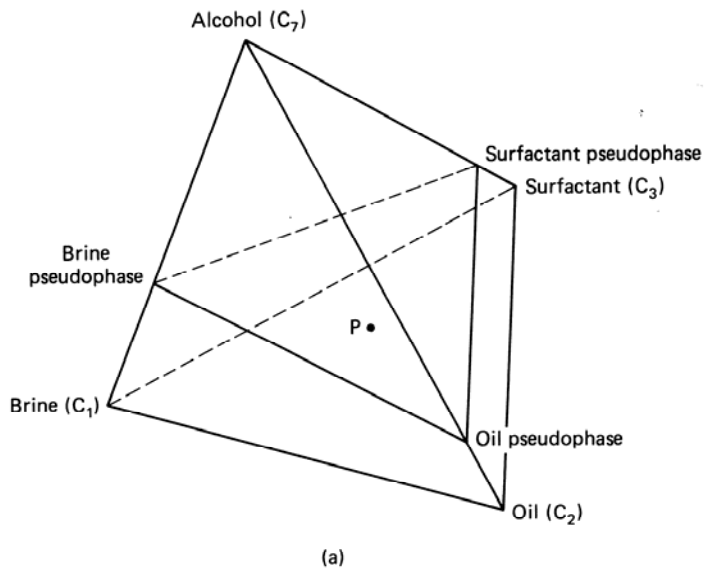
$$\text{Optimal salinity} \sim -\beta_6 f_6^3 \quad (9.8-1)$$

where β_6 is a positive constant. Moreover, ample experimental evidence (Baviere et al., 1981) suggests optimal salinity varies linearly with cosurfactant concentration.

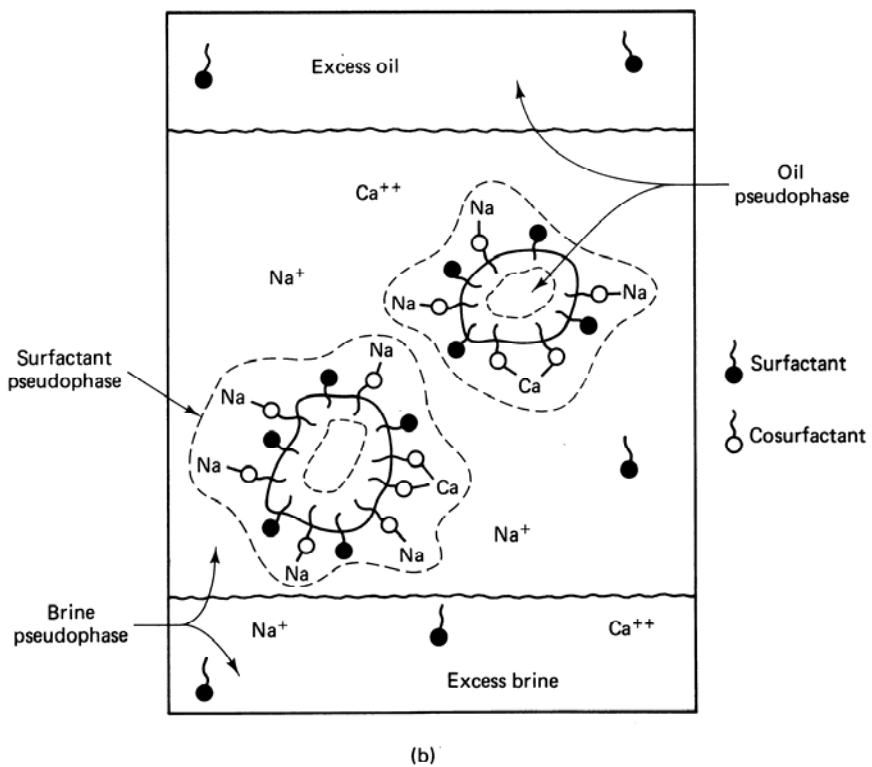
$$\text{Optimal salinity} \sim -\beta_7 f_7^3 \quad (9.8-2)$$

where f_7^3 is the fraction of the cosurfactant associated with the micelles. The constant β_7 can be positive if the cosurfactant is more water-soluble than the surfactant, and it can be negative otherwise. Equations (9.8-1) and (9.8-2) suggest the following combination for the optimal salinity expressed as the anion concentration in the aqueous phase:

$$C_{s1} = C_{s1}^* (1 - \beta_6 f_6^3)(1 + \beta_7 f_7^3) \quad (9.8-3)$$



(a)



(b)

Figure 9-17 Schematic representation of pseudophase theory for surfactant–brine–oil–cosurfactant systems

In this equation, C_{51}^* is the optimal anion concentration in the absence of divalents and cosurfactants. Equation (9.8-3) suggests a definition of effective salinity

$$C_{Se} = \frac{C_{51}}{(1 - \beta_6 f_6^3)(1 + \beta_7 f_7^3)} \quad (9.8-4)$$

C_{Se} is the effective salinity used as a normalizing factor in Sec. 9-7. The remaining tasks are to define f_6^3 and f_7^3

Cosurfactant Partitioning

In the following, we use C_i^j to designate pseudophase compositions. Let's estimate the pseudocomponent concentrations at point $P(C_1, C_2, C_3, C_7)$ in Fig. 9-17(a). If the pseudocomponents are the apexes of the indicated triangle,

$$C_7 = C_1 C_7^1 + C_2 C_7^2 + C_3 C_7^3 \quad (9.8-5)$$

That the pseudocomponent concentrations occupy the role of phase saturations in the equation accounts for why the theory is called the pseudophase theory. Now let's use partition coefficients to eliminate two of the pseudocompositions

$$K_{21}^7 = \frac{C_7^2}{C_7^1}, \quad K_{31}^7 = \frac{C_7^3}{C_7^1} \quad (9.8-6)$$

Ideally, the partition coefficients should be equal to the cosurfactant partition coefficients in the absence of surfactant (Prouvost, 1984). These substituted into Eq. (9.8-6) give the cosurfactant concentration in the aqueous pseudophase

$$C_7^1 = C_7 \left(\sum_{j=1}^3 C_j K_{j1}^7 \right) \quad (9.8-7a)$$

Because this pseudophase contains only cosurfactant and water

$$C_1^1 = 1 - C_7^1 \quad (9.8-7b)$$

Equations (9.8-7b) and (9.8-6) can be used to calculate all pseudophase compositions from overall compositions and the partition coefficients.

To use the equations of the previous section, we must express the overall and phase compositions in terms of the pseudocomponents. We define C_{Pi} as

$$C_{Pi} = \frac{\text{Volume of } i + \text{Volume of 7 associated with } i}{\text{Total volume}} \quad (9.8-8)$$

which gives

$$C_{Pi} = C_i (1 + C_7^i), \quad i = 1, 2, 3 \quad (9.8-9)$$

The C_{Pi} are overall concentrations and are to be used directly in the strict ternary representation. The equations collapse to the Sec. (9-6) equations when cosurfactant

and divalent concentrations are zero. Further, Eq. (9.8-9), summed over three phases, equals unity from Eq. (9.8-7a).

The fractional cosurfactant associated with the micelle follows directly from this also. By definition

$$f_7^3 = \frac{\text{Volume of 7 in pseudophase 3}}{\text{Volume of pseudophase 3}} \quad (9.8-10)$$

which is simply

$$f_7^3 = \frac{1}{1 + \frac{1}{C_7^3}} \quad (9.8-11)$$

also by definition.

Divalent Cation Association

Competition for anionic sites on the micelle surface is through electrical forces. Hence a cation exchange law of the following form applies:

$$\left(\frac{(C_9^3)^2}{C_6^3} = \beta^3 C_3^3 \frac{(C_9^3)^2}{C_6^3} \right)_1 \quad (9.8-12)$$

This equation is a form of Eq. (3.5-4) in which the constant (β^3) is multiplied by a factor that will convert the volume fraction C_3^3 into units of meq/L³ of pore volume. Equation (9.8-12) assumes the cosurfactant is nonionic and all the surfactant is available to exchange.

Two types of electroneutrality now apply: on the micelle surface

$$C_{61}^3 + C_{81}^3 = C_{31}^3 \quad (9.8-13a)$$

and in the bulk aqueous phase

$$C_{61} + C_{81} = C_{51} \quad (9.8-13b)$$

These form three equations in four unknowns, from which it becomes possible to solve for the bound divalents in terms of the unassociated species concentrations

$$C_{61}^3 = C_{31}^3 + \frac{1}{2} [r_{86}^3 - ((r_{86}^3)^2 + 4r_{86}^3 C_{31}^3)^{1/2}] \quad (9.8-14a)$$

where

$$r_{86}^3 = \beta^3 C_3^3 \frac{(C_{81}^3)^2}{C_{61}^3} \quad (9.8-14b)$$

Compare these equations to Eq. (3.5-7). Once the left side of Eq. (9.8-14a) is known, the fraction of the total divalents bound to the micelle follows from

$$f_6^3 = \frac{C_6^3}{C_3} \quad (9.8-15)$$

and C_{Se} can be estimated from Eq. (9.7-3).

The above theory will fit experimental data very well. Figure 9-16 shows the agreement between estimated and calculated phase boundaries for a system of petroleum sulfonate, decane, isobutanol, Na, and Ca. To construct this match, Prouvost (1984) assumed the above theory applies to phase boundaries as well as to optimal salinities. The theory and experiment agree well even though the SRD is far from ideal.

9-9 HIGH CAPILLARY NUMBER RELATIVE PERMEABILITIES

A transport property that deserves treatment in a separate section is the high capillary number relative permeability. In this section, we discuss two- and three-phase experimental results based on the work of Delshad et al. (1987) (see Sec. 3-3 for discussion of low capillary number relative permeabilities).

Few theoretical relations exist for relative permeabilities in general, much less for those at high capillary number. We do know the extreme values of relative permeability functions occur at residual phase saturations. The latter are functions of capillary number N_{vc} through the capillary desaturation curve (CDC) (see Sec. 3-4). Further, for very high values of N_{vc} , we expect the relative permeabilities to approach straight-line functions between zero and unit endpoints with no residual phase saturations. For low N_{vc} , the relative permeabilities should return to the two- or three-phase high IFT functions. The variation between these extremes is not well established.

High N_{vc} relative permeabilities are difficult to measure. In one type of experiment, the large N_{vc} may be attained by increasing the flow rate. This technique causes experiments to proceed rapidly since, as we saw in Sec. 3-4, N_{vc} must increase by several factors of 10 before a significant effect occurs. Such high rates are clearly unrepresentative of typical reservoir fluid velocities. If the high N_{vc} is established by lowering the IFT, the experiments tend to be dominated by transient composition changes. In principle, these transients could be analyzed by the method given in Sec. 9.10, but this requires knowing the relative permeabilities, whose measurement is the point of the experiment.

The most reliable measurement is of steady-state relative permeabilities using preequilibrated fluids. For micellar fluids in two-phase flow, this consists of displacing a composition on one end of a tie line with another on the same tie line at constant salinity. When the effluent and injected fractional flows are equal, and transients caused by nonideal phase behavior are gone, the relative permeability to the flowing phases may be calculated from the measured effluent cuts and pressure drop. A similar provision exists in the three-phase ideal systems where all

compositions are in equilibrium at constant salinity. Of course, such transients may take some time to die out; thus steady-state experiments can be time consuming. The uniform saturations established by such a procedure follow from material balance or, preferably, tracer data interpreted by a suitable numerical model (Delshad et al., 1987).

Despite these difficulties, high N_{vc} relative permeabilities for two-phase flow have been rather intensively measured, but three-phase data are rare. Figure 9-18 shows steady-state relative permeabilities to brine, oil, and microemulsion phases for both two- and three-phase flow. The permeable medium was strongly water wet in both cores A and B at high N_{vc} conditions. $N_{vc} = 0.01$ at the optimal salinity used in the experiments. The micellar system under test closely followed ideal phase behavior. From these high N_{vc} data, several observations can be made.

1. The residual phase saturations are nonzero. Of course, these values are points on the CDC. Except for the oleic phase, whose endpoint was already high in the water-wet medium, the endpoint relative permeabilities are substantially different from their low N_{vc} values.
2. The high N_{vc} relative permeabilities are not straight lines. The curves in these figures are the matches of the exponential forms Eq. (3.3-4) to the data. But the exponents n_1 and n_2 in these equations are not substantially different from their low N_{vc} values.
3. The two- and three-phase data follow essentially the same curves.
4. The relative permeability for all three phases are functions of their own saturations. This observation is at odds with the high N_{vc} behavior of three-phase gas, oil, and water flows (Stone, 1970).
5. Probably the most surprising conclusion is that the excess brine phase was not the most strongly wetting phase as it was under low N_{vc} conditions. This observation is supported by a variety of observations not present in Fig. 9-16. However, the microemulsion and excess brine residual phase saturations have about the same value at $N_{vc} = 0.01$.
6. The shape of the microemulsion curve is concave downward. This observation is highly atypical of relative permeabilities and can be explained only as wall or interfacial slippage.

For approximate calculation, let the exponential relative permeabilities of Eq. (3.3-4) approximate two-phase high N_{vc} behavior. Suppose the CDC of a type II(–) system is represented by Fig. 3-19, with $(N_{vc})_c$ and $(N_{vc})_t$ corresponding to the wetting state of phase j . We can define linear interpolants for the endpoints and the curvatures. For example, the endpoints vary according to

$$(k_{r2}^0)' = (k_{r2}^0) + \left(1 - \frac{S'_{3r}}{S_{3r}}\right)(1 - k_{r2}^0) \quad (9.9-1a)$$

$$(k_{r3}^0)' = (k_{r3}^0) + \frac{S'_{2r}}{S_{2r}}(1 - k_{r3}^0) \quad (9.9-1b)$$

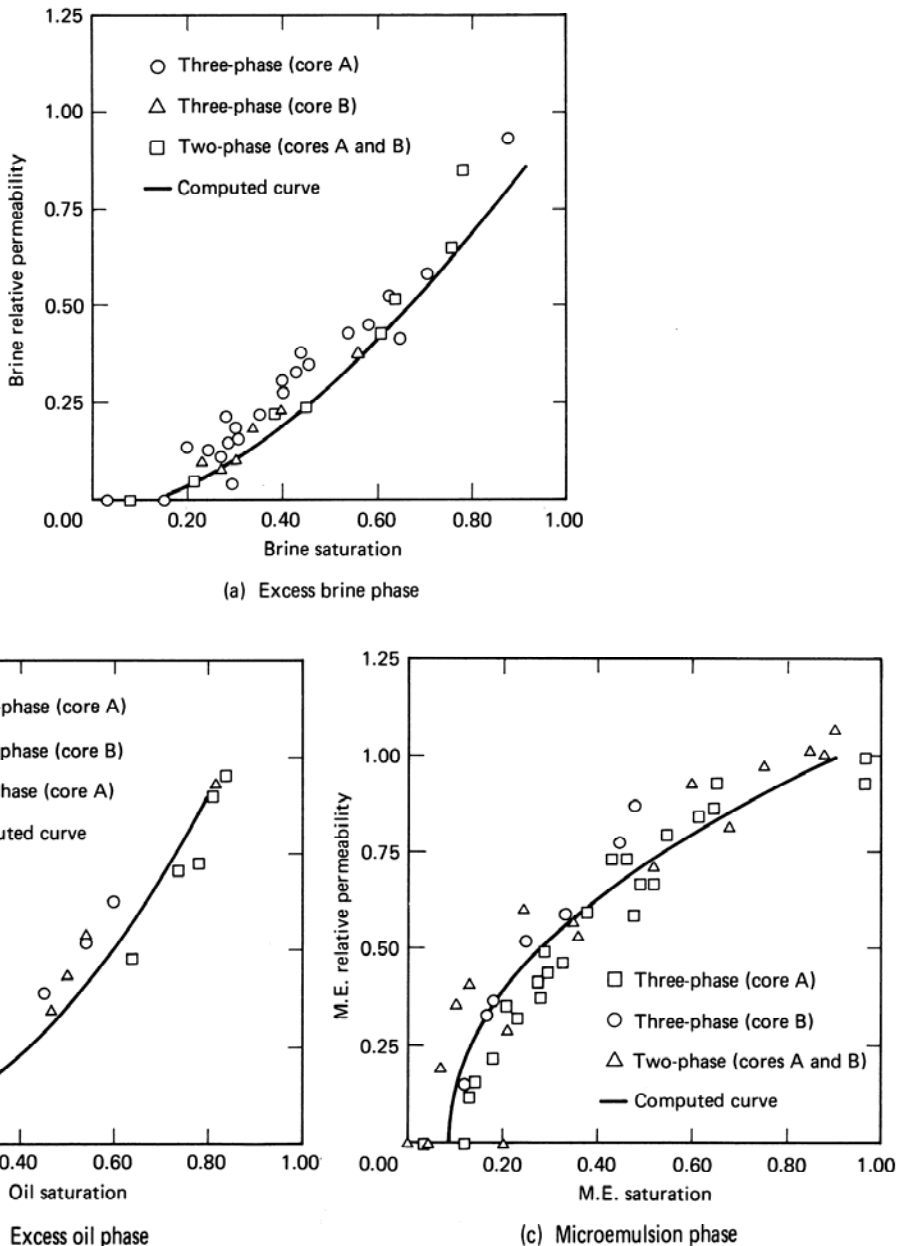


Figure 9-18 Two- and three-phase relative permeabilities (from Delshad et al., 1987)

where S'_{2r} and S'_{3r} are the high N_{vc} residual phase saturations. This approximate linear relation has been substantiated by Stegemeier (1976). The nonunit curvatures of the relative permeabilities seem to persist beyond the point of zero residual phase saturations; hence it seems reasonable that the logarithm of N_{vc} itself be used as an interpolating function

$$n'_j = n_j + (1 - n_j) \log \left[\frac{N_{vc}}{(N_{vc})_c} \right], \quad j = 2 \text{ or } 3 \quad (9.9-2)$$

Relations for type II(+) systems, where $j = 1$ or 3, follow analogous arguments.

We can now estimate two-phase relative permeabilities from phase behavior, a solubilization parameter correlation, the CDC curves, and low N_{vc} relative permeability curves. Suppose we know the overall composition of a type II(–) system that splits into two equilibrium phases. The phase compositions follow the ternary diagram. These can be converted to solubilization parameters using Eq. (9.5-1) and then into IFTs from the appropriate correlations. We use this to calculate N_{vc} , and the CDCs to estimate residual phase saturations. The high N_{vc} curves follow from Eqs. (9.9-1) and (9.9-2). If additional data are available about viscosities, dip angles, and densities, we can easily calculate phase fractional flows.

For three-phase flow, even such rough estimates are not warranted. Theoretical models by Hirasaki et al. (1983) and Delshad et al. (1987), though plausible in limiting senses, account neither for the intermediate wetting of the excess brine phase nor for the observation that the phase relative permeabilities are functions only of their own saturations. Clearly, we are hindered by a lack of understanding about the pore-level nature of high capillary number flows.

9-10 FRACTIONAL FLOW THEORY IN MICELLAR-POLYMER FLOODS

Fractional flow theory can be just as insightful for MP floods as for the solvent and polymer floods we covered in Secs. 7-7 and 8-4. In fact, there are so many similarities to those processes that we draw heavily on the material in those sections.

To make the analysis, we invoke the usual fractional flow assumptions: incompressible fluid and rock, one-dimensional flow, and no dissipative effects. In addition, we neglect the presence of the polymer drive (the polymer treatment can be added as an exercise), assume three-component MP floods with a step change in concentration at the origin of a time-distance diagram, and treat only those floods with constant phase behavior environment. Further, we neglect surfactant retention until later in this section where we invoke more restrictive assumptions about the phase behavior. To shorten the development, we cover only the high-salinity type II(+) floods. Fractional flow treatment for three-phase MP floods has not been extensively investigated (Giordano and Salter, 1984), but it could be so treated with the numerical technique of Sec. 5-7.

Ternary Landmarks

Figure 9-19(a) shows the basic phase and saturation behavior. This is very much like the behavior in Fig. 7-31 except that the miscibility gap extends entirely across the bottom edge of the ternary, and of course, water is explicitly included on the diagram.

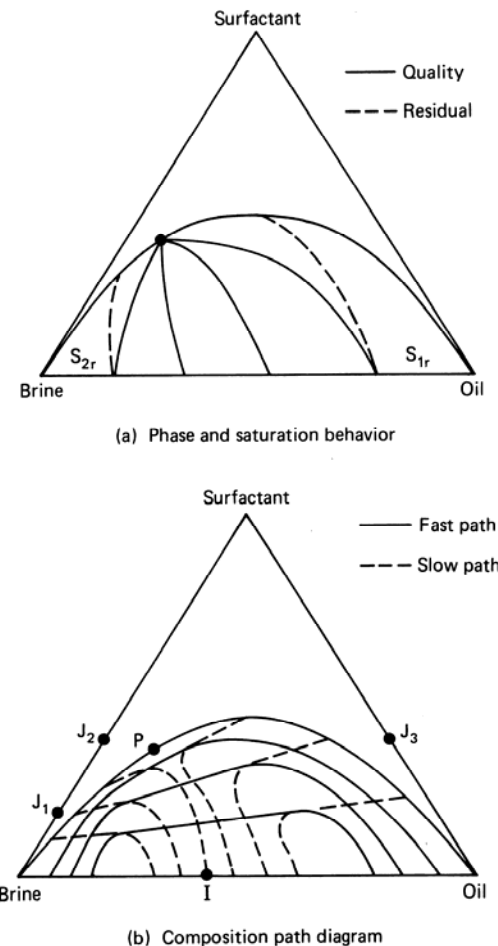


Figure 9-19 Ternary diagram and composition paths for micellar–polymer system

All phase diagrams in this section have exaggerated two-phase regions. One significant difference with solvent flooding is lines of residual oleic and aqueous phase saturations merge with the binodal curve at some distance from the plait point. This happens because the oleic-aqueous capillary number increases (IFT decreases) rapidly as the plait point is approached, which causes S_{2r} and S_{1r} to approach zero (see Sec. 3-4). For continuous surfactant injection, as we are treating here, this issue is entirely secondary. But for finite slugs in highly dissipative displacements—that is, the realistic cases—the rate of approach to zero S_{2r} is very important. The aqueous-oleic fractional flow curve follows from the large N_{vc} relative permeabilities we discussed in Sec. 9-9.

MP Flooding without Retention

The relative permeability behavior does not affect the qualitative features of the composition path diagram (Fig. 9-19b). The development in Sec. 7-7 applies directly: We see the presence of “hair-pin” fast paths along tie lines, slow paths on either side,

and a succession on nontie line paths. Because of the graphical possibilities, we assume the component distribution between phases is given by a family of straight lines intersecting at $C_3 = 0$ and $C_2 = C_2^0$ (the tie line envelope is a point on the C_3 axis)

$$C_{3j} = \eta(C_{2j} - C_2^0), \quad j = 1 \text{ or } 2 \quad (9.10-1)$$

from which we have $C_1^0 = 1 - C_2^0$. The parameter η is the slope of the phase distribution line.

To review briefly, the component velocities along a tie line are

$$v_{C_i} = \frac{dF_i}{dC_i}, \quad i = 1, 2, 3 \quad (9.10-2)$$

The nontie line paths carry the constant specific velocities given by

$$v_{\Delta C_i} = \frac{F_i - C_i^0}{C_i - C_i^0}, \quad i = 1, 2, 3 \quad (9.10-3)$$

At the tangent intersection of the tie line and nontie line paths, we must have

$$\frac{F_i - C_i^0}{C_i - C_i^0} = \frac{dF_i}{dC_i} \quad (9.10-4)$$

which defines the two singular curves and allows the location of the appropriate constructions on a fractional-flux-overall-concentration plot. Other paths include the binodal curve itself and the equivelocity curve where $f_1 = S_1$.

In Fig. 9-19(b), we illustrate behavior for fractional flux curves whose S-shape persists even to low IFT. Our task is to string together the paths so that the composition route leads to monotonically decreasing composition velocities.

We focus on the three different injection conditions. Condition J_1 is an aqueous (oil-free) surfactant solution below the critical tie line extension, J_2 is an aqueous surfactant solution above the extension, and J_3 is an oleic (brine-free) slug below the extension. Conditions J_1 and J_2 represent low- and high-concentration aqueous surfactant solutions, and condition J_3 is an oil-soluble solution. In each case, the initial condition will be at I , a uniform tertiary condition.

Figure 9-20 shows the composition route and the S_2 and C_3 profiles at fixed t_D for the low-concentration surfactant displacement. Starting at the injection condition, the composition route enters the two-phase region along a tie line extension, switches to the nontie line path at the second singular point on the tie line, switches again to the fast path along the ternary base, and then to the initial condition I . For typical fractional flux curves, this causes a shock to an oil bank saturation S_{2B} , and a mixed wave from S_{2B} to $S_2 = 0$. Following the tie line causes the curious effect that the flowing surfactant concentration can be greater than the injected concentration. The displacement can also be relatively inefficient if the spreading portion of the oil bank rear is large.

For the high-concentration surfactant displacement (Fig. 9-21), the composition route passes through the plait point, follows the equivelocity path to the

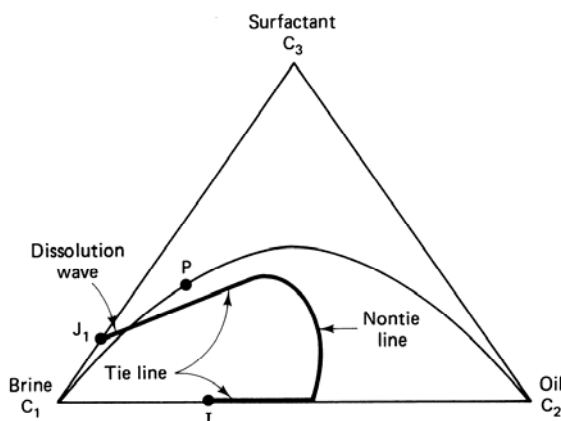
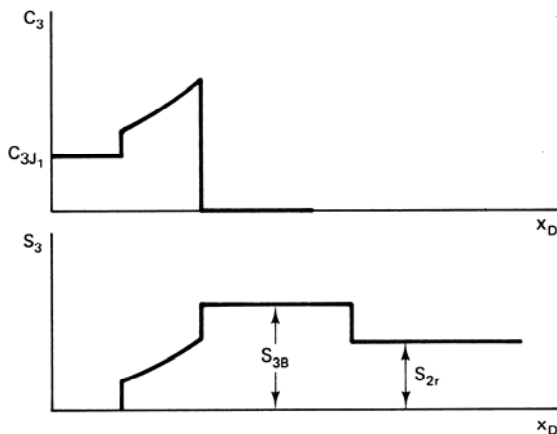


Figure 9-20 Composition route and profiles for low-concentration surfactant flood

oil bank saturation, and then on to the initial condition. This displacement is directly analogous to a condensing gas drive miscible displacement since the surfactant wave is indifferent and moves with unit specific velocity (compare this displacement with the lower panel in Fig. 7-35b). As such, it is highly efficient; however, the greater efficiency is bought with a higher surfactant concentration. The oil bank saturation is also somewhat lower than in Fig. 9-20.

The oleic surfactant behavior is shown in Fig. 9-22. Here the composition route also enters along a tie line extension, branches to a non-tie line path at the first singular point, and then on to the oil bank and the initial condition. In many respects, this displacement is the mirror image of that in Fig. 9-20. However, the ultimate microemulsion phase saturation is unity, meaning the oil bank saturation S_{2B} is between the initial and 1.0. The surfactant concentration decreases monotonically in this displacement, which as in Fig. 9-20, can also be inefficient.

There is great variety of behavior in the displacement character even under

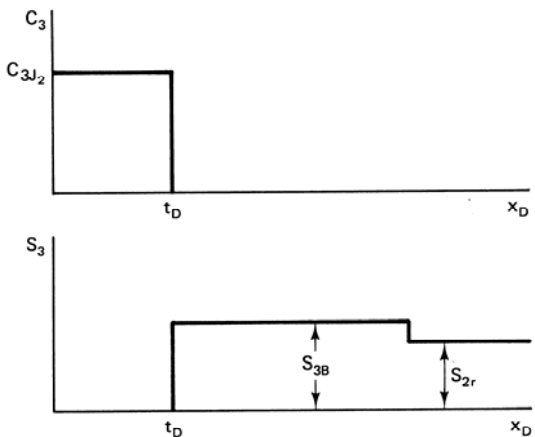


Figure 9-21 Composition route and profiles for high-concentration surfactant flood

the restrictive assumptions invoked here. Some of this variety is present in the constructions used to infer Figs. 9-20 through 9-23. The cases for type II(–) are analogous. The nature of the composition route does not change with the shape of the fractional flux curve even though the latter greatly affects the efficiency of the displacement.

MP Flooding with Retention

Adding retention complicates the analysis because the composition route no longer follow tie lines. But by making a few additional assumptions, we can develop a fractional flow solution that uses fractional flow curves instead of fractional fluxes.

Let us now analyze the type II(–) system where the right plait point is in the oil corner of the ternary, and the amount of solubilized oil in the microemulsion phase is negligible. The aqueous and microemulsion phase are now equivalent ($S_1 = S_3$). If the injected slug composition is below a tangent from the binodal curve at the

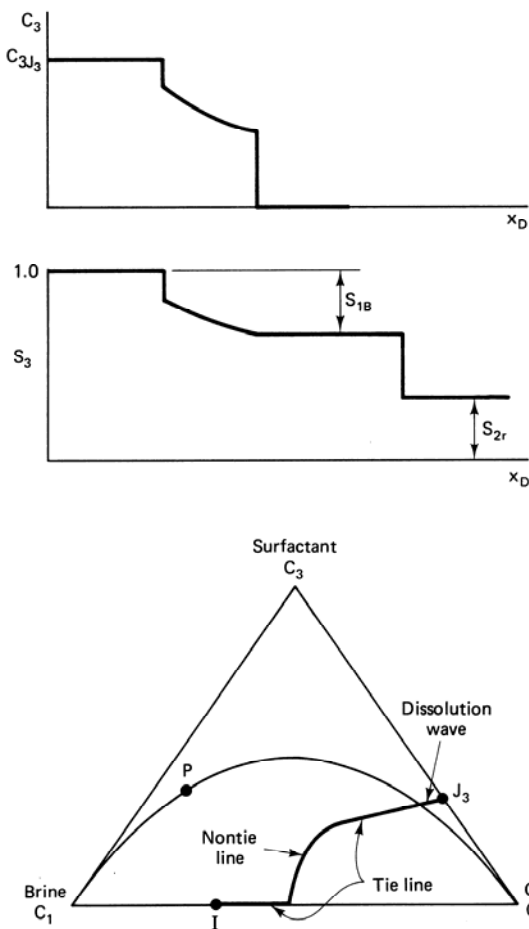


Figure 9-22 Composition route and profiles for high-concentration oleic surfactant flood

plait point, it must necessarily be on a tie line even if it contains no oil. Let the residual oil saturation on this tie line be S'_{2r} , the ultimate value of a low IFT (high N_{vc}) aqueous-phase fractional flow curve as shown in Fig. 9-24. This figure also shows the water-oil fractional flow curve f_1 along the tie line on the base of the ternary. Since this aqueous slug miscibly displaces the irreducible water, the velocity of the corresponding indifferent wave is

$$v_{C_3} = \frac{f_1^s}{S_1 + D_3} \quad (9.10-5)$$

from Eq. (5.4-8a). Note that f_1^s is the microemulsion (aqueous) phase high N_{vc} fractional flow. In this equation, D_3 is the surfactant's frontal advance loss given by

$$D_3 = \frac{1-\phi}{\phi} \frac{C_{3s}}{C_{3J} \rho_s} \quad (9.10-6)$$

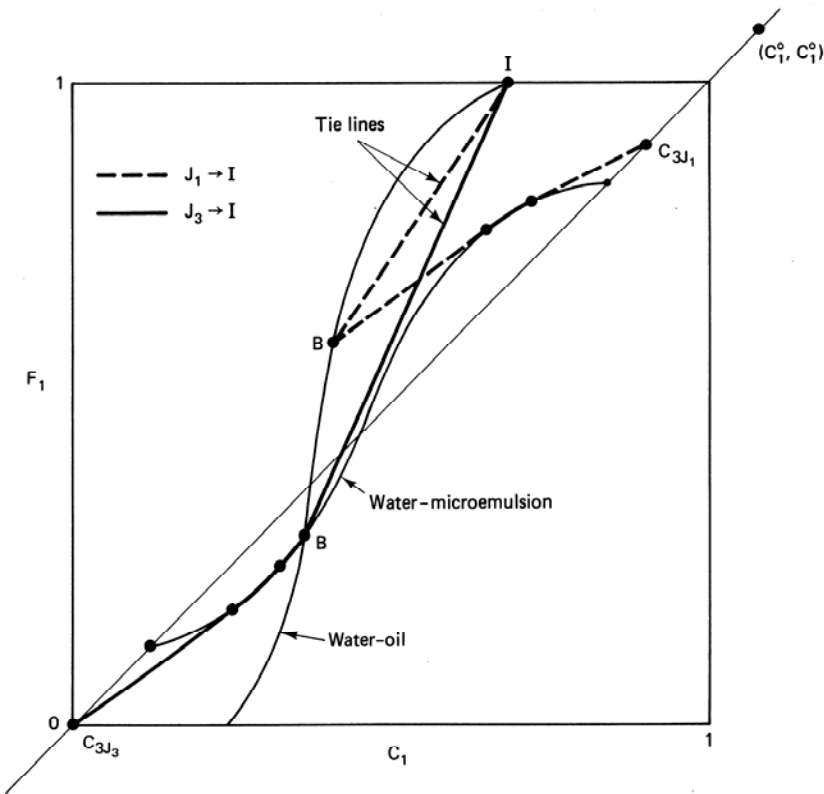


Figure 9-23 Fractional flux and composition routes for aqueous and oleic surfactant displacements

The most general case occurs when the rear of the oil bank travels as a mixed wave. At the leading edge of the spreading portion of this wave, the specific velocity in Eq. (9.10-5) must be equal to the specific oil velocity at some saturation S_1^* given implicitly by

$$\left(\frac{df_1^s}{dS_1} = \frac{f_1^s}{S_1 + D_3} \right)_{S_1^*} \quad (9.10-7)$$

The specific velocity of the shock portion of the oil bank rear is

$$v_{\Delta C_2} = \frac{f_{2B} - f_2^s(S_2^*)}{S_{2B} - S_2^*} \quad (9.10-8)$$

This must be equal to v_{C_3} evaluated at $S_2^* = 1 - S_1^*$. If the oil bank front is a shock, it travels with velocity given by

$$v_{\Delta C_2} = \frac{f_{2B} - f_{2I}}{S_{2B} - S_{2I}} \quad (9.10-9)$$

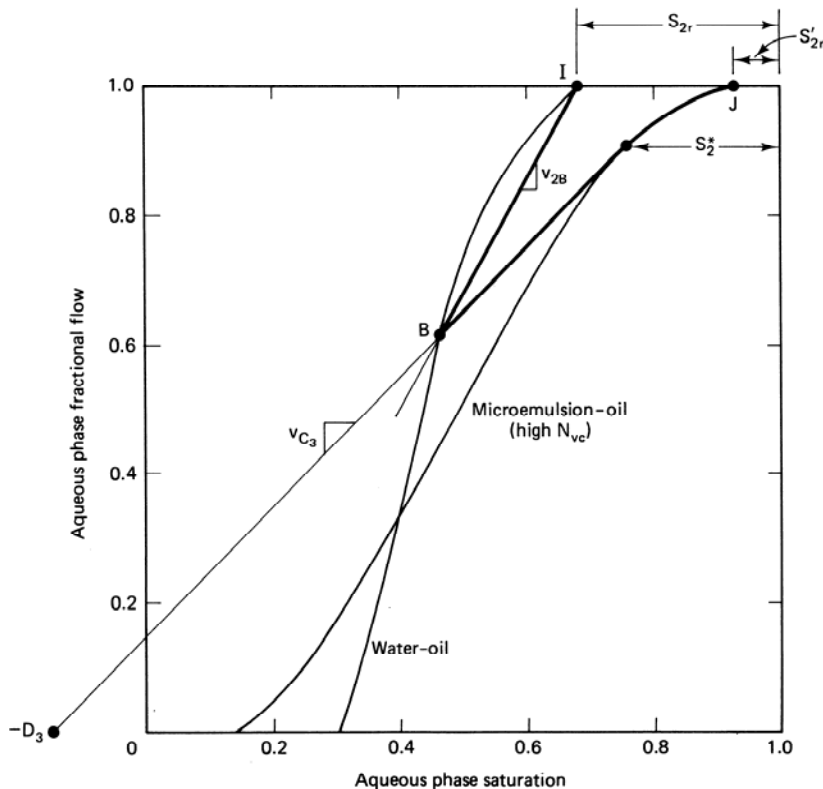


Figure 9-24 Graphical construction for simplified II(-) surfactant displacements

These equations are entirely suggestive of the polymer flooding construction in Sec. 8-4. This parallel is also apparent from comparing the construction given in Fig. 9-24 with the one in Fig. 8-10. The construction of the time-distance and profile diagrams corresponding to Fig. 9-24 is left as an exercise.

An issue not dealt with in Sec. 8-8 is the minimum slug size needed to satisfy retention. Let's suppose the surfactant displacement is pistonlike, that is, $S_{2l} = S'_{2r} = S_2^*$. The minimum surfactant slug size is attained when the similarly pistonlike surfactant-polymer front overtakes the surfactant front at the injection end of the medium. This gives a minimum surfactant slug size of $t_{Ds} = D_3$, meaning the frontal advance loss is an expression of the retention capacity of the medium expressed in units consistent with the slug size. Therefore, knowing D_3 is the beginning point in estimating surfactant requirement in MP flooding. The above result does not depend on the existence of a pistonlike surfactant front.

9-11 ROCK-FLUID INTERACTIONS

Brine salinity and hardness would have far less importance to MP flooding if the host permeable medium were unreactive. Unfortunately, in all but the most artificial cases, reservoir minerals provide an almost limitless source of monovalent and

divalent cations as well as ample sites for surfactant retention. Two sources of cations are mineral dissolution and cation exchange. Dissolution usually occurs at such a low level that it can be neglected in MP floods (but not in high-pH floods). Cation exchange is rarely negligible. For this reason, we discuss it at some length in this section. In the second half of the section, we deal with surfactant retention.

Cation Exchange

We treat the simplest case of monovalent–divalent exchange in single-phase flow in the absence of surfactant or oil. The displacement satisfies the fractional flow assumptions. (For more complicated treatment, see Pope et al., 1978.)

Each point in the permeable medium must satisfy solution electroneutrality

$$C_5 = C_6 + C_8 \quad (9.11-1a)$$

and electroneutrality on the clays

$$Z_v = C_{6s} + C_{8s} \quad (9.11-1b)$$

The units on all concentrations are in equivalents per unit pore volume, and the superfluous phase subscript has been dropped. These equations imply the monovalent, divalent, and anion concentrations are not independent; hence for convenience, we choose to proceed with the divalent and anion concentrations as the dependent variables. At local equilibrium, each point in the medium must also satisfy

$$\frac{C_{8s}^2}{C_{6s}} = K_N \frac{C_8^2}{C_6} \quad (9.11-2)$$

which is simply the cation exchange isotherm of Eq. (3.5-4). Using Eq. (9.11-1), we can express the adsorbed divalent concentration as

$$C_{6s} = Z_v \left(1 + \frac{K_N r}{Z_v} \left[\frac{1}{2} - \left(\frac{Z_v}{K_N r} + \frac{1}{4} \right)^{1/2} \right] \right) \quad (9.11-3a)$$

where

$$r = \frac{C_8^2}{C_6} = \frac{(C_5 - C_6)^2}{C_6} \quad (9.11-3b)$$

Equations (9.11-3) are the basic equilibrium representations.

Let's now consider the displacement of solution *I* by solution *J* under the above conditions. The coherence conditions (Eq. 5.6-14)

$$\left(1 + \frac{dC_{5s}}{dC_5} \right)^{-1} = v_{C_5} = v_{C_6} = \left(1 + \frac{dC_{6s}}{dC_6} \right)^{-1} \quad (9.11-4)$$

are satisfied at all points in the medium. Equation (9.11-4) implies

$$\frac{dC_{5s}}{dC_5} = \frac{dC_{6s}}{dC_6} = \lambda \quad (9.11-5)$$

where λ is the eigenvalue for this problem. In matrix form, Eq. (9.11-5) becomes

$$\begin{pmatrix} C_{55} & C_{56} \\ C_{65} & C_{66} \end{pmatrix} \begin{pmatrix} dC_5 \\ dC_6 \end{pmatrix} = \lambda \begin{pmatrix} dC_5 \\ dC_6 \end{pmatrix} \quad (9.11-6)$$

where $C_{65} = (\partial C_{6s} / \partial C_5)_{C_6}$, and so on. The matrix on the left side has a row of zeros because the anion does not adsorb. Solving Eq. (9.11-6) for the eigenvalues gives

$$\lambda^- = 0, \quad \lambda^+ = C_{56} \quad (9.11-7)$$

From this, it is obvious that $\lambda^+ > \lambda^-$ and that the wave corresponding to λ^- is faster than that corresponding to λ^+ from Eq. (9.11-4).

The eigenvector corresponding to each eigenvalue gives the concentration change across each wave. For the fast wave, inserting λ^- gives

$$C_{65}dC_5 + C_{66}dC_6 = 0 \quad (9.11-8a)$$

and from the slow wave, inserting λ^+ gives

$$dC_5 = 0 \quad (9.11-8b)$$

Immediately we see that the anion concentration is constant across the slow wave since $dC_5 = 0$. The fast wave interpretation is only a little less obvious. Equation (9.11-8a) is the change in C_5 and C_6 that would occur at constant C_{6s} . We can see this by setting the total differential dC_{6s}

$$dC_{6s} = C_{66}dC_6 + C_{65}dC_5 \quad (9.11-9)$$

equal to zero. The result (Eq. 9.11-9) is independent of the form of the exchange isotherm.

The coherent solution, therefore, predicts two waves: an indifferent salinity wave that moves at unit velocity across which the clay concentration remains constant and an exchange wave where the clay changes to be in equilibrium with the injected solution at constant anion concentration. The character of the latter wave depends on the direction in which the concentration velocity is increasing through Eqs. (9.11-3) and (9.11-4).

For example, consider Fig. 9-25(a), which shows the composition space for the two cation system plotted on a ternary representation. Lines of constant anion concentration are parallel to the right edge, and lines of constant clay composition are curves converging to the lower left corner. These curves are described by Eq. (9.11-3). Both sets of lines form the composition path diagram. The bold line segments $I-J'$ (salinity wave) and $J'-J$ (exchange wave) form the composition route. This particular sequence is selected because it is the only one for which the concentration velocities monotonically decrease from I to J . The exchange wave is spreading if the concentration velocity decreases from J' to J ; otherwise, it is a shock. Figure 9-25(b) shows a time-distance diagram for the former case.

To illustrate the accuracy of the above predictions, Fig. 9-26 shows the effluent histories of two laboratory core floods through which are flowing solutions containing only calcium (divalents), sodium (monovalents), and chloride (anion). In

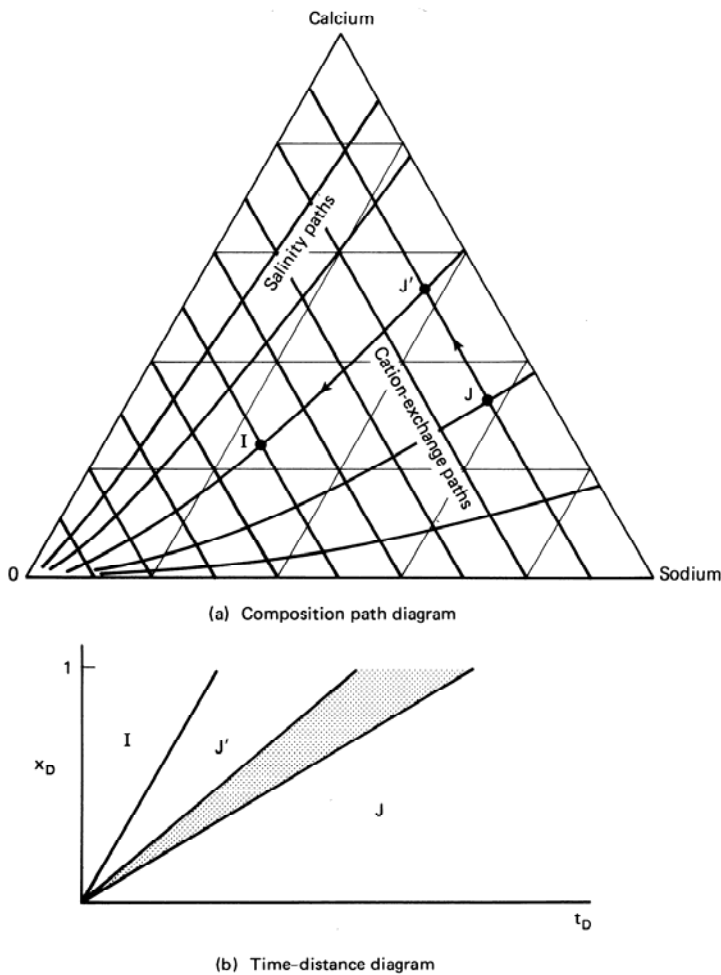


Figure 9-25 Diagrams for two exchanging cation case (from Pope et al., 1978)

both cases, the injected calcium was the same; hence in the absence of exchange, the effluent calcium concentration should not change. But because the anion concentration changes, cation exchange occurs, and the effluent calcium does change. In Fig. 9-26(a), the increased anion concentration causes calcium to be expelled from the clays. In Fig. 9-26(b), the reverse occurs. In both cases, the prediction based on the coherent treatment agrees well with the observed results. Calculated results including dispersion match even better (Lake and Helfferich, 1978).

These results hold immense practical significance for MP flooding in general and the use of low-salinity preflushes in particular. One of the intentions of a preflush is to remove divalent cations so that the slug can work more effectively. However, the above theory suggests the following hindrances:

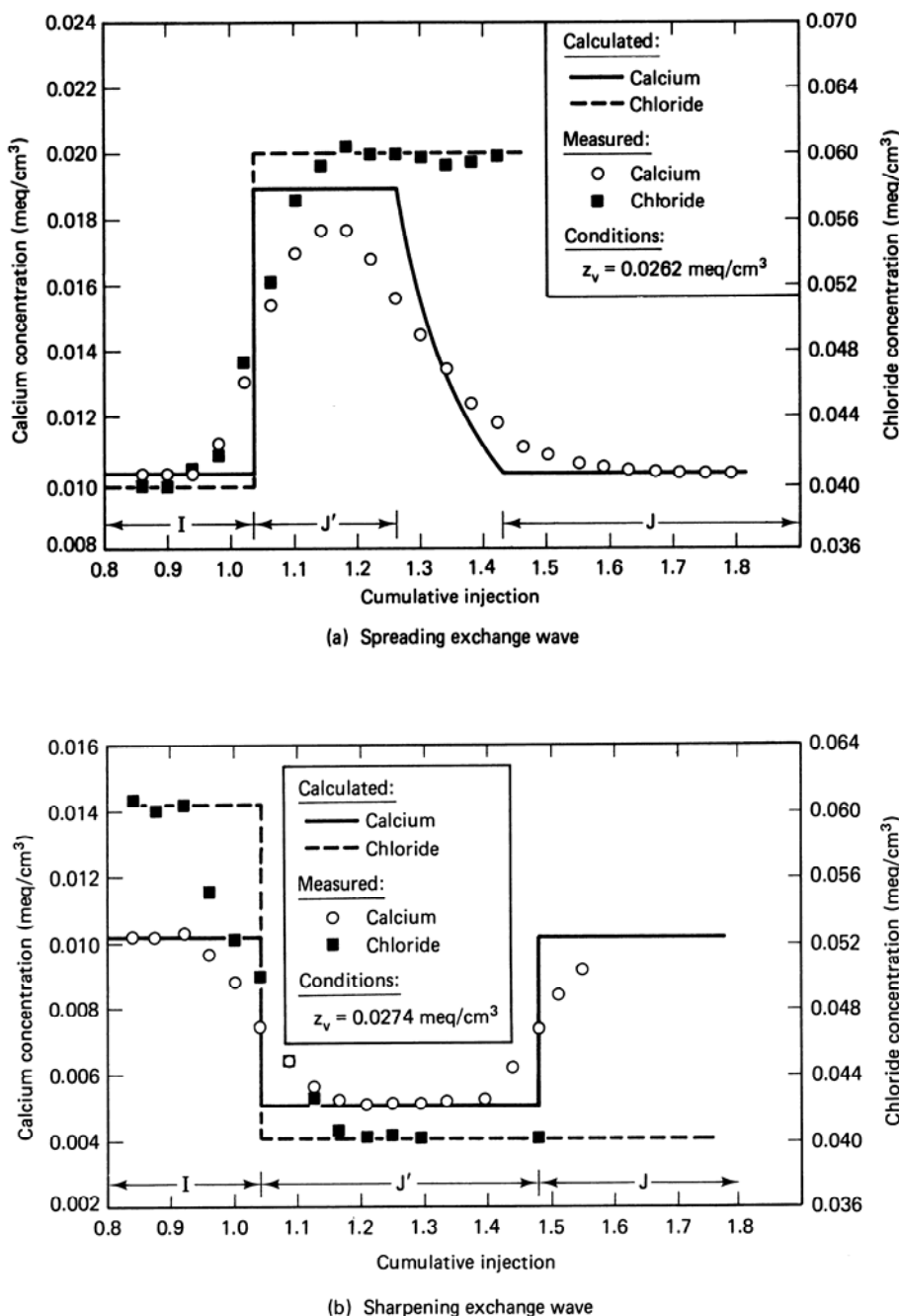


Figure 9-26 Comparison between theory and experiment for two exchanging cation displacement (from Pope et al., 1978)

1. It is entirely possible to inject a low-salinity preflush that actually loads the clays with divalent cations because changes in the ratio r determine clay loading. If r decreases, the clays will take up divalents, which regardless of the salinity, are available for subsequent release into solution.
2. Even if r decreases so that the clays unload divalents, this normally takes a large preflush because the exchange wave velocity is very slow at typical cation exchange capacities and brine concentrations.
3. If the injected solution is entirely devoid of divalents, the clays will still only partially unload because the dissolution of a small amount of divalent-containing minerals acts as a persistent source of hardness.

One philosophy for preflushes is to avoid upsetting the clays at all costs. Doing this is simple in principle: One just injects the preflush, slug, and polymer drive at the same r ratio as exists in the formation brine. But in practice, this procedure is complicated by dispersion-induced mixing (Lake and Helfferich, 1978) and by exchange of divalents with micelles (see Sec. 9-8).

Surfactant Retention

Surfactant retention is probably the most significant barrier to the commercial application of MP flooding. The problem here is one of selectivity. The surfactants should have good selectivity for oil–water interfaces, but they should also have poor selectivity for fluid–solid interfaces.

Surfactants are retained through four mechanisms.

1. On metal oxide surfaces (Fig. 9-27), the surfactant monomer will physically adsorb through hydrogen bonding and ionically bond with cationic surface sites. At higher surfactant concentrations, this association includes tail-to-tail interactions with the solution monomers, resulting in proportionally greater adsorption. At and above the CMC, the supply of monomers becomes constant, as does the retention. The Langmuir-type isotherm of adsorption versus overall surfactant concentration resembles the CMC plot in Fig. 9-4, which can be expressed as

$$C_{3s} = \frac{a_3 C_3}{1 + b_3 C_3} \quad (9.11-10)$$

where a_3/b_3 represents the plateau adsorption value. C_3 here is the surfactant concentration in the liquid phase wetting the substrate. The parameter b_3 is large, being related to the CMC, which is very small compared to practical surfactant concentrations (see Fig. 9-28). The surfactant isotherm therefore attains its plateau at such a low C_3 that it may be usefully represented as a step function. This form of retention should be reversible with surfactant concentration. The parameters a_3 and b_3 are functions of salinity since they depend on the number of surface sites available for adsorption.

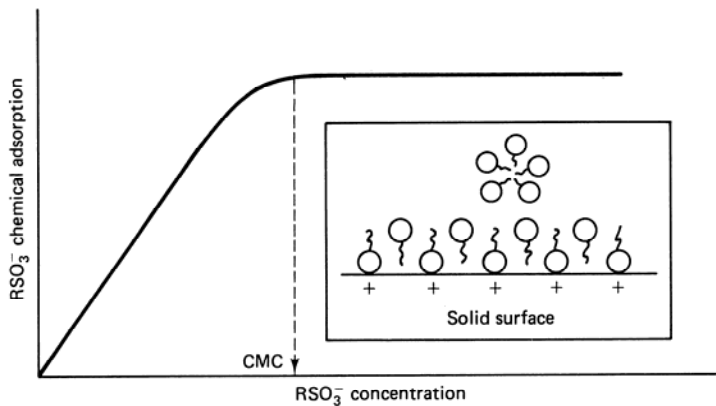


Figure 9-27 Surfactant adsorption on metal oxide surfaces (adapted from Harwell, 1983)

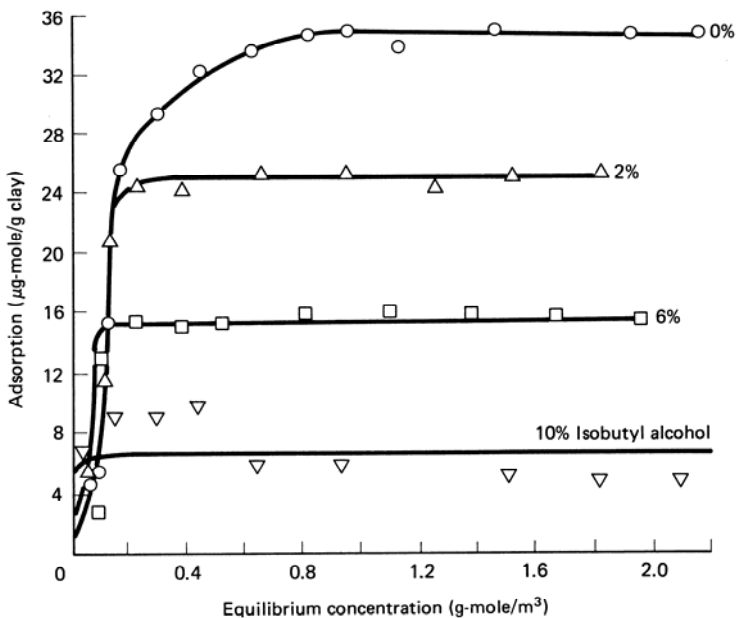
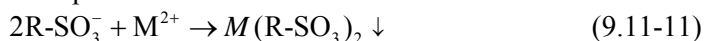


Figure 9-28 Effect of cosurfactant on surfactant retention. Surfactant is 4-phenyl dodecyl benzene sulfonate. (adapted from Fernandez, 1978)

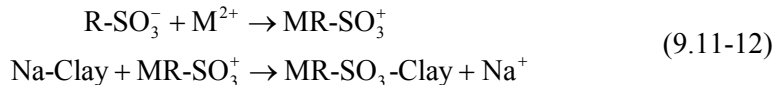
2. In hard brines, the prevalence of divalent cations causes the formation of surfactant–divalent complexes



which have a low solubility in brine. Precipitation of this complex will lead to retention. When oil is present, it can compete for the surfactant. Of course,

the precipitate must also compete with the micelles for the surfactant (Somasundrun et al., 1979).

3. At hardness levels somewhat lower than those required for precipitation, the preferred multivalent surfactant will be a monovalent cation that can chemically exchange with cations originally bound to the reservoir clays (Hill and Lake, 1978).



This effect is not unlike the divalent-micelle effect we discussed in Sec. 9-8. The surfactant bound to the clays will exhibit tail-tail interaction as in Fig. 9-27.

As a consequence of the ionic bonding and tail-tail interactions, adding a cosurfactant will reduce both types of retention (Fig. 9-28). Cosurfactants perform this service in two ways: (1) by filling surface sites that might otherwise be occupied by surfactant and (2) by mitigating the tail-to-tail associations. The retention expressed by Eq. (9.11-12) can also be lessened by filling the clay sites with a more preferred metal cation. This form of retention is reversible with both M^{2+} and surfactant concentration.

4. In the presence of oil in a II(+) phase environment, the surfactant will reside in the oil-external microemulsion phase. Because this region is above the optimal salinity, the IFT is relatively large, and this phase and its dissolved surfactant can be trapped. Figure 9-29 illustrates this phenomenon. The filled squares represent the surfactant injected, and the open squares the surfactant retained in a series of constant-salinity core floods. Retention increases smoothly with salinity (both a_3 and b_3 are functions of salinity) until 3% NaCl, at which point it increases so substantially that all the injected surfactant is retained. 3% NaCl is just above C_{Seu} for this system; hence the deviation can be nicely explained by phase trapping. A similar phase trapping effect does not occur in the II(-) environment because the aqueous mobility buffer miscibly displaces the trapped aqueous-external microemulsion phase. Using less than optimal salinities can, therefore, eliminate phase trapping. This form of retention is strongly affected by the MP phase behavior.

Most studies of surfactant retention have not made these mechanistic distinctions. Therefore, which mechanism predominates in a given application is not obvious. All mechanisms retain more surfactant at high salinity and hardness, which in turn, can be attenuated by adding cosurfactants. Precipitation and phase trapping can be eliminated by lowering the mobility buffer salinity at which conditions the chemical adsorption mechanism on the reservoir clays is predominant. In this event, there should be some correlation of surfactant retention with reservoir clay content. Fig. 9-30 attempts to make this correlation by plotting laboratory and field surfactant retention data against clay fraction. The correlation is by no means perfect since it

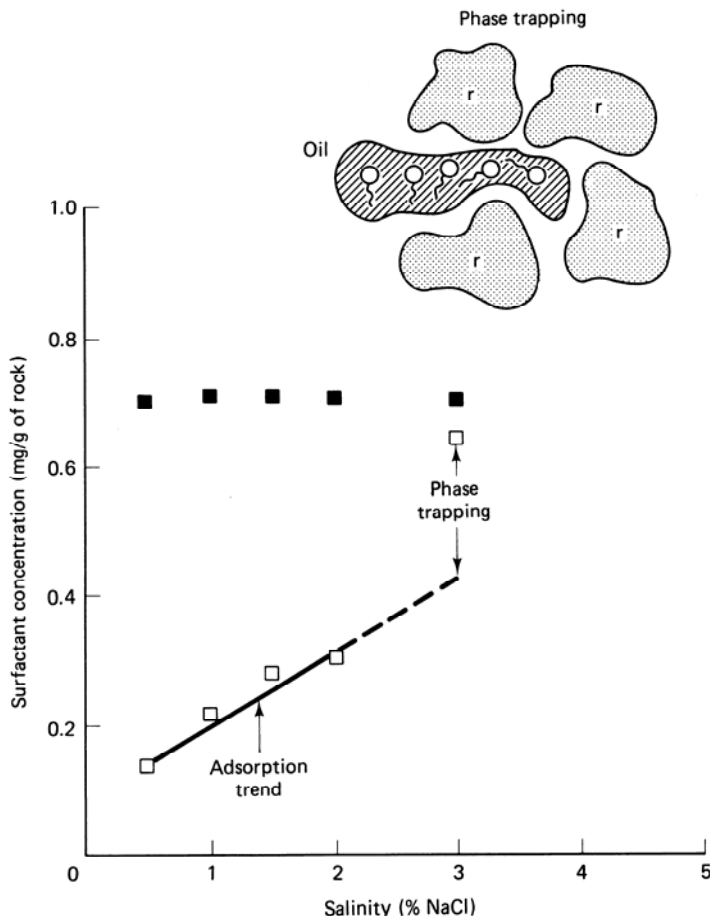


Figure 9-29 Surfactant retention caused by phase trapping; 3% NaCl is a type II(+) microemulsion system (from Glover, et al., 1979)

ignores variations in MP formulation and clay distribution as well as salinity effects. However, the figure does capture a general trend useful for first-order estimates of retention. In addition, note that the difference between lab- and field-measured retention is not significant. This observation implies that surfactant retention can be effectively measured in the laboratory.

A useful way to estimate the volume of surfactant required for an MP slug is through the dimensionless frontal advance lag D_3 defined in Eq. (9.10-6). C_{3s} is the surfactant retention from Fig. 9-30 (the plateau value a_3/b_3 on the appropriate isotherm), ϕ is the porosity, $C_{3,I}$ is the surfactant concentration in the MP slug, and ρ_s is the surfactant density. D_3 is a fraction that expresses the volume of surfactant retained at its injected concentration as a fraction of the floodable pore V_{pf} . For optimal surfactant usage, the volume of surfactant injected should be large enough to contact all V_{pf} but small enough to prevent excessive production of the surfactant.

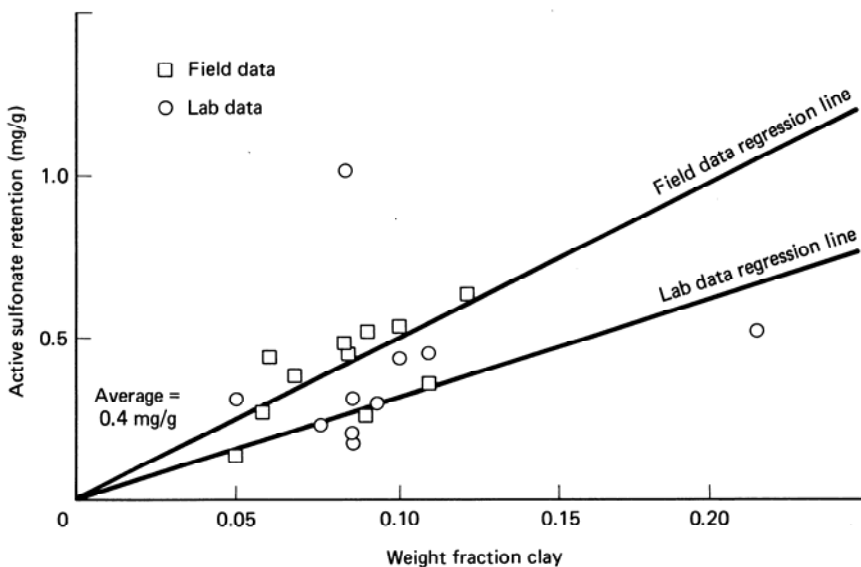


Figure 9-30 Overall surfactant retention correlated with clay content (adapted from Goldburg et al., 1983)

Besides wasting an expensive chemical, the produced surfactant can cause severe produced emulsions. Thus the MP slug size should be no less but not much greater than D_3 . The total amount of surfactant injected is independent of injected surfactant since, from Eq. (9.10-6), $D_3 C_{3J}$ is independent of C_{3J} .

9-12 TYPICAL PRODUCTION RESPONSES

In this section, we review responses of typical laboratory core and field flood showing the important features and expectations of MP flooding.

Laboratory Flood

Fig. 9-31 plots an effluent response of a typical MP flood in a Berea core showing oil cut, produced surfactant (Mahogany AA), cosurfactant, (isopropyl alcohol), polymer, and chloride anion concentrations. All concentrations have been normalized by their respective injected values. The chloride indicates the salinity in this flood. At the top of the figure is the phase environment of the produced fluids. The slug size is $t_{D_s} = 0.1$, and the horizontal axis is t_D , the volume of fluid injected since the start of the slug expressed as a fraction of the core's pore volume. There was no preflush. (For further details of this and similar core floods, see Gupta, 1980.)

Figure 9-31 shows a typical, though by no means optimal, oil recovery experiment. Before surfactant injection, the core was waterflooded so that it produces no oil initially. Oil breaks through at about $t_D = 0.2$, with relatively sustained cuts of

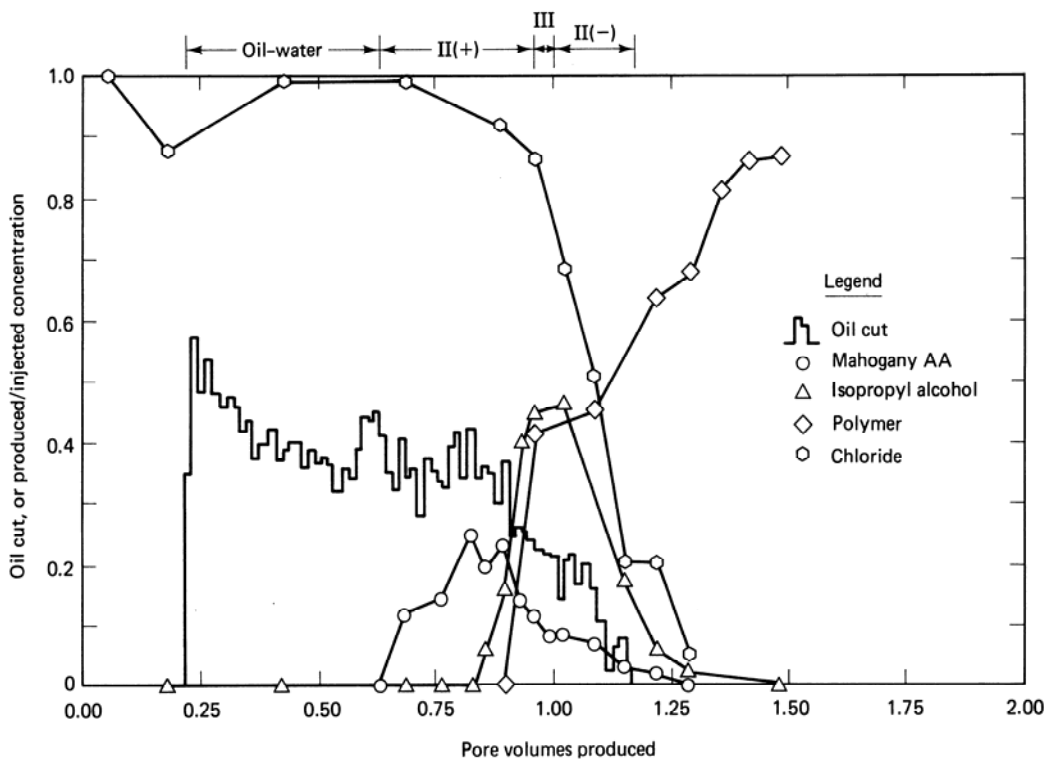


Figure 9-31 Typical core-flood produce response (from Gupta, 1980)

about 40% until about $t_D = 0.6$, at which point the surfactant appears. The behavior in this portion of the flood is consistent with the fractional flow theory in Sec. 9-10. About 60% of the produced oil is free of the injected chemicals. That 40% of the oil is produced with the surfactant indicates a viscous instability apparently caused by nonideal phase behavior. A well-designed flood will produce 80% to 90% of the oil ahead of the surfactant. Even here, though, the oil is invariably produced early and at fairly low cuts in laboratory experiments.

Surfactant breaks through at $t_D = 0.6$, reaches its maximum produced concentration of 30% of the injected concentration at $t_D = 0.8$, and ceases at $t_D = 1.5$. The total amount of surfactant produced is about one half that injected, which indicates substantial, though not excessive, retention.

The surfactant is preceding both the chloride and polymer by about 0.3 V_p . This separation indicates preferential partitioning of the cosurfactant between the aqueous and microemulsion phases (see Sec. 9-8 on phase behavior nonidealities). Though this did not drastically affect oil recovery, which is in excess of 90% of the residual oil, the separation is not a favorable indication for this design. A good MP design should show simultaneous production of all MP slug constituents as well as good oil recovery.

Field Response

As a field example, consider Fig. 9-32, which shows the produced fluid analyses of well 12-1 in the Bell Creek (Carter and Powder River counties, Montana) MP flood. This flood used a high oil content MP slug preceded by a preflush that contained sodium silicate to lessen surfactant retention and reduce divalent cation concentration. Well 12-1 was a producer in the center of an unconfined single five-spot pattern. (For further details on the flood, see Holm, 1982; Aho and Bush, 1982.)

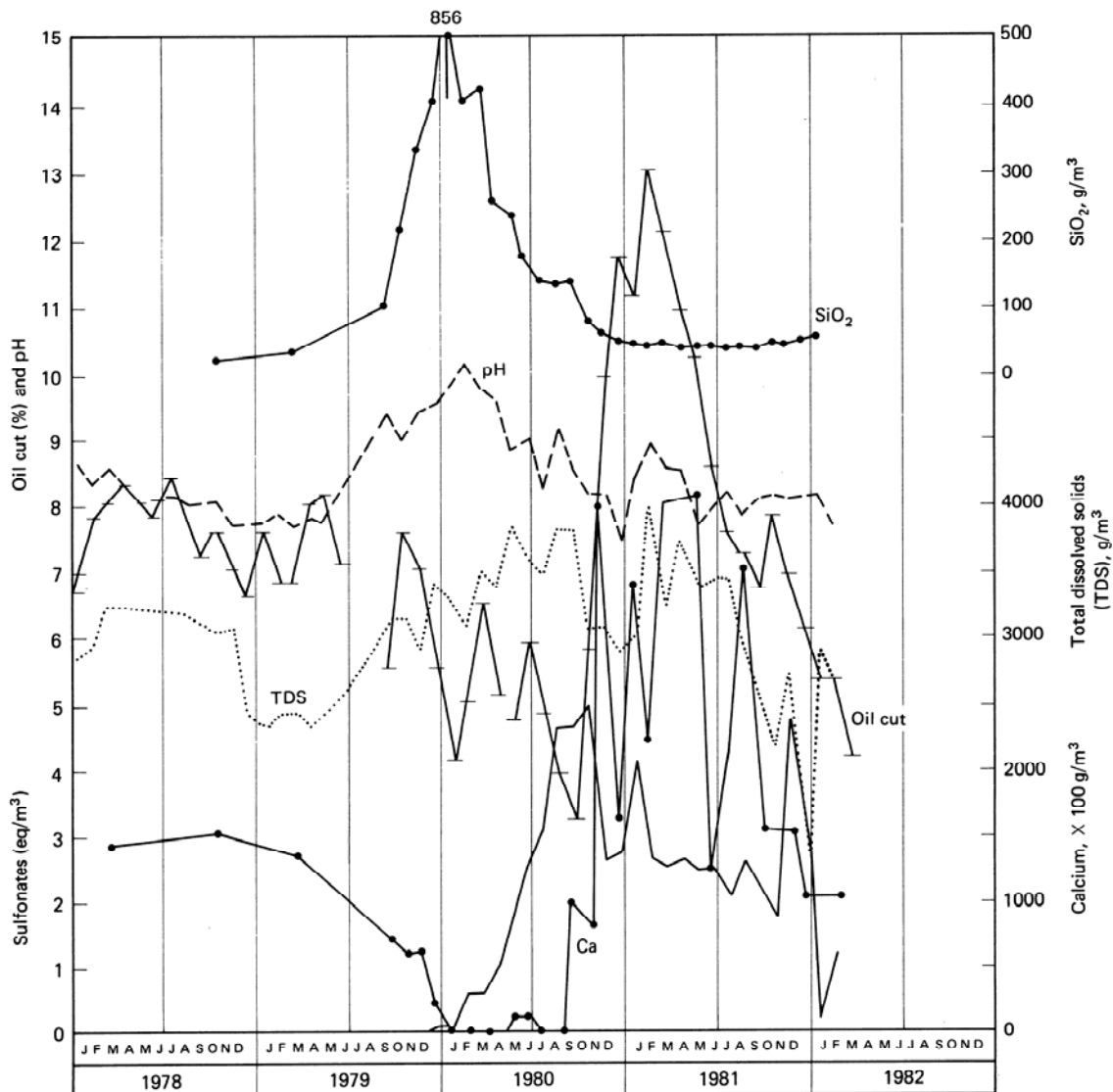


Figure 9-32 Production response from Bell Creek Pilot (from Holm, 1982)

Before MP slug injection in February, 1979, well 12-1 was experiencing low and declining oil cuts. Beginning in late 1980, MP oil response reversed the decline and reached peak cuts of about 13% about six months later. The pre-MP decline must be clearly established to accurately evaluate the MP oil recovery, an unnecessary step in evaluating the core flood. Moreover, compared to the core flood, there is no evident clean oil production; surfactant production actually preceded the oil response. Simultaneous oil and surfactant production is a persistent feature of field MP floods probably because of heterogeneities and dispersive mixing. The surfactant is preceding the oil in Fig. 9-32 because of preferentially water-soluble disulfonate components in the MP slug. The peak oil cut is invariably lower in field floods (13% in Fig. 9-32 versus nearly 60% in Fig. 9-31).

Other significant features in Fig. 9-32 are the evident presence of the preflush preceding the MP slug, inferred from the maxima in the pH and silicate concentrations, and the very efficient removal of the calcium cations ahead of the surfactant. But when oil production commenced, calcium rose roughly to its premicellar level.

Figure 9-33 shows ultimate oil recovery efficiency E_R (ultimate oil produced divided by oil in place at start of MP process) from a survey of more than 40 MP field tests correlated as a function of mobility buffer slug size t_{DMB} . Similar analyses on other process variables showed no or weak correlation (Lake and Pope, 1979). The strong correlation in Fig. 9-33 indicates the importance of mobility control in MP design. Though we have largely ignored mobility control in this chapter, it is

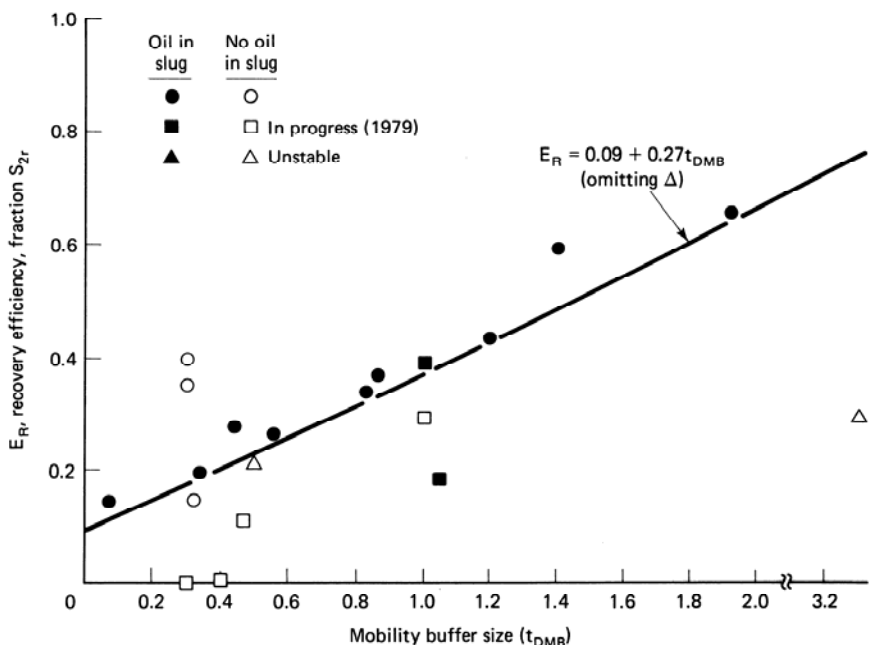


Figure 9-33 Recovery efficiencies from 21 MP field tests (adapted from Lake and Pope, 1979)

clearly an important variable. Note from Fig. 9-33 that the high oil content slugs have generally been driven by polymer drives larger than the high water content slugs.

Ultimate oil recovery efficiency averages about 30% of residual oil saturation in field tests (Fig. 9-33). Since oil recovery efficiency can be quite high in core floods, it seems that the peak oil cut and ultimate oil recovery efficiency in a technically successful MP field flood will average about one third of their respective values in core floods.

9-13 DESIGNING AN MP FLOOD

A successful MP flood must achieve three things for efficient oil recovery (Gilliland and Conley, 1975).

1. The MP surfactant slug must propagate in an interfacially active mode (i.e., at optimal conditions).
2. Enough surfactant must be injected so that some of it is unretained by the permeable media surfaces.
3. The active surfactant must sweep a large portion of the reservoir without excessive dissipation because of dispersion or channeling.

The first of these objectives is met through the formulation step of the MP design procedure; the second two objectives are met through scale up. Though there is considerable overlap, the formulation step consists mainly of test tube experiments and core floods; the scale-up steps consist mainly of core floods and numerical simulations.

Generating Optimal Conditions

There are three techniques for generating optimal conditions in MP floods.

1. Raise the MP slug optimal salinity to that of the resident brine salinity in the candidate reservoir. Philosophically, this procedure is the most satisfying of the three possibilities, and it is usually the most difficult. Though the subject of intensive research, surfactants having high optimal salinities that are not, at the same time, unstable at reservoir conditions, excessively retained by the solid surfaces, or expensive are yet to be discovered. Field successes with synthetic surfactants have demonstrated the technical feasibility of this approach (Bragg et al., 1982). A second way to make the optimal salinity of the MP slug closer to the resident brine salinity is to add cosurfactant. This approach is the most common implementation to date; however, as we

mentioned, there are penalties in surfactant–cosurfactant separation, loss of interfacial activity and expense.

2. Lower the resident salinity of a candidate reservoir to match the MP slug's optimal salinity. This common approach is the main purpose of the preflush step illustrated in Fig. 9-1. A successful preflush is appealing because, with the resident salinity lowered, the MP slug would displace oil wherever it goes in the reservoir, and retention would also be low. Preflushes generally require large volumes to significantly lower the resident salinity owing to mixing effects and cation exchange (see Sec. 9-11). With some planning, the function of preflush could be accomplished during the waterflood preceding the MP flood.
3. Use the most recent salinity gradient design technique for generating active MP slugs (Paul and Froning, 1973; Nelson and Pope, 1978; Hirasaki et al., 1983). This technique tries to dynamically lower the resident salinity to optimal during the course of the displacement by sandwiching the MP slug between the overoptimal resident brine and an underoptimal mobility buffer salinity. Table 9-4 illustrates the results of experimental core floods for different sequences of salinities. The experiment numbers on this table match the uncircled numbers in Fig. 9-8. Three core floods—numbers 3, 6, and 7—stand out both with respect to their low ultimate saturation and surfactant retention. The common feature of all these experiments is that the salinity of the polymer drive is underoptimal. In fact, no other variable, including, paradoxically, surfactant slug concentration, has such a similarly strong effect (Pope et al., 1982). The salinity gradient design has several other advantages: it is resilient to design and process uncertainties, provides a favorable environment for the polymer in the mobility buffer, minimizes retention, and is indifferent to the surfactant dilution effect.

TABLE 9-4 PHASE-ENVIRONMENT TYPE AND MP FLOOD PERFORMANCE FOR THE SALINITY-REQUIREMENT DIAGRAM IN FIG. 9-8 (FROM NELSON, 1982)

Chemical flood number	Phase type promoted by the			Residual oil saturation after chemical flood (% PV)	Injected surfactant retained by the core (%)
	Waterflood brine	Chemical slug	Polymer drive		
1	II(−)	II(−)	II(−)	29.1*	52
2	II(+) / III	II(+) / III	II(+) / III	25.2*	100*
3	II(+) / III	II(+) / III	II(−)	2.0†	61*
4	II(−)	II(−)	II(+) / III	17.6*	100*
5	II(−)	II(+) / III	II(+) / III	25.0	100
6	II(+) / III	II(−)	II(−)	5.6†	59†
7	II(−)	II(+) / III	II(−)	7.9*	73*
8	II(+) / III	II(−)	II(+) / III	13.7*	100*

* Average of duplicates

† Average of triplicates

Injecting Enough Surfactant

The first aspect of overcoming retention is to design the flood so that retention is as low as possible. This includes minimizing the chemical and physical adsorption effects discussed above and eliminating phase trapping by propagating the slug in a low-salinity environment. Cosurfactants and sacrificial agents in a preflush may also be appropriate. Once a low surfactant retention value is in hand, enough surfactant must be injected so that some of it transports to the production wells. As in polymer flooding, there are two aspects to this issue: the slug's surfactant concentration and the slug size.

Strong theoretical or practical reasons for selecting the slug surfactant concentration do not exist. The concentration must be large enough so that a type III region can form when the salinity is optimal but small enough so that the slug can be easily handled and transported. The latter requirement usually means the slug is single-phase and not excessively viscous and the surfactant does not precipitate.

Perhaps a more stringent lower bound on surfactant concentration is in its relative rate of propagation. The frontal advance loss of D_3 contains surfactant concentration in the denominator. This means the rate of slug propagation, as well as the maximum oil cut calculated from fractional flow theory (Fig. 9-24), decreases as concentration decreases. Because of the worth of the oil, the resulting delay in oil production is a liability to the process even if the ultimate oil recovery were unaffected. This argument suggests the concentration should be as large as possible, and the slug size should be correspondingly small. But extremely small slugs would seem to be sensitive to dispersive mixing in the reservoir.

Once the slug concentration is set, the slug size follows from the value of D_3 , as in Sec. 9-11. To satisfy retention, the slug size, based on floodable pore volume, must be somewhat larger than retention. Of course, how much larger is a strong function of the prevailing economics and reservoir characteristics. (For a graphical procedure, see Jones, 1972.)

Maintaining Good Volumetric Sweep

Figure 9-33 attests that the importance of this issue, particularly with respect to the mobility buffer, cannot be overstated.

The mobility control agent in the slug can be polymer or oil as in Fig. 9-13. Whatever the agent, it is of paramount importance that the slug-oil bank front be made viscously stable since small slugs cannot tolerate even a small amount of fingering. Thus we seek a slug less mobile than the oil bank it is to displace. To provide a margin of safety in estimating the oil bank mobility, use the minimum in the total relative mobility curves (see Sec. 3.3) to base the mobility control on. Such curves (Fig. 9-34) show that the minimum can be substantially less than the total relative mobility of either endpoint. Since these curves are subject to hysteresis, it is important that the relative permeability curves be measured in the direction of increasing oil saturation for tertiary floods.

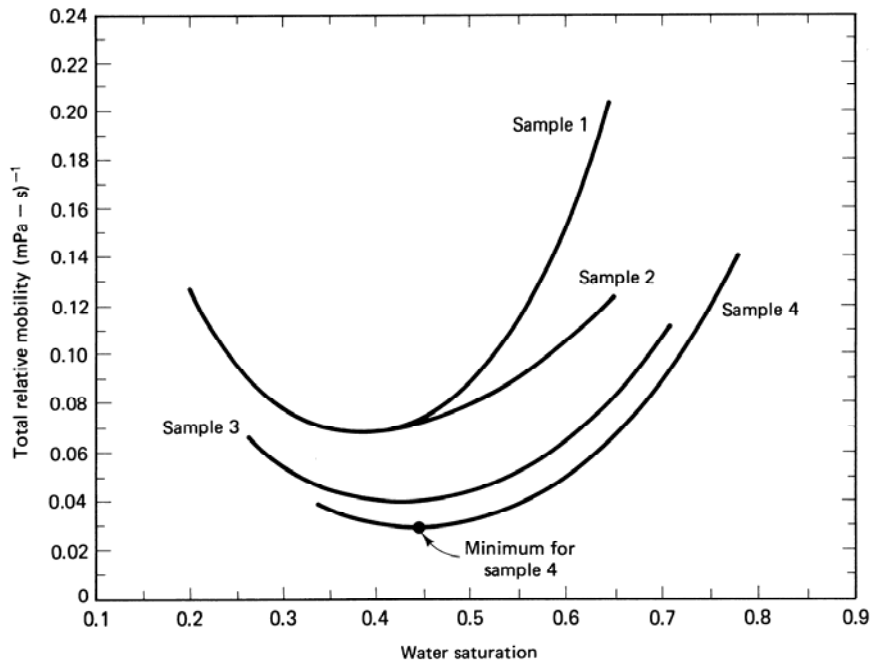


Figure 9-34 Total relative mobilities for samples of the same reservoir (from Gogarty et al., 1970)

Sizing the mobility buffer proceeds like the polymer drive we discussed in Sec. 8-5. Here the spike portion of the buffer must have mobility equal to or less than the slug mobility. Since the latter depends on the degree of oil desaturation, the buffer mobility cannot be designed independently of the slug.

9-14 MAKING A SIMPLIFIED RECOVERY PREDICTION

In the next few paragraphs, we describe a simple procedure to estimate oil recovery and oil rate-time curves for an interfacially active MP process. Since interfacial activity may be lost in innumerable ways, the procedure will be most accurate for processes that clearly satisfy the first design goal in Sec. 9-13. The procedure has two steps: estimating the recovery efficiency of an MP flood and then proportioning this recovery according to injectivity and fractional flow to give an oil rate-time curve. (For further details of the procedure, see Paul et al., 1982.)

Recovery Efficiency

The recovery efficiency E_R of a tertiary ($S_{2I} = S_{2R}$) MP flood is the product of a volumetric sweep efficiency E_V , a displacement efficiency E_D , and a mobility buffer efficiency E_{MB}

$$E_R = E_D E_V E_{MB} \quad (9.14-1)$$

Each quantity must be independently calculated.

Displacement efficiency. The displacement efficiency of an MP flood is the ultimate (time-independent) volume of oil displaced divided by the volume of oil contacted

$$E_D = 1 - \frac{S'_{2r}}{S_{2r}} \quad (9.14-2)$$

where S'_{2r} and S_{2r} are the residual oil saturation to an MP and a waterflood, respectively. S_{2r} must be known, but S'_{2r} can be obtained from a large slug (free from the effects of surfactant retention) laboratory core flood. Low values of S'_{2r} indicate successful attainment of good interfacial activity in the MP slug. If core flood results are not available, S'_{2r} may be estimated from a CDC using a “field” capillary number (Lake and Pope, 1978) based on the median velocity in a confined five-spot pattern.

$$N_{vc} = \frac{0.565q\sigma}{H_t \sqrt{A_p}} \quad (\text{dimensionless}) \quad (9.14-3)$$

Here, q is the volumetric injection rate and A_p is the pattern area. For approximate calculation, assume $\sigma = 1 \mu\text{N/m}$ in Eq. (9.14-3). The CDC chosen to estimate S'_{2r} should be consistent, as much as possible, with conditions of the candidate reservoir.

Volumetric sweep efficiency. Volumetric sweep efficiency E_V is the volume of oil contacted divided by the volume of target oil. E_V is a function of MP slug size t_{Ds} , retention D_3 , and heterogeneity based on the Dykstra-Parsons coefficient V_{DP} .

Consider the layered medium in Fig. 9-35 into which is injected an MP slug of size t_{Ds} . If the flow is apportioned by kh , and there is no crossflow, the slug size in layer l is

$$t_{Ds_l} = t_{Ds} \left(\frac{k}{\phi} \right)_l \left(\frac{\bar{\phi}}{\bar{k}} \right) = t_{Ds} F'_l \quad (9.14-4)$$

where Eq. (9.14-4) has introduced the derivative of the flow-capacity–storage-capacity curve (F - C curve) first discussed in Sec. 6-3. Besides invoking a continuous permeability–porosity distribution, using F - C curves implies the layers are arranged as decreasing (k/ϕ) . If $t_{Ds_m} > D_3$ in a particular layer m , it will be completely swept; otherwise, the layer’s volumetric sweep will be in proportion to t_{Ds_m}/D_3

$$E_{Vm} = \begin{cases} 1, & t_{Ds_m} > D_3 \\ \frac{t_{Ds_m}}{D_3}, & t_{Ds_m} \leq D_3 \end{cases} \quad (9.14-5)$$

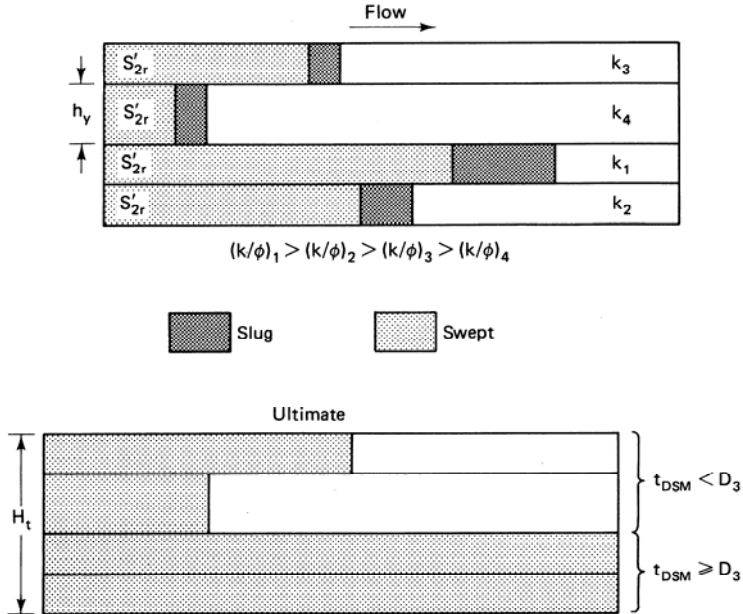


Figure 9-35 Schematic representation of MP slug sweep in a layered medium

Figure 9-35 illustrates this division. E_{Vm} summed over $n = 1, \dots, m, \dots, N_L$ layer after being weighted by $(\phi h)_m$ gives

$$E_V = C_m + \frac{t_{Ds}}{D_3} (1 - F_m) \quad (9.14-6)$$

To calculate E_V with t_{Ds} , D_3 , and F - C curve known, begin by finding the layer number m where $t_{Ds_m} = D_3$. This determines the coordinates $(F, C)_m$ in Eq. (9.14-6) to determine E_V . Equations (6.3-11) and (6.3-12) establish a relation between the F - C curves, the heterogeneity factor H_K , and V_{DP} for a lognormal continuous permeability distribution; thus E_V in Eq. (9.14-6) can be related directly to V_{DP} . Figure 9-36 shows this relationship. V_{DP} may be estimated from geologic study, matching the prior waterflood, or core data (see Table 6-1). The D_3 is from Eq. (9.10-6).

Mobility buffer efficiency. The mobility buffer efficiency E_{MB} is a function of E_V and V_{DP}

$$E_{MB} = (1 - E_{MBe}) \left[1 - \exp \left(\frac{-0.4t_{DMB}}{E_V^{1.2}} \right) \right] + E_{MBe} \quad (9.14-7a)$$

and

$$E_{MBe} = 0.71 - 0.6V_{DP} \quad (9.14-7b)$$

where E_{MBe} is the mobility buffer efficiency extrapolated to $t_{DMB} = 0$, and t_{DMB} is the mobility buffer volume, fraction V_{pf} . Equation (9.14-7) was obtained by numerical simulation.

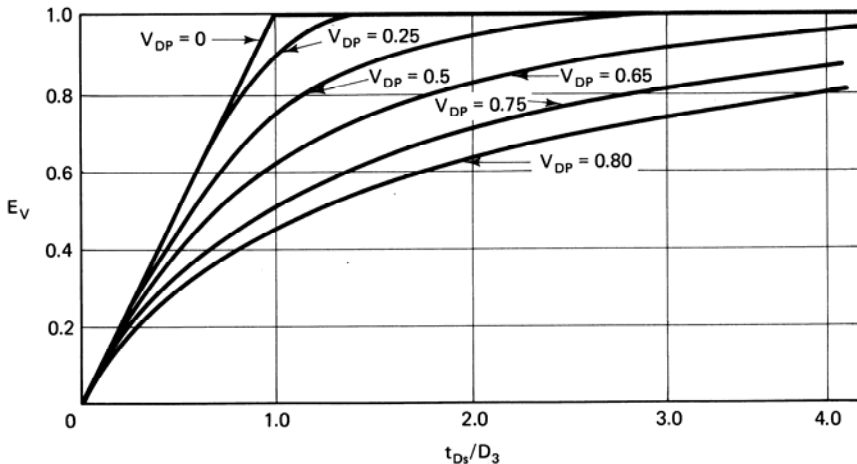


Figure 9-36 Effect of slug size–retention ratio on vertical sweep efficiency (from Paul et al., 1982)

The recovery efficiency E_R now follows from Eq. (9.14-1), which may be checked for reasonableness against Fig. 9-33.

Calculation of an Oil-Rate–Time Plot

The production function (oil rate q_2 versus time) is based on E_R and the following procedure. We assume the dimensionless production function is triangular with oil production beginning when the oil bank arrives. From here, q_2 increases linearly to a peak (maximum) oil cut when the surfactant breaks through and then decreases linearly to the sweep-out time. The triangular shape is imposed by the reservoir heterogeneity.

The first step is to calculate the dimensionless oil bank and surfactant breakthrough times for a homogeneous flood

$$t_{D_B} = \left(\frac{S_{2_B} - S_{2I}}{f_{2_B} - f_{2I}} \right) t_{D_s} \quad (9.14-8a)$$

$$t_{D_s} = 1 + D_3 - S'_{2r} \quad (9.14-8b)$$

where t_{D_B} is the dimensionless oil bank arrival time, and t_{D_s} is the surfactant arrival time. S_{2_B} and f_{2_B} may be estimated from the simplified fractional flow theory (see Sec. 9-10) or directly from laboratory experiments.

The second step is to correct these values for the heterogeneity of the candidate reservoir using the heterogeneity factor H_K defined in Eq. (6.3-11).

The corrected breakthrough times are now

$$\hat{t}_{D_B} = \frac{t_{D_B}}{H_K} \quad (9.14-9a)$$

$$\hat{t}_{Ds} = \frac{t_{Ds}}{H_K} \quad (9.14-9b)$$

and the peak oil cut f_{2pk} is

$$\hat{f}_{2pk} = \frac{\left(H_K - H_K \left(\frac{t_{D_B}}{t_{Ds}} \right)^{1/2} \right)}{(H_K - 1)} f_{2_B} \quad (9.14-10)$$

The symbol $\hat{\cdot}$ represents a quantity in a layered medium.

The final step is to convert the dimensionless production function to oil rate q_2 versus time t . This follows from

$$q_2 = q \hat{f}_2 \quad (9.14-11a)$$

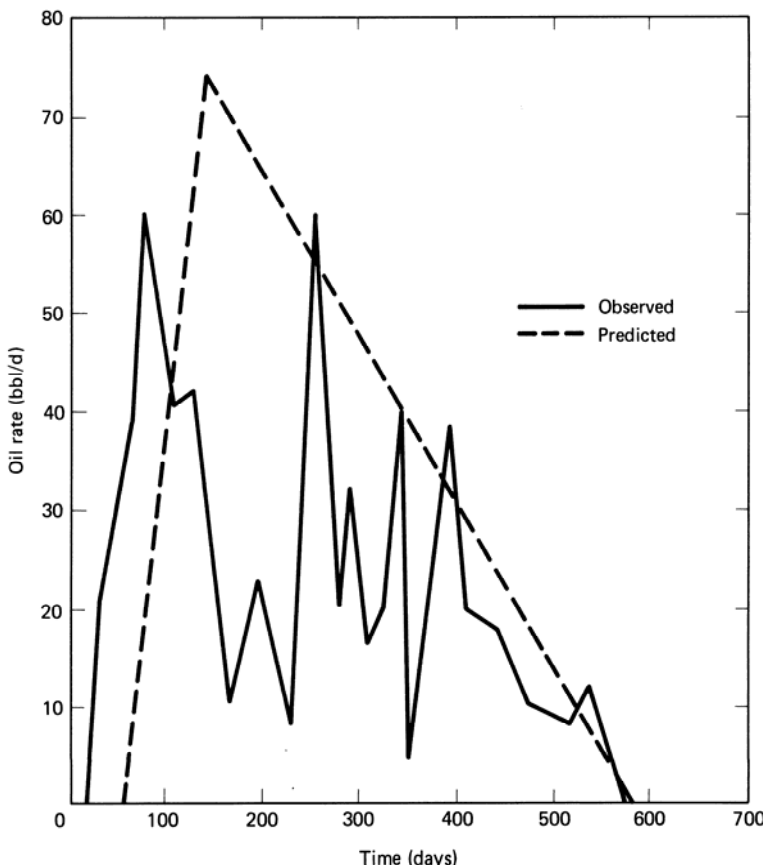


Figure 9-37 Comparison between predicted and observed oil-rate-time responses for the Sloss micellar-polymer pilot (from Paul et al., 1982)

$$t = \frac{V_{pf} \hat{t}_D}{q} \quad (9.14-11b)$$

Here \hat{f}_2 and \hat{t}_D are any points on the triangular oil recovery curve that begins at $(\hat{t}_{D_B}, 0)$, peaks at $(\hat{t}_{D_s}, \hat{f}_{2pk})$, and ends at $(\hat{t}_{D_{sw}}, 0)$. $\hat{t}_{D_{sw}}$, the dimensionless time at complete oil sweepout, is selected to make the area under the \hat{f}_2 - \hat{t}_D curve equal to E_R ,

$$\hat{t}_{D_{sw}} = \hat{t}_{D_B} + \frac{2E_R S_2}{\hat{f}_{2pk}} \quad (9.14-12)$$

Figure 9-37 compares the results of this procedure with the Sloss MP pilot.

9-15 CONCLUDING REMARKS

In terms of the number of design decisions required, micellar-polymer flooding is the most complicated enhanced oil recovery process. This complexity, along with reservoir heterogeneity and the need for a rather large capital investment, make micellar-polymer flooding a high-risk process. Consequently, recent years have seen a decline in interest in the process. The potential for the process is immense, however, even slightly exceeding that of thermal methods, at least in the United States. Moreover, both polymer and MP flooding seem uniquely suited for light-oil reservoirs in isolated areas of the world.

Reservoirs amenable to micellar-polymer flooding contain light- to medium-weight oils with moderate to high permeability. Since injectivity is essential in this process as in polymer flooding, we seek reservoirs with depth sufficient to tolerate high injection pressures but not so deep as to promote thermal degradation. Finally, the process is sensitive to high brine salinities, although this can be dealt with somewhat by suitable surfactant/polymer selection and design.

The important topics in this chapter deal with the association of interfacial activity with brine salinity and hardness through phase behavior, the importance of surfactant retention, and the need for good mobility control. In a sense, the design criteria given in Sec. 9-13 apply to all EOR processes, but it is only in micellar-polymer flooding that all criteria seem to apply with equal severity. Finally, the screening estimation of recovery in Sec. 9-14 is a useful yet simple tool for assessing the suitability of a reservoir and for estimating the risk associated with the process.

EXERCISES

- 9A. The Units of MP Flooding.** A particular petroleum sulfonate surfactant has an average molecular weight of 400 kg/kg-mole, a density of 1.1 g/cm³, and a monosulfonate-to-disulfonate mole ratio of 4. Express the overall surfactant concentration of a 5 volume percent aqueous solution in g/cm³, kg-moles/cm³, meq/cm³, mole fraction, and mass fraction.

- 9B.** *Surfactant Equilibria and Aggregation.* Relatively simple models can reveal much about surfactant equilibria. The surfactant is a monosulfonate in this problem.
- (a) The aggregation of surfactant monomers into micelles in a NaCl brine may be represented by the following reaction:



where N_A is the aggregation number. Using the definition for total surfactant (monomer + micelles), derive an expression between total and monomer sulfonate concentrations. If the equilibrium constant for Eq. (9B-1) is 10^{15} and $N_A = 10$, estimate the critical micelle concentration. The total sodium concentration is 10,000 g/m³.

- (b) Consider a more complicated situation where 0.3175 kg-moles/m³ monosulfonate surfactant solution is added to a NaCl brine. In a NaCl brine solution, five species can form: surfactant monomer (RSO_3^-), surfactant micelles [$(\text{RSO}_3\text{Na})_{N_A}$], free sodium-surfactant (RSO_3Na), precipitated sodium-surfactant ($\text{RSO}_3\text{Na}^\downarrow$), and free sodium (Na^+). Calculate the concentration of each species when the overall sodium concentration is 100 g/m³. Use the data in part (a) for the monomer-micelle reaction, and take the equilibrium constant for the sodium-sulfonate formation to 3×10^6 and the solubility product for the precipitate to be 10^{-8} .
- (c) Repeat the calculation of part (b) if the overall sodium concentration is 100,000 g/m³. What can you conclude about the effect of high salinities on surfactant precipitation?
- 9C.** *Phase Ratios for Hand's Rule.* In Sec. 4.4, we saw that flash calculations for vapor-liquid equilibria required using flash vaporization ratios or K -values. The analogous quantities for Hand's rule are *phase ratios* defined as

$$R_{ik}^j = \frac{C_{ij}}{C_{kj}} \quad (9\text{C}-1)$$

for components i and k . Nearly all the flash calculation can be formulated in terms of the phase ratios. Assume a type II(–) phase behavior ($j = 2$ or 3) in the following:

- (a) Show that the Hand equations for the binodal curve (Eq. 4.4-23) and the component distribution (Eq. 4.4-24) can be written as

$$R_{32}^j = A_H (R_{31}^j)^B, \quad j = 2 \text{ or } 3 \quad (9\text{C}-2)$$

$$R_{32}^2 = E_H (R_{31}^3)^F \quad (9\text{C}-3)$$

- (b) We can interchange the roles of phase concentrations and phase ratios. Show that the consistency relation $\sum_{i=1}^3 C_{ij} = 1$ reduces to

$$C_{ij} = \left(\sum_{k=1}^3 R_{ki}^j \right)^{-1}, \quad j = 2 \text{ or } 3 \quad (9\text{C}-4)$$

where $R_{ii}^j = 1$.

There are 18 phase ratios in two-phase systems. But only 4 of these are independent since

$$R_{ik}^j = (R_{ki}^j)^{-1} \quad \text{and} \quad R_{ik}^j = \frac{R_{im}^j}{R_{km}^j} \quad (9\text{C}-5)$$

As is consistent with the phase rule, specifying any one of these will determine the others and all phase concentrations through Eq. (9C-4). Solve for the phase concentrations when $R_{31}^2 = 5$. Take $A_H = 0.5$, $B_H = -1.5$, $E_H = 0.137$, and $F_H = 0.65$. Note that the phase ratios for the microemulsion phase are the same as solubilization parameters.

9D. *Using the Hand Equations*

- (a) For the Hand parameters $A_H = 2$, $B_H = -0.5$, $E_H = 600$, and $F_H = 2.3$, plot the binodal curve and at least two tie lines on triangular coordinates. Flash calculations in two-phase regions require an additional constraint over those in Exercise 9C. The constraint here is the equation of a tie line

$$S_1 = \frac{C_i - C_{i3}}{C_{i1} - C_{i3}}, \quad i = 1, 2, \text{ or } 3 \quad (9D-1)$$

for type II(+) systems (where $j = 1$ replaced $j = 2$ in Eqs. [9C-2] and [9C-3]). Any two of these may be used for a flash calculation, for example,

$$\frac{C_1 - C_{13}}{C_{11} - C_{23}} - \frac{C_2 - C_{23}}{C_{21} - C_{23}} = f \quad (9D-1)$$

The flash consists of picking the correct phase ratio (see Exercise 9C) so that $f = 0$ with the C_i known.

- (b) Calculate the compositions and amounts of each phase present if the overall composition C_i is $(0.45, 0.45, 0.1)$.
- 9E.** *Two-Phase Flash Calculation (Plait Point in Corner).* In a type II(+) system with the plait point in the brine corner, we have $C_{11} = 1$, and $C_{21} = C_{31} = 0$. The phase distribution Eq. (9.7-9) now becomes superfluous, as does the binodal Eq. (9.7-5) for the aqueous phase. The entire Hand representation collapses to

$$\frac{C_{33}}{C_{23}} = A_H \left(\frac{C_{33}}{C_{13}} \right)^{B_H} \quad (9E-1)$$

- (a) Show that the tie line equation for this special case reduces to

$$C_{23} = C_{33} \left(\frac{C_2}{C_3} \right) \quad (9E-2)$$

$$C_{13} = 1 - C_{33} \left[\frac{(1 - C_1)}{C_3} \right] \quad (9E-3)$$

which express the microemulsion phase concentrations as ratios of each other.

- (b) Show that Eqs. (9E-1) through (9E-3) may be used to solve explicitly for the surfactant concentration in the microemulsion phase as

$$\frac{1}{C_{33}} = \frac{1 - C_1}{C_3} + \left(\frac{C_3}{A_H C_2} \right)^{-1/B_H} \quad (9E-4)$$

- (c) For an overall composition of $C_i = (0.45, 0.45, 0.1)$, solve Eq. (9E-4) for the phase composition and the saturation of the aqueous phase. Take $A_H = 2$ and $B_H = -0.5$.

- (d) Compare the results of part (c) with the results of part (b) of Exercise 9D. What do you conclude about approximating this phase behavior with the plait point in one of the corners of the ternary?
- 9F.** *Equilibrium Calculations with Simplified Phase Behavior.* Use the simplified Hand representations with $B_H = -1$ and $F_H = 1$ in the following. Further, take the left and right oil coordinates of the plait point to be 0.05 and 0.95, respectively; the low-, optimal-, and high-salinity binodal curve heights to be 0.2, 0.1, and 0.2, respectively; and the lower- and upper-effective salinity limits to be 0.06% and 1.4% NaCl. The optimal salinity is at the midpoint between these two. Make all the calculations at a salinity of 0.08% NaCl where the phase environment is type III.
- Calculate the Hand parameter A_H and the coordinates of the two plait points and of the invariant point.
 - Plot the binodal curve and the three-phase region on a ternary diagram.
 - Calculate the phase concentrations and saturations at an overall concentration of $C_i = (0.65, 0.3, 0.05)$.
 - Repeat part (c) at an overall concentration of $C_i = (0.44, 0.44, 0.12)$. Plot both points on the diagram of part (b).
- 9G.** *Phase Behavior and IFT.* Fig. 9G shows the bottom half of six surfactant–brine–oil mixtures. These diagrams are on rectangular coordinates having a greatly expanded vertical scale. C_{Se} is the salinity in wt. % NaCl. In the following, the surfactant concentration is 0.05 volume fraction:
- Calculate and plot volume fraction diagrams at brine–oil ratios of 0.2, 1.0, and 5.
 - At a brine–oil ratio of 1, calculate and tabulate the solubilization parameters.
 - Use the correlation in Fig. 9-9 to convert the solubilization parameters to interfacial tensions. Plot these solubilization parameters against salinity, and estimate the optimal salinity.
 - Plot the IFTs in part (c) against salinity on semilog paper. Estimate the optimal salinity based on IFT and the optimal IFT.
 - Compare the optimal salinities in parts (c) and (d) to the midpoint salinity. The latter is the salinity halfway between C_{Seu} and C_{Sel} .
- 9H.** *Fractional Flow Construction for Type II(–) Systems.* Fig. 9H shows water fractional flux curves for a type II(–) MP system for which all tie lines extend to the common point $C_i^o = (0, 1, 1, 1, 0)$.
- Calculate and plot an overall water concentration (C_1) profile at oil bank breakthrough and an effluent water flux (F_1) for the following cases:

Case	Injected composition (J)			Initial composition (I)	
	C_2	C_3		C_1	C_2
1	0	0.10		0.66	0.34
2	0.97	0.03		0.66	0.34
3	0	0.10		0.20	0.80

For all cases, the displacement satisfies the fractional flow assumptions, the surfactant is not retained by the permeable medium, and the surfactant injection is

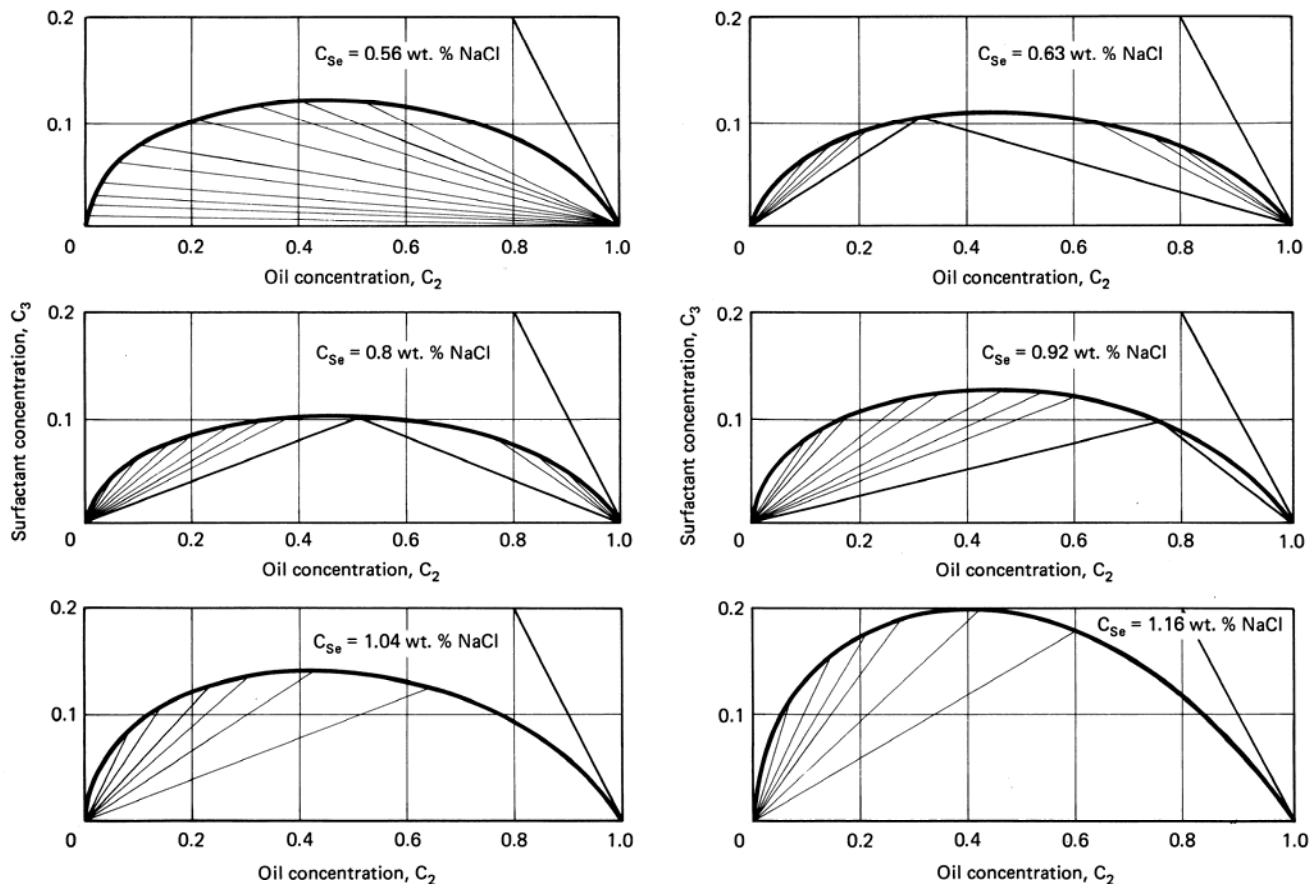


Figure 9G Ternary diagrams at various salinities (from Engleson, 1981)

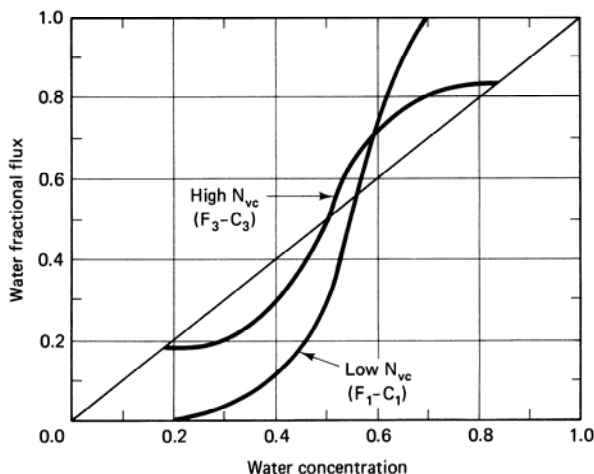


Figure 9H Water fractional flux for Exercise 9H

continuous. All injected compositions lie on extensions of the tie lines whose fractional flux curves are shown in the figure.

- (b) On the water concentration profiles of part (a), sketch (no calculation necessary) the microemulsion phase saturation S_3 profile.
- (c) On the water effluent histories of part (a), sketch the overall surfactant C_3 effluent history.
- 9I. *Two-Phase II(–) Fractional Flow.* Use the data in Figs. 9G and 9–9 in the following. Take the oil-free injected slug concentration to be 0.05 volume fraction surfactant, and the salinity to be constant at 0.56% NaCl. The surfactant is in an ideal mixture. The low N_{vc} relative permeability curves are given by

$$S_{2r} = 0.3, \quad k_{r2}^0 = 0.8, \quad n_2 = 1.5$$

$$S_{3r} = 0.2, \quad k_{r3}^0 = 0.1, \quad n_2 = 3$$

Phase 3 is water when N_{vc} . The displacement occurs at a superficial velocity of 10 $\mu\text{m}/\text{s}$. The microemulsion, oil, and water viscosities are 2, 5, and 1 mPa-s. The medium is horizontal. Use Fig. 3-19 as the capillary desaturation curve.

- (a) Estimate and plot the relative permeability curves corresponding to the tie lines the initial and injection conditions are on. Use the high N_{vc} relative permeabilities of Eqs. (9.9-1) and (9.9-2).
- (b) Estimate and plot the microemulsion fractional flow curves along the two tie lines in part (a).
- (c) Plot the time–distance diagram and a composition profile at oil bank breakthrough for this displacement if the injection is continuous surfactant. Use the simplified fractional flow analysis of Eqs. (9.10-5) through (9.10-9). Take $D_3 = 0.1$.
- 9J. *Slugs and Simplified Fractional Flow.* Use the simplified fractional flow of Eqs. (9.10-5) through (9.10-9) in the following. The displacement is a constant II(–) phase environment consisting of an oil-free surfactant slug followed by a polymer drive. The water-, oil-, and microemulsion-phase viscosities are 1, 5, and 10 mPa-s, respectively, and the relative permeability data at low and high N_{vc} are

	Oleic phase			Microemulsion phase		
	S_{2r}	k_{r2}^0	n_2	S_{3r}	k_{r3}^0	n_3
Low N_{vc}	0.3	0.8	1.5	0.2	0.1	5.0
High N_{vc}	0.05	0.9	1.2	0.1	0.6	2.5

- (a) Estimate the polymer solution viscosity in the mobility buffer if the mobility ratio between the slug and drive is to be 0.8. The polymer has no permeability reduction effect.
- (b) Calculate and plot the three aqueous-phase fractional flow curves (water–oil, microemulsion–oil, polymer-solution–oil) based on the data in part (a) and the polymer solution viscosity.
- (c) Estimate the minimum slug size required to entirely sweep the one-dimensional medium with slug. Take $D_3 = 0.2$ and $D_4 = 0.1$. There is no polymer in the slug.
- (d) Calculate and plot the time–distance diagram if the slug size is one half that estimated in part (c).
- (e) Calculate and plot saturation profiles at $t_D = 0.3$ and 0.8 for the conditions of part (d).
- 9K.** *Fractional Flow with Oil-Soluble Slug.* For this exercise, take the displacement to be constant type II(+) phase environment ($j = 1$ or 3) with the plait point in the brine corner. The surfactant is now dissolved in a predominantly oleic phase.
- (a) Show that the surfactant-specific velocity is analogous to Eq. (9.10-5)
- $$v_{\Delta C_3} = \frac{1 - f_1^s}{1 - S_1 + D_3} \quad (9K-1)$$
- and the oil bank saturation is given by the solution to
- $$v_{\Delta C_2} = \frac{C_{2J}f_1^s - f_{1B}^s - C_{3J}}{C_{2J}S_1 - S_{1B} - C_{3J}} = \frac{1 - f_1^s}{1 - S_1 + D_3} \quad (9K-2)$$
- (b) Illustrate the graphical solution of Eq. (9K-2) on an aqueous-phase fractional flow plot. What is the effect of injected oil concentration on the oil bank saturation? Justify this observation on physical grounds.
- (c) Figure 9K shows high- and low- N_{vc} fractional flow curves for a particular displacement. Based on these curves, calculate and plot an oleic-phase saturation profile at $t_D = 0.5$. Take $D_3 = 0.1$ and the surfactant injection to be continuous.
- 9L.** *Preflush Size Estimation.* The composition of an initial reservoir brine and a possible preflush solution are as follows:

Species	Reservoir brine (I), meq/cm ³	Preflush (J), meq/cm ³
Na^+	0.02	0.01
Ca^{2+}	0.06	0.005
Cl^-	0.08	0.015

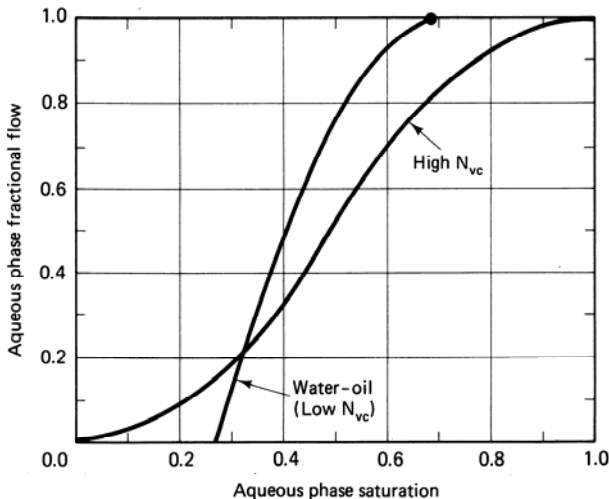


Figure 9K Aqueous-phase fractional flow curves for Exercise 9K

The cation exchange capacity of the reservoir is $Z_v = 0.05 \text{ meq/cm}^3$ of pore volume. The cation exchange satisfies Eq. (9.11-3) with $K_N = 0.1$. Assume single-phase flow of an ideal solution that contains only the species explicitly stated above.

- (a) Sketch this displacement in composition space as in Fig. 9-25a.
 - (b) Estimate the pore volumes of fluid J required to reduce the effluent calcium concentration to the injected value. What percentages of the clays are in the calcium form at this point?
 - (c) Calculate and plot the time-distance diagram for this displacement.
 - (d) State whether you think this would be an effective preflush for an MP flood.
- 9M.** *Importance of Mobility Control in MP Floods.* In the absence of other data, high N_{vc} relative permeabilities for a type II(–) system may be approximated by straight lines through the points $(S'_{3r}, 0)$ and $(1 - S'_{2r}, k_{r3}^0)'$ for the aqueous phase and through $(S'_{3r}, k_{r2}^0)'$ and $(1 - S'_{2r}, 0)$ for the oleic phase.
- (a) Plot two high- N_{vc} fractional flow curves for aqueous-phase ($j = 3$) viscosities of 5 and 50 mPa-s. Take $\mu_2 = 5$, $\mu_3 = 0.8 \text{ mPa-s}$, $S'_{3r} = 0.15$, $S'_{2r} = 0.05$, $(k_{r3}^0)' = 0.8$, and $(k_{r2}^0)' = 0.6$. The medium has no dip.
 - (b) Using the El Dorado relative permeabilities of Fig. 8L, illustrate the effects of good mobility control on an MP flood by calculating oil saturation profiles for the two cases in part (a) at $t_D = 0.3$. The frontal advance lag $D_3 = 0.16$. The injected aqueous surfactant is continuous.
- 9N.** *Performance Prediction.* Use the following information to perform a screening estimation of oil recovery on an MP project. The water–oil relative permeability data in Fig. 9K is appropriate.
- (a) Estimate the swept zone oil displacement efficiency E_D if the injection rate per pattern is $65 \text{ m}^3/\text{day}$. The pattern area is 8.1 hm^2 , and the formation thickness is 2 m. Take the IFT to be $1 \text{ } \mu\text{N/m}$, and use the CDC in Fig. 3-19 for the nonwetting phase.
 - (b) Calculate the volumetric sweep efficiency E_V . Take the Dykstra-Parsons coefficient to be 0.5, the slug size to be 0.16, and $D_3 = 0.12$.
 - (c) Estimate the recovery efficiency based on the above if the mobility buffer size is 0.8 PV.
 - (d) Calculate and plot the oil production rate versus time.